WIPP Library

March 17, 1995

Systems Prioritization Method - Iteration 2 Baseline Position Paper:

Repository Seals Program

F.D. Hansen, M.K. Knowles, J.R. Tillerson,
J.D. Schreiber, and P. Vaughn

Sandia National Laboratories
P.O. Box 5800
Albuquerque, NM 87185

950316

CONTENTS

1.0 INTRODUCTION 1

2.0 SEAL DESIGN BASIS 3
2.1 Impact of Regulations on Seal Design 3
2.2 Design Requirements 4

3.0 SHAFT SEAL SYSTEM DESIGN 5
3.1 Near-Surface Subsystems 6
3.1.1 Earthen Fill 6
3.1.2 Rustler Formation Subsystem 9
3.2 Salado Formation Subsystems 9
3.2.1 Upper Short-Term Seal 12
3.2.2 Upper Salt Column 12
3.2.3 Middle Short-Term Component 13
3.2.4 Middle Salt Column 13
3.2.5 Lower Short-Term Component 14
3.2.6 Lower Salt Column 14
3.2.7 Shaft Station Concrete Monolith 14

4.0 1992 PA, CURRENT PA AND BASELINE 15
4.1 1992 PA 15
4.2 Current PA Calculations 21
4.2.1 Revision to Shaft Seal Models 21
4.2.2 Panel Seal Performance 25
4.3 Seals Baseline Information 30

5.0 SUMMARY AND CONCLUDING REMARKS 37
5.1 Internal Issues 37
5.2 External Issues 38

6.0 REFERENCES 41

Figures

3-1. Representative WIPP shaft seal system. 7
3-2. Near-surface seal subsystems. 8
3-3. Salado Formation subsystem 10
4-1. 1992 Performance Assessment model. 16
4-2. North-south vertical cross section of model domain. 22
4-3. Long-term cumulative brine flow to shaft. 27
4-4. Early cumulative brine flow to shaft. 28
4-5. Long-term cumulative gas flow to shaft. 29
4-6. Ranges of permeabilities for seal materials. 31
4-7. Baseline permeabilities for shaft model elements. 34

Table

4-1. Seal System Input to PA 18

ACRONYMS

CAO	Carlsbad Area Office (DOE)
DOE	US Department of Energy
DRZ	Disturbed Rock Zone
EPA	US Environmental Protection Agency
NMVP	No-Migration Variance Petition
PA	Performance Assessment
PI	Principal Investigator
QA	Quality Assurance
RCRA	Resource Conservation and Recovery Act
SPM	System Prioritization Method
SPM-2	Systems Prioritization Methodology-2
SSSPT	Small-Scale Seal Performance Test
VOC	Volatile Organic Compound
WIPP	Waste Isolation Pilot Plant

1.0 INTRODUCTION

This paper presents the position of the seal system for the Waste Isolation Pilot Plant (WIPP). A process called Systems Prioritization has been implemented to determine priorities for WIPP project activities. To support Systems Prioritization Methodology (SPM), a series of position papers covering a wide range of technical investigations has been developed. The SPM has been implemented twice. The first interaction (SPM-1) basically assembled appropriate codes and ran through Performance Assessment (PA) calculations for compliance determination. Now, in support of SPM-2, the position papers have been updated based on the needs of the SPM and through incorporation of extensive technical, editorial, and programmatic comments. This paper is a baseline for SPM-2 calculations using PA codes which quantify expectations of meeting regulatory compliance today. The process of SPM included an elicitation of probabilities for various representations of the seal system. SPM-2 is expected to identify priority activities for compliance. Periodically in the future, PA will calculate the expected performance of the WIPP.

Seal performance parameters provide input to PA calculations, and in that respect, they contribute directly to regulatory compliance evaluations. In turn, PA makes certain modeling assumptions and simplifications to the seal system layout and performance parameters. This position paper summarizes the project position, including regulatory requirements, designs of the proposed seals system, PA calculations (1992 and ongoing), and seal-performance considerations impacting compliance. This version incorporates resolution of all comments received as of the publication date noted. Chapter 2.0 discusses the general relationship between regulatory requirements and seal-system design basis. Chapter 3.0 is a snapshot of the existing seal system design. In Chapter 4.0, the 1992 PA models are discussed along with the data base and assumptions. Current models of the panel seal performance are discussed in Chapter 4.0, which also provides the shaft seal baseline data for SPM. Chapter 5.0 summarizes several issues that warrant consideration in the Project Technical Baseline and compliance submittal. Chapter 6.0 contains a list of references.

2.0 SEAL DESIGN BASIS

The WIPP is authorized by the U.S. Congress (Public Law 96-164, 1979) and is designed as a full-scale, mined geological repository for the safe management, storage, and disposal of transuranic (TRU) radioactive wastes generated by Department of Energy (DOE) defense programs. Before disposing of radioactive wastes in the WIPP, the DOE must evaluate the repository based on various regulatory criteria for disposal of all waste components, and the U.S. Environmental Protection Agency (EPA) must certify that compliance with the regulatory criteria has been satisfactorily demonstrated. This section briefly describes the federal and state regulatory requirements in relation to the seal system performance and design.

2.1 Impact of Regulations on Seal Design

Regulations are used to guide development of the seal system design basis. Most components of the seal system design will not enter quantifiably into SPM because engineering design does not always translate into a PA calculation. The acceptability of the seal system design to the regulator is a compliance issue. In addition, regulations for seals and compliance thereto include many issues besides postclosure concerns of RCRA (Public Law 94-580, 1976) or *40 CFR 191* (U.S. EPA, 1985). Nonetheless, the regulations of concern to SPM also guide formation of seal design requirements. Therefore, it is clear that the extent to which the seal system (credibility, specifications, Title I design, etc.) meets the regulations is a compliance measure. The proposed seal system is predicated on interpretation of regulations with the intent to meet compliance.

Regulations from various sources are used for guidance in seal design. *40 CFR 191* requires the disposal system consist of natural and engineered barriers within the repository. *40 CFR 264* states that seals be designed to withstand forces expected to be present due to rock creep, hydraulic pressure, and probable collapses in the repository. Other guidance from regulations involves:

- Compatibility with the host rock,
- Locations to prevent leakage,
- Structural load-bearing capacity,
- Barriers included in drifts, panels, shafts, and drill holes,
- Protection of groundwater.

The regulations lead to a seal strategy that addresses long-term and short-term requirements. In addition, multiple components are used to address the diversity of seal concerns within the regulations.

2.2 Design Requirements

Preliminary design criteria for the WIPP sealing system have been assembled in a design requirements document and used in previous design efforts (Van Sambeek et al., 1992). When a design effort is undertaken, the first task is to develop the design basis which is attached to a design task file and becomes a quality assurance (QA) record. As the WIPP Project moves toward compliance submittal, careful interpretation of regulations is required because of the direct tie from regulation to design requirements. PA analyses also play a part in interpretation of functions of seal components, as discussed in this position paper. In some cases, the longevity requirements for certain components will be determined and defended through model calculations. Design requirements responsive to regulations thus evolve.

Occasionally, the reader will note reference to various "times" within the lexicon of the seals system, vis-à-vis 100 years, 10,000 years, 200 years, operational period, short term, and long term. For design work, the short term is 100 years, about the time needed for the long-term component to meet its functional requirements. The long term is 10,000 years according to regulations. During the 1992 PA calculations, an arbitrary division between short term and long term of 200 years was used. This difference has been reconciled, and in future calculations 100 years will be used as the design basis (and the seals baseline as discussed in Section 4.3) until analyses or some other considerations dictate otherwise. The difference between design assumptions of 100 years for the short-term components and 200 years used in 1992 PA calculations is not critical to development of PA techniques or to an evaluation of a breadth of scenarios. The distinction between 100 and 200 years is important to seal designs and durability arguments for the short-term components. Because assumptions made with respect to waste characteristics, available brine, corrosion and gas generation, and many other parameters and models input to compliance calculations also influence seal design, we expect these ''time'' considerations to be analyzed, evaluated, and refined.

3.0 SHAFT SEAL SYSTEM DESIGN

The seal system is designed to prevent water or brine from entering the repository and to prevent gases or brines from migrating out of the repository. The design requirements are derived from federal regulations and are grouped in terms of function and time. Concepts for accomplishing these requirements have appeared in waste management documents for more than 10 years. As experience was gained, details have been added to the basic strategy developed for the WIPP a decade ago (e.g., Stormont, 1984). This section describes the current reference seal system. Some discussion is given to the functional requirements derived from regulations and to the explanation of time-wise differences in various sealing strategies. Sealing functions are achieved by combinations of short- and long-term components. The seal system is a conservative design, exhibiting redundancy in function and number. Material development activities continue to tailor the seal components to match their service environment. In addition, construction methods, such as densification of salt by dynamic compaction, are being evaluated. Compliance with regulations is intimately tied to the seal system.

The various federal, state, and local statutes and agreements can be divided into three general periods for engineering performance requirements: 1) operational period, 2) short-term period, and 3) long-term period. The operational period extends over the time from operational bulkhead placement at the closure of the first filled panel to the time at which the last waste is placed and decommissioning commences. Various time estimates for the length of the operational period can be derived based on assumptions involving placement of waste. For purposes of this sealing strategy, the overall operational period is approximately 35 years. The sealing strategy for operational requirements is not sensitive to the time period; even if it were one-half or twice as long, it is likely that the same materials would be used. The short-term period has been given as 100 years in many documents, including the initial reference seal report (Nowak et al., 1990) and the No-Migration Variance Petition (NMVP) (Westinghouse Electric Corporation, 1990). The basic reasons for demarcating the short-term/long-term separation as 100 years are 1) about 100 years would be required after decommissioning of the WIPP facility for the emplaced salt to reconsolidate to a density and permeability over a sufficient length required for achieving long term sealing function, and 2) the site will be under institutional control for at least the first 100 years after closure. Should technical data or design approaches indicate that changes to the short-term/long-term time periods are necessary, requisite modifications to the design can be accommodated. The long-term period is the time between 100 and 10,000 years.

Seal materials are discussed in terms of their long- and short-term components. The single long-term component currently envisaged is reconsolidated salt, which is specifically engineered to achieve a seal function in approximately 100 years. The short-term materials include concrete, bentonite, grout, chemical seal rings, and potential alternatives, although the alternatives are not currently included in the reference seal design. These materials are selected and strategically placed in the shafts and drifts. Each seal component has a functional requirement to prevent the passageways from becoming preferred pathways for transport of brines or gases to or from the repository. Short-term components provide barriers to brine and groundwater inflow to the consolidating long-term members and to the repository. The composition of each selected seal is based on experience in the mining industry, assurance of function and longevity through test results, and compatibility with the stratigraphy in which the seal is placed.

In this section, individual components of the currently proposed seal system for a representative WIPP shaft are described, and the functional responsibilities assigned to each of the components are identified. The sealing system for a representative WIPP shaft is shown in Figure 3-1.

3.1 Near-Surface Subsystems

3.1.1 Earthen Fill

The near-surface subsystems include the materials near the earth's surface and components in the Rustler Formation to separate water-bearing units as shown in Figure 3-2A. Because significant inflows to shafts and boreholes are uncommon in the Dewey Lake Red Beds, the earthen fill is not required to retard groundwater movement. Its principal function is to prevent subsidence around the shafts. There are no limits placed on the effective life other than those that may be imposed if the surface cap (a monolith that fills the cross section of the shaft collar) is incorporated into the permanent site-markers system. The existing shaft collar and shaft liner will likely be retained to minimize the disturbance to the near-surface deposits. The concrete surface cap will deter entry into the shaft, and the earthen fill material will be compacted during placement to minimize the potential for subsidence.

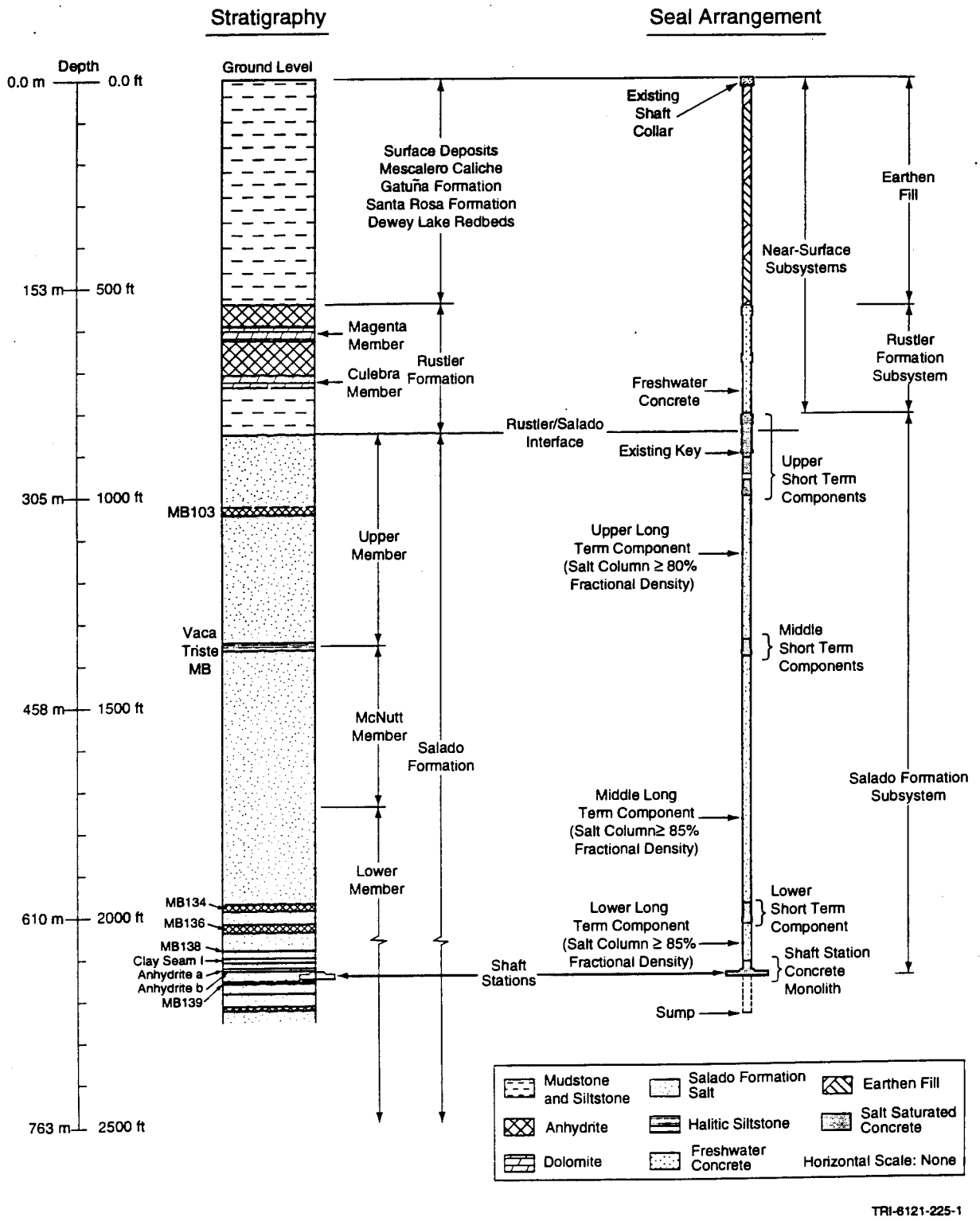

Figure 3-1. Representative WIPP shaft seal system.

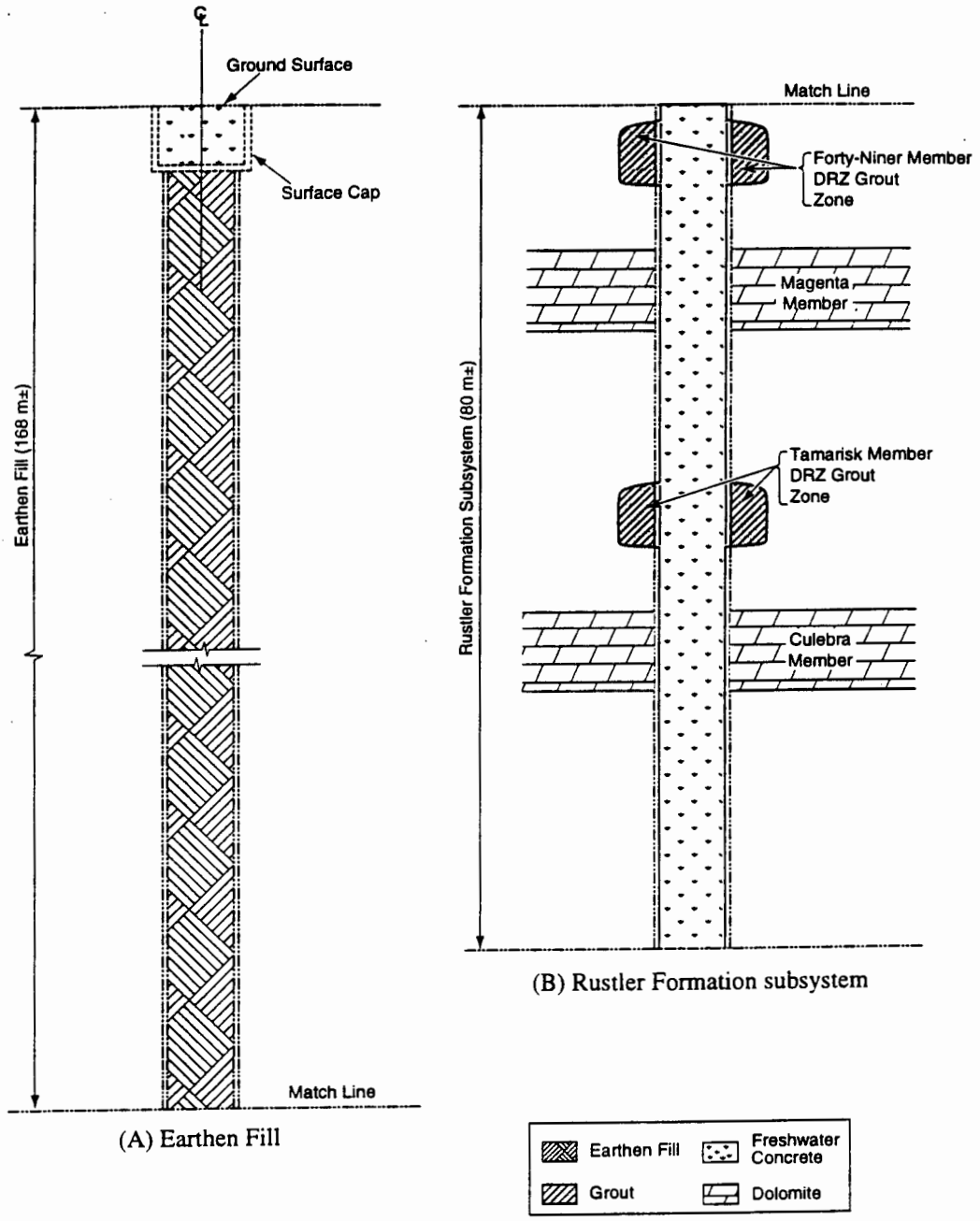

Figure 3-2. Near-surface seal subsystems.

3.1.2 Rustler Formation Subsystem

The principal function of the Rustler Formation seal subsystem (Figure 3-2B) is to ensure compliance with New Mexico state groundwater protection requirements. Within the site boundary, the total dissolved solids concentration in the Magenta range from approximately 4,000 to 25,000 mg/L; the Culebra groundwaters range from approximately 10,000 to greater than 200,000 mg/L; and the Rustler/Salado contact zone groundwaters are approximately 300,000 to 400,000 mg/L (Lappin et al., 1989). New Mexico state regulations require protection of groundwaters that have existing concentrations below 10,000 mg/L total dissolved solids. It is necessary for regulatory compliance to provide protection to the water-bearing zone in the Magenta Member. This requirement is satisfied by casting concrete of lower permeability than the surrounding rock through the entire length (80 m) shown in Figure 3-2B and by grouting.

3.2 Salado Formation Subsystems

The Salado Formation subsystem, shown in Figures 3-3A through 3-3D extends from a point just above the top of the Salado Formation to the terminus of each shaft. The air intake shaft and the exhaust shaft terminate at the floors of the drifts intersecting these shafts; the salt-handling shaft and the waste-handling shaft terminate in sumps that extend 34 and 38 m, respectively, below the floors.

The repository is required to meet the standards set forth in *40 CFR 191* and in *40 CFR 268* for undisturbed performance (U.S. EPA, 1992a). Undisturbed performance means the predicted behavior of a disposal system, including consideration of uncertainties in predicted behavior, if the disposal system is not disrupted by human intrusion or unlikely natural events. In the 1992 PA calculations, two contaminant flow paths are considered in the evaluation of the WIPP's undisturbed performance. In the first path, brine or gas may migrate through drifts or the disturbed rock zone (DRZ) to the shafts and then upward to the Culebra. The Culebra is the most permeable unit overlying the repository. Transport may then occur laterally in the Culebra toward the subsurface boundary. In the second path, migration may occur laterally toward the subsurface boundary within the anhydrite interbeds of the Salado Formation. The principal function of the Salado Formation subsystem is to prevent the transport of nonpermitted quantities of radionuclides or hazardous waste constituents from the repository to the ground surface, the Culebra, or other units above the Salado. There is no seal subsystem possible that would prevent lateral transport within the Salado Formation.

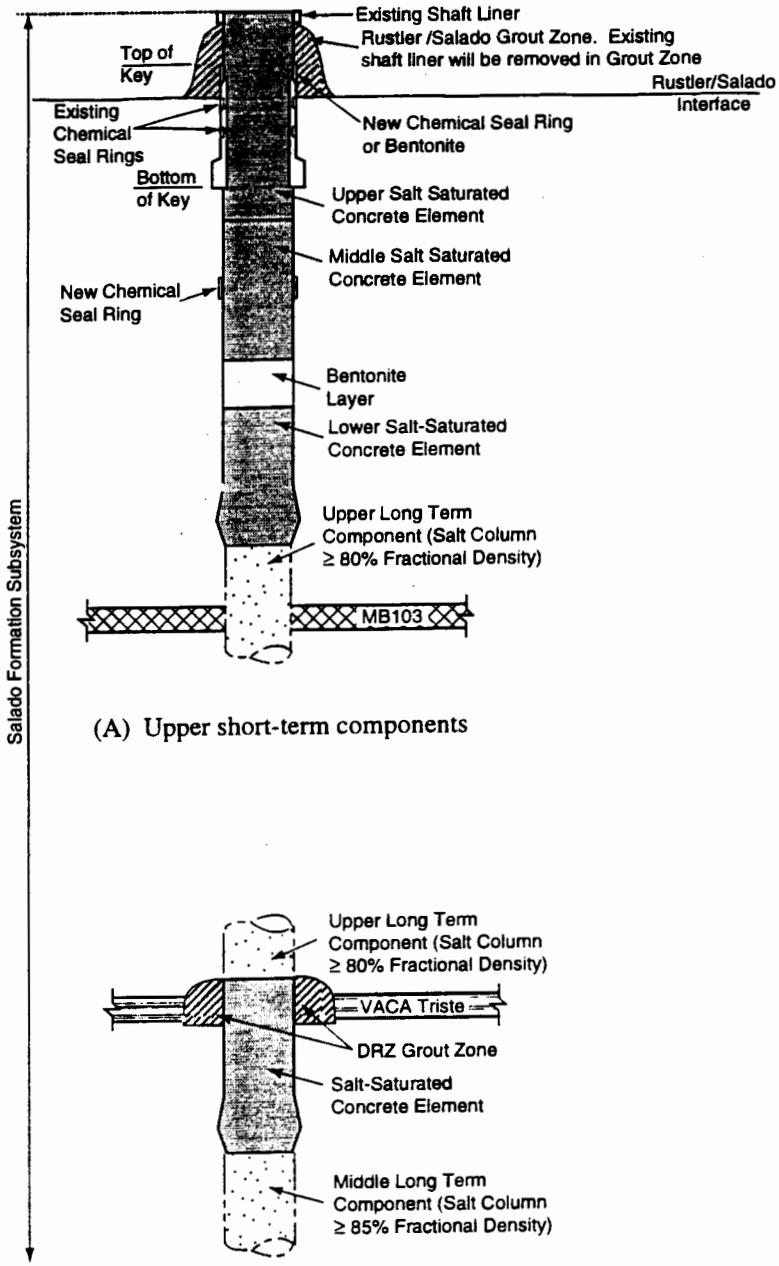

Figure 3-3. Salado Formation subsystem (Page 1 of 2).

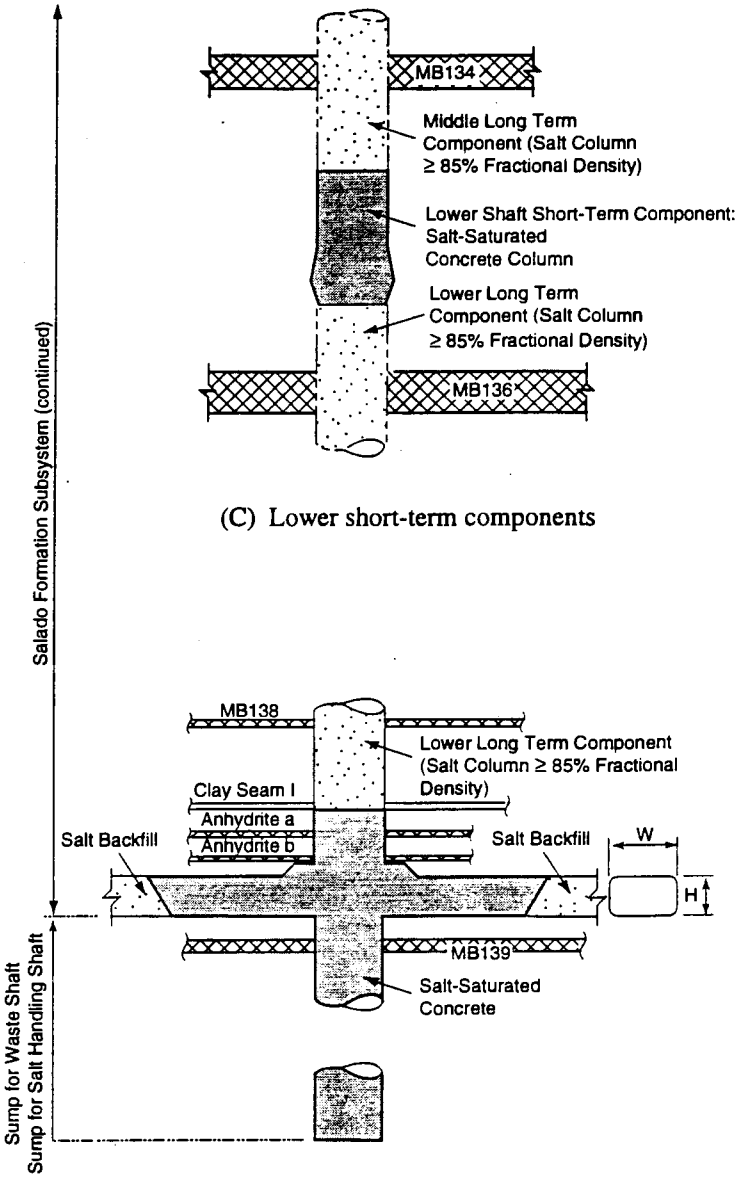

Figure 3-3. Salado Formation subsystem (Page 2 of 2).

3.2.1 Upper Short-Term Seal

The upper short-term components (shown in Figure 3-3A) are designed to limit the flow of brine from the Rustler Formation into the middle long-term salt component. Brine intrusion would also involve transmission through the entire upper salt column and the middle short-term salt-saturated concrete component before it could influence consolidation of the middle salt column. In time, the crushed salt in the middle salt column will be consolidated to nearly the same permeability as the host rock. Early estimates are that this will occur within about 100 years (Nowak et al., 1990). Although investigations on the time to consolidate are ongoing, this value of 100 years is assumed in the current conceptual design and is taken as the design life of the upper short-term component.

The upper short-term seal comprises eight elements:

- Existing Key,
- Upper Salt-Saturated Concrete Element,
- Rustler-Salado Grout Zone,
- New Upper Seal Ring — either Bentonite or Chemical,
- Middle Salt-Saturated Concrete Element,
- New Chemical Seal Ring,
- Bentonite Layer,
- Lower Salt-Saturated Concrete Element.

As can be witnessed in seal subsystems, the proposed design includes redundancy in number and utilization of different materials. Each seal component has been designed with contingencies for the types of materials used; usually the materials include industrial standards as well as alternatives. In coming years, the proposed design will be updated as analytical and experimental studies produce additional information.

3.2.2 Upper Salt Column

The upper salt column shown in Figures 3-1, 3-3A, and 3-3B does not have any compliance-related requirements. It is referred to as a long-term component because of expected compatibility of emplaced salt with existing salt. Although creep closure of the shaft is expected

eventually to consolidate the emplaced salt (estimated to have an initial density of 80% of intact WIPP salt) into a material with a permeability approaching that of intact WIPP salt, this will probably not occur in time to have a major long-term sealing impact, and no credit is taken for this component.

3.2.3 Middle Short-Term Component

The middle short-term component (shown in Figure 3-3B) is designed to limit flow of groundwater from the Vaca Triste and the overlying shaft into the middle salt column. Within 100 years, salt emplaced in the middle salt column is expected to consolidate to nearly the same permeability exhibited by the intact host rock salt. If the middle salt column were to become saturated, reconsolidation of the emplaced salt would be inhibited. Current design life of the middle short-term component is therefore about 100 years.

Two components comprise the middle short-term seal: grout in the Vaca Triste Marker Bed DRZ, and a salt-saturated concrete monolith. Because the concrete component is located approximately 412 m below the surface, creep closure of the Salado Formation is expected to create a seal between this component and the shaft wall rapidly after installation. Creep closure is also expected to heal the DRZ in the halite surrounding the rigid concrete component.

3.2.4 Middle Salt Column

The middle salt column (Figures 3-1, 3-3B, and 3-3C) in the current conceptual design is the sole long-term barrier in the seal system. Early estimates are that this component will become fully effective within 100 years after placement; creep closure of the shaft is expected to consolidate the high-density salt backfill (initial density >85% of intact WIPP host rock salt) into a material whose permeability is essentially equivalent to that of intact WIPP host rock salt. Investigations on the time to consolidate the emplaced salt are ongoing.

The current design proposes to compact crushed salt dynamically for this seal component. Other salt placement possibilities to achieve high initial density are considered as alternatives, such as stacking quarried salt blocks in the shaft. The engineered column of salt would fill the shaft cross section for approximately 180 m. In the 1992 PA, the height assumed for this barrier ranged from 30 to 100 m, with a median value of 65 m (WIPP PA, 1993b).

Effectiveness of the salt seal is anticipated to initiate at the lowest section and move upward with time, i.e., the effective length increases with time.

3.2.5 Lower Short-Term Component

The lower short-term component (shown in Figure 3-3C) is a salt-saturated concrete column. When the middle salt column is fully functional, there will no longer be a need for the lower short-term component or any other short-term components in the Salado. Therefore, the design life of the lower short-term component is 100 years. Because the concrete monolith is located approximately 604 m below the surface, creep closure of the Salado Formation is expected to achieve a seal between this component and the shaft wall soon after its installation. Creep closure is also expected to heal the DRZ in the halite surrounding this rigid component sufficiently to seal this zone.

3.2.6 Lower Salt Column

Creep closure of the shaft is expected to consolidate the high density (85%) salt backfill into a material with permeability that approaches that of intact WIPP host rock salt. The lower salt column adds length to the middle salt column. However, because the marker beds and clay seams are expected to enhance the DRZ in the vicinity of the shaft station, sealing functions are not currently assumed for either the lower shaft salt component or the shaft station concrete monolith.

3.2.7 Shaft Station Concrete Monolith

The principal purpose of the shaft station concrete monolith (shown in Figure 3-3D) is to stabilize the lower portion of the shaft walls and the back in the vicinity of the shaft station.

4.0 1992 PA, CURRENT PA AND BASELINE

The SPM initiated with a comparison between 1992 PA models and those being implemented today for PA calculations. For SPM calculations, a baseline of parameter values has been developed. This process has led to an evolution of input to PA. In this section, modeling efforts (1992 PA, current calculational approaches, and SPM) for PA as related to the seals program are discussed. Models involving simplifications of actual seal designs are used by PA for analyses. Key questions remain with respect to performance of the various seal components, especially in the WIPP setting over the times of interest to the regulators. Three separate views of the seals models are put forward to illustrate their evolution and performance in different repository scenarios. Model changes have involved terminologies that become confusing at times. Rules for SPM required the comparisons summarized in this section, regardless of inherent difficulties and potential confusion. First, the 1992 PA calculations are briefly discussed. Then, current PA simulations are summarized, including a PA evaluation of the efficacy of panel seals. Finally, the SPM baseline is given in Section 4.3.

4.1 1992 PA

Figure 4-1 depicts the domain used by PA in 1992 calculations for evaluation of long-term repository performance. The domain extends vertically from below the repository horizon in the Salado Formation to the top of the Culebra Member of the Rustler Formation. The total north-south length is approximately 47 km. The extent of the computational region prevents boundary conditions imposed at the edges of the grid from influencing the behavior of the region of interest. The width of elements out of the plane varies significantly in the x-direction to allow for variable storage volumes in the computational elements. Flow is confined to the vertical and north-south (not east-west) directions. Because of computational constraints, the detail is coarse but includes the major features believed to impact performance.

The PA conceptualization of the seal and shaft system is a simplification of the Reference Seal Design of Nowak et al. (1990). The shaft modeled in the PA conceptualization is actually an equivalent shaft having a cross-sectional area equal to the combined areas of all four shafts. This equivalent shaft is located at the position of the Waste Shaft (the shaft closest to the waste disposal areas). The cross-sectional area has little impact on long-term performance. This was investigated in the 1992 PA by varying the cross-sectional area from the smallest-diameter actual shaft to that of the equivalent shaft. The equivalent shaft is divided into two major regions,

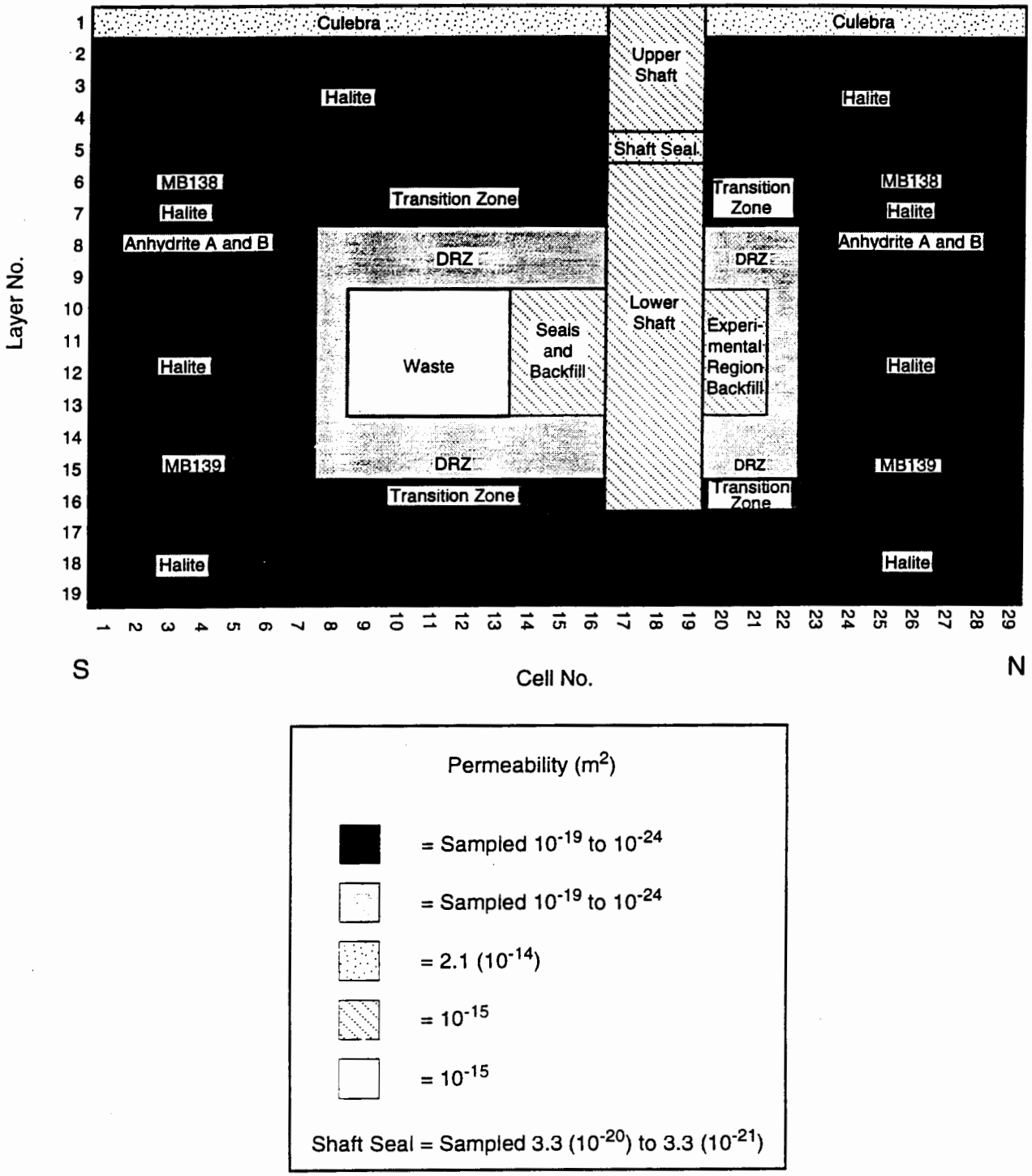

Figure 4-1. 1992 Performance Assessment model.

with a single seal between them. Length and permeability of the shaft seal were sampled for the 1992 PA calculations.

Examination of Figure 4-1 reveals that the waste disposal region of the repository consists of a single unit, with panel seals and backfill represented as a composite. The panel seals/backfill region extends approximately 311 m in the north-south direction. The simplified repository geometry used in 1992 PA modeling, including the excavated volumes of the waste disposal region, backfilled drifts, and the north-end experimental region, are consistent with the existing repository design. In addition, north-to-south lengths of the regions are preserved, as is their distance to the Waste Shaft. A horizontal DRZ lies above and below the repository and extends 1 to 2 m into the surrounding formation.

Inclusions of formations overlying the Culebra Dolomite should be considered because flow from a high-pressure brine reservoir may be sufficient to drive contaminants to the surface, rather than just into the Culebra. In the 1992 PA, the upper boundary of the model was the top of the Culebra and no flow above the Culebra was modeled. Modeling of the full repository as a single region resulted in several concerns. First, having two different conceptual models for the waste (a single panel for intrusion scenarios, and the full repository for undisturbed scenarios) in the 1992 PA raised questions about whether key features were being ignored. For example, the single-panel model ignored any probable contribution from adjacent panels to the total contaminant flow up an intrusion borehole. The single-panel model also did not include potential effects of panel seals on repository performance. Resolution of the issue of the efficacy of panel seals for long-term compliance requires investigation of the sensitivity of repository performance to the presence and properties of these seals. Section 4.2.2 discusses some of the calculations supporting the DOE/CAO position that panel seals have no long-term performance requirements.

The results of the 1992 PA calculations were reviewed in preparation of this position paper. Within the context of the formulation of a Project Technical Baseline, certain aspects of the 1992 conceptual model and parameter values are not defensible (for SPM) today by the DOE/Carlsbad Area Office (CAO). The principal areas of concern are: 1) formations above the Culebra to the ground surface should be modeled; 2) the full repository, in two segments, should be modeled in both undisturbed and human-intrusion scenarios; and 3) permeability values for seal systems should be increased. Permeability values for the seals baseline are discussed in Section 4.3. Revisions of the shaft and seal systems input parameters have been requested for contemporaneous calculations, as listed in Table 4-1. Implications of changes from 1992 PA

Table 4-1. Seal System Input to Performance Assessment (Page 1 of 3)

Conceptual Features	1992 Performance Assessment Key Characteristics[a] (Figure 4-1)	Values Used in Recent Seal Design Calculations (Figure 4-2)	Baseline Values for SPM Calculations
Culebra Shaft (Upper Shaft Seal, Element 9)	• 0-200 years • 7.7 m length; • fixed permeability (10^{-18} m^2) • fixed porosity (0.2)	• 0-200 years • extends downward through Rustler and 8.3 m into Salado Fm.; total length: 52 m • fixed permeability increased to 10^{-13} m^2 • fixed porosity increased to 0.28	• <100 years: sampled permeability (10^{-12} - 10^{-19} m^2) • length = 49 m
	• 200-10,000 years • sampled permeability (10^{-19} - 5×10^{-16} m^2) • sampled porosity correlated to permeability (0.01-0.09)	• 200-10,000 years • extends downward through Rustler and 8.3 m into Salado Fm.; total length: 52 m • permeability fixed at 10^{-13} m^2 • fixed porosity 0.28	• >100 years: permeability fixed at 10^{-12} m^2 • length = 49 m
Shaft Seal (Lower Shaft Seal, Element 8)	• 0-200 years • sampled length (30 - 100 m) • sampled permeability (10^{-19} - 5×10^{-16} m^2) • sampled porosity correlated to permeability (0.01-0.09)	• 0-200 years • fixed length (65 m) • fixed permeability (7.9×10^{-18} m^2) • fixed porosity (0.05)	• <100 years: 10^{-12} m^2 • length = 60 m
	• 200-10,000 years • sampled length (30 - 100 m) • different sampled permeability (10^{-19} - 5×10^{-16} m^2) • sampled porosity correlated to permeability (0.01-0.09)	• 200-10,000 years • fixed length (65 m) • sampled permeabilities (7.9×10^{-18} m^2) • fixed porosity (0.05)	• >100 years: sampled permeability 10^{-12} - 10^{-19} m^2 • length = 60 m

Table 4-1. Seal System Input to Performance Assessment (Page 2 of 3)

Conceptual Features	1992 Performance Assessment Key Characteristics[a] (Figure 4-1)	Values Used in Recent Seal Design Calculations (Figure 4-2)	Baseline Values for SPM Calculations
1992 Lower Shaft (Currently Bottom Shaft, Element 22)	• 0-200 years • extends from Lower Shaft Seal downward through MB139 • fixed permeability (10^{-15} m^2) • sampled porosity (0.01 - 0.075)	• 0-200 years • extends from Lower Shaft Seal downward through MB139 • fixed permeability (10^{-15} m^2) • sampled porosity (0.01 - 0.075)	• 10^{-12} m^2 (constant)
	• 200-10,000 years • sampled permeability (10^{-19} - 5×10^{-16} m^2) • different sampled porosity correlated to permeability (0.01-0.09)	• 200-10,000 years • extends from Lower Shaft Seal downward through MB139 • fixed permeability (10^{-15} m^2) • same sampled porosity as 0-200 yrs (0.01 - 0.075)	• 10^{-12} m^2 (constant)
1992 Shaft (Currently Lower Shaft, Element 5)	• 0-200 years • extends from bottom of Culebra Seal to top of Lower Shaft Seal • sampled permeability (10^{-19} - 5×10^{-15} m^2) • sampled porosity correlated to permeability (0.01-0.09)	• 0-200 years • extends from Upper Shaft Seal downward to Lower Shaft Seal • sampled permeability (10^{-19} - 10^{-15} m^2) • fixed porosity (0.05)	• 10^{-12} m^2 (constant)
	• 200-10,000 years • extends from bottom of Culebra Seal to top of Lower Shaft Seal • different sampled permeability (10^{-19} - 5×10^{-16} m^2) • different sampled porosity correlated to permeability (0.01-0.09)	• 200-10,000 years • extends from Upper Shaft Seal downward to Lower Shaft Seal • sampled permeability (10^{-21} - 10^{-18} m^2) • fixed porosity (0.05)	• 10^{-12} m^2 (constant)

Table 4-1. Seal System Input to Performance Assessment (Page 3 of 3)

Conceptual Features	1992 Performance Assessment Key Characteristics[a] (Figure 4-1)	Values Used in Recent Seal Design Calculations (Figure 4-2)	Baseline Values for SPM Calculations
Upper Shaft (Element 6)	• not used • no vertical flow above Culebra Seal or Shaft Seal 2 (beyond model boundary)	• 0-200 years • extends upward from top of Upper Shaft Seal to surface • fixed permeability (10^{-13} m^2) • fixed porosity (0.25)	• fixed permeability (10^{-13} m^2) • fixed porosity (0.25)
	• not used • no vertical flow above Culebra Seal or Shaft Seal 2 (beyond model boundary)	• 200-10,000 years • extends upward from top of Upper Shaft Seal to surface • fixed permeability (10^{-13} m^2) • fixed porosity (0.25)	• fixed permeability • fixed porosity (0.25)
Backfill/ Experimental Region	• 0-10,000 years • fixed permeability (10^{-15} m^2) • sampled porosity (0.01 - 0.075)	• 0-10,000 years • fixed permeability (10^{-15} m^2) • sampled porosity (0.01 - 0.075)	• no baseline
Panel Seal	• 0-10,000 years • sampled permeability (10^{-18} - 10^{-21} m^2) • sampled porosity (0.01 - 0.075) • sampled porosity correlated to permeability (0.05 - 0.09)	• 0-10,000 years • sampled permeability (10^{-18} - 10^{-21} m^2) • fixed porosity (0.07)	• 0-10,000 years • sampled permeability (10^{-15} - 10^{-20} m^2)

(a) Sandia WIPP Project. 1992. *Preliminary Performance Assessment for the Waste Isolation Pilot Plant, December 1992.* Volume 3: Model Parameters. SAND92-0700/3. Albuquerque, NM: Sandia National Laboratories.

to today's values and baseline values for SPM, discussed subsequently, are also summarized in Table 4-1. This table may facilitate compilation of the Project Technical Baseline.

PA has used ranges and distributions of parameters derived from the seal system. For the most part, realizations from PA could be called expected values or could be described in probabilistic terms. These values have been based on the assumption by the seals program that technology would continue to be developed so that seals with these properties could be constructed. One initial purpose of this paper was to establish seal-related parameters that could be defended today. The current understanding is to provide ranges of possible seal permeabilities and a sense of probabilities for each permeability (see Section 4.3). These numbers will be used in the Project Technical Baseline and in a SPM analysis. Parameter magnitudes and ranges for a defensible stance are different from those used in PA to date.

4.2 Current PA Calculations

4.2.1 Revision to Shaft Seal Models

Changes from the 1992 PA models proposed for current analyses of the seal systems are summarized in Table 4-1. The changes attempt to model the latest proposed design, construction, and performance over time (Chapter 3.0). In addition, some changes have been made so that the coarse PA model simulates the detailed design more accurately. A sensitivity study of the 1992 PA identified sampled parameters that had little or no influence on some key performance measures, especially gas migration distances. Thus, it was possible to eliminate some modeling details in the shaft and seals system; for example, porosity sampling was found not to be significant. It should be noted that several parameters used in the 1992 PA changed value at 200 years, although the design distinction between short- and long-term requirements is 100 years. As analyses are completed, expectations of performance will become less uncertain. For SPM, the design basis of 100 years for short-term component functional requirements will be used.

Figure 4-2 is the current model domain being used for PA calculations. The text below describes how each feature was incorporated in the analyses and why values were changed from 1992 PA. Although the seal-system design has matured over the last decade, many of the characteristics pertaining to each seal component are not well constrained. The following summarizes how the design features are currently being modeled.

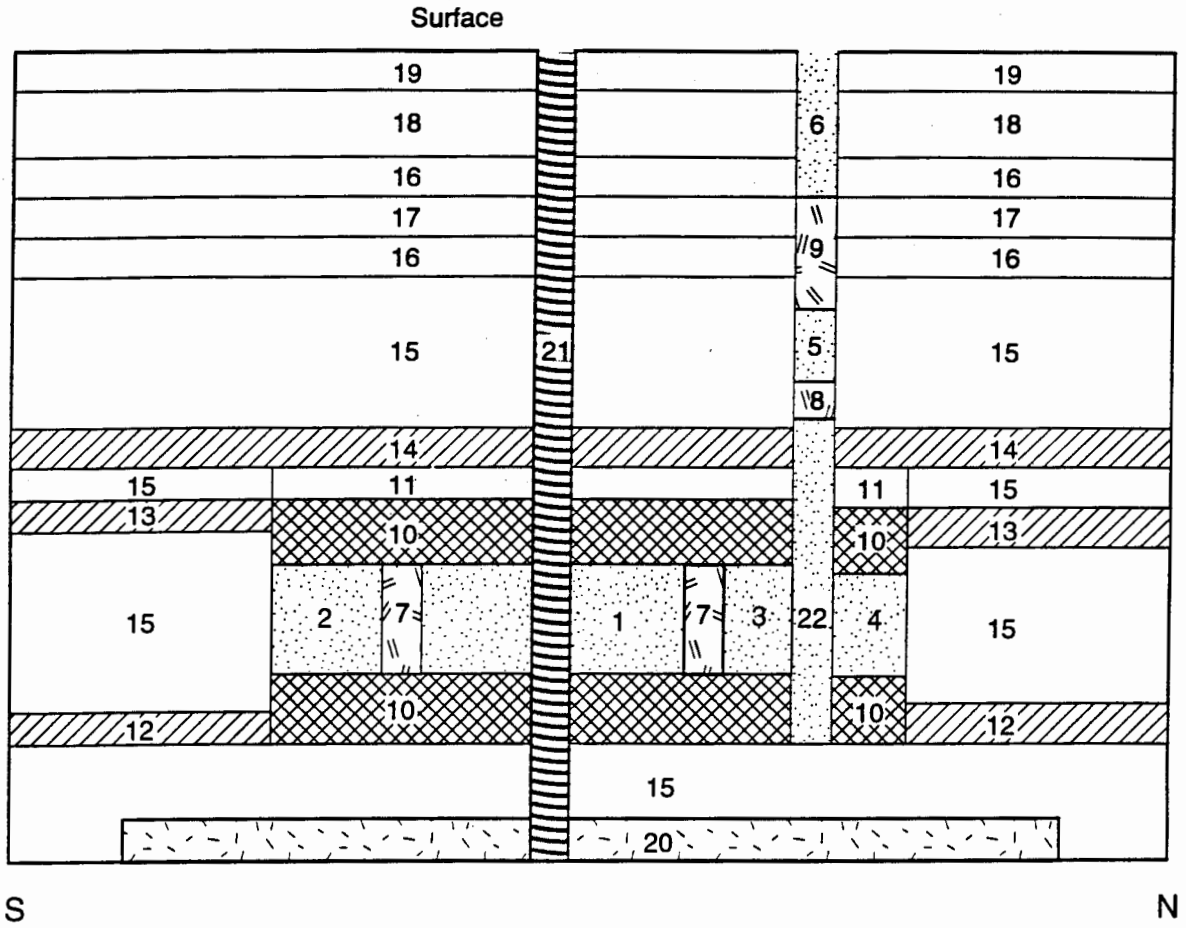

1 1 Equivalent Panel
2 Remaining Panels
3 Backfill Region
4 Experimental Region
5 Lower Shaft
6 Upper Shaft
7 Panel Seals
8 Lower Shaft Seal
9 Upper Shaft Seal
10 Disturbed Rock Zone
11 Transition Zone
12 MB 139
13 Anhydrite Layers A & B
14 MB 138
15 Intact Halite
16 Rustler (other than Culebra)
17 Culebra
18 Dewey Lake Red Beds
19 Santa Rosa
20 Castile Brine Pocket
21 Borehole
22 Bottom Shaft

TRI-6342-3801-2

Figure 4-2. North-south vertical cross section of model domain.

UPPER SHAFT SEAL

This shaft seal in the Culebra Member of the Rustler Formation was referred to as the Culebra Seal in the 1992 PA and is now labeled the Upper Shaft Seal (Element 9, Figure 4-2). In the 1992 PA, the properties of this seal changed at 200 years; the properties are considered constant in current calculations. In 1992, the Culebra was the upper boundary of the model region for two-phase flow modeling, and the rest of the Rustler Formation (specifically, the unnamed member) was combined with the Salado. Now, the upper boundary of the model is the ground surface, and the unnamed member is a separate and distinct region (Element 16, Figure 4-2). The shaft seal at the Culebra, rather than extending only through the thickness of the Culebra itself, is now modeled to extend downward from the top of the Culebra, through the bottom of the Rustler, and 8.3 m down into the Salado. Current PA calculations use these more realistic dimensions for the Upper Shaft Seal and increase the permeability of the seal five orders of magnitude, to 10^{-13} m^2, to represent a degraded concrete plug. A permeability of 10^{-13} m^2 approximates silty sand, a remnant of completely degraded concrete.

This paper recommends that the Upper Shaft Seal be further modified by PA to more accurately represent baseline calculations. First, the Upper Shaft Seal should have a short-term function to keep brine out of the reconsolidating salt lower in the shaft; second, the Upper Shaft Seal should be located at the Rustler/Salado contact, and not from the Culebra to the Salado. Baseline probabilities of permeabilities are given in Section 4.3.

SHAFT SEAL (LOWER SHAFT SEAL)

This shaft seal (Element 8) is located just above Marker Bed 138 (Element 14). For the 1992 PA calculations, the length (30 to 100 m), the permeability (10^{-19} to 5×10^{-16} m^2), and the porosity of the seal (0.01 to 0.09) were sampled variables during the first 200 years. None of these parameters was found to have a significant effect on the long-term undisturbed or disturbed performance of the repository. Consequently, these variables are not currently sampled, and mean values as listed in Table 4-1 are used: a permeability of 7.9×10^{-18} m^2, a length of 65 m, and a porosity of 0.05. In both the 1992 and current calculations, the properties remain at these levels for the remainder of the 10,000-year performance period. Whereas the distributions describing the permeability and porosity are the same for the first 200 years as they are for 10,000 years, the values selected will differ because of independent sampling. After 200 years, the current PA treats the porosity of this seal as an unsampled variable.

LOWER SHAFT

In 1992, the Lower Shaft was split into two regions: the Upper Shaft, and the Lower Shaft. In the current conceptual model, the Lower Shaft is also split into two regions, now renamed Lower Shaft and Bottom Shaft (Figure 4-2 model elements 5 and 22, respectively). In the 1992 PA, the portion of the shaft below the Shaft Seal, which is just above Marker Bed 138, was called the Lower Shaft. The same region is now called the Bottom Shaft. In 1992 PA and in today's calculations, the permeability of this portion of the shaft during the first 200 years was fixed at 10^{-15} m^2; whereas, the porosity was a sampled parameter. In the 1992 PA, at 200 years, the permeability was sampled over a range of lower values, simulating consolidation of the emplaced salt 10^{-16} to 10^{-19} m^2. In current analyses, the permeability and porosity are held constant for the Bottom Shaft element.

In 1992, the portion of the shaft between the Culebra Seal and the Shaft Seal was called the Upper Shaft. Now, the same region is called the Lower Shaft. In 1992, both permeability and porosity were sampled parameters and were changed at 200 years. In current analyses, for the first 200 years, the permeability is sampled from a range nearly the same as in 1992. In the case of porosity, the 1992 sensitivity analysis showed the undisturbed performance was not sensitive to shaft porosity. This is due to the small pore volume contained within the shaft as compared to the pore volume in the repository and experimental region. Thus, porosity in the Lower Shaft is not currently sampled. In both 1992 and current analyses, the sample range for permeability was reduced to simulate consolidation; the values used today are two orders of magnitude lower than the 1992 PA values (see Table 4-1).

The baseline modeling strategy for permeability distributions as discussed in Section 4.3 is quite different from either the 1992 PA or current modeling strategies. Because the Bottom Shaft element is in the proximity of marker beds and clay seams that may develop a maximal DRZ, no sealing credit is taken for the material in the Bottom Shaft. Because the long-term seal function is assigned to Element 8 of Figure 4-2, the Bottom Shaft (Element 22) and the Lower Shaft (Element 5) are simply assigned a constant permeability of 10^{-12} m^2 for 10,000 years.

UPPER SHAFT

The Upper Shaft as depicted in Figure 4-2 was not modeled in the 1992 PA because the upper flow boundary of the model was the top of the Culebra. An Upper Shaft element has been added to model formations up to the ground surface. No consolidation is assumed and properties

are not sampled. Permeability of 10^{-13} m^2 and porosity of 0.25 characterize this region for 10,000 years. If this element is retained in SPM calculations, no changes to these parameters are anticipated..

BACKFILL EXPERIMENTAL REGION

All properties are the same now as were used in 1992 PA: permeability of 10^{-15} m^2 and sampled porosity of 0.01 to 0.075. Backfill could provide structural stability and lessen the development of a damaged rock zone. This paper does not provide a baseline for backfill properties.

PANEL SEAL

The 1992 PA sensitivity analysis showed that panel seal porosity had little effect on undisturbed performance of the WIPP. The only change from 1992 is to fix the porosity at 0.07 instead of sampling over a range from 0.05 to 0.09. Implications of possible long-term functions of the panel seal are discussed in Section 4.2.2. When the panel seal permeability is modeled between 10^{-15} and 10^{-20} m^2, the permeability of the DRZ has far more influence on the flow of gas or brine.

4.2.2 Panel Seal Performance

One of the issues of particular interest within the WIPP Seals Program is the need and efficacy of long-term panel seals. This section outlines efforts made to date on achieving resolution of this issue. This section provides input to the Project Technical Baseline and conveys to the SPM group both the "state-of-the-technology," as well as the position that there is little sealing advantage gained by engineering long-term panel seals. Operational panel seals may be necessary for ventilation and worker safety, but these issues are not addressed here. Based on the results outlined in this section, it is concluded that panel seals do not add to containment and have only an operational purpose.

The evaluation of the sensitivity of repository behavior to long-term panel seal characteristics is an ongoing activity. The conceptual model and parameters for the analyses are based on

guidance received through interaction with PA staff. The parameters include both sampled and best-estimate values as inputs. Best-estimate values are used for those parameters that do not affect the panel seal sensitivity analyses, and may be obtained from a data base of values maintained by the WIPP PA. The conceptual model and grid of the WIPP region are illustrated in Figure 4-2.

Figure 4-3 illustrates the cumulative brine flows to the shaft for 10,000 years for a set of three simulations. The panel-seal permeability was initially specified as 6×10^{-18} m^2, which falls within the range of values used in the 1992 PA. Two additional simulations were run with permeabilities of 10^{-15} m^2 and 10^{-20} m^2. Although the presence of a low-permeability (10^{-20} m^2) panel seal in this conceptual model does reduce brine flow to the shaft, it should be recognized that this reduction is only 20% of the total brine flow to the shaft over a 10,000-year period. Plotting these same results over a shorter time scale (Figure 4-4), it is shown that brine flows during the first 400 years following seal emplacement will be toward the repository (flows toward the repository are negative in these figures). The predicted flow to the repository during the first 400 years is calculated to be less than 100 m^3. These calculations assume initially saturated surrounding formation and shaft and 0.2% halite porosity.

Using the most conservative estimates for gas-generation rates (i.e., within the upper 10% probability range for generation rates), the effects of panel-seal permeability on gas flow toward the base of the shaft is also being investigated. As shown in Figure 4-5, gas flows to the base of the shaft are very low during the first 400 years. Because the flows are low for this conservative calculation, it can be concluded that gas flows will be negligible for lower gas-generation rates. Based on these results, it is clear that the most recent PA conceptual models demonstrate that the effects of panel-seal permeability on brine and gas flows to the base of the shaft can be considered minimal for the first 400 years after decomissioning.

The issues of backfill consolidation and the effects of a borehole intrusion prior to 400 years have not been explicitly included in the sensitivity studies. In addition, the DRZ and anhydrite interbeds represented the principal pathway for fluid flow from the repository throughout the regulatory period. Further studies may demonstrate that the DRZ will heal, such that its permeability is reduced to that of the intact halite within decades of repository closure. The effects of these processes must be included in the assessment of the panel-seal design because the avenue of flow from a panel is largely through the DRZ.

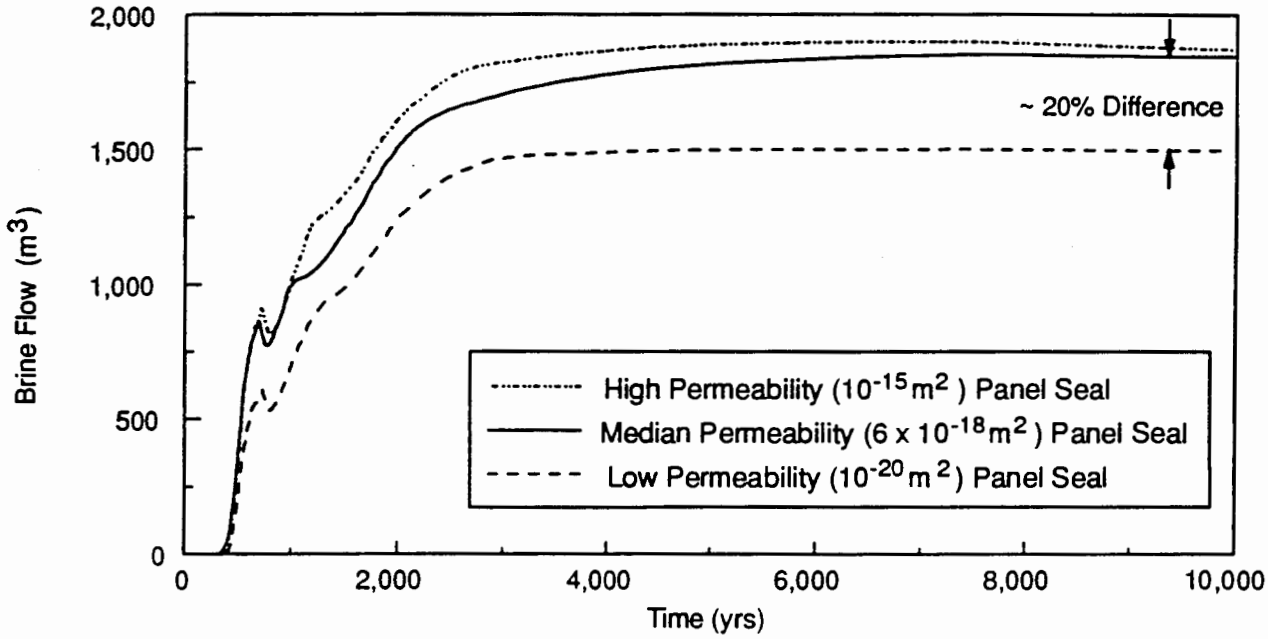

Figure 4-3. Long-term cumulative brine flow to shaft.

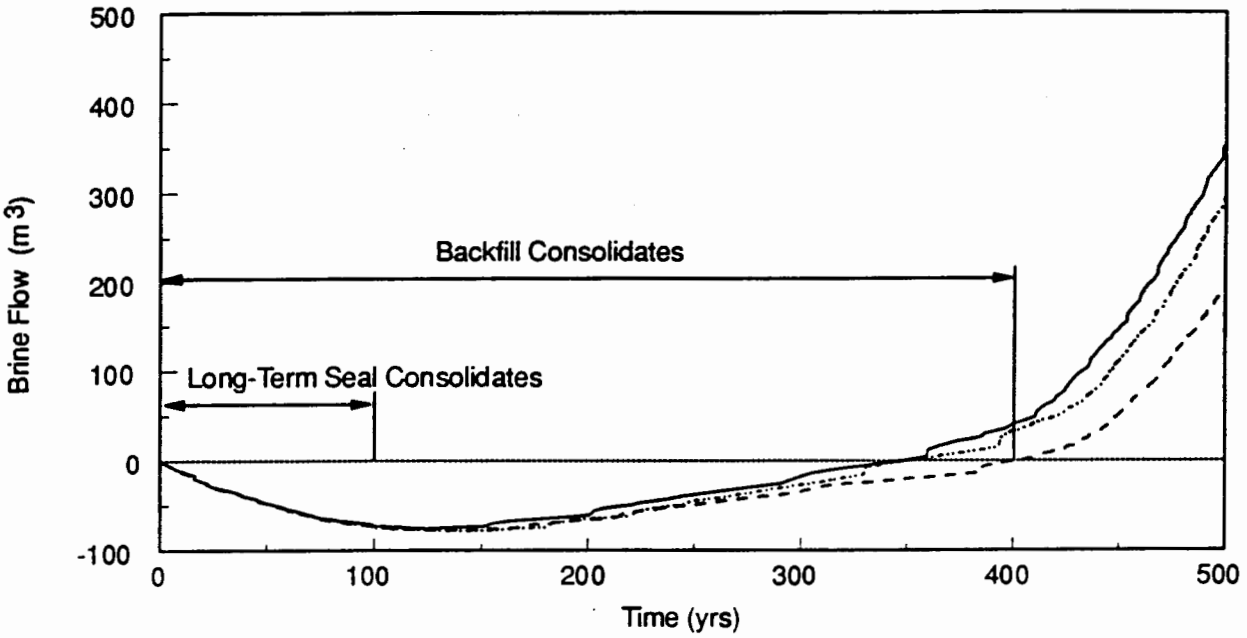

Figure 4-4. Early cumulative brine flow to shaft.

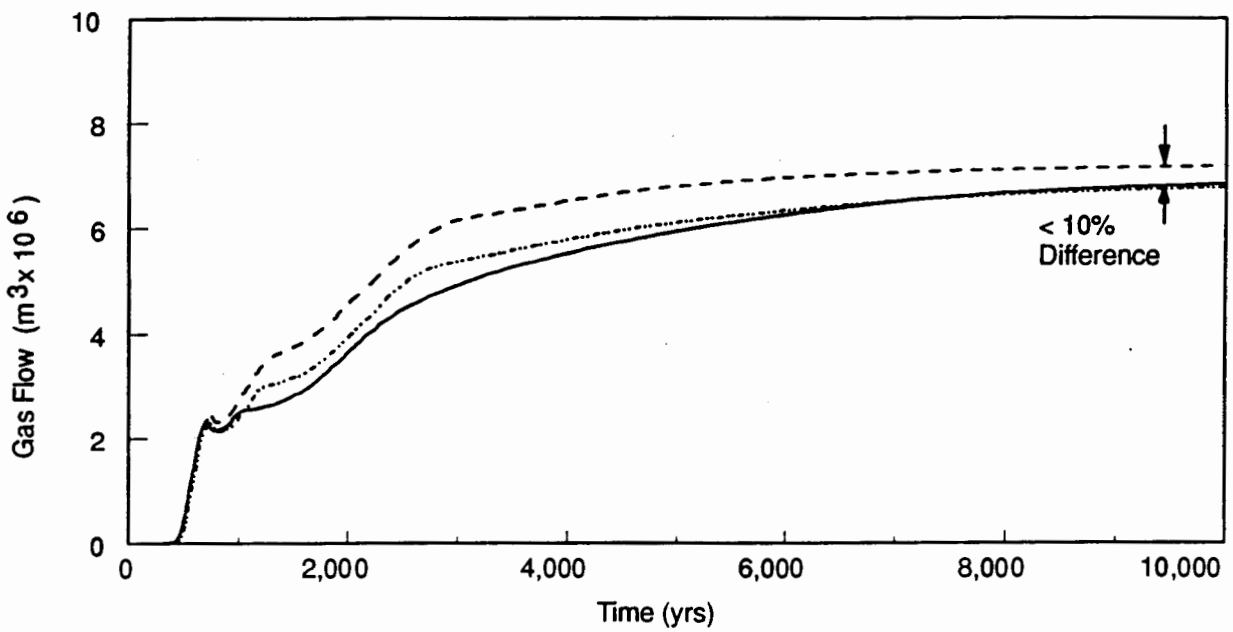

Figure 4-5. Long-term cumulative gas flow to shaft.

4.3 Seals Baseline Information

The process of systems prioritization has required a focus on PA calculations and direct input of the seals program to PA. As summarized, the 1992 PA was modified to capture certain aspects of the seal system and breach scenarios. Values for shaft-seal parameters, such as geometry, permeability, and porosity, were changed to achieve relatively more consistency in assumptions and to represent more accurately the proposed seal-system design. That is not to say that the current PA models and the nomenclature for elements of the grid shown in Figure 4-2 agree well with design components and baseline parameters. In fact, the nomenclature used in the two PA models is sometimes difficult to interpret in terms of the proposed seal system design. The SPM baseline has established a representation of the shaft seals that should enhance understanding of the modeling grid, the seals models, and the performance in different scenarios.

The seal-system design incorporates a strategy that includes short- and long-term seals. In general, upper short-term seals are designed to keep water or brine out of the shafts, thereby protecting the long-term salt seal as it reconsolidates. If gas generation is plausible during the life of the short-term components, the short-term seals located lower in the shaft columns would limit gas flow to the shaft, also protecting the long-term components. If gas or brine were to fill the shaft, the salt would possibly not reconsolidate to a lower permeability. A fundamental design consideration is that the shaft not become a preferred pathway for transmission of contaminants. Because short- and long-term performance of the shaft seal is integrally linked, shaft seal models (in particular permeabilities) have been closely scrutinized.

Three key considerations guided development of baseline permeability magnitudes and ranges. The first, as described above, is the linkage between short- and long-term performance of the shaft-seal components. Another key consideration is the data base used to support the project position with respect to permeabilities of full-scale seals. Yet another consideration is the relationship between the shaft seals and scenarios for repository performance. In particular, if shaft seals are assigned a relatively high permeability, then the repository probably would not develop significant gas pressures necessary to propagate horizontal fractures in the brittle anhydrite strata. The gas would escape via the shafts. Therefore, it is not sufficient for SPM to simply assign conservatively high permeabilities to shaft-seal components. A probability distribution that captures the possibility of very tight long-term shaft seals was felt to be more realistic.

It should be understood that magnitudes and ranges of permeabilities put forward in the baseline for SPM are based on sparse data. Figure 4-6 attempts to convey the variety of data bases and experiences pertinent to seal design and performance. Most notable is the fact that

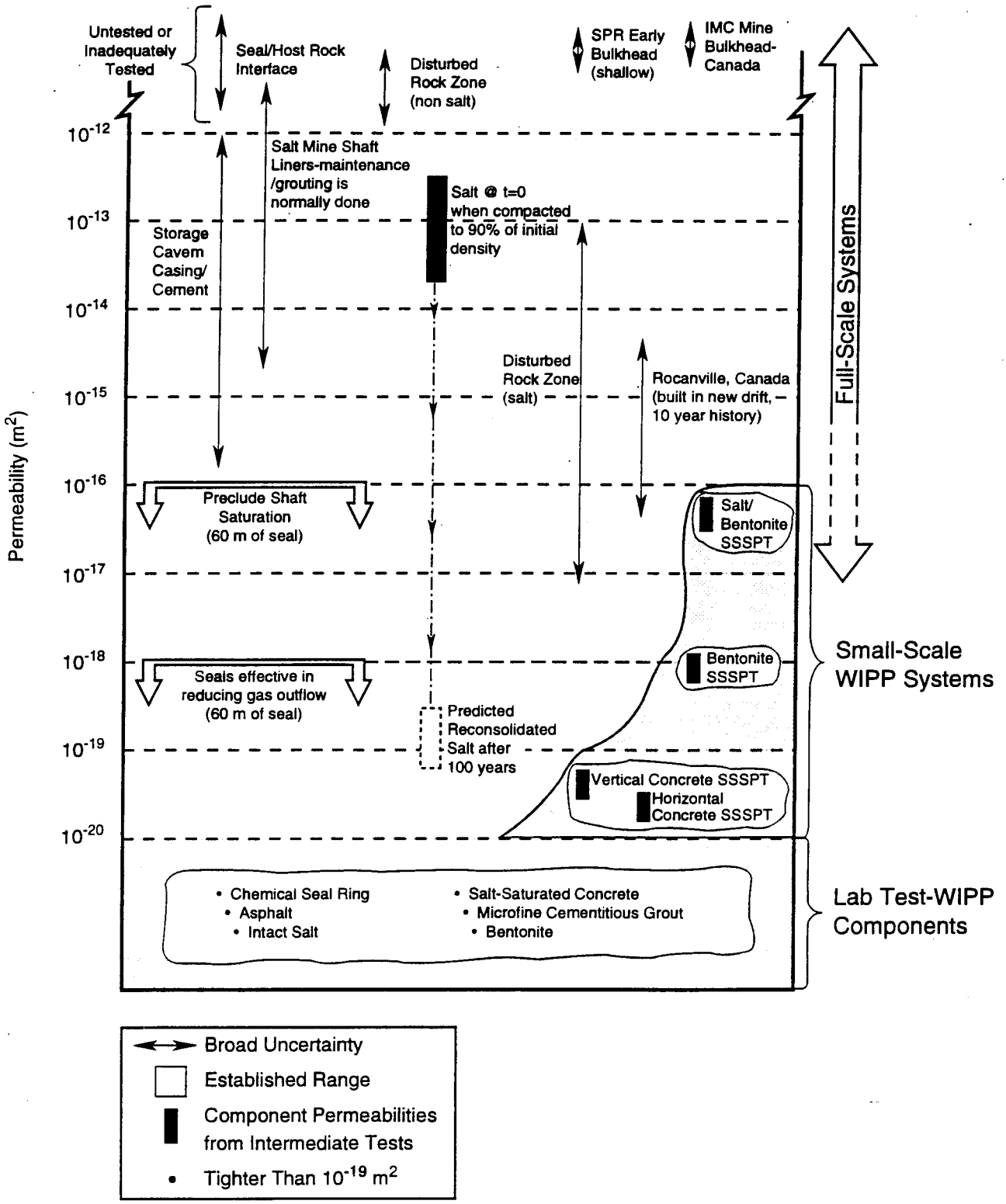

Figure 4-6. Ranges of permeabilities for seal materials.

no large seals have ever been built to the stringent regulations imposed on the WIPP site. Some of the seal material, reconsolidated crushed salt for example, is unique. Laboratory and intermediate-scale tests of seal material properties exist, and a search for analogs in the mining industry and oil and gas storage operations has been started, but the seals program does not have a quantified data base for large-scale seals. The vertical arrow to the right of Figure 4-6 shows the possible range of permeabilities that might be expected from full-scale seal systems. Indications are that some applications have resulted in relatively high permeabilities; the more challenging question is how impermeable can we argue the seals for WIPP will be.

Figure 4-6 also shows that laboratory-measured permeabilities of proposed seal material (such as concrete) are very low. Small, uncracked volumes of the short-term components are essentially impermeable. At an intermediate scale, represented by small-scale seals performance tests (SSSPTs) at the WIPP, concrete was shown to seal a borehole tightly. In other SSSPTs, materials such as salt/bentonite plugs and pure bentonite plugs achieved brine permeabilities of 10^{-16} m^2 and 10^{-18} m^2, respectively. All of the SSSPT series involved sealing and testing 0.9-m boreholes. The difficulty of extrapolating these tight permeabilities to the large-scale is a size effect.

The seal placed in a WIPP shaft is part of a system including 1) the large volume of seal material, 2) a DRZ, and 3) an interface between the host rock and the seal material. The permeabilities of each of these system components could range from very tight to highly permeable. Large volumes of any material, but particularly concrete, increase the likelihood of inherent imperfections such as cracks. The possibility of cracking can be mitigated by redundancy, use of differing materials, and due care during placement. Permeability of the interface zones can be reduced by using grout or flowable materials and will be reduced by pressure from the formation. A DRZ created around underground openings can be very transmissive, particularly near the skin. Field measurements have shown that a salt DRZ of 10^{-12} m^2 near the face is reduced to 10^{-15} m^2 at a depth of 1 m. Deteriorated ground near the skin may be mitigated by removal, and the salt DRZ at greater depth by healing. A non-salt DRZ may also be removed (somewhat) and then grouted. The processes of removal of bad ground surrounding a seal coupled with grouting should reduce the DRZ permeability as well as tighten the interface.

It is also important to the WIPP seal design to consider how well the seals need to function. Preliminary, moderately conservative calculations have been performed to quantify required shaft permeabilities. To prevent brine from filling the shaft, a permeability of about 10^{-16} m^2 is needed (see where this value plots on Figure 4-6). If gas is a concern during the short term,

the lower shaft short-term component would need to have a permeability of about 10^{-18} m^2 to mitigate gas flow up the shaft. One can readily observe that the materials data base comprising small- and intermediate-scale permeability measurements is much tighter than WIPP seals need to be; however, qualitative analog data suggest large-scale seals may be more permeable than required for WIPP seals. This type of argument, contrasting materials impermeable on a small scale with needed performance on a large scale, has led to the baseline permeability distribution discussed below.

The seal system has been simplified for the baseline into two common features: 1) a short-term seal and 2) a long-term seal. The short-term seal is intended to model all of the short-term components, both those at the Salado/Rustler contact designed to keep brine out of the shafts, and those nearer the base of the shaft seal designed to keep gas out of the shafts. The conceptual seal model for the baseline consists of short- and long-term permeabilities for shaft model elements. No long-term function is assigned to panel seals, in keeping with the current DOE position. The operational role of panel seals is based in part on the analyses discussed in Section 4.2.2. Baseline parameters for the shaft seals are to be estimated as follows:

- Seal permeability:
  - Calculations will sample on a value for seal permeability. That value will have a distribution between 10^{-12} m^2 and 10^{-19} m^2. The baseline sample distribution curve, sketched in Figure 4-7, has the following characteristics:
    - (a) a low point (i.e., a point of low permeability) at 10^{-19} m^2 with
    - (b) the probability of permeabilities less than 10^{-19} m^2 is 0.01 (1%)
    - (c) the probability of permeabilities lower than 10^{-15} m^2 is 0.50 (50%
    - (d) the probability of permeabilities lower than 10^{-14} m^2 is .95 (95%), and
    - (e) a high point (high permeability) at 10^{-12} m^2 with
    - (f) the probability of permeabilities lower than 10^{-12} m^2 is 0.99 (99%).
  - For the first 100 years:
    - (a) Set the short-term shaft seal permeability to the sampled value
    - (b) The long-term shaft seal permeability is assumed to be 10^{-12} m^2.
  - After 100 years:
    - (a) The short-term shaft seal permeability is assumed to be 10^{-12} m^2

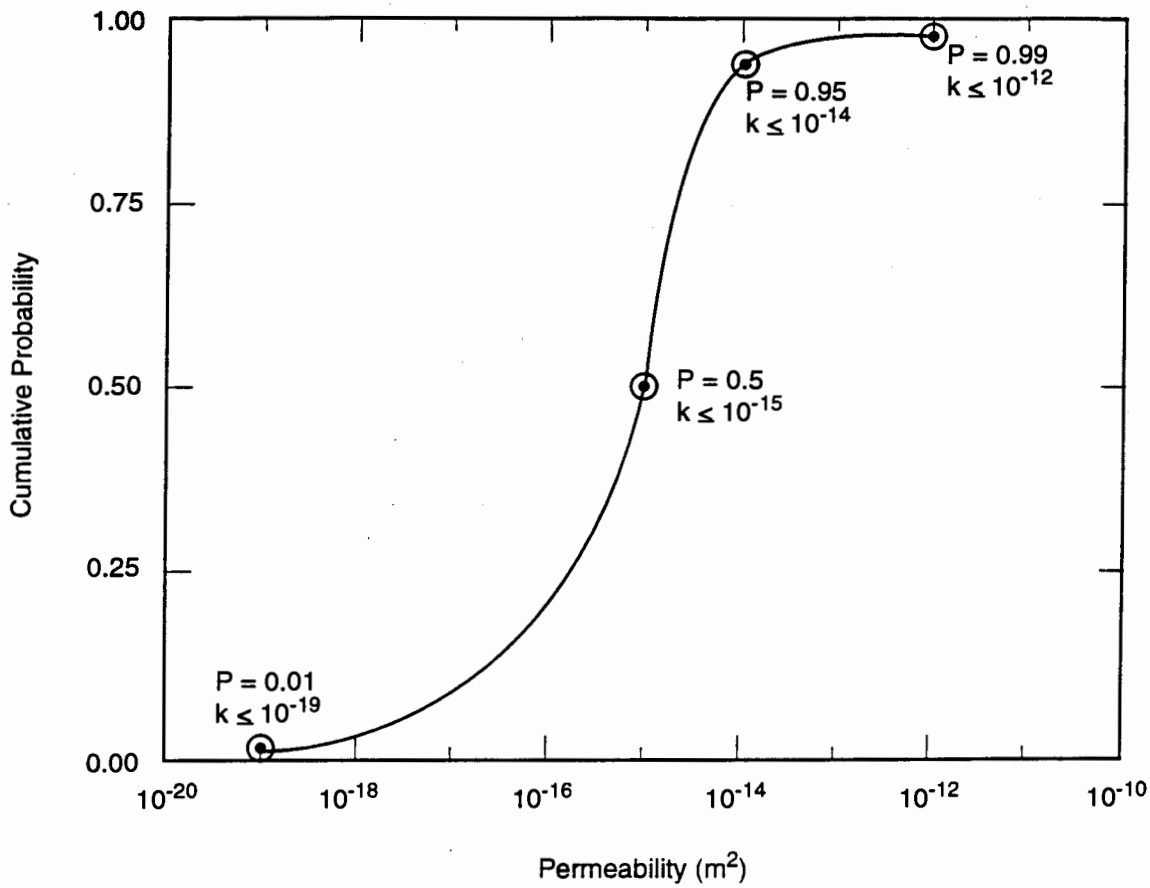

Baseline Parameters

- Sample Distribution

<100 yr
- Set Short-Term Seal to Sampled Permeability
- Set Long-Term Seal to 10^{-12} m^2

>100 yr
- Set Short-Term Seal to 10^{-12} m^2
- Set Long-Term Seal to Sampled Permeability

TRI-6121-276-0

Figure 4-7. Baseline permeabilities for shaft model elements.

(b) The long-term shaft seal permeability is set to sampled value.

- Length of the shaft seals:
  - Long-term salt seal length will be fixed at 60 m.
  - Short-term seal length for the four shafts average 49 m, based on the proposed design.

The PA model grid shown in Figure 4-2 does not include a lower short-term seal component located between Marker Bed 136 and Marker Bed 134. This particular short-term component would become important if significant gas is generated and no long-term seal is placed in the panels on closure of the facility. As discussed in more detail in Section 4.2.2, gas transmission to the shaft is modeled to be insignificant in the first 100 years, during which time the lower shaft salt seal will become effective. Therefore, to be completely consistent with current shaft-seal designs and the baseline parameter sampling, the lower short-term component should be included, but unless gas generation is profound, the lower short-term seal would not have compliance implications. If gas generation is a serious issue, additional design may be warranted.

5.0 SUMMARY AND CONCLUDING REMARKS

Designs, specifications, and drawings are available for a proposed reference seal system for the WIPP. The design concepts have matured over the years as design bases and design requirements have become better understood. A credible seal system is fundamental to establishing compliance with a regulator and to instill public confidence. PA uses parameter estimates provided by the seal-system group. Parametric inputs to PA calculations have been summarized for 1992 PA and in ongoing PA analyses. A baseline strategy for long-term and short-term seals has been developed in this position paper for the SPM. An elicitation process will develop probabilities that current repository isolation system activities will impact compliance.

This position paper has presented an overview of the development of the seal system for the WIPP facility and related PA analyses. The seal-system design group is engaged in several activities to improve materials, models, and data bases supporting the proposed design. SPM is proposed to evaluate activities quantifiably affecting regulatory compliance. Because the EPA is expected to request a well developed, defensible seal design, current design activities are thought to be necessary. Of the several issues discussed in the text, the following lists of internal and external issues warrant careful consideration.

5.1 Internal Issues

Assurance of long-term performance of salt components in shafts requires definitive information on a number of issues. Studies currently under way are meant to address the following:

- Degree of initial salt compaction,
- Adequacy of predictive models for consolidation, including:
  - — effects of parameter uncertainty on rates of creep closure,
  - — effects of backstress (including laboratory measurements and model predictions) on creep closure,
  - — characterization of DRZ: healing, time-dependent development, hydrologic properties.
- Adequacy of protection of compacted salt column during consolidation:

— properties and process control on salt-saturated concrete,

— data base and performance models (including longevity) of salt-saturated concrete, grout, chemical seal rings, and bentonite as emplaced in the WIPP environment,
  (1) effectiveness of grouting techniques,
  (2) effectiveness of chemical seal rings, particularly regarding swell pressures and longevity,
  (3) effectiveness of bentonite.

— assessment/demonstration of "system" short-term performance.

- Alternate materials for redundancy.

Functions and requirements for seal components (panel/drifts/shafts/boreholes) must be defined and evaluated prior to finalization of designs. Detailed designs sufficient for establishing emplacement feasibility and performance will require the following:

- Functions and requirements for seal components,
- Component designs (geometry, placement processes, materials specifications, etc.),
- Specifications of important processes related to construction/performance (salt-saturated concrete production, grout specifications, and placement, etc.),
- Hydrologic and structural design and performance calculations to ensure designs meet requirements.

5.2 External Issues

External issues will also significantly impact the WIPP seal-system program. Specific concerns relate to the lack of information on EPA and other stakeholder expectations regarding the extent of large-scale testing prior to compliance submittal and on the degree of detail in designs required for compliance submittal. In addition, the following topics continue to be uncertain within the seal-design effort:

- Regulatory interpretations of Resource Conservation and Recovery Act (RCRA) VOC compliance during postclosure,

- PA assumptions/results of RCRA VOC compliance, particularly regarding DRZ interconnection within repository and gas generation.

As can be seen from the above list of internal and external issues, a considerable body of work is in progress on design of the seal system, PA related to seal parameters, and actual parameter quantifications by way of testing. Currently, PA and system prioritization activities have provided defensible input for their calculations. The short-term seal must be effective for its entire functional period or the long-term reconsolidation of salt will be compromised. For the technical staff to tighten permeabilities and constrain distributions of input to PA, certain issues listed above must be resolved. We are currently working with the SPM group through the elicitation process to bracket improvements that could be gained by seal-system testing, by materials testing, and by technology development.

6.0 REFERENCES

Lappin, A.R., R.L. Hunter, D.P. Garber, and P.B. Davies, eds. 1989. *Systems Analysis, Long-Term Radionuclide Transport, and Dose Assessments, Waste Isolation Pilot Plant (WIPP), Southeastern New Mexico; March 1989.* SAND89-0462. Albuquerque, NM: Sandia National Laboratories.

Nowak, E.J., J.R. Tillerson, and T.M. Torres. 1990. *Initial Reference Seal System Design: Waste Isolation Pilot Plant.* SAND90-0355. Albuquerque, NM: Sandia National Laboratories.

Public Law 94-580. 1976. *Resource Conservation and Recovery Act of 1976.*

Public Law 96-164. 1979. *Department of Energy National Security and Military Applications of Nuclear Energy Authorization Act of 1980.*

Sandia WIPP Project. 1992. *Preliminary Performance Assessment for the Waste Isolation Pilot Plant, December 1992. Volume 3: Model Parameters.* SAND92-0700/3. Albuquerque, NM: Sandia National Laboratories.

Stormont, J.C. 1984. *Plugging and Sealing Program for the Waste Isolation Pilot Plant (WIPP).* SAND84-1057. Albuquerque, NM: Sandia National Laboratories.

U.S. EPA (Environmental Protection Agency). 1985. "40 CFR Part 191: Environmental Standards for the Management and Disposal of Spent Nuclear Fuel, High-Level and Transuranic Radioactive Wastes; Final Rule," *Federal Register.* Vol. 50, no. 182, 38066–38089.

U.S. EPA (Environmental Protection Agency). 1992a. "Land Disposal Restrictions," *Code of Federal Regulations 40, Part 268.* Washington, DC: Superintendent of Documents, U.S. Government Printing Office.

U.S. EPA (Environmental Protection Agency). 1992b. "Standards for Owners and Operators of Hazardous Waste Treatment, Storage, and Disposal Facilities," *Code of Federal Regulations 40, Part 264.* Washington, DC: Superintendent of Documents, U.S. Government Printing Office.

U.S. EPA (Environmental Protection Agency). 1993a. "Environmental Radiation Protection Standards for the Management and Disposal of Spent Nuclear Fuel, High-Level and Transuranic Radioactive Wastes," *Federal Register.* Vol. 58, no. 242, 66398–66416.

Van Sambeek, L.L., D.D. Luo, M.S. Lin, W. Ostrowski, and D. Oyenuga. 1993. *Seal Design Alternatives Study.* SAND92-7340. Albuquerque, NM: Sandia National Laboratories.

Westinghouse Electric Corporation. 1990. *Waste Isolation Pilot Plant No-Migration Variance Petition*. DOE/WIPP 89-003, Revision 1. Carlsbad, NM: Westinghouse Electric Corporation, Waste Isolation Division for U.S. Department of Energy.

WIPP PA. 1992a. *Preliminary Performance Assessment for the Waste Isolation Pilot Plant, December 1992. Volume 1: Third Comparison with 40 CFR 191, Subpart B*. SAND92-0700/1. Albuquerque, NM: Sandia National Laboratories.

WIPP PA. 1992b. *Preliminary Performance Assessment for the Waste Isolation Pilot Plant, December 1992. Volume 2: Technical Basis*. SAND92-0700/2. Albuquerque, NM: Sandia National Laboratories.

WIPP PA. 1993a. *Preliminary Performance Assessment for the Waste Isolation Pilot Plant, December 1992. Volume 4: Uncertainty and Sensitivity Analyses for 40 CFR 191, Subpart B*. SAND92-0700/4. Albuquerque, NM: Sandia National Laboratories.

WIPP PA. 1993b. *Preliminary Performance Assessment for the Waste Isolation Pilot Plant, December 1992. Volume 5: Uncertainty and Sensitivity Analyses of Gas and Brine Migration for Undisturbed Performance*. SAND92-0700/5. Albuquerque, NM: Sandia National Laboratories.

DISTRIBUTION

SNL WIPP Managers:

P. Brewer	(MS 1395)
W. Weart	(MS 1335)
S. Goldstein	(MS 1335)
A. Stevens	(MS 1341)
P. Davis	(MS 1345)
R. Lincoln	(MS 1341)
D.R. Anderson	(MS 1328)
D. Schafer	(MS 1341)
J. Holmes	(MS 1341)
P. Davies	(MS 1324)
W. Wawersik	(MS 0751)
J. Nowak	(MS 1320)
J. Tillerson	(MS 1322)
V. Harper-Slaboszewicz	(MS 1395)

6307 (MS 1345) Staff

S. Bertram
S. Bigger
T. Corbet
L. Hill
A. Lappin
P. Swift
T. Steinborn
J. Tollison
M. Wallace
M. Glora

6700 (MS 1395) Staff

S. Pickering
P. Sanchez

SNL PTB Position Paper Working Group Chairs

R. Beauheim	(MS 1324)
S. Howarth	(MS 1324)
N. Dhooge	(MS 1341)
F. Hansen	(MS 1322)
B. Butcher	(MS 1341)
M. Marietta	(MS 1328)
P. Swift	(MS 1345)
M. Fewell	(MS 1328)
L. Brush	(MS 1341)

Paper Authors and Others

K. Knowles	(MS 1322)
L.D. Hurtado	(MS 1322)
D. Borns	(MS 0750)
D. Holcomb	(MS 0751)
H. Morgan	(MS 0443)
M. Stone	(MS 0443)
E. Hoffman	(MS 0443)
R. Weatherby	(MS 0443)
B. Ehgartner	(MS 0706)
J. Linn	(MS 0706)

WIPP Library

March 17, 1995

Systems Prioritization Method - Iteration 2 Baseline Position Paper:

Hazardous Constituent Source Term for Modeling Contaminant Transport

DOE/WIPP-Draft-2083

Westinghouse Electric Corporation
Waste Isolation Division
Waste Isolation Pilot Plant
P.O. Box 2078
Carlsbad, New Mexico 88221

Hazardous Constituent Source Term for Modeling Contaminant Transport

March 17, 1995

DOE/WIPP-Draft-2083

Westinghouse Electric Corporation
Waste Isolation Division
Waste Isolation Pilot Plant
P.O. Box 2078
Carlsbad, New Mexico 88221

Executive Summary

This final draft of the hazardous constituent source term paper selects the headspace concentration limited model, described as an alternative conceptual model in the November 17 draft (Rev. 2) of the paper, as the baseline for the system prioritization method (SPM). Project participants are in agreement that conservative assumptions described in this report reasonably account for uncertainties in predicting quantities of hazardous constituents available for transport over the 10,000 year modeling period. The selected approach assumes hazardous constituents will exist in both the gas and brine phases at constant concentrations over time. No credit is taken for depletion of the RCRA source term through time dependent organic degradation and transport-related mechanisms, or depletion through sorption and immobilization of RCRA metal constituents within the repository. On a system basis, as described in the Salado Position Paper, SPM also assumes no attenuation of concentrations by chemical or physical processes along the travel path. Headspace gas analytical data for 536 drums of TRU mixed waste are used to derive the weighted average volatile organic compound (VOC) concentrations for the VOC source term, while saturated vapor concentrations are assumed for semi-volatile compounds. Thermodynamic equilibrium is retained as the approach for deriving the source term for hazardous constituents in the liquid phase.

TABLE OF CONTENTS

		Page
LIST OF TABLES		iii
1.0	INTRODUCTION	1
2.0	HAZARDOUS CONSTITUENTS IN TRU MIXED WASTE	2
	2.1 Waste Inventory	5
	2.2 Waste Forms	6
	2.3 Quantities of Hazardous Constituents	8
	2.3.1 Concentration of Hazardous Constituents in the Gas Phase	8
	2.3.2 Concentration of Hazardous Constituents in the Liquid Phase	11
3.0	CONCEPTUAL MODEL	16
	3.1 Baseline Assumptions	16
	3.2 Gas-Phase Source Term	18
	3.3 Liquid-Phase Source Term	19
4.0	FUTURE DEVELOPMENT ACTIVITIES	19
5.0	SUMMARY	20
6.0	REFERENCES	21

LIST OF TABLES

Table	Title	Page
2-1	List of Hazardous Constituents and CAS Numbers	3
2-2	Weighting Factors by TRUCON Code	7
2-3	Chemical Vapor Pressures at 27 °C and Gas-Phase Chemical Concentrations	10
2-4	Henry's Law Constant Parameters	14
2-5	Species Relevant to the Development of a Source Term for RCRA-Regulated Metals	15

1.0 Introduction

The Waste Isolation Pilot Plant (WIPP) is a transuranic (TRU) waste disposal repository designed to demonstrate the safe disposal of TRU waste resulting from defense activities of the United States. Transuranic mixed waste is TRU waste which has been contaminated with constituents regulated under the Resource Conservation and Recovery Act (RCRA). The Land Disposal Restrictions of the RCRA, codified in 40 CFR Part 268, prohibit the land disposal of TRU mixed waste unless the waste has been treated to meet specific regulatory standards. Pursuant to 40 CFR §268.6, the DOE may permanently dispose of TRU mixed waste without treatment if it is demonstrated, to a reasonable degree of certainty, that hazardous constituents will not migrate from the disposal unit in concentrations exceeding health-based levels for as long as the wastes remain hazardous. In order to demonstrate no migration, transport of hazardous constituents must be modeled, and the modeling results must be documented in a No-Migration Variance Petition (NMVP). The Environmental Protection Agency (EPA) has determined that a 10,000-year modeling period is adequate for demonstrating no migration.

The DOE has decided to demonstrate compliance with 40 CFR §268.6 through repository Performance Assessments (PA). Currently, the WIPP PA Department at Sandia National Laboratories (SNL) is responsible for providing the DOE with long-term conceptual model development and consequence modeling of the WIPP disposal system. In order to demonstrate compliance with 40 CFR §268.6 over the 10,000-year period of regulatory concern, SNL's system of PA codes will simulate the migration of hazardous, or RCRA-regulated, constituents. Evaluations of compliance with 40 CFR §268.6 will involve calculations assuming the undisturbed, or base-case, scenario by considering potential transport of hazardous constituents from the repository in both the gas and WIPP brine phases.

This report documents the current technical approach for defining the hazardous constituent source term for the post-closure period. The hazardous constituent source term to be used in transport modeling is the concentration of hazardous constituents in the transport media. Hazardous constituents present in TRU-mixed waste have been identified through waste characterization activities and include volatile organic compounds (VOCs), semi-volatile

organic compounds, and RCRA-regulated metals. Transport parameters, such as diffusion and sorption along contaminant pathways, are related to the actual migration of hazardous constituents and are outside the scope of this report.

The hazardous constituent source term must be developed for both the operational and post-closure phases of the NMVP. During disposal operations, the air pathway is the medium of interest. The approach for defining the operational source term will be to perform source emission calculations, the source being the individual waste containers. Each waste container, or drum of waste, will be fitted with a carbon composite filter (e.g., NFT-013 or NFT-020) to prevent the buildup of gases within the drum. For operational modeling purposes, the measured concentrations in the headspace of waste drums (i.e., drum headspace analyses) will be used to calculate the diffusion rates of VOCs across the drum filters and into the mine atmosphere. The headspace is the total void volume of a drum occupied by gases.

To demonstrate compliance with 40 CFR §268.6 over the long term (i.e., after closure of the repository), the transport of hazardous constituents via gas and/or brine must be evaluated. A source term must be developed to serve as input to the PA models. The hazardous constituent source term will be based on existing drum headspace data for VOCs and bounding assumptions for other RCRA-regulated constituents (semi-volatiles and metals).

2.0 Hazardous Constituents in TRU Mixed Waste

Hazardous constituents in TRU mixed waste are identified qualitatively through process knowledge and quantitatively through waste sampling and analysis activities. Knowledge of processes generating the waste has been documented by waste stream (DOE, 1990; DOE, 1991a). Table 2.1 lists hazardous constituents identified as target compounds selected for waste characterization in the RCRA Part B Permit Application Waste Analysis Plan (U.S. DOE, 1993). Per EPA guidance on 40 CFR 268.6, hazardous constituents listed in Appendix VIII of 40 CFR 261 are emphasized in this paper. However, for modeling purposes, SPM plans include screening all hazardous constituents listed in the RCRA Part B Permit Application on the basis of toxicity characteristics. Hazardous constituent source term indicator chemicals will be revised as additional information indicates the necessity.

TABLE 2-1

List of Hazardous Constituents and CAS Numbers

Volatile Organic Compounds (VOC)	CAS Number	Synonyms	Appendix VIII 40 CFR 261
Acetone	67-64-1	2-Propanone	
Benzene	71-43-2		▬
Bromoform	75-25-2	Tribromomethane	▬
n-Butyl alcohol	71-36-3	1-Butanol, Butanol	
Carbon disulfide	75-15-0	Carbon bisulfide	▬
Carbon tetrachloride	56-23-5		▬
Chlorobenzene	108-90-7		▬
Chloroform	67-66-3		▬
Cyclohexane	110-87-7		
Cyclohexanone	108-94-1		
1,1-Dichloroethane	75-34-3	Ethylidene chloride	
1,2-Dichloroethane	75-34-3	Ethylene dichloride	
1,1-Dichloroethylene (ene)	75-35-4	Vinylidene chloride	▬
(Z)-1,2-Dichloroethylene (ene)	540-59-0	cis 1,2-Dichloroethylene	▬
Ethyl acetate	141-78-6		
Ethyl benzene	100-41-4		
Diethyl ether	60-29-7	Ethyl ether, Ether	
2-Ethoxyethanol	110-80-5	Monoethyl ether	▬
Formaldehyde	50-00-0		▬
Hydrazine	302-01-2		▬
Isobutanol	78-83-1	Isobutyl alcohol	▬
Methanol	67-56-1	Methyl alcohol	
Methylene Chloride	75-09-2	Dichloromethane	▬

Modified after *Resource Conservation and Recovery Act Part B Permit Application* Waste Analysis Plan (U.S. DOE, 1993).

TABLE 2-1

List of Hazardous Constituents and CAS Numbers(cont.)

Volatile Organic Compounds (VOCs)	CAS Number	Synonyms	Appendix VIII 40 CFR 261
Methyl ethyl ketone	78-93-3	2-Butanone	▬
Methyl isobutyl ketone	108-10-1	4-Methyl-2-pentanone	
2-Nitropropane	76-46-9		▬
1,1,2,2-Tetrachloroethane	79-34-5		▬
Tetrachloroethylene (ene)	127-18-4	Perchloroethylene	▬
Toluene	108-88-3		▬
1,1,2-Trichloroethane	79-00-5		▬
1,1,1-Trichloroethane	71-55-6	Methyl chloroform	
Trichloroethylene (ene)	79-01-6		▬
Trichlorofluoromethane	75-69-4	Freon-11	▬
1,3,5-Trimethylbenzene	108-67-8	Mesitylene	
1,2,4-Trimethylbenzene	95-63-6	Pseudocumane	
1,1,2-Trichloro-1,2,2-trifluoroethane	76-13-1		
Vinyl chloride	75-01-4	Chloroethylene (ene)	▬
m-xylene p-xylene o-xylene	108-38-3 106-42-3 95-47-6	1,3-Dimethylbenzene 1,4-Dimethylbenzene 1,2-Dimethylbenzene	

Semi-volatile Organic Compounds	CAS Number	Synonyms	Appendix VIII 40 CFR 261
Cresols (o, m, p)	1319-77-3	Cresylic acid, Methyl phenol	▬
ortho-Dichlorobenzene	95-50-1	1,2-Dichlorobenzene	▬
1,4-Dichlorobenzene	106-46-7	p-Dichlorobenzene	▬
2,4-Dinitrotoluene	121-14-2		▬
Hexachloroethane	67-72-1		▬
Nitrobenzene	98-95-3		▬
Polychlorinated biphenyls (PCBs)	1336-36-3		▬
Pyridine	110-86-1		▬

Modified after *Resource Conservation and Recovery Act Part B Permit Application* Waste Analysis Plan (U.S. DOE, 1993a).

TABLE 2-1

List of Hazardous Constituents and CAS Numbers (cont.)

Metals	CAS Number	Synonyms	Appendix VIII 40 CFR 261
Arsenic	7440-38-2		▬
Barium	7440-39-3		▬
Beryllium	7440-41-7		▬
Cadmium	7440-43-9		▬
Chromium (IV only)	7440-47-3		▬
Lead	7439-92-1		▬
Mercury	7439-97-6		▬
Nickel (Nickel carboryl only)	7440-02-0		▬
Selenium	7782-49-2		▬
Silver	7440-22-4		▬
Thallium	7440-28-0		▬

Modified after *Resource Conservation and Recovery Act Part B Permit Application* Waste Analysis Plan (U.S. DOE, 1993a).

2.1 Waste Inventory

Transuranic waste results from plutonium reprocessing and fabrication; research and development; and decontamination and decommissioning activities. Since 1970, TRU waste has been placed in retrievable storage pending shipment to a permanent geologic repository. The anticipated inventory of TRU waste is defined as the sum of retrievably stored waste and currently projected (to be generated in the future) TRU waste volumes. TRUPACT-II (Transuranic Package Transporter-II) content (TRUCON) code waste volumes in the WIPP *Waste Analysis Plan* (DOE, 1990) are representative of the waste to be disposed of at the WIPP facility. Based on the volumes documented in the *Waste Analysis Plan*, the contribution of each waste stream, identified by TRUCON code, to the entire DOE inventory of TRU waste can be calculated. These values are referred to as weighting factors, the sum of which must be equivalent to 1.0. Table 2-2 lists the calculated weighting factors for each TRUCON code.

The DOE has developed the *Waste Isolation Pilot Plant Transuranic Waste Baseline Inventory Report* (BIR) (DOE, 1994a) which, when complete, will list the current anticipated inventory of TRU waste. The baseline inventory will be estimated using waste streams identified in recent information provided in the *Mixed Waste Inventory Report* (MWIR) (DOE, 1994b), supplemented with data from the *Nonradionuclide Inventory Database* and the 1993 *Integrated Database* (DOE, 1994c). Once the BIR is complete, a revised weighting scheme will be developed by Waste Matrix Code.

2.2 Waste Forms

Transuranic waste is packaged at the generator/storage sites in a primary confinement barrier (i.e., metal drum) and may include several layers of plastic, metal, and glass containers as well as adsorbents in the void spaces. Hazardous constituents contained in the waste at repository closure will exist in one or more physical states (solid, liquid, vapor), within solidified liquids and sludges, or sorbed onto cellulosics and other waste materials. Pursuant to the WIPP Waste Acceptance Criteria (WAC) (DOE, 1991b), waste containing free liquids is prohibited from shipment to the WIPP facility:

> Liquid waste will not be emplaced in the WIPP. TRU waste for emplacement in the WIPP shall contain as little residual liquid as is reasonably achievable. All internal containers (e.g., bottles, cans, etc.) must be well-drained, but may contain residual liquids. As a guideline, residual liquid in well-drained containers will be restricted to approximately one percent of the volume of the internal container. In no case shall the total liquid equal or exceed one volume percent of the waste container (e.g., drum or [standard waste box] SWB).

Real-time radiography (RTR) and visual examination are used to examine and verify the physical form of the waste and to certify conformance to the WAC. Experience at the Idaho National Engineering Laboratory (INEL) indicates a miscertifcation rate of only two percent, which includes all WAC operational safety and transportation-related criteria (EG&G, 1993). These administrative controls suggest that the presence of free liquids is not a controlling parameter in the conceptualization of the hazardous constituent source term.

TABLE 2-2

Weighting Factors by TRUCON Code

TRUCON Codes	Weighting Factor
111, 211	0.2302
112, 212	0.0308
113, 213	0.0038
114, 214	0.0214
115, 215	0.0076
116, 216	0.2104
117, 217	0.2042
118, 218	0.0183
119, 219	0.0445
121, 221	0.0028
122, 222	0.0035
123, 223	0.0255[a]
124, 224	0.0059
125, 225	0.1863
126, 226	0.0003

[a]This includes leaded rubber, listed as TRUCON 117 by Los Alamos National Laboratory.

The TRU waste inventory is classified according to 11 WIPP waste profiles based on the Waste Matrix Groups provided in the MWIR database. All TRU waste to be sent to the WIPP facility are represented by a WIPP waste profile, the highest tier of information describing acceptable waste forms. The Waste Matrix Groups from the MWIR are summarized in the BIR by the following acceptable WIPP waste profiles:

- Combustible Waste
- Filter Waste
- Graphite Waste
- Heterogeneous Waste
- Inorganic Non-Metal Waste
- Lead/Cadmium Metal Waste
- Uncategorized Metal Waste
- Salt Waste
- Soil
- Solidified Inorganic Waste
- Solidified Organic Waste

2.3 Quantities of Hazardous Constituents

Parameter values must be established for the conditions being modeled. Although some characterization data for VOCs in drum headspaces exist, actual quantities of hazardous constituents in the waste containers cannot be determined. In cases where data are not available, the maximum concentrations of hazardous constituents which could exist in the gas and/or liquid phases may be calculated. Many of the parameter values necessary for calculating these maximum quantities are readily available in the literature; others must be estimated over a range of repository conditions. In the absence of experimentally determined values, the EPA encourages the use of well-established and documented estimation techniques (EPA, 1986).

2.3.1 Concentrations of Hazardous Constituents in the Gas Phase

On-going waste characterization activities at the INEL and the Rocky Flats Plant (RFP) have provided actual headspace concentrations of VOCs for 536 drums of TRU mixed waste.

Analytical results have been weighted according to the TRUCON code volume ratios presented in Section 2.1. The average TRUCON-weighted headspace concentrations are presented in Table 2-3, specific to hazardous constituents listed in 40 CFR 261 Appendix VIII. Labeled as NA in Table 2-3, semi-volatile organic compounds and RCRA metals are not quantified through headspace analyses.

Weighted averages were calculated using the following equation:

$$\bar{x} = \sum_{i=1}^{t} w_i \bar{x}_i \tag{2-1}$$

where

$\bar{x}$	=	weighted average
$\bar{x}_i$	=	average for TRUCON code i
w_i	=	weighting factor for TRUCON code i
t	=	number of TRUCON codes,

and $\bar{x}_i$ is calculated by

$$\bar{x}_i = \frac{1}{n_i} \sum_{j=1}^{n_i} x_{ij} \tag{2-2}$$

where

n_i	=	number of samples in TRUCON code i
x_{ij}	=	analysis j for TRUCON code i.

The INEL is conducting a study to establish a relationship between headspace measurements and localized variations in concentrations that may occur in a typical drum of waste. The diffusion study is expected to establish whether headspace measurements are representative of the entire drum void space and whether concentrations over time indicate steady-state conditions. Although the results of this study have not yet been published, preliminary results suggest that headspace measurements are indicative of the presence of a constituent and that concentration gradients across inner layers of confinement are not significant.

TABLE 2-3

Chemical Vapor Pressures at 27 °C and Gas-Phase Chemical Concentrations

Chemical	Vapor Pressure at 27 °C (atm)[a]	Saturated Vapor Concentration (g/liter)	TRUCON Weighted Average Drum Headspace Concentration (g/liter)
Arsenic	NA	NA	NA
Barium	NA	NA	NA
Benzene	1.37E-01	4.34E-01	2.91E-05
Beryllium	NA	NA	NA
Bromoform (Tribromomethane)	8.84E-03[b]	9.07E-02	9.34E-05
Cadmium	NA	NA	NA
Carbon disulfide	5.12E-01	1.58E+00	8.00E-07[d]
Carbon tetrachloride	1.64E-01	1.02E+00	3.50E-03
Chlorobenzene	1.78E-02	8.13E-02	5.54E-05
Chloroform	2.82E-01	.37E+00	7.52E-05
Chromium	NA	NA	NA
Cresols	4.77E-04	2.09E-03	NA
1,4-Dichlorobenzene	2.68E-03	1.60E-02	NA
ortho-Dichlorobenzene	2.67E-03	1.59E-02	NA
(cis)-1,2-Dichloroethylene	2.90E-01	1.14E+00	3.57E-05
1,1-Dichloroethylene	7.89E-01[c]	3.11E+00	4.37E-05
2,4-Dinitrotoluene	6.71E-06[c]	4.96E-05	NA
2-Ethoxyethanol	1.49E-02[b]	5.45E-02	8.00E-07[d]
Formaldehyde	5.54E+00	6.75E+00	8.00E-07[d]
Hexachloroethane	1.00E-03[b]	9.61E-03	NA
Hydrazine	2.13E-02	2.77E-02	8.00E-07[d]
Isobutanol (Isobutyl alcohol)	1.84E-02	5.54E-02	8.00E-07[d]
Lead	NA	NA	NA
Mercury	NA	NA	NA
Methyl ethyl ketone	1.31E-01	3.84E-01	8.00E-07
Methylene chloride (Dichloromethane)	6.12E-01	2.11E+00	2.55E-03
Nickel	NA	NA	NA
Nitrobenzene	4.03E-04	2.01E-03	NA
2-Nitropropane	2.47E-02[b]	8.93E-02	8.00E-07[d]
PCBs	1.01E-07[c]	1.35E-06	NA
Pyridine	3.04E-02	9.76E-02	NA
Selenium	NA	NA	NA
Silver	NA	NA	NA
1,1,2,2-Tetrachloroethane	7.98E-03	5.44E-02	6.22E-05
Tetrachloroethylene	2.66E-02	1.79E-01	6.13E-05
Thallium	NA	NA	NA
Toluene	4.14E-02	1.55E-01	9.40E-05
1,1,2-Trichloroethane	3.27E-02	1.77E-01	8.00E-07[d]
Trichloroethylene	1.00E-01	5.33E-01	1.13E-04
Trichlorofluoromethane	1.09E+00	6.08E+00	8.00E-07[d]
Vinyl chloride	4.07E+00	1.03E+01	8.00E-07[d]

NA = Not applicable

[a]Values calculated from equations and coefficients in Reid et. al (1987)

[b]Values interpolated using Clausius-Clapeyron equation and values tabulated in Perry et. al (1984)

[c]Values are from EPA (1986)

[d]Data for constituent not available; value equal to one-half the sample quantitation limit

The maximum concentration of a hazardous constituent in the gas phase at a given temperature is equal to the saturated vapor concentration at that temperature. The vapor pressure is the pressure exerted by a chemical vapor in equilibrium with its solid or liquid form at any given temperature. The higher the vapor pressure, the more likely a chemical is to exist in a gaseous state. The saturated vapor pressure at 27° C for each Appendix VIII hazardous constituent is also listed in Table 2-3.

For the majority of the chemicals, the vapor pressure was estimated using the appropriate coefficients and estimation equations recommended in Reid et al. (1987). For the remaining chemicals, the Clausius-Clapeyron equation was used to estimate the vapor pressure at 27° C, given vapor pressure versus temperature data tabulated in Perry et al. (1984). The source of the vapor-pressure value for each chemical is indicated in Table 2-3. The saturated vapor concentration is calculated using the following relationship:

$$c_i = \frac{P_i^v \, M_i}{R \, T} \tag{2-3}$$

where,

c_i = saturated vapor concentration of chemical (i) in the gas phase [g/cm^3]

P_i^v = saturated vapor pressure of chemical (i) at 300.15 K [atm]

M_i = molecular weight of chemical (i) [g/mol]

R = gas constant [82.057 atm cm^3/(mol K)]

T = absolute temperature [300.15 K].

2.3.2 Concentrations of Hazardous Constituents in the Liquid Phase

For dilute solutions of gases in water, Henry's Law provides a good estimate of chemical concentration in the liquid phase (i.e., the source term in the liquid phase) by relating it to the chemical concentration in the gas phase (Reid et al., 1987). The Henry's Law constant for a gas in a liquid may be estimated by the equations of phase equilibrium or solution thermodynamics. The key parameter in phase equilibrium thermodynamics is fugacity. If agaseous phase and a liquid phase are in thermodynamic equilibrium, then for any component (i), the fugacities in both phases must be equal, and the following relation holds:

$$f_i^{gas} = f_i^{liquid} \tag{2-4}$$

where,

f_i^{gas} = gas-phase fugacity of component (i)

f_i^{liquid} = liquid-phase fugacity of component (i).

The fugacity of component (i) in each phase can be calculated as the product of other parameters. Specifically, the previous phase equilibrium relationship may be expressed as:

$$\varphi_i \, y_i \, P = H_{i,solvent} \, x_i \tag{2-5}$$

where,

φ_i = gas-phase fugacity coefficient of chemical (i)

y_i = mole fraction of chemical (i) in the gas phase

P = system (total) pressure

$H_{i,solvent}$ = Henry's Law constant for gas solute (i) in the solvent (water)

x_i = mole fraction of gas solute (i) in the solvent (water).

The Henry's Law constant of a gas in a solvent at any pressure can be evaluated using the Krichevsky-Kasarnovsky equation (Prausnitz, 1969), which takes the form:

$$H_i^{(P)} = H_{i,solvent}^{(P_{ref})} \exp\left[\frac{v_i^{\infty} \, (P - P_{ref})}{R \, T}\right] \tag{2-6}$$

where,

$H_i^{(P)}$ = Henry's Law constant of solute (i) in the solvent at the system pressure [atm]

$H_{i,solvent}^{(P_{ref})}$ = Henry's Law constant of solute (i) in the solvent evaluated at arbitrary reference pressure P_{ref} [atm]

v_i^{∞} = partial molar volume of solute (i) in the liquid phase at infinite dilution [cm^3/mol]

P = system or total pressure [atm]

P_{ref} = arbitrary reference pressure that is usually assumed to be equal to the saturated vapor pressure of the solvent (water or WIPP brine) at the temperature of the repository horizon [0.03 atm]

R = gas constant [82.057 atm cm^3/(mol K)]

T = absolute temperature [300.15 K].

Table 2-4 lists the parameters ($H_{i,solvent}^{(P\ ref)}$ and v_i^{∞}/RT) that are used to estimate the Henry's Law constant for each VOC and semi-volatile in water at 27° C as a function of total system pressure. The constants at atmospheric pressure were calculated from water solubility, vapor pressure, and molecular weight data for each chemical.

The solubilities of the 11 RCRA-regulated metals (listed in Table 2-5) in WIPP brine are a complex function of a number of parameters. These parameters include the ionic strength and the specific composition of the brine, radiolytic effects, microbial activity, generation of gases, and the pH/Eh values of the brine. Table 2-5 lists the major cations and anions, organic ligands, and gases that are expected to affect the source term for the RCRA-regulated metals. Materials that may be present in the waste matrix (e.g., cement) and repository brine will also impact the RCRA metal source term. The effects of these environmental parameters on solubility, mobilization or immobilization of metals will be evident as performance assessment and associated sensitivity analyses are completed. The most sensitive parameters will be identified through this process.

All these parameters will vary with time and have an uncertainty associated with their values. The uncertainty is usually defined by a statistical distribution type and the statistics of the distribution (e.g., mean value and variance). In order to derive a source term for the RCRA metals, the solubility in brine needs to be estimated over a range of chemical compositions. The range of compositions should be based on the uncertainties in the parameter values. The range may be established using a geochemical code. A geochemical code allows the uncertainties in the values of the input parameters to be propagated into a range of solubilities for each metal. The SNL WIPP PA Department uses Monte Carlo techniques with Latin Hypercube sampling to evaluate parameter uncertainties.

TABLE 2-4

Henry's Law Constant Parameters

Chemical	$H_{i,solvent}^{(P_{ref})}$ (atm)[a]	v_i^{∞}/RT (1/atm)[b]
Arsenic	NA	NA
Barium	NA	NA
Benzene	3.37E+02	3.91E-03
Beryllium	NA	NA
Bromoform (Tribromomethane)	4.09E+01	4.55E-03
Cadmium	NA	NA
Carbon disulfide	7.31E+02	2.36E-03
Carbon tetrachloride	1.84E+03	4.18E-03
Chlorobenzene	2.37E+02	4.69E-03
Chloroform	2.26E+02	3.60E-03
Chromium	NA	NA
Cresols	9.16E-02	4.71E-03
1,4-Dichlorobenzene	2.74E+02	5.53E-03
ortho-Dichlorobenzene	2.16E+02	5.53E-03
(cis)-1,2-Dichloroethylene	4.42E+02	3.41E-03
1,1-Dichloroethylene	1.87E+03	3.41E-03
2,4-Dinitrotoluene	2.80E-01	7.47E-03
2-Ethoxyethanol	7.39E-02	4.87E-03
Formaldehyde	2.30E+01	1.50E-03
Hexachloroethane	2.60E+02	6.43E-03
Hydrazine	1.10E-04	1.44E-03
Isobutanol (Isobutyl alcohol)	8.63E-01	4.14E-03
Lead	NA	NA
Mercury	NA	5.92E-04
Methyl ethyl ketone	1.94E+00	4.04E-03
Methylene chloride (Dichloromethane)	2.20E+02	2.81E-03
Nickel	NA	NA
Nitrobenzene	1.44E+00	5.33E-03
2-Nitropropane	7.13E+00	4.28E-03
PCBs	5.84E+01	1.14E-02
Pyridine	1.33E-01	3.83E-03
Selenium	NA	NA
Silver	NA	NA
1,1,2,2-Tetrachloroethane	2.54E+01	5.17E-03
Tetrachloroethylene	1.62E+03	4.40E-03
Thallium	NA	NA
Toluene	3.92E+02	4.82E-03
1,1,2-Trichloroethane	5.34E+01	4.45E-03
Trichloroethylene	6.61E+02	3.87E-03
Trichlorofluoromethane	7.50E+03	3.74E-03
Vinyl chloride	5.26E+03	2.50E-03

NA = Not applicable

[a]Values calculated from water solubility, vapor pressure, and molecular weight data (EPA 1986; Reid et. al 1987)

[b]Values based on summing group contributions to obtain critical volume and then using the estimation equation in Reid et. al (1987)

TABLE 2-5

Species Relevant to the Development of a Source Term for RCRA-Regulated Metals

- RCRA-Regulated Metals
  - Arsenic
  - Barium
  - Beryllium
  - Cadmium
  - Chromium
  - Lead
  - Mercury
  - Nickel
  - Selenium
  - Silver
  - Thallium

- Major Cations and Anions
  - Boron: B^{+3} probably present mainly as H_3BO_3
  - Bromide: Br^{-1}
  - Calcium: Ca^{+2}
  - Potassium: K^{+}
  - Magnesium: Mg^{+2}
  - Sodium: Na^{+}
  - Sulfate: SO_4^{2}

- Organic Ligands
  - Citric acid
  - Ethylenediaminetetraacetic acid (EDTA)
  - 8-Hydroxy-quinoline
  - 1-Thenoyl-3,3,3-trifluoroacetone (TTA)

- Gases
  - Oxygen
  - Nitrogen
  - Carbon Dioxide
  - Methane
  - Hydrogen

The EQ3/6 geochemical model, developed by Thomas Wolery at Lawrence Livermore Laboratories, is an example of a geochemical code that could be used in the analysis. The EQ3/6 model is a general purpose, versatile geochemical code, which can model the complex geochemical processes that result from interactions among the host rock, nuclear waste, groundwater, and gas. The code includes the Pitzer's equations for estimating the solubilities of species in concentrated brines such as those at the WIPP. The EQ3/6 code, or an equivalent, will be used to estimate metal solubilities. The requisite level of QA will be considered in selecting the code used for this task.

The steps in estimating the range of solubility values for the RCRA-regulated metals using a the EQ3/6 or equivalent code are summarized below:

1. Develop distribution types and parameters of the distribution (mean, variance, confidence intervals, etc.) for the concentration of major cation and anion species, organic ligands, and gases listed in Table 2-5 as well as for pH, Eh, total inorganic carbon, and ionic strength based on all available WIPP brine-related analyses. In cases where on interaction parameters are not available for a RCRA metal, reasonable and conservative assumptions will be made, as appropriate.

2. Create input file sets for the EQ3/6 suite of codes for each of the 11 RCRA-regulated metals to estimate the average metal solubility and to identify indicator metals.

3. Generate between 25 and 30 realizations or Latin Hypercube Samples (LHS) for each of the indicator metals, and execute the EQ3/6 suite of codes to develop a solubility distribution for each of the indicator metals.

4. Perform statistical analyses of the 25 to 30 solubility values for each metal to identify the distribution type and parameters of the distribution (mean, variance, confidence intervals, etc.).

3.0 Conceptual Model

The conceptual model for the hazardous constituent source term defines the expected behavior of VOCs, semi-volatiles, and metals within the WIPP disposal system after closure. In cases where waste characterization and physical property data are limited, and chemical transformation and release mechanisms are uncertain, certain bounding assumptions are made to develop the source term.

3.1 Baseline Assumptions

In order for hazardous constituents in the liquid, solid, or solidified liquid state to be released into the waste region, the waste drums must be breached. Prior to breaching of the drums,

the only release mechanism is diffusion of hazardous constituents in the vapor state through the drums filters. Because the integrity of the waste containers within the repository cannot be determined with certainty, it is conservatively assumed that all drums are breached instantaneously at repository closure.

Knowledge of the quantity of each hazardous constituent would allow depletion of the inventory to be accounted for in source-term estimates. In reality, depletion will likely occur as a result of microbial degradation and/or hazardous-constituent migration away from the repository in the gas and brine phases. Since information relative to future repository conditions that would affect such depletion mechanisms is imprecisely known, the following conservative assumptions are made:

- The migration of hazardous constituents away from the repository does not decrease the initial source term
- Degradation of hazardous constituents does not occur and, therefore, does not decrease the initial source term
- Hazardous constituents exist in the gas and brine phases at constant concentrations over time

Post-closure release mechanisms are the mechanisms by which hazardous constituents become mobile and available for transport from the waste region after repository closure. Several long-term chemical and physical processes described in the gas generation and disposal room position papers identify mechanisms that could affect VOC concentrations in the waste region. These processes include corrosion, decomposition/compression of sludges and waste, and microbial degradation. Degradation of substrates by these processes, if they occur, would liberate VOCs that are effectively immobilized in the short-term drum environment.

The impact of the release mechanisms on the post-closure VOC source term is speculative. For instance, anoxic corrosion of Fe and Al-alloy metals will result in corrosion products, which in themselves will act as a substrate for adsorption of VOCs. Degradation of cement and gypsum-based materials are known to decompose in the presence of brine, but Ca(OH) and other degradation products could also act as a substrate for continued adsorption of VOCs. Compression of the waste matrix to the extent necessary to release adsorbed VOCs (or physically bound within sludges) would occur only in the presence of low gas generation. Less gas generation would also reduce the driving force for VOC migration. Microbial degradation of cellulosics, plastics and rubbers is another potential release mechanism for

VOCs. Thermal desorption is inconsequential as a release mechanism, as repository temperatures are expected to remain constant at approximately 27° C.

It is believed that conservative assumptions used to model the post-closure VOC source term reasonably accounts for uncertainties in post-closure release mechanisms. Taking no credit for VOC source depletion and/or VOC degradation is more than conservative enough to bound any uncertainty accociated with this reasonable assumption. It is believed that these mechanisms will contribute insignificantly to the results of final transport modeling.

For each hazardous constituent present in the gas phase, its corresponding liquid-phase concentration may be calculated from its gas-phase concentration by assuming thermodynamic equilibrium. It is assumed that thermodynamic equilibrium is reached upon closure. In addition, it is conservatively assumed that the solubility of organics in brine is equivalent to their solubilities in water. In high salinity solutions such as the WIPP brine, most gases will be less soluble than in pure water because of the "salting-out" effect. Therefore, estimates of gas solubility in water will overestimate the actual solubility in brine.

3.2 Gas-Phase Source Term

The conceptual model for the hazardous constituent source term in the gas phase, for the purposes of transport modeling, is characterized by the following:

- Concentrations of VOCs are equivalent to the weighted average of measured headspace concentrations obtained from drum characterization data. These data have been obtained through sampling and analysis of wastes conducted at the INEL (243 drums) and the RFP (293 drums).

- Concentrations of semi-volatiles are equivalent to the saturated vapor concentrations, which are calculated from parameter values obtained from the literature.

- Metals do not exist in the gas phase.

The fundamental rationale for selecting the use of headspace measurements over the saturation vapor pressure model (presented in an earlier draft) is that the latter assumed VOC vapors in equilibrium with an infinite pool of liquid to serve as a future VOC source supply. As shown in Table 2-3, measured drum headspace concentrations are at least two orders of magnitude lower than the saturated vapor concentrations, indicating that free liquid organics are not present in the waste containers.

3.3 Liquid-Phase Source Term

For the purposes of transport modeling, the liquid-phase hazardous constituent source term is characterized by the following:

- Concentrations of VOCs and semi-volatiles in brine are governed by the laws of thermodynamic equilibrium between the gas and liquid phases. Henry's Law is used to calculate the liquid-phase concentration given the gas-phase concentration. Chemical-specific parameters (e.g., fugacity coefficients, Henry's Law constants) are readily available in the literature.

- Metal constituent concentrations are equivalent to their maximum solubilities in brine. These concentrations will be estimated using the EQ3/6 geochemical code, or equivalent.

4.0 Future Development Activities

The DOE plans to conduct several activities which will serve to refine the hazardous constituent source term. In order to obtain a statistical basis for the use of drum headspace data, additional knowledge of the waste drums and sampling practices is needed. This information is currently being pursued and includes the following:

- Date on which the sample was taken
- Whether or not the drum was vented prior to sampling
- When the drum was vented (if vented)
- Type of carbon composite filter installed on the drum
- Date on which the drum was packaged

The information listed above will be provided for each drum of waste. The objective is to subdivide each waste stream into categories of waste similar in age, drum configuration, and sampling practices. Within these categories, normal distributions of data are expected. In addition, waste characterization data/information obtained from other generator sites and waste streams will continue to be collected and added to the current source term data set.

An updated waste inventory definition will be needed to appropriately weight the waste characterization data set and provide the most accurate VOC gas-phase source term. Once the BIR is complete, this information will become available, and the data will be weighted by Waste Matrix Code rather than by TRUCON code (as described in Section 2.1).

Calculations for both an operational and long-term no-migration demonstration would allow bounding headspace concentrations to be determined. The basis for these calculations would be the regulatory limit for each constituent at the unit boundary. If the bounding headspace concentrations are orders of magnitude higher than weighted VOC concentrations, a comparison of the two levels will demonstrate that it is both a reasonable and conservative to use the headspace limited concept in transport modeling. This also supports selection of a subset of hazardous constituents for modeling on the basis of toxicty, as regulatory limits are based on health-based risk parameters.

Comparison of the bounding headspace concentrations with weighted headspace measurements also allows consideration of another stratgey: performance-based waste acceptance criteria (PBWAC). Criteria may be developed to prohibit the disposal of waste drums which exceed bounding headspace concentrations. Most likely, excluded drums would be derived from specific waste streams, such as sludges and solidified organics, and represent a small portion of the total inventory. If this approach is implemented, a gas-phase source term based on measured headspace concentrations for VOCs would not be necessary.

5.0 Summary

A hazardous constituent source term must be developed to model contaminant transport over the long term; the results of this modeling will provide the basis for a no-migration demonstration. For the postclosure phase, potential transport media include gas and brine. The hazardous constituent source term is defined as the concentrations of VOCs, semi-volatiles, and metals present in these media. Existing data and bounding assumptions serve as the bases for the hazardous constituent source term. The DOE will pursue additional information to further refine the data sets used in the development of the source term.

In the event that, through the PA models, gas and/or brine are not expected to reach the unit boundary in 10,000 years, the concentrations of hazardous constituents in these phases will become irrelevant. If there are no mechanisms by which hazardous constituents are transported to the unit boundary, a source term need not be defined.

6.0 References

EG&G, 1993. EG&G Engineering Design File, EDF Serial Number RWMC-675, Rev. 0, November 30, 1993.

Perry, R.H., D.W. Green, and J.O. Maloney, 1984. Perry's Chemical Engineers' Handbook, Sixth edition, New York, NY, McGraw-Hill Book Company.

Prausnitz, J.M., 1969. Molecular Thermodynamics of Fluid-Phase Equilibrium, Englewood Cliffs, NJ, Prentice-Hall, Inc.

Reid, R.C., J.M. Prausnitz, and T.K. Sherwood, 1987. The Properties of Gases and Liquids, Fourth edition, New York, NY, McGraw-Hill Book Company.

U.S. Department of Energy (DOE), 1990. Waste Isolation Pilot Plant No-Migration Variance Petition, Appendix B "Waste Analysis Plan," DOE/WIPP 89-003, Rev. 1, March 1990, Westinghouse Electric Corporation, Waste Isolation Division, Carlsbad, NM.

U.S. Department of Energy (DOE), 1991a. TRUPACT-II Content Codes (TRUCON), DOE/WIPP 89-004, Rev. 5, April 1991, Department of Energy, Carlsbad, NM.

U.S. Department of Energy (DOE), 1991b. Waste Acceptance Criteria for the Waste Isolation Pilot Plant, DOE-WIPP-069, Rev. 4, December 1991, Department of Energy, Carlsbad, NM.

U.S. Department of Energy (DOE), 1993. Resource Conservation and Recovery Act Part B Permit Application, DOE-WIPP-91-005, Rev. 3, Department of Energy, Carlsbad, NM.

U.S. Department of Energy (DOE), 1994a. U.S. Department of Energy Waste Isolation Pilot Plant Transuranic Waste Baseline Inventory Report, DOE/CAO-94-1005, Rev. 0, DOE Carlsbad Area Office, Carlsbad, NM..

U.S. Department of Energy (DOE), 1994b. Distribution of the Phase II Mixed Waste Inventory Report Data, Memorandum from Patty Bubar to Distribution, May 17, 1994 (includes data diskette [Version 1.00] of the draft User's Guide for National Data Base System for the Final Mixed Waste Inventory Report [May 1994] and Mixed Waste Inventory Report Database System User's Guide), Washington, D.C.

U.S. Department of Energy (DOE), 1994c. U.S. Department of Energy Integrated Database for 1993: U.S. Spent Fuel and Radioactive Waste Inventories, Projections, and Characteristics, DOE/RW-0006, Rev. 9, April 1994.

U.S. Environmental Protection Agency (EPA), 1986. Superfund Public Health Evaluation Manual, EPA/540/1-86/060, Washington, D.C, Environmental Protection Agency.

WIPP Library

March 17, 1995

Systems Prioritization Method - Iteration 2 Baseline Position Paper:

Performance Assessment Methodology

Mel Marietta

Sandia National Laboratories
Albuquerque, NM 87185

Contents

1 CONCEPTUALIZATION OF RISK FOR THE WIPP PERFORMANCE ASSESSMENT 1

1.1 Calculation of Risk 2
1.2 Characterization of Uncertainty in Risk 4
1.3 Risk and the EPA Limits 8

2 SELECTION OF SCENARIOS 12
2.1 Conceptual Basis for Scenario Development 12
2.2 WIPP Performance-Assessment Approach to Scenario Development 15

3 DETERMINATION OF SCENARIO PROBABILITIES 19

4 CALCULATION OF SCENARIO CONSEQUENCES 19

5 MONTE CARLO ANALYSIS TECHNIQUES 20

5.1 Selection of Variables and Their Ranges and Distributions 23
5.2 Generation of the Sample 25
5.3 Propagation of the Sample through the Analysis 25
5.4 Uncertainty Analysis 26
5.5 Sensitivity Analysis 26
5.6 System Prioritization 27

Figures

1 Estimated CCDF for consequence result cS 3
2 Example distribution of CCDFs obtained by sampling imprecisely known variables 5
3 Example summary curves from an estimated distribution of CCDFs 7
4 Decomposition of the sample space S into high-level subsets 13
5 Construction of a CCDF for comparison with the EPA release limits 16
6 Models used in the 1992 WIPP performance assessment 21
7 Distribution function for an imprecisely known analysis variable 24
8 Example of box plots (hypothetical results) 28

Tables

1 Release Limits for the Containment Requirements (U.S. EPA, 1985, Appendix A, Table 1) 10
2 Summary of Computer Models in the 1992 WIPP Performance Assessment . . . 22

Acronyms

CAMCON	Compliance Assessment Methodology Controller
CCDF	complementary cumulative distribution function
CDF	cumulative distribution function
CFR	Code of Federal Regulations
EPA	Environmental Protection Agency
IAEA	International Atomic Energy Agency
PA	performance assessment
PBWAC	performance-based waste-acceptance criteria
SPM	system prioritization methodology
VOC	volatile organic compound
WIPP	Waste Isolation Pilot Plant

1 CONCEPTUALIZATION OF RISK FOR THE WIPP PERFORMANCE ASSESSMENT

The Waste Isolation Pilot Plant (WIPP) performance assessment uses a conceptualization for risk similar to that developed for risk assessments for nuclear power plants. This conceptualization characterizes risk in terms of what can happen, how likely things are to happen, and the consequences of what can happen. This description provides a structure on which both the representation and calculation of risk can be based.[1]

Kaplan and Garrick (1981) have presented this representation of risk as a set of ordered triples. The WIPP performance assessment uses their representation and defines risk to be a set R of the form

$$R = \{(s_i,\ pS_i,\ \mathbf{cS}_i),\ i = 1, \ldots, nS\} \tag{1}$$

where

s_i = a set of similar occurrences

pS_i = probability that an occurrence in set s_i will take place

$\mathbf{cS}_i$ = a vector of consequences associated with s_i

nS = number of sets selected for consideration

and the sets s_i have no occurrences in common (i.e., the s_i are disjoint sets). This representation formally decomposes risk into what can happen (the s_i), how likely things are to happen (the pS_i), and the consequences of what can happen (the $\mathbf{cS}_i$). The s_i are scenarios in the WIPP performance assessment, the pS_i are scenario probabilities, and the vector $\mathbf{cS}_i$ contains performance measures associated with scenario si. Performance measures of interest are normalized EPA releases, dose and health effects for safety assessments, and concentrations of heavy metals and volatile organic compounds (VOCs) for hazardous waste assessments.

Risk results in R can be summarized with complementary cumulative distribution functions (CCDFs). These functions provide a display of the information contained in the probabilities pS_i and the consequences $\mathbf{cS}_i$. With the assumption that a particular consequence result cS in the vector $\mathbf{cS}$ has been ordered so that $cS_i \le cS_{i+1}$ for $i = 1, \ldots, , nS\text{-}1$, the CCDF for this consequence result is the function F defined by

[1] This position paper on Performance Assessment (PA) Methodology is taken largely from Chapter 3, Volume 2 of the 1992 WIPP PA documentation (WIPP PA Dept., 1992b). Additional information about this subject is provided in other published sources (Helton et al., 1992; 1993; Tierney, 1993).

$F(\mathbf{x})$ = probability that cS exceeds a specific consequence value x

$$= \sum_{j=i}^{nS} pS_j, \tag{2}$$

where i is the smallest integer such that $\mathbf{cS}_i > x$. As illustrated in Figure 1, F is a step function that represents the probabilities that consequence values on the abscissa will be exceeded. To avoid a broken appearance, CCDFs are usually plotted with vertical lines added at the discontinuities.

The steps in the CCDFs shown in Figure 1 result from the discretization of all possible occurrences into the sets $s_1,\ldots,s_{nS}$. Unless the underlying processes are inherently disjoint, the use of more sets s_i will tend to reduce the size of these steps and, in the limit, will lead to a smooth curve.

1.1 Calculation of Risk

The calculation of risk and its associated uncertainty begins with the determination of the sets s_i, which are the scenarios to be analyzed. Once these sets are determined, their probabilities pS_i, and associated consequences $\mathbf{cS}i$ must be determined. In practice, development of the s_i is an iterative process that must take into account the procedures required to determine the probabilities pS_i and the consequences $\mathbf{cS}_i$. For the WIPP performance assessment, the overall process is organized so that pS_i and $\mathbf{cS}_i$ are calculated by various models, with the configuration of these models depending on the individual s_i.

Use of these models requires values for many imprecisely known variables that can be represented by a vector

$$\mathbf{x} = [x_1, x_2, \ldots, x_{nV}] \tag{3}$$

where each x_j is an imprecisely known input required in the analysis and nV is the total number of such inputs. If the analysis has been developed so that each x_j is a quantity for which the overall analysis requires a single value, the representation for risk in Equation 1 can be restated as a function of $\mathbf{x}$:

$$\mathrm{R}(\mathbf{x}) = \{[S_i(\mathbf{x}), pS_i(\mathbf{x}), \mathbf{cS}_i(\mathbf{x})], i=1, \ldots, nS(\mathbf{x})\} \tag{4}$$

As $\mathbf{x}$ changes, so will $\mathrm{R}(\mathbf{x})$ and all summary measures that can be derived from $\mathrm{R}(\mathbf{x})$. Thus, rather than a single CCDF for each consequence contained in the vector $\mathbf{cS}$ shown in Equation 1, a distribution of CCDFs results from the possible values that $\mathbf{x}$ can represent (Figure 2).

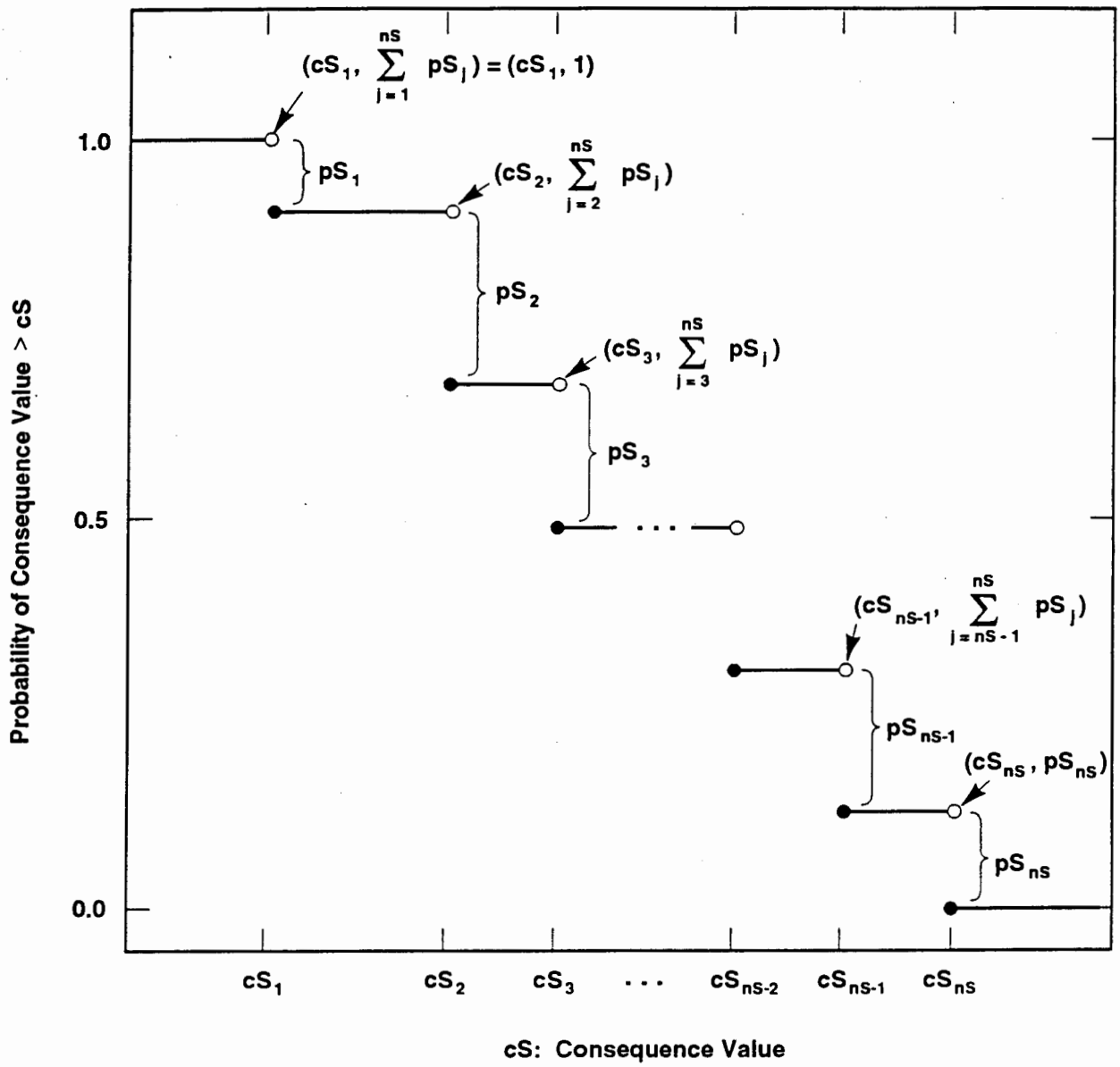

TRI-6342-730-5

Figure 1. Estimated CCDF for consequence result cS (Helton et al., 1991; Helton, 1993). The open and solid circles at the discontinuities indicate the points included on (solid circles) and excluded from (open circles) the CCDF.

Distributions can be assigned to the individual variables x_j in **x** to characterize uncertainty in our knowledge of the modeling system. Factors that affect uncertainty in risk results can be subdivided into those that affect imprecisely known variables, those related to the selection of conceptual and computational models, and those related to scenario selection. Each of these three sources of uncertainty has the potential to affect all three of the elements of the triple introduced in Equation 1. Uncertainty about imprecisely known variables may result from incomplete data or measurement uncertainty. Uncertainty in the actual choice of models used in the assessment primarily affects pS_i and $\mathbf{cS}_i$, but because of the complexity of the analysis, also has the potential to affect the definition of the s_i. Factors related to scenario selection can be further subdivided into completeness, aggregation, and stochastic variation. Completeness refers to the extent that a performance assessment includes all possible occurrences for the system under consideration. In terms of the risk representation in Equation 1, completeness deals with whether or not all possible occurrences are included in the union of the sets s_i. Aggregation refers to the division of the possible occurrences into the sets s_i. Resolution is lost if the s_i are defined too coarsely, (e.g., if nS is too small) or in some other inappropriate manner. Computational efficiency is affected if nS is too large. Stochastic variation is represented by the probabilities pS_i, which are functions of the many factors that affect the occurrence of the individual sets s_i.

Individual variables x_j may relate to each of these different types of uncertainty. For example, individual variables might relate to completeness uncertainty (e.g., the value for a cutoff used to drop low-probability occurrences from the analysis), aggregation uncertainty (e.g., a bound on the value for nS), model uncertainty (e.g., a 0-1 variable that indicates which of two alternative models should be used), variable uncertainty (e.g., a solubility limit or a retardation for a specific element), or stochastic uncertainty (e.g., a variable that helps define the probabilities for the individual S_i).

1.2 Characterization of Uncertainty in Risk

Characterization of the uncertainty in the results of a performance assessment requires characterization of the uncertainty in **x**, the vector of imprecisely known variables. This uncertainty can be described with a sequence of probability distributions

$$D_1, D_2, \ldots, D_{nV} \tag{5}$$

where D_j is the distribution developed for the variable x_j, $j=1, 2, \ldots, nV$, contained in **x**. The definition of these distributions may also be accompanied by the specification of correlations and various restrictions that further define the possible relations among the x_j. These distributions and other restrictions probabilistically characterize where the appropriate input to use in the performance assessment would most likely fall, given that the analysis is structured so that only one value can be used for each variable under consideration.

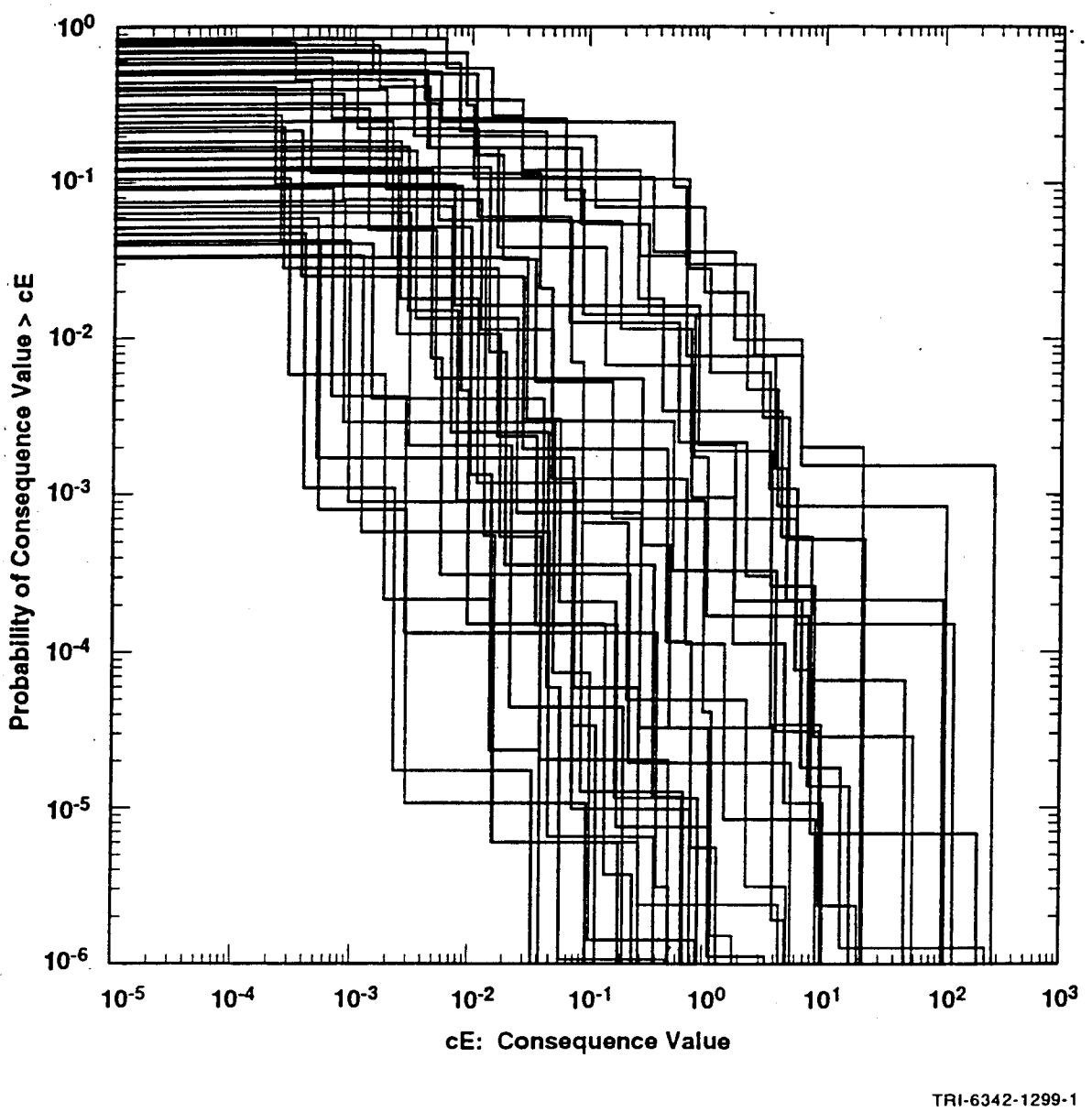

Figure 2. Example distribution of CCDFs obtained by sampling imprecisely known variables.

Once the distributions in Equation 5 have been developed, Monte Carlo techniques (Helton et al., 1992) can be used to determine the uncertainty in $R(\mathbf{x})$ from the uncertainty in $\mathbf{x}$. First, a sample

$$\mathbf{x}_k = [x_{k1}, x_{k2}, \ldots, x_{kv}, nV], \; k = 1, \ldots, nK \tag{6}$$

is generated according to the specified distributions and restrictions, where nK is the size of the sample. Performance-assessment calculations are then performed for each sample element $\mathbf{x}_k$, which yields a sequence of risk results of the form

$$R(\mathbf{x}_k) = \{[S_i(\mathbf{x}_k), pS_i(\mathbf{x}_k), \mathbf{cS}_i(\mathbf{x}_k)\}, \; i = 1, \ldots, nS(\mathbf{x}_k)\} \tag{7}$$

for $k = 1, \ldots, nK$. Each set $R(\mathbf{x}_k)$ is the result of one complete set of calculations performed with a set of inputs (i.e., $\mathbf{x}_k$) that the review process producing the distributions in Equation 5 concluded was possible. Further, associated with each risk result $R(\mathbf{x}_k)$ in Equation 7 is a probability or weight[2] that can be used in making probabilistic statements about the distribution of $R(\mathbf{x})$.

A single CCDF can be produced for each set $R(\mathbf{x}_k)$ of results shown in Equation 7, yielding a family of CCDFs of the form shown in Figure 2. The location of the distribution of CCDFs in Figure 2 relative to the regulatory criteria provides an assessment of the "assurance" with which 40 Code of Federal Regulations (CFR) 191.13(a) can be met as required in 191.13(b). In particular, the distribution of CCDFs in Figure 2 can be summarized with mean and percentile curves constructed in the following manner and illustrated in Figure 3. At each point on the abscissa in Figure 2, a vertical line is drawn through the nK exceedance probabilities from which the mean and various percentiles (e.g., 10%, 50%, 90%) can be determined. The curves in Figure 3 result from connecting the mean and percentile values obtained for individual consequence values. The percentile curves provide a probabilistic representation with respect to where the actual exceedance probability associated with a given consequence value is believed to be located. For example, the probability is 0.8 that the exceedance probability for a particular normalized release is located between the 10% and 90% percentile curves, with this probability deriving from the distributions in Equation 5.

Consideration of a family of CCDFs allows a distinction between the uncertainty that controls the shape of a single CCDF and the uncertainty that results in a distribution of CCDFs. The stepwise shape of a single CCDF reflects the fact that a number of different occurrences have a real possibility of taking place. This type of uncertainty is referred to as

[2] In random or Latin hypercube sampling, this weight is the reciprocal of the sample size (i.e., $1/nK$) and can be used in estimating means, cumulative distribution functions, and other statistical properties. This weight is often referred to as the probability for each observation (i.e., sample $\mathbf{x}_k$). However, this usage is not technically correct. If continuous distributions are involved, the actual probability of each observation is zero.

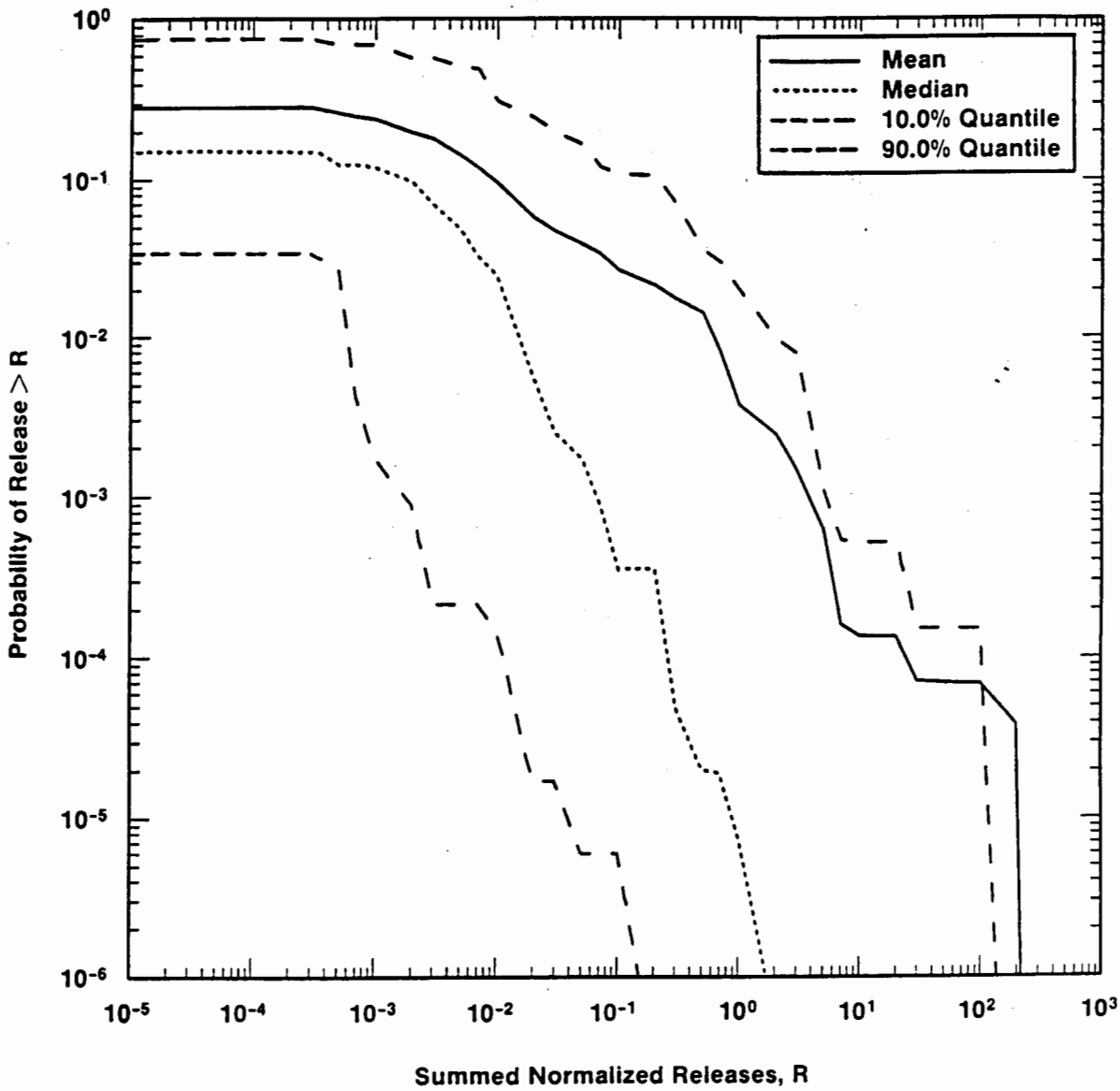

Figure 3. Example summary curves derived from an estimated distribution of CCDFs. The curves in this figure were obtained by calculating the mean and the indicated percentiles for each consequence value on the abscissa in Figure 2. The 90th-percentile curve crosses the mean curve due to the highly skewed distributions for exceedance probability. This skewness also results in the mean curve being above the median curve.

stochastic variation. A family of CCDFs arises from the fact that fixed, but unknown, quantities are needed in the estimation of a CCDF. The distributions that characterize what the values for these fixed quantities might be lead to a distribution of CCDFs, with each single CCDF reflecting a specific sample element $\mathbf{x}_k$.

Both Kaplan and Garrick (1981) and the International Atomic Energy Agency (IAEA, 1989) distinguish between these two types of uncertainty. Specifically, Kaplan and Garrick distinguish between probabilities derived from frequencies and probabilities that characterize degrees of belief. Probabilities derived from frequencies correspond to the probabilities pS_i in Equation 1, while probabilities that characterize degrees of belief (i.e., subjective probabilities) correspond to the distributions indicated in Equation 5. The IAEA report distinguishes between what it calls Type-A uncertainty and Type-B uncertainty. The IAEA report defines Type-A uncertainty to be stochastic variation; as such, this uncertainty corresponds to the frequency-based probability of Kaplan and Garrick and the pS_i of Equation 1. Type-B uncertainty is defined to be uncertainty that is due to lack of knowledge about fixed quantities; thus, this uncertainty corresponds to the subjective probability of Kaplan and Garrick and the distributions indicated in Equation 5. This distinction has also been made by other authors, including Vesely and Rasmuson (1984), Paté-Cornell (1986), and Parry (1988).

For a given conceptual model in the WIPP performance assessment, subjective uncertainty enters the analysis due to lack of knowledge about quantities such as solubility limits, retardation factors, and flow fields. In previous WIPP PAs, stochastic uncertainty entered the analysis through the assumption that future exploratory drilling will be random in time and space (i.e., follows a Poisson process). However, the rate constant in the definition of this Poisson process was assumed to be imprecisely known. Thus, subjective uncertainty can exist in a quantity used to characterize stochastic uncertainty.

1.3 Risk and the EPA Limits

In Title 40 of the CFR, the Environmental Protection Agency (EPA) has promulgated the following standard for the long-term performance of geologic repositories for high-level and transuranic (TRU) wastes (U.S. EPA, 1985):

191.13 Containment requirements.

(a) Disposal systems for spent nuclear fuel or high-level or transuranic radioactive wastes shall be designed to provide a reasonable expectation, based on performance assessments, that the cumulative releases of radionuclides to the accessible environment for 10,000 years after disposal from all significant processes and events that may affect the disposal system shall:

(1) Have a likelihood of less than one chance in 10 of exceeding the quantities calculated according to Table 1 (Appendix A of 40 CFR 191); and

(2) Have a likelihood of less than one chance in 1,000 of exceeding ten times the quantities calculated according to Table 1 (Appendix A of 40 CFR 191).

The term "accessible environment" means: "(1) The atmosphere; (2) land surfaces; (3) surface waters; (4) oceans; and (5) all of the lithosphere that is beyond the controlled area" (U.S. EPA, 1985, 191.12(k)). Further, "controlled area" means: "(1) A surface location, to be identified by passive institutional controls, that encompasses no more than 100 square kilometers and extends horizontally no more than five kilometers in any direction from the outer boundary of the original location of the radioactive wastes in a disposal system; and (2) the subsurface underlying such a surface location" (U.S. EPA, 1985, 191.12(g)). The preceding requirements refer to Table 1 (Appendix A of 40 CFR 191). This table is reproduced here as Table 1.

For a release to the accessible environment that involves a mix of radionuclides, the limits in Table 1 are used to define a normalized release (called normalized EPA release in this position paper) for comparison with the release limits. Specifically, the normalized EPA release for TRU waste is defined by

$$nR = \sum_i (Q_i / L_i)(1x10^6 Ci / C) \tag{8}$$

where

Q_i = cumulative release (Ci) of radionuclide i to the accessible environment during the 10,000-yr period following closure of the repository,

L_i = the release limit (Ci) for radionuclide i given in Table 1,

and

C = amount of TRU waste (Ci) emplaced in the repository.

The EPA expressly identifies the need to consider the impact of uncertainties in calculations performed to show compliance with the Containment Requirements. Specifically, Appendix C[3] of 40 CFR 191 suggests that

[3] This was originally promulgated as 40 CFR 191 Appendix B (U.S. EPA, 1985, p. 38088). It was subsequently remanded to the EPA (NRDC v. EPA, 824 F.2d 1258 [1st Cir. 1987]), and was repromulgated as 40 CFR 191 Appendix C (U.S. EPA, 1993, p. 66415). It is referenced as Appendix C throughout this position paper.

Table 1. Release Limits for the Containment Requirements (U.S. EPA, 1985, Appendix A, Table 1)

Radionuclide	Release limit L_i per 1000 MTHM* or other unit of waste (curies)
Americium-241 or -243	100
Carbon 14	100
Cesium-135 or -137	1,000
Iodine-129	100
Neptunium-237	100
Plutonium-238, -239, -240, or -242	100
Radium-226	100
Strontium-90	1,000
Technetium-99	10,000
Thorium-230 or -232	10
Tin-126	1,000
Uranium-233, -234, -235, -236 or -238	100
Any other alpha-emitting radionuclide with a half-life greater than 20 years	100
Any other radionuclide with a half-life greater than 20 years that does not emit alpha particles	1,000

* Metric tons of heavy metal exposed to a burnup between 25,000 megawatt-days per metric ton of heavy metal (MWd/MTHM) and 40,000 MWd/MTHM.

...whenever practicable, the implementing agency will assemble all of the results of the performance assessments to determine compliance with § 191.13 into a "complementary cumulative distribution function" that indicates the probability of exceeding various levels of cumulative release. When the uncertainties in parameters are considered in a performance assessment, the effects of the uncertainties considered can be incorporated into a single such distribution function for each disposal system considered. The Agency assumes that a disposal system can be considered to be in compliance with [section]

191.13 if this single distribution function meets the requirements of [section] 191.13(a) (U.S. EPA, 1985, p. 38088).

The representation for risk in Equation 1 provides a conceptual basis for the calculation of the complementary cumulative distribution function (CCDF) for normalized EPA releases specified in 40 CFR 191 Appendix C. Further, this representation provides a structure that can be used for both the incorporation of uncertainties and the representation of the effects of uncertainties.

A CCDF in the family of CCDFs that results from Equation 7 could be the appropriate choice for comparison against the EPA requirements, *if* $\mathbf{x}_k$ contained the correct variable values for use in determining the pS_i and $\mathbf{cS}_i$ *and if* the assumed conceptual models correctly characterize the disposal system. Increasing the sample size nK will, in general, produce a better approximation of the true distribution of CCDFs, but will not alter the fact that the distribution of CCDFs is conditional on the assumptions of the analysis.

If nK is large, displays of the complete family of CCDFs can be difficult to interpret. As discussed in the previous section, mean and percentile curves can be used to summarize the information contained in the family. Appendix C of 40 CFR 191 suggests that "the effects of the uncertainties considered can be incorporated into a single [CCDF]" (U.S. EPA, 1985; p. 38088), but 40 CFR 191 does not contain specific guidance on which curve should be compared to the Containment Requirements. In previous work, the mean curve has generally been proposed for showing compliance with § 191.13(a) (e.g., Cranwell et al., 1987, 1990; Hunter et al., 1986). Complete families of curves and the associated summary curves are presented in previous WIPP PAs. In the future, only mean curves will be compared to the Containment Requirements.

Whenever a distribution of curves is reduced to a single curve, information on uncertainty is lost. Replicated Monte Carlo analyses can be used to characterize the uncertainty in a mean CCDF or other summary curves. However, representing the uncertainty in an estimated value in this way is quite different from displaying the variability or uncertainty in the population from which the estimate is derived. For example, the uncertainty in the estimated mean curve in Figure 3 is less than the variability in the population of CCDFs that was averaged to obtain this mean (see Figure 2).

Because CCDFs are conditional on the assumptions of the analysis, they are also conditional on the choice of conceptual model. Previous WIPP performance assessments examined conceptual model uncertainty by repeating the complete Monte Carlo analysis for each alternative conceptual model and comparing mean CCDFs (WIPP PA Dept., 1992a, 1992b). Only those portions of the analysis specific to the alternative conceptual models (e.g., selected parameter values or computational models) are altered. All other models and parameter values are the same in each analysis, and the two conceptual models are thus

compared *ceteris paribus* (all other things being equal). The shift in the location of the CCDF provides a measure of the uncertainty introduced by the existence of alternative conceptual models and provides the Project guidance on which alternative conceptual models have the greatest potential to affect disposal-system performance. Previous ceteris paribus comparisons and sensitivity analysis results have motivated the Project to change direction in the experimental program (Beauheim and Davies, 1992; Brush, 1990; Gelbard, 1991; U.S. DOE, 1991).

2 SELECTION OF SCENARIOS

40 CFR 191 does not include the term scenario in its definition of performance assessment, referring instead only to events and processes that might affect the disposal system during the next 10,000 years. The various combinations of significant events and processes that define possible future states of the disposal system must be considered in a complete analysis. Combinations of events and processes are referred to as scenarios in Bertram-Howery and Hunter (1989), Marietta et al. (1989), Cranwell et al. (1990), Bertram-Howery et al. (1990), WIPP PA Division (1991), and WIPP PA Dept. (1992a, 1992b).

2.1 Conceptual Basis for Scenario Development

The scenarios s_i are obtained by subdividing a set s (the sample space) that contains all possible WIPP 10,000-year time histories beginning at the decommissioning of the facility. An important goal of the scenario development is to identify and remove from consideration those scenarios for which the impact on compliance with 40 CFR 191 Appendix C can be reasonably anticipated to be negligible due to low probability or low consequence, and those scenarios that are excluded by regulation.

Five subsets of s provide a starting point for scenario development (Figure 4). The reasoning behind selecting these subsets is provided in Section 4.2.3 of WIPP PA Dept. (1992b). First, the base-case subset s_B consists of all elements in s that fall within the bounds of what can be reasonably anticipated to occur over 10,000 years. For the WIPP, this represents the undisturbed performance of the disposal system. Second, a minimal disruption subset s_M consists of all elements in s that involve disruptions that result in no significant perturbation to the consequences associated with the corresponding elements in the base-case subset s_B. Third, a regulatory exclusion subset s_E consists of all elements in s that are excluded from consideration by regulatory directive (e.g., human intrusions more severe than the drilling of exploratory boreholes). Fourth, a low-probability subset s_L consists of elements of s not contained in s_B whose collective probability is small (e.g., the probability of s_L is less

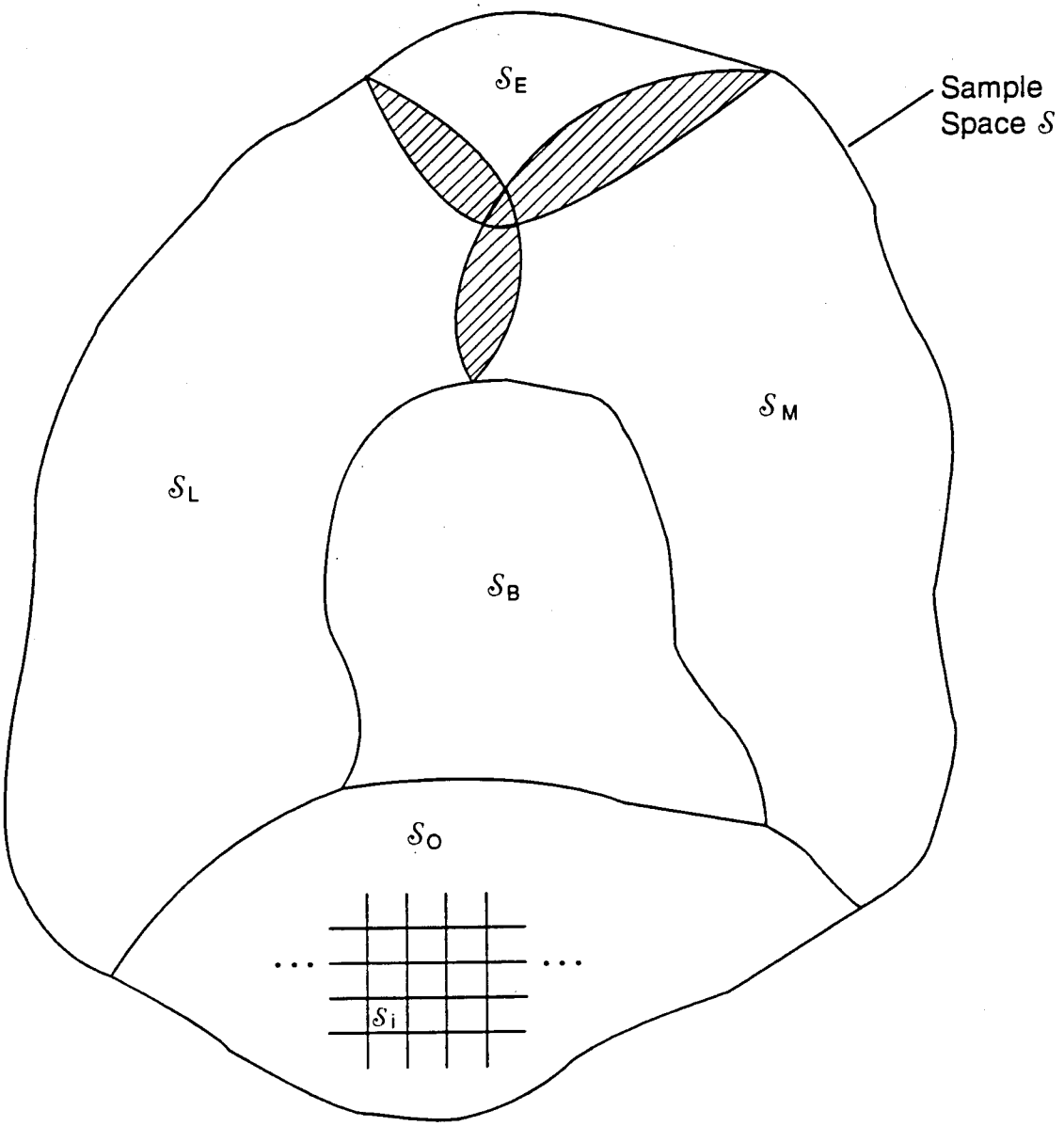

Figure 4. Decomposition of the sample space s into high-level subsets, where s_B designates the base-case subset, s_M designates a minimal disruption subset, s_E designates a regulatory exclusion subset, s_L designates a low-probability subset, and s_O designates $(s_B \cup s_M \cup s_E \cup s_L)^c$.

than 0.0001) regardless of their potential consequences. Everything that remains in s after the identification of s_B, s_M, s_E, and s_L, now becomes a fifth subset s_O, where the subscript O represents "Other." In set notation,

$$s_O = (s_B \cup s_M \cup s_E \cup s_L)^c \tag{9}$$

where the superscript c is used to designate the complement of a set.

Evaluation of compliance with the Containment Requirements of 40 CFR 191 Appendix C does not depend equally on each of the five subsets of s. By definition, elements of s_E are excluded from consideration. The relative contributions of the other four subsets to a hypothetical CCDF for the WIPP are shown in Figure 5. Releases associated with the base case s_B for the WIPP were zero for the previous analysis (see Chapter 5 of WIPP PA Dept., 1992a, and references cited there), and the consequences of both s_B and s_M therefore plot well below the EPA limits, at the extreme upper left of the CCDF. Consequences of s_L are by definition of sufficiently low probability (less than 10^{-4} in 10^4 years) that they plot below the EPA limits. High-consequence elements of s_L plot at the lower right of the CCDF. Compliance depends primarily therefore on the examination of s_O and partially on s_B, and specifically on a set of additional scenarios s_i, $i=1, \ldots, nS$, obtained by further refining (i.e., subdividing) the subset s_O. s_E, S_L, and s_M could be defined to be mutually exclusive, but this distinction is not important here so they are represented in Figure 4 with non-empty intersections. As described in Section 4.2.1 of WIPP PA Dept. (1992b), s_B and s_O are constructed to be mutually exclusive and to have empty intersections with s_M and s_L.

Although the scenarios that affect compliance for the WIPP come primarily from the set s_i, performance assessments must also include s_B. The overall pattern of Figure 5 can be seen in the results of the previous WIPP preliminary performance assessments, in which releases associated with the undisturbed base case s_B were zero. s_B determines the upper left of the CCDF and the remainder is determined by the s_i.

This analysis does not exclude S_L from consideration in the comparison with the EPA release limits. The contribution from s_L would always plot to the lower right of the CCDF, well below the EPA probability limits, and therefore would have little impact in a compliance decision. s_M is not included in WIPP PA so the probability of s_M is not accumulated as shown in Figure 5, i.e., only the probability of s_B is included. The net effect of excluding s_M is to raise the CCDF toward the probability limits; therefore, including s_M is conservative.

Consequences of s_M cannot be seen on the CCDF in Figure 5 because releases in the 1992 WIPP performance assessment from s_B are zero. Consequences of s_L are also not displayed directly in the results of the WIPP performance assessments as they would appear in the extreme lower right portion of the curve as an extension of the CCDF and would not impact a compliance evaluation.

Appendix C of 40 CFR 191 suggests that "... performance assessments need not consider categories of events or processes that are estimated to have less than one chance in 10,000 of occurring over 10,000 years" (U.S. EPA, 1985, p. 38088). By suitably defining the events and processes selected for consideration (i.e., by making nS sufficiently large), all probabilities can theoretically be made less than the specified bound. Conceptually, the WIPP performance assessment adds a level of conservatism by placing a bound on the total probability of all occurrences that are removed from detailed consideration (i.e., the probability pS_L for s_L) rather than the individual probabilities for a number of different scenarios. In practice, the distinction has no regulatory impact because, as discussed in Chapter 4 of WIPP PA Dept. (1992b), probabilities estimated for elements of s_L were substantially below the suggested probability cutoff for required inclusion.

2.2 WIPP Performance-Assessment Approach to Scenario Development

Recognition of the five subsets of s provides the basis for the WIPP performance assessment's approach to scenario development. Because s_B, s_E, s_L, and s_M may account for a large part of the sample space s and also have readily predicted effects on the CCDF used for comparison with the EPA release limits, s_B, s_E, s_L, and s_M are determined in the first stage of development before s_O is subdivided into the scenarios s_i shown in Figure 4.

The WIPP performance assessment uses a two-stage procedure for scenario development and the determination of scenario probabilities. The purpose of the first stage is to develop a comprehensive set of scenarios that includes all occurrences that might reasonably take place at the WIPP, and to determine the probabilities of these scenarios. The result of this stage is a set of scenarios that summarize what might happen at the WIPP. These scenarios provide a basis for discussing the future behavior of the WIPP and a starting point for the second stage of the procedure, which is the definition of scenarios s_i and the determination of the probabilities pS_i at a level of detail that is appropriate for use with the conceptual and computational models employed in the performance assessment.

The first stage of the analysis focuses on the determination of the sample space s and the subsets s_B, s_E, s_L, s_M and s_O. Major groupings of scenarios within s_O are also recognized at this time, and defined for reference purposes as summary scenarios. For previous PAs, this stage of the analysis uses a scenario-selection procedure suggested by Cranwell et al. (1990) that consists of the following five steps: (1) compiling or adopting a "comprehensive" list of events and processes that potentially could affect the disposal system, (2) classifying the events and processes to aid in completeness arguments, (3) screening the events and processes to identify those that can be eliminated from consideration in the performance assessment, (4) developing scenarios by combining the events and processes that remain after screening, and

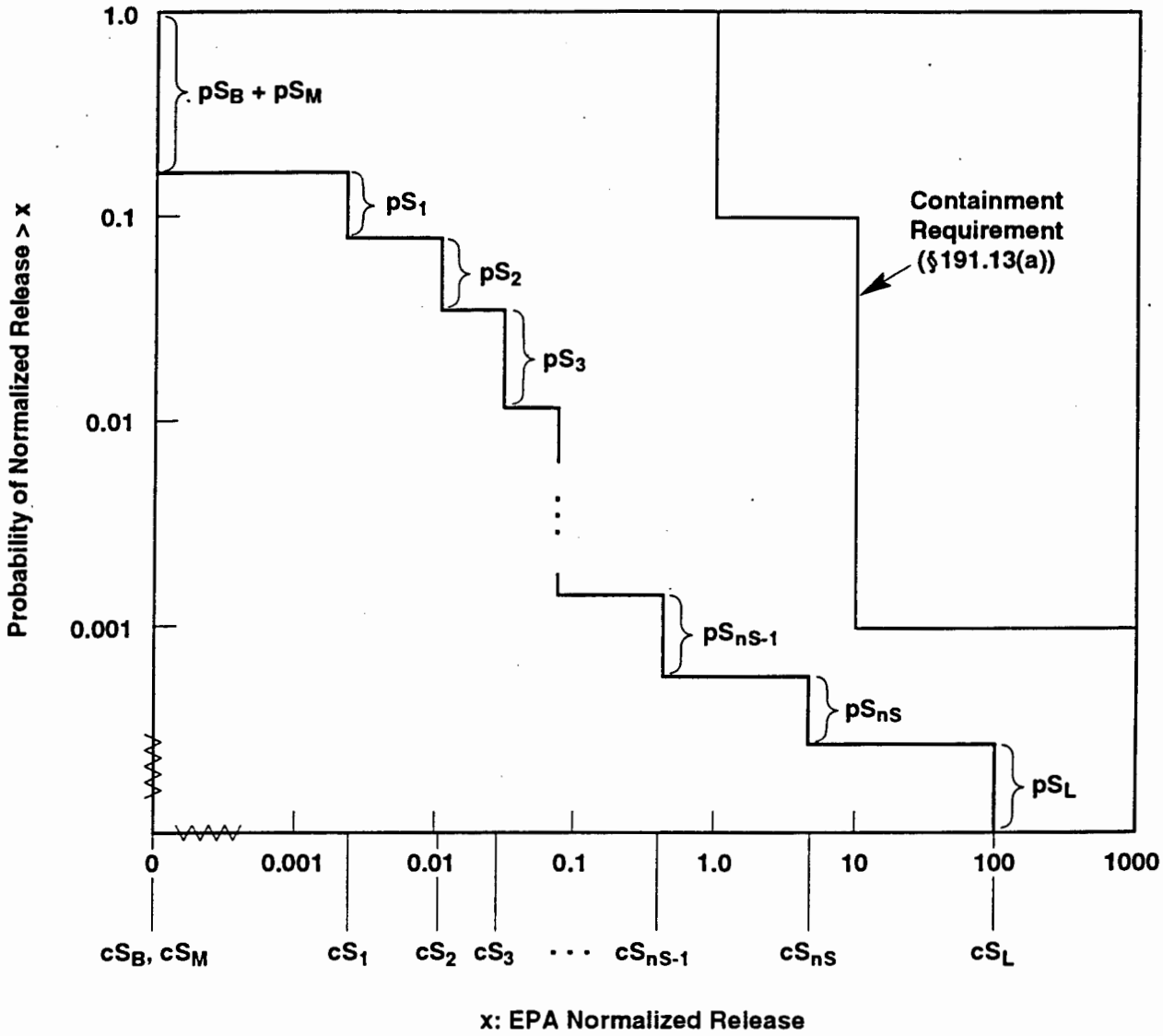

Notation: $pS_B, pS_M, pS_1, pS_2, \ldots, pS_{nS}, pS_L$ probability for corresponding scenario

$cS_B, cS_M, cS_1, cS_2, \ldots, cS_{nS}, cS_L$ consequence for corresponding scenario

$\mathcal{S}_1, \mathcal{S}_2, \ldots, \mathcal{S}_{nS}$ assumed to be ordered so that $cS_1 \leq cS_2 \leq \ldots \leq cS_{nS}$

TRI-6342-1278-0

Figure 5. Construction of a CCDF for comparison with the EPA release limits. Note that the location of cS_B at the lower left of the plot is correct for previous WIPP performance assessments, where no releases are predicted from the undisturbed base case, but is not a generic requirement for all sites.

(5) screening scenarios to identify those that have little or no effect on the shape or location of the mean CCDF.

The purpose of the first step is to develop the sample space s, which consists of all possible 10,000-year time histories that involve the identified events and processes. The sample space s is subdivided into the subsets s_B, s_E, s_L, s_M and s_O in Steps 2 and 3. The screening associated with Steps 2 and 3 also removes time histories from s that are physically unreasonable. In Step 4, a preliminary subdivision of the subset s_O into additional summary scenarios is accomplished through a two-part process. In the first part, subsets of s_O (i.e., scenarios) are defined that involve specific events or processes. However, these scenarios are not mutually exclusive. In the second part, is subdivided into mutually exclusive scenarios s_i by forming all possible intersections of the single event/process scenarios and their complements. The fifth and final step in the process is a screening of the scenarios s_i on the basis of probability, consequence, and physical reasonableness. The purpose of this screening is to determine if some of the s_i can be removed from the analysis.

A second stage of scenario development is necessary because the summary scenarios developed in the first stage are, in general, not defined at sufficiently fine levels of resolution for use in the construction of a CCDF that adequately displays the effects of stochastic, or Type-A, uncertainty (Section 1.2). The computational scenarios described in Section 4.2.4 of WIPP PA Dept. (1993b) represent a substantially finer subdivision of s_O than that used to construct the summary scenarios, but they are based on the same screening of events and processes conducted during the first stage of scenario development. As in previous scenario construction for preliminary performance assessments of the WIPP, inadvertent intrusion into the repository during exploratory drilling is the only disruptive event considered in the 1992 assessment. The computational scenarios reflect subdivisions based on time and number of intrusions, the activity of the waste intersected, and whether or not pressurized brine is encountered in the Castile Formation below the repository.

The determination of both scenarios and scenario probabilities is a complex process with significant uncertainties. To help assure that the WIPP performance assessment brings a broad perspective to this task, expert panels were formed to provide a diversity of views with respect to possible futures at the WIPP and the probability of human intrusion. The formation of these panels and the results obtained from their deliberations are documented in Hora et al. (1991) and the memorandum by Hora (1992) in Appendix A of Volume 3 of the 1992 WIPP PA documentation.

No inherently correct grouping exists of the possible time histories into scenarios; the probabilities associated with individual scenarios s_i can always be reduced by using a finer grouping. As long as low-probability s_i are not discarded, the use of more, but lower probability s_i will improve the resolution in the estimated CCDF shown in Figure 1. Because

a consequence must be calculated for each scenario s_i, the use of more s_i results in more detailed specification of the calculations that must be performed for each scenario.

For example, a scenario s_i for the WIPP might be defined by

$S_i = \{x$: x a single 10,000-year time history beginning at decommissioning of the facility under consideration in which a single borehole occurs$\}$. (10)

A more refined definition would be

$S_{ik} = \{x$: x a 10,000-year history at the WIPP beginning at decommissioning in which a single borehole occurs between $(k\text{-}1)\times 10^3$ and $k\times 10^3$ years and no boreholes occur during any other time interval$\}$. (11)

Then,

$$S_{ik} \subset S_i, k=1,\ldots,10, and\ S_i = \bigcup_{k=1}^{10} S_{ik} \tag{12}$$

Thus, s_i and $\cup_k s_{ik}$ contain the same set of time histories. However, the individual s_{ik} are smaller sets of time histories that are included in the larger set s_i. In terms of performance assessment, each s_{ik} describes a more specific set of conditions that must be modeled than does s_i. The estimated CCDF in Figure 1 could be constructed with either s_i or the s_{ik}, although the use of the s_{ik} would result in less aggregation error, and thus, provide better resolution in the resultant CCDF.

The s_i appearing in the definition of risk in Equation 1 should be developed to a level of resolution at which it is possible to view the analysis for each s_i as requiring a fixed, but possibly imprecisely known, vector $\mathbf{x}$ of variable values. When a set s_i is appropriately defined, it should be possible to use the same model or models and the same vector of variable values to represent every occurrence (e.g., a 10,000-year time history for the WIPP) in s_i. Scenario definition must permit the consequences $\mathbf{cs}_i$ appearing in Equation 1 to be calculated with reasonable efficiency, while holding the amount of aggregation error that enters the analysis to a reasonable level. Thus, although subdivision of s into a large number of s_i (e.g., on the basis of time of intrusion) may result in increased resolution in the estimate of $\mathbf{cs}$, it may also result in a computationally impractical analysis. Performance assessments balance these competing requirements.

3 DETERMINATION OF SCENARIO PROBABILITIES

The second element of the ordered triples shown in Equation 1 is the scenario probability pS_i. As with scenario definition, the probabilities pS_i have been developed at two levels of detail.

Preliminary probabilities for the summary scenarios have been developed by Marietta et al. (1989) and Guzowski (1991). Apostolakis et al. (1991) provide an additional discussion of techniques for determining probabilities in the context of performance assessment for radioactive-waste disposal.

Probabilities for the computational scenarios used in the construction of CCDFs are discussed in Chapter 5 of WIPP PA Dept. (1992b), and are based on the assumption that the occurrence of boreholes through the repository follows a Poisson process (i.e., are random in time and space) with a rate constant λ. Formulas for determining pS_i dependent on this assumption are derived in Chapter 5 of WIPP PA Dept. (1992b). The derivations are general and include both the stationary (i.e., constant λ) and nonstationary (i.e., time-dependent λ) cases. The 1992 performance assessment estimates consequences using both constant values for λ and time-dependent values derived from expert judgment.

4 CALCULATION OF SCENARIO CONSEQUENCES

The third element of the ordered triples shown in Equation 1 is the scenario consequence, $\mathbf{cS}_i$. Estimation of $\mathbf{cS}_i$ was done in the 1992 PA using a linked system of computational models described in greater detail in Chapters 7 and 8 of WIPP PA Dept. (1992b). Some modifications to these codes have provided additional capability since 1992. Present capability is discussed elsewhere in this technical baseline.

The models used in the WIPP performance assessment, as in other complex analyses, exist at four different levels. First, conceptual models provide a framework in which information about the disposal system can be organized and linked to processes that can be simulated with quantitative models. An adequate conceptual model is essential for both the development of the set s_o appearing in Equation 9 and the division of s_o into the scenarios s_i appearing in Equation 1. As defined in Chapter 2 of WIPP PA Dept. (1992b), alternative conceptual models can exist that are equally consistent with the available information. Consequences for each scenario must be estimated separately for each alternative conceptual model included in the analysis.

Second, mathematical models are developed to represent the processes at the site. The conceptual models provide the context within which these mathematical models must operate and define the processes they must characterize. The mathematical models are predictive in

the sense that, given known properties of the system and possible perturbations to the system, they predict the response of the system. Among the processes represented by these mathematical models are fluid flow, mechanical deformation, radionuclide transport in groundwater, removal of waste through intruding boreholes, and human exposure to radionuclides released to the surface environment. Mathematical models for these processes, and others, are described in Chapter 7 of WIPP PA Dept. (1992b).

Third, numerical models are developed to approximate the mathematical models. Most mathematical models do not have closed-form solutions and numerical procedures must be developed to provide approximations to the solutions of the mathematical models. In essence, these approximations provide "numerical models" that calculate results that approach the solutions of the original mathematical models. For example, Runge-Kutta procedures are often used to solve ordinary differential equations, and finite difference and finite element methods are used to solve partial differential equations. In practice, it is unusual for a mathematical model to have a solution that can be determined without the use of an intermediate numerical model. Numerical models used in the WIPP performance assessment are described in appendices to WIPP PA Dept. (1992b).

Fourth, the complexity of the system requires the use of computer codes to implement the numerical models. Figure 6 illustrates the sequence of linked codes used in the 1992 WIPP performance assessment. Each of the models appearing in this figure is briefly described in Table 2; more information is available in Chapter 7 and appendices of WIPP PA Dept. (1992b), and in references cited there.

5 MONTE CARLO ANALYSIS TECHNIQUES

As discussed in more detail by Helton et al. (1991) and in WIPP PA Dept. (1993a), the WIPP performance assessment uses Monte Carlo techniques for uncertainty and sensitivity analyses. In the context of this position paper, uncertainty analyses evaluate uncertainty in performance estimates that results both from the existence of alternative conceptual models and from the uncertainty about imprecisely known input variables. Sensitivity analyses determine the contribution of individual input variables to the uncertainty in model predictions. As used here, both these types of analyses provide information about the effects of subjective, or Type-B, uncertainty. The effects of stochastic, or Type-A, uncertainty are incorporated into the performance assessment through the scenario probabilities pS_i appearing in Equation 1.

Monte Carlo analyses involve five steps (1) selection of the variables to be examined and the ranges and distributions for their possible values, (2) generation of the samples to be analyzed, (3) propagation of the samples through the analysis, (4) uncertainty analysis, and (5) sensitivity analysis. These steps are described briefly in Sections 5.1 through 5.5. A more complete discussion can be found in Helton et al. (1991).

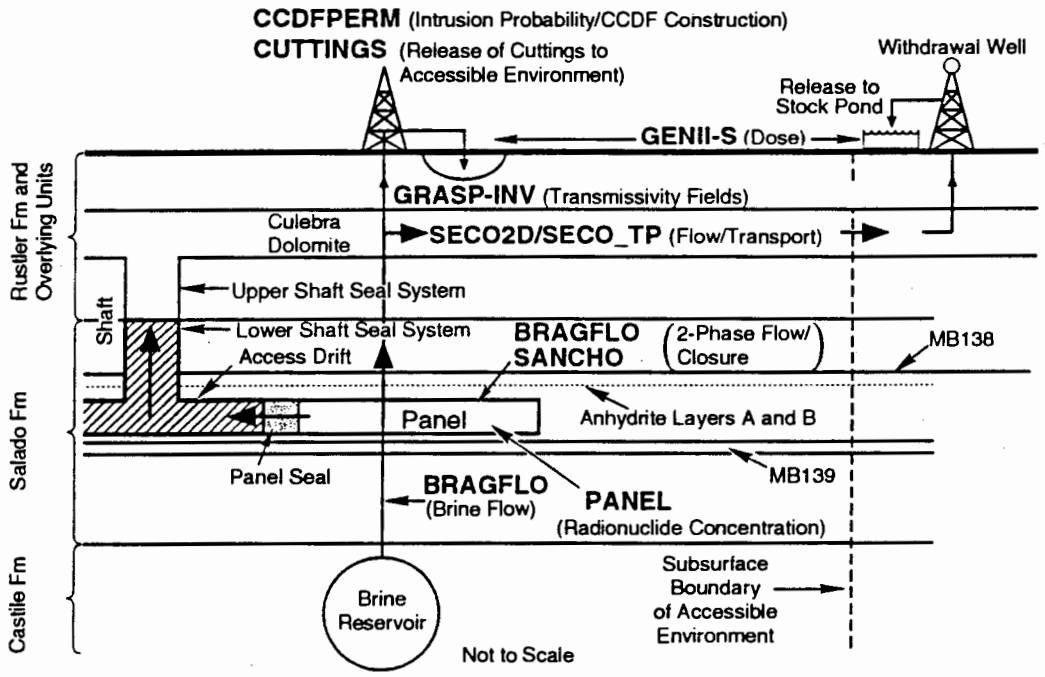

Figure 6. Models used in the 1992 WIPP performance assessment. The names for computer models (i.e., computer codes) are shown in capital letters.

Table 2. Summary of Computer Models Used in the 1992 WIPP Performance Assessment

Model	Description
BRAGFLO	Describes the multiphase flow of gas and brine through a porous, heterogenous reservoir. BRAGFLO solves simultaneously the coupled partial differential equations that describe the mass conservation of gas and brine along with appropriate constraint equations, initial conditions, and boundary conditions (Chapter 7 of WIPP PA Dept., 1992b).
CCDFPERM	Constructs probabilities for various computational scenarios associated with human intrusion by exploratory drilling (Section 1.4.2 of WIPP PA Dept., 1992b).
CUTTINGS	Calculates the quantity of radioactive material (in curies) brought to the surface as cuttings, spallings, and cavings generated by an exploratory drilling operation that penetrates a waste panel (Chapter 7 of WIPP PA Dept., 1992b).
GENII-S	Estimates potential radiation doses to humans from radionuclides in the environment (Leigh et al., 1993).
GRASP-INV	Automatically generates simulations of transmissivity fields (estimates of transmissivity values) conditioned on measured transmissivity values and calibrated to steady-state and transient pressure data at well locations using an adjoint sensitivity and pilot-point technique (LaVenue and RamaRao, 1992).
PANEL	Calculates rate of discharge and cumulative discharge of radionuclides from a repository panel through an intrusion borehole. Discharge is a function of fluid flow rate, nuclide solubility, and remaining inventory (Chapter 7 of WIPP PA Dept., 1992b).
SANCHO	Finite element program that solves quasistatic, large deformation, inelastic response of two-dimensional solids (Stone et al., 1985). Used in the 1992 performance assessment to determine porosity of the waste as a function of time and moles of gas generated (Section 1.4.7 of the Sandia WIPP Project, 1992).
SECO2D	Calculates single-phase Darcy flow for groundwater-flow problems in two dimensions. The formulation is based on a single partial differential equation for hydraulic head using fully implicit time differencing (Chapter 7 of WIPP PA Dept., 1992b).
SECOTP	Simulates fluid flow and transport of radionuclides in fractured porous media (Chapter 7 of WIPP PA Dept., 1992b).

5.1 Selection of Variables and Their Ranges and Distributions

Monte Carlo analyses use a probabilistic procedure for the selection of model input. Therefore, the first step in a Monte Carlo analysis is the selection of uncertain variables and of ranges and distributions that characterize the uncertainty in their possible values. These variables are typically input parameters to computer models, and the impact of the assigned ranges and distributions can be great. Analysis results are controlled in large part by the choice of input. Results of uncertainty and sensitivity analyses, in particular, strongly reflect the characterization of uncertainty in the input data.

As discussed in detail in the Sandia WIPP Project (1992), information about the ranges and distributions of possible values is drawn from a variety of sources, including field data, laboratory data, literature, and, in instances where significant uncertainty exists and site-specific information is unavailable or insufficient at the time of the analyses, subjective expert judgment. In general, data from these sources cannot be examined statistically and incorporated directly in performance-assessment analyses because data are rarely gathered with the specific model application in mind. Spatial and temporal scales over which the data are valid often do not match those of the models' applications, and in many cases, real site-specific data are simply not available and/or not reasonably obtainable. Data may be sparse or unavailable for several reasons. Measurements may be infeasible (e.g., drilling sufficient boreholes to determine the regional heterogeneity of transmissivity in overlying aquifers). Direct measurements would, in themselves, create risk (e.g., drilling of boreholes through the repository to determine the extent of an underlying brine reservoir). Measurements may be impossible (e.g., measuring future drilling technology). There could also be other reasons that data are sparce or unavailable.

The review process that leads from the available data to the construction of the cumulative distribution functions (CDFS) used in the performance-assessment analyses is described in detail in the Sandia WIPP Project (1992). In part, because of the nature of the available data and the type of analysis, this review process is unavoidably subjective and involves some judgment of the investigators and performance-assessment analysts.

The ultimate outcome of the review process is a distribution function $F(x)$ of the form shown in Figure 7 for each independent variable of interest. For a particular variable x_j, the function F is defined such that

$$\text{prob}(x < x_j \leq x+\Delta x) = F(x+\Delta x) - F(x) \tag{13}$$

That is, $F(x+\Delta x) - F(x)$ is equal to the probability that the appropriate value to use for x_j in the particular analysis under consideration falls between x and $(x + \Delta x)$.

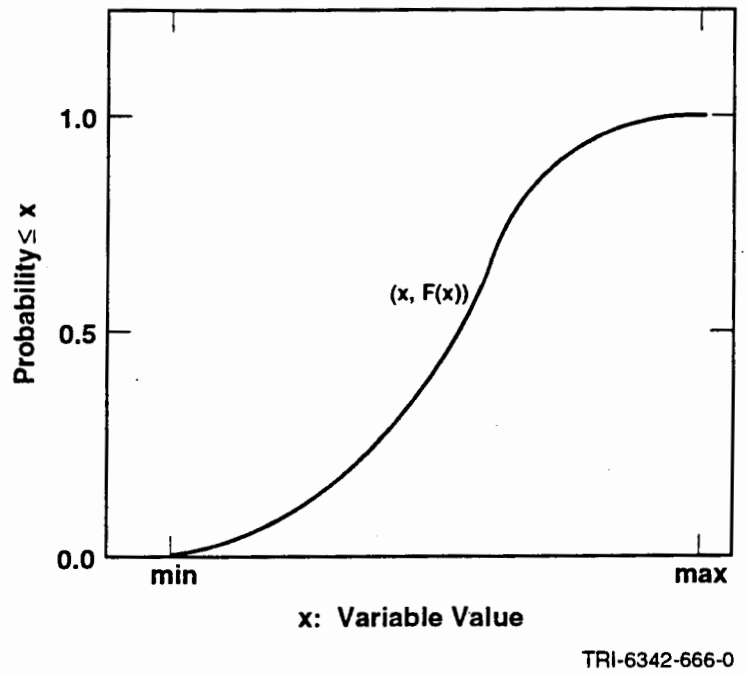

Figure 7. Distribution function for an imprecisely known analysis variable. For each value x on the abscissa, the corresponding value $F(x)$ on the ordinate is the probability that the appropriate value to use in the analysis is less than or equal to x (Helton et al., 1991).

5.2 Generation of the Sample

Various techniques are available for generating samples from the assigned distribution functions for the variables (McGrath et al., 1975; McGrath and Irving, 1975a,b), including random sampling, stratified sampling, and Latin hypercube sampling. As discussed in more detail in Helton et al. (1991), the WIPP performance assessment uses stratified sampling and Latin hypercube sampling.

Stratified sampling is a modification of random sampling in which a systematic coverage of the full range of possible values is forced by subdividing the sample space into strata with assigned probabilities. The decomposition of the subset s_0, shown in Equation 9, into scenarios s_i as indicated in Equation 1 is a form of stratified sampling in which the scenario probabilities pS_i are the strata probabilities. Stratified sampling provides for the inclusion of low-probability, but possibly high-consequence scenarios, and is used to incorporate stochastic, or Type-A, uncertainty into the WIPP performance assessment.

Latin hypercube sampling (McKay et al., 1979), in which the full range of each variable is subdivided into intervals of equal probability and samples are drawn from each interval, is used to incorporate subjective, or Type-B, uncertainty, into the WIPP performance assessment. Specifically, a Latin hypercube sample of size 70 was generated from the 49 variables that were sampled in the 1992 PA (see Tables 6.0-1, -2, and -3 in the Sandia WIPP Project, 1992). The restricted pairing technique of Iman and Conover (1982) was used to prevent spurious correlations within the sample.

5.3 Propagation of the Sample through the Analysis

The next step is the propagation of the sample through the analysis. Each element of the sample is supplied to the model as input, and the corresponding model predictions are saved for use in later uncertainty and sensitivity studies. The Compliance Assessment Methodology Controller (CAMCON) has been developed to facilitate the complex calculations and storage of the input and output files from each program (Rechard, 1989, 1992). This methodology incorporates databases, sampling procedures, model evaluations, data storage, uncertainty and sensitivity analysis procedures, and plotting capabilities into a unified structure.

Additional information on CAMCON and its use in the 1992 WIPP performance assessment is given in Chapter 1 of WIPP PA Dept. (1992b) and in Rechard (1992).

5.4 Uncertainty Analysis

Once a sample has been generated and propagated through a model, uncertainty in the model predictions can be interpreted directly from the CCDF. Stochastic, or Type-A, uncertainty, is represented by the steps in an individual CCDF. Subjective, or Type-B, uncertainty, can be represented either with a family of CCDFs or with a summary diagram showing mean and quantile curves, as shown in Figures 2 and 3.

Uncertainty in a predicted performance measure can be characterized with an estimated distribution function, which can be displayed as the above CCDF, a density function, a cumulative distribution function, or as box plots (Iman and Conover, 1982), as shown in Figure 8. The endpoints of the boxes in Figure 8 are formed by the lower and upper quartiles of the data, that is, $x_{.25}$ and $x_{.75}$. The vertical line within the box represents the median, $x_{.50}$. The sample mean is identified by the large dot. The bar on the right of the box extends to the minimum of $x_{.75} + 1.5(x_{.75} - x_{.25})$ and the maximum observation. In a similar manner, the bar on the left of the box extends to the maximum of $x_{.25} - 1.5(x_{.75} - x_{.25})$ and the minimum observation. The observations falling outside of these bars are shown with x's. Box plots display the same information as a distribution function in a reduced form (without explicit probabilities). They are convenient for presenting and comparing different distributions in a single figure, especially for displaying outliers (high consequence values).

5.5 Sensitivity Analysis

The final step in a Monte Carlo study is sensitivity analysis, which provides information about the sensitivity of the modeling system to uncertainty in specific input parameters. Sensitivity analyses can identify those parameters for which reductions in uncertainty (i.e., narrowing of the range of values from which the sample used in the Monte Carlo analysis is drawn) have the greatest potential to increase confidence in the estimate of disposal-system performance. However, because results of these analyses are inherently conditional on the models, data distributions, and techniques used to generate them, the analyses cannot provide insight about the correctness of the conceptual models and data distributions used. Qualitative judgment about the modeling system must be used in conjunction with sensitivity analyses to set priorities for performance-assessment data acquisition and model development.

Sensitivity analysis techniques used in the WIPP performance assessment include scatterplots and regression analysis, and are described in detail by Helton et al. (1991). Results of the 1992 sensitivity analyses are presented in WIPP PA Dept. (1993a, 1993b).

5.6 System Prioritization

Three annual iterations of the WIPP PA following the methodology described here have been completed and published. Each of these PAs is conditional on regulatory interpretation and the conceptual models and data elicited from the principal investigators involved in the experimental program. The elicitation process is described in the Sandia WIPP Project (1992). For selected conceptual models, each investigator was asked to characterize his/her degree of belief about where the appropriate value for a specific PA model-input parameter was located, based on currently available knowledge and informal expectations about the plausible outcome of his/her experimental activities. An evaluation of different experimental outcomes and the likelihoods that these outcomes may or may not occur was not formally included in the analyses.

The goal of the systems prioritization methodology (SPM) is to provide information about how these various activities, when viewed singly or in combination, can contribute to the successful demonstration of compliance with the long-term performance standards applicable to the WIPP repository. This objective is explicit and drives the SPM. The output from the SPM is the likelihood of demonstrating compliance given that certain activities (e.g., experiments, performance-based waste acceptance criteria (PBWAC) engineered alternatives) are undertaken, and given the costs in time and dollars necessary to undertake these activities. The decision analysis inherent in the SPM provides a logical approach to developing this information and presenting it in a form that facilitates decision making.

A key to the prioritization process is the relation between the output of the PA model and the regulatory requirements, and the use of decision analysis procedures to exercise the PA model to judge the likelihood that various activities will result in the demonstration of compliance. Information requirements of the SPM include potential outcomes of the various activities, their probabilities, and an evaluation of how such information will likely impact assessments of long-term repository performance.

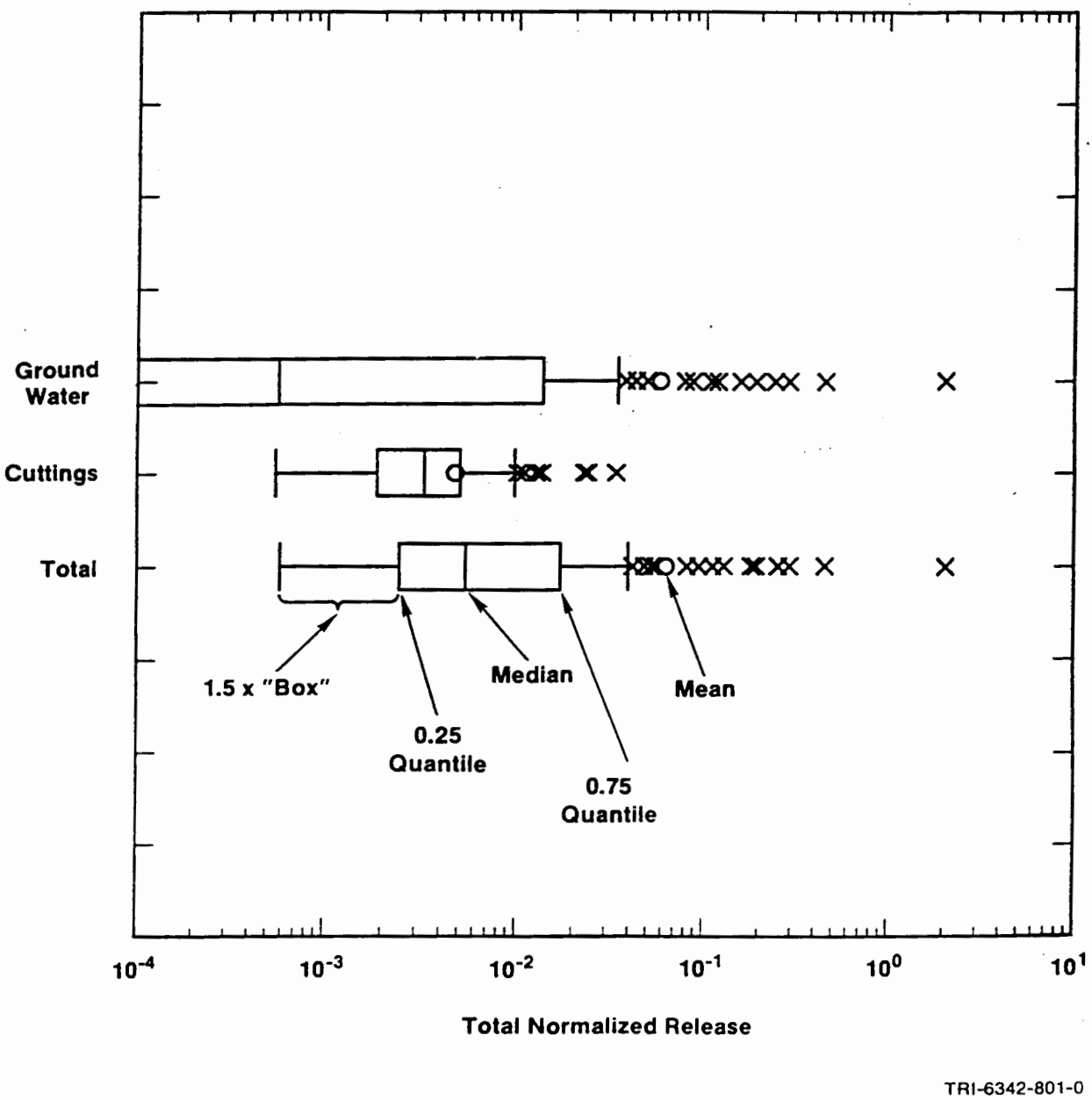

Figure 8. Example of box plots (hypothetical results).

6 References

Apostolakis, G., R.L. Bras, L.L. Price, J. Valdes, K.K. Wahi, and E. Webb. 1991. *Techniques for Determining Probabilities of Events and Processes Affecting the Performance of Geologic Repositories: Suggested Approaches*. NUREG/CR-3964, SAND86-0196. Albuquerque, NM: Sandia National Laboratories. Vol. 2.

Beauheim, R.L., and P.B. Davies. 1992. "Experimental Plan for Tracer Testing in the Culebra Dolomite at the WIPP Site." Revision A. Albuquerque, NM: Sandia National Laboratories.

Bertram-Howery, S.G., and R.L. Hunter, eds. 1989. *Preliminary Plan for Disposal-System Characterization and Long-Term Performance Evaluation of the Waste Isolation Pilot Plant*. SAND89-0178. Albuquerque, NM: Sandia National Laboratories.

Bertram-Howery, S.G., M.G. Marietta, R.P. Rechard, P.N. Swift, D.R. Anderson, B.L. Baker, J.E. Bean, Jr., W. Beyeler, K.F. Brinster, R.V. Guzowski, J.C. Helton, R.D. McCurley, D.K. Rudeen, J.D. Schreiber, and P. Vaughn. 1990. *Preliminary Comparison with 40 CFR Part 191, Subpart B for the Waste Isolation Pilot Plant, December 1990*. SAND90-2347. Albuquerque, NM: Sandia National Laboratories.

Brush, L.H. 1990. *Test Plan for Laboratory and Modeling Studies of Repository and Radionuclide Chemistry for the Waste Isolation Pilot Plant*. SAND90-0266. Albuquerque, NM: Sandia National Laboratories.

Cranwell, R.M., J.E. Campbell, J.C. Helton, R.L. Iman, D.E. Longsine, N.R. Ortiz, G.E. Runkle, and M.J. Shortencarier. 1987. *Risk Methodology for Geologic Disposal of Radioactive Waste: Final Report*. NUREG/CR-2452, SAND81-2573. Albuquerque, NM: Sandia National Laboratories.

Cranwell, R.M., R.V. Guzowski, J.E. Campbell, and N.R. Ortiz. 1990. *Risk Methodology for Geologic Disposal of Radioactive Waste: Scenario Selection Procedure*. NUREG/CR-1667, SAND80-1429. Albuquerque, NM: Sandia National Laboratories.

Gelbard, F. 1991. "Addendum Test Plan: Air Intake Shaft Performance Test. Addendum For Obtaining Cores In The Culebra for Radionuclide Retardation Studies." Albuquerque, NM: Sandia National Laboratories.

Guzowski, R.V. 1991. *Evaluation of Applicability of Probability Techniques to Determining the Probability of Occurrence of Potentially Disruptive Intrusive Events at the Waste Isolation Pilot Plant*. SAND90-7100. Albuquerque, NM: Sandia National Laboratories.

Helton, J.C. 1993. "Drilling Intrusion Probabilities for Use in Performance Assessment for Radioactive Waste Disposal," *Reliability Engineering and System Safety*. SAND93-7001J. Vol. 40, no. 3, 259-275.

Helton, J.C., J.W. Garner, R.D. McCurley, and D.K. Rudeen. 1991. *Sensitivity Analysis Techniques and Results for Performance Assessment at the Waste Isolation Pilot Plant*. SAND90-7103. Albuquerque, NM: Sandia National Laboratories.

Helton, J.C., J.W. Garner, R.P. Rechard, D.K. Rudeen, and P.N. Swift. 1992. *Preliminary Comparison with 40 CFR Part 191, Subpart B for the Waste Isolation Pilot Plant, December 1991—Volume 4: Uncertainty and Sensitivity Analysis Results*. SAND91-0893/4. Albuquerque, NM: Sandia National Laboratories.

Helton, J.C., M.G. Marietta, and R.P. Rechard. 1993. *Conceptual Structure of Performance Assessments Conducted for the Waste Isolation Pilot Plant*. SAND92-2285. Albuquerque, NM: Sandia National Laboratories.

Hora, S.C. 1992. Appendix A: "Probabilities of Human Intrusion into the WIPP, Methodology for the 1992 Preliminary Comparison," *Preliminary Performance Assessment for the Waste Isolation Pilot Plant, December 1992. Volume 3: Model Parameters*. Sandia WIPP Project. SAND92-0700/3. Albuquerque, NM: Sandia National Laboratories. A-69 through A-99.

Hora, S.C., D. von Winterfeldt, and K.M. Trauth. 1991. *Expert Judgment on Inadvertent Human Intrusion into the Waste Isolation Pilot Plant*. SAND90-3063. Albuquerque, NM: Sandia National Laboratories.

Hunter, R.L., R.M. Cranwell, and M.S.Y. Chu. 1986. *Assessing Compliance with the EPA High-Level Waste Standard: An Overview*. SAND86-0121, NUREG/CR-4510. Albuquerque, NM: Sandia National Laboratories.

IAEA (International Atomic Energy Agency). 1989. *Evaluating the Reliability of Predictions Made Using Environmental Transfer Models*. Safety Series Report No. 100. Vienna: International Atomic Energy Agency.

Iman, R.L., and W.J. Conover. 1982. "A Distribution-Free Approach to Inducing Rank Correlation Among Input Variables," *Communications in Statistics: Simulation and Computation*. Vol. B11, no. 3, 311-334.

Kaplan, S., and B.J. Garrick. 1981. "On the Quantitative Definition of Risk," *Risk Analysis*. Vol. 1, no. 1, 11-27.

LaVenue, A.M., and B.S. RamaRao. 1992. A *Modeling Approach to Address Spatial Variability within the Culebra Dolomite Transmissivity Field.* SAND92-7306. Albuquerque, NM: Sandia National Laboratories.

Leigh, C.D., B.M. Thompson, J.E. Campbell, D.E. Longsine, R.A. Kennedy, and B.A. Napier. 1993. *User's Guide for GENII-S: A Code for Statistical and Deterministic Simulations of Radiation Doses to Humans from Radionuclides in the Environment.* SAND91-0561. Albuquerque, NM: Sandia National Laboratories.

Marietta, M.G., S.G. Bertram-Howery, D.R. Anderson, K.F. Brinster, R.V. Guzowski, H. Iuzzolino, and R.P. Rechard. 1989. *Performance Assessment Methodology Demonstration: Methodology Development for Evaluating Compliance With EPA 40 CFR Part 191, Subpart B, for the Waste Isolation Pilot Plant.* SAND89-2027. Albuquerque, NM: Sandia National Laboratories.

McGrath, E.J., and D.C. Irving. 1975a. *Techniques for Efficient Monte Carlo Simulation. Volume II. Random Number Generation for Selected Probability Distributions.* ORNL-RSIC-38 (Vol. 2). Oak Ridge, TN: Oak Ridge National Laboratory.

McGrath, E.J., and D.C. Irving. 1975b. *Techniques for Efficient Monte Carlo Simulation. Volume III. Variance Reduction.* ORNL-RSIC-38 (Vol. 3). Oak Ridge, TN: Oak Ridge National Laboratory.

McGrath, E.J., S.L. Basin, R.W. Burton, D.C. Irving, and S.C. Jaquette. 1975. *Techniques for Efficient Monte Carlo Simulation. Volume I. Selecting Probability Distributions.* ORNL-RSIC-38. (Vol. 1). Oak Ridge, TN: Oak Ridge National Laboratory.

McKay, M.D., R.J. Beckman, and W.J. Conover. 1979. "A Comparison of Three Methods for Selecting Values of Input Variables in the Analysis of Output from a Computer Code," *Technometrics.* Vol. 21, no. 2, 239-245.

Parry, G.W. 1988. "On the Meaning of Probability in Probabilistic Safety Assessment," *Reliability Engineering and System Safety.* Vol. 23, no. 4, 309-314.

Paté-Cornell, M.E. 1986. "Probability and Uncertainty in Nuclear Safety Decisions," *Nuclear Engineering and Design.* Vol. 93, 2-3, 319-327.

Rechard, R.P. 1989. *Review and Discussion of Code Linkage and Data Flow in Nuclear Waste Compliance Assessments.* SAND87-2833. Albuquerque, NM: Sandia National Laboratories.

Rechard, R.P., ed. 1992. *User's Reference Manual for CAMCON: Compliance Assessment Methodology Controller Version 3.0.* SAND90-1983. Albuquerque, NM: Sandia National Laboratories.

Sandia WIPP Project. 1992. *Preliminary Performance Assessment for the Waste Isolation Pilot Plant, December 1992. Volume 3: Model Parameters.* SAND92-0700/3. Albuquerque, NM: Sandia National Laboratories.

Stone, C.M., R.D. Krieg, and Z.E. Beisinger. 1985. *SANCHO: A Finite Element Computer Program for the Quasistatic, Large Deformation, Inelastic Response of Two-Dimensional Solids.* SAND84-2618. Albuquerque, NM: Sandia National Laboratories.

Tierney, M.S. 1993. "3. PA Methodology Overview," *Initial Performance Assessment of the Disposal of Spent Nuclear Fuel and High-Level Waste Stored at Idaho National Engineering Laboratory. Volume 1: Methodology and Results.* Ed. R.P. Rechard. SAND93-2330/1. Albuquerque, NM: Sandia National Laboratories. 3-1 through 3-28.

U.S. DOE (Department of Energy). 1991. *Evaluation of the Effectiveness and Feasibility of the Waste Isolation Pilot Plant Engineered Alternatives: Final Report of the Engineered Alternatives Task Force.* DOE/WIPP 91-007, Revision 0. Carlsbad, NM: Waste Isolation Pilot Plant. Vols. 1-2.

U.S. EPA (Environmental Protection Agency). 1985. "40 CFR Part 191: Environmental Standards for the Management and Disposal of Spent Nuclear Fuel, High-Level and Transuranic Radioactive Wastes; Final Rule," *Federal Register.* Vol. 50, no. 182, 38066-38089.

Vesely, W.E., and D.M. Rasmuson. 1984. "Uncertainties in Nuclear Probabilistic Risk Analyses," *Risk Analysis.* Vol. 4, no. 4, 313-322.

WIPP PA (Performance Assessment) Department. 1992a. *Preliminary Performance Assessment for the Waste Isolation Pilot Plant, December 1992. Volume 1: Third Comparison with 40 CFR 191, Subpart B.* SAND92-0700/1. Albuquerque, NM: Sandia National Laboratories.

WIPP PA (Performance Assessment) Department. 1992b. *Preliminary Performance Assessment for the Waste Isolation Pilot Plant, December 1992. Volume 2: Technical Basis.* SAND92-0700/2. Albuquerque, NM: Sandia National Laboratories.

WIPP PA (Performance Assessment) Department. 1993a. *Preliminary Performance Assessment for the Waste Isolation Pilot Plant, December 1992 . Volume 4: Uncertainty*

and Sensitivity Analyses for 40 CFR 191, Subpart B. SAND92-0700/4. Albuquerque, NM: Sandia National Laboratories.

WIPP PA (Performance Assessment) Department. 1993b. *Preliminary Performance Assessment for the Waste Isolation Pilot Plant, December 1992. Volume 5: Uncertainty and Sensitivity Analyses of Gas and Brine Migration for Undisturbed Performance*. SAND92-0700/5. Albuquerque, NM: Sandia National Laboratories.

WIPP PA (Performance Assessment) Division. 1991. *Preliminary Comparison with 40 CFR Part 191, Subpart B for the Waste Isolation Pilot Plant, December 1991 — Volume 1: Methodology and Results*. SAND91-0893/1. Albuquerque, NM: Sandia National Laboratories.

WIPP Library

March 17, 1995

Systems Prioritization Method - Iteration 2 Baseline Position Paper:

Salado Formation Fluid Flow and Transport Containment Group

S. Howarth, K. Larson, T. Christian-Frear
R. Beauheim, D. Borns, D. Deal, A. L. Jensen, K. Knowles, D. Powers,
R. Roberts, M. Tierney, and S. Webb

Sandia National Laboratories
Albuquerque, NM 87185

EXECUTIVE SUMMARY

This paper establishes for the Salado Formation (1) the current baseline understanding used for Systems Prioritization Method (SPM) of the various processes affecting fluid flow and transport that may lead to releases from the Waste Isolation Pilot Plant (WIPP) disposal system, (2) the conceptual models developed to describe processes, (3) the assumptions made in mathematical and numerical process models, (4) experimental data available that support this understanding, and (5) the baseline numerical model to be used for Systems Prioritization Method - Iteration 2 (SPM-2). Containment issues related solely to fluid flow and transport in the Salado Formation are addressed in detail; rock mechanics, geophysics, and disposal room design are only considered as they relate to Salado fluid flow and transport. This paper replaces the Revision 1 document that was released on September 14, 1994, and the Revision 2 draft that was prepared December 22, 1994.

Two disposal system release scenarios are considered: 1) contaminant release driven by high, gas-generated pressure, and 2) human intrusion. Within the context of this paper, the term "disposal system release" is defined as any condition in which regulated waste or regulated waste constituents reaches the accessible environment. For the Salado, because the processes that impact the human intrusion scenario are similar to those that impact the high gas pressure scenario, a summary of how the human intrusion relates to Salado processes is included whereas the high gas pressure scenario is discussed in detail.

The Salado fluid flow and transport conceptual model for SPM-2 is composed of eight parts: 1) stratigraphy which incorporates geometry and dip, 2) salt creep, 3) fluid flow, 4) contaminant transport, 5) thermally driven fluid flow, 6) model initial conditions, 7) disturbed rock zone (DRZ), and 8) interbed fracturing. Each of these parts of the conceptual model is discussed in the paper. In addition, two processes were identified that are currently not evaluated in SPM-2 but are discussed here: 1) chemical reactions in the Salado, and 2) hydrogen diffusion. No process models or WIPP-specific data were identified for these two processes. There are three components or mechanisms that are potentially important in the fluid flow portion of the conceptual model: 1) far-field flow, 2) DRZ redistribution, and 3) clay consolidation. Data supporting each mechanism is available, and each likely occurs, although at different relative magnitudes and times, compared to the others, over the 10,000 year duration of performance assessment. At present, data is not available to demonstrate that any of the three mechanisms does not or will not occur.

The numerical model used for the SPM-2 Baseline is based on the far-field flow and DRZ redistribution mechanisms for calculating brine inflow, by agreement among WIPP Principal Investigators. The far-field flow and DRZ redistribution mechanisms for Salado flow are also used to calculate the flux of gas and brine entering interbeds, although these models are not used to calculate the outward movement of gas and brine in interbeds. The overall Salado model used for SPM-2 is similar to the 1992 PA models. Additional modifications and enhancements specified for the SPM-2 Baseline include the addition of dip and newly defined techniques for comparing brine and gas outflow to regulatory standards. Additional efforts have been specified as part of the Baseline Model to substantiate assumptions made during specification and implementation of the numerical model.

CONTENTS

Executive Summary iii

Acronyms x

1.0 INTRODUCTION 1
- 1.1 Background 2
- 1.2 Purpose and Scope 3
- 1.3 Performance Measures 4
- 1.4 Definitions/Terminology 4
- 1.5 Organization of Paper 6

2.0 PROCESSES AND MECHANISMS OF THE SALADO FORMATION IMPORTANT IN DISPOSAL SYSTEM RELEASE SCENARIOS 7
- 2.1 The SPM-2 Conceptual Model for Flow and Transport in the Salado Formation 7
  - 2.1.1 SPM-2 Conceptual Model for Natural Conditions 8
    - 2.1.1.1 Stratigraphy 8
    - 2.1.1.2 Salt creep 9
    - 2.1.1.3 Initial Conditions Developed For Conceptual Models . . . 9
    - 2.1.1.4 Fluid Flow 10
    - 2.1.1.5 Contaminant Transport 13
    - 2.1.1.6 Thermally Driven Fluid Flow 13
  - 2.1.2 SPM-2 Conceptual Model for Repository-Influenced Processes . . 13
    - 2.1.2.1 DRZ 14
    - 2.1.2.2 Interbed Fracturing 14
    - 2.1.2.3 Hydrogen Diffusion 15
    - 2.1.2.4 Chemical Reactions Within the Salado Formation 15
  - 2.1.3 Conceptual Model for Repository-Breach Scenarios 15
    - 2.1.3.1 Human-Intrusion Scenarios 16
    - 2.1.3.2 High-Pressure Repository Scenarios 17
- 2.2 SPM-2/PA Representation of Conceptual Model 17
  - 2.2.1 Stratigraphy 18
  - 2.2.2 Salt Creep 18
  - 2.2.3 Fluid Flow 20

2.2.4 Contaminant Transport 21
2.2.5 Initial Conditions 21
2.2.6 Thermally Driven Fluid Flow 21
2.2.7 DRZ 21
2.2.8 Interbed Fracturing 22

3.0 NUMERICAL MODELS OF SALADO PROCESSES AND MECHANISMS . . . 23
3.1 PA Models and Methods of Implementation 23
3.1.1 Stratigraphy 23
3.1.2 Salt Creep 23
3.1.3 Fluid Flow 23
3.1.4 Thermally Driven Fluid Flow 24
3.1.5 Initial Conditions 24
3.1.6 DRZ and Transition Zone 25
3.1.7 Other Numerical Models Developed Since 12/92 PA 25
3.1.7.1 Contaminant Transport 26
3.1.7.2 Interbed Fracturing 26

4.0 DATABASES AND TEST PROGRAMS DEVELOPED FOR CONCEPTUAL MODEL DEVELOPMENT AND PARAMETER DETERMINATION 29
4.1 Data Bases 29
4.2 Test Programs 29
4.2.1 Laboratory Test Program 29
4.2.2 Field Test Programs 34
4.2.2.1 Permeability Test Program 34
4.2.2.2 DRZ Observations and In-situ Tests 35
4.2.2.3 Large-Scale Brine Inflow Experiments 36
4.2.2.3.1 Brine Inflow Measurements 36
4.2.2.3.2 Analysis and Interpretation of Brine Inflow 36
4.2.2.4 Brine Sampling and Evaluation Program (BSEP) 36
4.2.2.4.1 Brine Flow to Boreholes 38
4.2.2.4.2 Brine Flow to Underground Openings 40
4.2.2.4.3 Laboratory Analysis of Brine Chemistry and Content 40
4.2.2.4.4 BSEP Mechanistic Models of Brine Inflow . 41
4.2.2.5 Small-Scale Brine-Inflow Experiments 42

4.2.2.6 Hydrofracture Experiments 46
4.2.2.7 Thermally Driven Fluid Transport 47
4.2.2.8 Geophysical Surveys and Fluid Flow 48

5.0 BASELINE SPM-2 MODEL FOR SALADO FLUID FLOW AND TRANSPORT CONTAINMENT 51
5.1. SPM-2 Baseline Model Overview 52
5.2 Model Enhancements 53
5.2.1 The Relative Permeability of Both Phases in the DRZ and Transition Zones = 1 54
5.2.2 Add a 1° dip to the BRAGFLO model. 54
5.2.3 Correlate the Threshold Displacement Pressure with Permeability 54
5.3 Necessary Efforts 56
5.3.1 Two-Dimensional/Three-Dimensional Comparison Study of Salado Fluid Flow 57
5.3.2 Discrete Fracture/Matrix Study of Brine Flow in Interbeds 57
5.3.3 Evaluation of Dissolved Gas Exsolution Effects 58
5.4 Post-Processing Techniques for Comparison to Regulatory Criteria 59
5.4.1 Brine Outflow Post-Processing 59
5.4.2 Gas Outflow Post-Processing 61
5.5 Tie-in to the Conceptual Model Components 63
5.5.1 Stratigraphy 63
5.5.2 Salt Creep 64
5.5.3 Contaminant Transport 64
5.5.4 Thermally Driven Fluid Flow 64
5.5.5 Model Initial Conditions 65
5.5.6 Disturbed Rock Zone 65
5.5.7 Hydrogen Diffusion 65
5.5.8 Chemical Reactions 65
5.6 Parameter Values and Distributions for the SPM-2 Baseline Model 66
5.7 SPM-2 Baseline Model Two-Phase Relationships 69

6.0 REFERENCES 73

APPENDIX A: Lincoln Memorandum A-1

APPENDIX B: 93/94 PA Memorandum B-1

APPENDIX C: 1993 WIPP PA Fracture Expert Group Meeting Minutes C-1

APPENDIX D: Larson and Davies Memorandum D-1

APPENDIX E: McTigue Memoranda E-1

APPENDIX F: Howarth Memorandum F-1

APPENDIX G: Summary of Test-Interpretation Results from In Situ Permeability and Pore Pressure Tests G-1

APPENDIX H: Results of McTigue Parameter Estimation for Small Scale Brine Inflow Tests H-1

APPENDIX I: Borns Memorandum I-1

Figures

1 North-South vertical cross-section of model domain 19
2 Cumulative brine into Room Q 37
3 Flow rate into Room Q 37
4 Example of brine inflow data (Hole DH 32) 39
5 A schematic of the small-scale brine inflow boreholes and the stratigraphic units tested in each borehole. 43
6 Schematic of DRZ and Transition Zone regions 55

Tables

1 Parameter Values Used in the 1992 PA for Halite and Polyhalite within Salado Formation near Repository 30
2 Hydrologic Parameter Values Used in the 1992 PA for Anhydrite Layers within Salado Formation 31
3 Summary of Number of Laboratory Tests for (FY93) MB139 Samples 33

Acronyms

AEC	Atomic Energy Commission
BRAGFLO	Brine and Gas Flow Code
BSEP	Brine Sampling and Evaluation Program
DC	Direct Current
DRZ	Disturbed Rock Zone
EdM	[French] École Nationale Supérieure des Mines de Paris
EM	Electromagnetic
EPA	Environmental Protection Agency
NAS-NRC	National Academy of Science-National Research Council
NUTS	Nuclide Transport System
ORNL	Oak Ridge National Laboratory
PA	Performance Assessment
PI	Principal Investigator
RCRA	Resource Conservation and Recovery Act
RH	Remote Handled
RIVM	[Dutch] National Institute of Publich Health and Environmental Protection
SPM-2	Systems Prioritization Method - Iteration 2
SSBI	Small Scale Brine Inflow
USGS	US Geological Survey
VAST	Vapor System Transport
VOC	Volatile organic compounds
WIPP	Waste Isolation Pilot Plant

1.0 INTRODUCTION

This position paper provides the information required by Waste Isolation Pilot Plant (WIPP) Systems Prioritization Methodology (SPM-2), a management tool, as requested in the June 10, 1994, memorandum from S. Goldstein, R. Lincoln, and P. Davis, entitled "Initiation of Systems Prioritization and Project Technical Baseline Efforts." SPM asked project Principal Investigators to

1. define disposal system release scenarios relevant to expertise areas, including location of documentation, alternatives, and assumptions;

2. define the process models for use by SPM-2, including location of documentation, model alternatives, and assumptions;

3. define current information and databases, including the location of documentation, and assess how well data support alternative process models proposed as part of (2);

4. assess whether the December 1992 Performance Assessment parameter distributions agree with experimental data, and include a description of alternative ranges and rationale for alternatives;

5. locate raw data;

6. locate documentation of techniques used to interpret raw data;

7. identify potential experiments to distinguish between alternative process models; and

8. include treatment, dispensation, or consideration of individual, stakeholder, and regulatory comments.

This document addresses the SPM-2 requests for topics in Salado Formation fluid flow and contaminant transport.

1.1 Background

Containment of waste for long-term compliance within the WIPP is dependent on various physical processes, including fluid flow and contaminant transport within the Salado Formation. Salt deposits, such as the Salado Formation, have been considered for nuclear waste disposal since the 1950s. National Academy of Sciences-National Research Council (NAS-NRC) (1957) recommended that the disposal of high-level nuclear waste in salt deposits be considered as the "most promising" method. The NAS-NRC committee chose salt deposits for several reasons: 1) their thermal properties, 2) their physical properties (e.g., creep deformation), and 3) the salt deposits' "very existence for hundreds of millions of years has demonstrated its isolation from circulating groundwater and the stability of the geologic formation in which it is located" (NAS-NRC, 1957). In 1962, the United States Geological Survey (USGS) described the Permian Basin (the sedimentary basin containing the Salado Formation that underlies portions of Kansas, Oklahoma, Colorado, Texas, and New Mexico) as a possible area for a waste repository. The Atomic Energy Commission (AEC) selected a Lyons, Kansas, salt site for a first US demonstration repository in 1970, and the NAS gave a conditional endorsement. However, the AEC rejected this site in 1972 due to fluid flow issues, such as loss of fluids in nearby solution mines and improperly plugged oil and gas wells. Following the rejection of the Lyons site, Oak Ridge National Laboratory (ORNL) selected the northern Delaware Basin as a possible location for the demonstration repository (Brokaw et al., 1972; Jones, 1973). One site in the Delaware Basin was rejected due to pressurized brine encountered in the preliminary drilling and commercial grade potash being present. The current site at Los Medaños was selected based on the following principal criteria: 1) continuity and predictability of strata, 2) thickness of salt, 3) extent of dissolution, 4) deformation, and 5) tectonics (Powers et al., 1978; U.S. DOE, 1980; Weart, 1983). Further studies have confirmed that several intrinsic properties of the Salado at the Los Medaños site make fluid flow difficult, and thus render the site favorable for the long-term containment of waste within the accessible environment. A few of the most important properties include low permeability, low porosity, and salt creep. Porosity and permeability may be increased by processes related to repository excavation and waste-generated gas. Under certain conditions, these processes have the potential to adversely affect waste containment.

With the excavation of the repository, some amount of damage has occurred. The permeability and effective (interconnected) porosity of the Salado Formation immediately surrounding the repository have been increased, thereby increasing the ability of brine to flow into the repository (Borns and Stormont, 1988; 1989). It is thought that some brine will flow into the repository after the operations phase is concluded. In the repository, brine may contact

the waste and/or be held by capillary forces in backfill material, if it is used. The importance of brine entering the repository depends on whether brine actually contacts waste. This may affect long-term repository performance in two principal ways: 1) brine provides a medium for transport of radionuclides and hazardous constituents dissolved or suspended in the liquid phase, and

2) brine provides an essential reactant for gas generation by anoxic corrosion of the metal waste and perhaps for some microbial reactions in the waste.

If gas generation occurs, it may have important effects because: 1) gas provides a medium and driving force for transport of volatile organic compounds, and/or driving force for contaminated brine release, and 2) gas may reach pressures that are high enough to cause fracturing of the formation, thus providing an enhanced pathway for brine and gas which might contain contaminants.

1.2 Purpose and Scope

Evaluating Salado Formation containment with respect to long-term compliance requires characterization of the various processes that might transport contaminants. This paper establishes the current SPM baseline understanding of the various processes affecting fluid flow and transport within the Salado Formation by outlining: 1) the conceptual models developed for SPM to describe Salado processes, 2) the assumptions made in SPM mathematical and numerical (process) models, 3) observations and experimental data available that support models, and 4) the numerical model that has been specified by Salado principal investigators (PIs) for use in SPM baseline calculations. This paper addresses the containment issues related solely to fluid flow and transport in the Salado Formation. Rock mechanics, geophysics, and disposal room design are only considered as they relate to Salado fluid flow and transport. The disposal system release scenarios, conceptual models, parameter distribution, and databases are the main categories for discussion. The specific topics addressed include:

- stratigraphy,
- salt creep,
- fluid flow mechanisms,
- contaminant transport mechanisms,
- thermally driven fluid flow,
- far-field conditions and model initial conditions,
- the disturbed rock zone (DRZ), and
- interbed fracturing.

1.3 Performance Measures

The performance measures for post-closure regulatory compliance upon which the discussion in this paper is based include: 1) radionuclide containment (*40 CFR 191.13(a)*) and 2) hazardous constituent concentration (*40 CFR 268.6*) requirements.

Performance measures are outlined in a memorandum authored by R.C. Lincoln and contained in Appendix A. This paper has assumed that the time period specified for performance projections is 10,000 years.

Compliance with Groundwater Protection Requirements (*40 CFR 191.16*) must be demonstrated. However, because no sources of groundwater exist in the Salado Formation at the WIPP within the maximum allowable extent of the special source of groundwater definition (WIPP Performance Appraisal (PA), 1992a), monitoring will not be required.

1.4 Definitions/Terminology

Accessible Environment: The region outside the disposal system, defined by regulatory boundaries established for waste containment.

Capillary Pressure: The pressure difference between the nonwetting-phase (in this case, gas) pressure and the wetting-phase (in this case, brine) pressure.

Conceptual Model: The aggregate of processes, properties and geometries considered in a compliance evaluation, based on insight into system behavior obtained by experiment or experience.

Current PA: The published Sandia Reports (WIPP PA, 1992a and b; WIPP PA, 1993a and b; Sandia WIPP Project, 1992), which document PA 1992 calculations.

Disposal System: The volume of rock and repository contained within the accessible environment boundaries, which may include portions of the shafts. For the purposes of this paper, the Disposal System is assumed to be the entire Salado Formation contained within the accessible environment boundary. Within the Disposal System, the location and concentration of regulated waste and waste constituents are not significant.

Disposal System Release: A condition in which regulated waste or regulated waste constituents reaches the accessible environment.

Effective Permeability: The permeability of a rock to one fluid phase flowing in the presence of another fluid phase which partially occupies the pore space.

High Pressure: Fluid pressure approaching lithostatic.

Lithostatic or Overburden Pressure: The total pressure resulting from the weight of the rock above a specified depth (approximately 14.8 MPa at the repository horizon).

Permeability (also referred to as intrinsic permeability): A macroscopic property of rock, determined by interpretation of experiments, that in part determines the flux of a single fluid phase that fully saturates the pore space across a specified area under an applied potential gradient. In this paper, permeability is expressed in units of m^2 unless otherwise noted.

Pore Pressure: The pressure of the fluid within the pore space of a rock.

Porosity (also referred to as effective or interconnected porosity): The ratio of interconnected, void volume to total volume of a rock sample, often expressed as a percentage.

Regulatory Boundary: The edge of the disposal system; the point at which the location and concentration of regulated waste and waste constituents become significant with respect to regulations.

Relative Permeability: A ratio of the effective permeability to the intrinsic permeability for a given fluid. The relative permeability is a function of the fluid saturation of the rock.

RCRA: The Resource Conservation and Recovery Act. Regulations promulgated under this law govern the management of hazardous wastes. The regulations apply to the WIPP as a disposal facility. When the term RCRA is used, we are referring to the following sections of the Code of Federal Regulations: *40 CFR 260*, *261*, *264*, *265*, *268*, and *270*, with special emphasis upon Part *268*, the Land Disposal Restrictions.

Scenario: An outline or synopsis of a sequence of events and/or processes.

Threshold Pressure: The lowest capillary pressure at which a nonwetting fluid will overcome and enter a wetting-phase-saturated porous medium.

1.5 Organization of Paper

This document consists of six sections, including this introductory section, and nine appendices. Section 2 discusses the scenarios for disposal system release and the SPM-2 conceptual model for fluid flow in the Salado. Section 3 discusses the SPM-2 mathematical and numerical models (process models) developed to simulate the significant processes. Section 4 presents observations, data, and information bases to support the models. Section 5 contains the baseline model proposed for Salado Fluid Flow and Transport in SPM-2 calculations. Section 6 lists references. The Appendices contain supporting documentation.

2.0 PROCESSES AND MECHANISMS OF THE SALADO FORMATION IMPORTANT IN DISPOSAL SYSTEM RELEASE SCENARIOS

The conceptual model for flow within the Salado Formation is the aggregate of processes, properties, and geometries considered to provide the technical basis for the SPM-2 calculations. SPM-2 process and numerical models are based on the conceptual model but make use of simplifying assumptions 1) to facilitate numerical implementation and 2) to reduce the computer resources necessary to complete the suite of simulations required. Simplifying assumptions are allowed by the regulations as stated, in the preamble to *40 CFR 191 (50 FR 38076c)*, "the appropriate test is a reasonable expectation of compliance based on practicably obtainable information and analysis." Simplifying assumptions are acceptable when: 1) their effects are known and accounted for, 2) their effects are known to be minor, or 3) they are reasonable with respect to an applicable regulation. The Salado flow and transport conceptual model is described in Section 2.1, together with a summary on disposal system release scenarios (2.1.3). Section 2.2 summarizes techniques that have been used in past PAs to numerically evaluate processes. Section 5 describes the model specified for use in the SPM-2 Baseline calculation. Evidence supporting the SPM-2 conceptual model is summarized in Section 4.

2.1 The SPM-2 Conceptual Model for Flow and Transport in the Salado Formation

A conceptual model is more general and more expansive than the mathematical and numerical models derived from it. All processes described by the mathematical and numerical models are part of the conceptual model; however, assumptions made to write an equation or implement a particular numerical scheme may be more limiting than the parent conceptual model. For example, to bound the effects of a particular process (e.g., interbed fracturing), assumptions may be made to write an equation that greatly simplifies the dynamics contained within the conceptual model. Similarly, a spatially varying parameter (e.g., permeability) may be represented with a single value rather than a range of values to simplify numerical models. Section 2.1.1 presents the conceptual model for natural conditions within the Salado Formation.

2.1.1 SPM-2 Conceptual Model for Natural Conditions

The WIPP Project recognizes that the Salado Formation is an environment within which stratigraphy, salt creep, fluid flow, contaminant transport, thermally driven fluid flow, and the present Salado Formation conditions all may influence the results of a compliance determination. The conceptual model for the Salado Formation considers these processes as part of the natural condition of the Formation. These factors are described in more detail below.

2.1.1.1 STRATIGRAPHY

The Salado Formation is a bedded salt deposit approximately 600 m thick that was deposited during the Late Permian. The repository is about 200 m above the base of the formation. The regional dip of the Salado Formation is about 1 degree southeast in the vicinity of the repository (Jarolimek et al., 1983)

Depositional models for the Salado have been presented by Lowenstein (1988) and Holt and Powers (1990). Individual beds formed as part of a depositional cycle that commonly began with flooding, resulting in basal claystones and sulfate beds that are commonly referred to as marker beds or interbeds. Halite beds above the sulfates are mainly pure halites that precipitated from standing bodies of water. With time, the evaporite lagoon or sea repeatedly dried up, with increasing frequency and magnitude as the depositional cycle continued. Most depositional cycles ended with a period of desiccation, perhaps lengthy, during which insoluble minerals were concentrated to form argillaceous halites. Renewed flooding introduced fresher water and precipitated additional sulfate beds. Complete depositional cycles are commonly a few meters thick. Individual marker beds, as well as many of the argillaceous units, are traceable over large areas through geophysical logs (e.g., Jones et al., 1960; Powers et al., 1988). The depositional environment was complex, and there are variations on this basic depositional cycle (Lowenstein, 1988; Holt and Powers, 1990).

The Salado stratigraphy is generally relatively simple over horizontal scales of hundreds of meters to kilometers, as indicated by the continuity of marker beds and many argillaceous horizons. Underground mapping units are traceable over the considerable area already excavated for the WIPP. There are many sedimentary features and mineralogical variations over short distances (generally less than 1 m); most of these are due to changes in water table level during deposition in the Permian and the complex surface accumulation of insoluble minerals during subaerial exposure of large areas, also in the Permian. In the upper parts of each depositional

cycle, lithology can vary within narrow limits along the same stratigraphic level because of these primary features.

2.1.1.2 SALT CREEP

Salt creep occurs naturally in halite-rich formations and is included in the conceptual model. Salt creep in response to redistribution of stresses influences pore pressures and Salado properties such as porosity and permeability. Because salt creeps, the walls of disposal rooms will move inward, fractures caused by excavation are expected to heal to some extent, and backfill, if used, is expected to assume near-intact properties within a relatively short period of time after closure. These properties are deemed desirable by the Project and were important in the decision to site the WIPP in the Salado Formation (Lappin et al., 1989; Weart, 1983; Powers et al., 1978). The effects of salt creep on pore pressure, porosity and permeability, and fluid flow are described in later sections of this report.

2.1.1.3 INITIAL CONDITIONS DEVELOPED FOR CONCEPTUAL MODELS

Notable features present in the Salado Formation are high pore pressure (Powers et al., 1978; Black et al., 1983; Skokan et al., 1989), low permeability (Beauheim et al., 1991; 1993a), and low porosity. Salt creep, in addition to diagenetic recrystallization and precipitation, may be responsible for these features. Pressure solution and recrystallization reduces porosity by dissolving minerals under high pressure at grain-grain contacts and depositing halite, gypsum, or anhydrite in low-pressure void space, either during diagenesis or creep (Borns, 1987). Porosity is further reduced if pore fluid pressures are different than lithostatic pressure, because salt crystals will deform under deviatoric stress generally into the lower-pressure, fluid-filled pore space, causing lower porosity and increased pore pressure. This will occur until either the pore pressure approaches lithostatic or durable minerals lining pore walls bear some of the lithostatic burden. As voids get smaller, permeability decreases rapidly because permeability is exponentially related to pore aperture. In general, pore pressures significantly different than hydrostatic, such as in the Salado Formation, will tend to be dissipated by flow processes; however, the rate at which fluid flow dissipates the high Salado pressure is extremely slow, even on geologic time scales, due to the extremely low permeability and thickness and stratification of the Salado Formation. Over time, salt creep in response to deviatoric stress acts to continuously maintain low porosity, low permeability, and high pore pressure. Some anomalous,

gas-charged, isolated zones of granular salt have relatively high porosity because of fluid pressure approaching lithostatic that cannot be dissipated by flow through surrounding units. The pore pressure in anhydrite interbed layers, which contain natural fractures (Borns, 1985), higher permeability, and far less susceptibility to creep than halite, is expected to be very close to that of surrounding halite because the anhydrites are thin and permeability of the anhydrites is not sufficient for equilibrium to be established with pore pressures at the edge of the Salado Formation.

The far-field pore pressure is assumed to be between hydrostatic (7.4 MPa) and lithostatic (14.8 MPa). Based on in-situ experiments, the far-field pore pressure within Marker Bed 139 is at least 12.8 MPa. The far-field pore pressure of other Salado units is expected to be similar to the pore pressure of Marker Bed 139. The far-field Salado pore pressure is elevated relative to hydrostatic due to salt creep, diagenesis, and in some areas gas generation during alteration of organic substances within the interbeds. The far-field pore pressures do not reach lithostatic because the pores (average 1 percent by volume) are propped by secondary minerals (averaging 1 to 5 percent by volume) whose intrinsic strength is sufficient to bear a portion of the lithostatic load.

2.1.1.4 FLUID FLOW

Observation of the response of pore fluids in the Salado Formation to changes in pressure boundary conditions (at walls in the repository, in boreholes without packers, in packer-sealed boreholes, or in laboratory core experiments) is complicated by low permeability and low porosity. Flow has been observed to walls in the repository, boreholes without packers, and packer-sealed boreholes, and has been induced in the laboratory. At certain places, flow is no longer observed where it once was; in others, flow has begun where it once was not observed. In many cases, observations and experiments must last for months or years to obtain useful results. In part because of design requirements such as duration, few quantitative data have been obtained for certain lithologic units within the Salado Formation. There is much direct, qualitative experience regarding the behavior of flow crossing the walls of the repository. There is some quantitative in-situ and laboratory data for isolated portions of the Salado lithology. There are three different mechanisms of flow supported by WIPP Project Staff based on the varied data that have been collected. Different predictions of brine inflow and the behavior of gas and brine in a high-pressure repository are obtained depending on which mechanism is assumed dominant. Because definitive data do not exist to rule out any of the mechanisms, the

conceptual model contains three different mechanisms for fluid flow in the Salado Formation. The relative importance of each mechanism remains a subject of debate among WIPP PIs.

One mechanism, far-field flow, is for flow from the far field in response to potentiometric gradients through naturally interconnected intergranular pore spaces. There is in-situ flow test evidence supporting this model in anhydrite interbeds and in impure halite units. In-situ flow test results from very pure halite are ambiguous with respect to this model: results can be interpreted either as extremely low permeability (near-complete absence of interconnected pore space); or as a lithology in which fluid is not responsive to applied pressure gradients. In the first case, potentiometric flow models can be used effectively with extremely low permeability values. In the second case, potentiometric flow models can also be used, however, with zero permeability specified for modeled regions representing pure halite. Laboratory tests on anhydrite core support the existence of interconnected, permeable pore space in anhydrite. Geophysical evidence, mostly electrical, is interpreted as showing a far-field source of brine which resaturates drained areas of the DRZ, and as showing ongoing flow around the repository (Appendix I; Borns, 1994). These interpretations support the far-field flow model.

Numerous parameters are necessary to describe flow in terms of potentiometric equations. These include parameters describing the rock formation such as porosity, permeability, density, rock compressibility, and other parameters describing fluid flow and fluid interactions such as relative permeability, capillary pressure, fluid compressibility, fluid density, and fluid viscosity. Within the conceptual model, few limits are imposed on the spatial variability or functional dependence of these properties. It is known, for example, that the pore structure and composition of the Salado Formation are not uniform, which leads to spatial heterogeneity in rock properties both by layering and within each layer. Fluid properties are known to be functions of pressure, temperature, chemical composition, and saturation.

A second mechanism, redistribution, proposes that interconnected pore spaces do not exist naturally in most lithologic units in the Salado Formation. Interconnected networks form due to fracturing and creep around excavations. Potentiometric flow occurs in interconnected networks, but because the interconnectedness is of limited extent, the volume of brine that can flow is less than that in the far-field flow mechanism. Rock damage consistent with the redistribution concept has been confirmed around the repository (Borns and Stormont, 1988; Borns and Stormont, 1989). A numerical model based on the redistribution concept was developed and applied to the Small-Scale Brine Inflow (SSBI) data set (McTigue, 1993). The

redistribution-based model allowed use of a more realistic capacitance for modeling the near-field formation response than did flow models using only far-field properties.

The third mechanism for fluid flow, clay consolidation, arises from observations recorded during more than nine years of underground observations during the Brine Sampling and Evaluation Program (BSEP). This mechanism proposes that the most significant source of brine flowing into the repository are clay layers exposed by excavation. According to this model, 1) clay layers consolidate and yield brine when stresses are redistributed near the excavation causing compression of the thin clay layers, and 2) flow through other lithologic units is negligible.

Estimates of the total potential brine inflow depend upon which combination of the three mechanisms in the conceptual model are assumed to dominate the fluid flow processes in the Salado Formation. For the far-field flow model, the long-term potential brine inflow is theoretically unlimited, but is practically limited by the low permeability of the formation and the expected short duration of time during which the fluid potential gradient will favor flow towards the repository. Small quantities of brine have often been predicted in past performance assessment calculations when low permeability far-field conditions have been sampled. Using best-estimate values, the quantities of brine inflow from far-field flow models to a single disposal room is on the order of 25 to 110 m^3. The quantity of brine that can be provided by the redistribution mechanism is limited by the quantity of brine initially present in the regions that will be altered by excavation-related stress redistribution. Preliminary estimates of the quantity of brine in a disposal room DRZ range from 28 m^3 (1-m-thick DRZ) to 151 m^3 (4-m-thick DRZ) per equivalent disposal room assuming 1 percent initial, intact porosity. These are maximum theoretical inflow values because some of the brine will remain in the pore structure and cannot flow or contact waste in the repository. Both the far-field and redistribution mechanisms have the potential to individually provide enough brine to fully corrode waste, which is estimated to require between 100 and 150 m^3 per disposal room of waste (Lappin et al., 1989). The clay consolidation mechanism likely provides much less brine to disposal rooms; it is likely that this mechanism would have for the most part ceased by the end of the disposal phase and brine inflow from clay consolidation during the period modeled by Performance Assessment would be negligible.

Multiphase flow (brine and gas) is a likely condition of the repository, immediately surrounding formation, and possibly the far-field. In addition to the naturally inflowing nitrogen

and any gases contained in the waste, air will be entrained in the storage rooms after sealing and closure. If sufficient additional volumes of gas are generated by anoxic corrosion, microbial activity, or radiolysis, it is possible that gas pressures could exceed lithostatic and might drive liquid and/or gas away from the excavations. Such flow might carry contaminants with them, so high-pressure scenarios might need to consider single-phase, two-phase or dissolved-phase flow away from the repository, which is most easily accommodated by the far-field flow and redistribution mechanisms.

2.1.1.5 CONTAMINANT TRANSPORT

Volatile organic compounds (VOCs) are the primary contaminants of concern for RCRA, however heavy metals in brine are also regulated by RCRA. Radionuclides are the concern for *40 CFR 191*. Transport of contaminants can occur in numerous ways. The following processes are included within the Salado flow and transport conceptual model: advection by porous media and fracture flow; dispersion caused by pore scale effects during advection; diffusion because of concentration gradients in fluid phases; and transport of mass adhered to colloid particles or microorganisms. Contaminant transport is mitigated in the conceptual model by decay processes and sorption of contaminants onto matrix materials.

2.1.1.6 THERMALLY DRIVEN FLUID FLOW

The Salado Formation has a high thermal conductivity and slow mass transport. Therefore, heat transport will be dominated by conduction. Radionuclide decay within the repository can affect the thermal conditions near the repository. These effects will be negligible in the far-field. Because thermal processes are intricately associated with the waste form and room processes, further discussion is beyond the scope of this paper.

2.1.2 SPM-2 Conceptual Model for Repository-Influenced Processes

Some features of the disposal system are expected to be affected by processes occurring due to repository effects. The processes included within the conceptual model are the formation of a zone of rock with disturbed properties around the repository (the DRZ), and increase of porosity and permeability of anhydrite interbeds if the repository attains high pressure because

of dilation of existing fractures or formation of new fractures. The conceptual models for these effects, and for chemical reaction and hydrogen diffusion, are presented below.

2.1.2.1 DRZ

The DRZ is the zone of rock in which the mechanical and hydrologic properties of rock have been changed in response to excavation. Since the existence of the DRZ was documented (Borns and Stormont, 1988; Borns and Stormont, 1989), the WIPP Project has postulated that the DRZ has impact in 1) gas and brine storage, 2) near-field hydrologic response of the Salado Formation, 3) design and performance of seals, and 4) repository design. The conceptual model for the DRZ involves complex processes, but the DRZ develops in response to the redistribution of stress around the excavation, stress relief, and rapid strain rates. The DRZ is characterized by fracturing at many scales, variable brine saturation, and increased porosity and permeability relative to intact Salado halite and anhydrite. The material and hydrologic properties of the DRZ and its extent are time dependent as the DRZ forms adjacent to the excavation, then extends outward into the formation, and eventually reverses to some degree with room closure and repressurization. Depending on its stage, the DRZ extends 1 to 5 m into the Salado. Some processes, such as shear fracturing in anhydrites, may not be completely reversible. The DRZ also varies laterally in character and extent along the excavation due to variations in the host salt and anhydrite, as well as excavation sequence, age, and method. The development of the DRZ and the time-dependent deformation of the DRZ drives coupled processes that affect changes in permeability and porosity in response to the growth and closure of fractures at many scales. The effects of the DRZ on Salado hydrology have also been discussed by Deal et al. (1991b).

2.1.2.2 INTERBED FRACTURING

Based on experimental evidence and an experience-based understanding of rock behavior (Mendenhall et al., 1991; Beauheim et al., 1993b), the repository is not expected to be able to contain pressures greater than lithostatic. Rather, gas generated pressure will be released through fractures in interbeds. The conceptual model for interbed fracturing is that if pressures approach lithostatic in the repository, fracturing or dilation of existing fractures will occur to the extent that gas will flow out of the repository and pressures will remain near or below lithostatic. Horizontal fractures within interbeds are expected to be the primary fracture orientation and location because natural horizontal fractures in the interbeds are existing planes of weakness

along which gas-generated pressure can propagate new fractures. Models of the repository that allow pressures much in excess of lithostatic pressure are not realistic.

2.1.2.3 HYDROGEN DIFFUSION

Hydrogen gas can move by diffusion through substances that are impenetrable to larger molecules. This diffusion process should not be confused with diffusion of VOCs and radionuclides through fluid phases, which is considered in the conceptual model. Because hydrogen is expected to be a major component of the gases generated in the repository, diffusion of hydrogen through the crystal matrix of halite rock would reduce maximum repository pressures and make repository releases caused by high pressure less severe or probable, such as gas hydrofracture.

2.1.2.4 CHEMICAL REACTIONS WITHIN THE SALADO FORMATION

Brines contained within the Salado Formation have high ionic strength may be highly reactive with solids. Because of negligible mass transport under natural conditions, pore fluids are likely to be in equilibrium with neighboring minerals. However, with fluid flow induced by repository pressures, and/or the presence of gas or contaminants expelled from the repository within the pore space, equilibrium between pore fluids and matrix rock could be disrupted and cause rock minerals to precipitate or dissolve. Chemical reactions could possibly alter the flow properties of the Salado Formation: dissolution could increase permeability locally and cause channeling, and precipitation and movement of fine particles could clog pore throats and hinder fluid flow. While the details of such chemical reactions have not been investigated, the overall quantities of flow in the Salado are expected to be quite small, and therefore, these processes are not currently thought likely to have major impact on flow.

2.1.3 Conceptual Model for Disposal System Release Scenarios

There are several scenarios in which regulated waste constituents could be transported to the regulatory boundaries. Only two broad groups of scenarios for disposal system release via the Salado Formation have a high likelihood of occurrence that they should be formally considered in the conceptual model upon which compliance determinations are based (see discussion in Guzowski, 1990): inadvertent human-intrusion scenarios, and repository-

pressurization scenarios. Inadvertent human intrusions are penetrations of the repository by a borehole or combination of boreholes from the surface that could result, depending on other factors, in vertical transport of regulated waste constituents to the surface, to water-bearing units overlying the Salado, or brine- or petroleum-bearing formations below the Salado. Repository-pressurization scenarios occur when the fluid pressure in the repository exceeds the pressure of fluids in pores in the surrounding Salado Formation, creating the potential for flow outward from the repository that could, under certain conditions, carry regulated waste laterally to the accessible environment. The conditions under which interbeds fracture is included is in the repository-pressurization scenario.

2.1.3.1 HUMAN-INTRUSION SCENARIOS

The consequences of human-intrusion scenarios are likely to be determined primarily by conditions in the borehole, the repository, and relatively permeable formations overlying and underlying the Salado (if penetrated) at the time of borehole penetration (Lappin et al., 1989; Reeves et al., 1991). Flow directly between an intruding borehole and the Salado Formation is expected to be of low consequence in the overall human-intrusion scenario because of the low permeability of the Salado Formation. Processes occurring within the Salado Formation may affect the condition of the repository prior to and after intrusion because brine and gas flow affect the brine volume and gas pressure in the repository. The mechanisms of brine and gas flow that over the long term affect repository conditions at the time of borehole penetration are described by and included within the high-pressure repository scenarios. Therefore, because the processes that affect the currently defined human-intrusion scenario are similar to those processes necessary to be included in the high-pressure repository scenario, the human-intrusion scenario will be discussed in summary fashion, whereas the high-pressure repository scenario will be described in detail.

The consequences of a human intrusion are significantly and directly influenced by the properties of the Salado Formation only if a borehole intersects a fracture in an anhydrite interbed that was created because of high repository pressure. Currently, SPM does not include this possibility in its suite of human-intrusion scenarios; however, intrusion into a transmissive, fractured region of anhydrite should be evaluated in scenario screening, and if its consequences are important, subsequently included in the suite of disposal system release scenarios. The properties of the borehole and how it is affected by physical and chemical interaction with the borehole walls and waste are beyond the scope of this paper.

2.1.3.2 HIGH-PRESSURE REPOSITORY SCENARIOS

Many mechanisms of waste transport must be considered to evaluate the likelihood and consequences of disposal system release due to high repository pressure. The conditions under which disposal system release may occur are grouped according to those that occur prior to fracturing of interbeds and those that could occur after fracturing. Prior to fracturing, or if fracturing does not occur, transport of contaminants dissolved in the fluids (if it occurs) must be dominated by advection with the bulk mass of fluid flowing through the natural pore spaces, because other processes acting without advection result in transport too slow for migration to the accessible environment in 10,000 years. Disposal system release due to diffusion along concentration gradients, dispersion, sorption, and colloid transport is exceedingly unlikely in the absence of advection. In unfractured interbeds, the mass transport capability of the Salado Formation is restricted and disposal system release may not occur even if significant quantities of contaminants move out of the repository into the Salado Formation within the disposal system.

If fracturing is caused by high repository pressure, advection of fluid through fractures will be the dominant mechanism for lateral contaminant transport. If fracturing occurs, interbeds will be more transmissive and transport to the regulatory boundary increases in likelihood, even though there may be significant flow interaction between fractures and matrix pores. Because of the significant difference between fractured and non-fractured interbed properties, the fractured-interbed advection-carried contaminant is considered to be the most important model to characterize.

2.2 SPM-2/PA Representation of Conceptual Model

Process models for many of the processes contained in the SPM-2 conceptual model have been developed for performance assessments. A general discussion of these process models follows, focusing on the PA model implementation used in the 1992 Performance Assessment calculations, the most recent complete PA calculations. Details about the mathematical and numerical methods used are presented in Section 3. The Salado Baseline Model for use in the SPM-2 calculations is based on the PA model described here and in Section 3, with important modifications. The SPM-2 model is further described in Section 5.

2.2.1 Stratigraphy

The 1992 PA used two lithologic types to describe the undisturbed Salado Formation. Each type was characterized by a set of properties (i.e., porosity and permeability) that were applied in the same manner throughout 1992 PA (WIPP PA, 1993a, Ch. 4 and 5). "Impure halite" denotes Salado beds dominated by halite and includes beds described as pure halite, argillaceous halite, or polyhalite. "Anhydrite" denoted Salado interbeds dominated by anhydrite that may include significant percentages of halite and clay beds, and includes numbered Marker Beds. Clay beds were not modeled explicitly. PA assumed horizontal stratigraphy and did not consider the effects of the natural dip of the Salado Formation or of lateral facies variations.

Whereas the Salado Formation has numerous interbeds composed of anhydrite, 1992 PA distinguished only three separate anhydrite strata in the numerical models—Marker Bed 138, a combination of anhydrites "a" and "b," and Marker Bed 139. The remainder of the Salado, except disturbed areas and shafts, was modeled as impure halite. The Salado stratigraphy as represented by 1992 PA is shown in Figure 1.

The PA model geometry combines two-dimensional and radial geometries. Use of this geometry is intended to represent both repository and far-field processes in a reasonable manner without having to resort to 3-dimensional techniques. The rooms, drifts, salt pillars, seals, backfill, waste, and four shafts comprising the repository are represented by a simplified two homogeneous regions and a single shaft. Information about the geometry of the repository and surrounding Salado Formation in PA models is contained in Figure 1, (WIPP PA, 1993a, Ch. 4 and 5), and Appendix B. Modifications to this geometry for the SPM-2 Baseline are described in Section 5.

2.2.2 Salt Creep

The effects of room closure on repository pressure and void volume were accounted for in 1992 PA models. Some of the near-field effects of salt creep were incorporated in assumptions about the DRZ and Transition Zone. The pore-scale effects of salt creep on fluid flow in the far field are not incorporated in the mathematical model used by PA. The mechanics of salt creep are more fully discussed in the Rock Mechanics position paper.

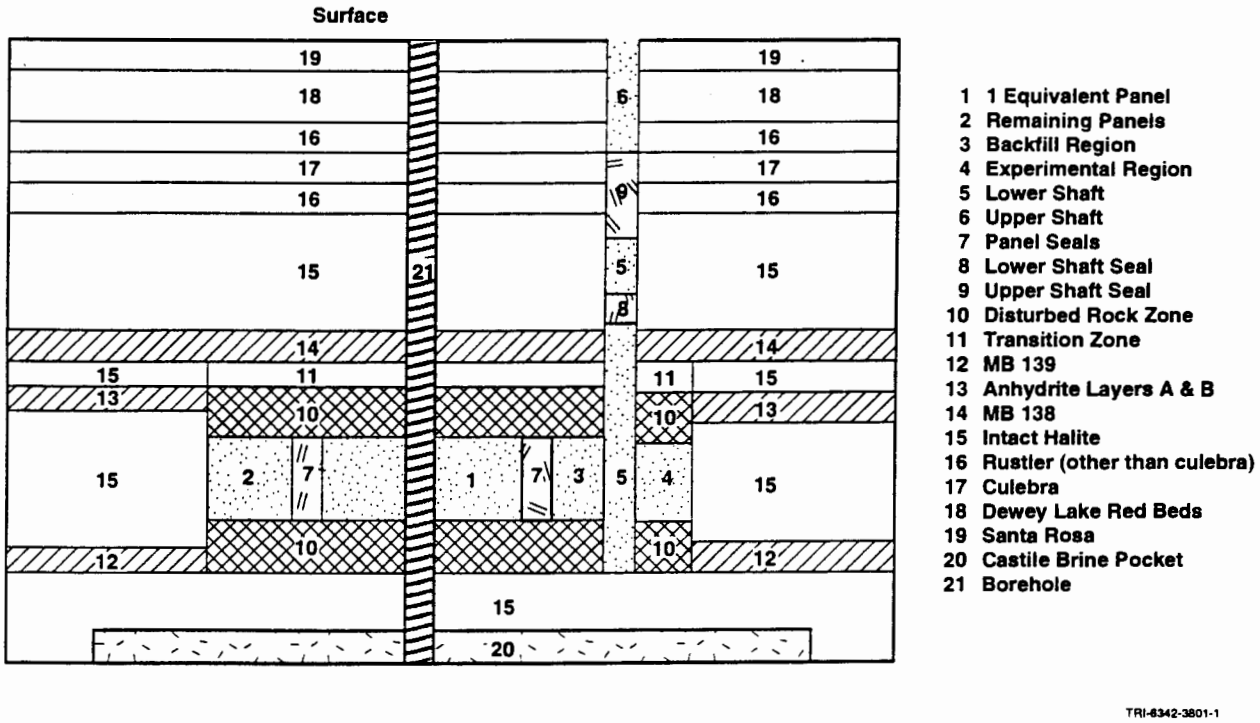

Figure 1. North-South vertical cross-section of model domain.

2.2.3 Fluid Flow

The fluid flow process model is based on a combination of the far-field and redistribution mechanisms described in the conceptual model section, by agreement among WIPP Principal Investigators (PIs). These mechanisms use flow which obeys Darcy's law, and differ in their description of rock properties as either intact or damaged. Darcy's law states that the fluid flux across a given area within a continuous system of pores will vary linearly with the gradient of hydraulic potential energy. The model does not specifically incorporate the coupling of fluid flow to rock deformation; however, it does incorporate pressure-dependent permeability for simulating hydrofractures.

The 1992 PA assumed that two fluid phases—hydrogen and brine—could be present in pore space. Because of the isothermal assumption, density and viscosity varied only as functions of pressure. The gas phase was assumed to be hydrogen and was therefore assigned the density and viscosity of pure hydrogen. Brine was assumed to be Salado Formation brine and had the appropriate density and viscosity. Both gas and brine were compressible, but they were immiscible. Brine did not contain dissolved gas, and gas does not contain brine vapor.

Interference between phases was assumed to follow standard principles of relative permeability and capillary pressure (Peaceman, 1977). Data on Salado-specific relative permeability and capillary pressure are not available. PA used two correlations for relative permeability and capillary pressure in their simulations: Brooks and Corey (Brooks and Corey, 1964) and van Genuchten/Parker (WIPP PA, 1993a, Parker et al., 1987). These correlations yield significantly different flow behavior, and the use of both was intended to incorporate the range of possible behavior into the 1992 PA simulations. Mean and median parameter values for the two correlations were based on tight sandstone (Morrow et al., 1986), an analog material. The 1992 PA used a large distribution for parameter values within these correlations to reflect the uncertainty about two-phase flow processes within the Salado.

Consistent with the use of a potentiometric conceptual model for fluid flow, the rock properties of the Salado Formation are described with parameters necessary in potentiometric flow equations. The 1992 PA approach assumed the properties of the rock and fluid were homogeneous and continuous and were represented by parameters with a single value within specified regions within one realization. Intergranular porosity was assumed to exist and be interconnected.

2.2.4 Contaminant Transport

Contaminant transport was not modeled in the Salado in the 1992 PA. Since then, PA has developed process models to describe the Salado transport of radionuclides and VOCs by advective transport, and radionuclide decay by first-order chains. In these new (post-1992 PA) models, radionuclides are transported as soluble constituents of the brine phase, and VOCs are transported within the gas phase. Since 1992, process models have also been developed to describe dispersion, diffusion, and sorption of VOCs and radionuclides.

2.2.5 Initial Conditions

The 1992 PA chose initial conditions for the Salado Formation to be consistent with the following expectations: 1) there is no regional scale flow, 2) pore pressures are elevated above hydrostatic from the surface but below lithostatic, and 3) permeability and porosity are low. Near the repository, initial conditions for the post-operational phase were modified to reflect the effects of the operational phase, DRZ development, and shafts and seals.

2.2.6 Thermally Driven Fluid Flow

The 1992 PA assumed isothermal conditions for the WIPP repository. Radionuclide decay will create some heat; however, it has been assumed that its thermal impact will be slight. An isothermal numerical model is used for flow calculations.

2.2.7 DRZ

The DRZ is the main flow path between the repository and the interbeds. The DRZ was conceptualized in the 1992 PA as a region around the excavated volume in which material properties of the rock have been altered from their original undisturbed state. These changes result from physical changes in the rock in response to deviatoric stresses created by the excavation, boreholes, and rock bolts. Both porosity and permeability were increased in the DRZ, allowing increased flow between the disposal region and the anhydrite interbeds. Pore volume added to the DRZ was assumed to be gas-filled initially, and pressures in the DRZ were

calculated using the two-phase flow models described in Section 2.1.1. A Transition Zone was included immediately above the DRZ in which permeability was increased but porosity was assumed to remain unchanged from its undisturbed value (see Figure 1). The Transition Zone was added as a conservative assumption to provide a pathway between the DRZ and rooms and the overlying interbeds.

2.2.8 Interbed Fracturing

Fracturing of interbeds was not modeled in the 1992 PA. A process model for interbed fracturing is available. It will be described in Section 3.1.7, Section 5, Appendix B, and Appendix C.

3.0 NUMERICAL MODELS OF SALADO PROCESSES AND MECHANISMS

3.1 PA Models and Methods of Implementation

This section describes the numerical models used for the 1992 PA calculations of fluid flow and contaminant transport within the Salado Formation. The section also includes a discussion of model geometry, boundary conditions, and initial conditions.

3.1.1 Stratigraphy

The stratigraphy and geometry of the 1992 PA model is illustrated in Figure 1. For further details, consult Section 5, Appendix B, WIPP PA, 1992a and b; Sandia WIPP Project, 1992; and WIPP PA, 1993a and b.

3.1.2 Salt Creep

The 1992 PA coupled flow with salt creep indirectly by incorporating changes in room porosity derived from look-up tables calculated elsewhere. PA incorporates only the impact of salt creep on room closure in its models. The effects of salt creep on pore pressure transients caused by fluid flow to or from the repository were disregarded in the long term; however, the model initial conditions reflected the impact of salt creep on present-day pore pressures, permeability, and porosity. The mechanics of salt creep are discussed in greater detail in the Rock Mechanics position paper.

3.1.3 Fluid Flow

The primary model used for flow calculations is BRAGFLO (BRine And Gas FLOw) (WIPP PA, 1992b). BRAGFLO simulates two-phase fluid flow (brine and gas) through a single-continuum porous medium in one, two, or three dimensions. BRAGFLO calculations of Salado fluid flow have been performed in one and two dimensions. The code uses spatially varying

meshes and solves the coupled nonlinear partial differential equations that describe the mass conservation of brine and gas using nonlinear Newton-Raphson iteration, automatic time-step controls, and either a direct or iterative solver.

Multiphase flow is simulated as simultaneous immiscible displacement in porous media. Regions within the model domain (waste, seals, and lithologic units) are represented as solid continuums of interconnected void space, and porosity is expressed as the ratio of void volume to total volume for each region. Flow occurs according to heuristic extensions of Darcy's law to two-phase conditions. Flow is assumed to be laminar, and fluids are viscous and Newtonian. Forces that affect fluid flow are those due to pressure, gravity, capillarity, and viscous shear. The saturation of a single phase is defined to be the ratio of phase volume to total void volume.

Additional features added to BRAGFLO specifically for Salado fluid flow calculations include the effect of halite creep dynamics (creep consolidation) on waste disposal room porosity; anisotropic permeabilities; rock compressibility effects; and kinetic or reaction-dependent gas generation as a function of fluid saturations.

3.1.4 Thermally Driven Fluid Flow

There was no heat generation, dissipation, or transport anywhere in the 1992 PA model, and any and all effects associated with the generation, dissipation, and transport of heat were considered to be insignificant. Parameters that may be functions of temperature were fixed with respect to a single reference temperature.

3.1.5 Initial Conditions

In the 1992 PA, the 10,000 year simulation started when the waste was isolated by seal emplacement. The initial conditions for the 10,000 year simulation were determined in part by expected far-field conditions, and in part by the results of a simulation of the operational phase which calculated the expected partial drying (dewatering) of the DRZ caused by repository ventilation during the operational phase. This preliminary period simulated 50 years for the undisturbed modeling of the full repository.

The important features of the initial conditions of the operational-phase simulation were: 1) no-flow in all lithologic regions; 2) atmospheric air pressure in the repository, 3) sampled brine pressures in the lithologic regions between 12 and 13 MPa, with an adjustment for the hydrostatic difference in pressure due to elevation difference between Marker Bed 139 and the unit being initialized, 4) permeability in the DRZ greater than intact rock, but less than the permeability of the DRZ in the 10,000 year simulation, 5) porosity in the DRZ the same as the far-field, 6) brine-saturated far-field, and 7) gas-saturated repository and DRZ.

The important features of the initial conditions for the 10,000 year simulation were: 1) atmospheric air pressure in the repository, 2) atmospheric brine and gas pressure in the DRZ, 3) DRZ porosity and permeability higher than far-field values, 4) partial brine saturation in the DRZ, mass of brine set according to the results of the operational phase simulation, 5) sampled initial water content of waste, 6) no flow in the far-field, 7) brine saturation in the far-field, and 8) gas saturation in the repository.

3.1.6 DRZ and Transition Zone

The DRZ was assumed to extend above the waste-emplacement panels to the top of anhydrites "a" and "b" and below the panels to 1 m below Marker Bed 139. The DRZ was assumed to extend laterally 1 m beyond the panel walls. The Transition Zone in which permeability was increased but porosity was unchanged was assumed to overly the DRZ, extending upwards from the top of anhydrites "a" and "b" to the base of Marker Bed 138 (see Figure 1). Parameter values assigned to these regions were discussed in Chapters 4 and 5 of Volume 4 of the 1992 PA (WIPP PA, 1993a).

3.1.7 Other Numerical Models Developed Since the 12/92 PA

Since the 1992 PA, several modeling methods have been developed for simulating contaminant flow and interbed fracturing in the Salado. These additional methods have not been implemented as yet but are available to be utilized.

3.1.7.1 CONTAMINANT TRANSPORT

The numerical model VAST (VApor System Transport) (Culver et al., 1991; Bear and Verruijt, 1987) may be used to quantify the spatial and temporal distribution of VOCs within the Salado. The VAST code simulates the transport of VOC in a known flow field with advective transport occurring only in the gas phase. The spatial discretization and flow field are determined from a BRAGFLO simulation. VOC transport does not influence in any manner the flow field calculated by BRAGFLO. This uncoupling of the two-phase flow field from VOC transport allows VOC modeling to be done as post-processing of a BRAGFLO simulation. The amount of VOC dissolved in either the liquid or gas phase is obtained by maintaining the VOC at its vapor pressure under the assumption of Dalton's law (Van Wylen and Sonntag, 1985). The dominant factor in the migration of VOC is assumed to be advection in the gas phase. The VOC is free to absorb to the solid interface according to a linear isotherm with a constant partitioning coefficient. VOCs are free to decay to other molecules according to a first-order decay equation with constant rate coefficient. Molecular diffusion and hydrodynamic dispersion are modeled according to Fick's law. VAST contains an inventory of 33 VOC compounds.

NUTS (NUclide Transport System) models the transport of radionuclides within the Salado Formation (Bear and Verruijt, 1987; Kazemi et al., 1976; Litvak, 1986; Shinta and Kazemi, 1993; Hill and Thomas, 1985). The model calculates the migration rate, distance, concentration, and level of radioactivity of radionuclides transported from the repository into surrounding formations. Processes considered by NUTS are advective transport, dispersion, diffusion, adsorption, radioactive decay, and solubility. Like VAST, NUTS uses the flow field calculated by BRAGFLO for the advective and dispersive transport of radionuclides. NUTS is capable of multi-dimensional, multi-continuum approximations to complex geometries.

3.1.7.2 INTERBED FRACTURING

The model implemented in BRAGFLO since the 1992 PA for pressure-dependent alteration of anhydrite interbeds assigns an alteration pressure such that when this pressure is reached, alteration of the unit begins (see Appendix B and Appendix C). Below this pressure, a lithologic unit has a constant permeability and compressibility, and the porosity is determined using the standard integral equation. Above the alteration pressure, the compressibility of the unit is assumed to increase linearly with pressure, which dramatically affects how rapidly porosity increases with increasing pore pressure. At pressures above the alteration pressure,

permeability increases by the magnitude of porosity increase raised to a power. This model is not verified for use at the WIPP, and other relationships, also unverified, can be formulated. Several alternative relationships have been formulated in the literature and in internal memoranda; one example of an alternative model in which permeability changes are correlated directly with fracture aperture was described by Larson and Davies and is attached as Appendix D. Although the Larson and Davies model has not been implemented, primarily because there are no data showing it to be better or worse than the present model, it illustrated uncertainty in the permeability correlation, and did influence the rationale for determining permeability parameters in the BRAGFLO model. The method now adopted for choosing permeability exponents in the BRAGFLO model allows the exponents to span a much larger range than was described in Appendices B and C, commensurate with the uncertainty in correlation of permeability with porosity.

4.0 DATABASES AND TEST PROGRAMS FOR CONCEPTUAL MODEL DEVELOPMENT AND PARAMETER DETERMINATION

Observations have been made and experiments have been conducted to justify the eight components of the conceptual model of the Salado Formation. Data supporting many of the eight components of the conceptual model have been previously referenced. At present, the data do not rule out any of the three mechanisms proposed to contribute to Salado fluid flow: far field flow, redistribution, and clay consolidation.

4.1 Data Bases

Parameters and parameter distributions used in numerical models employed in the 1992 preliminary PA (WIPP PA, 1992b; Sandia WIPP Project, 1992; WIPP PA, 1993a and b) are listed and rationalized in Sandia WIPP Project, 1992. The parameters of direct interest for this paper are the hydrologic parameters for halite and polyhalite within Salado Formation (Section 2.3 of Sandia WIPP Project, 1992) and the hydrologic parameters for anhydrite layers within Salado Formation (section 2.4 of Sandia WIPP Project, 1992). Of indirect interest are parameters used in the mechanical models of the Salado Formation (section 2.5 of Sandia WIPP Project, 1992). The parameters used in the 1992 PA for halite and anhydrite layers are respectively listed in Tables 1 and 2. Raw data resulting from experimental programs or non-PA modeling exercises are typically documented in SAND reports, or in limited-scope memoranda attached to general papers (as are attached to this document).

4.2 Test Programs

4.2.1 Laboratory Test Programs

Preliminary tests were performed on three groups of core samples from Marker Bed 139 of the Salado Formation during FY93 to provide data as part of the Salado Two-Phase Flow Laboratory Program. These preliminary laboratory experiments: 1) generated WIPP-specific porosity, single-phase permeability, and capillary pressure data, 2) provided information needed to design and implement planned tests to measure threshold pressure, capillary pressure, and relative permeability, and 3) will be used to evaluate the suitability of using tight gas sands

Table 1. Parameter Values Used in the 1992 PA for Halite and Polyhalite within the Salado Formation near the Repository

Parameter[a]	Median	Range		Units	Distribution Type	Source
Capillary Pressure (pc) and relative permeability (krw) Threshold displacement (correlated with permeability in 1992) pressure (pt)				Pa	Lognormal	Davies, 1991a, 1991b
Residual saturations						
Wetting Phase (Sbr)	**2×10^{-1}**	**0**	**4×10^{-1}**	**none**	**Uniform**	**Webb, 1992a, 1992b, Memos in Appendix A*; Davies and LaVenue, 1990**
Gas Phase (Sgr)	**$2 \times 10_{-1}$**	**0**	**4×10^{-1}**	**none**	**Uniform**	**Davies and LaVenue, 1990; Webb, 1992a, 1992b, Memos in Appendix A***
Brooks-Corey exponent (λ)	**0.7**	**0.2**	**10.0**	**none**	**Constructed**	**Davies and LaVenue, 1990; Webb, 1992a, 1992b, Memos in Appendix A***
Permeability (k)						
Log undisturbed	**-21.2**	**-24.0**	**-19.0**	**log(m^2)**	**Constructed**	**Gorham et al., June 15, 1992, Memo in Appendix A*; Howarth et al., 1991; Beauheim et al., 1991**
Log disturbed	-15.0	-15.0	-15.0	log(m^2)	Constructed	Gorham et al., June 15, 1992, Memo in Appendix A*; Howarth et al., 1991; Beauheim et al., 1991
Porosity (ϕ)						
Undisturbed	1×10^{-2}	1×10^{-3}	3×10^{-2}	none	Constructed	Powers et al., 1978; U.S. DOE, 1983
Specific Storage			1.4×10^{-6}	m^{-1}	Constructed	Beauheim, 1991

[a] Parameters in bold were sampled in the 1992 calculations
* Sandia WIPP Project, 1992

Table 2. Parameter Values Used in the 1992 PA for Anhydrite within the Salado Formation

Parameter[a]	Median	Range		Units	Distribution Type	Source
Capillary Pressure (pc) and relative permeability (krw) Threshold displacement pressure (pt) (correlated with anhydrite permeability)						**Section 2.3.1***
Residual saturations						
Wetting Phase (Sbr)	2×10^{-1}	0.0	4×10^{-1}	none	Uniform	**Section 2.3.1***
Gas Phase (Sgr)	$2 \times 10_{-1}$	0.0	4×10^{-1}	none	Uniform	**Section 2.3.1***
Brooks-Corey exponent (λ)	7×10^{-1}	2×10^{-1}	1×10^{1}	none	Constructed	**Section 2.3.1***
Log Permeability (k)						
Undisturbed	-19.3	-21.0	-16.0	$\log(m^2)$	Constructed	**Section 2.4.2***
Disturbed	-15.0			$\log(m^2)$	Constructed	section 2.4.2*
Pore Pressure	12.5	12.0	13.0	MPa	Uniform	**Section 2.4.3***
Porosity (ϕ)						
Undisturbed	1×10^{-2}	1×10^{-3}	3×10^{-2}	none	Constructed	**Section 2.4.4***
Disturbed	(correlated with undisturbed porosity)			none	Uniform	Section 2.4.4*
Specific Storage	1×10^{-6}	1×10^{-6}	1×10^{-6}	m^{-1}	Constructed	WIPP PA Division, 1991, Vol. 3, 2.4.8

[a] Parameters in bold were sampled in the 1992 calculations
* Sandia WIPP Project, 1992

correlations as a Salado analog for assessment of the long-term performance of the WIPP. Table 3 contains a summary of the number and types of tests performed. Total and effective porosity and gas and liquid steady-state single-phase permeability were measured as the test specimens were subjected to three different levels of hydrostatic confining stress while the pore pressure remained constant. Vertical and horizontal permeability were measured on adjacent cores and twelve capillary pressure tests were performed using the mercury injection and centrifuge techniques. Preliminary analysis of capillary pressure test results indicate a threshold pressure of less than 1 MPa.

The laboratory-measured effective porosity values range from 0.4 to 2.7 percent with a mean of 1.25 percent (see Appendix F). These values compare well with the range and mean values for porosity used in the 1992 PA; 0.1 to 3.0 percent and 1.25 percent, respectively. The laboratory-measured single-phase permeability values ranged from 8.4×10^{-16} to 5.5×10^{-20} m^2, depending on the stress conditions during the test (see Appendix F). The mean was approximately 3.5×10^{-18} m^2 at 6 MPa. These values are an order of magnitude higher on the low end of the permeability distribution curve than those used in the 1992 PA. Likewise, the mean laboratory-measured single-phase permeability was an order of magnitude higher than the mean used in the 1992 PA.

Liquid single-phase permeability data are also reported in Appendix F for three samples for which gas permeability was also measured. As expected, these data compare well with the Klinkenberg-corrected gas single-phase data at all confining stress levels. It should be noted that the liquid permeability test specimens were chosen using high gas permeability as the primary selection criterion. Single-phase permeability, whether gas or non-reactive-liquid, is considered to be an intrinsic property of the rock. Therefore, the conclusion should not be draw that liquid permeability of the Salado is more uniform or, on average, higher than the gas permeability.

Results indicate that both the porosity and single-phase permeability were reduced as increasing levels of confining stress were applied to the test specimen. Typically, permeability was reduced by less than an order of magnitude with an increase in confining stress from 2 to 10 MPa. Porosity reduction was less dramatic over the same pressure range; porosity was reduced by less than half a percent with an increase in confining stress from 2 to 10 MPa. These experimental results illustrate the stress dependence of porosity and permeability for Marker Bed 139 anhydrite. Correlations of porosity and permeability with stress may be coupled with stress distribution models to estimate the porosity and permeability distribution from excavation to far

Table 3. Summary of Number of Laboratory Tests (FY93) for MB139 Samples

Laboratory	RE/SPEC	TERRA TEK	Core Labs	Total Number of Tests Performed
Porosity				
Total	3	4	0	7
Effective	6	14	35	55
Permeability				
Gas	2	6	7 V*, 14 H**	29
Liquid	2	3	0	5
Capillary Pressure				
Hg Injection	0	0	6	6
Centrifuge	0	0	6	6

* V = vertical permeability tests (i.e., flow in direction perpendicular to MB 139 bedding plane)
** H = horizontal permeability tests (i.e., flow in direction parallel to MB 139 bedding plane)

field. Because the sample size used in laboratory experiments is not large enough to represent "average" far-field properties, the extremes observed in laboratory experiments may not be indicators of the average extremes appropriate for use in large-scale modeling.

Darcy flow was maintained during the permeability tests (i.e., flow rate was linearly proportional to pressure drop across the core). These results support the use of a potentiometric model for single-phase flow in the Salado anhydrite.

4.2.2 Field Test Programs

4.2.2.1 PERMEABILITY TEST PROGRAM

Hydraulic testing in the Salado Formation provides quantitative estimates of the hydraulic properties controlling brine flow through the Salado Formation and yield the best evidence demonstrating the far-field flow mechanism in the Salado. Tests performed include pressure-pulse tests, constant-pressure flow tests, and pressure-buildup/falloff tests. These tests, which are carefully designed to limit the effect of outside influences on the test interval, are interpreted using models based on potentiometric flow (Beauheim et al., 1991; 1993a). The tests influence rock as far as 10 m distant from the test zone and are not thought to significantly alter the pre-test conditions of most of the tested region. The stratigraphic intervals tested include halite (both pure and impure) and anhydrite with associated clay seams at distances from 1 to 23 m from excavations. Because tests close to the repository are within the DRZ, it is reasonable to use the results of the tests farthest from the repository as most representative of undisturbed conditions.

Fourteen tests have been performed in anhydrite, twenty-two in impure halite, and two in pure halite. Except in pure halite, values of permeability and specific storage are extracted from test data by a history-matching method. Interpreted permeabilities using a Darcy-flow model range from 2×10^{-20} to 7×10^{-18} m^2 for anhydrite intervals and from 1×10^{-23} to 4×10^{-18} m^2 for impure halite intervals. Interpreted formation pore pressures range from atmospheric to 12.5 MPa for anhydrite intervals, and from 0.3 to 9.7 MPa for impure halite. Tests in pure halite show no observable response, indicating either extremely low permeability ($< 10^{-23}$ m^2), or no flow whatsoever, even though appreciable pressures are applied to the test interval. Appendix G contains a summary of the results of field permeability tests to date.

4.2.2.2 DISTURBED ROCK ZONE OBSERVATIONS AND IN-SITU TESTS

The physical properties of the DRZ have been characterized by three approaches: visual observation, geophysical methods, and in-situ hydrologic testing (Borns and Stormont, 1988; 1989). Visual observations in drillholes and underground excavations indicate that gas and brine are found and fractures are common in the disturbed rock zone within the host rock in the immediate vicinity of the underground WIPP facility (Borns, 1985; Bechtel National, 1986; U.S. DOE, 1988). Fracturing occurs at many scales. Geophysical studies have utilized seismic refraction, seismic tomography, surface wave analysis, electromagnetic (EM) methods, and direct current (DC) methods (Borns and Stormont, 1989; Borns et al., 1990; Holcomb, 1988; Jung et al., 1991; Nelson, 1989; Pfeifer et al., 1989). In conjunction with the in-situ hydrologic tests, these studies define a DRZ extending to a depth of 1 to 5 m throughout the underground facility (Borns and Stormont, 1988; Stormont et al., 1991). The DC and EM methods indicate that fracture saturation and fracture density vary laterally along the excavations. These in-situ studies also demonstrate that microfracturing and desaturation of the pore space have occurred within the DRZ. The dilation that results from the microfracturing in the DRZ provides a component of the observed room closure. The processes involved in the development of the DRZ are complex, although they are basically related to stress relief and rapid strain rates. The redistribution of stress around the excavation with the development of the DRZ drives processes such as changes in permeability and porosity in response to fracture growth.

To evaluate fluid flow characteristics associated with the DRZ, gas-flow measurements were conducted in the Salado Formation immediately surrounding excavations. Measurements taken using small-diameter boreholes (5 to 15 cm) show that, within 1 to 2 m of the excavation, the halite shows very little resistance to fluid flow. Gas tracer tests (Stormont et al., 1987; Stormont, 1990) demonstrated that flow paths are consistent with the elliptical fracture pattern generally applied to describe fracture distribution around excavations. These tests have provided a qualitative description of the fluid flow properties of a DRZ at the WIPP. However, such a description does not provide PA with quantitative parameters necessary in numerical fluid-flow models, such as porosity, permeability, and initial saturation of the DRZ (these parameters are provided by in-situ flow tests in intervals close to the repository, and in stress-dependent laboratory core tests, as well as other programs). Models of the DRZ have been limited to constitutive modeling of the structural processes.

4.2.2.3 LARGE-SCALE BRINE INFLOW EXPERIMENTS

The Large-Scale Brine Inflow Test (Room Q) was designed to provide scaling information for brine inflow measurements from small-scale boreholes to repository size excavations and pore pressure and permeability data. Room Q is a nearly horizontal, circular drift centered in the same stratigraphic layer as the planned waste storage facility. Room Q is approximately 3 m in diameter and 108 m long, and a seal system composed of two bulkheads closes the room. The pore pressure and permeability data collected to date are included in Section 4.2.2.1, Jensen et al. (1993a), and Appendix G.

4.2.2.3.1 Brine Inflow Measurements

Measurement of brine inflow was made using three different methods: vacuuming the brine from natural sumps formed by depressions in the floor into pre-weighed flasks; manually absorbing brine with sponges; and vacuuming the brine from a prepared sump near the inner bulkhead using a remote collection device into pre-weighed flasks. From the July 1989 through May 1994, approximately 210 liters of brine were collected as shown in Figures 2 and 3.

4.2.2.3.2 Analysis and Interpretation of Brine Inflow

Interpretation of brine inflow into Room Q was addressed in two memoranda contained in Appendix E. McTigue's 1989 memorandum predicted the brine inflow into the room assuming radial flow. This model overestimated the amount of brine predicted when compared to the quantity of brine measured in early collections. McTigue made a second calculation using confined horizontal flow (reported in 1991 calculations). The 1991 calculations were made with the assumption that the brine is produced in a 1-m-thick layer of argillaceous halite that runs through the vertical midpoint of the room. This model appears to be more accurate in predicting brine flow when compared to brine accumulation collected from the room.

4.2.2.4 BRINE SAMPLING AND EVALUATION PROGRAM (BSEP)

Observational data on brine flow to underground workings and exploratory boreholes have been collected routinely since 1985 under the Brine Sampling and Evaluation Program

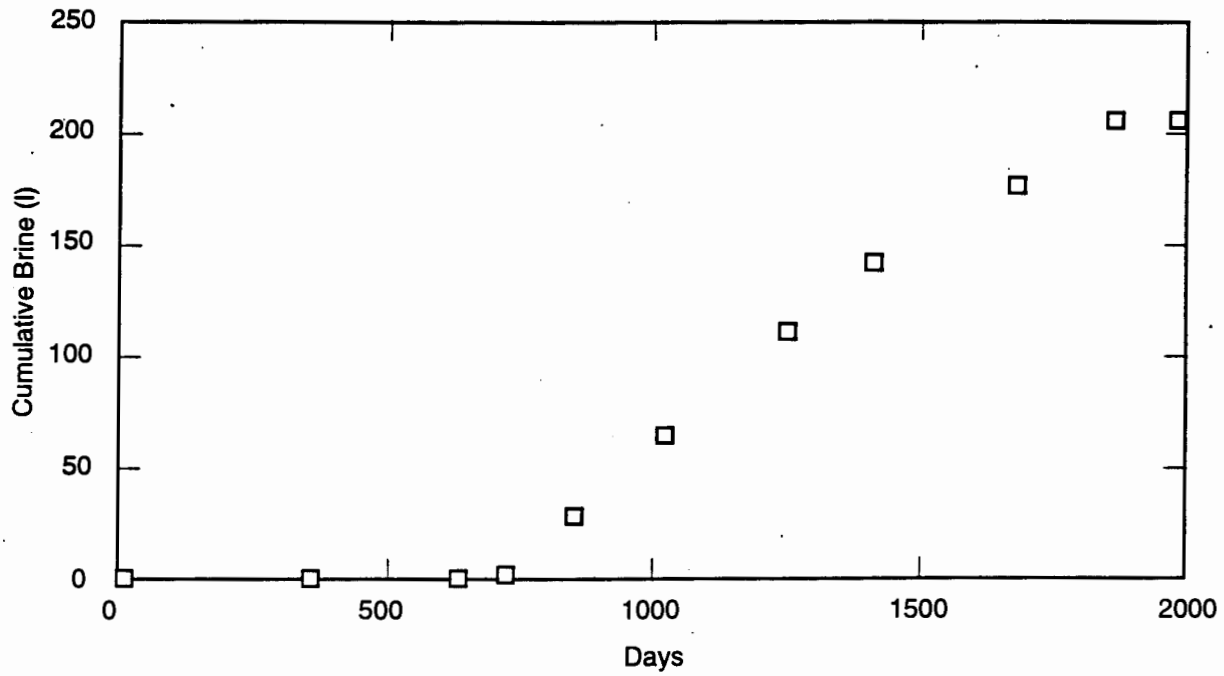

Figure 2. Cumulative brine into Room Q.

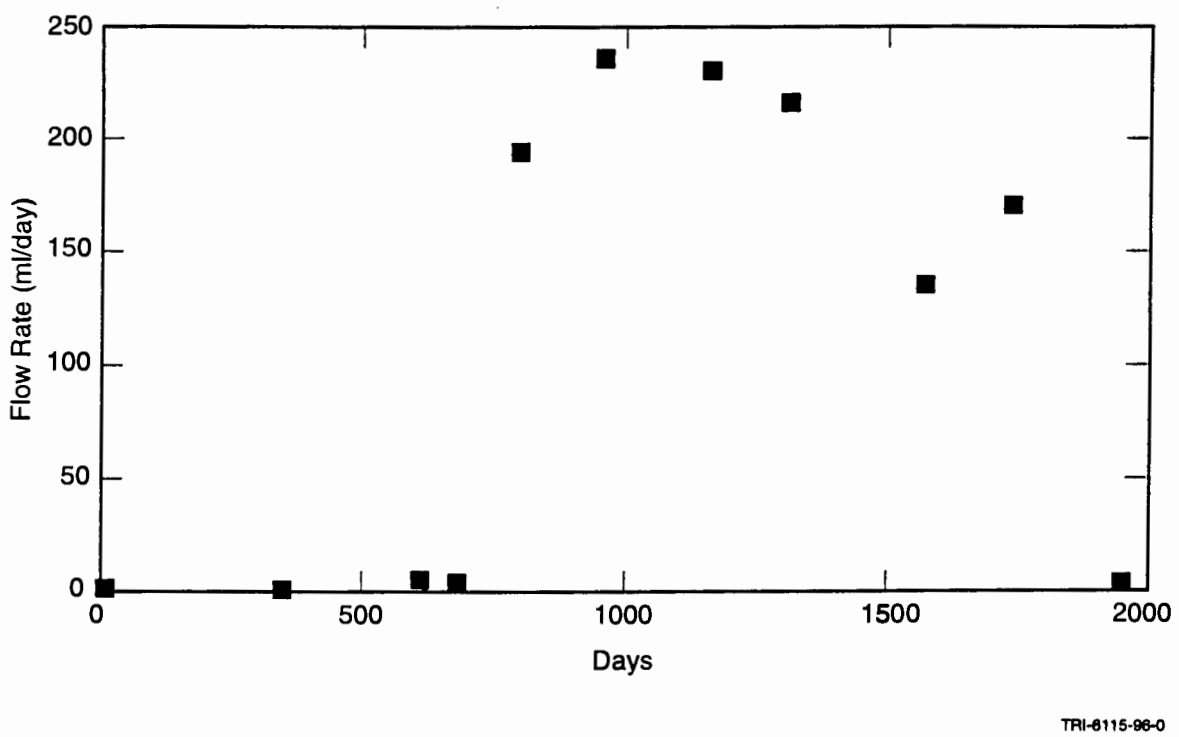

Figure 3. Flow rate into Room Q.

(BSEP). BSEP differs from the Room Q experiments and some other brine-flow programs because it collected observations from excavations and exploratory boreholes over the entire WIPP underground facility rather than from dedicated experimental areas alone.

BSEP provides a database of long-term measurements for the development of brine flow mechanistic models and for predictions of brine-flow rates to the WIPP facility during operation and after closure. A series of periodic reports to the DOE documents the brine-inflow observations (Deal, 1988; Deal and Case; 1987; Deal et al., 1987; 1989; 1991b; and 1993). Observations fall into three major groups—brine flow to boreholes, brine flow to underground openings, and laboratory measurements of brine chemistry and content in rock samples. The following sections describe the major findings and the current BSEP conceptual models.

4.2.2.4.1 Brine Flow to Boreholes

In 1985, BSEP inventoried all boreholes that had been drilled underground at the time. Of the over 1400 boreholes, seventy were chosen for detailed observation. An additional 49 holes have been added to the monitoring program since 1985 for a total 119 monitored holes. Of these holes, 89 were lost due to underground excavation or other experimentation or are located in currently inaccessible rooms. An additional 16 holes were dropped from the program because they are located in areas where construction activities introduced brine. Fifty-one holes did not produce or stopped producing measurable brine during the monitoring period. Thirteen holes have continuously produced brine. In these holes inflow rates may be as high as several hundred milliliters per day; however, most holes yield inflows of the order of tens of milliliters per day.

Nine of the thirteen holes that continuously produce brine were drilled shortly after their room locations were excavated in 1985. Inflow to these holes has been continuously monitored since drilling. For these nine holes, a period of days passed between the completion of drilling and the onset of brine inflow. The flow rates then rose over a period of several months, before beginning a slow rate decline (Figure 4). The exsolution of dissolved gases has been proposed as a mechanism for the observed early time behavior in these nine holes.

Most of the BSEP inflow observations do not directly distinguish the stratigraphic sources of brine flow within boreholes. Some boreholes are limited to the repository horizon and, in others, some stratigraphic units are close enough to the collar to be easily observed. Indirectly,

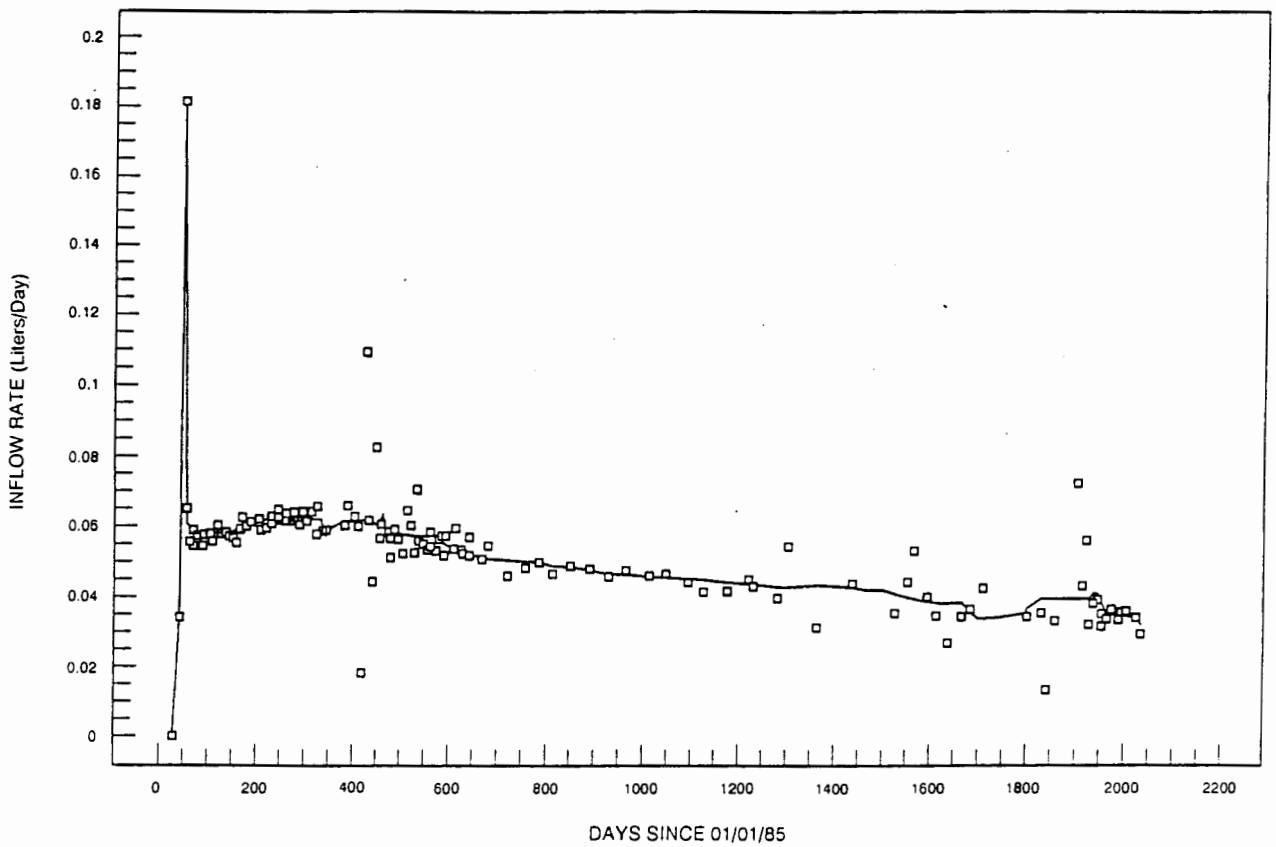

Figure 4. Example of brine inflow data (Hole DH 32).

however, electrical conductivity measurements on the walls of air-filled boreholes suggest that clay-rich units preferentially tend to be moister than the halites or anhydrites.

4.2.2.4.2 Brine Flow to Underground Openings

The observation of seepage on the walls of underground openings is a source of information on inflow to underground openings at the WIPP. All underground openings are geologically mapped by Westinghouse staff. Although the intent of the mapping is primarily for stratigraphic information, observations of seepage are sometimes included as well. Some of these seeps have been studied in detail as part of the BSEP effort.

The mapping of seepage from openings in an operating facility is complicated by several factors including the following: 1) drying of seepage by the ventilation system, 2) introduction of brine by construction activities for dust control, 3) the effects of dilation and multiphase flow in the DRZ, and 4) brine storage in fractures created in the footwall and crushed salt used for construction purposes.

Despite these limitations, the BSEP program has made several observations, and several seepage locations have been studied in detail. Mapping activities have shown that the seepage preferentially occurs associated with clay-rich layers. Where the ventilation evaporates the incoming brine, salt encrustations may form. Deal et al.(1993) collected and measured the mass of encrustations from several brine seeps. Sampling continued until the seepage stopped and no further encrustation growth was observed, which was generally within a three year period. Assuming the brine was near saturation, Deal et al. (1993) estimate brine inflow rates between 0.3 and 570 $ml/m^2/year$.

4.2.2.4.3 Laboratory Analysis of Brine Chemistry and Content

The possible sources of brine have been studied using chemical analysis and laboratory tests to extract brine from core and rock samples.

Chemical analysis is important to distinguish natural brine from that introduced by construction. Natural brine is high in bromine, boron, and magnesium, which are concentrated in residual water after precipitation of evaporate minerals during primary deposition. The brines

used for construction come from two sources. During shaft construction, brine was allowed to flow into the WIPP facility from the intersection of the shafts with permeable beds in the Rustler Formation above the repository horizon. Final grouting of the shafts sealed off this source, which no longer introduces water to the WIPP excavations. These brines are relatively high in strontium and low in bromine and magnesium. The construction work also used commercial brine produced by solution of Salado halites in municipal water to produce a predominantly NaCl brine with a high carbonate content.

The amount of moisture and brine that is potentially available in Salado rock for seepage has been measured by two methods. The moisture content was determined by measuring the change in weight of over 400 samples after heating them to over 90°C to vaporize the pore water. This moisture is assumed to represent the connected pore space that is available for brine flow through the rock. The average volume percent from these tests is 1.6 percent. Consolidation tests under lithostatic loading provided brine content information for sample of clays from the excavations. The brine volumes extracted from the clay samples comprised between 25 and 29 percent of the original sample volumes (Deal et al., 1993).

4.2.2.4.4 BSEP Mechanistic Models of Brine Inflow

The BSEP's PIs initially proposed that brine seepage was driven by a transient far-field radial flow system that resulted from the excavation of WIPP openings (Deal and Case, 1987; Deal and Bills, 1994). As additional data on brine seepages accumulated, the BSEP PIs felt that they were not able to observe as much brine as predicted from those assumptions, and proposed that there may not be a far-field source. They proposed that the observed brine seepages resulted from redistribution of brine within the developing DRZ (Deal et al., 1989). More recently they have proposed, as the main source of brine inflow underground, the dewatering of clays due to excavation-related consolidation (Deal et al., 1993). The basis for the BSEP model consists of observations of seepage from clay-rich strata and the laboratory measurements of brine volumes extracted during consolidation tests on clay samples. The laboratory data indicate the brine content in the clays may be sufficient to account for the inflow rates observed in the BSEP program at the WIPP, provided excavation-induced consolidation occurs. Implementation of the BSEP mechanistic model would possibly affect assessments of repository performance by predicting lower brine inflows to the disposal rooms than the those predicted by the potentiometric flow model.

4.2.2.5 SMALL-SCALE BRINE-INFLOW (SSBI) EXPERIMENTS

Small-scale brine-inflow experiments were conducted at the facility horizon from September 1987 to June 1993. The objective of this experimental program was to provide data for use in the development and validation of a mechanistic model for brine inflow into the repository. Seventeen boreholes in Room D (10 boreholes), Room L4 (2 boreholes), and the Room Q access drift (5 boreholes) were monitored for brine accumulation (see Figure 5). The borehole diameters ranged from approximately 5 to 90 cm and the lengths varied from 3 to 6 m. The boreholes intersected numerous lithologic units surrounding the repository at various inclinations. The experiments consisted of regular collection and weighing of the accumulated brine. The frequency of collection was weekly from September 1987 through October 1989, and then monthly or quarterly from then on (no collection occurred when the experiment was suspended from approximately September 1990 to May 1991). The data collection program through June 1991 is detailed in Finley et al. (1992). Documented evaluation of some of the experimental data (from September 1987 through mid-January 1990) was completed by McTigue (1993).

The brine inflow boreholes test all stratigraphic units within or close to the waste facility horizon, except anhydrite "b" and clay G. Figure 5 shows all the boreholes and their related stratigraphy. All stratigraphic units labeled in the figure are described in detail in Deal et al. (1989).

The excavation of the Q access drift was completed in November 1988 and was roughly 5 months old when the 5 boreholes in the floor of the Q access drift (QPB01, QPB02, QPB03, QPB04, and QPB05) were drilled. These five boreholes were drilled specifically to investigate the possibility of brine transport between an area where brine had accumulated beneath the Air Intake Shaft and Room Q. The five boreholes are 5 cm in diameter and roughly 3 m deep so that all five penetrate Marker Bed 139 located between 1.5 to 2.4 m below the floor of the drift.

Room D is situated within a set of stratigraphic units about 6 m above the waste facility horizon (see Figure 5). There are 10 brine-inflow boreholes drilled from Room D. Eight of the boreholes (DBT10, DBT11, DBT12, DBT13, DBT14, DBT15, DBT31, and DBT32) are collared in the center of the floor of the room and extend down through the waste facility horizon. The other two boreholes (DBT16 and DBT17) in the room are collared in the east rib and slope

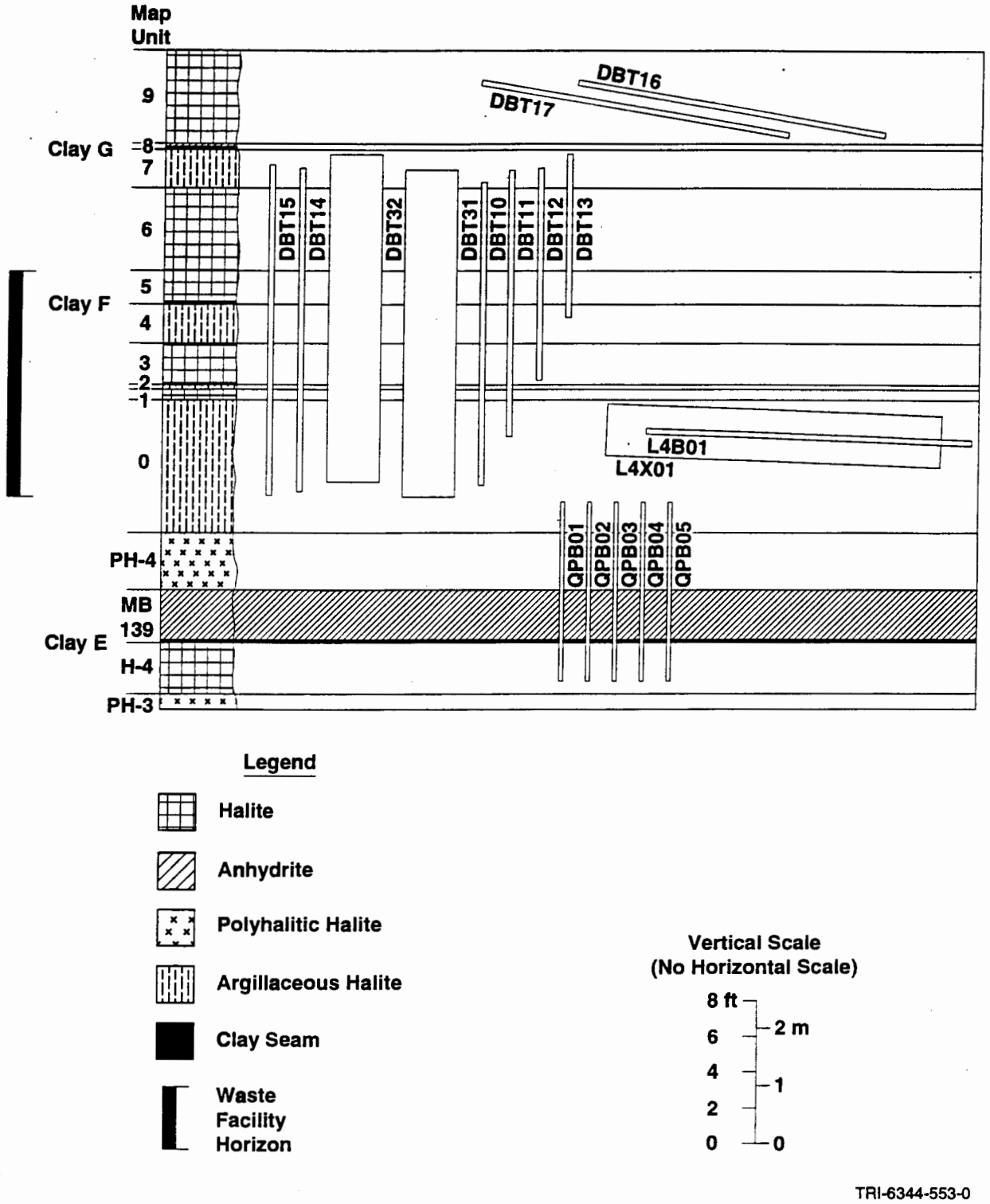

Figure 5. A schematic of the small-scale brine inflow boreholes and the stratigraphic units tested in each borehole.

down to the east at 10 degrees. These two rib boreholes are contained within a relatively pure halite stratigraphy (Map Unit 9) situated between anhydrites "a" and "b" (see Figure 5).

Excavation of Room L4 was completed in March 1989, and the two brine-inflow boreholes (L4X01 and L4B01) were drilled in May 1989. These two boreholes are sub-horizontal and are contained within the upper argillaceous portion of Map Unit 0 (see Figure 5). They are both approximately 6 m deep and angled down to the north at about 2 degrees. L4X01 is 90 cm in diameter and L4B01 is 10 cm.

There is considerable variability in the responses of the 17 brine-inflow boreholes; however, with the exception of the two boreholes in the rib of Room D (DBT16 and DBT17), all monitored holes yielded some brine. The cumulative brine mass collected in the boreholes range from 7 to 37 kg for the eight boreholes in the floor of Room D (DBT10, DBT11, DBT12, DBT13, DBT14, DBT15, DBT31, and DBT32) from September 1987 to April 1993 and from 1.8 to 2.4 kg for the two boreholes in the face of Room L4 (L4X01 and L4B01) from May 1989 through April 1993. The inflows for the boreholes located in Q access drift are the most variable. Cumulative brine mass for these five boreholes ranges from 5 to 372 kg for the period from April 1989 to April 1993.

McTigue (1993) analyzed the data from the experiment by assuming a simple model for radial, cylindrical Darcy flow into a long hole due to relaxation of ambient pore-water pressure assuming a homogeneous, isotropic medium. It was further assumed that the initial pressure was uniform and the flow was normal to the hole axes. An exact, analytical solution for the linear diffusion problem corresponding to the model configuration was formulated. Numerical simulations representing the solution of flux and volume determination were used to fit the data for each borehole. Three methods of history matching of the model response to the data yielded estimates of two parameters that characterize the magnitude of the flow and the timescale over which it evolves. Assuming a value for the far-field pressure, the parameters can be related to the permeability and hydraulic diffusivity of the formation. The parameter estimations yielded effective values of permeability and diffusivity because the sampling scale of the data was on the order of the borehole; rates of brine seeping from individual horizons were not measured.

The three-history matching procedures used by McTigue involved fitting with analytical equations the full-flux data, the late-time flux data, and the cumulative-volume data. The resulting estimated parameters from these fits are shown in Appendix H. The solutions were

based on the assumptions that the viscosity of the brine was 2.1 x 10^{-3} Pa·s and the far-field pressure was 10.0 MPa. For those data that were consistent with the model predictions (data that show a decaying trend of brine inflow), inferred permeabilities were on the order of 10^{-22} to 10^{-21} m^2. The relatively small range in inferred permeability values suggests that the magnitude of flow (measured fluxes) can be predicted by the model. The inferred diffusivities typically ranged from 10^{-10} to 10^{-8} m^2/s. The large scatter in the inferred diffusivity indicates that it is difficult to match the idealized model history to the observed evolution of the flow. The McTigue (1993) model predicts flows that decrease with time; however, late time flow data from many of the tests were not considered in McTigue's analysis and may reflect property changes due to excavation closure.

Gelbard (1992) derived a two-dimensional (r-z) analytical model to evaluate McTigue's (1993) one-dimensional approach to interpretation of the SSBI tests. He concluded that McTigue's neglect of the vertical dimension should cause an error or no more than a factor of two in the interpreted properties.

Data from some of the SSBI experiments were also evaluated by Dutch and French teams as part of the INTRAVAL program. INTRAVAL is a cooperative international project organized to evaluate conceptual and mathematical models for groundwater flow and radionuclide transport to aid in performance assessment of radioactive waste repositories. The INTRAVAL studies use information from laboratory tests, field experiments, and natural analog studies as input for mathematical models, which in turn attempt to validate the underlying conceptual models and study the model validation process. The objective of the INTRAVAL study was to determine whether a Darcy-flow model of brine flow through evaporites could accurately simulate the SSBI experiments and, by extension, be used to predict the rates and volumes of brine inflow to the WIPP repository.

The team from the [Dutch] National Institute of Public Health and Environmental Protection (RIVM) used a numerical model with two-dimensional axially symmetric coordinates to simulate approximately the first two years of brine inflow to holes DBT10, 11, 12, and 13 (Hassanizadeh et al., 1994). The boundary and initial conditions were similar to these used by McTigue (1993): horizontal no-flow boundaries at the tops and bottoms of the boreholes and an initial and constant far-field pore pressure of 10 MPa. The Dutch team defined a single value of specific capacitance, 3.0 x 10^{-11} Pa^{-1}, from constitutive properties of halite and assigned this value throughout their model domain. The strata penetrated by each borehole were categorized

as either pure or impure halite based on core logs. Differences in brine inflow to the four holes were assumed to be due to the different thicknesses of pure and impure halite penetrated by the holes and to the two types of strata having different permeability. Hassanizadeh et al. (1994) determined that the values of pure and impure halite permeability that provided the best match to the data from all the holes (not necessarily the data from any individual hole) are 4 x 10^{-22} m^2 and 4 x 10^{-21} m^2, respectively.

The team from the [French] Ecole Nationale Superieure des Mines de Paris (EdM) used a two-stage numerical modeling approach to simulate the brine-inflow test in DBT10, 9, 12, and 13. (Ait Chalal et al., 1993). They first simulated the relaxation of the pore-pressure field caused by brine flow to Room D after it was excavated and then simulated the SSBI tests conducted within the relaxed pore-pressure field. The French team identified a single value at specific capacitance, 6.7 x 10^{-11} Pa^{-1} from fitting to the DBT13 brine-inflow data and used that value to simulate the other brine-inflow tests. Categorizing strata as either pure or impure halite in the same manner as the Dutch team, Ait Chalal et al. (1993) estimated the permeability of pure halite to be 3.4 x 10^{-13} m/sec and that of impure halite to be 1.8 x 10^{-14} m/sec.

The INTRAVAL teams concluded that Darcy flow models could replicate the SSBI data in a consistent and reasonable manner. Discrepancies between the data and simulations were attributed to inadequate representation in the model of processes modifying the pore-pressure field in addition to the experiments themselves, such as flow to the excavations and ongoing deformation of the rock around the excavations. Therefore, refinements of the basic Darcy-flow model were suggested rather than replacement with a fundamentally different model

4.2.2.6 HYDROFRACTURE EXPERIMENTS

There were three separate experiments conducted to investigate conditions of fracture formation and fracture properties within the Salado. One experiment described hydrofractures for the facility horizon salt (Wawersik and Stone, 1985). Pressure-dependent permeability in Marker Bed 138 was observed in the second test, which was performed as part of the Salado far-field permeability testing program (Beauheim, 1993). The third experiment coupled permeability and hydrofracture tests performed in Marker Bed 139 and Marker Bed 140 and were designed to address five questions: 1) What are the pressures needed to initiate and extend interbed fractures? 2) Will fracturing occur by reopening and interconnecting pre-existing fractures

and/or by forming discrete new fractures? 3) Is the combination of the in-situ stress state and pre-existing weakness planes in the interbed such that fracturing will be contained within the marker beds or might newly developed fractures break out of the marker bed? 4) How does fracture development change interbed permeability and storage capacity? 5) Are the post-fracturing permeability and storage capacity of the marker beds constant or are they dependent on pressure? The experimental sequence in each test hole consisted of an initial pressure-buildup period to establish the formation pore pressure, a pre-fracture permeability test, hydrofracturing, and post-fracture permeability tests. The post-fracture tests included both constant-pressure injection and withdrawal to evaluate post-fracture permeability under different pressure conditions.

The following is a brief discussion of the preliminary results from the tests performed in Marker Bed 139 (Beauheim et al., 1993b). Fracturing took place when the fluid pressure in Marker Bed 139 exceeded the assumed total local in-situ stress normal to the fracture plus the tensile strength of the rock. At two test locations, fracturing was associated with horizontal fracture development primarily along pre-existing, partially or fully healed fractures in the bottom third of the 1 m thick marker bed. Fracture development by hydraulic fracturing created new storage capacity because 67 percent of the hydraulic fracture fluid injected was retained in the formation. Hydraulic fracturing also resulted in a net increase in permeability and specific storage of Marker Bed 139 over pre-test conditions. Both properties exhibited a strong pressure-dependence assumed to be caused by changes in fracture aperture as a function of fluid pressure in the fracture. The permeabilities and specific storage remained higher than pre-fracture conditions even when pore pressures were reduced during withdrawal tests, presumably because of incomplete fracture closure as manifested by the high retention of fracture fluid at the end of hydraulic-fracturing tests.

4.2.2.7 THERMALLY DRIVEN FLUID TRANSPORT

Numerical simulations of heat generation by RH waste were made in the U.S. DOE (1980). Experimental studies of the thermal response of the Salado Formation were conducted by the WIPP Experimental Program (Tyler et al., 1988) in the simulated heated room experiment. Based on the results of these studies, it is possible that a small thermal gradient will form in the host salt in the immediate vicinity of the repository in response to RH emplacement into ribs. The RH waste could possibly raise the temperature in the host salt to approximately 35 to 40°C (U.S. DOE, 1980). The resulting thermal gradients might drive the transport of

water vapor by thermally driven diffusion and by pressure gradients. Under these conditions, flow cells may form, extending from the DRZ into the room in the vicinity of the RH waste emplacements. Because this process is intricately linked to the waste form and room contents, further detailed discussion is beyond the scope of this paper, which focuses on fluid flow in the Salado Formation.

4.2.2.8 GEOPHYSICAL SURVEYS AND FLUID FLOW

The following discussion is summarized from a memorandum by D. Borns that is included as Appendix I in this paper. Electric current flow takes place through ionic conduction in pore networks or conduction through conducting minerals. In evaporites, ionic conduction through pore networks dominates as the mechanism. Mineral conduction in the Salado is possible; however, the time-dependent variations observed in resisitivity are more consistent with ionic flow through a deforming pore network because the distribution of conductive minerals in the matrix does not vary significantly with time. The electrical current flow induced or observed is therefore assumed to be supported by an interconnected, partially (greater than 70 percent) to completely brine-saturated pore network. Based on this assumption, the resistivity of the pore network can be related to the porosity, pore saturation, tortuosity of the network, and composition of the pore fluid. The observations from a variety of surface-to-depth measurements and three separate WIPP underground geophysical investigations provide strong support for the existence of an interconnected, permeable network at the large scale in the Salado Formation.

Extensive efforts to measure the resistivity of the Salado Formation have been made due to oil and gas reserves, the GNOME experiment, and the WIPP site. The large-scale resisitivity of the Salado ranges between 100 and 1000 ohm-m, commensurate with a brine content of 1 to 3 percent throughout the bulk of the formation (Skokan et al., 1989).

In a WIPP analysis, Poiseuille's equation was used to estimate variations in permeability from electrical data acquired along the length of a borehole for the Salado Two-Phase Flow Laboratory Program that was drilled to assess anhydrite core damage and properties restoration (Howarth, 1993). The calculated permeabilities match closely the range for anhydrite and halite determined in laboratory and field experiments. This result suggests that the interconnected pore network model represents electrical current flow in the Salado.

Room Q resistivity data were collected from 1989 through 1993. The resistivity array was sensitive to changes in resisitivity up to four m away from the excavation. The behavior observed over the 2.6 years of data collection suggests that the DRZ can resaturate over a 2.6 year period. This suggests that there is a source of brine external to the DRZ that with time is able to resaturate the porosity of the DRZ.

Self-potentials have been routinely measured in Room Q as a background check for electrical surveys. Self potential measures the background current flow when induced sources are turned off. Self potential is commonly induced by ionic current flow accompanying fluid flow in rocks. As such, self potential is often used to detect leaks in man-made structures. In the WIPP underground, observed self potential may not indicate natural far-field flow due to perturbations like shafts and excavations. The distribution of self-potentials suggests that layer stratified ionic flow is occurring around the Room Q excavation.

5.0 SPM-2 BASELINE MODEL FOR SALADO FLUID FLOW AND TRANSPORT CONTAINMENT

The SPM-2 Salado Baseline Model for the Salado Formation Fluid Flow and Transport Containment (Baseline Model) is described in this section. The Baseline Model is based on the PA BRAGFLO model described in Section 3. However, modifications to this model are specified in this section. The Baseline Model is a set of modeling assumptions and input parameters providing one possible basis for compliance-related model predictions. It is based on the numerical models used in the 1992 Performance Assessment, with extensive modifications both in model configuration and input parameters. The modifications are one way to account for uncertainty that is known to exist but has not been incorporated in previous performance assessment efforts.

The Baseline Model makes use of and is supported by existing data and knowledge, as well as highly probable projected results from a limited suite of efforts deemed necessary to support certain implementing assumptions, consistent with guidance received during the SPM process. These efforts are also described in this section. The Baseline Model honors data and supporting information that is available today and certain projected results, and attempts to encompass the potential impact of known uncertainty (i.e. known lack of understanding or characterization) of processes likely to occur. No factors have been introduced to account for "unknown" uncertainty, or the possibility of new knowledge acquired in the future modifying present findings.

The principle of conservatism was applied during the development of the Baseline Model. Because of the coupling between physical processes and the resulting lack of clear relationship between parameters and regulatory criteria, and because of the stochastic methodology used in the Baseline Model, the principle of conservatism was applied both in the sense of "is the uncertainty captured?" and "is this a justified position?" The first interpretation, which is most easily applied to estimated data ranges within a given model, was most useful in cases where existing data or understanding was available; the second interpretation was most useful in cases where bounding assumptions were made, due to lack of reasonable characterization of a particular process or lack of development of alternatives that are acceptable under SPM-2 guidance.

Although all flow interactions of the Salado Formation must be captured either explicitly or by assumption in the Baseline Model, the model was developed with primary emphasis on the

three fundamental regulatory-related questions of fluid flow in the Salado Formation: 1) how much brine will enter the repository?; 2) how far will gas move from the repository?; and 3) how far will brine move from the repository?. Brine contributes to gas generation in the repository, and thus brine inflow must be characterized by the Baseline Model because it provides vital parameters to the disposal room model. Outflow of gas containing VOCs and of brine containing dissolved radionuclides are of direct regulatory concern.

Present data support the use of BRAGFLO and associated numerical models, as described in the 1992 PA and modified by Section 3 and Appendix B of this paper, with additional modifications listed below, for brine inflow calculations. However, it is believed that the present data and characterization do not support explicit calculation in SPM-2 of brine movement distances or gas movement distances, as described below, following SPM-2 guidance. Therefore, an alternative method based on post-processing of BRAGFLO calculations is specified for comparison of brine and gas outflow to regulatory criteria, for the purposes of SPM-2 calculations. Post-processing is defined here as the analysis of numerical data created by a completed flow simulation to develop conclusions that are not based on the algorithms in the flow simulation computer code.

The Baseline Model was developed to address the three fundamental fluid flow issues described above rather than to address each of the eight portions of the conceptual model described in Sections 2 and 3 of this paper. Therefore, this description of the Baseline Model will not be organized around the components of the conceptual model. Rather, aspects of the conceptual model will be mentioned as appropriate throughout this description of the baseline model.

5.1 SPM-2 Baseline Model Overview

The Baseline Model is based on BRAGFLO and associated numerical models as described in WIPP PA 1992 (WIPP PA, 1992a and b; WIPP PA, 1993a and b; Sandia WIPP Project, 1992), and as modified by Appendix B, Section 2, Section 3, and this section of this paper. A fundamental modification to the WIPP PA 1992 (WIPP PA, 1992a and b; WIPP PA, 1993a and b; Sandia WIPP Project, 1992) model is the altered anhydrite model component (Appendix B and Appendix C), which is retained for use in the Baseline Model. Certain enhancements and revised performance measures are defined for the Baseline Model below; however the basic

BRAGFLO model (Appendix B), nodalization, layering, and panel and repository representations are retained.

BRAGFLO is the basis of the Baseline Model because it is the best model for Salado fluid flow currently available for performance assessment. It has demonstrated capabilities for modeling multiphase flow in the context of both 1) specific process interactions (room closure, gas generation, brine consumption, human intrusion, etc.) and 2) project-related demands (Quality Assurance, stochastic framework), that are necessary for a performance assessment of the WIPP repository. These capabilities are lacking in available alternative models. Modifications to the configuration of BRAGFLO are specified in the following section to assure that the uncertainty associated with the BRAGFLO characterization of the repository and formation is captured by the model outputs. Modifications can be grouped into three categories: 1) model enhancements by use of newly-added or newly-enabled governing equations, 2) change of parameter ranges from historical (i.e., WIPP PA 1992) values to updated values (reflecting new data and/or better characterization of uncertainty), and 3) the use of post-processing techniques where BRAGFLO in this Baseline Model configuration is not currently capable of capturing the range of uncertainty required by SPM-2 guidance.

To summarize, the SPM-2 Baseline Model emphasizes the three fundamental questions of Salado fluid flow – brine inflow, brine outflow, and gas outflow. The Baseline Model will numerically estimate brine inflow using BRAGFLO in a configuration modified from, but still similar to, those used in recent performance assessments (see Appendix B). The Baseline Model will also numerically estimate the quantity of brine and gas outflow using BRAGFLO. However, the configuration of BRAGFLO used for the Baseline Model does not capture uncertainty required by SPM-2 guidance for estimating movement of brine and gas from the repository to the accessible environment. Therefore, the quantity of brine and gas reaching the boundary will be calculated in SPM-2 by post-processing BRAGFLO results.

5.2 Model Enhancements

The following model enhancements to the BRAGFLO model (WIPP PA, 1992, as modified by Appendix B, and Section 3) are specified as part of the Baseline Model.

5.2.1 The Relative Permeability of Both Phases in the DRZ and Transition Zones = 1

The DRZ and Transition Zone region definitions are depicted in Figure 6. These regions will have time-varying properties due to DRZ formation and shrinkage, room consolidation, possible room expansion, and possible fracturing due to high gas pressure. These time-varying properties have not been quantified in a model usable by PA, nor can the effects of these time-varying properties on fluid flow be predicted accurately. The DRZ and Transition Zone are modeled with a constant, high permeability relative to intact units of the Salado Formation. The saturation of this region with brine is expected to vary over time as brine inflow, gas exsolution, brine outflow, and gas outflow occurs. Relative permeability is sensitive to saturation, and therefore, the relative permeability to brine may be very low under certain saturation conditions. Low brine relative permeability in the DRZ and Transition Zones is generally thought to be less conservative than high brine relative permeability because low brine relative permeability restricts brine flow to the repository. Relative permeabilities in the deforming, time-varying DRZ and Transition Zones are unknown. Therefore, use of a constant high relative permeability is specified for both phases in the Baseline Model.

The DRZ and Transition Zones are expected to fracture in response to possible high, gas generated pressure. Although the effective permeability (relative permeability times intrinsic permeability) of the DRZ and Transition Zones is assumed to be higher than intact, far-field permeabilities of the Salado Formation, the possibility exists that fractured DRZ may have even higher effective permeability. Higher DRZ and Transition Zone permeability favors gas and brine outflow into the far-field Salado Formation. Thus there is uncertainty whether the assumption used for DRZ and Transition Zone permeabilities is conservative with respect to gas and brine outflow. To address this uncertainty, as part of the Baseline Model, an investigation of the possible effects of fracturing in the DRZ is specified. It is expected that the study will confirm the Baseline Model assumption; it may even allow a less conservative assumption be implemented. This additional effort is one of four specified with the Baseline Model. The other three efforts will be described in Section 5.3.

5.2.3 Add a 1° dip to the BRAGFLO model

Dip has been found to affect gas migration distance and brine inflow under conditions of elevated (i.e., above natural) interbed permeability. In one case, brine inflow was calculated to increase 75 percent into the disposal region after interbeds were altered using the current PA

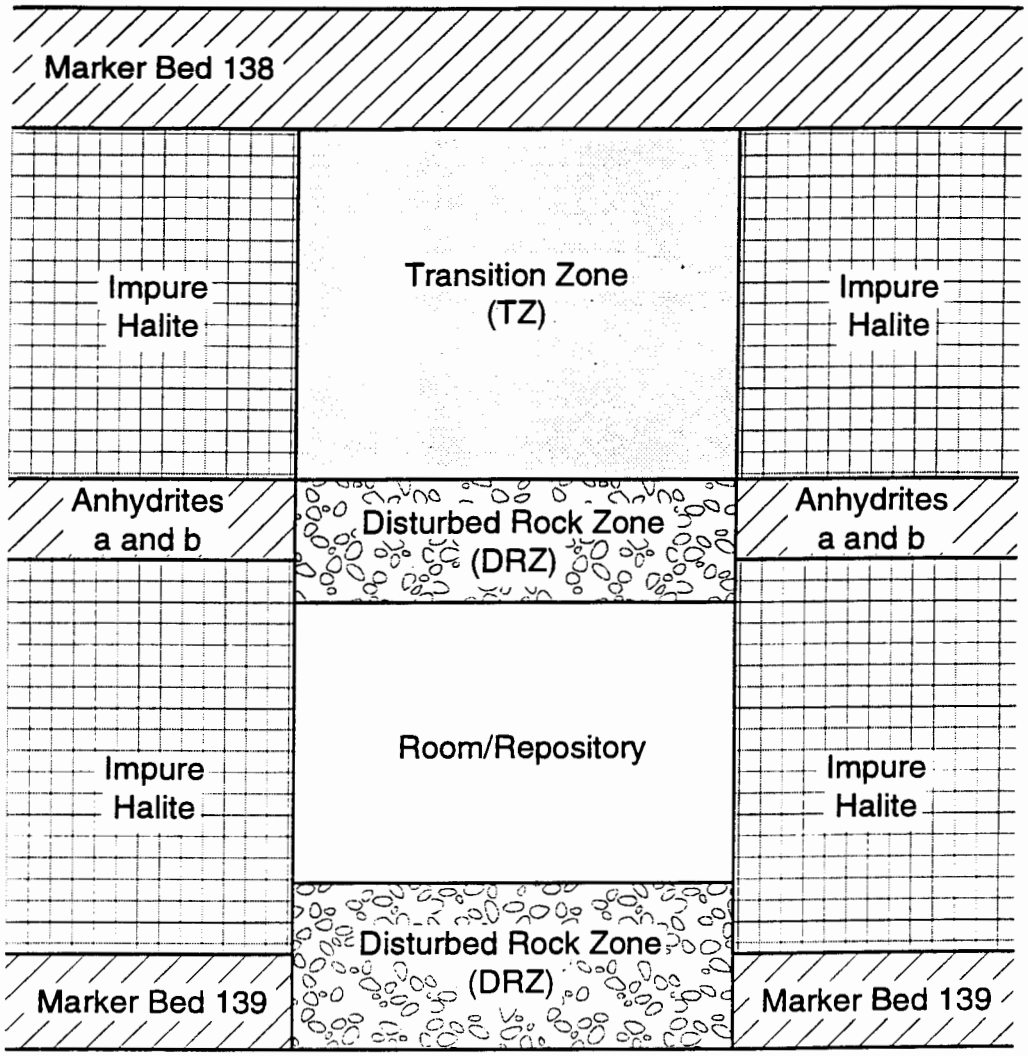

Figure 6. Schematic of DRZ and Transition Zone Regions.

model of interbed fracture (Appendix C, modified for dipping stratigraphy). Elevated interbed permeability will occur if interbeds fracture or dilate in response to high gas pressure in the repository. Because interbed fracture appears a likely response to high repository pressure, and because interbed fracture with dip may increase brine inflow, dip should be included in the Baseline Model calculation.

The general layout specified for the Baseline Model for the repository and Salado Formation requires the use of two repository discretizations, one with the modeled panel region higher than the rest-of-repository region and one with the panel region lower. The interbed fracturing model will need to be modified due to the inclusion of dip. A recommended modification is to make the fracture parameters specific to each element or node, not a constant value. This model enhancement should allow the possibility of countercurrent flow in the interbed and increased brine inflow to the room when interbed alteration occurs.

5.2.3 Correlate the Threshold Displacement Pressure with Permeability

The threshold displacement pressures of the interbeds, DRZ, and Transition Zone should be correlated with their respective permeabilities through the Davies correlation (Davies, 1991), including uncertainties. This should be done both prior to and after fracturing occurs in every element composing these regions. Previously with the interbed alteration model, zero capillary pressure was assumed in the interbeds for all time, to accommodate the anticipated threshold displacement pressure in fractured interbeds. Salado PIs believe that zero capillary pressure for intact interbeds is not physically reasonable. Use of the Davies correlation is justified because it is based on the best available information on the expected behavior of threshold displacement pressure in the Salado Formation.

5.3 Necessary Efforts

In some instances positions in the Baseline Model are justified based on expected outcomes of additional efforts. The nature of the additional efforts is such that they can potentially be completed within about a year from initiation, and that their outcomes are reasonably certain but not yet demonstrated. Four such necessary efforts have been identified for the Salado Baseline Model; one was described above for the DRZ and Transition Zone permeability assumptions. The other three are discussed here.

5.3.1 Two-Dimensional/Three-Dimensional Comparison Study of Salado Fluid Flow

The hybrid two-dimensional/three-dimensional BRAGFLO configuration has not been numerically compared with more conventional three-dimensional nodalizations. Therefore, it is unknown whether the configuration of BRAGFLO effectively simulates three-dimensional flow, which is required for a realistic estimate of brine inflow. The BRAGFLO configuration is a two-dimensional model in which the volumes of elements and their connection areas have been altered, in an approach thought to be consistent with the assumption of radial flow. Although this approach is standard for modeling radial flow to a borehole, features in the repository configuration specified for the Baseline Model cause concern that the model may behave more like a two-dimensional model than a three-dimensional model. As a limited part of a modeling study, brine inflow in a three-dimensional, single-room model was found to be 2 to 3 times higher than in a two dimensional, single-room model. Because the BRAGFLO geometry has not been shown to accurately simulate three dimensional brine flow to the repository, there is concern that it may generally underestimate brine inflow, possibly by as much as a factor of 2 or 3.

As part of the Baseline Model, an explicit comparison of two-dimensional to three-dimensional repository geometry is specified to verify the assumption that the current PA description of the repository is adequate. This study is solely for verification of the BRAGFLO geometry and is independent of adding dip to the BRAGFLO model. This study will however yield insight into the three-dimensional mechanics of brine outflow which may allow other assumptions contained in the Baseline Model to be modified.

5.3.2 Discrete Fracture/Matrix Study of Brine Flow in Interbeds

It is expected that some of the contaminated brine that can potentially flow out of the repository will flow through the matrix of interbeds, or adjacent halite-rich units, rather than through fractures. This conclusion, however, depends upon the nature of fractures in the anhydrite and the two-phase characteristics of the fractures, matrix, and adjacent halite units. The maximum value for the range of brine storage (discussed below) within the disposal system takes into account that some contaminated brine will flow in the matrix of the interbeds or adjacent halite units and not be available for transport laterally through fractures to the accessible environment. This assumption is both uncertain and non-conservative with respect to the regulations, and therefore requires justification. As part of the Baseline Model, a discrete

fracture/matrix study of brine and gas transport in fractured interbeds is specified. Because the actual fracture geometry and two-phase flow relations that will result from fractures caused by high gas pressure are uncertain, the modeling effort will use a wide variety of possible fracture geometries and two-phase flow relations in order to span the range of possible conditions. This effort must also be pursued in conjunction with the effort specified in Section 5.3.1. Even though there is uncertainty in the model parameters in the specified study, it is extremely likely that at least some contaminated brine will flow into anhydrite matrix and adjacent halite regardless of the assumptions used, as long as the assumptions are bound by known physical characteristics. It is therefore expected with high probability that the Baseline Model assumptions will be verified by the modeling effort.

5.3.3 Evaluation of Dissolved Gas Exsolution Effects

The current BRAGFLO model does not include gas dissolved in high-pressure formation brine. In reality, as formation brine depressurizes near the repository, dissolved gas exsolves, providing additional impetus for brine inflow. Webb (1992) studied this effect on brine inflow to a constant pressure borehole. Dissolved gas exsolution increased the rate of brine inflow sufficiently to introduce uncertainty about the BRAGFLO assumption. The impact on the repository will probably be less than predicted by Webb for an open borehole because the repository pressurization due to gas generation and creep closure makes flow to the repository more difficult than flow to an open borehole. For numerical reasons, the implemented Baseline Model will not incorporate gas exsolution. In the Baseline Model, it is assumed that the effects of gas phase exsolution will be negligible. This assumption needs to be verified through a repository-scale model that incorporates gas exsolution as one of the processes occurring in the Salado Formation. This effort could likely be conducted in close cooperation with the two-dimensional/three-dimensional model effort described above.

In this effort, the gas solubility can be modeled with a Henry's constant of 4×10^{10} Pa as suggested in Webb (1992) based on the study of Cygan (1991). The calculation should be started with brine fully saturated with dissolved gas, and no free gas phase (Beauheim et al., 19931). The effect of dissolved gas on the brine density and viscosity can be neglected because it is considered to be minor. The dissolved gas can be assumed to be pure nitrogen because this is the predominant naturally-occurring gas observed in the Salado formation.

5.4 Post-Processing Techniques for Comparison to Regulatory Criteria

The Baseline Model configuration does not capture uncertainty required by SPM-2 associated with gas and brine lateral flow and transport to regulatory criteria. The primary issues are: 1) the representation of flow by a two-dimensional approximation which assumes radial flow may not be reasonable for flow in a dipping formation occurring due to the buoyant force, 2) the panel/rest-of-repository representation of the disposal areas may not allow reasonable resolution of the locations of brine and gas outflow, 3) lack of verified Salado-specific two-phase curves yields uncertainty in flow dynamics that is not entirely captured by varying between Brooks-Corey and van Genuchten/Parker, 4) the dynamics of fracture formation (or dilation) are only partially characterized, 5) the dynamics of WIPP fracture flow are only partially characterized, 6) the Baseline Model configuration is unable to capture channeling and fingering dynamics, and 7) the porous-medium representation of multiphase fracture flow in the Baseline Model has not been verified as reasonable for regulatory purposes. Uncertainty in the response of the formation to high gas pressure in the repository (fracture characterization) is important because if migration of gas and especially brine to the lateral boundary occurs, it will almost certainly be through interbeds (or in other layers in the formation) whose permeability has been increased by dilation of existing fractures or the formation of new fractures.

Because the Baseline Model cannot be used for direct estimation of contaminant movement distances and/or rates in SPM-2, assumptions must be made about how contaminants might be transported to the boundary. For the Baseline Model, these assumptions take the form of post-processing of BRAGFLO results to estimate the quantities of gas and brine that reach the boundary, the time they reach the boundary, and their concentration. Although the methods for both gas and brine are similar, the post-processing method prescribed for quantifying transport of each phase is discussed separately in the following sections.

5.4.1 Brine Outflow Post-Processing

While brine may flow out of the repository and into the surrounding formation due to local formation depressurization, it will not reach the far-field until the pressure exceeds the far-field pore pressure. For post-processing, the far-field pressure is called the brine containment pressure, P_{bc}. If brine flows towards the accessible environment, fluid storage within the Salado Formation will delay and possibly prevent its arrival. Brine storage may occur in fractures, the surrounding matrix, and/or adjoining lithologic layers (e.g. the impure halite adjacent to

anhydrite interbeds). Brine storage is included in the Baseline Model, and its method of calculation is described below.

As a part of the BRAGFLO simulation, brine flux out of the repository must be recorded on a frequent interval, such that the record of brine flow can be recreated by a post-processor. For maximum flexibility in post-processing and for use in SPM-2 Activity Sets, the fluxes between repository and adjacent regions must be recorded, as well as the flux between adjacent regions, the Transition Zone, and all interbed layers. The concentration of contaminants in brine must also be recorded, so that a detailed history of mass flux, concentration and time can be recorded. This is necessary for calculating integrated releases, as detailed below.

The amount of brine that can be stored between the repository and accessible environment boundary is uncertain but bounded. It is assumed that all brine outflow from the repository moves into Marker Bed 139, because the likely stratification of brine under gas in the repository makes brine outflow to other interbeds above the repository unlikely. It is also assumed the known uncertainty in how brine flows within Marker Bed 139, and between Marker Bed 139 and adjacent halite-rich rock, can be addressed with a sampled parameter, C_b, which is defined in the following paragraph.

If $P_{repository} > P_{bc}$ at any time, the total fluid mass reaching the boundary in 10,000 years is given by

$$M_{brine\ at\ boundary} = M_{leaving\ repository} - M_{brine\ storage}$$

where

$$M_{brine\ storage} = C_b\ \rho_b\ \phi\ \pi\ r^2\ h_b$$

and $C_b = 10^{-3}$ to 2; log uniform distribution
$\phi = 0.01$ (MB139 porosity)
r = distance to regulatory boundary
h_b = MB 139 thickness
ρ_b = density of brine

$M_{leaving\ repository}$ is the mass of contaminated brine that actually enters interbeds. Contaminated brine is assumed to exist in the waste disposal panels, and in the DRZ

immediately below the waste disposal panels. Only brine that has been in either of these two regions and subsequently enters interbeds is accumulated in the term $M_{leaving\ repository}$. $M_{brine\ storage}$, although cast in radially symmetric terms, is intended to account for several uncertainties, all of which are incorporated in the term C_b. The rationale behind the minimum value selected for C_b is based on the assumption that brine, if it is to reach the boundary, will flow through fractures. Fractures will likely 1) propagate up dip in a limited arc from the repository, 2) be of small aperture, and 3) channelize brine flow. The extent to which these processes will limit the ability of brine to access all of the pore volume in MB 139 has been estimated by assigning an order-of-magnitude factor to each, and multiplying them for a final factor. A factor of 10^{-2} was assigned due to directional propagation (which can be thought of as a wedge-shaped fracture 150 m wide at the accessible environment boundary); a factor was not assigned for brine flow confined to the fracture aperture based on the expected results of the discrete fracture/matrix modeling study, and a factor of 10^{-1} was assigned to account for likely channeling of brine that does flow within the fracture. Thus, the minimum storage volume for brine is estimated to be 10^{-3} times the intact pore volume of Marker Bed 139 between the repository and the accessible environment boundary. The maximum value of C_b, 2, is based on the possibility of significant flow of brine in the interbed matrix (or existing, undilated fractures), some flow into adjacent, impure halite units, and dilation of the interbed fractures creating new pore volume. The distribution for C_b shall be lognormal between 10^{-3} and 2, giving a mean/median value of approximately 4×10^{-2}.

The median brine storage using this post-processing technique has been estimated as approximately 9×10^6 kg or 7,500 m^3 of brine. Due to the sampling method and large range about the median value, some realizations may have storage volumes as low as about 180 m^3, and some as much as about 360,000 m^3.

5.4.2 Gas Outflow Post-Processing

Gas, like brine, cannot reach the far field without first exceeding the resident pressure of far-field fluids. Additionally, gas must overcome the threshold displacement pressure to displace brine from pores. The range for interbed threshold displacement pressure is 0 to 2 MPa greater than the far-field pore pressure (Beauheim et al., 1994). Therefore, for lateral gas flow to the accessible environment, the Baseline Model will as a precondition require repository pressures to exceed the far-field brine pore pressure at the repository horizon (a sampled value), plus a normally-distributed threshold displacement pressure of between 0 and 2 MPa. This

pressure is called the gas containment pressure, P_{gc}. Unless the pressure in the repository exceeds this pressure, no gas will reach the lateral accessible environment.

If $P_{repository} > P_{gc}$ at any time, a post-processing step to calculate gas reaching the accessible environment must be performed. Similarly to brine, the mass of gas reaching the boundary is:

$$M_{gas\ at\ boundary} = M_{leaving\ repository} - M_{gas\ storage}$$

where

$$M_{gas\ storage} = C_g\ \rho_g\ \phi\ \pi\ r^2\ h_g$$

and $C_g = 10^{-1}$ to 10^{-6} (fractured interbeds); 1/3 to 10^{-3} (unfractured interbeds)
$\phi = 0.01$
r = distance to regulatory boundary
h_g = composite thickness of anhydrites a, b, and marker bed 138
ρ_g = density of gas (at P_{gc})

The uncertainty associated with lateral gas flow to the accessible environment begins with all of the uncertainty associated with brine flow (because gas is also a fluid), but is greater, due to the greater mobility of gas (lower viscosity), reduced ability of gas to enter the matrix and adjacent units (threshold pressure is assumed to be high based on the correlation with permeability), the buoyant drive for gas flow directed up-dip, and the likely dominance of fracture flow for gas movement. Gas flow in fractures remain uncharacterized for the WIPP. These uncertainties are significantly greater than those associated with brine flow. Because of these uncertainties, the range of gas storage in the disposal system is uniformly lower than for brine. It was decided to evaluate the gas-storage parameter in terms of fractured (high pressure) interbeds, and unfractured interbeds. For fractured interbeds, the maximum (most favorable) value was determined by assigning a factor of 1 for flow direction (assuming radial fractures), a factor of 0.5 based on the relation between marker bed thickness and likely fracture aperture, and factor of 0.3 for fingering/channeling effects. The resulting factor of 1/15 was rounded to 1/10 for numerical simplicity. For fractured interbeds, the minimum (least favorable) value was

determined by assigning a factor of 10^{-2} for directed fractures, a factor of 1/5 for fracture aperture, a factor of 10^{-2} for fingering and channeling, and a factor of 10^{-2} to account for uncertainty in two-phase flow properties. The resulting minimum value is 10^{-6}. The sampled values on this range are specified to be lognormally distributed. For unfractured interbeds, the maximum value of 1/3 was assigned assuming radial flow through porous media with viscous fingering and channeling. The minimum value of 10^{-3} was determined by assigning 0.1 factor for two-phase flow property uncertainty (no fractures means less uncertainty), a factor of 0.1 to account for the possibility of increased fingering and channeling, and a factor of 0.1 to account for likely up-dip flow due to buoyancy.

5.5 Tie-in to the Conceptual Model Components

This section provides additional links between the conceptual and the Baseline Model. Eight components of the conceptual model were described in Sections 2, 3, and 4: 1) stratigraphy, 2) salt creep, 3) fluid flow, 4) contaminant transport, 5) thermally driven fluid flow, 6) model initial conditions, 7) disturbed rock zone, and 8) interbed fracturing. In addition, two components were described as unevaluated: 9) hydrogen diffusion and 10) chemical reactions. Also, there has been little direct reference to components of the process model presented in Section 3, other than the required modifications that are being specified. Those aspects of the conceptual model that were not discussed in detail previously in Section 5 are addressed here.

5.5.1 Stratigraphy

The Baseline Model utilizes stratigraphy similar to that described in Section 3 for the process model. Based on a detailed study on this subject, this stratigraphic representation is reasonable for brine inflow and for calculating the flux of brine and gas out of the repository. It may not be reasonable for calculating brine and gas movement in the interbeds away from the repository because it does not allow channeling. This concern contributed to the implementation of post-processing techniques described in sections 5.4.1 and 5.4.2.

5.5.2 Salt Creep

The Baseline Model does not account for the effects of salt creep in response to changes in pore-fluid pressure on fluid flow other than those accommodated by the effects of elastic compressibility of the rock matrix on porosity. The dramatic effects of salt creep in the DRZ and regions near the repository are accounted for in the DRZ assumptions. The salt-creep response to far-field pore pressure changes is less significant than fracturing, channeling, fingering, buoyancy, and fluid pressure gradients on the 10,000-year time scale. Due to the many assumptions and post-processing techniques adopted for far-field flow, this effect is neglected in the Baseline Model.

5.5.3 Contaminant Transport

All aspects of uncertainty in contaminant transport, and all processes described in the Conceptual Model, are accommodated in the post-processing steps described. In the post-processing, there is no credit taken for sorption, decay, or other path, exposure, and/or travel-time dependent processes. The effects of dispersion, diffusion, and colloid transport, which modify contaminant movement, are accommodated in the C_b and C_g sampled parameters. The development of a method for incorporating the favorable effects of radionuclide decay along the flow path within the brine outflow post-processing technique is under consideration.

5.5.4 Thermally Driven Fluid Flow

The Baseline Model retains the assumption of isothermal conditions for the Salado Formation. Thus, thermally driven fluid flow is not included in the physics of the model. The uncertainty introduced by not considering thermally driven fluid flow is considered to be captured within the range of brine inflow as calculated by the model, consistent with the observed differences between thermally-driven and isothermal brine inflow experiments in the WIPP underground (Nowak et al., 1988).

5.5.5 Model Initial Conditions

Uncertainty in initial conditions was associated with long-term movement of contaminants. Because of the post-processing assumptions that have been implemented in the Baseline Model, the uncertainty associated with initial conditions is considered addressed.

5.5.6 Disturbed Rock Zone

The Baseline Model has altered the Section 3 description of the DRZ and Transition Zone such that the effective permeability of these regions will remain high regardless of their respective saturations. This new assumption must be verified by an additional modeling effort.

5.5.7 Hydrogen Diffusion

Diffusion of hydrogen through the crystalline structure of minerals in the Salado Formation would decrease the repository pressure and the saturation of gas along VOC transport pathways. This will decrease gas migration, increasing confidence in compliance, and thus can be conservatively ignored in the Baseline Model.

5.5.8 Chemical Reactions

Concern about the effects of chemical reactions stems primarily from a lack of understanding about their effects on flow pathways for contaminants. Because post-processing assumptions are used to determine brine and gas storage (and, hence, contaminant storage), chemical reaction between repository fluids and the host rock can be neglected in the Baseline Model.

5.6 Parameter Values and Distributions for the SPM-2 Baseline Model

The parameter values necessary for the Baseline Model and their distributions are summarized below:

Impure Halite

Threshold Pressure	50 MPa; fixed
Permeability	10^{-20} to 10^{-24} m^2; median 10^{-21} m^2
Porosity	0.001 to 0.03; median 0.01
Specific Storage	10^{-7} to 10^{-5} m^{-1}; median 10^{-6} m^{-1}
Initial Pore Pressure	Hydrostatic; datum at MB 139 relative to shaft

Discussion: The high value of impure halite threshold pressure will prevent any gas from entering the impure halite. The permeability range includes the values obtained from field tests. The effect of explicit representation of all the layers compared to the impure halite representation used by PA has been investigated but detailed results are not yet available for release. The difference between explicit representation and an impure halite permeability of 10^{-21} m^2 on brine inflow, repository pressure, and gas migration, however, was not significant.

Anhydrite

Apply interbed alteration model	
Threshold Pressure	Correlated with local permeability according to Davies correlation (Davies, 1991) with uncertainty
Initial Permeability	10^{-17} to 10^{-20} m^2; median 10^{-19} m^2
Max. Frac. Permeability	10^{-9} m^2
Initial Porosity	0.001 to 0.03; median 0.01
Max. Fractured Porosity	Initial porosity + 0.01
Specific Storage	10^{-7} to 10^{-5} m^{-1}; median 10^{-6} m^{-1}
Initial Pore Pressure (MB 139)	12.0 to 13.0 MPa; median 12.5 MPa at repository elevation, adjusted hydrostatically for dip

Fracture Initiation Pressure	Sampled value ranging from 1 MPa lower than lithostatic pressure to lithostatic pressure, uniform distribution
Full Fracture Pressure	Initiation pressure + 2.5 MPa

Discussion: Dilation or fracturing in the anhydrite interbeds is expected if the repository reaches pressures approaching lithostatic. Therefore, the fracture initiation pressure has been varied from 1 MPa below lithostatic up to lithostatic. The maximum porosity and permeability values specified in the fracturing model are thought to be upper limits. Uncertainty in the applicability of the current interbed fracture model is a significant factor in the prediction of fluid migration away from the repository. Therefore, calculated fluid migration distances are not used as performance measures in the Baseline Model, as discussed in section 5.4.

Anhydrite permeability has been measured in the field and in the laboratory. The permeability over the entire interbed thickness is used in the BRAGFLO model. While the field values measure the permeability on this scale, the laboratory measurements are more local. The maximum local permeability measured in the laboratory is about 1.6×10^{-16} m^2. Based on these measurements, an upper bound of 10^{-17} m^2 for the entire interbed thickness has been specified. Anhydrite porosity values, while higher locally as seen in laboratory measurements, are from 0.001 to 0.03 over the entire interbed thickness.

DRZ

Threshold Pressure	Correlated with local permeability with uncertainty
Initial Permeability	10^{-15} m^2
Initial Porosity	Impure halite value
Maximum Fractured Porosity	Initial porosity + 0.01
Specific Storage	10^{-5} m^{-1}
Relative Permeability (gas)	1.0
Relative Permeability (brine)	1.0

Discussion: The permeability is higher than the anhydrite due to damage caused by repository effects. Relative permeabilities are fixed at 1.0 to prevent possible low brine saturations from blocking flow.

Transition Zone

Threshold Pressure	Correlated with local permeability with uncertainty
Initial Permeability	10^{-15} m^2
Initial Porosity	Impure halite value
Maximum Fractured Porosity	Initial porosity + 0.01
Specific Storage	10^{-5} m^{-1}
Relative Permeability (gas)	1.0
Relative Permeability (brine)	1.0

Discussion: The Transition Zone parameters and rationale are similar to the DRZ. The Transition Zone is between the DRZ and MB 138.

All Regions and Materials

Sample on the two-phase characteristic curves; make all regions the same curve set with region-specific values

2/3 mixed Brooks and Corey; 1/3 mixed van Genuchten/Parker

van Genuchten/Parker saturation definition changed from 1992 PA, the appropriate equations are summarized in Section 5.7,

Gas Residual Saturation	0. to 0.4 - Uniform distribution; median 0.2
Brine Residual Saturation	0. to 0.6 - Uniform distribution; median 0.3
Brooks and Corey Parameter(λ)	0.2 to 10.0 - Median 0.7
van Genuchten/Parker m	$m = \lambda/(1+\lambda)$

Discussion: There are no two-phase characteristic curve data for WIPP-specific materials. In order to address this lack of data, the use of two widely-used models, Brooks and Corey and van Genuchten/Parker, are recommended. A

"mixed" variation of each model as summarized in Section 5.7 improves the best overall data-model comparison for non-WIPP data. The Brooks and Corey model gives better agreement with data than van Genuchten/Parker, so it is given a higher weight. The large range on the Brooks and Corey parameter, λ, is based on Mualem (1976) who fit the capillary pressure data for 45 different soils. The λ values ranged from a low of 0.19 to 11.67. The value of 11.67 seems to be an outlier; the next two highest values are 6.24 and 8.35; therefore, a range of from 0.2 to 10. has been specified. The mean value of 0.7 is from fitting the Morrow et al. (1986) tight gas sands data which had a permeability of 2.4-4.3 x 10^{-17} m^2 and porosity of 0.12, and gas relative permeability data.

5.7 SPM-2 Baseline Model Two-Phase Relationships

The mixed Brooks and Corey and the mixed van Genuchten/Parker two-phase characteristic curves are recommended, as detailed below.

Brooks and Corey

The original definition of effective saturation is

$$S_e = \frac{S - S_r}{1 - S_r}$$

where S_r is the residual wetting phase saturation.

The modified Brooks and Corey model redefines the effective saturation as

$$S_e' = \frac{S - S_r}{S_c - S_r} .$$

where S_c is 1 - S_{gr}.

The mixed approach uses both effective saturation definitions as follows

$$P_c = \frac{P_t}{S_e^{1/\lambda}}$$

$$k_{r,w} = S_e^{(2+3\lambda)/\lambda}$$

$$k_{r,nw} = \left(1 - S_e'\right)^2 \left(1 - S_e'^{(2+\lambda)/\lambda}\right) .$$

The mixed Brooks and Corey model is recommended over the original and modified approaches.

<u>van Genuchten/Parker</u>

The effective saturation used by van Genuchten is

$$S_e = \frac{S - S_r}{S_s - S_r}$$

where S, S_r, and S_s are the saturation, residual liquid saturation, and full saturation value, respectively.

In the original implementation, the value of S_s is set equal to 1.0, so

$$S_e = \frac{S - S_r}{1 - S_r} .$$

Similar to Brooks and Corey, a modified saturation definition can be defined as

$$S_e' = \frac{S - S_r}{S_c - S_r}$$

where S_c is defined above.

The mixed van Genuchten/Parker model is similar to mixed Brooks and Corey as both effective saturation values are used.

The restricted form of the van Genuchten water retention equation ($m = 1 - 1/n$) gives the capillary pressure equation

$$P_c = \frac{1}{\alpha}\left(S_e^{-1/m} - 1\right)^{1-m} .$$

van Genuchten used the Mualem wetting phase relative permeability expression to get

$$k_{r,w} = S_e^{1/2}\left(1 - \left(1 - S_e^{1/m}\right)^m\right)^2 .$$

van Genuchten (1978, 1980) did not address nonwetting phase relative permeabilities. The Parker extension is currently recommended with the modified saturation definition similar to Brooks and Corey, or

$$k_{r,nw} = \left(1 - S_e'\right)^{1/2}\left(1 - S_e'^{1/m}\right)^{2m}$$

6.0 REFERENCES

Ait Chalal, A., S-M. Tijani, and G. Vouille. 1993. *Modelling of the Small Scale Brine-Inflow Experiments*. Paris, France: Centre de Géotechnique et D'Exploitation du Sous-Sol.

Bear, J., and A. Verruijt. 1987. *Modeling Groundwater Flow and Pollution*. Boston, MA: D. Reidel Publishing Co. 168-177.

Beauheim, R.L. 1993. "Conceptual Hydrologic Models of the Salado Formation Derived from Experimental Observations," *Presentation to the NAS WIPP Review Panel. Denver, CO, September 16, 1993*. (Copy on file at the Sandia WIPP Central Files, Sandia National Laboratories, Albuquerque, NM.)

Beauheim, R.L., G.J. Saulnier, Jr., and J.D. Avis. 1991. *Interpretation of Brine-Permeability Tests of the Salado Formation at the Waste Isolation Pilot Plant Site: First Interim Report*. SAND90-0083. Albuquerque, NM: Sandia National Laboratories.

Beauheim, R.L., R.M. Roberts, T.F. Dale, M.D. Fort, and W.A. Stensrud. 1993a. *Hydraulic Testing of Salado Formation Evaporites at the Waste Isolation Pilot Plant Site: Second Interpretive Report*. SAND92-0533. Albuquerque, NM: Sandia National Laboratories.

Beauheim, R.L., W.R. Wawersik, and R.M. Roberts. 1993b. "Coupled Permeability and Hydrofracture Tests to Assess the Waste-Containment Properties of Fractured Anhydrite," *International Journal of Rock Mechanics and Mining Sciences & Geomechanics Abstracts*. Vol. 30, no. 7, 1159-1163.

Beauheim, R.L., S.M. Howarth, P. Vaughn, S.W.Webb, and K.W. Larson. 1994. "Integrated Modeling and Experimental Programs to Predict Brine and Gas Flow at the Waste Isolation Pilot Plant," *Geoval 94, Paris, France, October 11-14, 1994*. SAND94-0599C. Albuquerque, NM: Sandia National Laboratories.

Bechtel National, Inc. 1986. *Design Validation Final Report*. DOE-WIPP-86-010. San Francisco, CA: Bechtel National, Inc.

Beraun, R. 1989. "Numerical Brine Flow Modeling to an Isolated WIPP Disposal Room," *Systems Analysis, Long-Term Radionuclide Transport, and Dose Assessment, Waste Isolation Pilot Plant (WIPP), Southeastern New Mexico; March 1989*. Eds. A.R. Lappin, R.L. Hunter, D.P. Garber, and P.B. Davies. SAND89-0462. Albuquerque, NM: Sandia National Laboratories. A-71 through A-82.

Black, S.R., R.S. Newton, and D.K. Shukla. 1983. *Results of Site Validation Experiments*. TME 3177, Rev. 2.0. Albuquerque, NM: U.S. Department of Energy. Vol. 2.

Borns, D.J. 1985. *Marker Bed 139: A Study of Drillcore From A Systematic Array*. SAND85-0023. Albuquerque, NM: Sandia National Laboratories.

Borns, D.J. 1987. *Rates of Evaporite Deformation: The Role of Pressure Solution*. SAND85-1599. Albuquerque, NM: Sandia National Laboratories.

Borns, D.J., and J.C. Stormont. 1988. *An Interim Report on Excavation Effect Studies at the Waste Isolation Pilot Plant: The Delineation of the Disturbed Rock Zone*. SAND87-1375. Albuquerque, NM: Sandia National Laboratories.

Borns, D.J., and J.C. Stormont. 1989. "The Delineation of the Disturbed Rock Zone Surrounding Excavations in Salt," *Rock Mechanics as a Guide for Efficient Utilization of Natural Resources, Proceedings of the 30th U.S. Symposium, West Virginia University, Morgantown, WV, June 19-22, 1989*. Ed. A.W. Khair. SAND88-2230C. Brookfield, VT: A.A. Balkema. 353-360.

Borns, D.J., M.C. Pfeifer, H.T. Andersen, and C.K. Skokan. 1990. "Electrical Methods to Delineate Fluid Flow In Situ in Bedded Salt," *Society of Exploration Geophysicists. Workshop on Permeability, Fluid Pressure Seals in the Crust, Denver, CO, August 5-8, 1990*. SAND90-1685A. Albuquerque, NM: Sandia National Laboratories.

Brace, W.F. 1977. "Permeability from Resistivity and Pore Shape," *Journal of Geophysical Research*. Vol. 82, no. 23, 3343-3349.

Brokaw, A.L., C.L. Jones, M.E. Cooley, and W.H. Hays. 1972. *Geology and Hydrology of the Carlsbad Potash Area, Eddy and Lea Counties, New Mexico*. Open-File Report 4339-1. Denver, CO: U.S. Geological Survey.

Brooks, R.H., and A.T. Corey. 1964. *Hydraulic Properties of Porous Media*. Hydrology Paper No. 3. Fort Collins, CO: Colorado State University.

Butcher, B.M., and F.T. Mendenhall. 1993. *A Summary of the Models Used for the Mechanical Response of Disposal Rooms in the Waste Isolation Pilot Plant with Regard to Compliance with 40 CFR 191, Subpart B*. SAND92-0427. Albuquerque, NM: Sandia National Laboratories.

Culver, T.B., C.A. Shoemaker, and L.W. Lion. 1991. "Impact of Vapor Sorption on the Subsurface Transport of Volatile Organic Compounds: A Numerical Model and Analysis," *Water Resources Research*. Vol. 27, no. 9, 2259-2270.

Cygan, R.T. 1991. *The Solubility of Gases in NaCl Brine and a Critical Evaluation of Available Data*. SAND90-2848. Albuquerque, NM: Sandia National Laboratories.

Davies, P.B. 1991. *Evaluation of the Role of Threshold Pressure in Controlling Flow of Waste-Generated Gas into Bedded Salt at the Waste Isolation Pilot Plant*. SAND90-3246. Albuquerque, NM: Sandia National Laboratories.

Davies, P.B., and A.M. LaVenue. 1990. Appendix A: "Memo 11: Additional Data for Characterizing 2-Phase Flow Behavior in Waste-Generated Gas Simulations and Pilot Point Information for Final Culebra 2-D Model (SAND89-7068/1)," *Data Used in Preliminary Performance Assessment of the Waste Isolation Pilot Plant (1990)*. R.P. Rechard, H. Iuzzolino, and J.S. Sandha. SAND89-2408. Albuquerque, NM: Sandia National Laboratories. A-139 through A-156.

Davies, P., K. Larson, G. Freeze, and S. Webb. 1993. "Numerical Implementation of Conceptual Hydrologic Models to Understand Flow System Behavior and Model Limitations," *Presentation to the NAS WIPP Review Panel, Denver, CO, September 16, 1993*. (Copy on file at the Sandia WIPP Central Files, Sandia National Laboratories, Albuquerque, NM.)

Deal, D.E. 1988. "Brine Seepage into the Waste Isolation Pilot Plant (WIPP) Excavations," *Waste Management '88, Waste Processing, Transportation, Storage and Disposal, Technical Programs and Public Education, Tucson, AZ, February 28-March 3, 1988*. Ed. R.G. Post. Tucson, AZ: University of Arizona. Vol. 2, 649-657.

Deal, D.E., and R.A. Bills. 1994. "Conclusions After Eleven Years of Studying Brine at the Waste Isolation Pilot Plant," *Waste Management '94, Tucson, AZ, March 2, 1994.* Albuquerque, NM: IT Corporation; Carlsbad, NM: U.S. Department of Energy, Carlsbad Area Office. (Copy on file at the Sandia WIPP Central Files, Sandia National Laboratories, Albuquerque, NM.)

Deal, D.E., and J.B. Case. 1987. *Brine Sampling and Evaluation Program, Phase I Report.* DOE-WIPP 87-008. Carlsbad, NM: Westinghouse Electric Corporation.

Deal, D.E., and W.M. Roggenthen. 1989. "The Brine Sampling and Evaluation Program (BSEP) at WIPP: Results of Four Years of Brine Seepage Data," *Waste Management '89, Waste Processing, Transportation, Storage and Disposal, Technical Programs and Public Education, Tucson, AZ, February 26-March 2, 1989.* Ed. R.G. Post. Tucson, AZ: University of Arizona. Vol. 1, 405-406.

Deal, D.E., J.B. Case, R.M. Deshler, P.E. Drez, J. Myers, and J.R. Tyburski. 1987. *Brine Sampling and Evaluation Program Phase II Report.* DOE-WIPP-87-010. Carlsbad, NM: Westinghouse Electric Corporation.

Deal, D.E., R.J. Abitz, D.S. Belski, J.B. Case, M.E. Crawley, R.M. Deshler, P.E. Drez, C.A. Givens, R.B. King, B.A. Lauctes, J. Myers, S. Niou, J.M. Pietz, W.M. Roggenthen, J.R. Tyburski, and M.G. Wallace. 1989. *Brine Sampling and Evaluation Program, 1988 Report.* DOE-WIPP-89-015. Carlsbad, NM: Westinghouse Electric Corporation.

Deal, D.E., R.J. Abitz, D.S. Belski, J.B. Clark, M.E. Crawley, and M.L. Martin. 1991a. *Brine Sampling and Evaluation Program, 1989 Report.* DOE-WIPP-91-009. Prepared for U.S. Department of Energy by IT Corporation and Westinghouse Electric Corporation. Carlsbad, NM: Westinghouse Electric Corporation, Waste Isolation Division.

Deal, D.E., R.J. Abitz, J. Myers, J.B. Case, M.L. Martin, W.M. Roggenthen, and D.S. Belski. 1991b. *Brine Sampling and Evaluation Program, 1990 Report.* DOE-WIPP-91-036. Prepared for U.S. Department of Energy by IT Corporation and Westinghouse Electric Corporation. Carlsbad, NM: Westinghouse Electric Corporation, Waste Isolation Division.

Deal, D.E., R.J. Abitz, J. Myers, M.L. Martin, D.J. Milligan, R.W. Sobocinski, P.P.J. Lipponer, and D.S. Belski. 1993. *Brine Sampling and Evaluation Program, 1991 Report*. DOE-WIPP-93-026. Prepared for U.S. Department of Energy by IT Corporation and Westinghouse Electric Corporation. Carlsbad, NM: Westinghouse Electric Corporation, Waste Isolation Division.

Ehgartner, B. 1991. *Structural Analyses and Design of a Concrete Liner that Limits The Disturbed Rock Zone Around Underground Openings in Salt*. SAND90-2702. Albuquerque, NM: Sandia National Laboratories.

Finley, S.J., D.J. Hanson, and R. Parsons. 1992. *Small-Scale Brine Inflow Experiments--Data Report Through 6/6/91*. SAND91-1956. Albuquerque, NM: Sandia National Laboratories.

Gelbard, F. 1992. *Exact Analysis of a Two-Dimensional Model for Brine Flow to a Borehole in a Disturbed Rock Zone*. SAND92-1303. Albuquerque, NM: Sandia National Laboratories.

Guzowski, R.V. 1990. *Preliminary Identification of Scenarios That May Affect the Escape and Transport of Radionuclides From the Waste Isolation Pilot Plant, Southeastern New Mexico*. SAND89-7149. Albuquerque, NM: Sandia National Laboratories.

Hassanizadeh, S.M., G.M. van der Giessen, H. Holtman, and P.N. Mollema. 1994. *INTRAVAL Phase 2, Test Case WIPP-I Modeling Brine Migration In Rock Salt*. Final Report 715206003. Bilthoven, The Netherlands: National Institute of Public Health and Environmental Protection. (Copy on file at the Sandia WIPP Central Files, Sandia National Laboratories, Albuquerque, NM.)

Hill, A.C., and G.W. Thomas. 1985. "A New Approach for Simulating Complex Fractured Reservoirs," *Proceedings, Eighth SPE Symposium on Reservoir Simulation, Dallas, TX, February 10-13, 1985*. SPE 13537. Ed. L.C. Young. Richardson, TX: Society of Petroleum Engineers of AIME. Vol. 8, 429-440.

Holcomb, D.J. 1988. "Cross-Hole Measurements of Velocity and Attenuation to Detect a Disturbed Zone in Salt at the Waste Isolation Pilot Plant," *Key Questions in Rock Mechanics: Proceedings of the 29th U.S. Symposium, University of Minnesota, Minneapolis, MN, June 13-15, 1988*. Eds. P.A. Cundall, R.L. Sterling, and A.M. Starfield. SAND87-3016C. Brookfield, VT: A.A. Balkema. 633-640.

Holt, R.M., and D.W. Powers. 1990. *Geologic Mapping of the Air Intake Shaft at the Waste Isolation Pilot Plant*. DOE-WIPP 90-051. Carlsbad, NM: Westinghouse Electric Corporation.

Howarth, S.M. 1994. "Test Plan: Two-Phase Flow Laboratory Program for the Waste Isolation Pilot Plant." Albuquerque, NM: Sandia National Laboratories.

Jarolimek, L., M.J. Timmer, and R.F. McKinney. 1983. *Geotechnical Activities in the Exploratory Shaft -- Selection of the Facility Interval, Waste Isolation Pilot Plant (WIPP) Project, Southeastern New Mexico*. TME 3178. Albuquerque, NM: U.S. Department of Energy, Waste Isolation Pilot Plant.

Jensen, A.L., C.L. Howard, R.L. Jones, and T.P. Peterson. 1993a. *Room Q Data Report: Test Borehole Data from April 1989 through November 1991*. SAND92-1172. Albuquerque, NM: Sandia National Laboratories.

Jensen, A.L., R.L. Jones, E.N. Lorusso, and C.L. Howard. 1993b. *Large-Scale Brine Inflow Data Report for Room Q Prior to November 25, 1991*. SAND92-1173. Albuquerque, NM: Sandia National Laboratories.

Jones, C.L., C.G. Bowles, and K.G. Bell. 1960. *Experimental Drill Hole Logging in Potash Deposits of the Carlsbad District, New Mexico*. U.S. Geological Survey Open File Report 60-84. [Denver, CO]: U.S. Geological Survey.

Jung, Y., A. Ibrahim, and D. Borns. 1991. "Mapping Fracture Zones in Salt: High-Resolution, Cross-Gallery Seismic Tomography," *Geophysics: The Leading Edge of Exploration*. Vol. 10, no. 4, 37-39.

Kazemi, H., L.S. Merrill, Jr., K.L. Porterfield, and P.R. Zeman. 1976. "Numerical Simulation of Water-Oil Flow in Naturally Fractured Reservoirs," *Society of Petroleum Engineers Journal*. Vol. 16, no. 6, 317-326.

Lappin, A.R., R.L. Hunter, D.P. Garber, and P.B. Davies, eds. 1989. *Systems Analysis, Long-Term Radionuclide Transport, and Dose Assessments, Waste Isolation Pilot Plant (WIPP), Southeastern New Mexico; March 1989.* SAND89-0462. Albuquerque, NM: Sandia National Laboratories.

Litvak, B.L. 1986. "Simulation and Characterization of Naturally Fractured Reservoirs," *Reservoir Characterization Technical Conference, Dallas, TX, April 29-May 1, 1985.* Eds. L.W. Lake and H.B. Carroll, Jr. Orlando, FL: Academic Press. 561-584.

Lowenstein, T.K. 1988. "Origin of Depositional Cycles in a Permian 'Saline Giant': The Salado (McNutt Zone) Evaporites of New Mexico and Texas," *Geological Society of America Bulletin*. Vol. 100, no. 4, 592-608.

McTigue, D.F. 1993. *Permeability and Hydraulic Diffusivity of Waste Isolation Pilot Plant Repository Salt Inferred from Small-Scale Brine Inflow Experiments*. SAND92-1911. Albuquerque, NM: Sandia National Laboratories.

Mercer, J.W. 1983. *Geohydrology of the Proposed Waste Isolation Pilot Plant Site, Los Medaños Area, Southeastern New Mexico*. Water-Resources Investigations Report 83-4016. Albuquerque, NM: U.S. Geological Survey.

Morrow, N.R., J.S. Ward, and K.R. Brower. 1986. *Rock Matrix and Fracture Analysis of Flow in Western Tight Gas Sands - 1985 Annual Report*. DOE/MC/21179-2032. Socorro, NM: New Mexico Institute of Mining and Technology, New Mexico Petroleum Recovery Research Center.

Mualem, Y. 1976. "A New Model for Predicting the Hydraulic Conductivity of Unsaturated Porous Media," *Water Resources Research*. Vol. 12, no. 3, 513-522.

Munson, D.E., S.V. Petney, T.L. Christian-Frear, J.R. Ball, R.L. Jones, and C.L. Northrop-Salazar. 1991. *18 W/m² Mockup for Defense High-Level Waste (Rooms A): In Situ Data Report: Vol. II - Thermal Response Gages (February 1985 - June 1990)*. SAND90-2749. Albuquerque, NM: Sandia National Laboratories.

NAS-NRC (National Academy of Sciences-National Research Council). 1957. *The Disposal of Radioactive Waste on Land, Report of the Committee on Waste Disposal of the Division of Earth Sciences*. Publication 519. Washington, DC: National Academy of Sciences - National Research Council.

Nelson, P.P., M. Lopez, K.H. Stokoe II, and C.J. Roblee. 1989. "In Situ Evaluation of Rock Mass Stiffness for Underground Openings Using Surface Wave and Borehole Seismic Methods." *Proceedings, Seventh Annual Workshop on Mine Systems Design and Ground Control, Generic Mineral Technology Center, Virginia Polytechnic Institute*. 35-46. (Copy on file at the Sandia WIPP Central Files, Sandia National Laboratories, Albuquerque, NM.)

Nowak, E.J., D.F. McTigue, and R. Beraun. 1988. *Brine Inflow to WIPP Disposal Rooms: Data, Modeling, and Assessment*. SAND88-0112. Albuquerque, NM: Sandia National Laboratories.

Nowak, E.J., S.J. Finley, and C.L. Howard. 1990. *Implementation of Initial Tests in the Brine Inflow Room (Room Q) of the Waste Isolation Pilot Plant*. SAND90-0611. Albuquerque, NM: Sandia National Laboratories.

Parker, J.C., R.J. Lenhard, and T. Kuppusamy. 1987. "A Parametric Model for Constitutive Properties Governing Multiphase Flow in Porous Media," *Water Resources Research*. Vol. 23, no. 4, 618-624.

Peaceman, D.W. 1977. *Fundamentals of Numerical Reservoir Simulation*. New York, NY: Elsevier.

Pfeifer, M.C., H.T. Andersen, and C.K. Skokan. 1990. "Permanent DC-Resistivity Arrays To Monitor the Development of a Disturbed Rock Zone Around Underground Excavations," *SAGEEP '90, 3rd Symposium on the Application of Geophysics to Engineering and Environmental Problems, Colorado School of Mines, Golden, CO, March 12-15, 1990.* Denver, CO: Society of Engineering & Exploration Geophysicists.

Powers, D.W., S.J. Lambert, S-E. Shaffer, L.R. Hill, and W.D. Weart, eds. 1978. *Geological Characterization Report, Waste Isolation Pilot Plant (WIPP) Site, Southeastern New Mexico.* SAND78-1596. Albuquerque, NM: Sandia National Laboratories. Vols. 1-2.

Powers, D.W., M. Martin, and R.M. Holt. 1988. "Siliciclastic-Rich Units of the Permian Salado Formation, Southeastern New Mexico," *Abstracts with Programs, Geological Society of America, Denver, CO, October 31 - November 3, 1988.* Vol. 20, no. 7, A174.

Reeves, M., G.A. Freeze, V.A. Kelley, J.F. Pickens, D.T. Upton, and P.B. Davies. 1991. *Regional Double-Porosity Solute Transport in the Culebra Dolomite Under Brine-Reservoir-Breach Conditions: An Analysis of Parameter Sensitivity and Importance.* SAND89-7069. Albuquerque, NM: Sandia National Laboratories.

Sandia WIPP Project. 1992. *Preliminary Performance Assessment for the Waste Isolation Pilot Plant, December 1992. Volume 3: Model Parameters.* SAND92-0700/3. Albuquerque, NM: Sandia National Laboratories.

Shinta, A.A., and H. Kazemi. 1993. "Tracer Transport in Characterization of Dual-Porosity Reservoirs," *Reservoir Engineering Proceedings, SPE Annual Technical Conference and Exhibition, Houston, TX, October 3-6, 1993.* SPE 26636. Richardson, TX: Society of Petroleum Engineers. 285-299.

Skokan, C.K., M.C. Pfeifer, G.V. Keller, and H.T. Andersen. 1989. *Studies of Electrical and Electromagnetic Methods for Characterizing Salt Properties at the WIPP Site, New Mexico.* SAND87-7174. Albuquerque, NM: Sandia National Laboratories.

Snow, D.T. 1968. "Rock Fracture Spacings, Openings, and Porosities," *Journal of the Soil Mechanics and Foundations Division, Proceedings of the American Society of Civil Engineers*. Vol. 94, no. SM1, 73-91.

Snow, D.T. 1965. "A Parallel Plate Model of Fractured Permeable Media." Ph.D. dissertation. Berkeley, CA: University of California.

Stormont, J.C., and J.J.K. Daemen. 1991. "Laboratory Study of Gas Permeability Changes in Rock Salt During Deformation," *International Journal of Rock Mechanics and Mining Sciences & Geomechanics Abstracts*. Vol. 29, no. 4, 325-342.

Stormont, J.C., E.W. Peterson, and P.L. Lagus. 1987. *Summary of and Observations About WIPP Facility Horizon Flow Measurements Through 1986.* SAND87-0176. Albuquerque, NM: Sandia National Laboratories.

Stormont, J.C., C.L. Howard, and J.J.K. Daemen. 1991. *In Situ Measurements of Rock Salt Permeability Changes Due to Nearby Excavation*. SAND90-3134. Albuquerque, NM: Sandia National Laboratories.

Truskowski, M.G., and H.T. Andersen. 1993. "Resistivity Changes Over Time Related To Modeled Fluid Flow In Room-Q of the Waste Isolation Pilot Plant," *SAGEEP '93, Symposium on the Application of Geophysics to Engineering and Environmental Problems, San Diego, CA, April 18-22, 1993*. Englewood, CO: Environmental and Engineering Geophysical Society (EEGS). 545-558.

TSC-D'Appolonia. 1983. *Quarterly Geotechnical Field Data Report October 1983*. WIPP-DOE-177. Compiled for the U.S. Department of Energy by TSC-D'Appolonia Consulting Engineers. Albuquerque, NM: U.S. Department of Energy, Waste Isolation Pilot Plant Project Office.

Tyler, L.D., R.V. Matalucci, M.A. Molecke, D.E. Munson, E.J. Nowak, and J.C. Stormont. 1988. *Summary Report for the WIPP Technology Development Program for Isolation of Radioactive Waste*. SAND88-0844. Albuquerque, NM: Sandia National Laboratories.

U.S. DOE (Department of Energy). 1980. *Final Environmental Impact Statement, Waste Isolation Pilot Plant*. DOE/EIS-0026. Washington, DC: U.S. Department of Energy.

U.S. DOE (Department of Energy). 1988. *Geotechnical Field Data and Analysis Report, July 1986 through June 1987.* DOE/WIPP 87-017. Carlsbad, NM: Westinghouse Electric Corporation.

U.S. EPA (Environmental Protection Agency). 1985. "40 CFR Part 191: Environmental Standards for the Management and Disposal of Spent Nuclear Fuel, High-Level and Transuranic Radioactive Wastes; Final Rule," *Federal Register.* Vol. 50, no. 182, 38066-38089.

U.S. EPA (Environmental Protection Agency). 1986. "Land Disposal Restrictions," *Code of Federal Regulations 40, Part 268.* Washington, DC: Superintendent of Documents, U.S. Government Printing Office. (As amended and published in the most recent *Code of Federal Regulations.*)

van Genuchten, M.Th. 1980. "A Closed-Form Equation for Predicting the Hydraulic Conductivity of Unsaturated Soils," *Soil Science Society of America Journal.* Vol. 44, no. 5, 892-898.

van Genuchten, R. 1978. *Calculating the Unsaturated Hydraulic Conductivity with a New Closed-Form Analytical Model.* Research Report 78-WR-08. Princeton, NJ: Princeton University, Department of Civil Engineering.

Van Wylen, G.J., and R.E. Sonntag. 1985. *Fundamentals of Classical Thermodynamics.* 3rd ed. New York, NY: John Wiley & Sons, Inc. 414-415.

Walsh, J.B., and W.F. Brace. 1984. "The Effect of Pressure on Porosity and the Transport Properties of Rock," *Journal of Geophysical Research.* Vol. 89, no. B11, 9425-9431.

Wawersik, W.R., and C.M. Stone. 1985. *Application of Hydraulic Fracturing to Determine Virgin In Situ Stress State Around Waste Isolation Pilot Plant--In Situ Measurements.* SAND85-1776. Albuquerque, NM: Sandia National Laboratories.

Weart, W.D. 1983. *Summary Evaluation of the Waste Isolation Pilot Plant (WIPP) Site Suitability.* SAND83-0450. Albuquerque, NM: Sandia National Laboratories.

Webb, S.W. 1992. *Brine Inflow Sensitivity Study for Waste Isolation Pilot Plant Boreholes: Results of One-Dimensional Simulations*. SAND91-2296. Albuquerque, NM: Sandia National Laboratories.

WIPP PA (Performance Assessment) Department. 1992a. *Preliminary Performance Assessment for the Waste Isolation Pilot Plant, December 1992. Volume 1: Third Comparison with 40 CFR 191, Subpart B*. SAND92-0700/1. Albuquerque, NM: Sandia National Laboratories.

WIPP PA (Performance Assessment) Department. 1992b. *Preliminary Performance Assessment for the Waste Isolation Pilot Plant, December 1992. Volume 2: Technical Basis*. SAND92-0700/2. Albuquerque, NM: Sandia National Laboratories.

WIPP PA (Performance Assessment) Department. 1993a. *Preliminary Performance Assessment for the Waste Isolation Pilot Plant, December 1992. Volume 4: Uncertainty and Sensitivity Analyses for 40 CFR 191, Subpart B*. SAND92-0700/4. Albuquerque, NM: Sandia National Laboratories.

WIPP PA (Performance Assessment) Department. 1993b. *Preliminary Performance Assessment for the Waste Isolation Pilot Plant, December 1992. Volume 5: Uncertainty and Sensitivity Analyses of Gas and Brine Migration for Undisturbed Performance*. SAND92-0700/5. Albuquerque, NM: Sandia National Laboratories.

Witherspoon, P.A., J.S.Y. Wang, K. Iwai, and J.E. Gale. 1980. "Validity of Cubic Law for Fluid Flow in a Deformable Rock Fracture," *Water Resources Research*. Vol. 16, no. 6, 1016-1024.

APPENDIX A:
LINCOLN MEMORANDUM

R.C. Lincoln to P.A. Davis, "Second Draft Performance Measures for the WIPP Systems Prioritization," June 27, 1994. Internal SNL Memorandum.

Distribution w/1 attachment:
6300 D. E. Ellis
6303 W. D. Weart
6305 S. A. Goldstein
6306 A. L. Stevens
6305 N. H. Prindle
6307 F. T. Mendenhall
6307 S. G. Bertram
6308 W. Beyeler
6308 D. Rudeen
6141 R. C. Lincoln
6342 D. R. Anderson
6347 D. R. Schafer
6348 J. T. Holmes
6351 R. E. Thompson
6352 S. E. Sharpton
6115 P. B. Davies
6117 W. R. Wawersik
6119 E. J. Nowak
6121 J. R. Tillerson
6700 P. Brewer
6743 V. Harper-Slaboszewicz
SWCF CO/SP WBS 1.1.7.2

Sandia National Laboratories

date: June 27,1994

Albuquerque, New Mexico 87185

to: P. A. Davis, Org. 6307

from: R. C. Lincoln, Org. 6308

subject: Second Draft Performance Measures for the WIPP System Prioritization

S. Bertram implemented a 6307 review of the draft performance measures defined in my June 20, 1994, memo. After that review she asked that I modify the proposed performance measures. This memo formally transmits the second draft of the WIPP System Prioritization Performance Measures. The major differences are that 1) these performance measures are digital in nature and only indicate compliance or non-compliance, and 2) the post-closure RCRA performance measure averages hazardous constituent concentrations over a smaller region of space and includes both gas and liquid phase transport of hazardous constituents.

Attached to this memo is a draft of Performance Measures for the WIPP System Prioritization. These two performance measures are designed to indicate either compliance or non-compliance for both radionuclide and hazardous constituent post-closure regulatory compliance. The definition of these performance measures specifically excludes any consideration of operational time scale regulatory compliance requirements as a part of the system prioritization effort and also excludes from this effort undisturbed performance related to 40 CFR 191 (specifically the dose requirements of 191.15, Subpart B, and the Environmental Standards for Ground-Water Protection of Subpart C).

Please review the draft performance measures and arrange for review by CAO and WID. We will continue developing the system prioritization analysis using these draft performance measures. Comments received prior to July 9, 1994, will have the potential to impact the September 30, 1994, analysis. It will be very difficult, if not impossible, to change the performance measures after July 9 and meet the September milestone. If the performance measures do not represent the regulatory requirement the system prioritization will result in a flawed decision matrix being the basis for potential CAO decisions. Therefore, it is critical that CAO, WID and EPA review the performance measures in a timely manner.

Note that implementing the post-closure RCRA performance measure may require a health based level (for soil) for any hazardous constituent identified in the WIPP inventory. This may require implementing the EPA procedure for hazardous constituents not included in 55 FR 30865 through 55 FR 30868. We need to identify what organization (other than 6308) is responsible for implementing this procedure consistent with the system prioritization schedule.

PERFORMANCE MEASURES FOR THE WIPP SYSTEM PRIORITIZATION

Implementation of the WIPP system prioritization requires the definition of a performance measure for each regulatory requirement that will be addressed by the analysis. These definitions of performance measures assume that the regulatory requirements to be addressed by the WIPP system prioritization will be the radionuclide containment requirement of 40 CFR 191, Subpart B, section 191.13(a), and the hazardous constituent concentration requirement of 40CFR268.6 with health based levels for soil as defined in 55 FR 30865 through 55 FR 30868.

The scope of the system prioritization effort has been defined as post-closure regulatory compliance. Based on this scope definition operational time scale RCRA requirements and 40 CFR 191, Subpart A, requirements will not be included in the analysis. The focusing of system prioritization on the post-closure radionuclide containment portion of 40 CFR 191 is based on the results of prior modeling of undisturbed performance. This modeling has indicated that radionuclide releases without human intrusion are very small. Based on these prior modeling results the system prioritization analysis will not address 40 CFR 191, Subpart B, section 191.15 (Individual protection requirements) and 40 CFR 191, Subpart C (Environmental Standards for Ground-Water Protection).

RADIONUCLIDE CONTAINMENT PERFORMANCE MEASURE

Radionuclide containment regulatory compliance will be assumed when the mean CCDF meets the requirements of 40 CFR 191, Subpart B, section 191.13 (a).

HAZARDOUS CONSTITUENT CONCENTRATION PERFORMANCE MEASURE

Post-closure hazardous constituent concentration regulatory compliance will be assumed when the hazardous constituent concentration calculated at the unit boundary is less than the health based level for soil (as defined in 55 FR 30865 through 30868) for each hazardous constituent. Hazardous constituents transported to the unit boundary by gas will be compared with the health based levels. The anhydrite interbed pathway will use from the top of marker bed 138 to the bottom of marker bed 139 and gas available porosity for concentration calculations. The shaft pathway will use the model shaft diameter and the gas available porosity for concentration calculations. The focusing of system prioritization on hazardous constituent transport by the gas phase is based on the results of prior modeling of undisturbed performance. This modeling has indicated that contaminated brine does not reach the unit boundary. The hazardous constituent concentrations will be calculated from the larger of the mean or median of the multiple deterministic concentration calculations to include the effect of parameter uncertainty.

APPENDIX B:
93/94 PA MEMORANDUM

Dan Stoelzel, Palmer Vaughn, Jim Bean, and Jim Schreiber to Rip Anderson, "Summary of 1993-94 Preliminary Undisturbed Repository Calculations," February 21, 1994. Internal SNL Memorandum.

date: February 21, 1994

to: Rip Anderson

from: Dan Stoelzel, Palmer Vaughn, Jim Bean, Jim Schreiber

subject: Summary of 1993-94 WIPP Preliminary Undisturbed Repository Calculations

1994 Performance of Untreated Wastes for the Undisturbed Repository: Comparison to 1992 PA. Preliminary Results & Sampled Consequences vs. Mean / Median Calculation

1. Model Conceptualization:
The model set-up for the 1994 calculations is summarized in Table 1. The grid layout is essentially unchanged from that used in the 1992 calculations (see Figures 1, 2, and 3), with the exception being an increase in stratigraphy from the Castile to the surface (same as for the intrusion scenarios). This did not affect gas migration to the surface, since the gas stopped at the lower shaft seal for all the calculations. In addition, the waste region is divided into two areas, labeled Repository and Panel. The fluid and material parameters for the two waste areas are exactly the same, the only difference being that the Panel volume represents one excavated panel (the North Equivalent Panel), and the Repository volume contains the waste for the remaining panels in the proposed site. The "Entire Repository" is the Panel and the Repository together. This conceptualization of the waste region was not done for previous PA's and should provide a better representation of fluid flow within the entire repository.

2. Description of the Input Parameters and Changes from the 1992 Model:
Tables 2 through 6 describe the input variables used for the 50 calculations performed for this study. Twenty three of the variables were sampled over a specified range. One additional calculation was made (the "Example Calculation"), in which the input variables were determined by a "best guess" within the distribution of values for each parameter: either the median (for rock properties) or the mean (for the remaining parameters such as corrosion rates and waste inventory). This calculation was made to show the non-linear relationship that exists between the input parameters and the model consequences after 10,000 years. As expected, the results from the "example" run did not match the mean or median of the consequences from the 50 runs with sampled input parameters. Major changes from the 1992 PA models are described below:

A. Fracturing of the anhydrite layers is approximated based on pressure dependent alterations to the rock compressibility, permeability and porosity of the affected layers. The intact compressibility, permeability and porosity are increased when the brine pressure is above the fracture pressure of 12.6 MPa to a maximum value calculated at 15.0 MPa (the alteration zone). The full fracture permeability and porosity (upper limit at 15.0 MPa) are shown on Table 5. The fracture model was explained in a previous memo from Sam Key (RE/SPEC) dated 3-Sep-1993. Essentially, anhydrite compressibility is increased linearly to a maximum value, based on the increase in pore pressure due to gas generation. Porosity (ϕ) is related to compressibility, and absolute permeability (k_{abs}) is related to porosity, hence, ϕ and k_{abs} also increase within the anhydrite layers as pressure increases. This is shown in Figures 4 and 5. The methodology adopted for this model was reviewed by the Fracture Expert Group, and deemed reasonable for a "first effort". It was also recognized by the group that experimental data is needed to support the model or any alternative.

B. Permeability and porosity data were provided by Rick Beauheim and Susan Howarth. The anhydrite intact (absolute) permeability was modified for the 1994 assessment. The median value was increased slightly from 5.0×10^{-20} m^2 to 6.3×10^{-20} m^2, with the sample range reduced from five orders of magnitude to three orders of magnitude, mainly at the high end. This is in contrast to the 1992 range of permeabilities, which were arbitrarily extended to 1×10^{-16} m^2 to "approximate" fracturing in the anhydrite. The anhydrite median porosity was increased from 1.0% in 1992 to 1.4% in the current calculations. These changes, along with the fracture model, resulted in an overall increase in gas migration distances in the anhydrite, and a decrease in repository pressures.

C. The permeability of the lower shaft seal (<200 years) was changed from a sampled range of 1×10^{-19} m^2 - 5×10^{-16} m^2 to a fixed value of 8×10^{-18} m^2, as recommended by Ray Finley. This greatly

reduced gas migration up the shaft, and diverted gas to MB 138 instead. For the 1994 undisturbed calculations, gas flow did not go past the top of the Salado Formation.

D. The disturbed rock zone (DRZ) porosity was changed from a sampled value designed to be slightly greater than the halite porosity (although not to exceed the maximum allowable halite porosity of 0.1% to 6.0%); to a fixed value of 1.5%. This had the effect of reducing the available gas storage in the DRZ. These changes were made as a result of recommendations by Dept. 6115 and others.

E. The values for initial liquid (brine) saturation in the waste were reduced from a sampled range of 0% - 14% (7.0% median) to 0.04% - 5.2% with a 0.44% median. These values are based on a Westinghouse analysis of free liquid content in EG&G / INEL waste, and a study done by Barry Butcher to estimate the brine content in the backfill and residual liquid in the cellulosics. This new range lowered the volumes of gas generated, since there was less initial brine available for reaction.

F. The gas generation submodel parameters were also changed (see Table 5). New estimates were provided by Larry Brush. The range of values for inundated corrosion rate was increased significantly (from a maximum of 2 mol/drum/year to 150 mol/drum/year), and the range for humid corrosion rate was greatly reduced (with a median value of zero). This caused an increase in gas generation for wet environments, and lower gas generation in humid environments.

3. Preliminary Results:

A. Pressures in the Waste: Figure 6 shows a time plot of the volume averaged Panel pressures for all 50 calculations. The Repository pressures are nearly identical, and are therefore not shown. The affects of the fracture model and higher anhydrite permeability are seen as the gas is allowed to flow more easily into the anhydrite and most of the pressures peak below the fracture upper pressure limit of 15.0 MPa. The pressure behaved differently in the 1992 calculations, in which half of the realizations remained above the 14.8 MPa lithostatic pressure to 10,000 years, many in the 20 MPa range. For the current calculations, the average pressure peaks at 14.7 MPa and declines to 13.5 MPa after 10,000 years, which is much closer to the far-field pressure (12.5 MPa) than was reached by the 1992 calculations. For one third of the current realizations, pressures reach levels higher than lithostatic, usually within the first 1,500 years, and then decline rapidly. The reason for this is still under investigation, but is probably a result of the interaction between the fracturing model and the two phase flow behavior within the DRZ and anhydrite layers. It is possible that the effective permeability for gas (as defined by the relative permeability model used for each consequence) may be restricting the gas flow leaving the repository at low gas saturations. Figure 7 shows a histogram of the Panel pressures at 10,000 years. The majority of the pressures ended in the 12 to 14 MPa range, whereas the 1992 pressures ended in a fairly even distribution from 6 to 22 MPa. The pressure resulting from the Example Calculation peaked slightly lower than the average of the consequences, (14.0 MPa compared to 14.7 MPa), but was very close to the mean after 10,000 years.

B. Brine Saturation in the Waste: Brine saturation is important, as it is needed for the corrosion and biodegradation processes in gas generation. Figure 8 shows brine saturation behavior over time for the Panel (the Repository saturations were nearly identical). This pattern is similar to the one seen in the 1992 calculations, with a rapid, early increase in saturation as the reduction in porosity due to creep closure results in an increase in brine saturation, and a small amount of brine flows in from the DRZ and anhydrite layers. Brine saturation then drops rapidly as it is consumed in the corrosion process. The brine saturations in the waste remain higher through time for the 1992 calculations due to higher initial brine saturations, and increased brine inflow from the surrounding DRZ and anhydrite layers. Note that the Example Calculation brine saturation remains fairly close to the median of the 50 consequences.

C. Brine Flow in the Waste: As in the 1992 calculations, net brine flow was generally *into* the Repository; however, the volume of brine inflow was less for the 1994 runs. In the 1992 calculations, several realizations exceeded 10,000 m^3 brine inflow, whereas the 1994 runs had only a few exceeding 5,000 m^3 brine inflow to the Repository (see Figure 9). This discrepancy may be in part due to the lower DRZ porosity in the 1994 model, which reduced the available brine volume in the rock surrounding the waste region, as well as the lower permeability in the intact anhydrites, which are the major pathways

for brine inflow. The updated representation of the undisturbed model may also have an influence on fluid flow, especially that of the brine. In the 1992 mesh the waste is one continuous region, whereas in the 1994 conceptualization, the waste region is split into two distinct areas: the Panel and the Repository, separated by a panel seal. For the majority of the calculations, the net brine flow was *out of* the Panel (Figures 10, 11, and 12). As in the 1992 calculation, the main pathway for brine flow is in the anhydrite layers. The brine flowing into the waste region most likely originates from the South, since the brine from the Northern layers has a greater distance to travel to reach the waste and must pass through a lower permeability backfill and seal region. Brine flowing from the South is partially diverted to the Repository on its way to the Panel. This is illustrated in Figure 13, which shows the brine inflow to the Panel for all realizations. The brine volumes flowing into the Panel were extremely low, with the average of the 50 consequences being 152 m^3 and the median 15 m^3. Hence, fluid flow through the system is influenced by the conceptualization of the repository, especially on how the panels are represented within the waste region. For the Example Calculation, the net brine flow for the Repository was 1,890 m^3 inward, which fell between the mean and median values of the 50 consequences, whereas the Example net brine flow for the Panel, 224 m^3 outward, was somewhat less than the mean and median values. In addition figure 13 shows that the brine flowing into the Panel for the Example Calculation (7 m^3) is considerably lower than the mean and median of the consequences.

D. Gas Generation: Changes in the gas generation model, along with a reduction in available brine for reaction, resulted in less gas generation than in the 1992 calculations. Figure 14 shows total gas generated over time for the Entire Repository. At 10,000 years, cumulative gas produced ranged from 146 to 1,107 mol/drum, or 2.9×10^6 m^3 to 22.0×10^6 m^3, compared to 160 to 1600 mol/drum, (3.0×10^6 to 32.0×10^6 m^3) for the 1992 PA (all gas volumes are measured at reference conditions of 300.15 K and 101.325 kPa). For comparison, the range of gas that could theoretically be generated if all reactants were consumed, based on maximum and minimum inventory and stoichiometry, would be 860 to 1940 mol/drum (17.1×10^6 m^3 to 38.6×10^6 m^3). The gas generated as a result of the corrosion process is shown in Figure 15. Two distinct patterns are evident. At high corrosion rates, gas production rises rapidly until the available brine is consumed, at which point the gas generation either stops or slows down dramatically. The rapid gas generation causes a steep increase in repository pressure above the far-field pore pressure of 12.5 MPa, which restricts brine flow into the repository to limit reaction even more. The other major trend is a slow, steady increase in gas generation. Because the repository pressure does not rise as rapidly in these scenarios, it is possible to have a steady influx of brine. Figure 16 shows iron content in the Panel over time (similar curves were observed for iron content in the Repository). Figure 17 is a histogram of the iron remaining at 10,000 years. Note that none of the calculations resulted in 100% iron consumption, unlike the 1992 results, in which 26% of the scenarios resulted in complete iron consumption. Gas production resulting from biodegradation also follows two distinct trends (Figure 18). On average, the biodegradation rates are higher than the corrosion rates, hence, about 50% of the scenarios resulted in 100% consumption of the cellulosics (Figures 19 and 20). Because there was a smaller inventory of cellulosics than metals, the volume of gas produced by biodegradation was about half of that resulting from corrosion. The total gas generated in the Example Problem closely matched the median value of gas generation for the 50 consequences. However, the Example Problem was lower in gas resulting from corrosion, and higher in gas resulting from biodegradation than the mean and median of the 50 consequences.

E. Gas Migration: Table 7 summarizes gas migration distances in each of the anhydrite layers for all 50 realizations and the shaft. The maximum distance reached by the gas within each anhydrite layer was determined by adding together the x-dimensions of the grid blocks containing gas leading away from the edge of the repository. The distance reached in the farthest most grid block containing gas was determined by proportioning the x-dimension of that grid block by its S_{gmax} / S_{gr} ratio. Because of the rectangular flaring concept used to describe the geometry of the anhydrite layers, the pore volumes increase in the grid cells leading away from the repository (note the Δx and Δz dimensions in Figures 3, 4, and 5). Therefore the coarseness of the mesh around the Land Withdrawal Boundary (LWB) affects the calculation of the gas migration distances to some degree. It is planned to run a set of calculations in a model with a finer mesh leading away from the repository to improve the resolution of the migration distances. For the current calculations, eighteen of the fifty realizations (36%) had gas reach the LWB at 2,400 meters. Gas migration distance was also highly dependent on the relative-permeability sub-model used to determine two phase flow, as well as the permeability and porosity

changes resulting from the fracture model. Approximately one third (16 out of 50) of the scenarios used the Van Genuchten / Parker (VG/P) submodel, and the remaining two thirds used the Brooks-Corey (B-C) relationship to determine relative permeability. Each of the models requires two key parameters to determine the shape of the relative permeability curves: a residual brine saturation (S_{br}) and a pore size distribution parameter (λ). In addition, the Brooks-Corey model requires a residual gas saturation (S_{gr}). All three of these parameters were sampled to create fifty different relative permeability curves. Figures 21 and 22 show the relative permeability curves used for realization #6, which uses the VG/P model, and realization #16, which uses the B-C model. The importance of S_{gr} becomes obvious when comparing these two models. For the VG/P curves, gas is mobile as soon as it enters the grid block (the k_{rg} curve in Figure 21). For the B-C model, gas must first exceed S_{gr} before it can move through the grid block (compare the k_{rg} curve in Figure 22), creating gas storage proportional to (grid block pore volume) x S_{gr} for each grid block within the anhydrite layers. This is why 14 of the 16 realizations using the VG/P model had gas reach the LWB since the gas was able to move freely through the layers, even at low gas saturations. Only 4 of the 34 realizations using the B-C model reached the LWB, as the gas mobility was restricted by the residual gas storage inherent in the relative permeability model. Note that the four B-C calculations (realizations 17, 18, 27, and 37) that reached the LWB had relatively low residual gas saturations (< 10%), meaning lower gas storage. Similarly, the increase in anhydrite permeability due to the fracture flow model assisted flow out of the repository, offsetting the increase in gas storage resulting from higher fracture porosities. It would appear that the two-phase flow properties, specifically the permeability changes due to the fracture model and relative permeability models, have a greater impact on gas migration distance than do the other sampled properties such as gas generation (i.e. corrosion rates) and porosities. Many of the realizations in which large amounts of gas were generated have relatively short migration distances due to their high residual gas saturations. Because of the fracture model, at least half of the calculations had gas volumes of 1×10^6 m^3 or more escape the repository into the anhydrite layers, but very few of those had gas make it to the LWB due to their mobility as defined by their fluid's relative permeabilities. This is illustrated by figures 23, 24, and 25 for Anhydrite A&B South. Of the top six realizations with gas escaping the repository, only one (realization #6) had significant amounts of gas escape to the LWB. A similar pattern was seen for the other anhydrite layers. These gas migration results differ significantly from the 1992 calculations. Only 6 out of 70 scenarios (9%) had gas reach the LWB, in spite of the larger amounts of gas generated. Gas migration up the shaft was insignificant (Figure 26) compared to the 1992 PA. The gas that may have otherwise escaped up the shaft appears to have been diverted laterally into MB 138, as gas migration occurred there (see Table 7), where it had not been apparent in the 1992 PA. The maximum migration distance reached for the Example Problem was 866 meters from the repository edge in Anhydrite A&B South. This was significantly less than the mean and median distances of the 50 consequences for that layer. Once again, this illustrates the extreme non-linearity of the system, and the value of the Monte-Carlo sampling method when experimental input data is unavailable. It should be noted that the effects of capillarity are not accounted for in this model due to lack of capillary pressure data. The gas (and brine) migration distances may change significantly if capillary pressure were added to the model.

4. Conclusions:

A. For the 1994 undisturbed PA, gas migration to the Land Withdrawal Boundary is influenced by fluid flow parameters such as relative permeability, as well as altered rock properties caused by the fracturing model.

B. The incorporation of a fracture approximation sub-model played a major role in reducing repository pressures and allowing more gas to escape.

C. The reduced lower shaft seal permeability effectively stopped gas flow through the shaft to the Culebra, but in diverting the gas away from the shaft, an increase in lateral migration to MB 138 resulted.

D. Using a mean or median value for input parameters in lieu of accurate experimental data may lead to significant inaccuracies in model results when compared to the statistical findings (maximum, minimum, mean, median, etc.) resulting from Monte Carlo uncertainty analysis, due to the non-linearities inherent in the system.

Table 1. Summary of Conceptual Models Associated with Repository and Salado Fluid Flow in Performance Assessment.

Geometry/ Stratigraphy (PA)	Fluid Flow and Storage in Host Rock	Repository Processes	Seal/Shaft Treatment	Multi-Phase, Porous Media Flow
• Repository with DRZ, Salado to surface, three anhydrite interbeds	• Intact halite and anhydrite - Darcy flow model • DRZ (P. Davies) - provide communication through enhanced permeability only • Altered anhydrite (Fracture Expert Group, R. Beauheim) - rock compressibility increases with pore pressure and is reflected in permeability and porosity changes	• Disposal room consolidation (B. Butcher) - pressure based porosity surface • Gas generation - linear correlation/ average stoichiometry model (P. Davies) - corrosion of Ferrous Metals; biodegradation of Cellulosics (L. Brush)	• Hydrologic properties specified in two time periods (panel and shaft) (J. Tillerson)	• Standard assumptions common in multi-phase flow literature (J. Bear) • Two-phase behavior based on literature values (P. Davies)

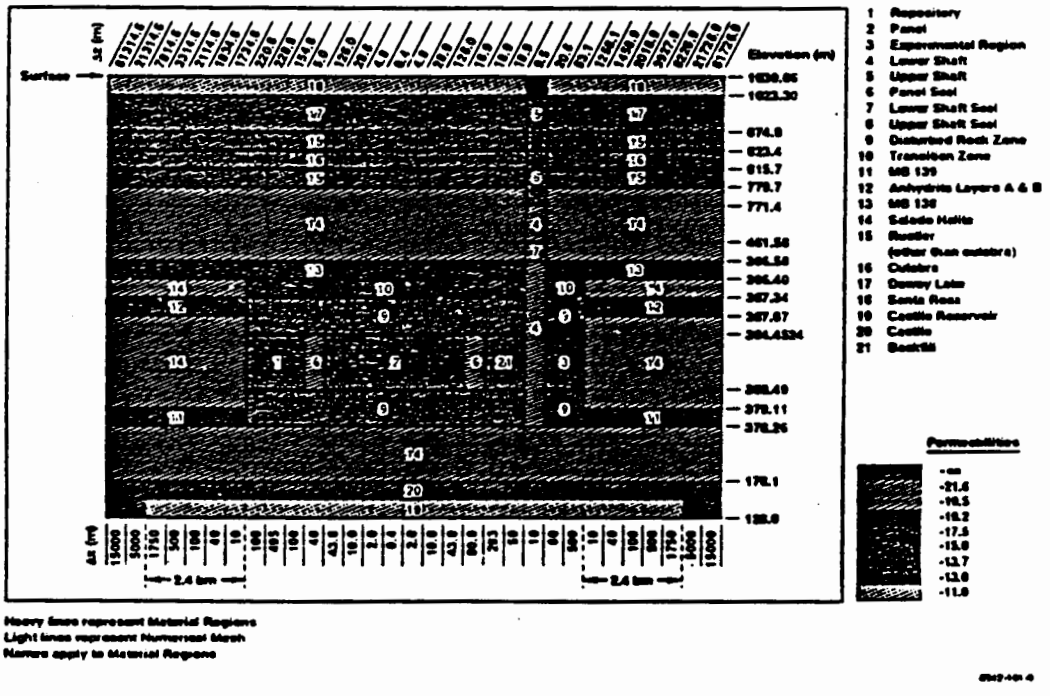

Figure 1. Material Permeabilities for 1994 Undisturbed Repository Simulations.

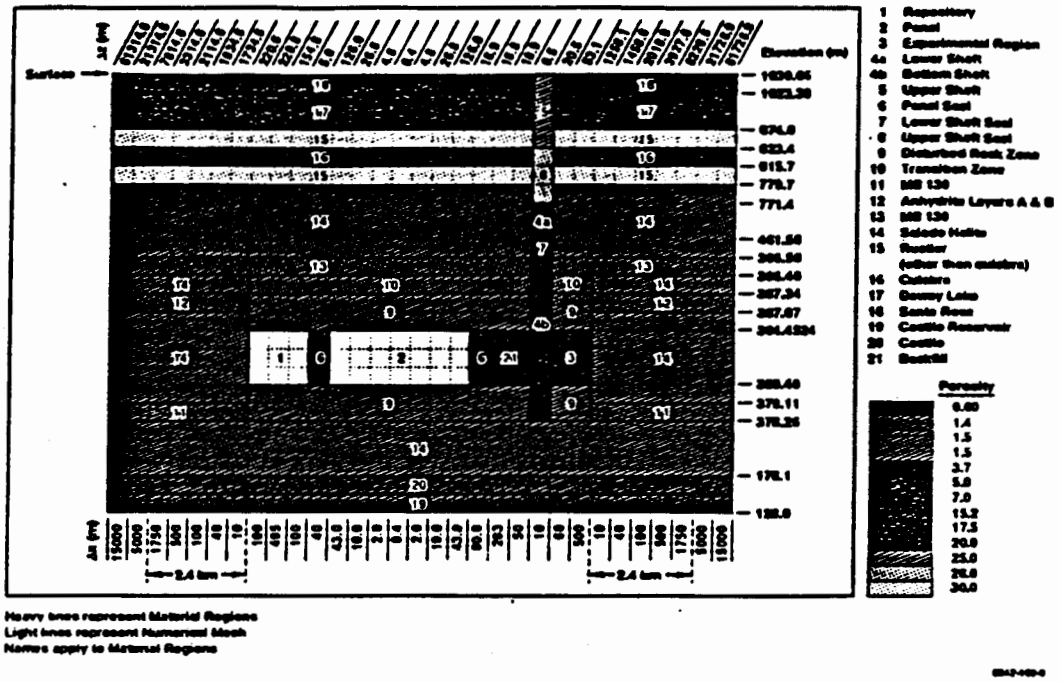

Figure 2. Material Porosity for 1994 Undisturbed Repository Simulations.

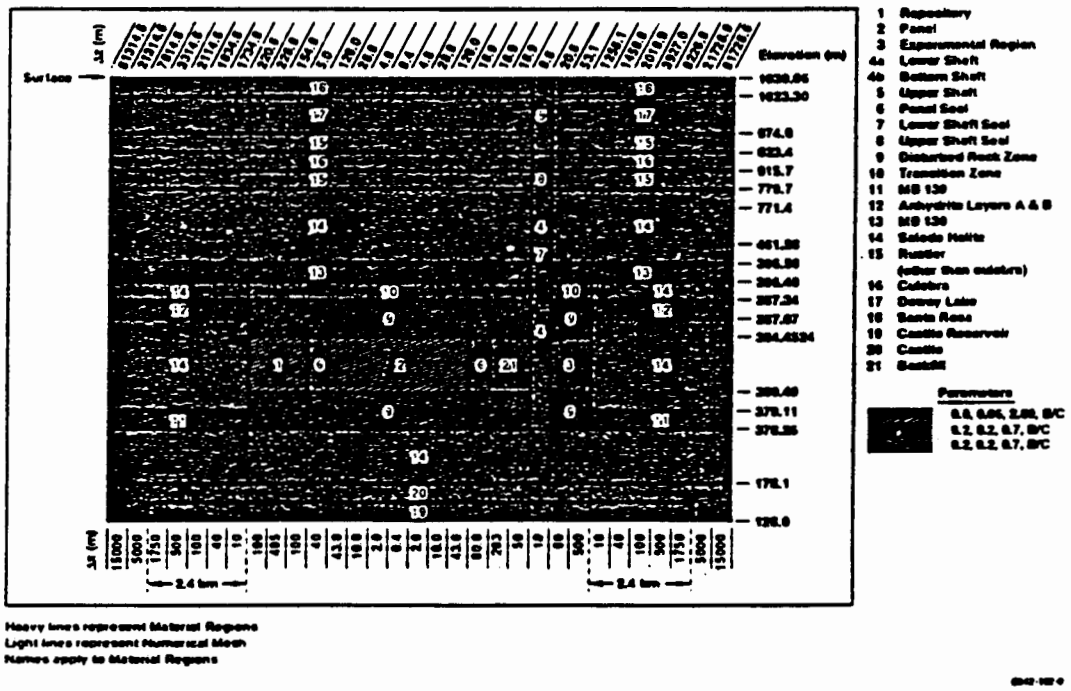

Figure 3. Two Phase Flow Parameters for 1994 Undisturbed Simulations.

Table 2. Material Permeabilities for 1994 Undisturbed Repository Simulations.

Material Name	Time Period Other Than >0 yr	Sampled	Log (Permeability) [Log (m^2)] Range Minimum	Maximum	Example Calculation
Impermeable		N	--	--	-∞
Halite		Y	-22.4	-20.2	-21.6
Panel Seals Lower Shaft Lower Shaft Seal	 (>200 yr) (>200 yr)	Y	-21.0	-18.0	-19.5
Anhydrite A & B MB138 MB139 Transition Zone		Y	-20.0	-18.0	-19.2
Rustler (other than Culebra)		N	--	--	-17.5
DRZ Experimental Backfill Bottom Shaft Dewey Lake Red Beds		N	--	--	-15.0
Culebra		N	--	--	-13.7
Waste Disposal Region Upper Shaft Upper Shaft Seal		N	--	--	-13.0
Castile Brine Pocket Santa Rosa		N	--	--	-11.0
Lower Shaft	(<200 yr)	Y	-19.0	-15.0	-17.0
Lower Shaft Seal	(<200 yr)	N	--	--	-17.1

Table 3. Material Porosities for 1994 Undisturbed Repository Simulations.

Material Name	Sampled	Range		Porosity [% of Material Volume]		
		Minimum	Maximum	Mean	Median	Example
Castile	N	–	–	0.55	0.50	0.60
Anhydrite A & B MB138 MB139	Y	0.4	2.7	1.4	1.4	1.4
Halite Transition	N	–	–	1.5	1.0	1.5
DRZ	N	–	–	1.0	1.5	1.5
Experimental; Backfill Bottom Shaft	Y	1.0	7.5	3.7	3.7	3.7
Power Shaft Lower Shaft Seal	N	–	–	5.0	5.0	5.0
Panel Seal	N	–	–	7.0	7.0	7.0
Culebra	Y	9.5	25.2	15.2	15.2	15.2
Santa Rosa	N	–	–	17.5	13.0	17.5
Dewey Lake	N	–	–	20.0	20.0	20.0
Upper Shaft	N	–	–	25.0	25.0	25.0
Upper Shaft Seal	N	–	–	28.0	28.0	28.0
Rustler (not Culebra)	N	–	–	30.0	30.0	30.0

Table 4. Two Phase Flow Parameters for 1994 Undisturbed Simulations.

Material Region	Parameter Name	Sampled/ Fixed	Range Minimum	Range Maximum	Mean	Median	Example
Halite	Residual Gas Saturation	F	–	–	0.2	0.2	0.2
Transition	Residual Brine Saturation	F	–	–	0.2	0.2	0.2
Culebra	Pore Distribution Parameter	F	–	–	5.1	0.7	0.7
Rest of Rustler	Sub-Model	F	–	–	B/C	B/C	B/C
Dewey Lake							
Santa Rosa							
Panel Seals							
Shaft Seals							
Shaft Fill							
Anhydrite A & B	Residual Gas Saturation	S	0	0.4	0.2	0.2	0.2
MB138	Residual Brine Saturation	S	0	0.4	0.2	0.2	0.2
MB139	Pore Distribution Parameter	S			5.1	0.7	0.7
DRZ	Sub-Model	S	B/C	VG/P	B/C	B/C	B/C
Waste Disposal Area	Residual Gas Saturation	F	–	–	0.0	0.0	0.0
	Residual Brine Saturation	F	–	–	0.06	0.06	0.06
	Pore Distribution Parameter	F	–	–	2.89	2.89	2.89
	Sub-Model	F	–	–	B/C	B/C	B/C

Notes
Threshold Displacement Pressure Correlated to Permeability Except in Anhydrite.
Threshold Displacement Pressure of Anhydrite is Assumed to be Zero.

Table 5. Altered Anhydrite Flow Parameters.

Name	Sampled/ Fixed	Range Minimum	Range Maximum	Mean	Median	Example
Log (Full Fracture Permeability limit) [log (m^2)]	S	-9	-13	-11	-11	-11
Full Fracture Porosity limit [% volume]	F	–	–	.10	.10	.10

Table 6. Gas Generation Parameters.

Name	Sampled/ Fixed	Range Minimum	Range Maximum	Mean	Median	Example
Initial Brine Saturation (% void) In Waste Disposal Area	S	0.03	5.16	2.6	0.36	0.36
Corrosion Rates (mol/drum/yr)						
Humid	S	0.0	0.096	3.8×10^{-3}	0.0	0.0 Median
Inundated	S	0.0	150.0	30.6	0.6	0.6 Median
Biodegradation Rates (mol/drum/yr)						
Humid	S	0.0	1.0	0.18	0.1	0.1 Median
Inundated	S	0.0	5.0	1.8	1.0	1.0 Median
Gas Stoichiometry (mol gas/mol reactant)						
Corrosion	S	1.0	1.33	1.17	1.17	1.17 Median
Biodegradation	S	0.0	1.67	.835	.835	.835 Median
Inventory (Volume Fraction)						
Metals	S	.321	.521	.421	.421	.421 Median
Cellulose	S	.272	.472	.372	.372	.372 Median

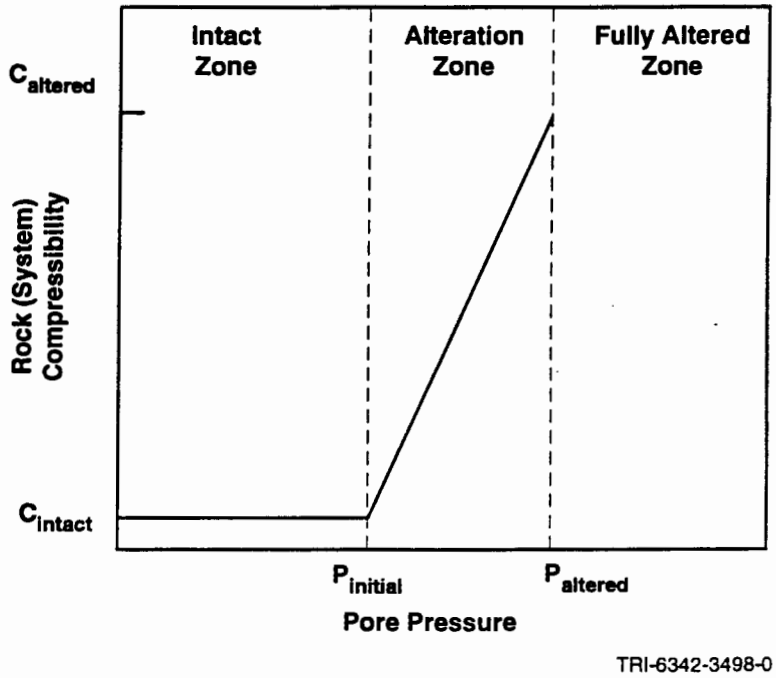

Figure 4. Compressibility Dependencies on Pore Pressure.

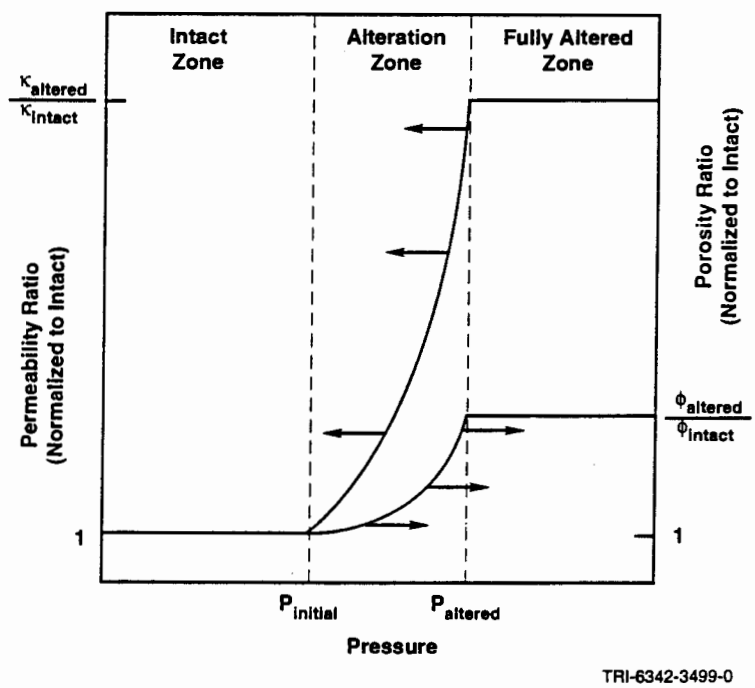

Figure 5. Permeability and Porosity Dependencies on Pore Pressure.

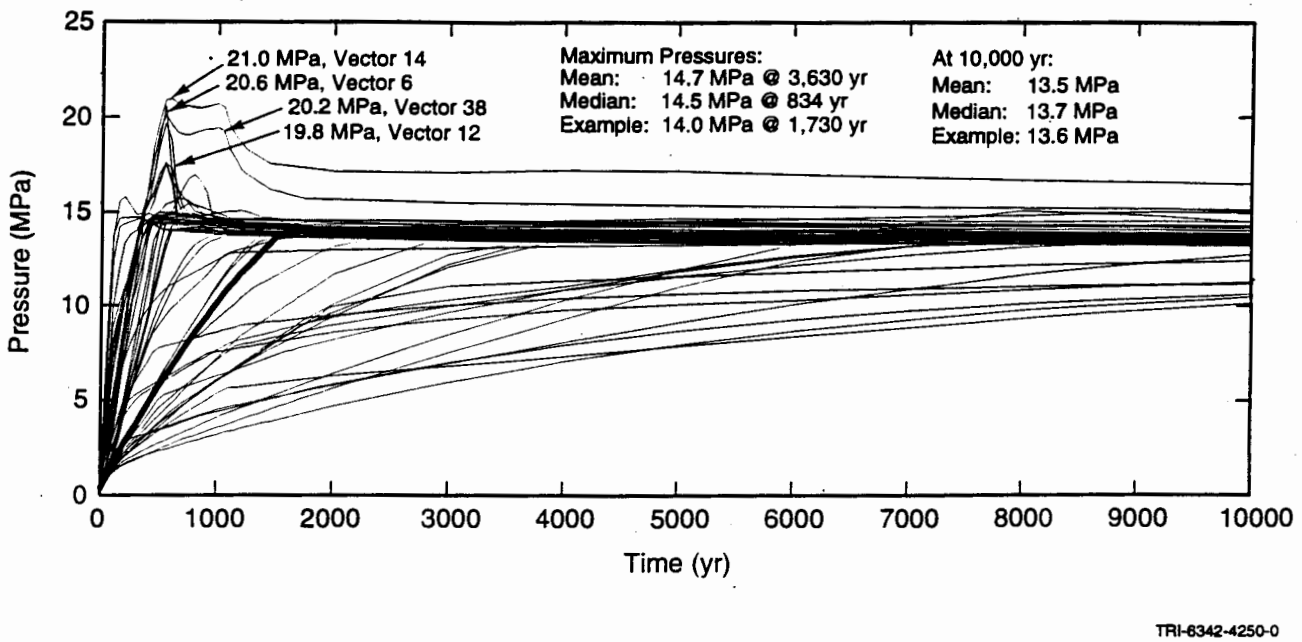

TRI-6342-4250-0

Figure 6. Volume Average Pressure in the Panel.

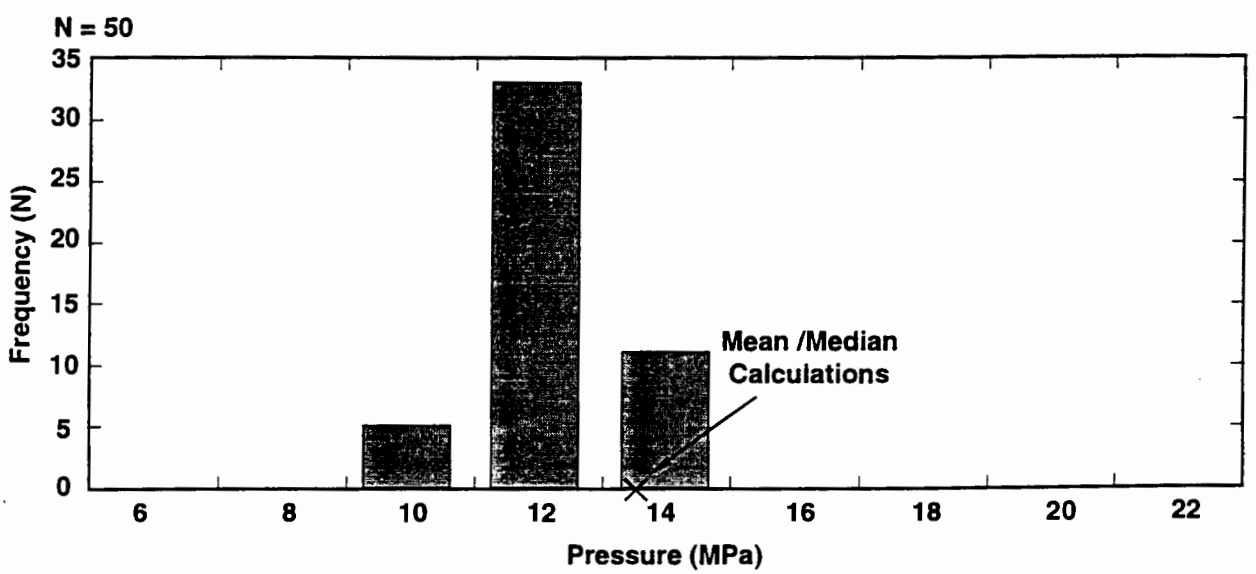

TRI-6342-4251-0

Figure 7. Volume Average Panel Pressure at 10,000 yr.

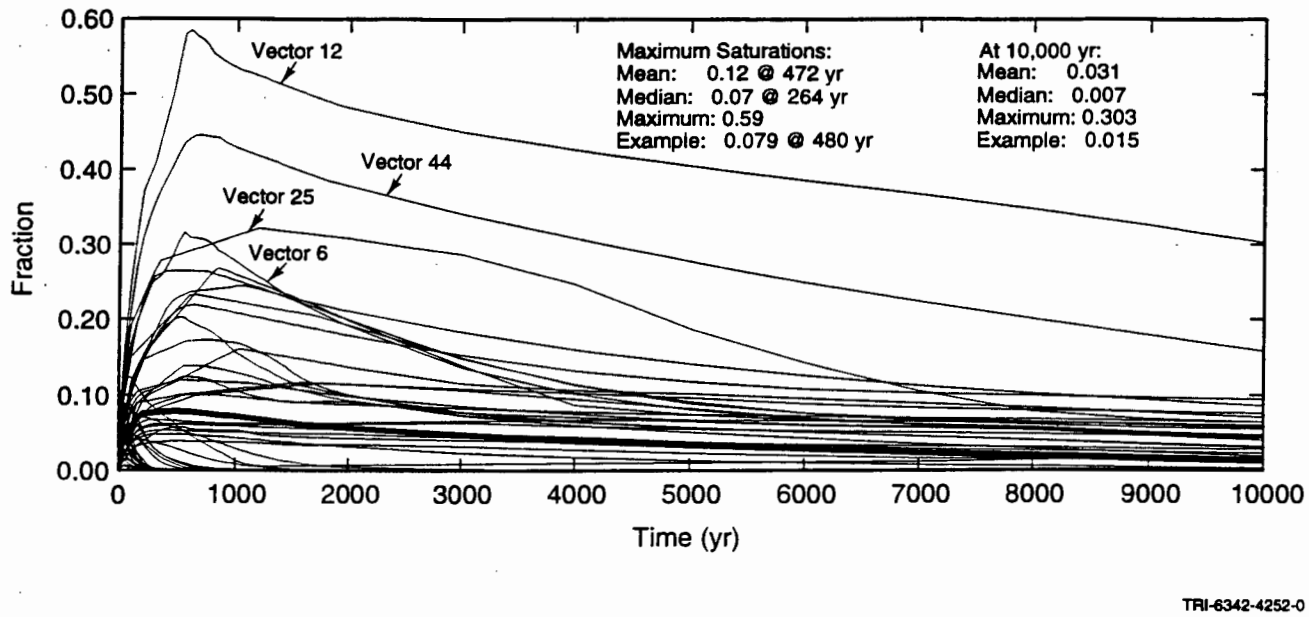

Figure 8. Volume Average Brine Saturation in the Panel.

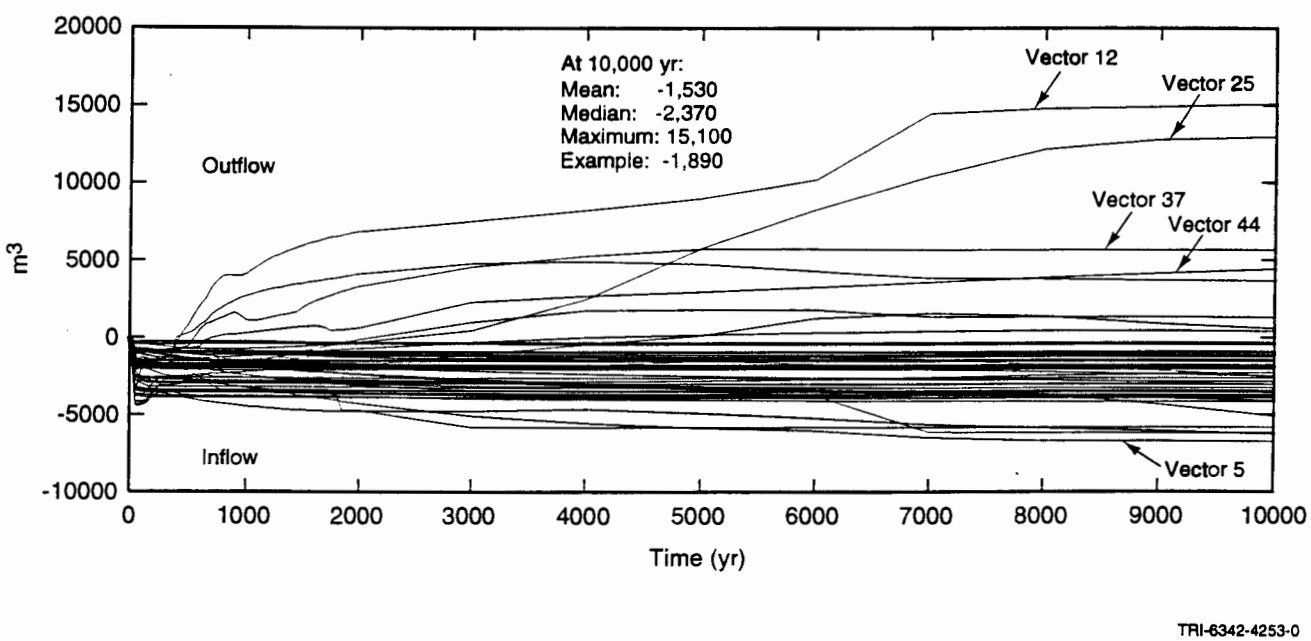

Figure 9. Net Brine Flow Out of (or Into) the Repository.

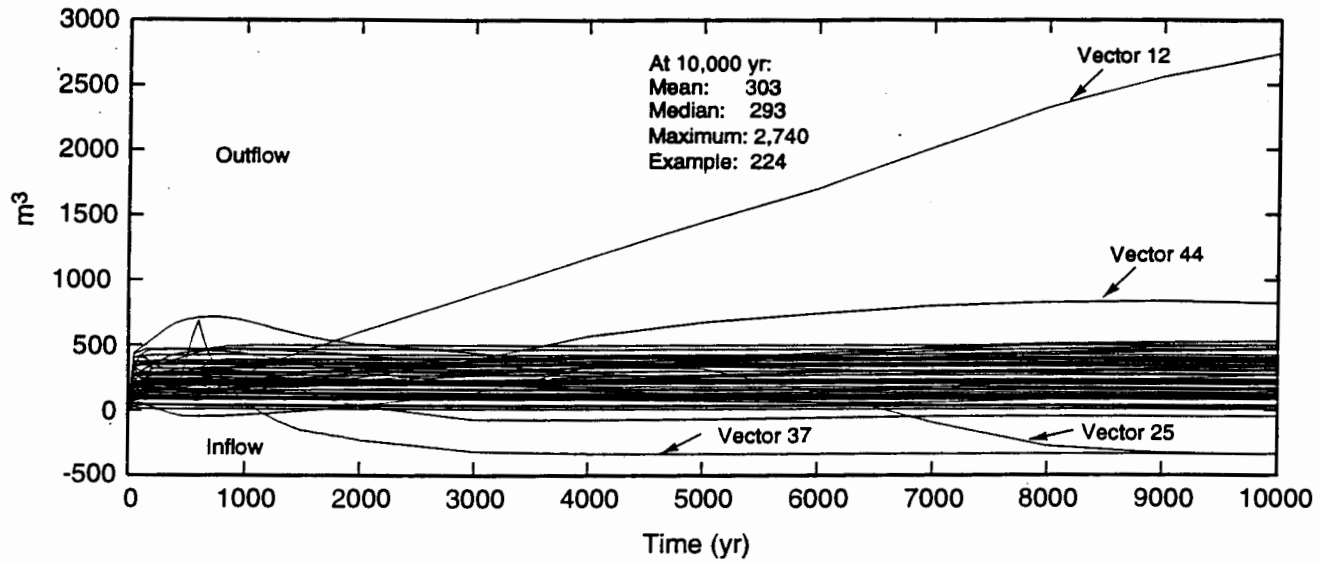

Figure 10. Net Brine Flow Out of (or Into) the Panel.

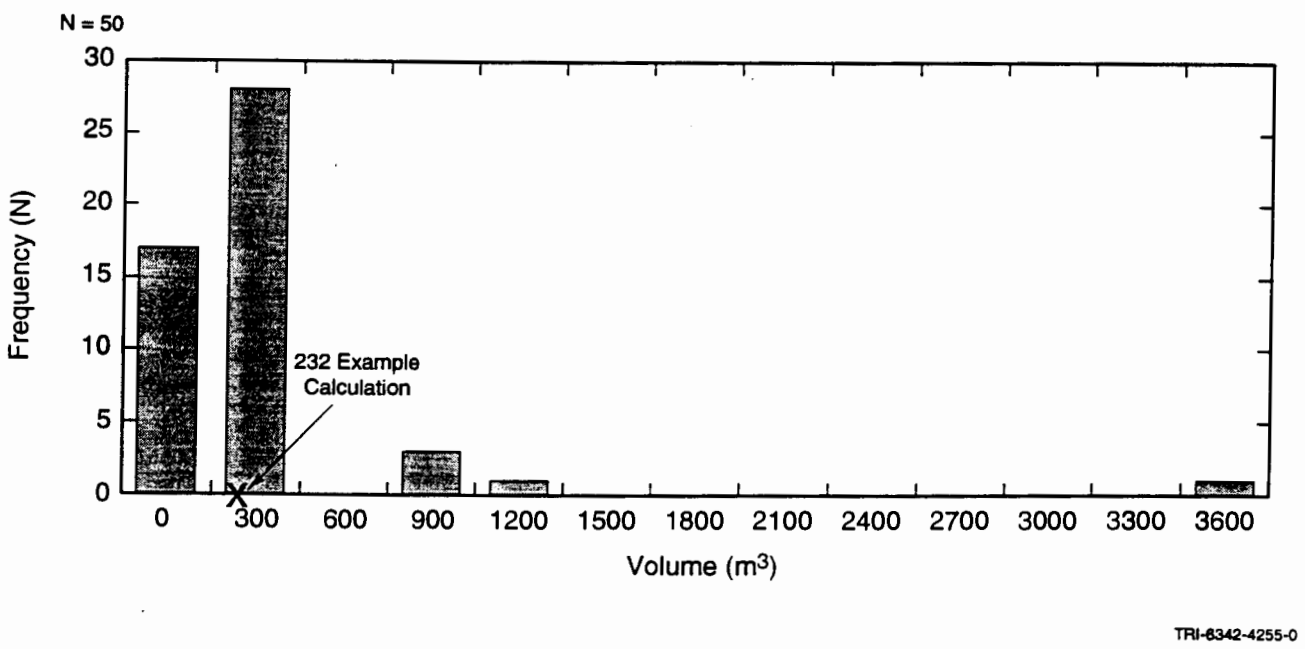

Figure 11. Brine Outflow from Panel After 10,000 yr.

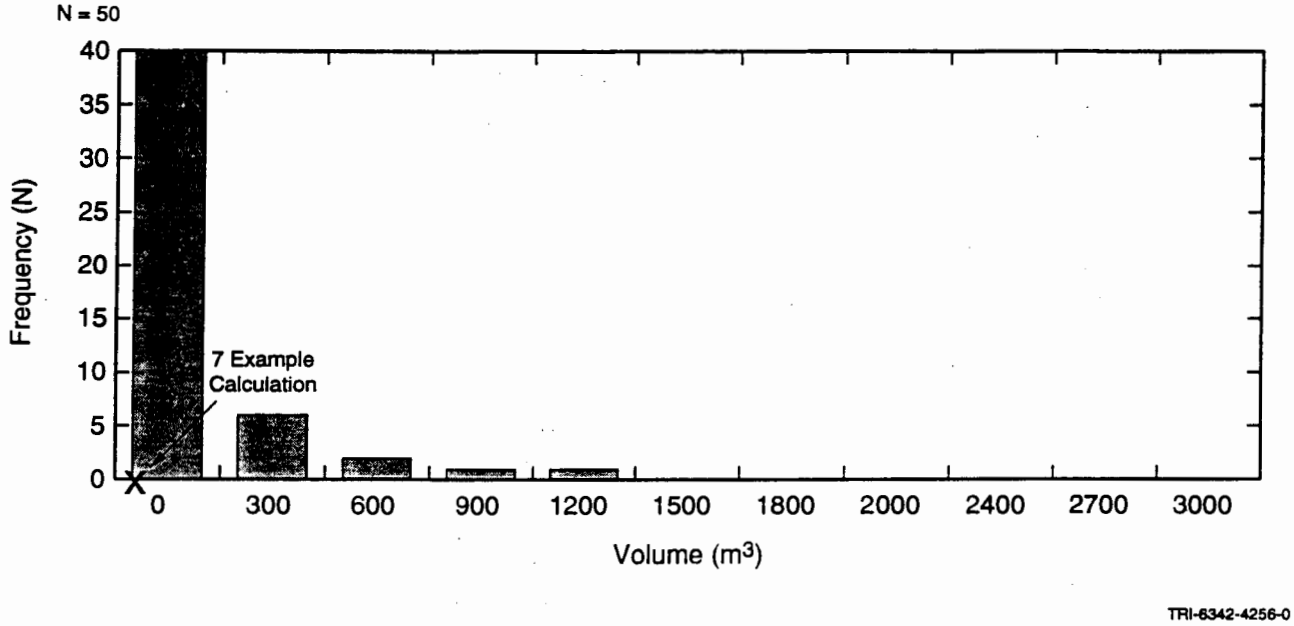

Figure 12. Brine Inflow to Panel After 10,000 yr.

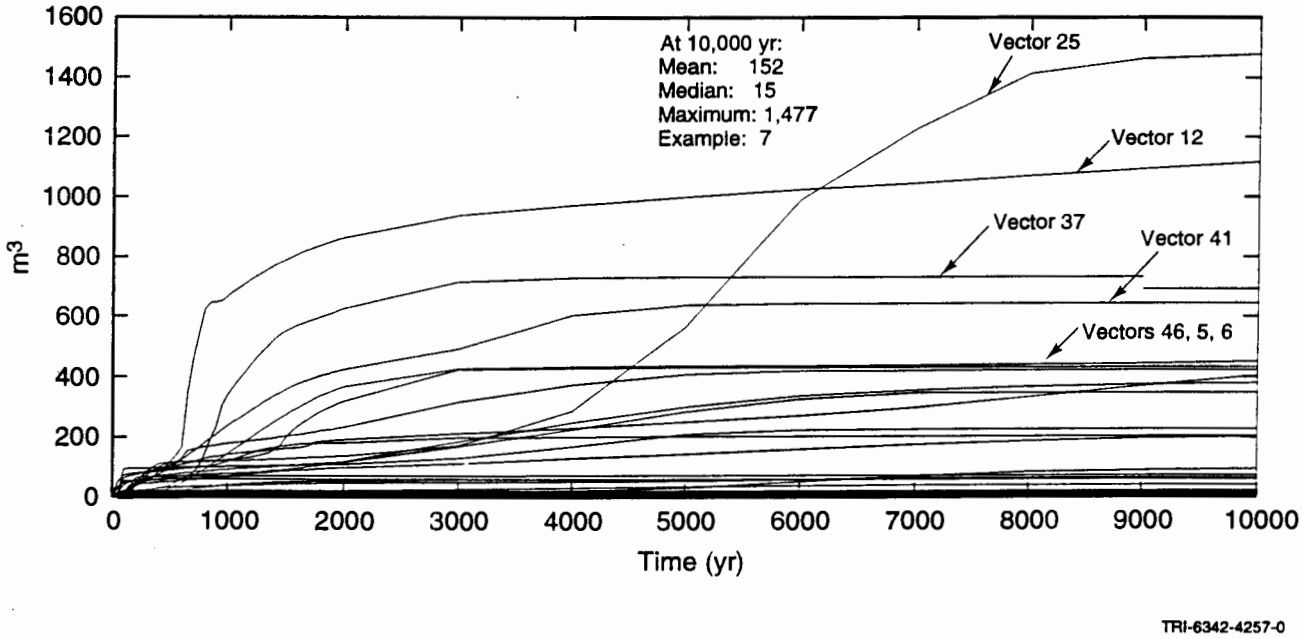

Figure 13. Total Brine Flowing Into the Panel.

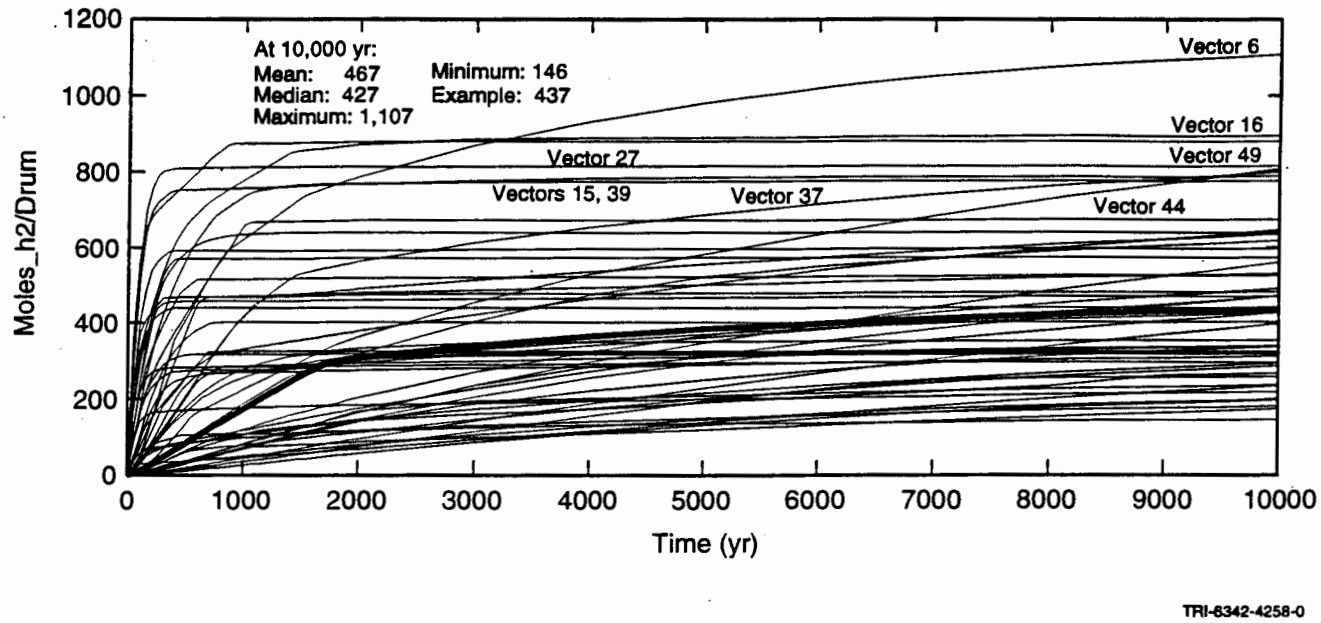

Figure 14. Total Gas Generated in the Entire Repository.

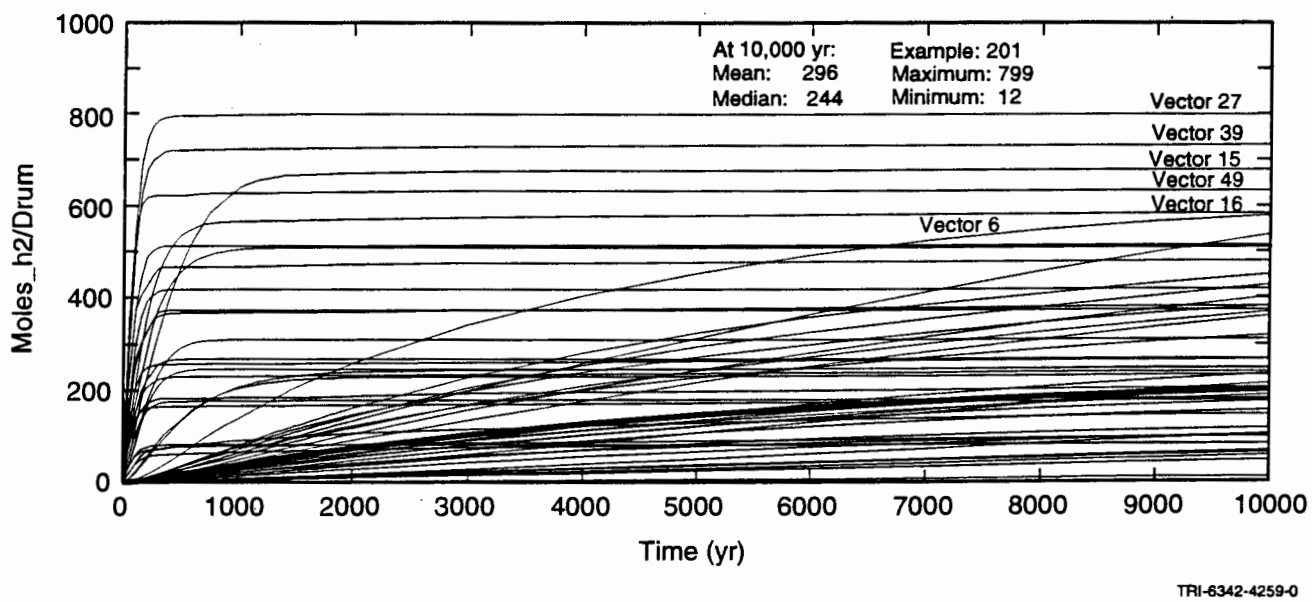

Figure 15. Total Gas Generated from Corrosion in the Entire Repository.

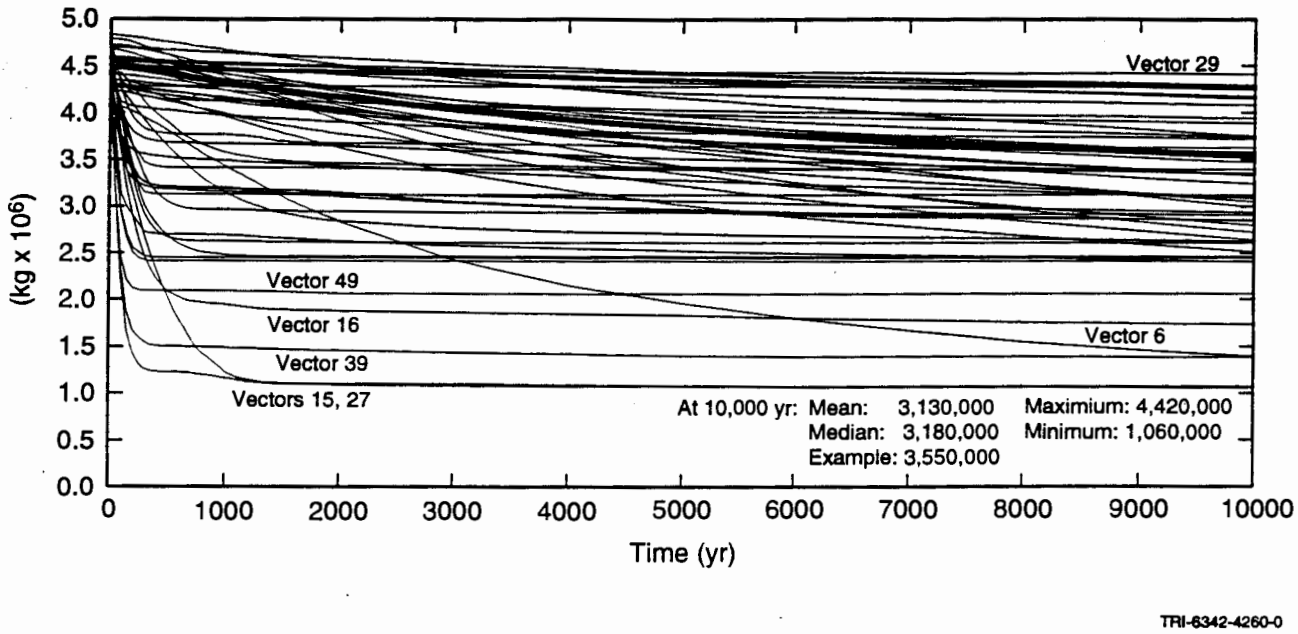

Figure 16. Ferrous Metals in the Panel.

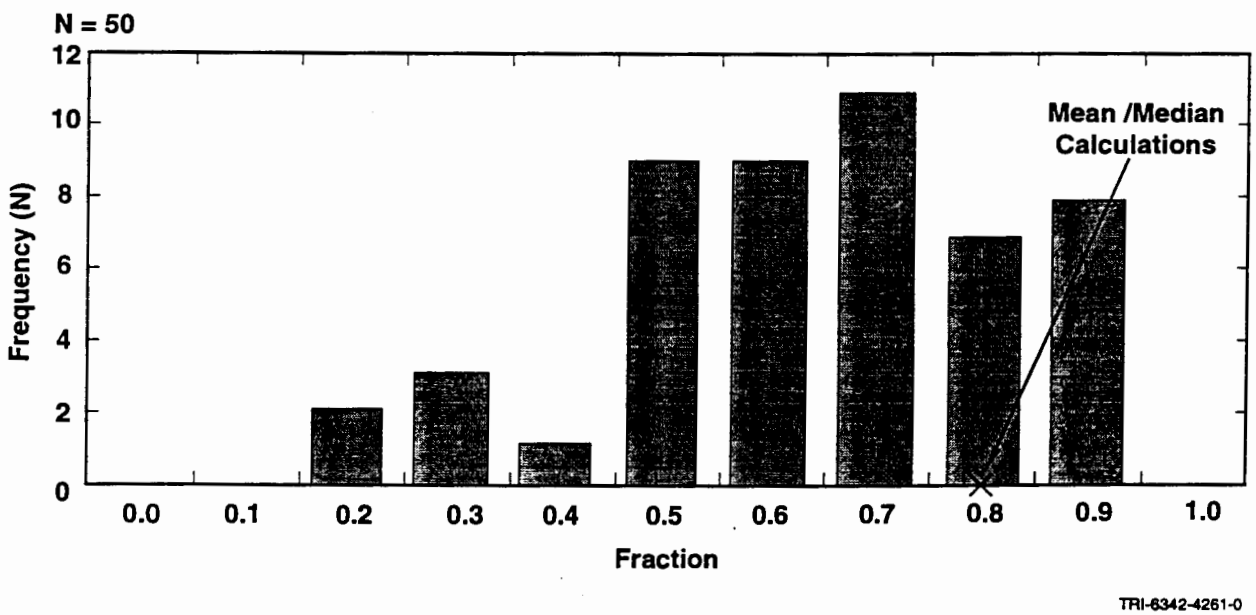

Figure 17. Ferrous Metal Remaining in Panel After 10,000 yr.

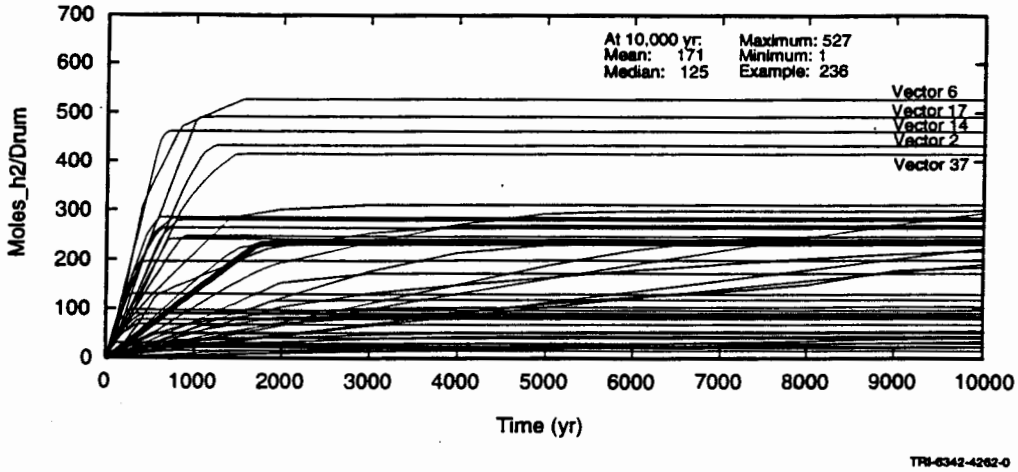

Figure 18. Total Gas Generated from Biodegradation in the Entire Repository.

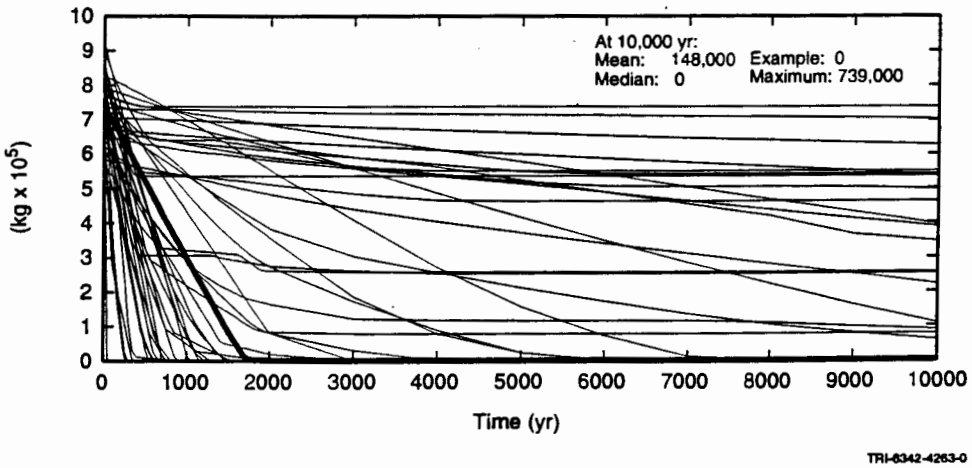

Figure 19. Cellulosics in the Panel.

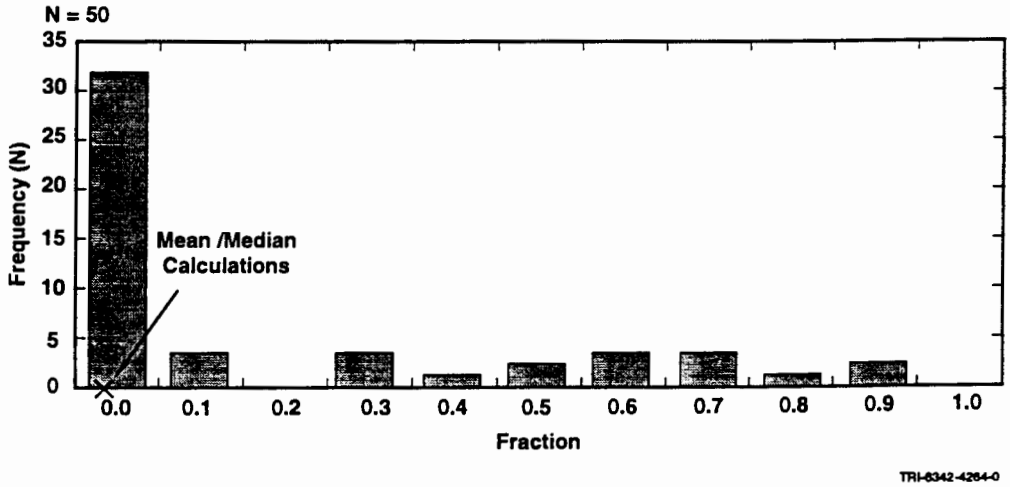

Figure 20. Cellulosics Remaining in Panel After 10,000 yr.

Table 7. Gas Migration Distances.

			Gas Migration						
	Sampled Value		Outward (m)						Upward (m)
Vector #	S_{gr}	K_r Model	MB139 S.	MB139 N.	Anh AB S.	Anh AB N.	MB138 S.	MB138 N.	Shaft
1	0.061	VG/P	2,400	151	2,400	2,400	1,046	2,400	116
2	0.181	B-C	90	0	1,158	1,032	1,004	1,196	15
3	0.134	B-C	664	0	905	723	10	778	31
4	0.112	B-C	0	0	0	0	0	0	0
5	0.122	B-C	0	0	50	0	0	0	0
6	0.278	VG/P	2,401	150	2,403	2,401	2,403	2,403	15
7	0.196	VG/P	2,404	2,400	2,405	2,403	2,405	2,403	75
8	0.078	B-C	0	0	0	0	0	0	0
9	0.142	B-C	32	0	650	485	650	650	0
10	0.391	B-C	301	0	660	660	41	596	65
11	0.327	B-C	0	0	32	0	0	0	2
12	0.380	B-C	0	0	1,183	769	857	999	4
13	0.222	B-C	317	0	651	407	728	803	7
14	0.291	B-C	0	0	739	0	0	71	0
15	0.344	VG/P	2,400	150	2,400	2,400	2,400	2,400	0
16	0.347	B-C	877	0	1,044	1,006	1,157	1,152	111
17	0.068	B-C	1,844	0	2,400	2,400	2,400	2,400	39
18	0.022	B-C	2,400	0	2,400	0	1,811	2,400	0
19	0.175	B-C	36	0	820	0	0	98	17
20	0.265	B-C	0	0	0	0	0	0	0
21	0.259	VG/P	2,404	650	2,405	2,403	2,400	2,403	0
22	0.283	B-C	43	0	177	158	0	7	0
23	0.366	VG/P	2,400	0	2,401	2,400	2,400	2,400	20
24	0.308	B-C	181	0	318	275	8	184	0
25	0.094	B-C	1	0	86	0	0	0	0
26	0.039	B-C	0	0	5	0	0	0	0
27	0.027	B-C	2,400	0	2,400	2,400	2,400	2,400	33
28	0.004	VG/P	0	0	2,517	2,409	1,678	2,401	0
29	0.086	B-C	0	0	157	84	0	6	0
30	0.100	VG/P	2,403	0	2,404	2,401	2,401	2,400	0
31	0.051	VG/P	650	0	1,255	779	738	940	4
32	0.146	B-C	835	0	1,286	1,224	652	900	5
33	0.165	B-C	912	0	1,567	831	790	1,332	8
34	0.246	B-C	0	0	699	0	0	50	3
35	0.188	VG/P	2,400	0	2,400	715	650	667	4
36	0.232	VG/P	650	0	652	652	0	50	0
37	0.011	B-C	682	0	2,402	2,400	2,401	2,400	63
38	0.297	B-C	0	0	1,897	0	1	960	0
39	0.376	VG/P	2,401	152	2,403	2,402	2,400	2,403	58
40	0.208	B-C	924	0	1,129	926	817	1,124	2
41	0.317	B-C	145	0	1,267	933	545	691	0
42	0.252	B-C	36	0	381	0	0	5	0
43	0.156	B-C	650	0	657	652	0	669	2
44	0.043	VG/P	0	0	2,403	2,401	2,403	2,403	26
45	0.333	B-C	0	0	4	1	0	0	0
46	0.238	B-C	49	0	1,638	59	1,046	1,213	109
47	0.392	VG/P	2,400	0	2,400	2,400	650	2,400	5
48	0.117	VG/P	2,401	650	2,401	2,400	652	2,400	0
49	0.358	B-C	882	0	1,317	29	40	798	6
50	0.204	VG/P	2,401	650	2,401	2,400	650	2,400	45
Mean	0.201	N/A	888	99	1,315	1,016	853	1,135	18
Median	0.200	N/A	483	0	1,219	719	650	920	3
Maximum	0.392	N/A	2,404	2,400	2,517	2,409	2,405	2,403	116
Example	0.200	B-C	667	0	866	717	571	713	4

Vector = 6
S_{gr} = 0.278
S_{br} = 0.0101
Lambda = 1.39
S_b @ S_{gr} = 0.722

Brine Sat	Eff Sat (SE)	K_{rg}	K_{rw}
0	-0.010203	1	0
0.0101	0	1	0
0.05	0.0403071	0.975083	1.09E-06
0.1	0.0908173	0.935603	2.68E-05
0.15	0.1413274	0.889475	0.000154
0.2	0.1918376	0.838117	0.00052
0.25	0.2423477	0.782574	0.001321
0.3	0.2928579	0.723727	0.002828
0.35	0.343368	0.662372	0.005388
0.4	0.3938782	0.599258	0.009443
0.45	0.4443883	0.535109	0.015547
0.5	0.4948985	0.470643	0.024399
0.55	0.5454086	0.406584	0.036874
0.6	0.5959188	0.34368	0.054091
0.62	0.6161228	0.319014	0.062617
0.65	0.6464289	0.282708	0.077502
0.7	0.6969391	0.224502	0.109038
0.75	0.7474492	0.169971	0.15137
0.8	0.7979594	0.120142	0.208397
0.85	0.8484695	0.07622	0.286295
0.9	0.8989797	0.039725	0.39625
0.95	0.9494898	0.012822	0.564516
1	1	0	1

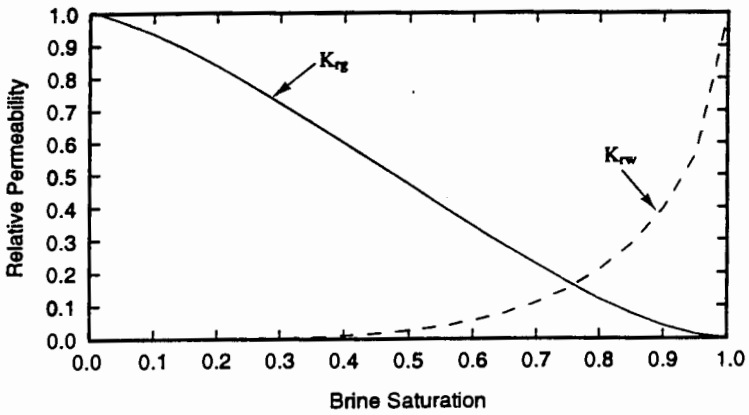

TRI-6342-4265-0

Figure 21. Van Genuchten/Parker Brine-Water Relative Permeability Curves for Vector Number 6.

Vector = 16
S_{gr} = 0.347
S_{br} = 0.085
Lambda = 2.3
S_b @ S_{gr} = 0.653

Brine Sat	Eff Sat (SE)	K_{rg}	K_{rw}
0	-0.092896	1	0
0.05	-0.038251	1	0
0.085	0	1	0
0.1	0.0163934	0.946819	1.23E-07
0.15	0.0710383	0.770597	3.6E-05
0.2	0.1256831	0.60395	0.000327
0.25	0.1803279	0.453488	0.001322
0.3	0.2349727	0.323421	0.003682
0.35	0.2896175	0.216152	0.00827
0.4	0.3442623	0.132504	0.016142
0.45	0.3989071	0.071853	0.028546
0.5	0.4535519	0.032206	0.046913
0.55	0.5081967	0.010262	0.072857
0.6	0.5628415	0.001457	0.108169
0.625	0.5901639	0.000219	0.129946
0.653	0.620765	0	0.158022
0.7	0.6721311	0	0.214942
0.75	0.726776	0	0.290858
0.8	0.7814208	0	0.385045
0.85	0.8360656	0	0.500154
0.9	0.8907104	0	0.639002
0.95	0.9453552	0	0.804569
1	1	0	1

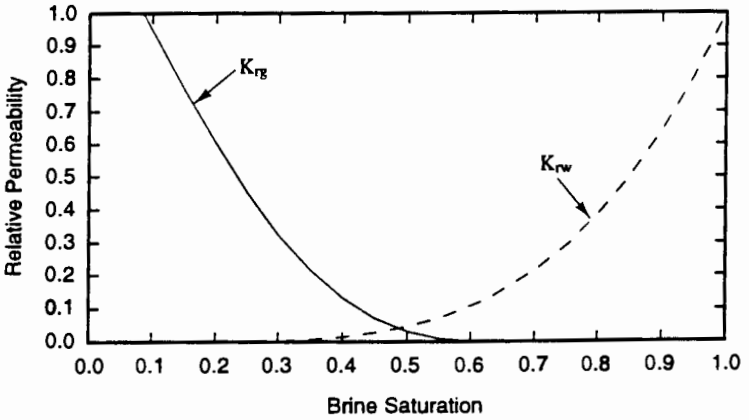

TRI-6342-4266-0

Figure 22. Brooks-Corey Brine-Water Relative Permeability Curves for Vector Number 16.

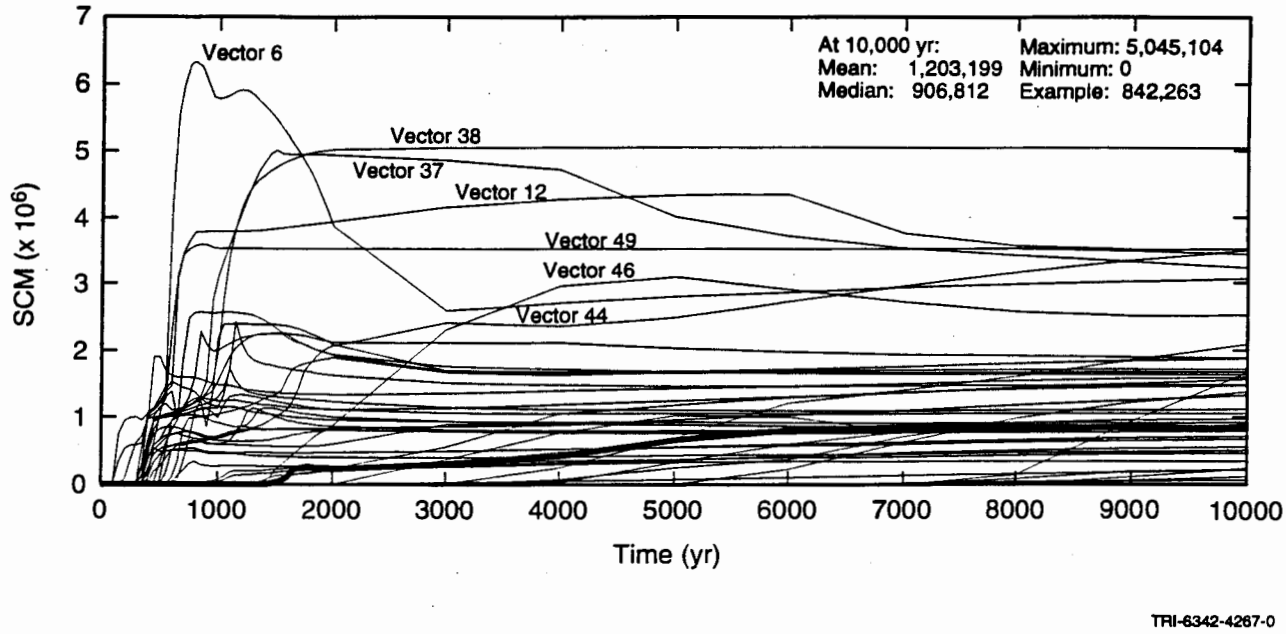

Figure 23. Cumulative Gas Flow Entering Anhydrite A & B South from the Repository Interface.

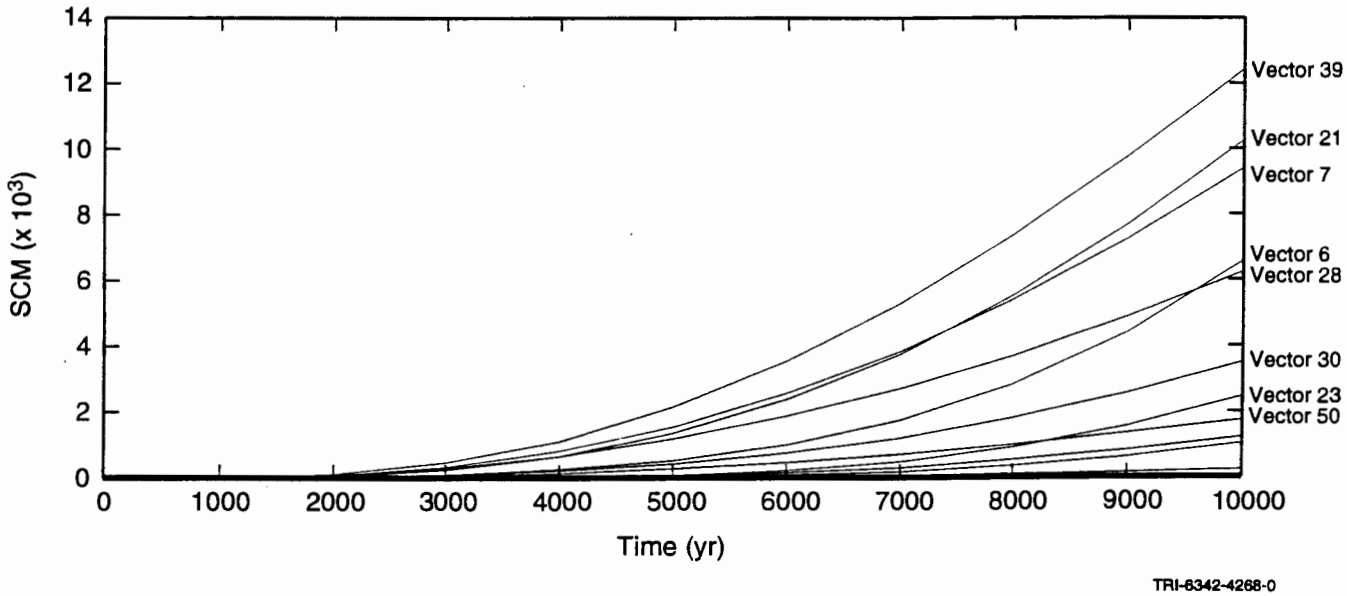

Figure 24. Cumulative Flow of Gas Out Anhydrite A & B South at 2.4 km Boundary.

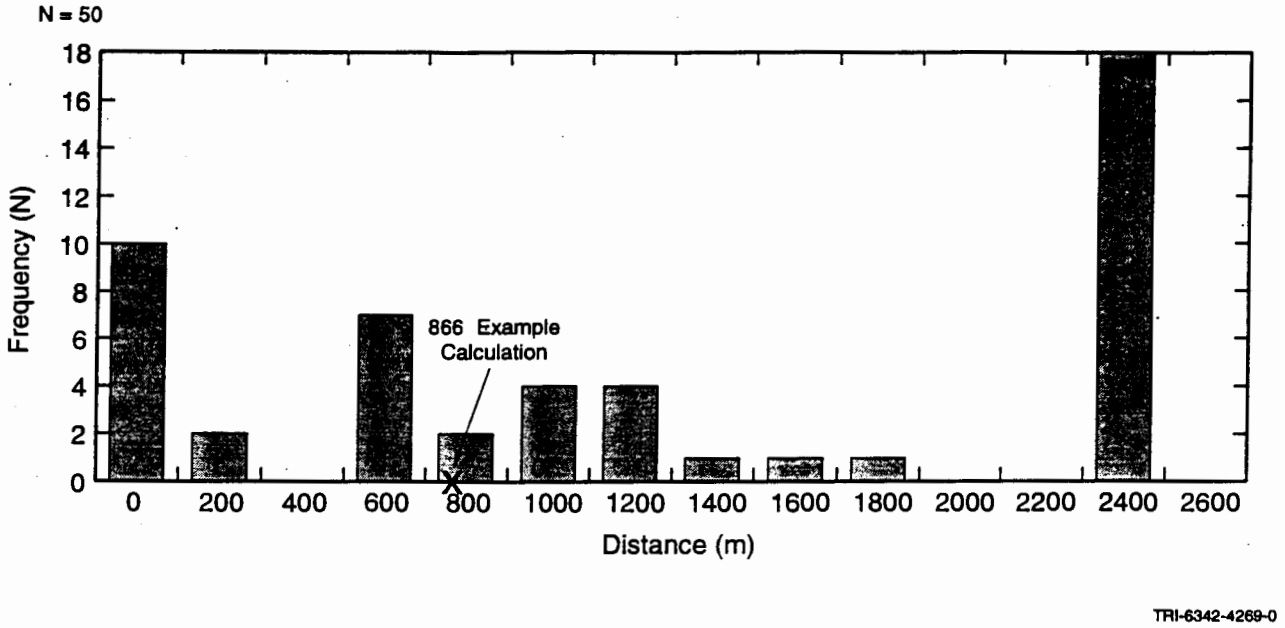

Figure 25. Gas Migration Distance: Anhydrite A & B South.

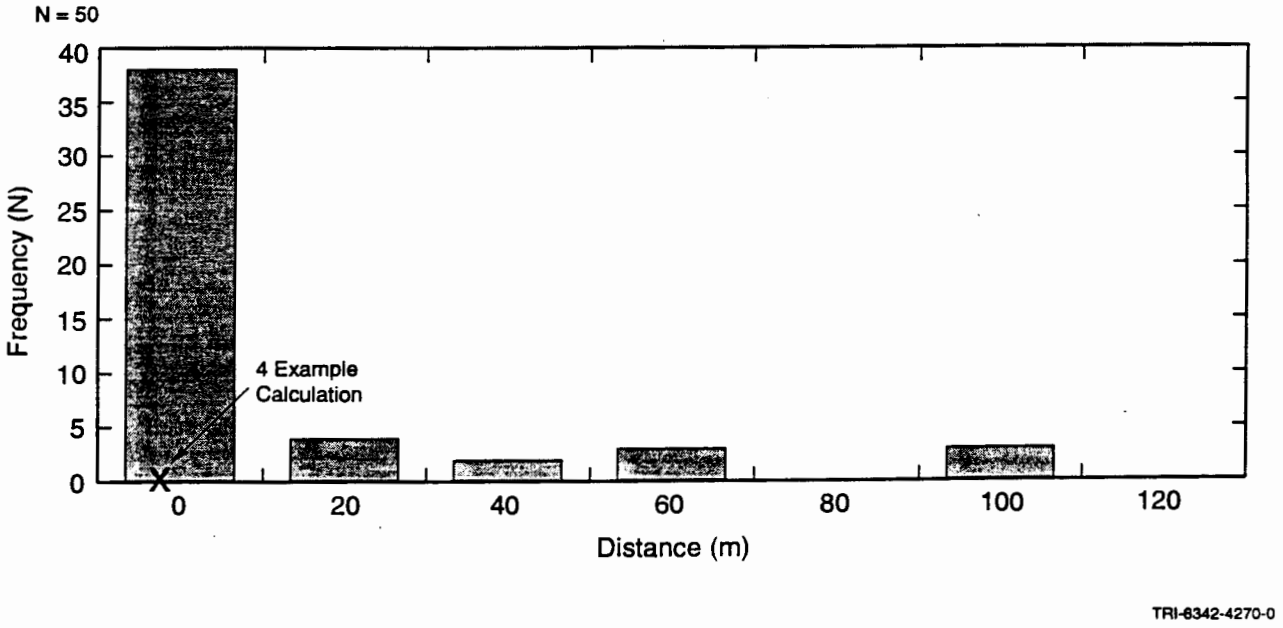

Figure 26. Gas Migration Distance: Up Through the Shaft.

Copy to:

6115/MS1324	P. B. Davies
6115/MS1324	R. L. Beuheim
6115/MS1324	S. M. Howarth
6115/MS1324	S. W. Webb
6115/MS1324	C. Larson (INTERA)
6117/MS0751	W. R. Wawersik
6119/MS1320	E. J. Nowak
6121/MS1322	J. R. Tillerson
6303/MS1335	W. E. Weart
6305/MS1335	S. A. Goldstein
6307/MS1345	P. A. Davis
6307/MS1345	A. R. Lappin
6319/MS1333	R. R. Richards
6342/MS1328	J. Bean
6342/MS1328	M. G. Marietta
6342/MS1328	L. C. Sanchez
6342/MS1328	J. Schreiber
6342/MS1328	D. Stoelzel
6342/MS1328	P. N. Swift
6345/MS1341	R. C. Lincoln
6347/MS1341	D. R. Schafer
6348/MS1341	J.T. Holmes
6348/MS1341	L. H. Brush
6743/MS1395	V. Harper-Slaboszewicz
6352/MS1330	SWCF WBS 1.1.6.2.5 PA
6342/MS1328	P. Vaughn

APPENDIX C:
1993 WIPP PA FRACTURE EXPERT GROUP MEETING MINUTES

Previous drafts of the White Paper included the Agenda of the Fracture Expert Group Meeting from March 23-25, 1993. Further work has resulted in preparation of formal documentation of the PA fracture model. It is contained in SAND94-0381 (see below for citation), which is in management review and will be released shortly. Therefore, the Agenda from the Fracture Expert Group has been deleted from this text.

Key, S, M. Fewell, P. Vaughn, M. Lord, and D. Labreche. In Management Review. *Background and Basis for the Fluid Flow Model Incorporated in BRAGFLO for Representing Pore Pressure-Induced Alterations in Permeability and Porosity in the Anhydrite Interbeds Above and Below the WIPP Repository Horizon.* SAND94-0381. Albuquerque, NM: Sandia National Laboratories.

APPENDIX D:
LARSON AND DAVIES MEMORANDUM

Kurt Larson and Peter Davies to Martin Tierney, "Justification for Larger Exponential Multiplier in Fractured Interbed Permeability Correlation for 1994 Performance Assessment Calculations," October 11, 1993. Internal SNL Memorandum. This memorandum was prepared to document concerns about the power-law assumption in the PA interbed alteration model which correlates permeability with porosity. In response, PA began to sample on the maximum fracture permeability rather than the exponential multiplier. Neither the PA model nor the model described here have been verified, and no data have been identified that could currently distinguish the better of the two. An experiment is planned which may allow the choice of one of these or an alternative. Other memoranda were issued contemporaneously with this one expressing similar concerns. The reference in this memorandum to Fewell on page 1 is incorrect; the correct reference is Key (SAND94-0381), which is in management review. This is the same reference now provided in lieu of Appendix C.

Sandia National Laboratories
Albuquerque, New Mexico 87185

date: October 11, 1993

to: Martin Tierney, 6342

from: Kurt Larson, 6115 (INTERA) Kurt Larson
Peter Davies, 6115 Pete Davies

subject: **Justification for Larger Exponential Multiplier in Fractured Interbed Permeability Correlation for 1994 Performance Assessment Calculations**

Introduction

Division 6342 has developed and implemented in the BRAGFLO multiphase simulator a model for the effects on fluid flow of fracture dilation in predominantly anhydrite interbeds (Fewell, in preparation). The functional form of the model has been reviewed by the Fracture Expert Group, which has endorsed it as a reasonable first approximation. The conceptual model assumes that a fractured element (nodal block) is composed of matrix except for single or multiple fractures extending across the element. A single, horizontal fracture conceptualization is shown in Figure 1. Element-average properties are formulated as follows: compressibility is a linear function of pore pressure; porosity is an integral function of compressibility; and permeability is a function of the magnitude of porosity change raised to a power. The exact permeability equation is:

$$k_e = k_0 \left(\frac{\phi_e}{\phi_0}\right)^J \qquad (1)$$

where k_e is the element-average intrinsic permeability, k_0 is the undisturbed intrinsic permeability, ϕ_e is the element-average porosity, ϕ_0 is a reference porosity, and J is an exponent, currently with a best-estimate value of 3. The porosity-permeability correlation will hereafter be refered to as the Porosity Model.

The Performance Assessment model accounts for the two likely important effects of fractures: effects on storage through porosity change, and effects on transmissive properties through

effects on storage through porosity change, and effects on transmissive properties through permeability change. Although the validity of the linear correlation of compressiblity with pressure is not known, the formulation of the dependence of porosity on compressibility has a sound basis. The best-estimate value of the exponent J, 3, in the Porosity Model is based on a parallal plate model, but the validity of the correlation with the magnitude of porosity change is unknown.

The form of the fracture permeability correlation used in the current Performance Assessment model is different from that suggested by theoretical consideration of fracture permeability. In most cases, fracture permeability is expressed as a function of fracture aperture, which has little relation to the porosity of elements in BRAGFLO, which contain both matrix and fractures. To illustrate the differences between the current Performance Assessment Model and theoretical considerations, an alternative approach for correlating the permeability of an element to porosity change will be developed here. The alternative approach uses an intermediate step to relate porosity change to fracture dilation, and then uses theoretical and geometric assumptions to derive the associated element-average permeability. The alternative approach will be referred to as the Aperture Model. The Aperture Model is generally supported by theoretical consideration of fracture permeability, and yields significantly different element-average intrinsic permeabilities than the Porosity Model.

Conceptual Approach

For practical reasons, Performance Assessment has adopted an effective continuum approximation model for simulating the effects of fractures on fluid flow. The effective continuum approximation assumes that a representative elemental volume (REV) exists within which flow processes can be represented with homogeneous values for porosity, permeability, and compressibility. In a dilating, fractured rock, it is likely that most of the dilation occurs in fracture apertures and that the matrix porosity is unchanged. In an REV approach, the distinction between fracture aperture and matrix porosity is lost. Similarly, the REV permeability represents a macroscopic quantity, but REV permeability changes are likely due to increases in fracture aperture or connectivity, a microscopic phenomena. The distinction between REV properties and actual physical processes indicates that functions relating change in one REV property to another must be based upon consideration of the processes occuring at the microscopic scale within an REV.

Intrinsic Permeability and Flow-Channel Aperture

There is both theoretical and experimental evidence that intrinsic permeability varies as a function of the square of a measure of the aperture of flow channels. For example, the Navier-Stokes equations applied to parallel plates yields (Bear, p. 692),

$$k = \frac{b^2}{12} \tag{2}$$

where b is the aperture of the space between the plates and k is its intrinsic permeability. In sediments, experimentally-determined permeability can often be expressed as a function of a measure of the mean grain diameter squared (Bear, 1972, pp. 133-134). The implication of the above comments about element porosity and the functional relationship between aperture and permeability suggest that if changes in REV porosity can be associated with fracture aperture changes, a highly defensible correlation between REV porosity and REV permeability could be formulated.

Element-Average Porosity and Fracture Aperture

The BRAGFLO numerical simulator requires use of element-average properties for compressibility, porosity, and permeability to simulate flow in fracture-altered interbeds. However, fractures in an element are discrete structures with properties quite different than the matrix. The element-average porosity, which is currently determined by the pressure-compressibility-porosity correlation, represents voids in the porous matrix and fracture apertures. Assuming horizontal fractures, the element-average porosity can be expressed as

$$\phi_e = \frac{(a_m\phi_m + na_f)\,l}{(a_m + na_f)\,l} \tag{3}$$

where ϕ_e is the element-average porosity, ϕ_m is the matrix porosity (assumed constant), a_m is the cross-sectional area of matrix perpendicular to the flow direction, a_f is the average cross-sectional area of a fracture perpendicular to the flow direction, n is the number of fractures, and l is the length of the element. Assuming a unit depth of the element and cancelling,

$$\phi_e = \frac{(h\phi_m + nb)}{h + nb} \tag{4}$$

where h is the height of the matrix, and b is the aperture of an individual fracture. After correlating element porosity, ϕ_e, with compressibility (pressure), nb and ϕ_m are the only unknown terms:

$$nb = \frac{h(\phi_m - \phi_e)}{\phi_e - 1} \tag{5}$$

Intrinsic Permeability of Elements Affected by Fracturing

Assuming that fractures are horizontal and transect the element, the arithmetic average technique is appropriate for calculating the average properties of an element from its discrete members. The arithmetic average is based upon assumptions that flow is parallel to the fracture-matrix interface and the potential field for flow is the same in the matrix as in fractures. Element-average intrinsic permeability is then given by:

$$k_e = \frac{nbk_f + hk_m}{nb + h} \tag{6}$$

where k_f is the fracture intrinsic permeability and k_m is the matrix intrinsic permeability. Assuming $h >> nb$,

$$k_e = \frac{nbk_f}{h} + k_m \tag{7}$$

Finally, substituting the theoretical permeability of the aperture between parallel plates (Equation 2) for the fracture intrinsic permeability k_f,

$$k_e = \frac{nb^3}{12h} + k_m \tag{8}$$

A formulation for the intrinsic permeability of a fracture network alone, similar to the first right-side term in Equation 8, is presented by Freeze and Cherry (1979, pp. 74-75). The permeability predicted with equations 5 and 8 can be calculated easily with assumptions about n and k_m and compared to the Porosity Model prediction.

Comparison of the Porosity Model and Aperture Model

The difference between the Aperture Model and the Porosity Model is the degree of permeability change associated with interbed dilation. A graphical comparison of permeability versus porosity was prepared to illustrate this difference in behavior under different assumptions about critical input parameters (Figure 2). As shown in Figure 2, the Aperture Model has a rapid increase in permeability once fracture dilation begins regardless of the number of active

fractures, whereas the Porosity Model has a gradual and nearly linear increase in permeability. The Porosity Model requires values of J of about 40 to attain permeabilities similar to the Aperture model at a porosity of 0.02 if the initial porosity (matrix porosity) is 0.01. However, it is apparent from the graph that the two conceptual models are incompatible, i.e. no selection of parameters can make the shape of the porosity-permeability correlation in the Aperture Model look like that in the Porosity model. Because of this difference, it is important to assess whether the effects the difference warrant adopting a new correlation for use in Performance Assessment calculations.

Propagation of dilation-altered interbed properties away from the repository for both the Aperture Model and the Porosity Model depends upon the rate of flow in previously affected elements. Because the Aperture Model predicts permeabilities orders of magnitude larger than the Porosity Model, use of the Aperture Model will likely indicate increased lateral gas migration distance and lower fracture porosity than use of the Porosity Model. The actual impact on a repository scale requires numerical evaluation. Because lateral gas migration is of concern for regulatory compliance and is an important performance measure, it appears that the differences between the Aperture Model and Porosity Model may be quite significant.

The dependence of fracture propagation on fracture permeability may not be as strong as the above paragraph suggests, however. Because fracture permeability increases so much with even moderate dilation, it is likely that properties of the fractured rock, such as fracture toughness, determine to greater extent than fracture permeability whether fractures become long and thin or short and fat. Fracture geometry is important because it affects the near-repository storage volume available for waste-generated gas in the interbeds. For this reason, it is vitally important that the pressure-compressibility-porosity correlation be able to reasonably predict fracture propagation and dilation. The present model is in part controlled by assumptions about fracture permeability but is equally affected by the assumption of a linear response of element compressibility to pressure changes. If fractures cannot propagate easily due to rock properties, fractures that do form might be short and fat regardless of how permeable they become. Calibration of the pressure-compressibility-porosity correlation to experimental results should mitigate concern about whether the method used to model fracture propagation and dilation is adequately accurate.

Recommendation

Fracturing will cause dramatic changes in the flow properties in interbeds. Both propagation/dilation and fracture permeability need to be depicted reasonably accurately before an assessment of the importance of fractures in repository performance can be made. The Aperture Model predicts much larger changes in permeability than the Porosity Model and is likely the more defensible of the two. Due to time constraints, the Performance Assessment Division cannot adopt a new correlation between porosity change and permeability for the 1994 Round of calculations. Is is recommeded that the Performance Assessment Division adopt a distribution function that allows J to reach values as high as 40 or 50 for 1994 calculations. For future rounds of calculations, it is recommended that Performance Assessment adopt a new correlation between porosity change and element permeability, based upon consideration of how element porosity change affects fracture aperture. The model may be similar to the one above or to one of several reported in literature.

References

Bear, Jacob, 1972. *Dynamics of Fluids in Porous Media*. American Elsevier, New York.

Fewell, M. E. in preparation. Background and basis for the fluid flow model incorporated in BRAGFLO for representing pore-pressure-induced alterations in permeability and porosity in the anhydrite beds above and below the WIPP repository horizon (Marker Beds 138 and 139).

Freeze, R. Allan and John. A. Cherry 1979. *Groundwater*. Prentice-Hall, New Jersey.

Distribution:

RE/SPEC Sam Key

6115 P. B. Davies

6115 R. L. Beauheim

6115 S. W.Webb

6115 S. A. Howarth

6115 K. Larson

6115 G. Freeze

6116 D.Borns

6117 W. Wawersik

6305 A. Lappin

6342 Mel Marietta

6342 M. Fewell

6342 P. Vaughn

6345 F. Mendenhall

6345 B. Butcher

6345 W. Gerstle/UNM

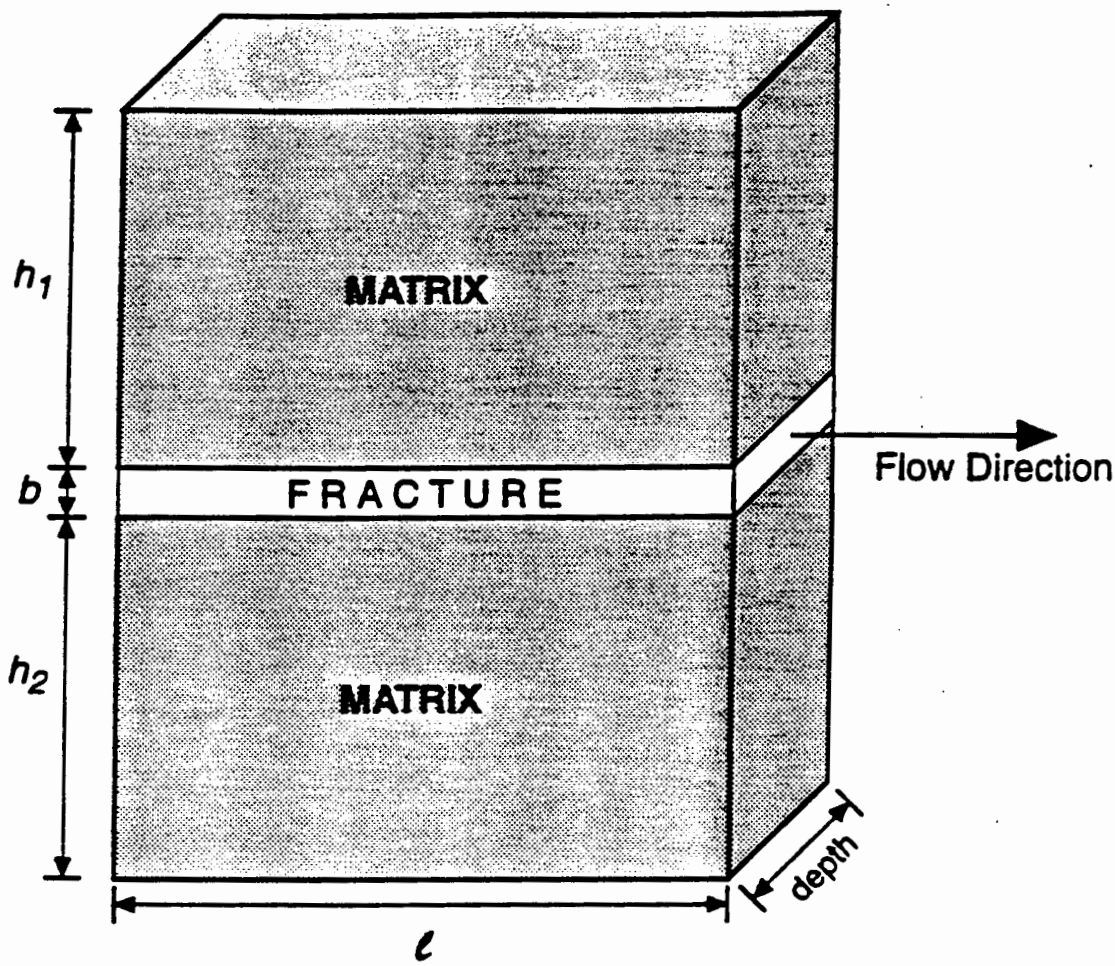

Figure 1. Schematic representation of a fractured element following the conceptual model. From the development in the text, $h = h_1 + h_2$.

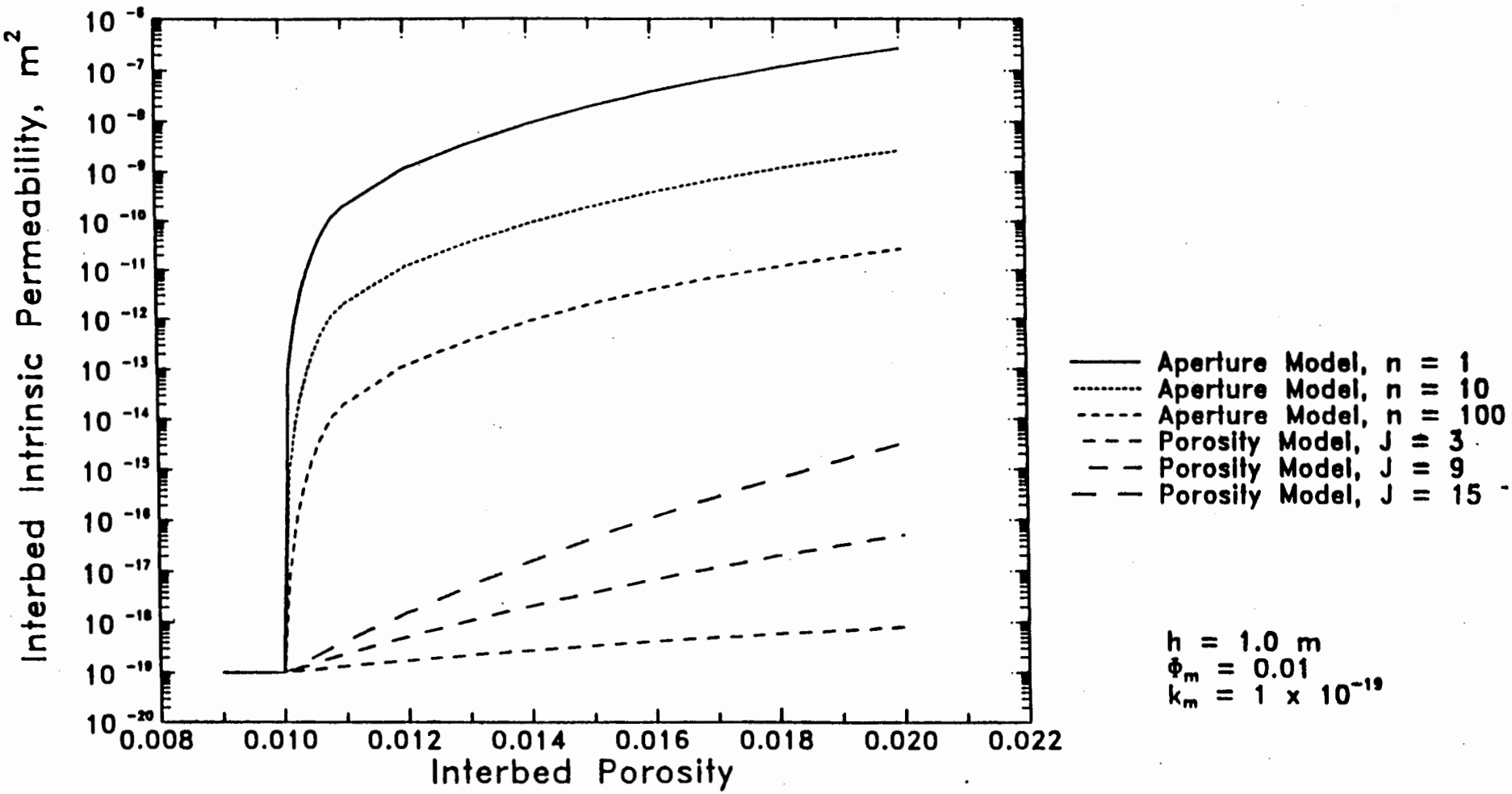

Figure 2. Relationship between change in interbed porosity due to fracture dilation and interbed intrinsic permeability for two conceptual models. Because the behavior of the two sets of curves are inherently different, there is no parameter selection that can make one conceptual model behave as the other.

APPENDIX E:
McTIGUE MEMORANDA

D.F. McTigue to Distribution, "Horizontal Darcy Flow to Room Q," June 24, 1991. Internal SNL Memorandum.

D.F. McTigue to Distribution, "Calculations of Brine Flux and Cumulative Brine Volume for Room Q, Based on a Darcy Flow Model," April 3, 1989. Internal SNL Memorandum.

ROUGH DRAFT

Sandia National Laboratories
Albuquerque, New Mexico 87185

date: August 2, 1990

to: Distribution

from: D. F. McTigue, 1511

subject: A Model for Brine Inflow Due to Salt "Damage"

Preview Summary

The purpose of this memo is to summarize possible inconsistencies in modeling brine flow in salt as a classical problem of transport in a porous medium. The framework of an alternative modeling approach that appears to resolve these inconsistencies is outlined. The principal points to be developed are:

- Data for flow to boreholes in WIPP Room D are represented well *qualitatively* by the classical model. However, the capacitance indicated by fitting model calculations to the field data is orders of magnitude larger than that expected on the basis of the compressibilities of salt and brine. That is, the decay of the brine flux into the boreholes takes place over a time scale that is much too long to be explained in terms of the processes assumed in the development of the classical model.

- The classical model invokes an unbounded domain of interconnected porosity. This concept is contradicted by both mechanical arguments and geochemical observations.

- A new conceptual model is outlined in which the undisturbed salt is assumed to contain brine only in unconnected porosity. "Damage" associated with deformation upon the introduction of mined cavities can result in the development of a local zone of interconnected porosity characterized by finite permeability. "Healing" can occur as creep closure of interconnected pores isolates them again.

- A sample calculation shows that this model can capture the long time scale observed in the field data, even though the value for the capacitance used is the small one expected for the compressibility of the system. The long time scale enters through the evolution of the connected porosity field as the salt creeps toward the hole.

1 Introduction

It has been observed that brine seeps from the walls of fresh excavations and accumulates in drillholes in the WIPP facility. The cumulative magnitude of this seepage is of concern because of possible effects on room closure, backfill consolidation, gas generation, and related performance-assessment issues. Due to the time scale of interest — tens to hundreds of years — predictive models must be invoked, and this, in turn, requires identification of the predominant transport processes involved.

1.1 The Classical, Hydrological Model

A few predictive calculations have been performed (*e.g.*, [1, 2]) based on what will be referred to in this memo as the "classical, hydrological model." The classical model views the salt as a fluid-saturated, porous medium with an interconnected network of pores. In its undisturbed state, the fluid is taken to be at some initial pressure, usually assumed to be between hydrostatic ($\sim$ 6 MPa) and lithostatic ($\sim$ 15 MPa) for the repository depth. Excavations may perturb this initial pressure via their effect on the mean stress field. The principal influence of an excavation, however, is to introduce faces at zero (atmospheric) pressure. Flow is driven toward these faces by the resulting pressure gradients. The pore pressure near the excavation thus relaxes in a transient process that has a diffusion-like character.

The transient evolution of the pore-pressure field requires that the medium have a finite "capacitance," *i.e.*, the ability of an element of salt to change its fluid mass content. In a saturated medium, this capacitance is due to changes in fluid density, porosity, and/or matrix dilatation. For elastic rock and fluid, then, the capacitance is directly related to the compressibilities of the porous matrix and the individual fluid and solid constituents.

Classical, hydrological problems can often be cast as initial-value problems for the pore-pressure field (or, equivalently, for the "head"), which is governed by a linear diffusion equation:

$$\frac{\partial p}{\partial t} - \frac{k}{\mu C}\nabla^2 p = 0, \tag{1}$$

where p is the pressure, k is the permeability, μ is the fluid viscosity, and C is the capacitance. For flow to a borehole embedded in an unbounded domain, one can construct by dimensional analysis a characteristic time for the diffusive relaxation of the pore pressure:

$$t_D \equiv \frac{a^2 \mu C}{k}, \tag{2}$$

where a is the borehole radius.

1.2 Possible Contradictions in the Classical Model

1.2.1 *Empirical Observations from Field Tests at the WIPP*

Results of fitting the classical hydrological model to data for brine accumulation in a hole in Room D have been presented previously [3]. A fit to data for 500 days from hole DBT10 (Figure 1) yielded a hydraulic diffusivity of $c = k/\mu C = 3.1 \times 10^{-11}$ m^2/s and the combination $kp_0/\mu a = 3.2 \times 10^{-11}$ m/s, where p_0 is the initial pressure. For the known values $a = 0.051$ m and $\mu = 1.6 \times 10^{-3}$ Pa·s, and the assumed initial pressure $p_0 = 1.0 \times 10^7$ Pa [4, 5], this fit yields $k = 2.6 \times 10^{-22}$ m^2 and $C = 5.1 \times 10^{-9}$ Pa^{-1}. The inferred permeability is very small, but not exceptional in comparison to independent determinations [4, 5]. The inferred capacitance, however, is very large in comparison to estimates calculated on the basis of the known compressibilities of salt and brine. A calculation based on the well-established theory for linear, porous, elastic media [2] yields an estimate of $C \simeq 7.8 \times 10^{-12}$ Pa^{-1}, some three orders of magnitude smaller than that inferred from the field data.

Stated in somewhat different terms, the observed characteristic time for the decay of the flux[1] to hole DBT10 is of the order of 200 days. From equation (2) above, the expected characteristic time based upon the classical model and independent estimates of material properties is of the order of only hours to tens of hours.

Thus, the field observations of brine seepage into boreholes in Room D pose a dilemma. The classical Darcy-flow model yields very good fits to some data in terms of qualitative behavior. However, the material parameters inferred from the fits are difficult to reconcile with the assumptions underlying the model. In particular, the data indicate a very large apparent capacitance that cannot be explained by the elastic compressibilities of the salt and brine. Arguments have been presented previously [6] that suggest that the presence of a highly compressible gas phase in the pore fluid is not sufficient to resolve this contradiction.

Another possibility, which was suggested previously [3], and is developed explicitly in the present memo, is that the long time scale revealed by the data enters through other transport mechanisms not addressed by the classical model. In particular, it is noted that the deformation of the salt in the neighborhood of a hole or excavation evolves over a longer time scale. Thus, some sort of coupling between the creep deformation of the salt and the brine flow may introduce the longer time scale in a natural fashion.

1.2.2 *Conceptual Contradictions*

The classical model invokes a ubiquitous network of interconnected porosity. In salt, however, this view encounters both mechanical and geochemical contradictions. In a creeping medium, it can be argued that the equilibrium condition approached after sufficiently great time must be isolated domains of pore fluid at lithostatic pressure. Flow of fluid to "drained" boundaries and creep closure of open pore networks would tend to seal off local, isolated regions of fluid. Geochemical evidence supports this view. Detailed

[1] The decay time is defined here as the time at which the flux falls off to e^{-1} times the maximum observed value.

analyses of the chemical composition of brines from the WIPP [7, 8] show considerable variability, even among samples collected within close proximity of one another. This, too, suggests that fluid domains in the salt are isolated from one another, in order that molecular diffusion not homogenize the brines. These two paradoxes, posed by the assumption of a persistent, interconnected pore network, are discussed in more detail in the following sections.

1.2.2.1 Mechanical Paradox

Salt is typically represented as a nonlinear, Maxwell-like, viscoelastic material (*e.g.*, [9]). That is, under an applied deviatoric stress, there is an instantaneous, elastic deformation, followed by nonlinear, rate-dependent creep. This type of material creeps at vanishingly small deviatoric stress. Although salt may exhibit a finite threshold stress below which the established creep relations do not hold, it seems reasonable to assert that this threshhold is very small.

The *volumetric* deformation of rock salt is usually taken to be purely elastic; *i.e.*, models typically neglect any rate-dependent, volumetric creep. The creep response of the salt is thus taken to be that of an *incompressible*, nonlinear (*e.g.*, power-law) fluid. For many purposes, such as cavity-closure calculations, this assumption is reasonable. The volumetric response of individual salt crystals is indeed elastic under most conditions of interest, and the void fraction in the aggregate rock salt is so small (typically of the order of 1% by volume in WIPP salt), that the inelastic closure of voids can contribute little to the overall deformation. However, if one is to consider the coupling of rock deformation and fluid flow, the mechanisms of volume change are all-important.

Even if the individual salt crystals are regarded as incompressible in creep, volumetric creep of the bulk aggregate can occur by the opening or closing of voids. On a *local*, microscopic scale, it is shearing deformation that allows macroscopic, volumetric creep. Consider, for example, connected porosity in the form of a domain between plane, parallel walls that are separated by solid asperities. Let us idealize the asperities as an array of circular cylinders that bridge the gap (Figure 2). In the absence of any fluid, a load applied normal to the plane walls is carried by the cylinders; on average, if the force per unit area of the plane walls is σ, the force per unit area of the asperities is $\sigma/(1-\phi)$, where ϕ is the area fraction of void ($1-\phi$ is the area fraction of solid asperities). Each asperity then appears locally as a sample in a triaxial creep test. The incompressible material in the asperities undergoes volume-preserving deformation, while the void space in the gap is reduced. Thus, local shearing deformation accomodates the bulk volumetric deformation. If the asperities creep under any applied load, then the voids will ultimately be closed down.

Now reconsider the foregoing when a fluid fills the void space entirely (only saturated systems are addressed here). The pressure in the fluid acts as a "back stress" against the parallel plane walls of the idealized pore network. Thus, the "effective stress" across the plane is $-(\sigma-p)$, and the "effective stress" across each asperity is $-(\sigma-p)/(1-\phi)$.

When $\sigma > p$, the load is shared by the pressurized fluid and the deviatorically-loaded asperities; the latter deform by creep, decreasing the void volume. This, in turn, requires the fluid volume contained in the element under consideration to decrease, by an increase in density, by net outflow through a "drained" boundary, or by some combination of both. When $\sigma = p$, the load is entirely born by the pressurized fluid and an *isotropic* stress in the asperities, and no further deformation occurs. This "equilibrium" configuration implies that there are no "drained" boundaries on the porosity domain; the porosity is thus "isolated."

There is no particular limitation, in this view, on the size of such a domain of "isolated" porosity containing fluid at a pressure equal to (minus) the mean stress in the rock. The size of isolated domains would depend upon the detailed history of the consolidation of the salt/brine system. For this reason, it can be expected that domains of isolated porosity may be quite heterogeneous. This is consistent with the highly variable response encountered in various borehole tests performed in the WIPP. For example, while some pressure-decay tests show behavior easily interpreted in terms of the classical porous-medium model, others show essentially the response of an impermeable, solid body [4].

These arguments, then, suggest that such a system will approach an equilibrium configuration in which isolated domains of porosity may persist, containing fluid at lithostatic pressure. As long as interconnected paths exist through the medium to boundaries at lower pore pressure, fluid will be squeezed out, and porosity will be eliminated, resulting in the "sealing-off" of isolated domains.

1.2.2.2 Geochemical Paradox

Stein, Krumhansl, and Kimball [7, 8] have analyzed the composition of brines sampled from various localities in the WIPP. Many of these samples were collected in small holes drilled into faces from which visible seepage was observed. An important finding in these studies is that the brine chemistry is highly variable, even among samples separated by distances of the order of tens of centimeters. If these brines were derived from an interconnected pore network, one would expect that molecular diffusion would have eliminated any significant contrasts in brine composition over the very long existence of the formation. For example, the characteristic diffusion length, L_D, scales like $L_D \sim \sqrt{\mathcal{D}t}$, where $\mathcal{D}$ is the diffusivity. The effective diffusivity in a porous medium is often represented as the product of the molecular diffusivity, $\mathcal{D}_m$, and the tortuosity, T, *i.e.*, $\mathcal{D} = \mathcal{D}_m T$. Molecular diffusivities are typically of the order of $\mathcal{D}_m \sim 10^{-9}$ m^2/s; a very small tortuosity might be of the order of $T \sim 10^{-2}$, giving $\mathcal{D} \sim 10^{-11}$ m^2/s. Over a period of 230 Ma, the diffusion length, L_D, is thus of the order of hundreds of meters. The observation that compositional differences persist in the brines over short length scales and very long time, then, suggests strongly that the brine in undisturbed salt is in local, isolated domains.

2 A "Damage" Model

The following presents a development for a model that couples the creep deformation of the salt and the flow of brine. The model is exploratory in nature; it is intended primarily as a demonstration of how some of the phenomenology described in the foregoing sections might be put into a sound model framework. The goal is to eliminate some of the contradictions that seem to arise in application of the classical, porous-medium model.

2.1 Mass Balances

Consider a system comprised of N constituents. The balance of mass for each constituent α takes the classical form

$$\frac{\partial \rho_\alpha}{\partial t} + \nabla \cdot (\rho_\alpha \mathbf{v}_\alpha) = c_\alpha, \tag{3}$$

where ρ_α is the mass per unit volume of the mixture, $\mathbf{v}_\alpha$ is the velocity, and c_α is the rate of creation of mass due to an internal source. In order that the total mass of the system be conserved, it is required that

$$\sum_{\alpha=1}^{N} c_\alpha = 0, \tag{4}$$

i.e., the sum of the mass sources over the N constituents must vanish. Thus, c_α represents the exchange of mass between various constituents of the mixture. Note that the density, ρ_α, can be decomposed into the product of the material density (mass of the constituent per unit volume of the constituent), γ_α, and the volume fraction of the constituent, ϕ_α:

$$\rho_\alpha = \gamma_\alpha \phi_\alpha. \tag{5}$$

It is convenient to note that the porosity, ϕ, is related to the solid volume fraction simply by:

$$\phi = 1 - \phi_s. \tag{6}$$

Furthermore, because the volume fractions must sum to unity, the total porosity must be equal to the sum of the fluid volume fractions:

$$\phi = \sum_{\alpha=2}^{N} \phi_\alpha, \tag{7}$$

where the αs from 2 to N represent the $N-1$ fluid constituents.

The system considered here is comprised of a porous solid matrix, denoted by $\alpha = s$, and two fluid constituents: fluid in isolated pores, denoted by $\alpha = is$, and fluid in interconnected pores, denoted by $\alpha = cn$. The isolated and interconnected fluid are comprised of the same material, so that $\gamma_{is} \equiv \gamma_{cn} \equiv \gamma_f$, where γ_f is the density of the fluid. It is assumed at the outset that the constituents are incompressible; *i.e.*, γ_f and γ_s are material constants. This restriction is easily relaxed; it is made here for simplicity,

and to isolate the effects of bulk deformation of the matrix. Finally, the solid matrix is assumed to exchange no mass with the fluid constituents, so that

$$c_s = 0. \tag{8}$$

However, fluid can be exchanged between the isolated and interconnected fractions; *i.e.*, isolated porosity can become interconnected by "damage" to the salt, or interconnected pores can become isolated by some "healing" mechanism. Thus, the remaining mass exchange terms, restricted by (4), are written in the form:

$$-c_{is} = c_{cn} = \gamma_f \Gamma, \tag{9}$$

where Γ is a volume exchange rate, whose functional form is yet to be specified. For the remainder of the discussion, ϕ_{is} and ϕ_{cn} will be referred to as the isolated and connected porosity, respectively. Equation (7) in this case simply states that $\phi = \phi_{is} + \phi_{cn}$, *i.e.*, the total porosity is the sum of the isolated and connected porosities.

Under the foregoing definitions and assumptions, the mass balances (3) for the solid, isolated fluid, and connected fluid, respectively, reduce to:

$$-\frac{\partial \phi}{\partial t} + \nabla \cdot [(1-\phi)\mathbf{v}_s] = 0, \tag{10}$$

$$\frac{\partial \phi_{is}}{\partial t} + \nabla \cdot (\phi_{is}\mathbf{v}_{is}) = -\Gamma, \tag{11}$$

$$\frac{\partial \phi_{cn}}{\partial t} + \nabla \cdot (\phi_{cn}\mathbf{v}_{cn}) = \Gamma. \tag{12}$$

The isolated fluid must move passively with the solid,[2] so that

$$\mathbf{v}_{is} = \mathbf{v}_s. \tag{13}$$

Substitution of (13) into (11), and summation of the three mass balances to obtain a mass balance for the system as a whole yields:

$$\nabla \cdot [\mathbf{v}_s + \phi_{cn}(\mathbf{v}_{cn} - \mathbf{v}_s)] = 0. \tag{14}$$

This simply states that the dilatation rate of the solid skeleton, $\nabla \cdot \mathbf{v}_s$, is balanced by the divergence of the flow of interconnected fluid relative to the solid. That is, expansion of the solid, which, for γ_s constant, can be accomplished only by increasing the porosity, must be accompanied by a net inflow of fluid.

The fluid flux is defined as the volume flow rate per unit area of interconnected fluid relative to the solid, *i.e.*, a classical Darcy velocity:

$$\mathbf{q} = \phi_{cn}(\mathbf{v}_{cn} - \mathbf{v}_s). \tag{15}$$

[2]This statement can be made more formally in terms of the momentum balances for the constituents.

For small volumetric strain, the dilatation rate of the solid is approximately equal to the volumetric strain rate:

$$\nabla \cdot \mathbf{v}_s \simeq \frac{\partial \epsilon}{\partial t}, \tag{16}$$

where ϵ is the infinitesimal (Cauchy) volume strain (defined here as negative in compression).

Substitution of (15)–(16) into (11), (12), and (14) yields:

$$\frac{\partial \phi_{is}}{\partial t} = -\Gamma - \phi_{is}\frac{\partial \epsilon}{\partial t} - \mathbf{v}_s \cdot \nabla \phi_{is}, \tag{17}$$

$$\frac{\partial \phi_{cn}}{\partial t} = \Gamma + (1 - \phi_{cn})\frac{\partial \epsilon}{\partial t} - \mathbf{v}_s \cdot \nabla \phi_{cn}, \tag{18}$$

$$\frac{\partial \epsilon}{\partial t} = -\nabla \cdot \mathbf{q}. \tag{19}$$

The last two terms on the RHS of (17) and (18), of the form $-\phi_\alpha(\partial\epsilon/\partial t) - \mathbf{v}_s \cdot \nabla\phi_\alpha$, are products of small quantities. For the purpose of the present illustrative development, it suffices to neglect these terms, although they are not difficult to implement in a numerical solution. In this case, (17) and (18) reduce to:

$$\frac{\partial \phi_{is}}{\partial t} = -\Gamma, \tag{20}$$

$$\frac{\partial \phi_{cn}}{\partial t} = \Gamma + \frac{\partial \epsilon}{\partial t}, \tag{21}$$

which simply state that isolated porosity is destroyed at the rate Γ (20), and connected porosity is created due to the conversion of isolated porosity at a rate Γ and due to dilatation (21). Note that total porosity, $\phi_{is}+\phi_{cn}$, is not conserved; a net loss of connected porosity results from pore closure ($\partial\epsilon/\partial t < 0$). Finally, it is reiterated that equation (19) shows that dilatation (compaction) is balanced by fluid inflow (outflow).

2.2 Constitutive Models

Constitutive models are now required for the exchange rate Γ, the volume strain, ϵ, and the flux, $\mathbf{q}$. Simple models that capture the character of the important processes are posed here. It is emphasized that these are somewhat *ad hoc*, and are put forward here principally to explore the general behavior of the system.

2.2.1 *Volumetric Deformation of the Matrix*

In traditional problems of hydrology, it often suffices to consider only elastic deformation of the porous matrix. However, in salt, it is reasonable to suppose that some volumetric creep occurs, as well. This sort of process has not been studied extensively; most creep modeling for salt assumes rate-dependent behavior only in the deviatoric deformation. For simplicity, it is assumed here that the matrix behaves as a Maxwell viscoelastic material:

$$\frac{\partial \epsilon}{\partial t} = -\frac{1}{K}\frac{\partial}{\partial t}(p_c - p) - \frac{1}{\kappa}(p_c - p), \tag{22}$$

where K is the drained bulk modulus of the porous matrix, p_c is the confining pressure (minus the mean total stress) and κ is the bulk viscosity of the porous skeleton. This is an "effective-stress law," in the sense that the volumetric deformation is related to the *difference* between the confining and fluid pressures, or the "effective pressure," $p_{eff} = p_c - p$. The limit $\kappa \to \infty$ recovers the classical, elastic model.

The mean stress, or confining pressure, thus appears explicitly in the governing equations for the fluid flow. In general, the mean stress varies spatially and temporally in the vicinity of an excavation. If one believes that the brine has little effect on the overall deformation of the salt, then the coupling is "one-way," *i.e.*, the deformation influences the fluid flow, but not *vice versa*. In this case, the stress field in the rock can be obtained from an independent calculation. However, if "two-way" coupling is deemed important, the entire system, including the momentum balance for the solid, along with appropriate constitutive models, must be solved together. For present purposes, the former course is taken.

It is acknowledged that this linear model for the volumetric creep is quite unrealistic; for example, one would expect some sort of strain hardening to occur — *i.e.*, the rate of pore closure should decrease rapidly as the connected porosity is eliminated. In the present case, it is necessary to apply the restriction that (22) holds only when $\phi_{cn} > 0$, while $\partial\epsilon/\partial t = 0$ if $\phi_{cn} = 0$. Furthermore, one would expect that, as in the power-law creep model for the shearing deformation of salt, the "viscosity," κ, depends on the stress level (see discussion, *e.g.*, in [3]). Nonetheless, the linear, viscoelastic model given by (22) captures the effect of creep closure of pores due to a pore pressure less than the confining pressure.

2.2.2 *Fluid Flux*

The fluid flux, q, is assumed to follow Darcy's law:[3]

$$\mathbf{q} = -\frac{k}{\mu}\nabla p. \tag{23}$$

Equation (23) neglects the gravitational body force. It is expected that the permeability will be a strongly-varying function of the connected porosity. For present purposes, a simple power law is adopted:

$$k = C\phi_{cn}^{n_k}, \tag{24}$$

where C is a constant. The appropriate value for the exponent n_k has not been established for salt. The value $n_k = 3$ is an approximation of the widely-used Blake-Kozeny correlation [*e.g.*, 10]. Rumpf and Gupta [11] suggest $n_k = 4.5$ for very low permeability. Equation (24) assures that the permeability vanishes altogether when the connected porosity vanishes. Note that (23) and (24) assume an isotropic medium; this can be relaxed in a more general model.

[3] Equation (23) is not a constitutive equation *per se*; rather, it is a statement of the momentum balance for the continuous fluid, along with constitutive assumptions for the fluid stress and the forces of interaction between the fluid and solid.

2.2.3 *Volumetric Exchange: The "Damage" Model*

It is assumed that the conversion of isolated porosity to connected porosity is related to the macroscopic, shearing deformation of the salt. That is, following the introduction of an excavation or borehole, non-zero deviatoric stresses cause the salt to deform in shear. This shearing is assumed to cause isolated pores to link up and form a connected network. A simple model that captures this effect is developed from the assumption that the isolated porosity is related to the creep strain by

$$\phi_{is} = \phi_{is0} \exp(-\beta \epsilon') \tag{25}$$

where ϕ_{is0} is the initial value of the isolated porosity in the undeformed state, β is a constant, and ϵ' is the creep strain, a measure of the magnitude of the shear strain:

$$\epsilon' = \left(\frac{2}{3}\epsilon_c : \epsilon_c\right)^{1/2}, \tag{26}$$

where ϵ_c is the creep-strain tensor. Equation (25) states that the isolated porosity takes a value ϕ_{is0} in the undeformed state, and is eliminated completely by large deformation ($\epsilon' \to \infty$). Substitution of (25) into (20) shows that Γ takes the form:

$$\Gamma = \phi_{is0}\beta \exp(-\beta\epsilon')\frac{\partial \epsilon'}{\partial t}. \tag{27}$$

Thus, the rate of conversion of isolated porosity to connected porosity depends on the magnitude and the rate of shear deformation.

Substitution of (22)–(27) into (19)–(21) gives:

$$\frac{\partial \phi_{is}}{\partial t} = -\phi_{is0}\beta \exp(-\beta\epsilon')\frac{\partial \epsilon'}{\partial t}, \tag{28}$$

$$\frac{\partial \phi_{cn}}{\partial t} = \phi_{is0}\beta \exp(-\beta\epsilon')\frac{\partial \epsilon'}{\partial t} - \frac{1}{K}\frac{\partial}{\partial t}(p_c - p) - \frac{1}{\kappa}(p_c - p), \tag{29}$$

$$\frac{\partial p}{\partial t} - \frac{KC}{\mu}\nabla \cdot (\phi_{cn}^{n_k}\nabla p) = \frac{\partial p_c}{\partial t} + \frac{K}{\kappa}(p_c - p). \tag{30}$$

Note that equation (30) recovers the linear diffusion equation of classical hydrology when the connected porosity takes some constant value, $\phi_{cn} = \phi_{cn0}$, the confining stress is constant, and the bulk viscosity is infinite. The fluid diffusivity is then simply $k_0 K/\mu =$ constant (where $k_0 = C\phi_{cn0}^{n_k}$ is the permeability), implying a capacitance of K^{-1}. It was noted previously [6] that the capacitance due solely to the salt compressibility, K^{-1}, even if augmented by additional compressibility of the fluid and solid constituents, appears to be much too small to reconcile field data for the brine flux to open boreholes. In particular, if one defines a characteristic time $a^2\mu/k_0 K$ for the linear diffusion problem, where a is the characteristic length scale for the opening (*e.g.*, borehole radius), it proves to be very small compared to the observed characteristic time for the decay of the fluid

flux. An interesting feature of equation (30), however, is the presence of the source terms on the right-hand side, representing the generation of pore pressure by increases in confining stress and by creep closure of the pores. The latter is appealing, since it allows the "squeezing out" of fluid by volumetric creep. This process will proceed until the pore pressure rises to the confining pressure and the "effective pressure" vanishes. It is clear, also, that this simple model introduces several new time scales into the problem. First, there is a time scale associated with the evolution of the mean stress field around the opening. Second, there is a viscoelastic relaxation time, κ/K, associated with the creep closure of pores. Finally, the permeability field evolves in time, as well, through its dependence on the growth of ϕ_{cn}. It is possible, then, that the evolution of the fluid flux may be limited, not by the permeability, but by the rate of production of interconnected porosity by the shearing deformation and/or by the rate of pore closure by volumetric creep.

In order to complete the foregoing model, one must solve for the creep strain and mean stress fields. If one assumes that the fluid transport processes do not affect the overall creep processes, then the creep strain and mean stress can be calculated independently.

3 Flow to a Borehole

Consider now the one-dimensional, radial flow to a long borehole. An independent calculation of the creep strain and mean stress, neglecting any coupling with the brine transport, has been provided by H. S. Morgan (1521), based on an elastic-plastic, power-law creep model [*e.g.*, 9, 12]. The calculation assumes that a circular hole is introduced into an unbounded region at zero time; the far-field stress is isotropic and equal to the overburden, $p_c = 15.0$ MPa. The inner boundary, at radius $r = a$ is traction-free. Rather than attempt to represent the full solution in detail, the general trend of the solution is parameterized in the simple form:

$$\epsilon' = A_\epsilon \left(\frac{r}{a}\right)^{-n_\epsilon} t^{m_\epsilon}, \tag{31}$$

where A_ϵ, n_ϵ, and m_ϵ are constants. A crude fitting exercise using the results of the more elaborate numerical calculation for the deformation yields the approximate values: $A_\epsilon = 8.0 \times 10^{-8}$ s$^{-0.6}$, $n_\epsilon = 2.0$, and $m_\epsilon = 0.6$ (with t given in seconds). The mean stress relaxes around the hole, and is also parameterized in the form

$$p_c = p_{c0} - A_\sigma \left(\frac{r}{a}\right)^{-n_\sigma} t^{m_\sigma}, \tag{32}$$

where p_{c0} is the initial, undisturbed mean stress. Again, a rough fit to the calculated values gives: $A_\sigma = 3.0 \times 10^3$ Pa s$^{-0.46}$, $n_\sigma = 1.5$, and $m_\sigma = 0.46$ (with t given in seconds).

Table 1. Estimated Material Properties for WIPP Salt.

Property	Symbol	Eq.	Value	Units	Source
Drained Blk. Mod.	K	(22)	20.7	GPa	[7]
Brine Viscosity	μ	(23)	1.6×10^{-3}	Pa·s	[2]
Porosity	ϕ_α	(5)	0.01	—	[2]
Shear-Strain Coeff.	A_ϵ	(31)	8.0×10^{-8}	$s^{-0.6}$	*
Shear Radial Exponent	n_ϵ	(31)	2.0	—	*
Shear Time Exponent	m_ϵ	(31)	0.6	—	*
Initial Mean Stress	p_{c0}	(32)	15.0	MPa	*
Mean-Stress Coeff.	A_σ	(32)	3.0×10^3	Pa $s^{-0.46}$	*
Stress Radial Exponent	n_σ	(32)	1.5	—	*
Stress Time Exponent	m_σ	(32)	0.46	—	*
Bulk Viscosity	κ	(22)	4.0×10^{17}	Pa·s	†
Perm. Coeff.	C	(24)	1.0×10^{-11}	m^2	†
Perm. Expon.	n_k	(24)	4.5	—	†
"Damage" Coeff.	β	(25)	2.0×10^3	—	†

*Obtained by fit to results calculated by H. S. Morgan (1521).
†Obtained by fit of model calculation to field data provided by S. J. Finley (6332).

4 Calculations and Results

Equations (28)–(30), along with the parameterized shear strain and confining stress models (31) and (32), were integrated using the method of lines. This scheme uses a centered-difference approximation to resolve the spatial gradients in (30), and a backward-difference solver for the time integrations. The semi-infinite domain from $r = a$ to $r \to \infty$ was mapped onto a finite region by a coordinate transformation (see, *e.g.*, [13]).

Results are shown in Figures 3–9. The simulation assumes a hole of radius $a = 0.05$ m (4" diameter). Figure 3 shows the creep strain calculated using equation (31). The strain

is maximum at the borehole wall, increases with time, and propagates outward. After 1 y, the effect is significant a few hole radii away. Figure 4 shows the confining pressure (or the magnitude of the mean stress), p_c, calculated using equation (32). The confining pressure is minimum at the borehole wall, decreases with time, and the relaxed zone propagates outward. The effect is significant over a region comparable to that influenced by the shear strain.

Figure 5 shows the evolution of the isolated porosity field, obtained by integration of (28). The isolated porosity takes the undisturbed value ϕ_{iso} in the far field, is eliminated quickly at the borehole wall, and diminishes in time, with the disturbed zone propagating outward. The zone in which the isolated porosity has been converted to connected porosity extends much further outward than does the sheared zone shown in Figure 3. This is simply a consequence of the highly nonlinear model relating the two (25). It is emphasized that this feature of the model is rather *ad hoc*; a different choice for the function Γ (27) could change these results significantly.

The connected porosity field is shown in Figure 6. The initial condition in the undisturbed salt is zero connected porosity, and this condition is maintained in the far field. The zone of connected porosity propagates outward in time. In a zone within a few radii of the borehole wall, the connected porosity reaches values slightly less than the original isolated porosity due to the creep pore closure accounted for in the model. In particular, near the wall, where the pore pressure vanishes, the sink term for connected porosity due to pore closure (*cf*, eq. 29), $-(p_c - p)/\kappa$, is a maximum.

Figure 7 shows the corresponding permeability field, calculated from the connected porosity by means of (24). The permeability vanishes entirely in the far field where ϕ_{cn} vanishes. Only at the borehole wall, where the shearing is greatest, does the permeability reach its maximum value associated with full conversion of isolated to connected porosity. Immediately outward from the wall, the creep closure of connected pores has reduced the permeability to about 80% of the maximum possible value.

Finally, Figure 8 shows the evolution of the pore pressure field. Here the difference from the classical, linear diffusion problem is evident. The far field remains at lithostatic pressure, and the relaxation front remains relatively steep as it propagates outward. The pressure rise is primarily in material outside the zone in which the permeability has increased significantly. That is, the pore pressure relaxes rapidly in the high-permeability region, and it is the evolution of connected porosity and associated permeability that controls the outward propagation of the front. This is where the longer time scale associated with the creep deformation affects the fluid flow. The near-wall pressure gradient decreases monotonically throughout this calculation.

The computed flux at the wall is shown in Figure 9 for comparison with the data from DBT10. The value of the parameter β in the "damage" model was varied to obtain a good match to the data. The interesting feature of the calculation shown is that the elastic capacitance ($C = K^{-1}$) used is the very small value expected based on the compressibility

of the salt. Thus, the classical, poroelastic relaxation time is still in the problem, and takes its small expected value. If this were the only time scale in the problem, the flux would fall off very rapidly compared to the observed behavior. However, as discussed above, the flux falls off over a time scale of hundreds of days because of the coupling to the creep deformation and the evolution of finite permeability.

5 Omissions from the Model

The model outlined here is, of course, highly idealized. Numerous additional processes may have significant, or even dominant, effects on the transport of brine in salt. Some of the phenomena that have been discussed on occasion could be incorporated within the general model structure as given here.

Omitted processes include:

- shear-induced dilatation or compaction,
- multiphase flow (e.g. air imbibition),
- exsolution of dissolved gas,
- precipitation and dissolution of salt and effects on permeability,
- vapor phase transport (drying),
- *etc.*

6 Summary

A model has been outlined that attempts to address some of the conceptual inconsistencies that may be present in representing salt as a classical, porous medium. This development is motivated by several observations:

1. The measured flow to open boreholes in the WIPP evolves over a very long time scale (of the order of hundreds of days). In the context of the classical model, this implies a very large capacitance, and, in turn, a very large compressibility for the system. It is difficult to reconcile this with independent estimates of the salt and brine compressibilities.
2. The usual concept of salt as a material that creeps under vanishingly small deviatoric stress is difficult to reconcile with the persistence of a ubiquitous, interconnected pore network, which is essential to the classical model.

3. The observation of variable brine chemistry over short length scales presents a further argument against the presence of extensive, interconnected porosity in the undisturbed salt. Molecular diffusion would be expected to homogenize the brines over the very long time available.

References

1. Nowak, E. J., D. F. McTigue, and Beraun, R., Brine Inflow to WIPP Disposal Rooms: Data, Modeling, and Assessment, **SAND88–0112**, September 1988.

2. McTigue, D. F., Calculations of bine flux and cumulative brine volume for Room Q, based on a Darcy-flow model, Memo to Distribution, April 3, 1989.

3. McTigue, D. F., Observations on brine flow mechanisms in WIPP repository salt based on data from a Room D borehole, Memo to Distribution, March 15, 1989.

4. Peterson, E., K. Lie, and P. Lagus, Brine-flow and gas-flow test summary, presented at Meeting on Salado Hydrology, Sandia National Laboratories, Albuquerque, NM, October 12, 1989.

5. Peterson, E., P. Lagus, and K. Lie, WIPP Horizon Free Field Fluid Transport Characteristics, **SAND87–7164**, December 1987.

6. McTigue, D. F., Effects of large capacitance on calculated brine volume due to Darcy flow, Memo to Distribution, October 27, 1989.

7. Stein, C. L., and J. L. Krumhansl, A model for the evolution of brines in salt from the Salado Formation, Southeastern New Mexico, *Geochimica et Cosmochimica Acta*, **52**, 1988, 1037–1046.

8. Krumhansl, J. L., K. M. Kimball, and C. L. Stein, Intergranular Fluid Compositions from the Waste Isolation Pilot Plant (WIPP), Southeastern New Mexico, **SAND90–0584**, in review, May 1990.

9. Krieg, R. D., Reference Stratigraphy and Rock Properties for the Waste Isolation Pilot Plant, **SAND83–1908**, January 1984.

10. Bird, R. B., W. E. Stewart, and E. N. Lightfoot, *Transport Phenomena*, Wiley, New York, 1960, p. 199.

11. Rumpf, H., and A. R. Gupta, *Chem. Ing. Techn.*, **43**, 1971, 367*ff*.

12. Morgan, H. S., and C. M. Stone, Pretest Reference Calculation for the Overtest for Simulated Defense High Level Waste (WIPP Room B In Situ Experiment), **SAND85–0213**, April 1985.

13. Nowak, E. J., and D. F. McTigue, Interim Results of Brine Transport Studies in the Waste Isolation Pilot Plant (WIPP), SAND87–0880, April 1987.

14. McTigue, D. F., Coupled rock deformation and pore fluid flow for salt based on linear poroelasticity, Memo to Distribution, March 2, 1990.

dfm:1511

Key Words: **Waste Isolation Pilot Plant (WIPP), brine inflow, damage, creep, coupled model**

Copy to:

1510 E. H. Barsis (acting)
1511 D. K. Gartling
1511 P. L. Hopkins
1511 D. F. McTigue (day file)
1512 E. H. Barsis (acting)
1513 D. W. Larson
1520 L. W. Davison
1521 H. S. Morgan
1521 J. G. Arguello
1521 C. M. Stone
1521 J. R. Weatherby
1530 J. R. Asay
1533 S. T. Montgomery
1550 C. W. Peterson
6340 W. D. Weart
6340 S. Y. Pickering
6341 R. C. Lincoln
6342 D. R. Anderson
6342 W. E. Beyeler
6342 R. P. Rechard
6343 T. M. Schultheis
6344 E. Gorham
6344 R. L. Beauheim
6344 P. B. Davies
6344 S. J. Finley
6344 A. L. Jensen
6344 S. W. Webb
6345 A. R. Lappin
6345 B. M. Butcher
6345 F. T. Mendenhall
6346 J. R. Tillerson
6346 D. E. Munson
6346 E. J. Nowak

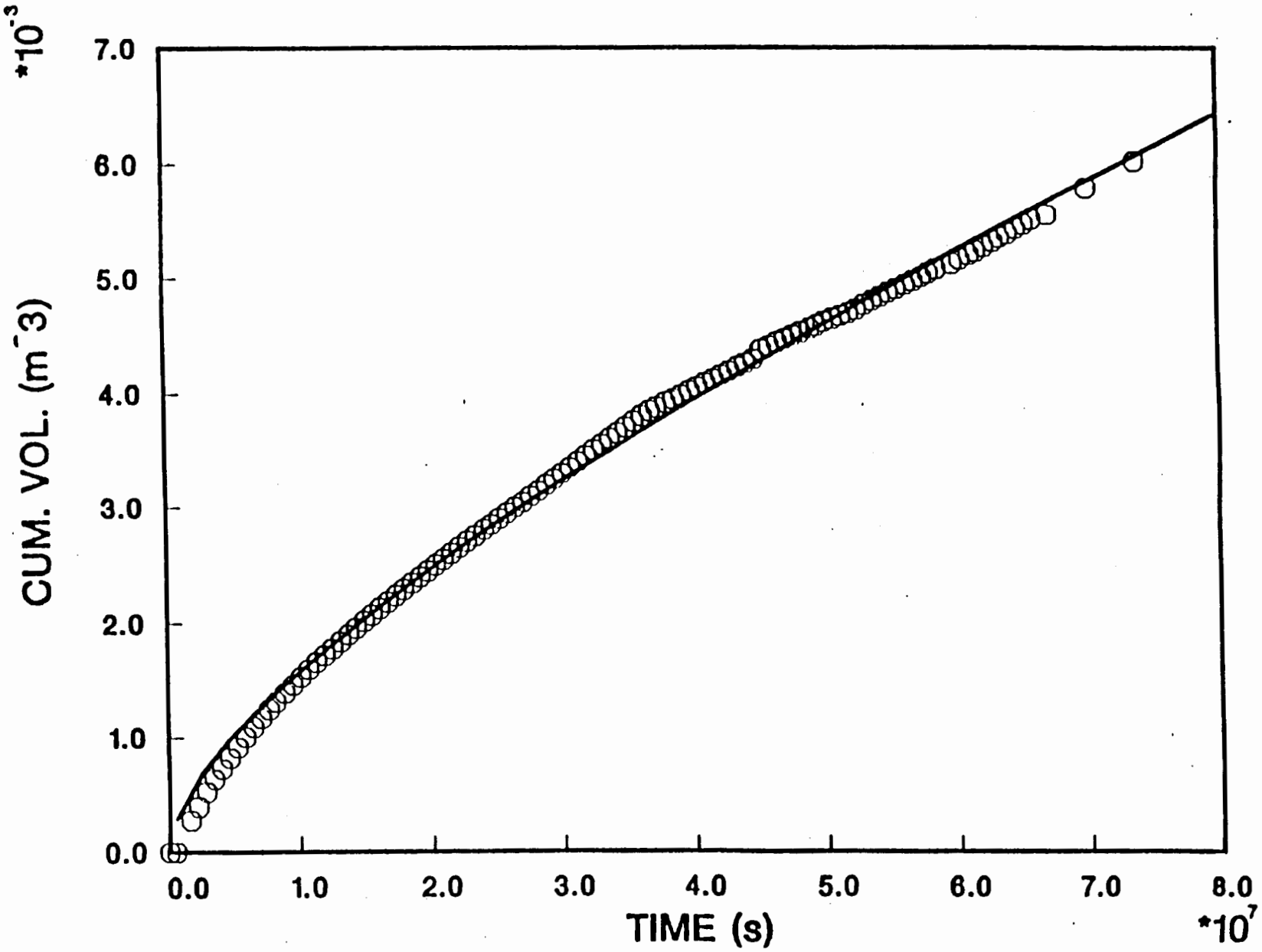
*10^-3
7.0
6.0
5.0
4.0
3.0
2.0
1.0
0.0
CUM. VOL. (m^3)
0.0
1.0
2.0
3.0
4.0
5.0
6.0
7.0
8.0
TIME (s)
*10^7

DBT10 FIT

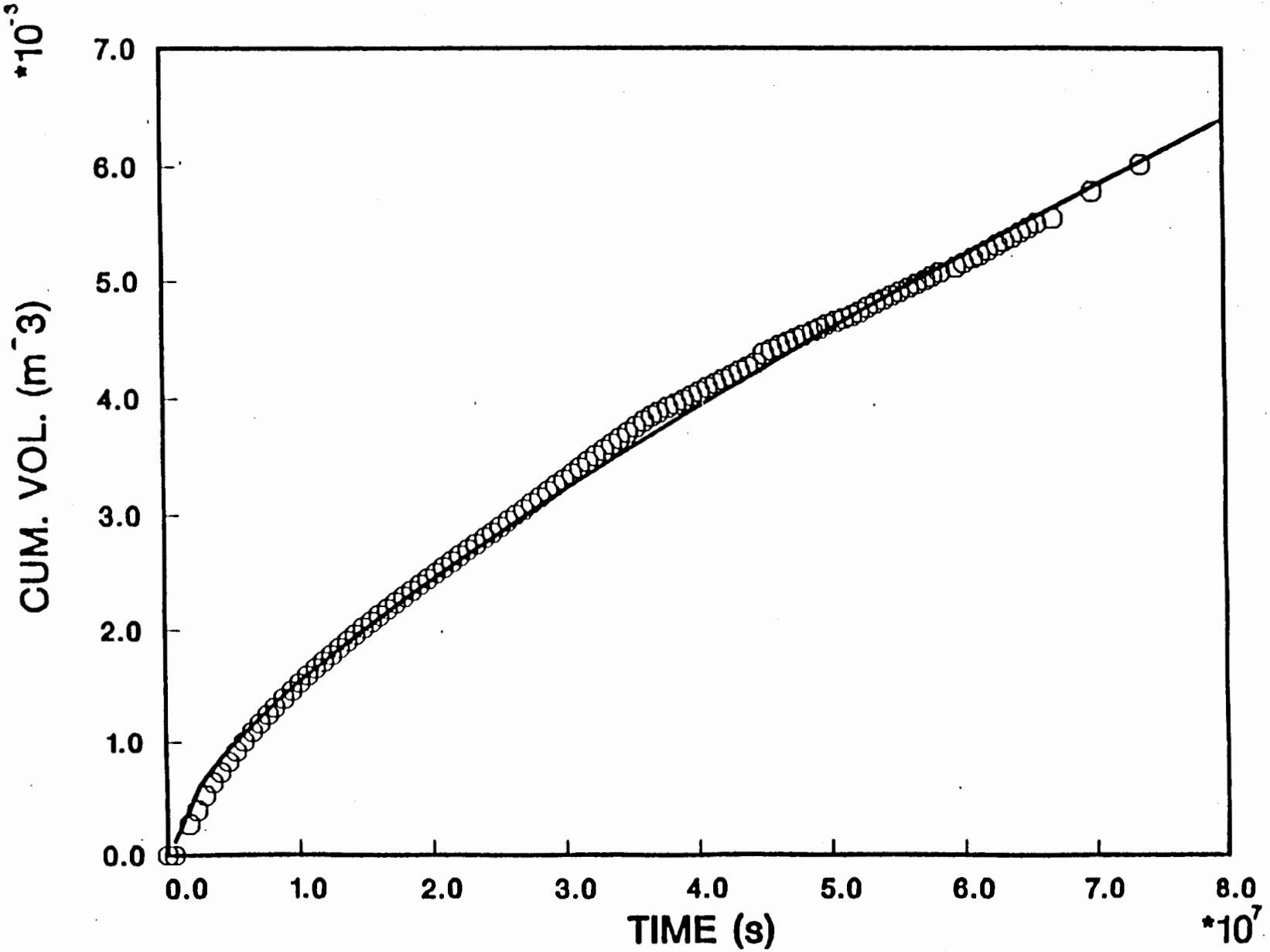
*10^-3
7.0
6.0
5.0
4.0
3.0
2.0
1.0
0.0
CUM. VOL. (m^3)
0.0
1.0
2.0
3.0
4.0
5.0
6.0
7.0
8.0
TIME (s)
*10^7

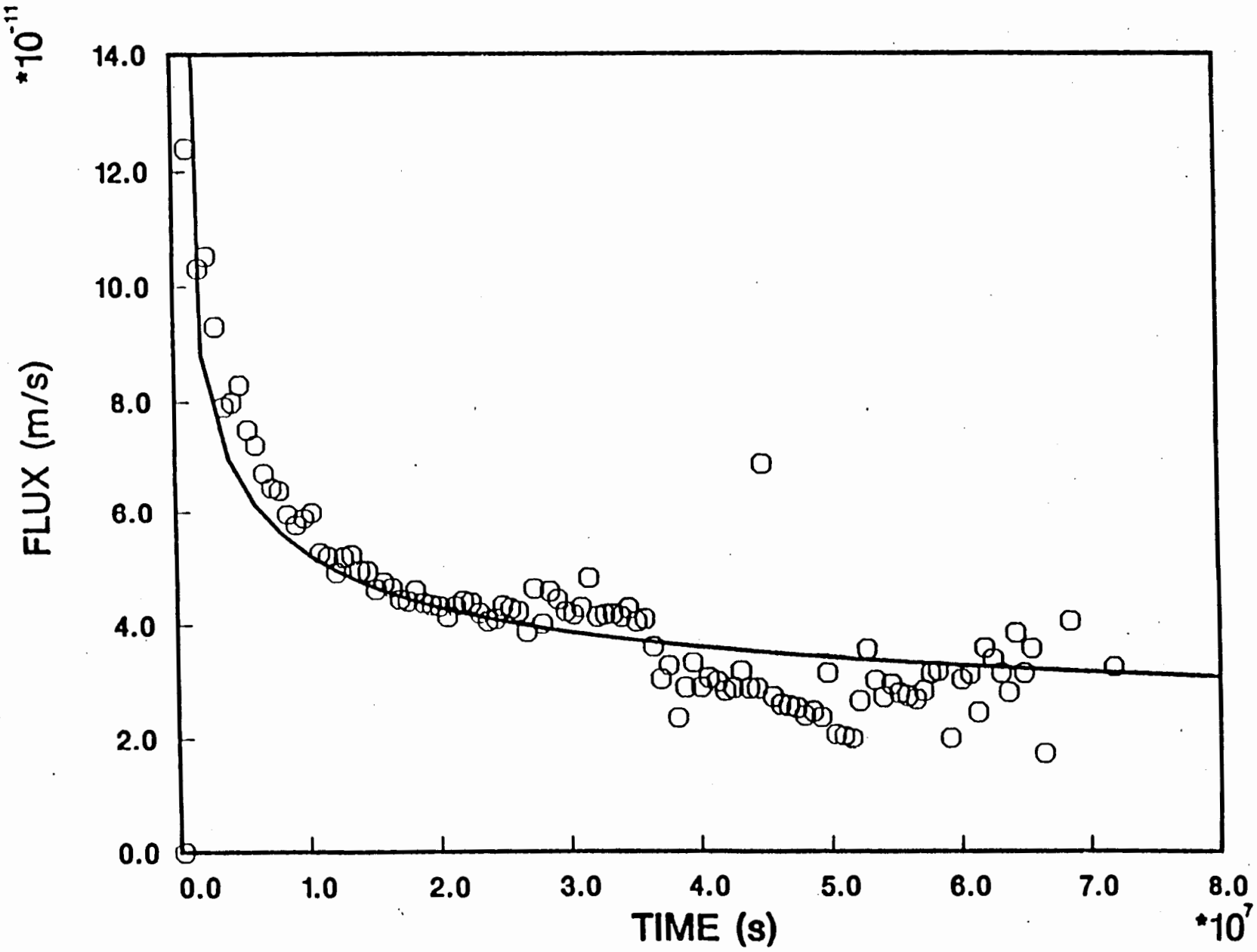
*10^-11
14.0
12.0
10.0
8.0
6.0
4.0
2.0
0.0
FLUX (m/s)
0.0
1.0
2.0
3.0
4.0
5.0
6.0
7.0
8.0
TIME (s)
*10^7

CREEP STRAIN

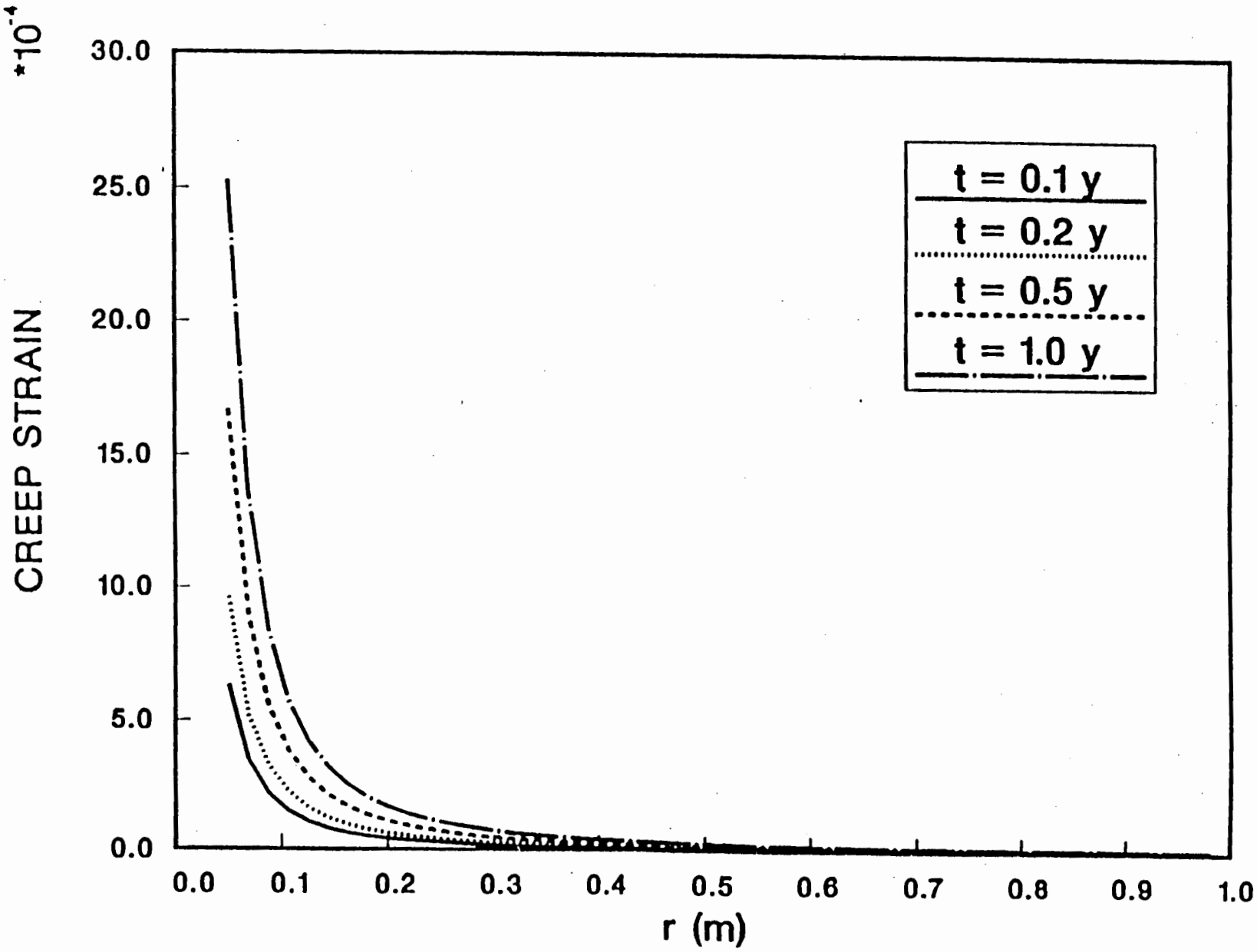

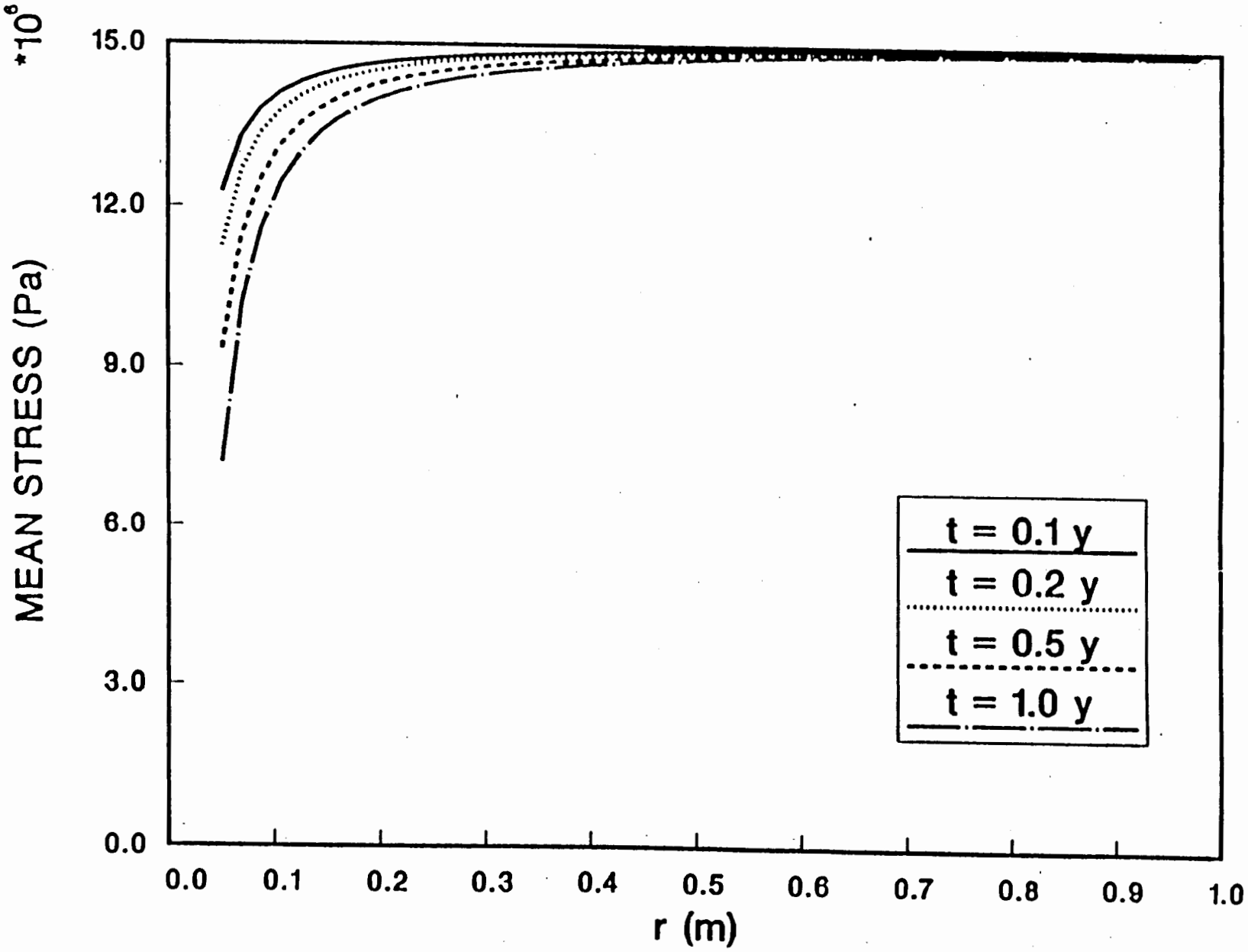
*10^6
MEAN STRESS (Pa)
15.0
12.0
9.0
6.0
3.0
0.0
0.0
0.1
0.2
0.3
0.4
0.5
0.6
0.7
0.8
0.9
1.0
r (m)
t = 0.1 y
t = 0.2 y
t = 0.5 y
t = 1.0 y

ISOLATED POROSITY

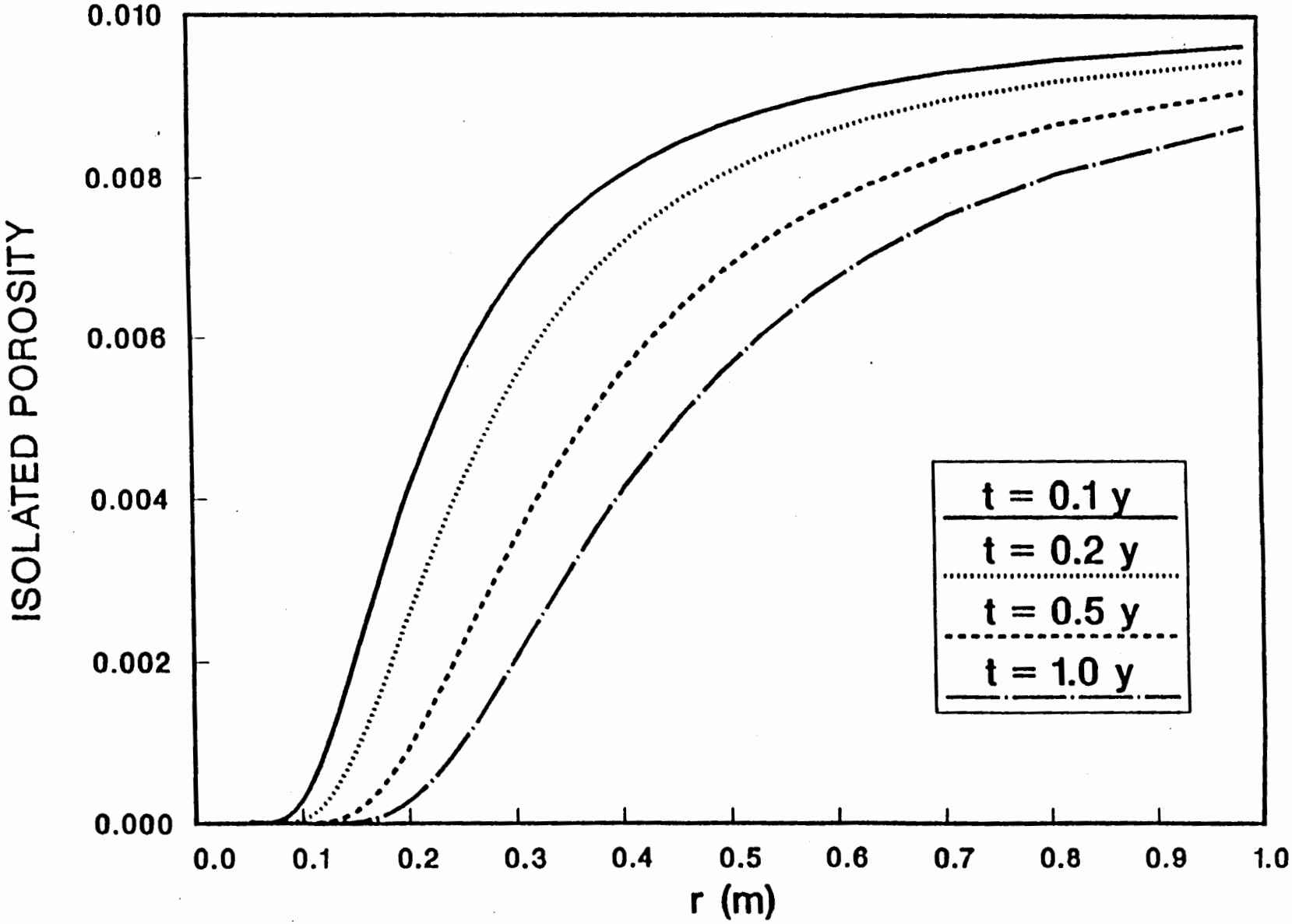

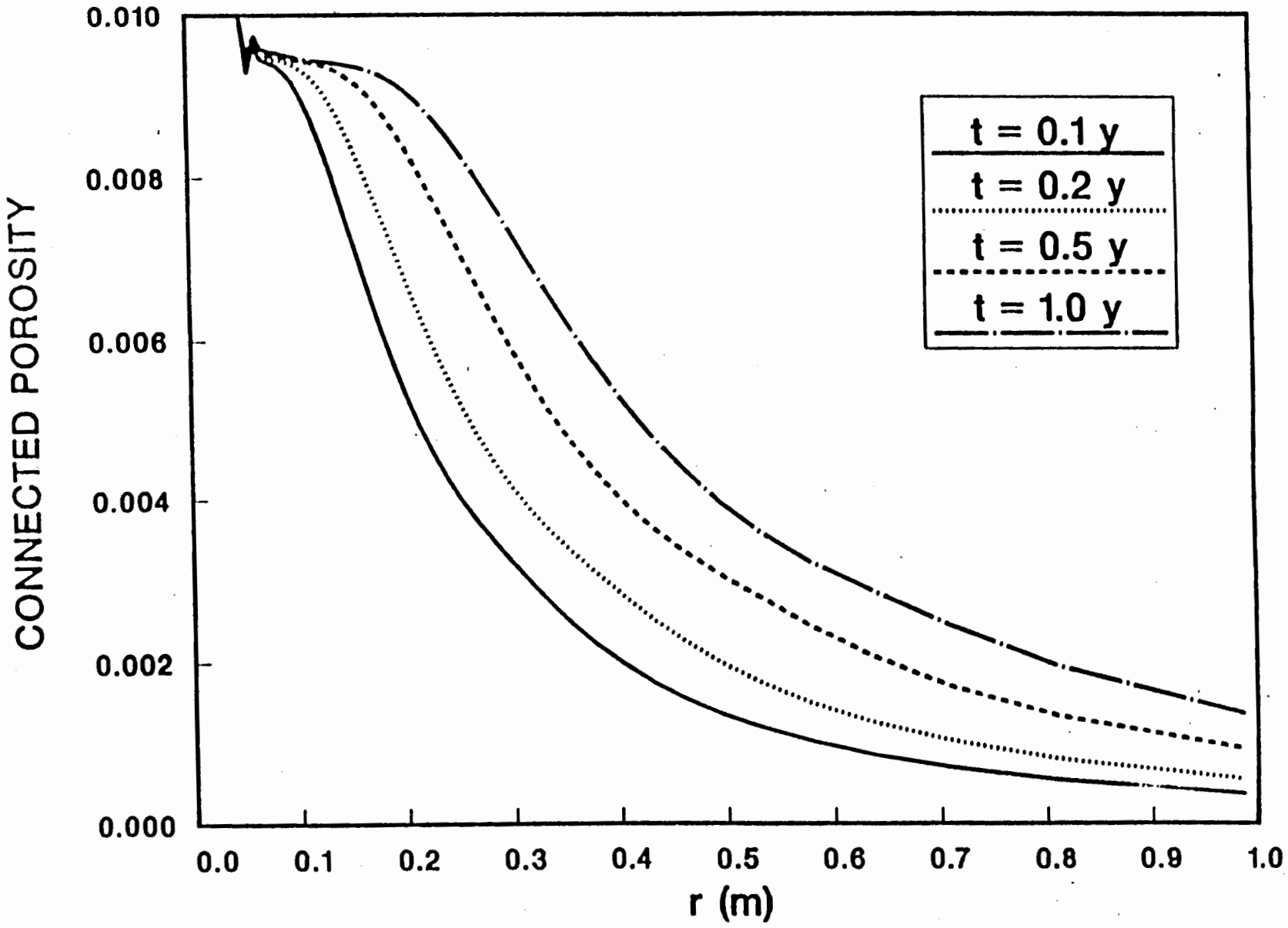
CONNECTED POROSITY
0.010
0.008
0.006
0.004
0.002
0.000
0.0
0.1
0.2
0.3
0.4
0.5
0.6
0.7
0.8
0.9
1.0
r (m)
t = 0.1 y
t = 0.2 y
t = 0.5 y
t = 1.0 y

PERMEABILITY

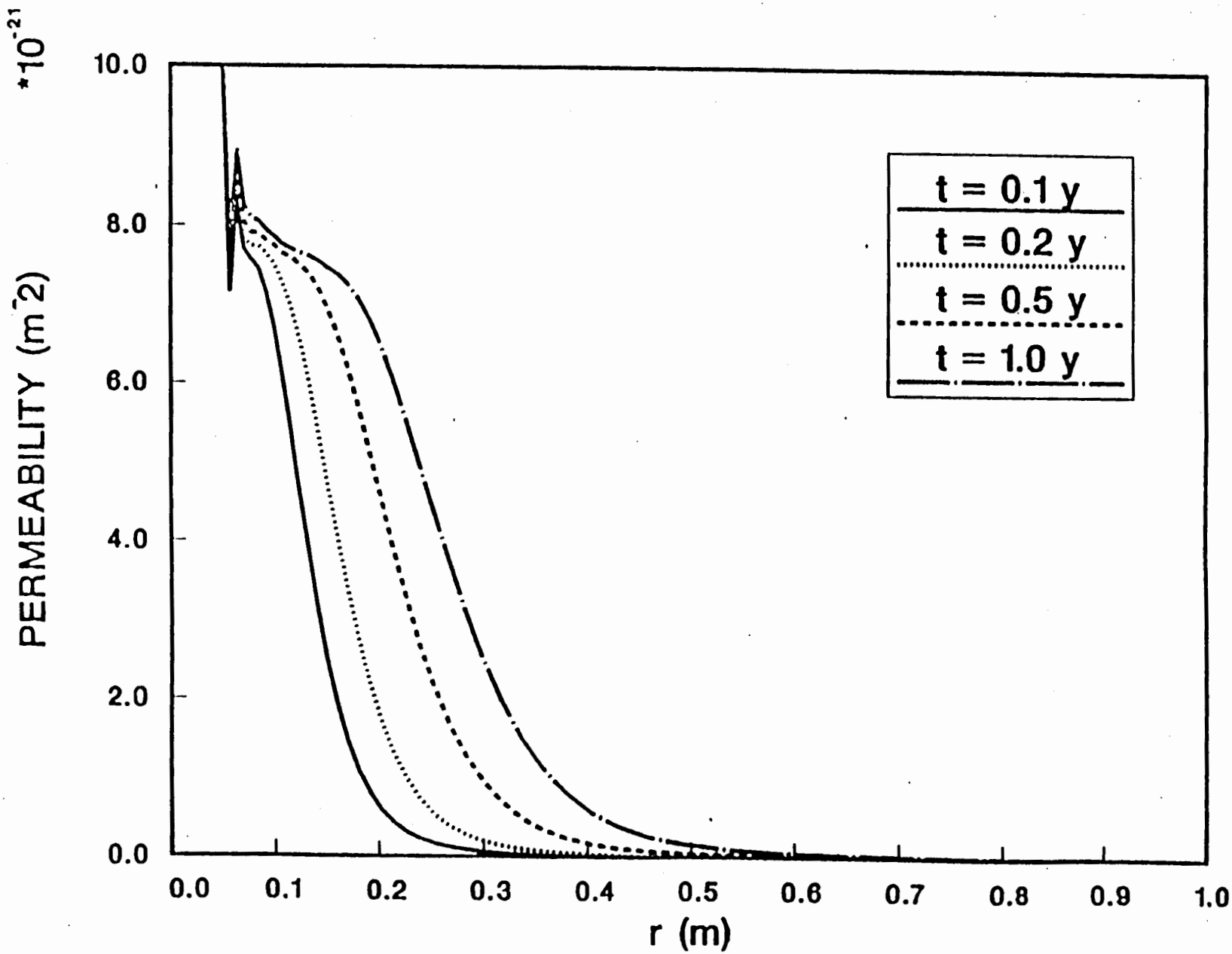

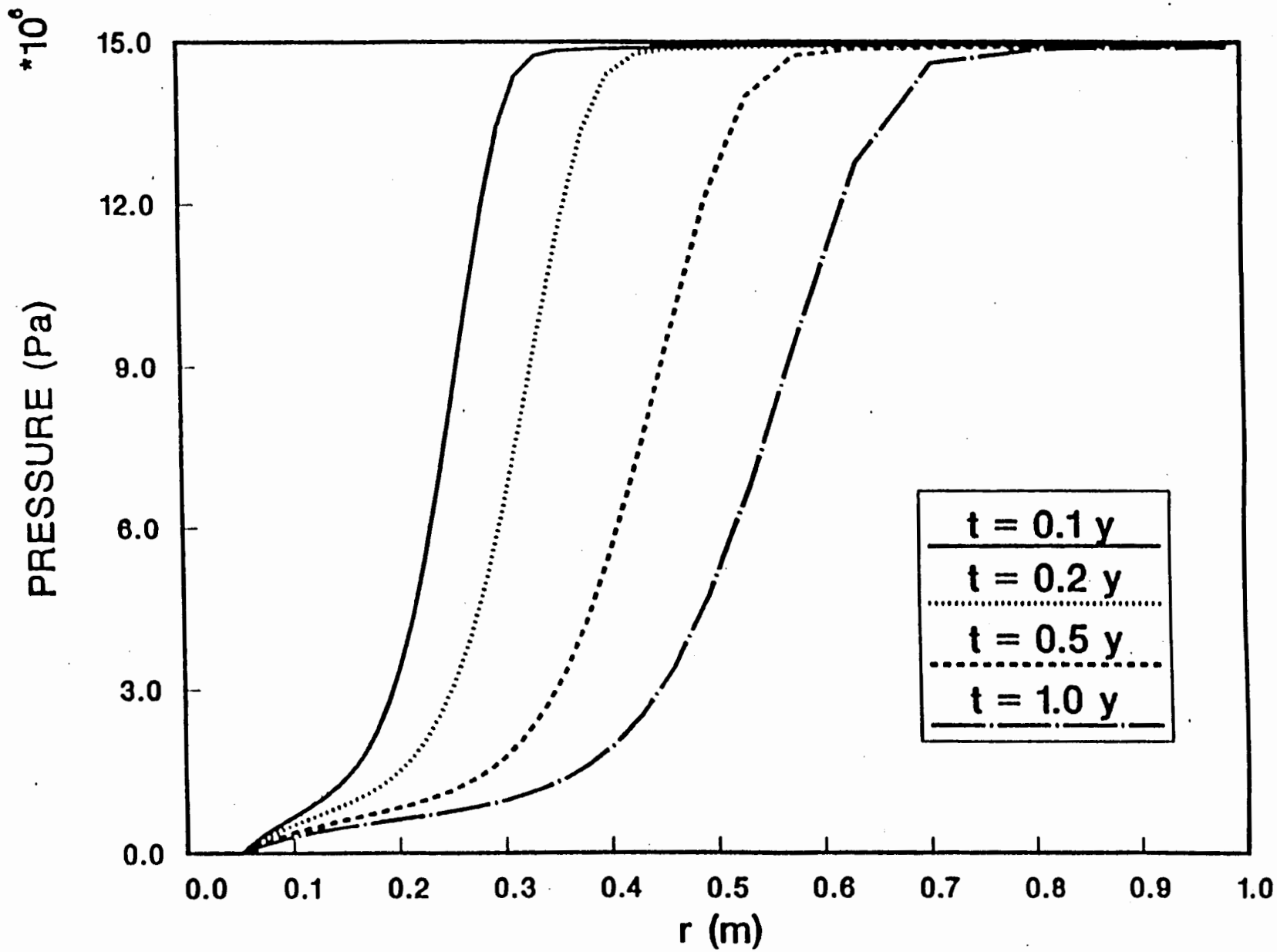
*10^6
15.0
12.0
9.0
6.0
3.0
0.0
PRESSURE (Pa)
0.0
0.1
0.2
0.3
0.4
0.5
0.6
0.7
0.8
0.9
1.0
r (m)
t = 0.1 y
t = 0.2 y
t = 0.5 y
t = 1.0 y

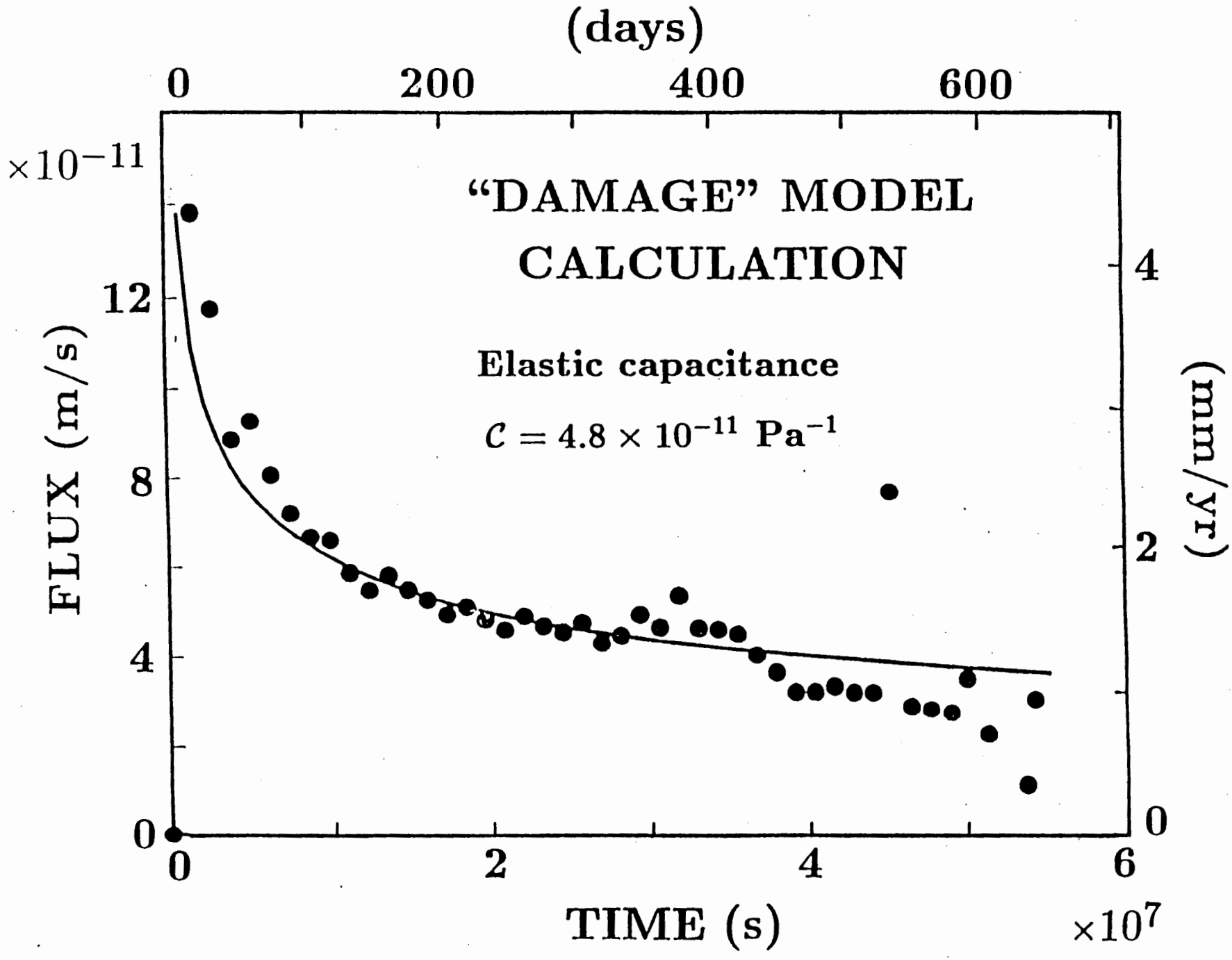
(days)
0
200
400
600
"DAMAGE" MODEL
CALCULATION
Elastic capacitance
$\mathcal{C} = 4.8 \times 10^{-11}$ Pa^{-1}
$\times 10^{-11}$
12
8
4
0
FLUX (m/s)
4
2
0
(mm/yr)
0
2
4
6
TIME (s)
$\times 10^{7}$

Fri.

Jim –

Here's the memo I talked about. As I noted, there's lots more to do —— This doesn't allow for dilatation due to stress relief (the microstructure changes, in this story, due only to shearing), imbibition of room air, etc. Nor does it consider the "damage" due to the room, later penetrated by a hole. Nonetheless, it makes the point that there can be much stronger coupling between rock deformation & brine flow.

Dave

Sandia National Laboratories
Albuquerque, New Mexico 87185

date: June 24, 1991

to: Distribution

from: D. F. McTigue, 1511

subject: Horizontal Darcy Flow to Room Q

Introduction

This memo reports order-of-magnitude estimates of brine seepage to Room Q assuming horizontal, Darcy flow confined to argillaceous halite. The calculation is in response to questions raised by the National Academy of Sciences (NAS) WIPP Panel at meetings held in Albuquerque on June 2 and June 4.

Susan Howarth (6344) reported at the NAS meeting that approximately 1.8 liters of brine were collected in Room Q in March 1991, representing the measurable accumulation since December 1990. With improved seals, approximately 3 to 7 liters of brine accumulated in the room from March to May 1991. She noted that even the latter volume is one to two orders of magnitude less than the quantities predicted by early calculations [1] based on radial Darcy flow to the room. The calculations referred to considered a range of properties and initial conditions. Permeabilities of 10^{-21} m^2 and 10^{-20} m^2 were assumed; the hydraulic diffusivity was computed based on the known elastic properties of the brine and salt, and fell in the corresponding range of about 10^{-7} m^2/s to 10^{-6} m^2/s. Initial pressures of 6 MPa and 15 MPa were assumed. These calculations predicted that, 21 months after mining (the approximate age of Room Q in April 1991), the flux to the room would be in the range 2–24 ml per day per meter length, or about 0.22 to 2.6 liters per day for the 109 m long room. The average inflow rate observed for the period March to May 1991 was of the order of 0.03 to 0.08 liters per day. The higher estimate for the observed accumulation rate (0.08 ℓ/d) is about one third of the lowest predicted rate (0.22 ℓ/d), while the lower estimate for the observed rate (0.03 ℓ/d) is only about 1% of the high prediction (2.6 ℓ/d).

Several other presentations to the NAS Panel showed evidence that brine seepage in the salt may be confined to certain lithologies, most notably anhydrite interbeds (*e.g.*, Marker Bed 139) and argillaceous halite. In this case, the effective permeability of the salt might be regarded as highly anisotropic, with flow predominantly in horizontal planes. The radial flow calculations performed previously would then be inappropriate. NAS Panel members asked how calculations based on the assumption of horizontal flow only compare

Table 1. Sample Calculations of Horizontal Brine Flow.

Quantity	Symbol	Units	Case 1	Case 2
Permeability	k	m^2	1.0×10^{-21}	1.0×10^{-22}
Capacitance	C	Pa^{-1}	1.0×10^{-11}	6.2×10^{-10}
Diffusivity	c	$m^2\ s^{-1}$	6.2×10^{-8}	1.0×10^{-10}
Initial pressure	p_0	Pa	1.0×10^{7}	1.0×10^{7}
Viscosity	μ	Pa·s	1.6×10^{-3}	1.6×10^{-3}
Volume flux*	$\lvert q \rvert A$	$m^3\ s^{-1}$	4.1×10^{-10}	10.2×10^{-10}

*Compare to observed: $\sim 6.3 \times 10^{-10}\ m^3/s$

Case 2 considers a much larger capacitance, as suggested by recent analysis of data for seepage to open boreholes (*i.e.*, at atmospheric pressure), as presented to the NAS Panel by Sharon Finley (6344). Typical values for the diffusivity found in that study are of the order of $c \sim 10^{-10}\ m^2/s$, and the inferred permeabilities tend toward relatively low values of order $k \sim 10^{-22}\ m^2$, implying a large capacitance ($C \sim 6.2 \times 10^{-10}\ Pa^{-1}$). These values are shown in Table 1 as Case 2. The effects of smaller permeability and smaller diffusivity are offsetting to some extent, particularly since the effect of a large change in diffusivity is weakened by the square-root dependence. Thus, the predicted flux for Case 2 is only 2.5 times greater than that in Case 1, and is still in order-of-magnitude agreement with the observed value.

It is emphasized that the two cases considered here were chosen to be representative of properties assumed or inferred for the salt in various aspects of the WIPP program. Other properties or combinations of properties that also appear to be reasonable do not yield the same agreement of predicted and observed brine flux. For example, consider a permeability of order $10^{-20}\ m^2$ and diffusivity of order $10^{-9}\ m^2/s$, which are not exceptional estimates from recent fits to data for seepage to boreholes [5]. These properties yield, with (1), a volume flow rate of about $3.3 \times 10^{-8}\ m^3/s$, a factor of 50 times greater than the rate accounted for by the brine collected.

Conclusions

In response to a question asked by the NAS WIPP Panel, simple calculations for horizontal brine flow to Room Q have been carried out. For reasonable choices of material properties, rough agreement is obtained with the observed flow rate estimated from the

2. Nowak, E. J., and D. F. McTigue, Interim Results of Brine Transport Studies in the Waste Isolation Pilot Plant (WIPP), **SAND87–0880**, Sandia National Laboratories, Albuquerque, NM, May 1987.

3. Krieg, R. D., Reference Stratigraphy and Rock Properties for the Waste Isolation Pilot Plant (WIPP) Project, **SAND83–1908**, Sandia National Laboratories, Albuquerque, NM, January 1984.

4. Sumino, Y., and O. L. Anderson, Elastic Constants of Minerals, *CRC Handbook of Physical Properties of Rocks*, **III**, R. S. Carmichael, ed., CRC Press, Boca Raton, FL, 1984, 39–138.

5. Kaufman, D. W., ed., *Sodium Chloride; The Production and Properties of Salt and Brine*, ACS Monograph **145**, American Chemical Society, Washington, D. C., 1960, 609.

6. Black, S. R., R. S. Newton, and D. K. Shukla, eds., Results of the Site Validation Experiments, Vol./ II, Supporting Document 10, Brine Content of Facility Interval Strata, U. S. Department of Energy, Waste Isolation Pilot Plant, 1983.

7. Peterson, E. W., P. L. Lagus, and K. Lie, WIPP Horizon Free Field Fluid Transport Characteristics, **SAND87–7164**, Sandia National Laboratories, Albuquerque, NM, December 1987.

DFM:1511

Table 4. Calculated Cumulative Volume.

	Cumulative Volume (liters/m)			
Time (months)	Case 1	Case 2	Case 3	Case 4
1	0.218	0.545	0.965	2.412
2	0.343	0.857	1.524	3.811
3	0.445	1.112	2.005	5.012
4	0.534	1.336	2.443	6.106
5	0.617	1.541	2.853	7.131
6	0.693	1.733	3.242	8.106
7	0.765	1.914	3.616	9.041
8	0.834	2.086	3.978	9.945
9	0.901	2.252	4.329	10.823
10	0.965	2.412	4.672	11.679
11	1.026	2.566	5.006	12.516
12	1.087	2.717	5.334	13.335
13	1.145	2.864	5.656	14.140
14	1.203	3.007	5.973	14.932
15	1.259	3.147	6.285	15.711
16	1.314	3.284	6.592	16.480
17	1.368	3.419	6.895	17.238
18	1.421	3.552	7.195	17.988
19	1.473	3.682	7.491	18.728
20	1.524	3.811	7.784	19.461
21	1.575	3.937	8.075	20.186
22	1.625	4.062	8.362	20.905
23	1.674	4.186	8.647	21.617
24	1.723	4.308	8.929	22.322

Sandia National Laboratories
Albuquerque, New Mexico 87185

date: April 3, 1989

to: Distribution

from: D. F. McTigue, 1511

subject: Calculations of Brine Flux and Cumulative Brine Volume For Room Q, Based on a Darcy-Flow Model

1 Introduction

Room Q is to be mined at the WIPP in order to perform a carefully controlled brine-inflow test at large scale. It is to have a circular cross section, 1.524 m (5 ft) in radius. An attempt will be made to collect all brine that arrives at the tunnel wall over a period of approximately two years, providing data for cumulative brine volume and average brine flux at the wall. The test-room configuration does not purport to represent a waste-storage room.

This memo summarizes calculations of the expected brine inflow to Room Q based on a classical Darcy flow model. The model simply states that the circular tunnel introduces a face at zero (atmospheric) pressure into a region of pore water at some initial pressure p_0. The initial pressure is expected to be between hydrostatic and lithostatic for the repository depth. Flow is driven toward the tunnel wall by the diffusion-like process of Darcy flow. Because the diffusivity is small, and the ratio of tunnel radius to length is small, it is reasonable to approximate the flow as one-dimensional (radial). Although this model is highly idealized, it has been shown previously [1] to reproduce observed brine fluxes in the WIPP to the correct order of magnitude.

2 The Classical Darcy Flow Model

It has been shown previously [2] that the magnitude of the Darcy flux to a circular tunnel or borehole is given by

$$|q|(t) = \frac{kp_0}{\mu a}\,\frac{4}{\pi^2}\int_0^\infty \frac{\exp(-cu^2t/a^2)}{J_0^2(u)+Y_0^2(u)}\,\frac{du}{u}, \tag{1}$$

where k is the permeability, p_0 is the initial brine pressure, μ is the brine viscosity, a is the radius of the hole, and c is the brine diffusivity. One can avoid having to integrate over

total brine in a typical sample is in interconnected pores. There is at present no strong argument for one choice over another, and, in any case, the influence on the calculations is not large. In particular, the two changes discussed here tend to be offsetting; the greater incompressibility of the brine tends to decrease the calculated capacitance, while the increased porosity increases the capacitance. For $k = 1.0 \times 10^{-21}$ m^2, the previous estimates yield a diffusivity of $c = 1.1 \times 10^{-7}$ m^2/s, while the properties in Table 1 yield $c = 0.8 \times 10^{-7}$ m^2/s. Other things being equal, an order-of-magnitude increase in ϕ_0 results in a 30% decrease in the diffusivity, while the 80% increase in K_f results in a 30% increase in the diffusivity. These changes do not affect the scale of the brine flux; they affect only the time scale over which the flux falls off. Thus, their overall effect on the present estimates of brine inflow is relatively small.

The radius used in the calculations is $a = 1.524$ m. Initial pressures were set to 6.0 MPa (approximately hydrostatic) and 15.0 MPa (approximately lithostatic) for the cases calculated, and permeabilities were set to 10^{-21} m^2 and 10^{-20} m^2. The four cases treated are summarized in Table 2.

Table 1. Estimated Material Properties for WIPP Salt.

Property	Symbol	Value	Units	Source
Drained Blk. Mod.	K	20.7	GPa	[3]
Shear Modulus	G	12.4	GPa	[3]
Poisson's Ratio	ν	0.25	—	[3]
Solid Blk. Mod.	K_s	23.5	GPa	[4]
Fluid Blk. Mod.	K_f	3.7	GPa	[5]
Viscosity	μ	1.6×10^{-3}	Pa·s	[5]
Porosity	ϕ_0	0.01	—	[6]
Permeability	k	$(1.0\text{–}10.0) \times 10^{-21}$	m^2	[7]
Undrained Bulk Mod.	K_u	22.6	GPa	
Undrained Poiss. Rat.	ν_u	0.268	—	
Skempton Coeff.	B	0.719	—	
Diffusivity	c	$(0.8\text{–}8.0) \times 10^{-7}$	m^2/s	

APPENDIX F:
HOWARTH MEMORANDUM

S. Howarth to R. Beauheim, "Laboratory-measured Values for Porosity and Permeability from Preliminary Laboratory Tests Performed on Marker Bed 139 Cores," September 9, 1994. Internal SNL Memorandum.

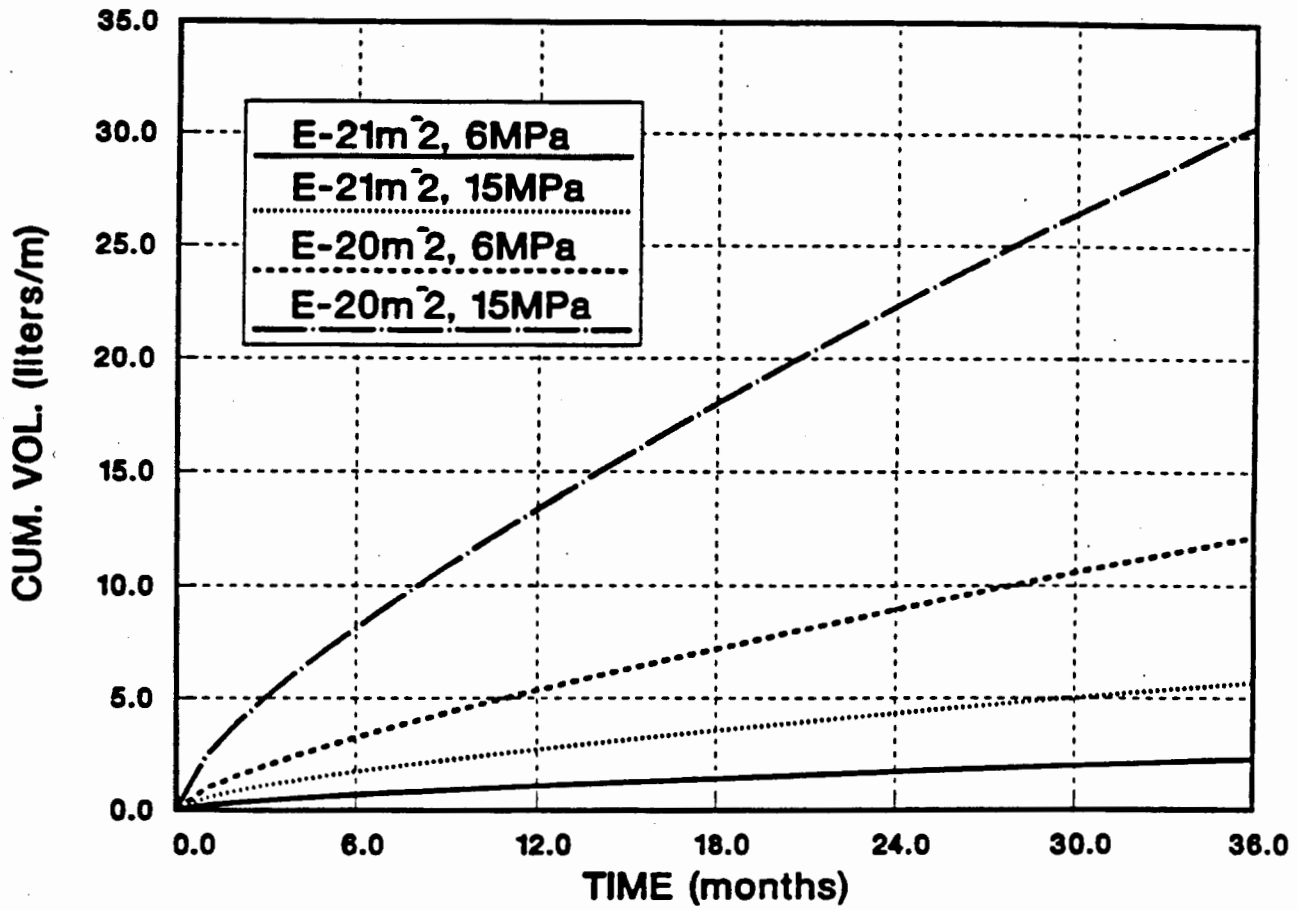

Figure 2. Calculated cumulative brine volume for a circular tunnel of radius 1.524 m (5 ft); volume is given in liters per meter length of the tunnel; four cases correspond to permeabilities $k = 10^{-21}$ and 10^{-20} m^2 and initial pressures $p_0 = 6.0$ and 15.0 MPa.

Sandia National Laboratories

Albuquerque, New Mexico 87185

to: R. Beauheim, 6115

from: S. Howarth, 6115

date: September 9, 1994

subject: Laboratory-measured Values for Porosity and Permeability from Preliminary Laboratory Tests Performed on Marker Bed 139 Cores

Preliminary tests were performed on three groups of core samples from Marker Bed 139 of the Salado Formation during FY93 to provide data to support the development of the numerical models used to predict the long-term hydrological and structural response of the WIPP to waste-generated gas as part of the Salado Two-Phase Flow Laboratory Program. These preliminary laboratory experiments: 1) generated WIPP-specific porosity, single-phase permeability, and capillary pressure data, 2) provided information needed to design and implement planned tests to measure threshold pressure, capillary pressure, and relative permeability, and 3) will be used to evaluate the suitability of using tight gas sands correlations as a Salado analog for assessment of the long-term performance of the WIPP. Total and effective porosity and gas and liquid steady-state single-phase permeability were measured as the test specimens were subjected to three different levels of hydrostatic confining stress while the pore pressure remained constant. Darcy flow was maintained during the permeability tests (i.e., the graph of flow rate versus pressure drop across the core was linear). Vertical and horizontal permeability were measured on adjacent cores.

Table 1 contains a summary of the porosity and permeability data results received from two (TerraTek and RE/SPEC) of the three laboratories that performed preliminary tests on Marker Bed 139 samples. Preliminary results from the third laboratory (Core Laboratories) are within the same ranges as the results contained in Table 1. Once QA of the Core Laboratories data is complete, Table 1 will be updated to incorporate all porosity and permeability data from the Preliminary Tests.

The laboratory-measured effective porosity values range from 0.4 to 2.7% with a mean of 1.25% (see Table 1). These values compare well with the range and mean values for porosity used in the 1992 PA; 0.1 to 3.0% and 1.25%, respectively. The laboratory-measured single-phase permeability values ranged from 8.4×10^{-16} to 5.5×10^{-20} m^2, depending on the stress conditions during the test (see Table 1). The mean was approximately 3.5×10^{-18} m^2 at 6 MPa. These values are an order of magnitude higher on the low end of the permeability distribution curve than those used in the 1992 PA. Likewise, the mean laboratory-measured single-phase permeability was an order of magnitude higher than the mean used in the 1992 PA.

Liquid single-phase permeability data are also reported in Table 1 for three samples for which gas permeability was also measured. As expected, these data compare well with the Klinkenberg-corrected gas single-phase data at all confining stress levels. It should be noted that the liquid permeability test specimens were chosen using high gas permeability as the primary selection criterion. Single-phase permeability, whether gas or non-reactive-liquid, is considered to be an intrinsic property of the rock. Therefore, one should not draw the conclusion that liquid permeability of the Salado is more uniform or, on average, higher than the gas permeability. Thus, for single-phase permeability of the Salado anhydrite, the range and mean values detailed in the preceding paragraph should be used.

Results indicate that the both porosity and single-phase permeability were reduced as increasing levels of confining stress were applied to the test specimen. Typically, permeability was reduced by less than an order of magnitude with an increase in confining stress from 2 to 10 MPa. Porosity reduction was less dramatic over the same pressure range; porosity was reduced by less than half a percent with an increase in confining stress from 2 to 10 MPa. These experimental results illustrate the stress dependence of porosity and permeability for Marker Bed 139 anhydrite.

Copy to:

6115 Davies, P.
6115 Webb, S.
SWCF-A:WBS1141;HYD/TPF

Table 1. Porosity and Permeability Data from Preliminary Laboratory Tests on Marker Bed 139 Cores

Lab	Sample Number	Sample Bulk Volume (cc)	Total Porosity (%)	Effective Porosity (%)	Klinkenberg- Corrected Gas Permeability (m^2) Under Net Hydrostatic Confining Stress (MPa)	Liquid Permeability (m^2) Under Net Hydrostatic Confining Stress (MPa)
R/S	P3X11-5-2-SP1T	12.62	2.8		3.2×10^{-18} (2 Mpa) 1.7×10^{-18} (6 Mpa) 1.4×10^{-18} (10 Mpa)	
R/S	P3X11-5-3-SP3T	14.97	2.2		1.6×10^{-17} (2 Mpa) 8.9×10^{-18} (6 Mpa) 5.1×10^{-18} (10Mpa)	
R/S	P3X10-6-SP2T	14.59				
TT	E1X08-A	822.24		1.87	8.4×10^{-18} (2 Mpa) 5.8×10^{-18} (6 Mpa) 5.1×10^{-18} (10Mpa)	6.8×10^{-18} (2 Mpa) 5.8×10^{-18} (6 Mpa) 5.4×10^{-18} (10Mpa)
TT	E1X08-B	776.83		0.49	1.3×10^{-17} (2 Mpa) 7.5×10^{-18} (6 Mpa) 4.7×10^{-18} (10Mpa)	
TT	E1X08-C	819.62		1.01	4.6×10^{-18} (2 Mpa) 2.6×10^{-18} (6 Mpa) 2.0×10^{-18} (10Mpa)	3.7×10^{-18} (2 Mpa) 2.4×10^{-18} (6 Mpa) 1.8×10^{-18} (10Mpa)
TT	E1X08-EP1	83.47	1.4	1.29		
TT	E1X08-EP2	84.39	0.6	0.75		
TT	E1X08-EP3	83.54	0.4	0.42		
TT	E1X08-EP4	83.35	1.6	1.60		
TT	E1X07-D	803.84		0.73	1.5×10^{-19} (2 Mpa) 6.0×10^{-20} (6 Mpa) 5.5×10^{-20} (10Mpa)	
TT	E1X07-E	843.08		1.55	8.4×10^{-16} (2 Mpa) 3.1×10^{-16} (6 Mpa) 1.6×10^{-16} (10Mpa)	

Lab	Sample Number	Sample Bulk Volume (cc)	Total Porosity (%)	Effective Porosity (%)	Gas Permeability (m^2) Under Net Hydrostatic Confining Stress (Klinkenberg Corrected)	Liquid Permeability (m^2) Under Net Hydrostatic Confining Stress
TT	E1X07-F	815.25		1.00	1.1×10^{-18} (2 Mpa) 7.0×10^{-19} (6 Mpa) 5.8×10^{-19} (10Mpa)	1.1×10^{-18} (2 Mpa) 6.2×10^{-19} (6 Mpa) 5.2×10^{-19} (10Mpa)
TT	E1X07-EP5	84.85		1.92		
TT	E1X07-EP6	84.04		2.73		
TT	E1X07-EP7	83.73		0.55		
TT	E1X07-EP8	84.52		1.57		
Total Number of Data Points			6	14	8 at each Confining Stress	3 at each Confining Stress
Range of Data			0.4 to 2.8%	0.42 to 2.73%	2 MPa: 1.5×10^{-19} - 8.4×10^{-16} 6 MPa: 6.0×10^{-20} - 3.1×10^{-16} 10MPa: 5.5×10^{-20} - 1.6×10^{-16}	2 MPa: 1.1×10^{-18} - 6.8×10^{-18} 6 MPa: 6.2×10^{-19} - 5.8×10^{-18} 10MPa: 5.2×10^{-19} - 5.4×10^{-18}
Mean			1.5%	1.25%	6.6×10^{-18} (2 Mpa) 3.5×10^{-18} (6 Mpa) 2.5×10^{-18} (10Mpa)	3.0×10^{-18} (2 Mpa) 2.0×10^{-18} (6 Mpa) 1.7×10^{-18} (10Mpa)

R/S = RE/SPEC laboratory, Rapid City, South Dakota
TT = TerraTek laboratory, Salt Lake City, Utah

APPENDIX G:
SUMMARY OF TEST-INTERPRETATION RESULTS FROM IN SITU PERMEABILITY AND PORE PRESSURE TESTS

Appendix G. Summary of Test-Interpretation Results from In Situ Permeability and Pore Pressure Tests

Test Internal (meters from excavation)	Hole	Zone	Map Unit	Test	Analysis Method	Average Permeability k (m^2)	Formation Pore Pressure p_f (MPa)	Data Reference	Interpretation Reference
8.63 - 10.06	L4P51-B	test	anhydrite "c"	PB	Interpret/2	5.1×10^{-20}	5.17	a	b
				all	GTFM	6.4×10^{-20}	5.21	a	b
6.75 - 7.79		guard	H-2	SI	–	–	>3.25	a	b
4.14 - 5.56	L4P52-A	test	anhydrite "a"	PB	Interpret/2	6.4×10^{-20}	6.50	a	b
				all	GTFM	6.0×10^{-20}	6.75	a	b
2.27 - 3.32		guard	anhydrite "b"	SI	–	–	>3.5	a	b
8.70 - 10.15	S1P71-B	test	anhydrite "c"	all	GTFM	8.0×10^{-20}	5.12	a	b
6.82 - 7.87		guard	H-2	SI	–	–	>4.2	a	b
2.15 - 3.18	S1P72-A	guard	0, PH-4	all	GTFM	1.8×10^{-21}	4.08	a	b
3.38 - 4.80	S1P73-A	test	anhydrite "a"	SI	–	–	0	a	b
0.85 - 2.49		guard	anhydrite "b"	SI	–	–	0	a	b
9.92 - 11.32	S1P73-B	test	MB138	PW2	type curve	4.9×10^{-20}	–	a	b
				CPW	type curve	1.8×10^{-20}	–	a	b
				PB	Interpret/2	4.9×10^{-20}	4.29	a	b
				all	GTFM	4.9×10^{-20}	4.37	a	b
8.04 - 9.09		guard	AH-1	SI	Horner	–	2.55	a	b
10.68 - 15.39	SCP01-A	test	MB139	CPW2	type curve	5.8×10^{-20}	–	a	b
				PB2	Interpret/2	5.1×10^{-20}	12.40	a	b
				all	GTFM	7.1×10^{-20}	12.55	a	b

Test Interval (m)	Hole	Zone	Map Unit	Test	Analysis Method	Average Permeability k (m^2)	Formation Pore Pressure P_f (MPa)	Data Reference	Interpretation Reference
2.09 - 5.58	C2H01-A	Test	0 - 5	All	GTFM	9.1×10^{-19}	0.54	c	d
		Test	4 - 5	All	GTFM	3.5×10^{-18}	0.56	c	d
4.50 - 5.58	C2H01-B	Test	0	All	GTFM	6.9×10^{-21}	3.22	c	d
2.92 - 4.02		Guard	0 - 4		GTFM	2.5×10^{-21}	4.17	c	d
6.63 - 8.97	C2H01-C	Test	MB139	All	GTFM	1.2×10^{-18}	8.16	c	d
9.47 - 10.86	C2H02	Test	MB139	All	GTFM	1.0×10^{-19}	9.43	c	d
7.76 - 9.14	C2H03	Test	9	All	GTFM	$< 10^{-21}$	?	c	d
3.33 - 4.75	L4P51-A	Test	PH-3, Clay D	All	GTFM	7.9×10^{-21}	2.81	c	d
3.74 - 5.17	S0P01	Test	PH-3, Clay D	All	GTFM	1.1×10^{-20}	4.52	c	d
1.86 - 2.91		Guard	MB139	All	GTFM	7.4×10^{-18}	0.56	c	d
3.12 - 4.56	S1P71-A	Test	PH-3, Clay D	All	GTFM	7.0×10^{-20}	3.01	c	d

Test Interval (m)	Hole	Zone	Map Unit	Test	Analysis Method	Average Permeability k (m^2)	Formation Pore Pressure P_f (MPa)	Data Reference	Interpretation
24.49 - 26.37 (12.3) ***	QPP01	Test	MB138	All	GTFM	8.4×10^{-20}**	10.4**	e	f
23.20 - 24.05 (6.2)	QPP02	Test	12 - 13	All	--	?	?	e	f
22.45 - 23.35	QPP03	Test	anhydrite "b"	All	GTFM	7.8×10^{-20}*	12.4*	e	f
(2.9)		Test	anhydrite "b"	All	GTFM	7.8×10^{-20}**	6.9**	e	f
23.69 - 24.54 (1.9)	QPP04	Test	6 - 7	All	--	?	?	e	f
22.08 - 22.98	QPP05	Test	6	All	GTFM	3.6×10^{-23}*	6.5*	e	f
(0.8)		Test	6	All	GTFM	4.1×10^{-20}**	0.3**	e	f
25.29 - 26.64	QPP11	Test	H1	All	GTFM	5.3×10^{-22}*	5.5*	e	f
(12.3)		Test	H1	--	--	--	7.4**	e	f
23.35 - 24.20	QPP12	Test	H3	All	GTFM	2.7 x 10-22*	9.6*	e	f
(6.2)		Test	H3	All	GTFM	2.7×10^{-22}**	9.6**	e	f
22.54 - 23.44 (3.3)	QPP13	Test	MB139	All	GTFM	7.3×10^{-20}**	8.1**	e	f
22.35 - 23.20	QPP14	Test	MB139	All	GTFM	2.1×10^{-23}*	8.0*	e	f
(2.1)		Test	MB139	All	GTFM	2.0×10^{-23}**	8.0**	e	f
22.14 - 23.04	QPP15	Test	0 - PH4	All	GTFM	1.1×10^{-23}*	7.5*	e	f
(1.0)		Test	0 - PH4	All	GTFM	3.1×10^{-22}**	3.1**	e	f
23.18 - 24.54 (12.0)	QPP21	Test	2 - 3	All	GTFM	8.8×10^{-23}*	3.9*	e	f
		Test	2 - 3	All	GTFM	1.5×10^{-21}**	5.0**	e	f
22.25 - 23.10 (5.9)	QPP22	Test	3	All	GTFM	1.3×10^{-21}**	3.2**	e	f

Test Intraval (m)	Hole	Zone	Map Unit	Test	Analysis Method	Average Permeability k (m^2)	Formation Pore Pressure P_f (MPa)	Data Reference	Interpretation
21.99 - 22.89 (3.0)	QPP23	Test	3	All	GTFM	1.2×10^{-20}**	3.5**	e	f
22.01 - 22.86 (1.6)	QPP24	Test	1 - 2	–	–	?	?	e	f
21.96 - 22.86 (1.0)	QPP25	Test	2 - 3	All	GTFM	7.0×10^{-21}**	2.2**	e	f

Key:PB = pressure-buildup test
SI = shut-in pressure buildup
PW = pulse-withdrawal test
CPW = constant-pressure withdrawal test
* = before mining of Room Q
** = after mining of Room Q

a = Stensrud, W.A., T.F. Dale, P.S. Domski, J.B. Palmer, R.M. Roberts, M.D. Fort, G.J. Saulnier, Jr., and A.L. Jensen. 1992. *Waste Isolation Pilot Plant Salado Hydrology Program Data Report #2.* SAND92-7072. Albuquerque, NM: Sandia National Laboratories.

b = Beauheim, R.L., R.M. Roberts, T.F. Dale, M.D. Fort, and W.A. Stensrud. 1993. *Hydraulic Testing of Salado Formation Evaporites at the Waste Isolation Pilot Plant Site: Second Interpretive Report.* SAND92-0533. Albuquerque, NM: Sandia National Laboratories.

c = Saulnier, G.J., Jr., P.S. Domski, J.B. Palmer, R.M. Roberts, W.A. Stensrud, and A.L. Jensen. 1991. *WIPP Salado Hydrology Program Data Report #1.* SAND90-7000. Albuquerque, NM: Sandia National Laboratories.

d = Beauheim, R.L., G.J. Saulnier, Jr., and J.D. Avis. 1991. *Interpretation of Brine-Permeability Tests of the Salado Formation at the Waste Isolation Pilot Plant Site: First Interim Report.* SAND90-0083. Albuquerque, NM: Sandia National Laboratories.

e = Jensen, A.L., C.L. Howard, R.L. Jones, and T.P. Peterson. 1993. *Room Q Data Report: Test Borehole Data from April 1989 through November 1991.* SAND92-1172. Albuquerque, NM: Sandia National Laboratories.

f = Domski, June 29, 1994. Memo.

*** = Approximate post-mining distance from Room Q to test interval.

APPENDIX H:
RESULTS OF McTIGUE PARAMETER ESTIMATION FOR SMALL SCALE BRINE INFLOW TESTS

Results of McTigue (1993) parameter estimation based on three different history matches. Different hole histories due to extension or enlargement are indicated by the alpha character (A,B,C) following the borehole identification.

Borehole	Comments	History Fit Used	Inferred Permeability ($m^2 x 10^{-21}$)	Inferred Diffusivity ($m^2/s \times 10^{-10}$)
DBT10	Good data; Deleted initial zero and one outlier data points.	Full Flux Late-Time Flux Cum. Vol	0.38 0.83 0.67	0.47 22.80 3.11
DBT11	Good data; Deleted initial zero data point.	Full Flux Late-Time Flux Cum. Vol.	1.49 2.07 1.61	35.09 508.00 57.70
DBT12	Good data; Deleted initial zero data point	Full Flux Late-Time Flux Cum. Vol.	0.84 2.60 0.85	101.73 1.45×10^7 141.00
DBT13	Good data; No data deleted	Full Flux Late-Time Flux Cum. Vol.	0.23 0.44 0.30	0.59 22.80 1.50
DBT14 A	Deleted initial zero and all data for increasing flux (t > ~146 days)	Full Flux Late-Time Flux Cum. Vol.	1.02 0.47 0.82	278.10 49.40 133.00
DBT14 B	Deleted initial zero and all data for increasing flux (t > ~178 days)	Full Flux Late-Time Flux Cum. Vol.	2.93 — —	433.61 — —
DBT15 A	Good data; No data deleted	Full Flux Late-Time Flux Cum. Vol.	0.42 0.46 0.61	1.85 11.50 4.28
DBT15 B	Good data; Deleted first three data points.	Full Flux Late-Time Flux Cum. Vol.	0.24 1.28 0.18	1.27 133.00 0.66
DBT16	No observed brine inflow			
DBT17	No observed brine inflow			
DBT31 A	Deleted initial data; Deleted all data for erratic flow (t > 152 days)	Full Flux Late-Time Flux Cum. Vol.	1.18 1.22 —	4.05 29.8 —
DBT31 B	No fit obtained; increasing flow rate.			
DBT31 C	Fit only for period of declining flux from 196 to 335 days.	Full Flux Late-Time Flux Cum. Vol.	0.004 — —	0.003 — —
DBT32 A	No fit obtained; increasing flow rate.			
DBT32 B	Not fit obtained; increasing flow rate.			

DBT32 C	Fit only to period of declining flux from 203 to 322 days.	Full Flux Late-Time Flux Cum. Vol.		
L4B01		Full Flux Late-Time Flux Cum. Vol.	0.09 0.14 0.19	0.58 13.60 44.00
L4X01	No full flux fit or cum. vol. fit obtained; data showed linear decline to zero flux.	Full-Flux Late-Time Flux Cum. Vol.	0.34	626.00
QPB01	Deleted data from t> ~384 days when flow began to increase.	Full Flux Late-Time Flux Cum. Vol.	1.88 1.26 0.002	110.04 42.60 536.00
QPB02	Deleted data from t> ~46 days when flow rate began to decrease rapidly to 0 and then increased.	Full Flux Late-Time Flux Cum. Vol.	32.13 28.70 14.40	11.58 41.30 9.62
QPB03	Deleted all data from t> ~221 days when flow rate began to increase.	Full Flux Late-Time Flux Cum. Vol.	1.91 1.56 —	6388.00 4300.00 —
QPB04	No fit obtained; no discernible period of continuously decreasing flux.			
QPB05	No fit obtained; no discernible period of continuously decreasing flux.			
Room D	Summation of data from DBT10, DBT11, DBT12, DBT13, DBT15A, DBT15B, DBT31A, DBT32A	Full Flux Late-Time Flux Cum. Vol.	0.57 — —	9.82 — —

APPENDIX I:
BORNS MEMORANDUM

David J. Borns to Paul Davis, "Implications of Geophysical Surveys in the WIPP Underground on the Interpretation of the Relative Roles of the Three Proposed Conceptual Models for Salado Fluid Flow." October 3, 1994. Internal SNL Memorandum.

Sandia National Laboratories

Albuquerque, New Mexico 87185-0750

date: October 3, 1994

to: Paul Davis, Org. 6307/MS-1345

from: David J. Borns, Org. 6116/MS-0750

subject: Implications of Geophysical Surveys in the WIPP Underground on the Interpretation of the Relative Roles of the Three Proposed Conceptual Models for Salado Fluid Flow

Introduction

The Technical Baseline Document for Salado Fluid Flow proposes three conceptual models for the observed brine inflow at the repository level. The three models are *1. Far-field Flow, 2. Redistribution of brine with the pore structure of the Disturbed Rock Zone, and 3. Clay consolidation within the Disturbed Rock Zone.* As we witnessed at the stakeholder's meeting in Carlsbad on 29 October, the relative roles and importance of these models for fluid flow appear unclear. The strategy to test these models remains uncertain..

However, observations based on geophysical surveys, predominantly electrical, suggest that *Far-Field Flow* is the dominant mechanism. In summary, these observations are:

1. The Disturbed Rock Zone (DRZ) is observed to resaturate in a sealed room, Room Q. This observation suggests that there is a source of brine external to the DRZ that with time is able to resaturate the porosity of the DRZ.
2. The Salado halites and interbeds can support electrical current flow, which suggests that even in low permeability units there exists an interconnected pore structure to support ionic flow. Measured resistivities in the Salado halites and interbeds have successfully predicted permeabilities.
3. Distinct electrical self potentials within the individual map units of the facility horizon suggest that far field flow is ongoing around the excavation.

In the remainder of this memo, I will elaborate on these points in detail.

Electrical Methods

The flow of electrical current in rocks takes place through ionic conduction in the pore space or conduction through conducting minerals. In rocks of the upper crust including evaporites, ionic conduction in the pore space dominates as a mechanism. For the units of the Salado, clays possibly act as a conducting mineral, which facilitates electrical flow in addition to ionic flow. To support current flow as a mineral conductor, the clays must link as a continuous phase in the rock matrix or along a pore channel pore. Since clays comprise less that 5% of Salado halites and anhydrite, where a modal distribution of greater than 30% is generally required to form a continuous phase in the matrix, mineral conductance in the matrix probably is limited to the clay interbeds. Clays lining pore networks, such as

diagenetic dewatering conduits, or fractures may support mineral conductance rather than ionic flow. The time dependent variations in resistivity are, however, more consistent with ionic flow in pore network of the Salado units since the clay distribution in the matrix and pores does vary significantly with time. The measured resistivities of the Salado units range from hundred to a thousand ohm-m. In comparison, the measured resistivities of domal salts range from tens of thousands to hundred of thousand ohm-m. Therefore, our assumption is that the electrical current flow that we induce or observe is supported by an interconnected partially (probably greater than 70%) to completely brine saturated pore network. Based on this assumption, we can relate the resistivity to the porosity, pore saturation and the tortuosity of the pore network and chemistry of the pore fluid. Brace (1977) utilized resistivity methods to determine permeabilities of tight crystalline rocks undergoing deformation in a laboratory.

At WIPP, we have used Poiseuille's equation as developed by Brace to estimate variations in permeability along the length of a borehole for the Salado Two-Phase Flow Laboratory Program: anhydrite core damage assessment and properties restoration (Howarth, 1993). In Figure 1, resistivity measurements where made in and between two vertical boreholes (E25 and E26) that penetrate Marker Bed 139. From these measurements, we calculated permeabilities for the halite and anhydrite intercepted by the boreholes (Borns and others, 1994). The calculated permeabilities duplicate the range for anhydrite and halite determined in laboratory and field experiments (Howarth, 1993). *This suggests that the interconnected pore network model represents the electrical current flow in the Salado.*

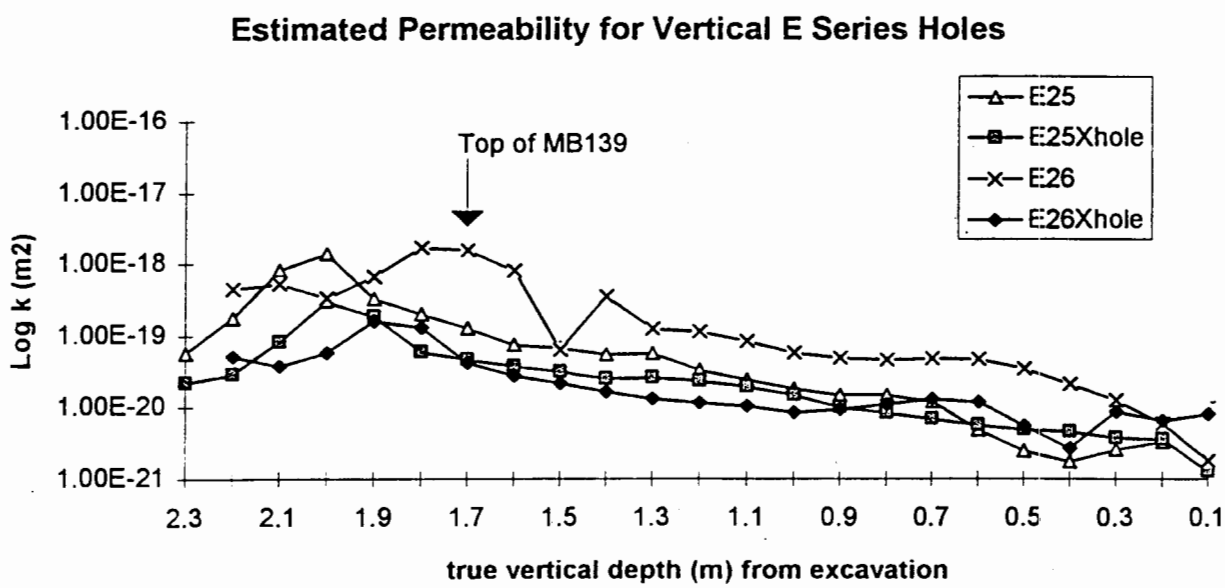

Figure 1: Calculated Permeabilities from Resistivity Surveys in Halite and Anhydrite beneath the Repository Floor

Room Q Arrays

We emplaced two electrical arrays in Room Q in the autumn of 1989 and have monitored the electrical response (changes are resistance and self potential) around Room Q through August 1993 (Pfeifer and others, 1989; Jensen and others 1992; Truskowski, 1994).These are sensitive to changes in electrical properties in a region four meters radially outward from the excavation. Figures 3 a, b, and c show the change in resistance along a series of lines parallel to the length of Room Q *along the **centerline** of the array, Ring 13 (Fig. 3a), on the **floor** (Fig. 3b), the **rib** (Fig. 3c), and the **roof** (Fig. 3d)*. Along the x-axis is time sine 1/1/90 to 8/20/93 (0 to 2.63 fractional years). From these plots, apparently the resistance increased (blue and yellow contours) in the first six months after we had access to the room (12/89). This increase is interpreted to mirror desaturation of the DRZ based on forward modeling (Pfeifer and others, 1989). After this increase, the resistance decreases (toward red contours) for two years. Based on forward modeling, this decrease in resistance is interpreted to represent *resaturation* of the DRZ. At 2 years, a rapid rise in resistance especially in the floor occurs followed by a decrease in resistance. Again based on modeling, this behavior is interpreted as a fracture opening between the floor and the far field electrode. In turn this fracture resaturated resulting in the decrease in resistance.

Another way to view the changes around Room Q with time is a series of graphs showing the percentage change in resistance between an index measurement (6/20/90 in most analyses) and the date of a following measurement. Figure 4 displays the cylindrical surface of Room Q projected onto a plane with the floor at Row 13, the rib at Row 9, and the roof at Row 3. These figures show the change in resistance for the periods **a) 3/11/90 to 6/22/90** (the period within a year of excavation and before an effective seal was installed), **b) 6/22/90 to 8/14/90** (the period for which access was beginning to be limited and partially seals were in place); **c) 6/22/90 to 8/12/91** (a period covering over a year of operation); and **d) 6/22/90 to 8/20/93** (a period covering the last documented measurement of the array in Room Q). These figures covering almost three years of the room's history show the initial increase in resistance with the opening of the DRZ and its desaturation (Figure 4a) and the subsequent reduction in resistance with resaturation of the DRZ (Figures 4b, c, and d). *In conclusion, we observe that the field data suggests that the DRZ can resaturate over a 2.6 year period.*

Figure 3a: Resistance change with time for all electrodes along Ring 13 (centerline of array) in Room Q

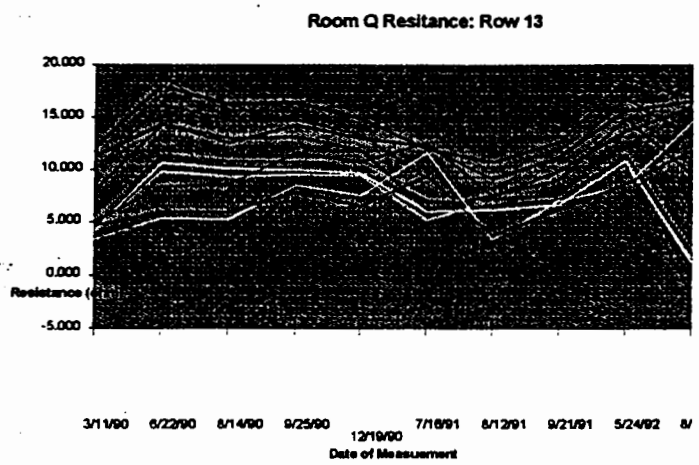

Figure 3b: Change in resistance with time along Room Q floor

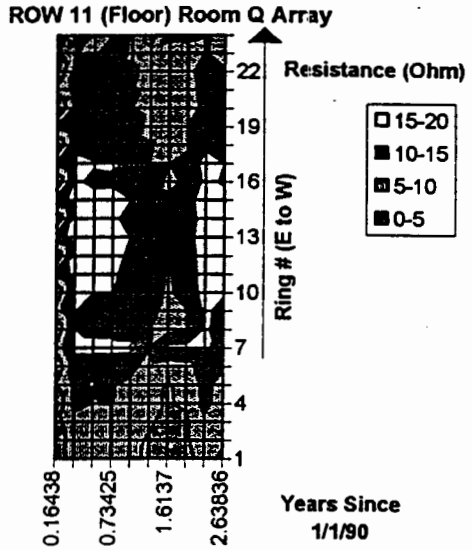

Figure 3c: Change in resistance with time along Room Q rib

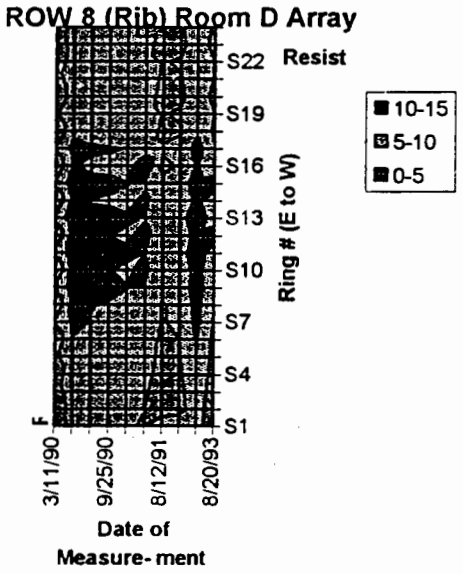

Figure 3d: Change in resistance with time along Room Q roof

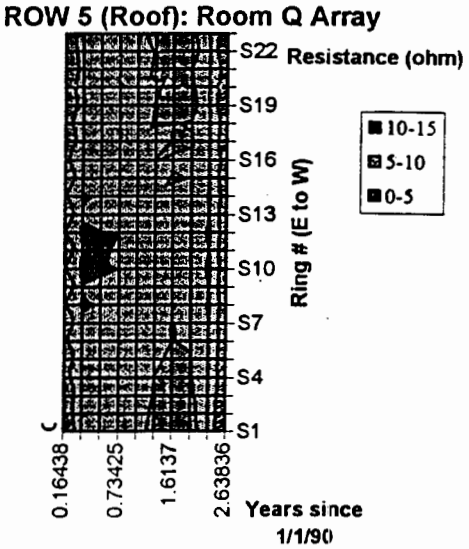

Figure 4a: Change in resistance (resistance increasing with development and desaturation of DRZ)

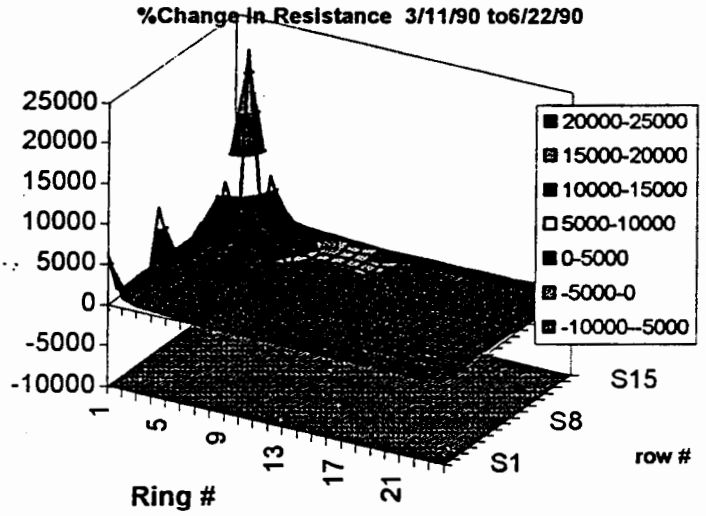

Figure 4b: Change in resistance (resistance decreasing with resaturation of DRZ)

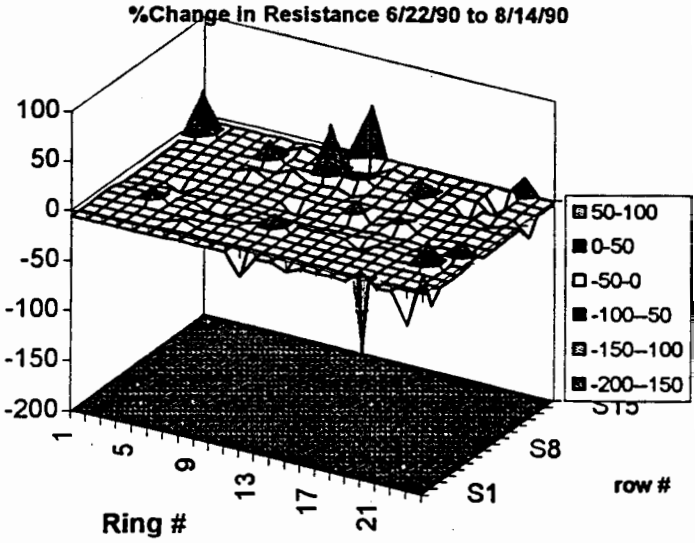

Figure 4c: Change in resistance (resistance decreasing with resaturation of DRZ)

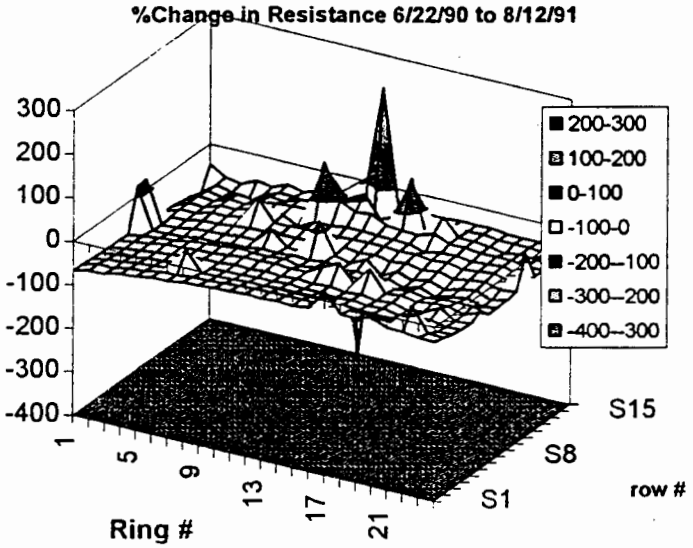

Figure 4d: Change in resistance (resistance decreasing with resaturation of DRZ; zone of higher resistance may reflect the opening of a secondary fracture[s] in the floor)

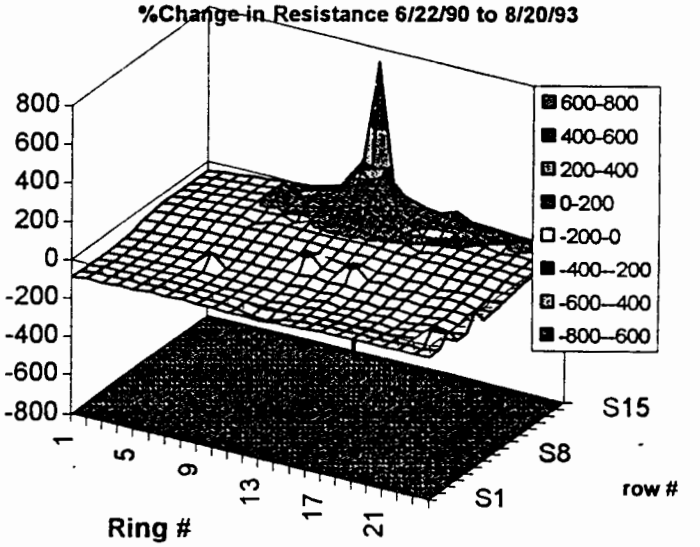

Self Potential Surveys in Room Q

We measure electrical self potential regularly as a background check for electrical surveys in Room Q and elsewhere in the underground. The self potential measures the background current flow when our induced sources are turned-off. This self potential is commonly induced by ionic flow accompanying fluid flow in rocks. As such, the self potential is used to detect zones of fluid flow (e.g., leaks in man made structures). In the WIPP underground, the self potential may not be totally natural and may reflect perturbations in the electrical field due to the shafts and underground mine operations. However, the observed self potentials show that the ionic flow occurs in the pore network of the Salado. Figure 3 shows the self potentials measured in the electrical arrays of Room Q.

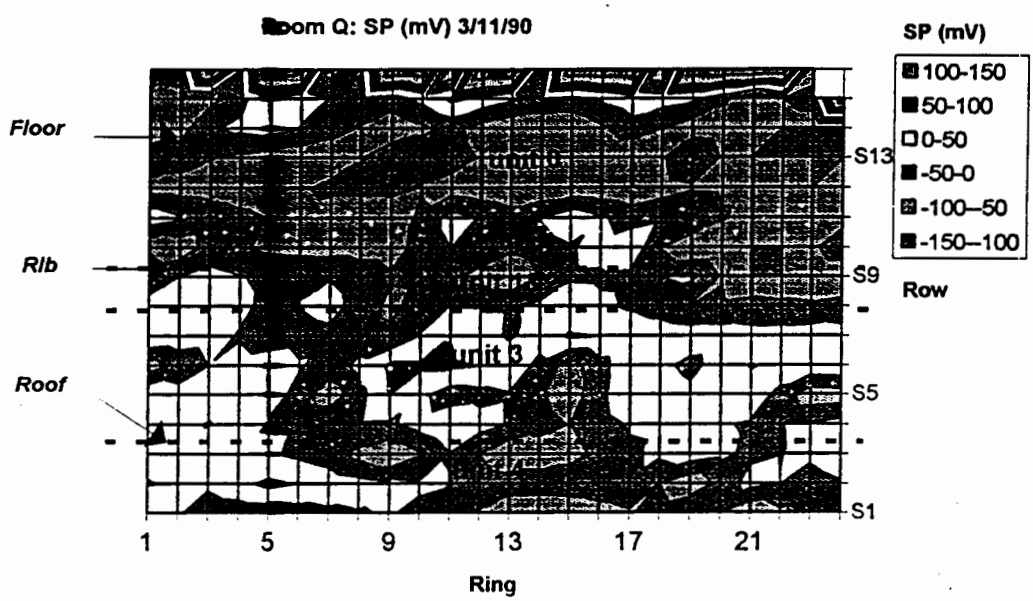

Figure 4: Self Potential (SP) measured in Room Q on 3/11/90. Figure represents the cylindrical surface of room projected onto a planar surface. The intersection of the excavation with the map units is marked by the dotted lines. The relative positions of the floor, rib and roof are marked by arrows.

observed in Room Q related to the map units. These map units represent the sedimentary layering of the Salado as marked by variations in texture and clay content. **Map Unit 0** has a distinct self potential, which is 100 mV greater than **Map Unit 3**. The boundary between these two units is horizontal and corresponds to the relatively thinner **Map Units 1 and 2**. *The distribution of self potentials suggests that layer stratified ionic flow is occurring around the Room Q excavation.*

References:

Borns, D. J., H. T. Andersen, and D. I. Neuman, 1994, Electrical Resistance Measurements of Boreholes: E3X23, E3X24, E3X25, E3X26, E3X27, and E3X28 in Alcove E300N90:Field Test Portion of the Core Damage Assessment Study for the Salado Two-Phase Flow Laboratory Program, Sandia Report, SAND94-1200, Sandia National Laboratories, Albuqerque, New Mexico

Brace, W. F., 1977, Permeability and Resistance and Pore Shape, Journal of Geophysical Research, 82, 3343-3349

Howarth, S., 1993, Conceptual Plan: Two Phase Flow Laboratory Program for the Waste Isolation Pilot Plant, Sandia Report, SAND93-1197, Sandia National Laboratories, Albuquerque, New Mexico

Jensen, A. L., R. L. Jones, E. N. Lorusso, and C. L. Howard, 1991, Large-scale brine inflow data report for Room Q prior to November 25, 1991, Sandia Report, SAND92-1173, Sandia National Laboratories, Albuqerque, New Mexico

Pfeifer, M. C., D. J. Bornsm C. K. Skokan, H. T. Andersen, and J. Starrett, 1989, Geophysical methods to monitor development of the disturbed rock zone around underground excavation in bedded salt, Procedding of the Symposium on the Application of Geophysics to Engineering and Environmental Problems (SAGEEP), Golden, CO, March 1989, SAND89-7055A

Truskowski, M. G., 1994, Detecting material proerty changes and fluid flow using a stationary DC resistance grid, M.S. Thesis, Colorado School of Mines, Golden, CO.

March 17, 1995

WIPP Library

Systems Prioritization Method - Iteration 2 Baseline Position Paper:

Gas Generation in the Waste Isolation Pilot Plant

L. H. Brush

Sandia National Laboratories
Albuquerque, NM 87185-1341

ABSTRACT

Gas generation by transuranic (TRU) waste is an important issue because gas will, if produced in significant quantities, affect the performance of the Waste Isolation Pilot Plant (WIPP) with respect to Environmental Protection Agency (EPA) regulations for long-term isolation of radioactive and chemically hazardous waste. If significant gas production occurs, it will also affect, and will be affected by, other processes and parameters in WIPP disposal rooms. The processes that will produce gas in WIPP disposal rooms are corrosion, microbial activity and radiolysis (the chemical dissociation of molecules by ionizing radiation). This position paper describes these processes and the models, assumptions, and data used to predict gas generation in the repository.

CONTENTS

EXECUTIVE SUMMARY iv

1.0 OVERVIEW OF GAS GENERATION UNDER EXPECTED WIPP CONDITIONS 1
1.1 Significance of Gas Generation in the WIPP 1
1.2 Interactions between Gas Generation and Other Processes Expected in the WIPP 1
1.3 Summary of Current Understanding of WIPP Gas-Generation Processes . . . 3
1.3.1 Corrosion 4
1.3.2 Microbial Activity 6
1.3.3 Radiolysis 8
1.3.4 Processes that Consume Gas 8

2.0 WIPP COMPLIANCE-RELATED GAS-GENERATION ISSUES 9
2.1 Interactions between Gas Generation and Other Processes Expected in the WIPP 9
2.2 Summary of WIPP Gas-Generation Models and Assumptions 9
2.3 Summary of WIPP Gas-Generation Data 11
2.3.1 Gas-Generation Data Used in the 1991 and 1992 Performance-Assessment Calculations 11
2.3.2 Gas-Generation Data Submitted for the 1993 Performance-Assessment Calculations and the Systems-Prioritization-Method-2 Calculations 11
2.3.3 Sources of Gas-Generation Data 12
2.3.4 Sources of Interpretations of Gas-Generation Data 13

3.0 REFERENCES 15

APPENDIX A: HISTORY OF WIPP STUDIES OF GAS GENERATION A-1

APPENDIX B: REVIEW OF WIPP-RELATED LABORATORY STUDIES OF GAS GENERATION B-1

APPENDIX C: REVIEW OF WIPP GAS-GENERATION MODELS C-1

APPENDIX D: WIPP GAS-GENERATION DATA USED IN THE 1991 AND 1992 PERFORMANCE-ASSESSMENT CALCULATION D-1

APPENDIX E: WIPP GAS-GENERATION DATA SUBMITTED FOR THE 1993 PERFORMANCE-ASSESSMENT CALCULATION AND THE SYSTEMS-PRIORITIZATION-METHOD-2 CALCULATIONS E-1

ACRONYMS

ANL	Argonne National Laboratory
ASTM	American Society for Testing and Materials
BNL	Brookhaven National Laboratory
CH	contact-handled
DOE	Department of Energy
ELP	Enhanced Lab Program
EPA	Environmental Protection Agency
PA	performance assessment
PNL	Pacific Northwest Laboratory
SPR	Strategic Petroleum Reserve
TRU	transuranic
VOC	volatile organic compound
WIPP	Waste Isolation Pilot Plant
XRD	x-ray defraction

EXECUTIVE SUMMARY

Gas generation by transuranic waste is an important issue because gas will, if produced in significant quantities, affect the performance of the Waste Isolation Pilot Plant (WIPP) with respect to Environmental Protection Agency regulations for long-term isolation of radioactive and chemically hazardous waste (see 1.1). (In this position paper, "gas generation" refers to both production and consumption of gas.)

If significant gas production occurs, it will also affect, and will be affected by, other processes and parameters in WIPP disposal rooms (see 1.2). These include: (1) the H_2O content of the repository; (2) room closure; (3) the chemical conditions that will affect the actinide source term; and (4) transport and, perhaps, generation of volatile organic compounds.

The processes that will produce gas in WIPP disposal rooms are: (1) corrosion (see 1.3.1 and B.1); (2) microbial activity (see 1.3.2 and B.2); (3) radiolysis (the chemical dissociation of molecules by ionizing radiation) (see 1.3.3 and B.3). From the standpoint of expected gas-production rates, the most important processes are corrosion and microbial activity. Radiolysis will not produce gas at rates comparable to those expected for corrosion and microbial activity. Gas-consuming processes include reaction with cementitious materials and dissolution in brine (see 1.3.4).

Oxic corrosion (oxidation of metals by molecular O_2) of steels and other Fe-base alloys in the waste containers (drums and boxes) and the waste will significantly affect the O_2 content of WIPP disposal rooms, but not their overall gas or H_2O content (see 1.3.1 and B.1.1). After depletion of the O_2 initially present, and in the absence of radiolytically produced O_2, anoxic corrosion (oxidation of metals by H_2O or H_2S) of steels and other Fe-base alloys will consume significant quantities of H_2O and produce significant quantities of H_2 if: (1) sufficient H_2O is present; (2) significant microbial activity (resulting in passivation by microbially produced CO_2 or H_2S) does not occur; (3) in the event of microbial activity, consumption of CO_2 by reaction with cementitious materials or other processes depassivates steels and other Fe-base alloys. High pressure will accelerate anoxic corrosion of steels and other Fe-base alloys. Anoxic corrosion of Al and Al-base alloys in the waste will produce significant quantities of H_2 and consume significant quantities of H_2O if sufficient H_2O is present.

Microbial consumption of substrates such as cellulosics and, perhaps, plastics and rubbers will generate significant quantities of gas in WIPP disposal rooms via any of the three potentially significant respiratory pathways (see 1.3.2 and B.2.4) if all of the following conditions are met: (1) microorganisms capable of carrying out these respiratory pathways are present when the

repository is filled and sealed (see B.2.1.1); (2) these microbes survive for a significant fraction of the 10,000-year period of performance of the repository (see B.2.1.3); (3) sufficient H_2O is present in the waste or brine (see B.2.1.4); (4) sufficient electron acceptors (oxidants) are present and available (see B.2.1.6); (5) enough nutrients, especially N and P, are present and available (see B.2.1.7). If these conditions are met, high pressure will not preclude microbial gas generation or even inhibit it significantly, even when it increases to 150 atm (lithostatic pressure at the depth of the repository). Because of uncertainties as to whether the conditions listed above will be satisfied, significant microbial gas generation is possible, but by no means certain (see 1.3.2 and B.2.1). Aerobic microbial activity (respiration using molecular O_2 as the electron acceptor) will significantly affect the O_2 content of the repository, but not its gas or H_2O content (see 1.3.2 and B.2.3). After depletion of the O_2 initially present and in the absence of radiolytic O_2, anaerobic microbial activity (respiration using NO_{3-}, Mn(IV) oxides and hydroxides, Fe(III) oxides and hydroxides, SO_{42-}, organic acids or CO_2 as the electron acceptor) will produce various gases and, perhaps, consume CO_2 and H_2 (see B.2.4). If significant microbial activity occurs (see 1.3.2 and B.2.1), anaerobic microbial activity will be much more important than aerobic respiration from the standpoint of the gas and H_2O contents of the repository.

Radiolysis of H_2O in the waste and brine will significantly affect the O_2 content of WIPP disposal rooms, but not their overall gas or H_2O content (see 1.3.3 and B.3.1). Radiolysis of cellulosics, plastics, and rubbers in the waste (or, in the case of plastics, the liners of the waste containers) will produce a variety of gases, but at rates lower than radiolysis of H_2O in the waste and brine (see 1.3.3 and B.3.2).

Consumption of gases (especially CO_2) by various reactions with constituents of cementitious materials or proposed backfill materials, or dissolution of gases (especially CO_2 and H_2S) in brine, will remove gas from the repository (see 1.3.4 and B.4).

The reaction-path gas-generation model (see 2.2 and C.3) is the most defensible WIPP gas-generation model. This model is more defensible than the average-stoichiometry model (see 2.2 and C.2), the gas-production model used in the multi-phase flow code Brine and Gas Flow for the 1992 PA calculations.

Several assumptions are necessary to predict gas generation in WIPP disposal rooms (see 2.2). These include: (1) which corrosion product will form during anoxic corrosion of steels and other Fe-base alloys in the absence of CO_2 and H_2S (see B.1.2); (2) the hydration number x of $(Fe,Mg)(OH)_2.xH_2O$, one of two likely corrosion products under CO_2- and H_2S-free conditions (see B.1.2); (3) whether microorganisms capable of carrying out potentially significant

respiratory pathways (see 2.3.2 and B.2.4) will be present when the repository is filled and sealed (see B.2.1.1); (4) whether these microbes will survive for a significant fraction of the 10,000-year period of performance of the repository (see B.2.1.3); (5) whether these microbes will consume significant quantities of plastics and rubbers (see B.2.1.5); (6) whether sufficient electron acceptors will be present and available (see B.2.1.6); (7) whether enough nutrients will be present and available (see B.2.1.7); (8) the stoichiometry of the overall reaction for each significant respiratory pathway (see B.2.4).

Appendix D describes the gas-production rates used in the average-stoichiometry model for the 1992 PA calculations. However, the most defensible gas-production rates currently available are those used in the average-stoichiometry model in 1993. Appendix E describes these data, which were submitted for the 1993 PA calculations and the Systems-Prioritization-Method-2 calculations.

1.0 OVERVIEW OF GAS GENERATION UNDER EXPECTED WIPP CONDITIONS

1.1 Significance of Gas Generation in the WIPP

Gas generation by transuranic (TRU) waste is an important issue because gas will, if produced in significant quantities, affect the performance of the Waste Isolation Pilot Plant (WIPP) with respect to Environmental Protection Agency (EPA) regulations for long-term isolation of radioactive and chemically hazardous waste. (In this position paper, "gas generation" refers to both production and consumption of gas.) For example, several of the processes that produce gas will consume H_2O present in the waste at the time of emplacement or in any brine that enters the repository after filling and sealing. This will in turn decrease the H_2O content of the repository and retard or even completely eliminate additional gas production by reactions that consume H_2O. Furthermore, the increased pressure caused by this gas production will retard or prevent additional brine inflow and outflow. Therefore, gas production will decrease the quantity of H_2O present in the repository, or even remove it entirely. Because most plausible scenarios for radionuclide release from the repository involve dissolution or suspension of these radionuclides in brines, decreasing the quantity of H_2O present will improve the performance of the repository with respect to the EPA regulations for radioactive waste constituents and other contaminants transported by brine.

On the other hand, gas will, if present in sufficient quantities, enhance the permeability of the rock surrounding WIPP disposal rooms and serve as a carrier for the small quantities of volatile organic compounds (VOCs) present in the waste at the time of emplacement. Therefore, the rates at which major gases are produced will affect the performance of the repository with respect to the EPA regulations for chemically hazardous waste. Furthermore, radiolysis (the chemical dissociation of molecules by ionizing radiation) and microbial activity, two of the processes that will generate gas in the repository (see 1.3), could also produce or consume VOCs.

1.2 Interactions between Gas Generation and Other Processes Expected in the WIPP

If significant gas generation occurs, it will affect, and will be affected by, other processes and parameters in WIPP disposal rooms. These include: (1) the H_2O content of the repository; (2) room closure; (3) the chemical conditions that affect the actinide source term; (4) transport and, perhaps, generation of VOCs. Gas generation is significant from the standpoint of its

effects on these processes and parameters to the extent that they affect compliance with EPA regulations for radioactive and chemically hazardous waste.

Gas generation will significantly affect, and will be significantly affected by, the H_2O content of the waste at the time of emplacement, brine inflow and outflow and, hence, the H_2O content of WIPP disposal rooms. Brush and Anderson (1989) demonstrated that processes such as anoxic corrosion of steels and microbial degradation of cellulosics could affect the H_2O content of the repository as significantly as inflow of intergranular brines from the surrounding Salado Formation. Subsequently, results obtained from laboratory studies of gas generation have shown that the H_2O content of the repository will affect gas-production rates, or even determine whether gas production occurs at all (see 1.3.1, 1.3.2, B.1.2 and B.2.4).

Gas production will retard room closure by pressurizing WIPP disposal rooms. It will thus reduce the rate and the extent to which room closure decreases the porosity and permeability of the waste and its susceptibility to erosion and spalling during human intrusion. However, gas production, H_2O consumption, and concomitant precipitation of salts from brine will decrease the porosity and permeability of the waste and increase its strength. Room closure will affect gas generation by rupturing waste containers (drums and boxes) and exposing their contents to materials and conditions different from those within the containers (brine, gas with a different composition or humidity, salt and, perhaps, bentonite and other backfill materials, microorganisms in other containers or outside the containers, electron acceptors and nutrients in other containers, etc.). Furthermore, room closure will also affect gas generation by decreasing the connected porosity available for brine inflow and outflow and the permeability of the waste. However, pressurization caused by room closure will not impede gas generation (see B).

Finally, gas generation will affect chemical conditions such as the O_2 content of the repository[1] and the pH of any brine present. These parameters will, in turn, affect the

---

[1] In general, the concept of Ih as an intrinsic thermodynamic parameter is invalid in aqueous, geochemical systems at a temperature of 30°C, the expected temperature of WIPP disposal rooms after filling and sealing. This is because the kinetics of most oxidation-reduction (redox) reactions are so slow at this temperature that they rarely reach equilibrium. Therefore, the Eh calculated from the activity ratio (roughly equivalent to the concentration ratio) of one redox couple rarely agrees with those calculated from other couples, or with the value measured with an Eh electrode (see, for example, Lindberg and Runnels, 1984). Microbial activity, however, catalyzes redox reactions such as recution of NO_3., MN(IV) oxides and hydroxides, Fe(III) oxides and hydroxides, and $SO_4$2- in natural system (see B.2.4). If significant microbial activity occurs in WIPP disposal rooms (see 1.3.2 and B.2.1), it will catalyze at least some of these recox reactions and, to some extent, render Eh a meaningful parameter. Nevertheless, this position paper uses "O_2 content of the repository" instead of "Eh" to avoid giving the impression that the WIPP Project assumes that significant microbial activity will occur and catalyze redox reactions in the repository.

solubilities of the actinide elements, their sorptive properties, the extent to which they form colloids, and, hence, the actinide source term.

The O_2 content of the gaseous phase in WIPP disposal rooms at the time of filling and sealing will be similar to that of an equivalent volume of air. Subsequently, oxic corrosion (see 1.3.1 and B.1.1) and aerobic microbial activity (see 1.3.2 and B.2.3) will consume O_2. Radiolysis of H_2O in the waste and brine will produce O_2 (see 1.3.3 and B.3.1), but not as fast as oxic corrosion and microbial activity will consume it. Therefore, the repository will become anoxic after filling and sealing.

Reactions between brine and the waste in WIPP disposal rooms will increase or decrease the pH significantly from the mildly acidic values reported for intergranular brines from the Salado Formation at or near the stratigraphic horizon of the repository by Deal and Case (1987) and Deal et al. (1989a, 1989b, 1991a, and 1991b). Microbial production of CO_2 or H_2S will decrease the pH of the brine to acidic values. Reactions between brine and $Ca(OH)_2$ in hydrated cementitious materials used to remove liquids from sludges, grouts used in seals, or grouts proposed to reduce the permeability of the waste (see Butcher, 1990) will increase the pH to basic values. Reactions between brine and CaO, a possible backfill material proposed to remove CO_2, would also increase the pH to basic values. Brush (see E) estimated that, because of these reactions, the pH in various parts of the repository will vary between about 3 and 12.

1.3 Summary of Current Understanding of WIPP Gas-Generation Processes

The processes that will produce gas in WIPP disposal rooms are: (1) corrosion (see 1.3.1 and B.1); (2) microbial activity (see 1.3.2 and B.2); (3) radiolysis (see 1.3.3 and B.3). From the standpoint of the gas-production rates expected in WIPP disposal rooms, the most important processes are corrosion and microbial activity. Brush (see E) concluded that radiolysis will not produce gas at rates comparable to those expected for corrosion and microbial activity. However, radiolysis will be important from the standpoint of the O_2 content of the repository. This parameter will, in turn, affect the actinide source term (see 1.2). Gas-consuming processes include reaction with cementitious materials and dissolution in brine.

Subsections 1.3.1, 1.3.2 and 1.3.3 summarize the results of studies of corrosion, microbial activity, and radiolysis carried out for the WIPP Project by Telander and Westerman (1993), Francis and Gillow (1994), and Reed et al. (1993), respectively, and the results of studies conducted for applications other than the WIPP Project. Appendix B reviews these studies in detail.

1.3.1 Corrosion

Oxic corrosion (oxidation of metals by molecular O_2) will consume O_2 and H_2O in WIPP disposal rooms (see B.1.1). Oxic corrosion of steel waste containers (drums and boxes), Fe-base alloys in the waste, and other metals in the waste, such as Al and Al-base alloys, will significantly affect the O_2 content of the repository. Oxic corrosion of these metals will be important because this process is, along with aerobic microbial activity, one of the two major processes that will consume O_2 in the repository. Radiolytically induced uptake by plastics, and perhaps rubbers, and oxidation of dissolved, reduced species such as Fe^{2+} produced by dissolution of Fe(II)-bearing corrosion products, will also consume O_2, but these processes will be less significant than oxic corrosion and aerobic microbial activity. The O_2 content of the repository will, in turn, affect other important processes and parameters. These include: (1) how soon the repository becomes anoxic after filling and sealing; (2) whether gas is produced or consumed by corrosion of metals; (3) which gases are produced or consumed by microbial degradation of cellulosics and, perhaps, plastics and rubbers; and (4) the actinide source term (see 2.2). However, oxic corrosion will not affect the overall gas or H_2O content of the repository significantly because the quantity of O_2 in the repository at the time of filling and sealing and that produced thereafter by brine radiolysis will be small (see B.1.1), thus limiting the extent of oxic corrosion relative to that of anoxic corrosion (see below).

After depletion of the O_2 initially present in WIPP disposal rooms, and in the absence of radiolytically produced O_2, anoxic corrosion (oxidation of metals by H_2O or H_2S) will consume H_2O, CO_2, and H_2S, and produce H_2 (see B.1.2). Anoxic corrosion of steels and other Fe-base alloys will consume significant quantities of H_2O and produce significant quantities of H_2 if: (1) sufficient H_2O is present in the waste at the time of emplacement (either as an aqueous phase or an interlayer constituent of clay minerals such as vermiculite) or sufficient brine enters the repository after filling and sealing; (2) significant microbial activity (see 1.3.2 and B.2.1) (and concomitant passivation) does not occur (microbial activity will produce CO_2 or CO_2 and H_2S, which will passivate steels and other Fe-base alloys and thus prevent additional H_2 production and H_2O consumption from anoxic corrosion of these metals); (3) in the event of microbial activity and passivation, consumption of CO_2 or H_2S depassivates steels and other Fe-base alloys. High pressure will accelerate anoxic corrosion of steels and other Fe-base alloys. Anoxic corrosion of Al and Al-base alloys will produce significant quantities of H_2 and consume significant quantities of H_2O if sufficient H_2O is present in the waste or brine (neither CO_2 nor H_2S passivates Al and Al-base alloys). Other metals subject to oxic or anoxic corrosion might include (but are not necessarily limited to) Pb, Pu, and U.

In the absence of CO_2 and H_2S, anoxic corrosion of steels and other Fe-base alloys by intergranular Salado-Formation brines with a neutral or nearly neutral pH will occur at a rate of 0.99 μm of steel per year, and produce H_2 at a rate of 0.10 mole per m^2 of steel per year (see B.1.2). Acidic conditions, high N_2 partial pressure, and, presumably, high total pressure will increase these rates significantly; basic conditions and high H_2 partial pressures will decrease them significantly (see B.1.2 and E for discussions of the effects of pressure and pH, respectively). How much H_2 will be produced will depend on: (1) the quantity of steels and other Fe-base alloys in the repository; (2) the quantity of aqueous H_2O present; (3) which corrosion product forms (see B.1.2). If sufficient steels, other Fe-base alloys, and H_2O are available, CO_2 and H_2S are absent, and $(Fe,Mg)(OH)_2.xH_2O$ is the corrosion product, anoxic corrosion of steels and other Fe-base alloys and concomitant H_2 production will continue until the H_2 fugacity increases to its equilibrium value of about 60 atm. (When a chemical reaction reaches equilibrium, the forward and backward rates of that reaction are equal, and the reaction "stops.") However, the equilibrium H_2 fugacity for $Fe3O_4$, the other possible anoxic corrosion product in the absence of CO_2 and H_2S, is about 400 atm. Therefore, if Fe_3O_4 forms, anoxic corrosion and H_2 production will continue even if the H_2 fugacity increases to its highest possible value of roughly 150 atm (lithostatic pressure at the depth of the repository).

If sufficient CO_2 or H_2S is present, anoxic corrosion of steels and other Fe-base alloys will stop prior to producing significant quantities of H_2 and consuming significant quantities of H_2O, even if brine is present, because of passivation by the adherent corrosion product $FeCO_3$, FeS, or, perhaps, FeS_2 (see B.1.2). Because microbial activity in WIPP disposal rooms will produce CO_2 and/or H_2S (in addition to other gases such as N_2, H_2 and CH_4), significant microbial activity will, if it occurs (see 1.3.2 and B.2.1), passivate steels and other Fe-base alloys, and thus prevent additional H_2 production and H_2O consumption from anoxic corrosion of these metals. High CO_2 partial pressures will not depassivate steels and other Fe-base alloys.

Under humid conditions (gaseous, but not aqueous, H_2O present), anoxic corrosion of steels and other Fe-base alloys will not occur (see B.1.2). Therefore, anoxic corrosion in WIPP disposal rooms will be self-limiting. Small quantities of brine in the repository will initiate anoxic corrosion, which will produce H_2, consume H_2O, increase the pressure, and prevent additional brine inflow or even cause brine outflow, thus precluding additional anoxic corrosion.

1.3.2 Microbial Activity

Microbial activity in WIPP disposal rooms will consume O_2 and, perhaps, CO_2 and H_2, and produce gases such as CO_2, N_2O, N_2, H_2S, H_2 and, perhaps, CH_4 (see B.2). It is unclear how microbial activity will affect the H_2O content of the repository. Microbial consumption of substrates such as cellulosics and, perhaps, plastics and rubbers will produce significant quantities of gas via any of three potentially significant respiratory pathways (see B.2.4) if all of the following conditions are met: (1) microorganisms capable of carrying out these respiratory pathways are present when the repository is filled and sealed (see B.2.1.1); (2) these microbes survive for a significant fraction of the 10,000-year period of performance of the repository (see B.2.1.3); (3) sufficient H_2O is present in the waste or brine (see B.2.1.4); (4) sufficient electron acceptors (oxidants) are present and available (see B.2.1.6); (5) enough nutrients, especially N and P, are present and available (see B.2.1.7). If these conditions are met, high pressure will not preclude microbial gas generation or even inhibit it significantly, even when it increases to 150 atm (lithostatic pressure at the depth of the repository). Subsection B.2.1 considers these and other issues in detail and concludes that, although significant microbial gas production is possible, it is by no means certain.

If significant microbial activity occurs in WIPP disposal rooms (see above and B.2.1), there are additional uncertainties as to its effects on the gas and H_2O contents of the repository. The most important issues are: (1) whether microorganisms will consume significant quantities of plastics and rubbers during the 10,000-year period of performance of the repository (see B.2.1.5); (2) the stoichiometry of the overall reaction for each significant respiratory pathway, especially the number of moles of electron acceptors, nutrients, gases, and H_2O consumed or produced per mole of substrate consumed (see B.2.4).

Brush and Anderson (1989) and Brush (1990) used the conceptual model of sequential consumption of electron acceptors by microorganisms in natural environments (see B.2.2) and estimates of which electron acceptors will be present in significant quantities in the repository after filling and sealing to determine which microbial respiratory pathways will be significant if microbial activity occurs (see above and B.2.1). They also predicted the overall equation for each potentially significant microbial process (see B.2.3 and B.2.4).

Aerobic microbial activity (respiration using molecular O_2 as the electron acceptor) will consume O_2 and produce CO_2 and H_2O in WIPP disposal rooms (see B.2.3). Aerobic microbial consumption of cellulosics and, perhaps, plastics and rubbers will significantly affect the O_2 content of the repository. Aerobic microbial activity will be important because this process is,

along with oxic corrosion of metals, one of the two major processes that will consume O_2 in the repository. The O_2 content of the repository will, in turn, affect the actinide source term (see 1.2). However, aerobic microbial activity will not affect the overall gas or H_2O content of the repository significantly, because the quantity of O_2 in the repository will be small, thus limiting the extent of aerobic microbial activity relative to that of anaerobic microbial activity (see below and B.2.4).

After depletion of the O_2 initially present, and in the absence of radiolytic O_2, anaerobic microbial activity (respiration using NO_3^-, Mn(IV) oxides and hydroxides, Fe(III) oxides and hydroxides, SO_4^{2-}, organic acids or CO_2 as the electron acceptor) will produce CO_2, N_2O, N_2, H_2S, H_2, and, perhaps, CH_4, and possibly consume CO_2 and H_2 (see B.2.4). If significant microbial activity occurs in WIPP disposal rooms (see above and B.2.1), anaerobic microbial activity will be much more important than aerobic respiration from the standpoint of the gas and H_2O contents of the repository because there will be much more NO_3^-, SO_4^{2-}, and CO_2 present than O_2. The most important anaerobic processes will be: (1) denitrification, which consumes NO_3^- as the electron acceptor and produces CO_2, N_2O and N_2; (2) SO_4^{2-} reduction, which consumes SO_4^{2-} as the electron acceptor and produces CO_2 and H_2S; (3) methanogenesis, which consumes organic acids or CO_2 as the electron acceptor and produces CH_4 and CO_2 or uses CO_2 and H_2 and makes CH_4. Whether denitrification, SO_4^{2-} reduction, and methanogenesis will be significant will depend on whether the microorganisms responsible for each of these processes survive long enough for conditions to become conducive to that process, and the relative quantities of electron acceptors present. The rates at which these processes will produce or consume gas will depend on whether conditions are humid or inundated, the concentrations of electron acceptors such as NO_3^-, SO_4^{2-}, organic acids or CO_2, the concentrations of nutrients such as N and P, the dissolved Pu concentration and other factors. Microbial reduction of Mn(IV) and Fe(III) oxides and hydroxides will be insignificant relative to denitrification, SO_4^{2-} reduction, and methanogenesis because there will be limited quantities of Mn(IV) and Fe(III) oxides and hydroxides present. It is unclear how anaerobic microbial consumption of cellulosics will affect the H_2O content of the repository (see B.2.4.1). It is also unclear how microbial consumption of plastics and rubbers will affect the H_2O content of the repository. Quantification of the effects of microbial activity on the repository H_2O content is essential to predict the extent of gas production from anoxic corrosion (see 1.3.1 and B.1.2) and brine radiolysis (see 1.3.3 and B.3.1), both of which consume H_2O, and the quantity of brine available for the transport of radioactive waste constituents and other contaminants subject to aqueous-phase transport (see 1.1).

1.3.3 Radiolysis

In this position paper, "radiolysis" refers to α radiolysis, the chemical dissociation of molecules by α particles emitted during the radioactive decay of the actinide elements in TRU waste. Because molecular dissociation caused by other types of radiation will be insignificant in a TRU-waste repository such as the WIPP, this report considers only α radiolysis.

Radiolysis of H_2O in the waste and brine in WIPP disposal rooms will consume H_2O, and produce H_2 and O_2 or other oxidizing, O-bearing species (see B.3.1). Radiolysis of H_2O will significantly affect the O_2 content of the repository. Brine radiolysis will be important because this process is the only major process that will produce O_2 in the repository. The O_2 content of the repository will, in turn, affect the actinide source term (see 1.2). However, based on calculations using the results of laboratory studies of brine radiolysis, estimates of the quantities of brine that could be present in the repository after filling and sealing, and estimates of the solubilities of Pu, Am, Np, Th, and U in WIPP brines (see E), radiolysis of H_2O will not significantly affect the overall gas or H_2O content of the repository.

Radiolysis of cellulosics, plastics, and rubbers in the waste and, in the case of plastics, the container liners will produce a variety of gases (see B.3.2). However, radiolysis of these materials will produce gas at rates lower than radiolysis of H_2O in the waste and brine.

1.3.4 Processes that Consume Gas

Consumption of gases (especially CO_2) by various reactions with constituents of cementitious materials or proposed backfill materials, or dissolution of gases (especially CO_2 and H_2S) in brine will remove gas from WIPP disposal rooms (see B.4).

Although the WIPP Project has carried out few studies of gas-consuming processes, reaction of CO_2 with $Ca(OH)_2$ in hydrated cementitious materials, or with proposed backfill materials such as CaO, will consume more gas than dissolution in brine. This is because the gases produced by corrosion, microbial activity, and radiolysis will not dissolve to a significant extent in WIPP brines (see Cygan, 1991), and because there will not be sufficient brine present to consume significant quantities of these relatively insoluble gases.

2.0 WIPP COMPLIANCE-RELATED GAS-GENERATION ISSUES

This section describes the gas-generation models and assumptions required for performance assessment (PA) calculations. It also discusses the gas-generation and related data required for these calculations. A description of the interactions between gas generation and other processes appears in 1.2.

2.1 Interactions between Gas Generation and Other Processes Expected in the WIPP

Subsection 1.2 explains how gas generation will affect, and be affected by, other processes and parameters in WIPP disposal rooms.

2.2 Summary of WIPP Gas-Generation Models and Assumptions

The reaction-path model currently being developed by Brush et al. (1994) is the most defensible WIPP gas-generation model. Although still incomplete (see C.3), this model is more defensible than the average-stoichiometry model, the gas-production model used in the multi-phase flow code Brine and Gas Flow (BRAGFLO) for the 1992 PA calculations (see C.2). The reaction-path model is more defensible because it includes: (1) additional gas-generation processes; (2) additional reactions simulating these processes; (3) interactions among gas-generation processes. Because of these additional features, the reaction-path model predicts gas-generation in WIPP disposal rooms more realistically than the average-stoichiometry model. For example, the reaction-path model includes several gas-consuming processes and reactions not included in the average-stoichiometry model. These include consumption of CO_2 by $Ca(OH)_2$ (in cementitious materials) and CaO (a proposed backfill material) (see B.4), and consumption of CO_2 and H_2 by microbial methanogenesis (see B.2.4). Therefore, if there are sufficient quantities of cementitious materials in the TRU waste emplaced in the repository, if CaO is used as a backfill material, or if laboratory studies of microbial activity imply that methanogenic consumption of CO_2 and H_2 is significant under expected repository conditions, the reaction-path model will predict that significantly less gas will be present. Furthermore, the reaction-path model includes passivation of steels and Fe-base alloys by microbially produced CO_2 and H_2S, the most important interaction among gas-generation processes observed in laboratory studies since the development of the average-stoichiometry model. Consequently, the reaction-path model will predict that anoxic corrosion will stop prior to producing significant quantities of H_2 and consuming significant quantities of H_2O, even if brine is present. Moreover, because the

reaction-path model includes oxic corrosion, aerobic microbial activity and radiolysis (three gas-generation reactions or processes not included in the average-stoichiometry model), it can predict the O_2 content of the repository as a function of time. The O_2 content of the repository will, in turn, affect the actinide source term.

Because it contains the additional features described above, incorporation of the reaction-path model in BRAGFLO will also result in more realistic predictions of the interactions among gas generation, brine inflow and outflow, and room closure. (BRAGFLO also includes a room-closure model.)

Several assumptions are necessary to predict gas generation in WIPP disposal rooms. These include: (1) which corrosion product will form during anoxic corrosion of steels and other Fe-base alloys in the absence of CO_2 and H_2S (see B.1.2); (2) the hydration number x of $(Fe,Mg)(OH)_2.xH_2O$, one of the two most likely corrosion products under CO_2- and H_2S-free conditions (see B.1.2); (3) whether microorganisms capable of carrying out potentially significant respiratory pathways (see 1.3.2 and B.2.4) will be present when the repository is filled and sealed (see B.2.1.1); (4) whether these microbes will survive for a significant fraction of the 10,000-year period of performance of the repository (see B.2.1.3); (5) whether these microbes will consume significant quantities of plastics and rubbers (see B.2.1.5); (6) whether sufficient electron acceptors (oxidants) will be present and available (see B.2.1.6); (7) whether enough nutrients, especially N and P, will be present and available (see B.2.1.7); (8) the stoichiometry of the overall reaction for each significant respiratory pathway, especially the number of moles of electron acceptors, nutrients, gases, and H_2O consumed or produced per mole of substrate consumed (see B.2.4).

Ongoing laboratory studies of gas generation will not eliminate the need for these assumptions. Although it might be possible to determine which corrosion product will form during anoxic corrosion of steels and other Fe-base alloys in the absence of CO_2 and H_2S, it will probably not be possible to eliminate the need for most of these assumptions about microbial gas generation (see B.2.1.3, B.2.1.5, B.2.1.6, B.2.1.7, and B.2.4). Furthermore, it will be difficult to defend any of the possible outcomes, conditions, or reactions listed above to the exclusion of the other. Therefore, it will be necessary to carry out probabilistic calculations based on all possible combinations of these outcomes, conditions, or reactions.

WIPP Performance Assessment Division (1991) and Sandia WIPP Project (1992) described the average-stoichiometry gas-production model in detail. However, they did not describe the reaction-path model. Brush et al. (1994) provided a preliminary description of the

latter model. WIPP Performance Assessment Division (1991) and Sandia WIPP Project (1992) described some, but not all, of the assumptions listed above.

2.3 Summary of WIPP Gas-Generation Data

This subsection describes the gas-production and related data used in the 1992 PA calculations, data submitted for the Systems Prioritization Method-2 calculations, the sources of these data, and the interpretation of these data.

2.3.1 Gas-Generation Data Used in the 1991 and 1992 Performance-Assessment Calculations

Brush (see D) provided the gas-generation rates used in the average-stoichiometry gas-production model (see C.2) for the 1992 PA calculations. (Actually, Brush provided these data for the 1991 PA calculations, but PA personnel used them for both their 1991 and 1992 calculations because experimental data obtained between 1991 and 1992 did not justify any changes.) These are the most recent gas-production rates used in a complete set of PA calculations. They are also the most recent rates described in PA reports (WIPP Performance Assessment Division, 1991; Sandia WIPP Project, 1992). Although Brush (see D) recommended best estimates and ranges of gas-production rates, he did not specify how these rates are distributed within these ranges. WIPP Performance Assessment Division (1991) described the distributions that PA personnel assumed for these parameters. WIPP Performance Assessment Division (1991) also discussed how PA personnel converted these rates from the units given below to those used in the average stoichiometry model.

2.3.2 Gas-Generation Data Submitted for the 1993 Performance-Assessment Calculations and the Systems-Prioritization-Method-2 Calculations

The most defensible gas-production rates currently available were provided by Brush (see E) for use in the average-stoichiometry model for the planned 1993 PA calculations. (Although PA personnel used these rates for preliminary calculations pertaining to undisturbed conditions, they did not carry out a complete set of calculations in 1993, and have not described these rates in any of their reports to date.) Brush also submitted these data for the Systems-Prioritization-Method-2 calculations.

The gas production rates provided by Brush (see E) in 1993 are significantly different from those he provided for the 1992 Pa calculations (see D). These differences, described in detail below, arose mainly because in 1993: (1) Brush estimated rates of oxic corrosion of steels and other Fe-base alloys and concomitant O_2 consumption, not just anoxic corrosion and H_2 production; (2) Brush used data from 12- and 24-month, low-pressure, anoxic-corrosion experiments with steels (Telander and Westerman, 1993), not just 3- and 6-month results; (3) Brush estimated the effects of more factors on the ranges of H_2-production and anoxic-corrosion rates of steels and other Fe-base alloys; (4) Brush used data from Reed et al. (1993) and estimates of actinide solubilities summarized by Trauth et al. (1992) to estimate H_2- and O_2-production rates from radiolysis of WIPP brines. Brush (see E) reviewed data on microbial gas-production from Francis and Gillow (1994) in addition to the results summarized by Molecke (1979), Sandia Laboratories (1979), and Brush (see D). However, the gas-production rates reported by Francis and Gillow (1994) have all fallen within the range estimated previously by Brush (see D). There is probably no justification, at least on the basis of the results obtained by Francis and Gillow (1994), for reducing the previously-estimated range. On the other hand, there is no justification for extending it. Therefore, Brush (see E) recommended using the microbial gas-production rates provided previously.

2.3.3 Sources of Gas-Generation Data

Brush (see E) used several primary sources of gas-production and related data obtained by the WIPP Project. (This list of primary sources from the late 1970s is not necessarily complete.) Molecke (1979) provided very limited data on oxic and anoxic corrosion of steel, and no description of the experiments that yielded them. Telander and Westerman (1993) described laboratory studies of anoxic corrosion of steels and other metals carried out at Pacific Northwest Laboratory (PNL) since November 1989. They emphasized the effects of factors such as inundated and humid conditions, the composition of the gaseous phase and pressure on corrosion of ASTM A 360 and ASTM A 570 steels, the low-C steels that simulate the contact-handled TRU waste drums and boxes, respectively, and concomitant H_2 production. Caldwell et al. (1987) described laboratory studies of microbial activity carried out at the University of New Mexico during the late 1970s. Francis and Gillow (1994) discussed laboratory studies of microbial activity conducted at Brookhaven National Laboratory (BNL) since May 1991. They emphasized the effects of factors such as inoculation, amendment with nutrients and/or NO_3^- (an electron acceptor), and addition of bentonite (a proposed backfill material) on gas production from microbial degradation of papers under inundated conditions. Kosiewicz et al. (1979), Zerwekh (1979), and Kosiewicz (1981) described laboratory studies of radiolysis performed at Los Alamos National Laboratory. Reed et al. (1993) described

laboratory studies of brine radiolysis at Argonne National Laboratory (ANL), especially the effects of brine composition and dissolved Pu concentration on the Gvalues (the number of molecules of a radiolytic dissociation product per 100 eV of absorbed dose) for radiolysis. Stein and Krumhansl (1986), Deal and Case (1987), Stein and Krumhansl (1988), and Deal et al. (1989a, 1989b, 1991a and 1991b) studied intergranular Salado-Formation brines at or near the stratigraphic horizon of WIPP disposal rooms. Popielak et al. (1983) studied fluids from brine reservoirs in the Castile Formation, which could enter the repository in the event of human intrusion. Although Brush (see E) did not use these data directly, Brush (1990) used the results of these studies to plan laboratory studies of gas generation.

Brush (see E) also used several primary sources of gas-production and related data obtained for applications other than the WIPP Project. Uhlig and Revie (1963) provided data used to estimate the effects of pH on the O_2-consumption, H_2-production, and corrosion rates for oxic and anoxic corrosion of steels and other Fe-base alloys. Wikjord et al. (1980), Haberman and Frydrych (1988), and Simpson and Schenk (1989) studied the effects of various factors on anoxic corrosion of steels and other Fe-base alloys. Although Brush (see E) did not use their results directly, their studies led to a greater understanding of anoxic corrosion of these materials under conditions expected in WIPP disposal rooms. Grauer et al. (1991) provided additional data used to estimate the effects of pH on the H_2-production and corrosion rates for anoxic corrosion of steels and other Fe-base alloys. Froelich et al. (1979) and Berner (1980) provided the conceptual model of sequential usage of electron acceptors applied by Brush and Anderson (1989) and Brush (1990) to determine which microbial respiratory pathways are potentially significant under expected WIPP conditions. Brush (1990) used these results to plan laboratory studies of microbial gas generation. Brush et al. (1994) also incorporated this conceptual model and the overall reactions for the microbial processes of Berner (1980) in the reaction path gas-generation model.

2.3.4 Sources of Interpretations of Gas-Generation Data

Several secondary sources summarized, reviewed, or interpreted the "raw" data obtained by the WIPP Project (see 2.3.3). Molecke (1979) summarized and interpreted data from studies of corrosion, microbial activity, radiolysis, and "thermal degradation" carried out for the WIPP Project and other applications during the 1970s. Sandia Laboratories (1979) briefly reviewed gas generation by these processes from the standpoint of the WIPP waste-acceptance criteria. Brush et al. (1991a) reviewed and interpreted preliminary data from laboratory studies of gas generation carried out for the WIPP Project after these studies were restarted in 1989. These included studies of: (1) anoxic corrosion of steels and other Fe-base alloys conducted by

Westerman and his colleagues at PNL; (2) halophilic microorganisms from the WIPP Site and vicinity performed by Vreeland and his students at West Chester University; (3) microbial consumption of cellulose carried out by Grbic-Galic and her students at Stanford University (this study did not yield any useful results); (4) radiolysis of brine and plastics conducted by Reed and his colleagues at ANL. Brush et al. (1991b) also reviewed and interpreted preliminary data from these studies. Brush (see D) provided gas-production rates for anoxic corrosion, microbial activity, and radiolysis for the 1992 PA calculations. WIPP Performance Assessment Division (1991) described the distributions that PA personnel assumed for the ranges of anoxic-corrosion and microbial gas-production rates provided by Brush (see D), and discussed how PA personnel converted these rates from his units to those used in the average stoichiometry model. (Sandia WIPP Project, 1992, used the same rates and distributions for the 1992 PA calculations.) Brush et al. (1993) reviewed and interpreted data from the following laboratory studies carried out for the WIPP Project since 1989: (1) anoxic corrosion of steels and other Fe-base alloys at PNL; (2) microbial consumption of papers conducted by Francis and his colleagues at BNL; (3) brine radiolysis at ANL. Brush (see E) provided gas-production rates for anoxic corrosion, microbial activity, and radiolysis for the planned 1993 PA calculations. PA personnel have not described these data in any of their reports.

3.0 REFERENCES

Berner, R.A. 1980. *Early Diagenesis: A Theoretical Approach.* Princeton, NJ: Princeton University Press.

Brush, L.H. 1990. *Test Plan for Laboratory and Modeling Studies of Repository and Radionuclide Chemistry for the Waste Isolation Pilot Plant.* SAND90-0266. Albuquerque, NM: Sandia National Laboratories.

Brush, L.H., and D.R. Anderson. 1989. "Potential Effects of Chemical Reactions on WIPP Gas and Water Budgets," *Systems Analysis, Long-Term Radionuclide Transport, and Dose Assessments, Waste Isolation Pilot Plant (WIPP), Southeastern New Mexico; March 1989.* Eds. A.R. Lappin, R.L. Hunter, D.P. Garber, and P.B. Davies. SAND89-0462. Albuquerque, NM: Sandia National Laboratories. A-3 through A-30.

Brush, L.H., D. Grbic-Galic, D.T. Reed, X. Tong, R.H. Vreeland, and R.E. Westerman. 1991a. "Preliminary Results of Laboratory Studies of Repository Chemistry for the Waste Isolation Pilot Plant," *Scientific Basis for Nuclear Waste Management XIV, Materials Research Society Symposium Proceedings, Boston, MA, November 26-29, 1990.* Eds. T. Abrajano, Jr. and L.H. Johnson. SAND90-1031C. Pittsburgh, PA: Materials Research Society. Vol. 212, 893-900.

Brush, L.H., M.A. Molecke, A.R. Lappin, R.E. Westerman, X. Tong, J.N.P. Black, D. Grbic-Galic, R.E. Vreeland, and D.T. Reed. 1991b. "Laboratory and Bin-Scale Tests of Gas Generation for the Waste Isolation Pilot Plant," *Waste-Generated Gas at the Waste Isolation Pilot Plant: Papers Presented at the Nuclear Energy Agency Workshop on Gas Generation and Release from Radioactive Repositories.* Eds. P.B. Davies, L.H. Brush, M.A. Molecke, F.T. Mendenhall, and S.W. Webb. SAND91-2378. Albuquerque, NM: Sandia National Laboratories. 2-1 through 2-14.

Brush, L.H., M.A. Molecke, R.E. Westerman, A.J. Francis, J.B. Gillow, R.H. Vreeland, and D.T. Reed. 1993. "Laboratory Studies of Gas Generation for the Waste Isolation Pilot Plant," *Scientific Basis for Nuclear Waste Management XVI, Materials Research Society Symposium Proceedings, Boston, MA, November 30-December 4, 1992.* Eds. C.G. Interrante and R.T. Pabalan. SAND92-2160C. Pittsburgh, PA: Materials Research Society. Vol. 294, 335-340.

Brush, L.H., J.W. Garner, and L.J. Storz. 1994. "Development of a Gas Generation Model for the Waste Isolation Pilot Plant," *Scientific Basis for Nuclear Waste Management XVII, Materials Research Society Symposium Proceedings, Boston, MA, November 29-December 3, 1993.* Eds. A. Barkatt and R.A. Van Konynenburg. SAND93-1145C. Pittsburgh, PA: Materials Research Society. Vol. 333, 241-246.

Butcher, B.M. 1990. *Preliminary Evaluation of Potential Engineered Modifications to the Waste Isolation Pilot Plant (WIPP).* SAND89-3095. Albuquerque, NM: Sandia National Laboratories.

Caldwell, D.E., R.C. Hallet, M.A. Molecke, E. Martinez, and B.J. Barnhart. 1988. *Rates of CO_2 Production from the Microbial Degradation of Transuranic Wastes Under Simulated Geologic Isolation Conditions*. SAND87-7170. Albuquerque, NM: Sandia National Laboratories.

Cygan, R.T. 1991. *The Solubility of Gases in NaCl Brine and a Critical Evaluation of Available Data*. SAND90-2848. Albuquerque, NM: Sandia National Laboratories.

Deal, D.E., and J.B. Case. 1987. *Brine Sampling and Evaluation Program Phase I Report*. DOE-WIPP-87-008. Carlsbad, NM: U.S. Department of Energy Waste Isolation Pilot Plant.

Deal, D.E., J.B. Case, R.M. Deshler, P.E. Drez, J. Myers, and J.R. Tyburski. 1989a. *Brine Sampling and Evaluation Program Phase II Report*. DOE-WIPP-87-010. Carlsbad, NM: U.S. Department of Energy Waste Isolation Pilot Plant.

Deal, D.E., R.J. Abitz, D.S. Belski, J.B. Case, M.E. Crawley, R.M. Deshler, P.E. Drez, C.A. Givens, R.B. King, B.A. Lauctes, J. Myers, S. Niou, J.M. Pietz, W.M. Roggenthen, J.R. Tyburski and M.G. Wallace. 1989b. *Brine Sampling and Evaluation Program 1988 Report*. DOE-WIPP 89-015. Carlsbad, NM: U.S. Department of Energy Waste Isolation Pilot Plant.

Deal, D.E., R.J. Abitz, D.S. Belski, J.B. Clark, M.E. Crawley, and M.L. Martin. 1991a. *Brine Sampling and Evaluation Program 1989 Report*. DOE-WIPP 91-009. Carlsbad, NM: U.S. Department of Energy Waste Isolation Pilot Plant.

Deal, D.E., R.J. Abitz, J. Myers, J.B. Case, D.S. Belski, M.L. Martin, and W.M. Roggenthen. 1991b. *Brine Sampling and Evaluation Program 1990 Report*. DOE-WIPP 91-036. Carlsbad, NM: U.S. Department of Energy Waste Isolation Pilot Plant.

Francis, A.J., and J.B. Gillow. 1994. *Effects of Microbial Processes on Gas Generation Under Expected Waste Isolation Pilot Plant Repository Conditions*. SAND93-7036. Albuquerque, NM: Sandia National Laboratories.

Froelich, P.N., G.P. Klinkhammer, M.L. Bender, N.A. Luedtke, G.R. Heath, D. Cullen, P. Dauphin, D. Hammond, B. Hartman, and V. Maynard. 1979. "Early Oxidation of Organic Matter in Pelagic Sediments of the Eastern Equatorial Atlantic: Suboxic Diagenesis," *Geochimica et Cosmochimica Acta*. Vol. 43, no. 7, 1075-1090.

Grauer, R., B. Knecht, P. Kreis, and J.P. Simpson. 1991. "Hydrogen Evolution from Corrosion of Iron and Steel in Intermediate Level Waste Repositories," *Scientific Basis for Nuclear Waste Management XIV, Materials Research Society Symposium Proceedings, Boston, MA, November 26-29, 1990*. Eds. T.A. Abrajano, Jr. and L.H. Johnson. Pittsburgh, PA: Materials Research Society. Vol. 44, 295-302.

Haberman, J.H., and D.J. Frydrych. 1988. "Corrosion Studies of A216 Grade WCA Steel in Hydrothermal Magnesium-Containing Brines," *Scientific Basis for Nuclear Waste Management XI, Materials Research Society Symposium Proceedings, Boston, MA, November 30-December 3, 1987.* Eds. M.J. Apted and R.E. Westerman. Pittsburgh, PA: Materials Research Society. Vol. 112, 761-772.

Kosiewicz, S.T. 1981. "Gas Generation from Organic Transuranic Wastes. I. Alpha Radiolysis at Atmospheric Pressure," *Nuclear Technology*. Vol. 54, no. 1, 92-99.

Kosiewicz, S.T., B.L. Barraclough, and A. Zerwekh. 1979. *Studies of Transuranic Waste Storage Under Conditions Expected in the Waste Isolation Pilot Plant (WIPP), December 15, 1978 - March 15, 1979.* LA-7775-PR. Los Alamos, NM: Los Alamos Scientific Laboratory.

Molecke, M.A. 1979. *Gas Generation from Transuranic Waste Degradation: Data Summary and Interpretation.* SAND79-1245. Albuquerque, NM: Sandia National Laboratories.

Popielak, R.S., R.L. Beauheim, S.R. Black, W.E. Coons, C.T. Ellingson, and R.L. Olsen 1983. *Brine Reservoirs in the Castile Formation, Waste Isolation Pilot Plant Project, Southeastern New Mexico*. TME 3153. Carlsbad, NM: U.S. Department of Energy WIPP Project Office.

Reed, D.T., S. Okajima, L.H. Brush, and M.A. Molecke. 1993. "Radiolytically-Induced Gas Production in Plutonium-Spiked WIPP Brine," *Scientific Basis for Nuclear Waste Management XVI, Materials Research Society Symposium Proceedings, Boston, MA, November 30-December 4, 1992.* Eds. C.G. Interrante and R.T. Pabalan. SAND92-7283C. Pittsburgh, PA: Materials Research Society. Vol. 294, 431-438.

Sandia Laboratories. 1979. *Summary of Research and Development Activities in Support of Waste Acceptance Criteria for WIPP.* SAND79-1305. Albuquerque, NM: Sandia National Laboratories.

Sandia WIPP Project. 1992. *Preliminary Performance Assessment for the Waste Isolation Pilot Plant, December 1992. Volume 3: Model Parameters.* SAND92-0700/3. Albuquerque, NM: Sandia National Laboratories.

Simpson, J.P., and R. Schenk. 1989. "Corrosion Induced Hydrogen Evolution on High Level Waste Overpack Materials in Synthetic Groundwaters and Chloride Solutions," *Scientific Basis for Nuclear Waste Management XII, Materials Research Society Symposium* Proceedings, *Berlin, Germany, October 10-13, 1988,* Eds. W. Lutze and R.C. Ewing. Pittsburgh, PA: Materials Research Society. Vol. 127, 389-396.

Stein, C.L., and J.L. Krumhansl. 1986. *Chemistry of Brines in Salt from the Waste Isolation Pilot Plant (WIPP), Southeastern New Mexico: A Preliminary Investigation*. SAND85-0897. Albuquerque, NM: Sandia National Laboratories.

Stein, C.L., and J.L. Krumhansl. 1988. "A Model for the Evolution of Brines in Salt from the Lower Salado Formation, Southeastern New Mexico," *Geochimica et Cosmochimica Acta*. Vol. 52, 1037-1046.

Telander, M.R., and R.E. Westerman. 1993. *Hydrogen Generation by Metal Corrosion in Simulated Waste Isolation Pilot Plant Environments*. SAND92-7347. Albuquerque, NM: Sandia National Laboratories.

Trauth, K.M., S.C. Hora, R.P. Rechard, and D.R. Anderson. 1992. *The Use of Expert Judgment to Quantify Uncertainty in Solubility and Sorption Parameters for Waste Isolation Pilot Plant Performance Assessment*. SAND92-0479. Albuquerque, NM: Sandia National Laboratories.

Uhlig, H.H., and R.W. Revie. 1963. *Corrosion and Corrosion Control: An Introduction to Corrosion Science and Engineering*. New York, NY: John Wiley and Sons.

Wikjord, A.G., T.E. Rummery, F.E. Doern, and D.G. Owen. 1980. "Corrosion and Deposition During the Exposure of Carbon Steel to Hydrogen Sulphide-Water Solutions," *Corrosion Science*. Vol. 20, no. 5, 651-671.

WIPP Performance Assessment Division. 1991. *Preliminary Comparison with 40 CFR Part 191, Subpart B for the Waste Isolation Pilot Plant, December 1991. Volume 3: Reference Data*. Eds. R.P. Rechard, A.C. Peterson, J.D. Schreiber, H.J. Iuzzolino, M.S. Tierney, and J.S. Sandha. SAND91-0893/3. Albuquerque, NM: Sandia National Laboratories.

Zerwekh, A. 1979. *Gas Generation from Radiolytic Attack of TRU-Contaminated Hydrogenous Waste*. LA-7674-MS. Los Alamos, NM: Los Alamos National Laboratory.

APPENDIX A: HISTORY OF WIPP STUDIES OF GAS GENERATION

APPENDIX A: HISTORY OF WIPP STUDIES OF GAS GENERATION

The Waste Isolation Pilot Plant (WIPP) Project carried out laboratory studies of gas generation during the late 1970s to support the development of transuranic (TRU) waste-acceptance criteria. Molecke (1978) provided plans for these studies, and Molecke (1979) summarized the results of this work. For the most part, these studies comprised single-process experiments on microbial activity and radiolysis with nonradioactive and some radioactive simulated TRU waste. There was very little work on anoxic corrosion. Based on laboratory measurements carried out on samples obtained by drilling from the surface, the permeability of the Salado Formation appeared to be high enough for rapid migration of gas from the repository, even given the highest gas-production rates summarized by Molecke (1979). Furthermore, Environmental Protection Agency regulations for chemically hazardous waste constituents did not apply at the time these studies were conducted. Therefore, the WIPP Project terminated studies of gas generation in 1979.

In 1987, preliminary performance-assessment (PA) calculations on the effects of human intrusion identified inflow of intergranular brine from the Salado Formation as a concern for the long-term performance of the repository. In early 1988, L. H. Brush and D. R. Anderson of Sandia National Laboratories began to examine the possible effects of processes such as anoxic corrosion of steels and microbial degradation of cellulosics on the H_2O content of the repository. Brush and Anderson (1989a) concluded that these processes could affect its H_2O content as significantly as brine inflow. Furthermore, they concluded that these processes could also produce significant quantities of gas. Meanwhile, in situ measurements in the WIPP underground workings had revealed by this time that the permeability of the Salado Formation was much lower than believed in the late 1970s.

Systems analysis carried out by Lappin et al. (1989), which used these new permeabilities, gas-generation assumptions from Brush and Anderson (1989a, 1989b and 1989c), and the rates-and-potentials gas-production model of Lappin et al. (1989) (see C.1), demonstrated that gas, if present in significant quantities, will affect the overall performance of the repository.

Therefore, the WIPP Project restarted laboratory studies of gas generation in February 1989. These studies have comprised mainly single-process experiments on anoxic corrosion, microbial activity, and radiolysis, mostly with nonradioactive, simulated contact-handled (CH) TRU waste (see B). Brush (1990) presented detailed plans for these studies. Brush et al. (1991a, 1991b and 1993), Reed et al. (1993), Telander and Westerman (1993), and

Francis and Gillow (1994) described these ongoing studies and most of the results obtained from them to date.

The WIPP Project also started to plan large-scale, multi-process tests with CH TRU waste at about the same time it restarted laboratory studies with simulated waste. Molecke (1990a and 1990b) and Molecke and Lappin (1990) provided detailed plans for these bin-scale and alcove tests. Lappin et al. (1991) provided additional justification for them.

The WIPP Project has also developed and used models to predict gas-generation by TRU waste (see C). For their 1989 systems analysis, which demonstrated that significant quantities of gas will affect repository performance, Lappin et al. (1989) used the rates-and-potentials gas-production model (see C.1). WIPP Performance Assessment Division (1991) developed the average-stoichiometry gas-production model (see C.2) and incorporated it in the multi-phase flow code Brine and Gas Flow (BRAGFLO), which also simulates room closure. Incorporation of the average-stoichiometry model in BRAGFLO thus coupled this gas-production model with the hydrologic and geomechanical models used for PA. Brush (see D) reviewed laboratory studies of gas generation carried out for the WIPP Project during the late 1970s, laboratory studies conducted for the WIPP Project since 1989, and similar studies for other applications. WIPP Performance Assessment Division (1991) and Sandia WIPP Project (1992) used these data in the average-stoichiometry model for the 1991 and 1992 PA calculations, respectively. In 1992, work began on the reaction-path gas-generation model (see C.3), which includes more gas-generation processes than the average-stoichiometry model and the interactions among these processes. Brush et al. (1994) provided a brief description of this model, which will replace the average stoichiometry model in BRAGFLO.

On October 21, 1993, the US Department of Energy (DOE) canceled the bin and alcove tests prior to their initiation in the WIPP underground workings. This decision was based, at least in part, on the results of the Independent Technical (Red Team) Review of these tests (U.S. DOE Office of Environmental Restoration and Waste Management, 1993). The DOE also announced that an Enhanced Laboratory Program (ELP) will replace the bin and alcove tests.

In late 1993, the WIPP Project began planning the ELP. This program will comprise multi-process experiments with radioactive (Pu-doped) simulated waste and multi-process tests with actual CH TRU waste. Once started, both the simulated and CH TRU-waste tests will continue for about two to five years.

REFERENCES

Brush, L.H. 1990. *Test Plan for Laboratory and Modeling Studies of Repository and Radionuclide Chemistry for the Waste Isolation Pilot Plant.* SAND90-0266. Albuquerque, NM: Sandia National Laboratories.

Brush, L.H., and D.R. Anderson. 1989a. "Potential Effects of Chemical Reactions on WIPP Gas and Water Budgets," *Systems Analysis, Long-Term Radionuclide Transport, and Dose Assessments, Waste Isolation Pilot Plant (WIPP), Southeastern New Mexico; March 1989.* Eds. A.R. Lappin, R.L. Hunter, D.P. Garber, and P.B. Davies. SAND89-0462. Albuquerque, NM: Sandia National Laboratories. A-3 through A-30.

Brush, L.H., and D.R. Anderson. 1989b. "First Meeting of the WIPP PA Source Term Group," *Systems Analysis, Long-Term Radionuclide Transport, and Dose Assessments, Waste Isolation Pilot Plant (WIPP), Southeastern New Mexico; March 1989.* Eds. A.R. Lappin, R.L. Hunter, D.P. Garber, and P.B. Davies. SAND89-0462. Albuquerque, NM: Sandia National Laboratories. A-31 through A-50.

Brush, L.H., and D.R. Anderson. 1989c. "Second Meeting of the WIPP PA Source-Term Group," *Systems Analysis, Long-Term Radionuclide Transport, and Dose Assessments, Waste Isolation Pilot Plant (WIPP), Southeastern New Mexico; March 1989.* Eds. A.R. Lappin, R.L. Hunter, D.P. Garber, and P.B. Davies. SAND89-0462. Albuquerque, NM: Sandia National Laboratories. A-51 through A-59.

Brush, L.H., D. Grbic-Galic, D.T. Reed, X. Tong, R.H. Vreeland, and R.E. Westerman. 1991a. "Preliminary Results of Laboratory Studies of Repository Chemistry for the Waste Isolation Pilot Plant," *Scientific Basis for Nuclear Waste Management XIV, Materials Research Society Symposium Proceedings, Boston, MA, November 26-29, 1990.* Eds. T. Abrajano, Jr. and L.H. Johnson. SAND90-1031C. Pittsburgh, PA: Materials Research Society. Vol. 212, 893-900.

Brush, L.H., M.A. Molecke, A.R. Lappin, R.E. Westerman, X. Tong, J.N.P. Black, D. Grbic-Galic, R.E. Vreeland, and D.T. Reed. 1991b. "Laboratory and Bin-Scale Tests of Gas Generation for the Waste Isolation Pilot Plant," *Waste-Generated Gas at the Waste Isolation Pilot Plant: Papers Presented at the Nuclear Energy Agency Workshop on Gas Generation and Release from Radioactive Repositories.* Eds. P.B. Davies, L.H. Brush, M.A. Molecke, F.T. Mendenhall, and S.W. Webb. SAND91-2378. Albuquerque, NM: Sandia National Laboratories. 2-1 through 2-14.

Brush, L.H., M.A. Molecke, R.E. Westerman, A.J. Francis, J.B. Gillow, R.H. Vreeland, and D.T. Reed. 1993. "Laboratory Studies of Gas Generation for the Waste Isolation Pilot Plant," *Scientific Basis for Nuclear Waste Management XVI, Materials Research Society Symposium Proceedings, Boston, MA, November 30-December 4, 1992.* Eds. C.G. Interrante and R.T. Pabalan. SAND92-2160C. Pittsburgh, PA: Materials Research Society. Vol. 294, 335-340.

Brush, L.H., J.W. Garner, and L.J. Storz. 1994. "Development of a Gas Generation Model for the Waste Isolation Pilot Plant," *Scientific Basis for Nuclear Waste Management XVII, Materials Research Society Symposium Proceedings, Boston, MA, November 29-December 3, 1993.* Eds. A. Barkatt and R.A. Van Konynenburg. SAND93-1145C. Pittsburgh, PA: Materials Research Society. Vol. 333, 241-246.

Francis, A.J., and J.B. Gillow. 1994. *Effects of Microbial Processes on Gas Generation Under Expected Waste Isolation Pilot Plant Repository Conditions.* SAND93-7036. Albuquerque, NM: Sandia National Laboratories.

Lappin, A.R., R.L. Hunter, D.P. Garber, and P.B. Davies, eds. 1989. *Systems Analysis, Long-Term Radionuclide Transport, and Dose Assessments, Waste Isolation Pilot Plant (WIPP), Southeastern New Mexico; March 1989.* SAND89-0462. Albuquerque, NM: Sandia National Laboratories.

Lappin, A.R., C.A. Gotway, M.A. Molecke, R.L. Hunter, and E.N. Lorusso. 1991. *Rationale for Revised Bin-Scale Gas-Generation Tests with Contact-Handled Transuranic Wastes at the Waste Isolation Pilot Plant.* SAND90-2481. Albuquerque, NM: Sandia National Laboratories.

Molecke, M.A. 1978. *Waste Isolation Pilot Plant Transuranic Wastes Experimental Characterization Program: Executive Summary.* SAND78-1356. Albuquerque, NM: Sandia National Laboratories.

Molecke, M.A. 1979. *Gas Generation from Transuranic Waste Degradation: Data Summary and Interpretation.* SAND79-1245. Albuquerque, NM: Sandia National Laboratories.

Molecke, M.A. 1990a. "Test Plan: WIPP Bin-Scale CH TRU Waste Tests." Albuquerque, NM: Sandia National Laboratories.

Molecke, M.A. 1990b. "Test Plan: WIPP In Situ Alcove CH TRU Waste Tests." Albuquerque, NM: Sandia National Laboratories.

Molecke, M.A., and A.R. Lappin. 1990. *Test Plan Addendum #1: Waste Isolation Pilot Plant Bin-Scale CH TRU Waste Tests.* SAND90-2082. Albuquerque, NM: Sandia National Laboratories.

Reed, D.T., S. Okajima, L.H. Brush, and M.A. Molecke. 1993. "Radiolytically-Induced Gas Production in Plutonium-Spiked WIPP Brine," *Scientific Basis for Nuclear Waste Management XVI, Materials Research Society Symposium Proceedings, Boston, MA, November 30-December 4, 1992.* Eds. C.G. Interrante and R.T. Pabalan. SAND92-7283C. Pittsburgh, PA: Materials Research Society. Vol. 294, 431-438.

Sandia WIPP Project. 1992. *Preliminary Performance Assessment for the Waste Isolation Pilot Plant, December 1992. Volume 3: Model Parameters.* SAND92-0700/3. Albuquerque, NM: Sandia National Laboratories.

Telander, M.R., and R.E. Westerman. 1993. *Hydrogen Generation by Metal Corrosion in Simulated Waste Isolation Pilot Plant Environments*. SAND92-7347. Albuquerque, NM: Sandia National Laboratories.

U.S. Department of Energy. Office of Environmental Restoration and Waste Management. 1993. *Independent Technical Review of the Bin and Alcove Test Programs at the Waste Isolation Pilot Plant*. DOE/EM-0130T. Washington, DC: U.S. Department of Energy.

WIPP Performance Assessment Division. 1991. *Preliminary Comparison with 40 CFR Part 191, Subpart B for the Waste Isolation Pilot Plant, December 1991. Volume 3: Reference Data*. SAND91-0893/3. Eds. R.P. Rechard, A.C. Peterson, J.D. Schreiber, H.J. Iuzzolino, M.S. Tierney, and J.S. Sandha. Albuquerque, NM: Sandia National Laboratories.

APPENDIX B: REVIEW OF WIPP-RELATED LABORATORY STUDIES OF GAS GENERATION

CONTENTS OF APPENDIX B

B.1 Corrosion B-4
B.1.1 Oxic Corrosion of Steels and Other Iron-Base Alloys B-4
B.1.2 Anoxic Corrosion of Steels and Other Iron-Base Alloys B-5
B.1.2.1 Effects of Anoxic Corrosion on the Water Content of WIPP Disposal Rooms B-18
B.2 Microbial Activity B-19
B.2.1 Significant Issues Pertaining to Microbial Activity in WIPP Disposal Rooms B-19
B.2.1.1 Presence of Microorganisms in WIPP Disposal Rooms B-19
B.2.1.2 Sterilization of the Waste and Other Contents of WIPP Disposal Rooms B-21
B.2.1.3 Long-term Survival of Microorganisms in WIPP Disposal Rooms B-22
B.2.1.4 Presence of Water in WIPP Disposal Rooms B-22
B.2.1.5 Biodegradability of Substrates in WIPP Disposal Rooms B-22
B.2.1.6 Presence and Availability of Electron Acceptors in WIPP Disposal Rooms B-23
B.2.1.7 Presence and Availability of Nutrients in WIPP Disposal Rooms B-24
B.2.2 Sequential Consumption of Electron Acceptors B-24
B.2.3 Aerobic Microbial Activity B-26
B.2.4 Anaerobic Microbial Activity B-29
B.2.4.1 Effects of Anaerobic Microbial Activity on the Water Content of WIPP Disposal Rooms B-33
B.3 Radiolysis B-35
B.3.1 Radiolysis of Water in the Waste and Brine B-35
B.3.2 Radiolysis of Cellulosics, Plastics and Rubbers B-37
B.4 Processes that Consume Gas B-38
B.5 References B-39

Figures

Figure B-1. Pressures measured during 24-month, low-pressure corrosion experiments started with initially pure N_2 and CO_2. . . . . B-8
Figure B-2. Pressures measured during low-pressure corrosion experiments started at various CO_2 partial pressures. B-12
Figure B-3. Pressures measured during low-pressure corrosion experiments started with initially pure H_2S B-13
Figure B-4. Pressures measured during high-pressure corrosion experiments started with initially pure CO_2 . . . . . B-17
Figure B-5. Total quantities of gas produced in aerobic microbial experiments with cellulose B-30
Figure B-6. Total quantities of gas produced in aerobic microbial experiments with cellulose and bentonite B-30
Figure B-7. Total quantities of gas produced in anaerobic microbial experiments with cellulose B-34

Figure B-8. Total quantities of gas produced in anaerobic microbial experiments with cellulose and bentonite B-34

Tables

Table B-1. Composition of Brines Used for Laboratory Studies of Corrosion, Microvial Activity, and Radiolysis B-7
Table B-2. Corrosion Rates of Different Steel Alloys and Heats under Inundated Conditions with Initially Pure N_2 at Low Pressure (m/year) B-8
Table B-3. Corrosion Rates of Different Steel Alloys and Heats under Inundated Conditions with Initially Pure CO_2 at Low Pressure (m/year) B-11
Table B-4. Conditions in the Low-Pressure Experiments to Obtain Additional Information on the CO_2 Passivation Requirement B-12
Table B-5. Conditions in and Results from High-Pressure Experiments with Steels . . . B-15
Table B-6. Composition of the Mixed Inoculum Used in Long-Term Microbial Gas-Generation Experiments at BNL. B-28
Table B-7. Microbial Populations in Brines from Nash Draw and G Seep B-28

APPENDIX B: REVIEW OF WIPP-RELATED LABORATORY STUDIES OF GAS GENERATION

This section reviews Waste Isolation Pilot Plant (WIPP)-related studies of gas generation. It emphasizes laboratory studies carried out by the WIPP Project since 1989. However, it includes some theoretical calculations conducted by the WIPP Project during that period, and results from studies performed for applications other than the WIPP Project. Molecke (1979) summarized the results of laboratory studies of gas generation carried out during the late 1970s to support the development of transuranic (TRU) waste-acceptance criteria.

Subsections 1.3.1, 1.3.2, and 1.3.3 summarize the results of these studies.

B.1 Corrosion

Oxic corrosion of steels and other Fe-base alloys, Al and Al-base alloys, and possibly other metals will consume O_2 and H_2O in WIPP disposal rooms. After depletion of the O_2 initially present in the repository, and in the absence of radiolytically produced O_2, anoxic corrosion of these metals will produce H_2, and consume H_2O, CO_2, and H_2S.

B.1.1 Oxic Corrosion of Steels and Other Iron-Base Alloys

Brush and Anderson (1989) concluded that oxic corrosion will not have a significant, direct effect on the gas and H_2O contents of WIPP disposal rooms. They concluded, based on their 1988 estimate of the quantity of steel in the contact-handled (CH) TRU waste drums to be emplaced in the repository and the assumption that oxic corrosion will be the only O_2-consuming process, that the O_2 in mine air trapped in the repository at the time of filling and sealing will only be sufficient to oxidize about 0.4 to 1.1% of the drums, depending on the initial void volume assumed. Inclusion of the Fe-base alloys in the CH TRU waste, the steels or other Fe-base alloys used for remote-handled (RH) TRU waste canisters and plugs, and the Fe-base alloys contained in RH TRU waste would, of course, somewhat decrease the estimated range given above. Whether oxic corrosion will be important also depends on the rate of O_2 production from radiolysis of H_2O in the waste and brine. The radiolytic O_2-production rate depends, in turn, on the quantity of H_2O in the waste and the quantity of brine in the repository (both of which will probably vary with time), and the dissolved and suspended concentrations of the important actinide elements in TRU waste. The estimates of actinide solubilities presented by

Trauth et al. (1992) and of the quantities of brine from Brush (see E) imply that brine radiolysis will produce O_2 at such low rates that oxic corrosion will continue to be unimportant throughout the 10,000-year period of performance of the repository.

The most likely oxic-corrosion reaction under inundated conditions in WIPP disposal rooms is:

$$4Fe + 2H_2O + 3O_2 \Leftrightarrow 4\gamma FeO(OH) \qquad (B.1)$$

In this reaction, Fe represents the Fe in steels and other Fe-base materials and γFeO(OH) is lepidocrocite. This reaction is the most likely of many possible reactions because γFeO(OH) was the most abundant phase observed during posttest x-ray-diffraction (XRD) analysis of the corrosion products from oxic, inundated, corrosion experiments carried out for the Strategic Petroleum Reserve (SPR) Project. Fe_3O_4 (magnetite) was also a major corrosion product and βFeO(OH) was a minor product. (The identity of the polymorph of FeO(OH), or even whether FeO(OH) or Fe_3O_4 is the dominant composition of oxic corrosion products, will not affect predictions of gas generation significantly, because oxic corrosion will be a minor process.) It is unclear whether oxic corrosion will occur under humid conditions and, if so, which erosion product(s) will form. (The SPR Project did not carry out any corrosion experiments under humid conditions.)

B.1.2 Anoxic Corrosion of Steels and Other Iron-Base Alloys

Because the WIPP Project had carried out very little work on anoxic corrosion during the 1970s, Brush (1990) used thermodynamic calculations and kinetic results from laboratory studies carried out for applications other than the WIPP Project to determine the possible behavior of steels and other Fe-base alloys under expected WIPP conditions. He concluded that, from the standpoint of the gas and H_2O contents of the repository, the most important issues were: (1) whether anoxic corrosion of these materials will produce H_2 and consume H_2O at the same rates under humid conditions as expected for inundated conditions; (2) how H_2 and gases produced by microbial activity (the other major gas-production processes) will affect anoxic corrosion; (3) the effects of pressure on anoxic corrosion; (4) the effects of pH. Brush (1990) recognized that these issues also apply to anoxic corrosion of other metals, especially Al and Al-base alloys.

R. E. Westerman and his colleagues at Pacific Northwest Laboratory (PNL) have carried out laboratory studies of anoxic corrosion of low-C steels for the WIPP Project since

November 1989. Telander and Westerman (1993) described low-pressure (about 5 to 20 atm) and high pressure (about 36 to 73 atm) experiments conducted for periods of three to 24 months. The objectives of the low-pressure experiments conducted in seal-welded containers were to determine the effects of humid and inundated conditions, the composition of the gaseous phase, and different steel alloys and heats on the H_2-production and corrosion rates. The objective of the low-pressure experiments conducted in autoclaves was to quantify the effect of crushed salt on the corrosion rate. The objectives of the high-pressure autoclave runs were to determine the effects of pressure, gaseous-phase composition, and different steel alloys and heats on the corrosion rate.

For most of their low-pressure experiments, Telander and Westerman (1993) used 2-L, Hastelloy C-22, seal-welded containers. Hastelloy C-22, a corrosion-resistant, Ni-Cr-Mo alloy, did not corrode in any of these runs. Telander and Westerman (1993) used two heats each of the low-C steels American Society for Testing and Materials (ASTM) A 366 and ASTM A 570 for these experiments. Cold-rolled ASTM A 366 steel simulates the CH TRU waste drums to be emplaced in WIPP disposal rooms; hot-rolled ASTM A 570 steel simulates the CH TRU waste boxes. They placed 24 specimens, six of each heat, with a total surface area of 0.60 to 0.64 m^2 in each container. For their humid runs, they suspended the electrically insulated specimens above 0.25 L of synthetic Brine A (see Table B-1). Although Brine A was initially developed to simulate fluids equilibrated with K^+- and Mg^{2+}-bearing minerals in the overlying potash-rich zones of the Salado Formation prior to entering the repository (Molecke, 1983), it is also similar in composition to intergranular brines from the Salado Formation at or near the stratigraphic horizon of the WIPP underground workings (Stein and Krumhansl, 1986 and 1988; Deal et al., 1989a and 1989b; Brush, 1990; Deal et al., 1991a and 1991b). For their inundated runs, Telander and Westerman (1993) added 1.34 to 1.39 L of Brine A to the containers. This immersed the tops of the specimens to a depth of about 6 mm. They then added enough N_2 or CO_2 to the headspaces (1.74 L in the humid containers and 0.63 L in the inundated containers) to pressurize them to about 10 atm. Telander and Westerman (1993) carried out duplicate 3-, 6-, 12-, and 24-month runs at 30 $\pm$ 5°C for each combination of conditions (humid or inundated, initially pure N_2 or CO_2).

In low-pressure, inundated experiments started with initially pure N_2 in the headspace above Brine A, Telander and Westerman (1993) reported that the pressures increased at a nearly constant rate due to H_2 production, probably from the reaction:

$$Fe + (x + 2)H_2O \Leftrightarrow Fe(OH)_2.xH_2O + H_2 \qquad (B.2)$$

Table B-1. Composition of Brines Used for Laboratory Studies of Corrosion, Microbial Activity, and Radiolysis

Element or Chemical Property	Brine A[1]	DH36[2]	G Seep[2]	ERDA-6[3]
Alkalinity (mM)[4]	ND[5]	11.9	12.0	43
B^{3+} (mM)[6]	20	137	144	63
Br^- (mM)	10	ND[5]	17.1	11
Ca^{2+} (mM)	20	9.60	7.68	12
Cl^- (M)	5.35	5.37	5.10	4.8
K^+ (mM)	770	472	350	97
Mg^{2+} (mM)	1,440	817	630	19
Na^+ (M)	1.83	3.67	4.11	4.87
pH (std. units)	6.5	6.0	6.1	6.17
Specific gravity	1.2	1.22	1.23	1.216
SO_{42-} (mM)	40	173	303	170
TDS (mg/L)[7]	306,000	346,000	355,000	330,000
TIC (mM)[8]	10	0.0139	0.0115	16

1 Synthetic brine described by Molecke (1983); composition similar to intergranular brines from the Salado Formation at or near the stratigraphic horizon of the WIPP underground workings.
2 Brine collected from the WIPP underground workings; composition from Brush (1990).
3 Brine from a reservoir in the Castile Formation; composition from Popielak et al. (1983).
4 Reported as equivalent HCO_{3-}, but probably reflects mainly B(III) species.
5 Not determined.
6 Probably present mainly as H_3BO_3 and HB_4O_{7-} or H_3BO_3 and $B(OH)_{4-}$.
7 Total dissolved solids.
8 Total inorganic C.

Figure B-1 shows the (averaged) results from the duplicate 24-month runs. The results from separate, duplicate 3-, 6-, and 12-month runs were similar at any given time, and are not shown here. The H_2-production and corrosion rates decreased somewhat with time. Posttest analysis of the headspace gases from the 3-, 6-, 12-, and 24-month runs yielded average H_2-production rates of 0.19, 0.21, 0.16, and 0.10 mole per m^2 of steel per year, respectively. The corrosion rates, determined independently by gravimetric (weight-loss) analysis of replicate steel specimens, did not vary significantly from heat to heat of the same alloy, or from alloy to alloy (see Table B-2). The average corrosion rates for the 3-, 6-, 12-, and 24-month runs were 1.96, 1.72, 1.23, and 0.99 μm of steel per year. The ratios of moles of H_2 produced to moles of

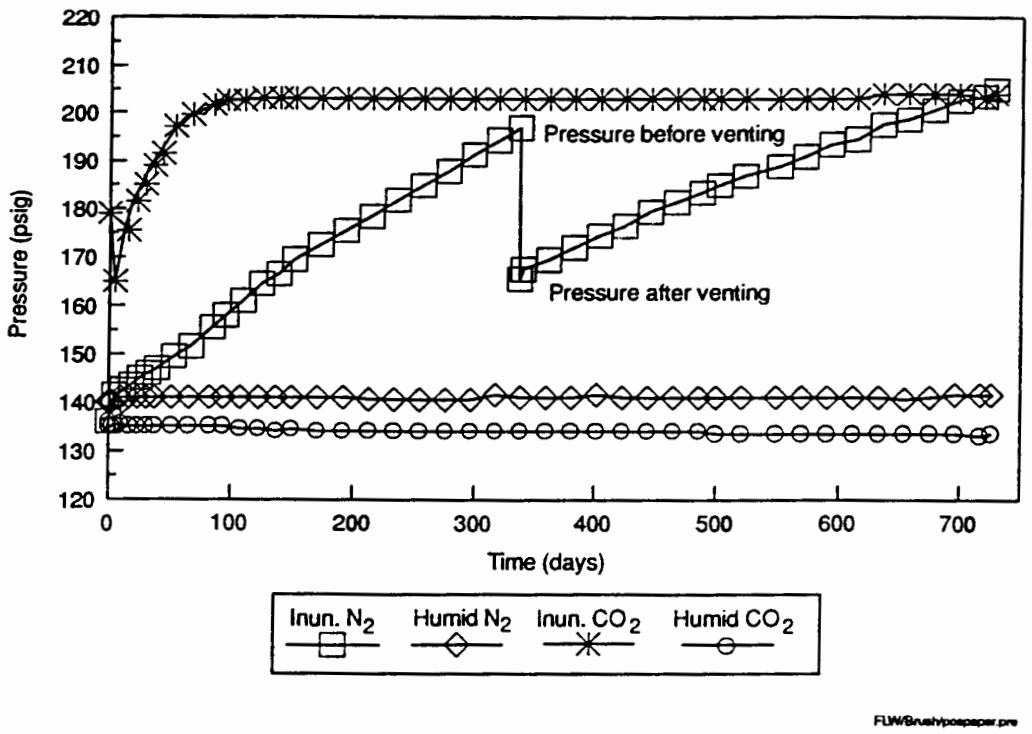

Figure B-1. Pressures measured during 24-month, low-pressure corrosion experiments started with initially pure N_2 and CO_2.

Table B-2. Corrosion Rates of Different Steel Alloys and Heats under Inundated Conditions with Initially Pure N_2 at Low Pressure (μm/year)

Run Time (months)	Alloy and Heat				
	ASTM A 366, Lot J	ASTM A 366, Lot K	ASTM A 570, Lot L	ASTM A 570, Lot M	Average
3	1.94 ± 0.16	2.03 ± 0.26	2.10 ± 0.19	1.79 ± 0.16	1.96 ± 0.22
6	1.61 ± 0.07	1.65 ± 0.37	1.81 ± 0.04	1.71 ± 0.08	1.72 ± 0.13
9	1.05 ± 0.05	1.26 ± 0.04	1.31 ± 0.04	1.29 ± 0.03	1.23 ± 0.11
12	0.95 ± 0.05	1.14 ± 0.08	0.91 ± 0.04	0.95 ± 0.04	0.99 ± 0.11

metal consumed in the 3-, 6-, 12-, and 24-month runs were 0.65, 0.83, 0.90 and 1.0. It is unclear why these ratios were less than the expected value of unity in the 3-, 6-, and 12-month runs, or why they increased and eventually attained unity in the 24-month runs. However, dissolution of H_2 in brine and uptake of H_2 by corrosion products were probably more

significant in the 3-, 6-, and 12-month experiments than in the 24-month runs because less H_2 was produced in the short-term runs. It is also unclear why the H_2-production and corrosion rates decreased by about a factor of two from the 3- to the 24-month runs. Possible explanations include: (1) pretest preparation (surface grinding) of the specimens resulted in initially rapid rates, which decreased as surficial material was removed by corrosion; (2) some inhibition of Reaction B.2 occurred due to accumulation of a thin film of the corrosion product on the surfaces of the steel specimens (however, PNL personnel have observed no such film); and (3) depletion of a reactant, perhaps in Brine A. Posttest analysis of the Brine A used for these runs revealed no changes in the concentrations of its major constituents. The corrosion product, which could not be identified by XRD analysis, but probably had the composition $Fe(OH)_2.xH2O$ or $(Fe,Mg)(OH)_2.xH_2O$, did not adhere to the specimens in these experiments. Therefore, H_2 production and corrosion will continue at these rates under inundated conditions unless the waste prevents this corrosion product from sloughing off or salts precipitated from brine during corrosion isolate the steels.

Brush (1990) calculated that $Fe(OH)_2$, the apparent corrosion product of the inundated experiments with initially pure N_2, is unstable with respect to Fe_3O_4 below an H_2 fugacity (roughly equivalent to the partial pressure) of about 100,000 atm. Therefore, significant quantities of steels and other Fe-base alloys might corrode via the reaction

$$3Fe + 4H_2O \Leftrightarrow Fe_3O_4 + 4H_2 \qquad \text{(B.3)}$$

if Fe_3O_4 eventually nucleates and replaces $Fe(OH)_2$. Telander and Westerman (1993) did not observe Fe_3O_4 in anoxic experiments that lasted for up to 24 months. However, Fe_3O_4 was among the corrosion products observed in oxic, inundated, corrosion experiments carried out for the SPR Project. Therefore, oxic corrosion may produce Fe_3O_4, which may then serve as nuclei for Reaction B.3.

Whether Reaction B.2 or B.3 is predominant in the absence of CO_2 and H_2S could be an important issue if sufficient H_2O is available to corrode enough steel to produce high H_2 partial pressures in WIPP disposal rooms. Brush (1990) calculated that, if sufficient steels, other Fe-base alloys, and H_2O are available, Reaction B.2 will reach equilibrium at an H_2 fugacity of about 60 atm, but that Reaction B.3 will continue until the H_2 fugacity is 400 atm. Simpson and Schenk (1989) calculated similar equilibrium H_2 fugacities for these reactions (about 100 and 500 atm, respectively) under conditions expected for a Swiss high-level-waste repository in granite. The results of Brush (1990) and Simpson and Schenk (1989) both suggest that the equilibrium H_2 fugacity for Reaction B.2 is well below lithostatic pressure at the depth of WIPP disposal rooms (about 150 atm), but that of Reaction B.3 is well above lithostatic pressure.

However, Telander and Westerman (1993) reported data from high-pressure experiments (see below), which imply that Reaction B.2 will continue to an H_2 fugacity of at least 70 atm.

No detectable H_2 production or corrosion occurred in the 3-, 6-, 12-, and 24-month humid experiments with initially pure N_2, except for very limited corrosion of the bottom 10% of the specimens splashed with brine during the pretest preparation procedures (see Figure B-1). These results suggest that anoxic corrosion in the repository will be self-limiting. Small quantities of brine in the repository will initiate anoxic corrosion, which will produce H_2, consume H_2O, increase the pressure, prevent additional brine inflow, or even cause brine outflow, thus precluding additional anoxic corrosion.

In low-pressure, inundated experiments started with initially pure CO_2 in the headspace above Brine A, the pressures decreased from initial values of about 12 atm because of continuing dissolution of CO_2 in Brine A (see Figure B-1). The pretest preparation procedures used by Telander and Westerman (1993), which included manual agitation of the seal-welded containers during CO_2 addition, apparently did not saturate Brine A with CO_2 prior to the start of these runs. After saturation, the pressures increased rapidly due to the reaction

$$Fe + H_2O + CO_2 \Leftrightarrow FeCO_3 + H_2. \qquad (B.4)$$

The pressures increased, despite the fact that Reaction B.4 did not affect the total quantity of gas in the system (aqueous and gaseous phases), because H_2 is significantly less soluble in brine than CO_2. Therefore, consumption of relatively soluble CO_2 and production of relatively insoluble H_2 resulted in a net increase in the quantity of gas in the gaseous phase. The corrosion rates, H_2-production rates, and pressurization rates in these experiments were higher than those in the inundated runs with initially pure N_2, at least initially. For example, Telander and Westerman (1993) reported average, 3-month corrosion rates of 8.76 μm per year for all four heats of steel (see Table B-3), and H_2-production rates of 1.10 mole per m^2 per year in the runs with initially pure CO_2, and average, 3-month corrosion rates of 1.96 μm per year (see Table B-2) and H_2-production rates of 0.19 mole per m^2 per year in the runs with initially pure N_2. Furthermore, heat-to-heat and alloy-to-alloy variations in the corrosion rates were greater in the experiments with initially pure CO_2 than in the runs with initially pure N_2. The rapid corrosion rates, H_2-production rates, and pressure increases in the runs with initially pure CO_2 probably resulted from acidic conditions caused by CO_2 dissolution in the brine. After about three or four months, however, the pressures stopped increasing due to passivation of the steel specimens. Posttest XRD analysis demonstrated that passivation resulted from formation of the adherent corrosion product $FeCO_3$ (siderite) by Reaction B.4. Although no $CaCO_3$ was observed in the diffractograms, posttest analysis of the Brine A used for these runs revealed that the

Table B-3. Corrosion Rates of Different Steel Alloys and Heats under Inundated Conditions with Initially Pure CO_2 at Low Pressure (μm/year)

Run Time (months)	Alloy and Heat				
	ASTM A 366, Lot J	ASTM A 366, Lot K	ASTM A 570, Lot L	ASTM A 570, Lot M	Average
3	12.7 ± 0.3.1	9.59 ± 1.02	5.29 ± 0.85	7.41 ± 2.43	8.76 ± 3.44
6	8.47 ± 1.91	7.91 ± 2.50	3.82 ± 0.74	5.00 ± 0.90	6.31 ± 2.54
9	3.68 ± 0.70	3.58 ± 0.78	1.72 ± 0.20	2.69 ± 2.61	2.91 ± 1.00
12	1.63 ± 0.34	1.85 ± 0.43	1.12 ± 0.49	1.26 ± 0.20	1.46 ± 0.47

dissolved Ca concentration decreased, perhaps due to some substitution of Ca for Fe in $FeCO_3$. In these low-pressure experiments, passivation by $FeCO_3$ consumed 0.42 mole of CO_2 per m^2 of steel. The results of other experiments (see below) imply that the quantity of CO_2 required for passivation depends on the CO_2 partial pressure and pH, and varies from about 0.16 to at least 0.42 mole of CO_2 per m^2 of steel.

As in the case of the low-pressure, humid experiments with initially pure N_2, no detectable corrosion occurred in the 3-, 6-, 12-, and 24-month humid runs with initially pure CO_2 except for very limited corrosion of the bottom 10% of the specimens splashed with brine during the pretest preparation procedures (see Figure B-1).

To obtain additional information on the CO_2 passivation requirement, Telander and Westerman (1993) carried out another series of low-pressure experiments in seal-welded containers identically to the low-pressure runs with initially pure N_2 and CO_2 (see above), except that they started these runs with initial CO_2 partial pressures of 7.6, 3.8, 1.5, 0.76, 0.39, and 0.00 atm, respectively (see Table B-4). The quantities of CO_2 in these experiments were equivalent to about 0.76, 0.38, 0.15, 0.076, 0.038, and 0.000 times that required for passivation in the first set of runs with inundated conditions and initially pure CO_2 (see above). (They added enough N_2 to the headspaces of the last three containers to pressurize them to slightly above 1 atm.) Pressure measurements from the first two containers imply that passivation occurred in about four to five months (see Figure B-2), somewhat longer than the three to four months required in the first set of runs. These results show that as the CO_2 partial pressure increases, the quantity of CO_2 required for passivation increases, but the time required decreases. In the third, fourth, and fifth containers, formation of $FeCO_3$ began, but did not result in passivation, presumably because there was not enough CO_2 in these containers to form a thick enough film of $FeCO_3$.

Table B-4. Conditions in the Low-Pressure Experiments to Obtain Additional Information on the CO_2 Passivation Requirement

Seal-Welded Container #	Initial CO_2 Pressure (atm)	Moles of CO_2 per m^2 of Steel	Initial N_2 Pressure (atm)
33	7.6	0.32	0.0
34	3.8	0.16	0.0
35	1.5	0.063	0.0
36	0.75	0.032	2.0
37	0.39	0.016	2.0
38	0.00	0.000	3.1

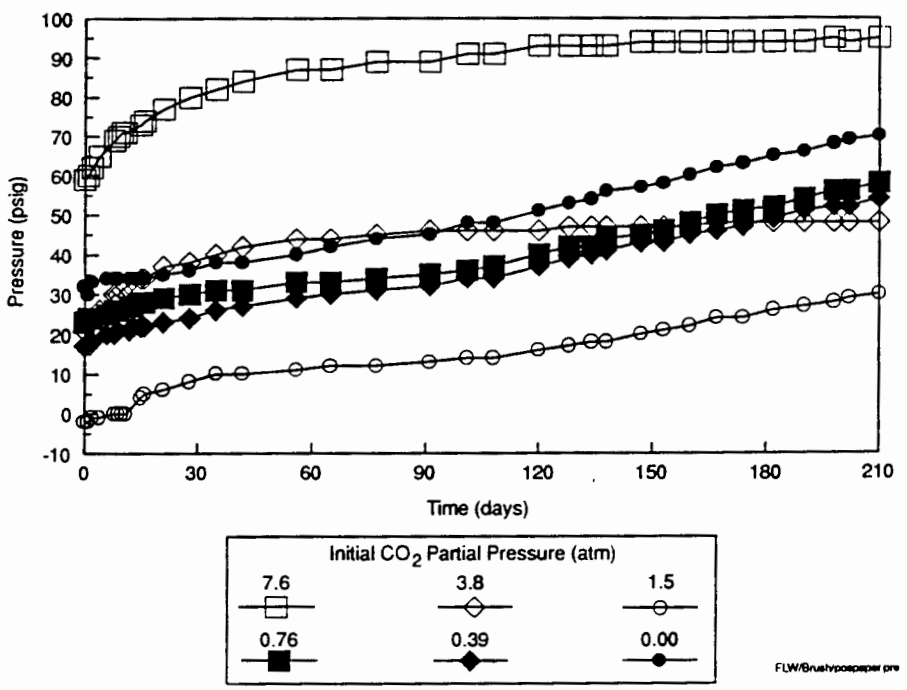

Figure B-2. Pressures measured during low-pressure corrosion experiments started at various CO_2 partial pressures.

Telander and Westerman (1993) carried out low-pressure experiments with initially pure H_2S identically to the low-pressure runs with initially pure N_2 and CO_2 (see above), except that the initial H_2S pressure was only about 5 atm. In the duplicate, inundated experiments, anoxic corrosion produced some H_2 initially by the reaction

$$Fe + H_2S \Leftrightarrow FeS + H_2. \tag{B.5}$$

The pressures increased, despite the fact that Reaction B.5 did not affect the total quantity of gas in the system, because H_2 is less soluble in brine than H_2S (see Figure B-3). However, the pressures stopped increasing after a few days due to passivation. Posttest XRD analysis revealed that FeS_{1-x} (mackinawite) was the passivating corrosion product under these conditions. This is surprising in view of results from studies for applications other than the WIPP Project (for example, Wikjord et al., 1980), which identified Fe sulfides with higher S/Fe ratios, such as $Fe_{1-x}S$ (pyrrhotite), and FeS_2 (pyrite) as the passivating phases in H_2S-bearing systems, but found that mackinawite is nonprotective. In these low-pressure runs, the passivation requirement was 0.056 moles of H_2S per m^2 of steel. In view of these published results, there is at least one more potentially significant anoxic-corrosion reaction:

$$Fe + 2H_2S \Leftrightarrow FeS_2 + 2H_2. \tag{B.6}$$

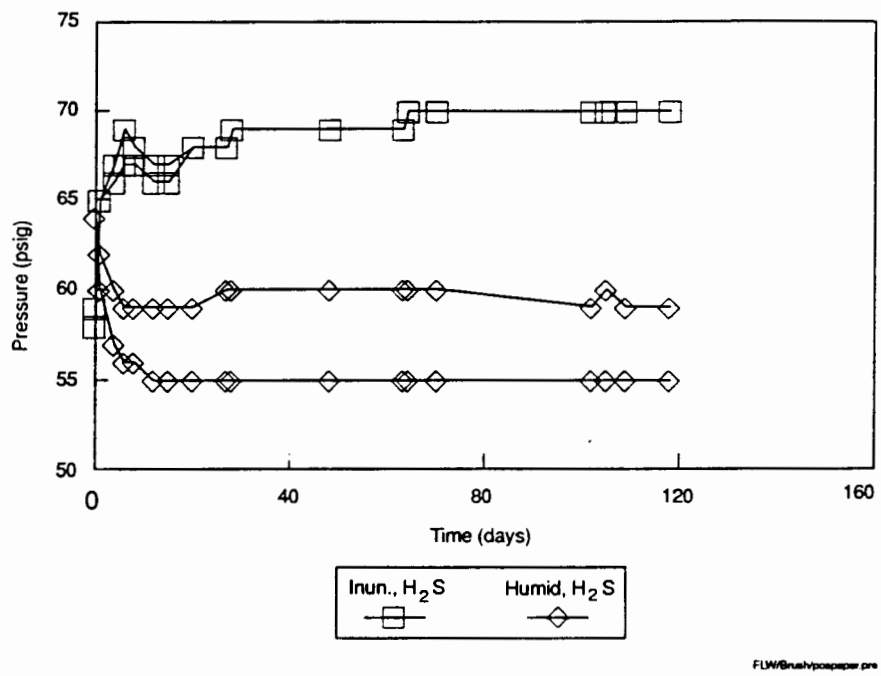

Figure B-3. Pressures measured during low-pressure corrosion experiments started with initially pure H_2S.

It is unclear whether this reaction (or any other reaction that produces a sulfide with a higher S/Fe ratio than mackinawite) will result in passivation of steels under expected WIPP conditions. However, it is clear that passivation of steels and other Fe-base alloys by $FeCO_3$ and FeS is a real phenomenon under some combinations of conditions expected in WIPP disposal rooms. On the other hand, results obtained during the development of the reaction-path gas-generation model (see C.3) suggest that depassivation is also possible, especially if consumption of CO_2 by $Ca(OH)_2$ (in hydrated cementitious materials) and CaO (a proposed backfill material) decrease the partial pressure of CO_2 below values required to stabilize $FeCO_3$.

Telander and Westerman (1993) carried out high-pressure experiments in 3.8-L, Hastelloy C autoclaves. Hastelloy C is a corrosion-resistant Ni-Cr-Mo alloy similar to Hastelloy C-22, the alloy used for the seal-welded containers in the low-pressure experiments described above. Telander and Westerman (1993) tested two heats of ASTM A 366 steel in the runs with initially pure N_2 and H_2, and two heats each of ASTM A 366 and ASTM A 570 steels in the runs with initially pure CO_2. They placed a total of 10 specimens, five of each heat, with a total surface area of 0.20 m^2 in the autoclaves with initially pure N_2 and H_2 and a total of 16 specimens, four of each heat, with a total surface area of 0.10 m^2 in the autoclaves with initially pure CO_2. Telander and Westerman (1993) added 2.8 L of Brine A (see Table B-1) to the autoclaves with initially pure N_2 and H_2, and 3.1 L of the same brine to the autoclaves with initially pure CO_2, enough to completely immerse the specimens. They then added sufficient N_2, H_2, or CO_2 to the headspaces (1.0 L in the autoclaves with initially pure N_2 or H_2, and 0.7 L in the autoclaves with initially pure CO_2) to pressurize them to either about 35 or 70 atm. They did not conduct duplicate runs under high-pressure, inundated conditions, or any runs under high-pressure, humid conditions.

In a six-month experiment with initially pure N_2 at a pressure of 73 atm, the average corrosion rate of two heats of ASTM A 366 steel was 2.96 μm per year (see Table B-5). This value was 82% higher than the average corrosion rate of 1.63 μm per year reported by Telander and Westerman (1993) for the same heats of ASTM A 366 steel in the six-month, low-pressure (about 10-atm) run with initially pure N_2 (see Table B-2). Because the total surface area of the steel specimens and the sensitivity of the pressure gauges used in the high-pressure experiments were less than those used in the low-pressure runs, and because the headspace volume of the autoclaves was greater than that of the (inundated) seal-welded containers, they did not report H_2-production rates for the high-pressure runs. Westerman et al. (1987) observed a similar increase in the corrosion rate of mild steel in experiments pressurized with Ar in a laboratory study carried out for the Salt Repository Project (SRP) for commercial spent fuel and high-level waste. Telander and Westerman (1993) proposed that the corrosion rate is proportional to the N_2 and Ar partial pressures because the portion of the cathodic reaction that controls the

Table B-5. Conditions in and Results from High-Pressure Experiments with Steels

Initially Pure Gas	Initial Pressure (atm)	Run Time (months)	ASTM A 366, Lot J	ASTM A 366, Lot K	ASTM A 570, Lot L	ASTM A 570, Lot M	Average
N_2	73	6	2.76[1]	3.17[2]	ND[3]	ND[3]	2.96[4]
H_2	35	12	0.20[5]	0.25[6]	ND[3]	ND[3]	0.22[4]
H_2	70	6	0.32[7]	0.40[8]	ND[3]	ND[3]	0.36[4]
H_2	69	12	0.20[9]	0.27[10]	ND[3]	ND[3]	0.24[4]
CO_2	36	6	22.1[11]	24.9[12]	36.0[13]	35.8[14]	29.7[4]

1 Standard deviation was 0.24 μm/year.
2 Standard deviation was 0.04 μm/year.
3 Not determined.
4 Standard deviation not determined.
5 Standard deviation was 0.01 μm/year.
6 Standard deviation was 0.02 μm/year.
7 Standard deviation was 0.01 μm/year.
8 Standard deviation was 0.04 μm/year.
9 Standard deviation was 0.01 μm/year.
10 Standard deviation was 0.03 μm/year.
11 Standard deviation was 1.8 μm/year.
12 Standard deviation was 1.0 μm/year.
13 Standard deviation was 1.3 μm/year.
14 Standard deviation was 1.7 μm/year.

overall rate of this reaction contains an activated complex with a molar volume smaller than that of the reactants that form this complex. However, in the absence of experimental confirmation of the cathodic reaction mechanism, this explanation is speculative. Because N_2 and Ar are inert gases, it is reasonable to assume that high N_2 and Ar partial pressures have the same effect on the corrosion and H_2-production rates as total pressure. Therefore, high total pressures in WIPP disposal rooms will increase the corrosion rate of steels and other Fe-base alloys and the concomitant H_2-production rate. XRD analysis of the nonadherent corrosion product implies that it was similar to the unidentifiable corrosion product formed in the low-pressure experiments with initially pure N_2. Chemical analysis of the corrosion product from this high-pressure run revealed that the cations consisted of 88% Fe and 12% Mg. Therefore, its composition was probably $(Fe_{0.88}Mg_{0.12})(OH)_2.xH_2O$.

In a 12-month experiment started with pure H_2 at a pressure of 35 atm, the average corrosion rate of two heats of ASTM A 366 steel was 0.22 μm per year (see Table B-5), 81% lower than the average corrosion rate of 1.16 μm per year observed with the same heats

of ASTM A 366 steel in the 12-month, low-pressure run with initially pure N_2 (see Table B-2). Doubling the initial H_2 pressure did not result in an additional decrease in the average corrosion rates. The latter results imply that Reaction B.2 will not stop at an H_2 fugacity of about 60 atm in WIPP disposal rooms, as predicted by Brush (1990). The most likely reason for this incorrect prediction is that Brush (1990) used a free energy of formation for pure $Fe(OH)_2$ (amakinite) for his calculation, but the corrosion product formed under these conditions has a significantly different composition or crystal structure and, hence, a significantly different free energy of formation. The average corrosion rates of two heats of ASTM A 366 steel were 0.36 and 0.24 μm per year in a 6- and a 12-month run, respectively. These rates were 78 and 79% lower than the average corrosion rates of 1.63 and 1.16 μm per year observed with the same materials in the 6- and 12-month, low-pressure runs with initially pure N_2. Telander and Westerman (1993) speculated that doubling the H_2 pressure did not decrease the average corrosion rate further because the effect of increasing the total pressure was equal, but opposite, to that of increasing the H_2 pressure. Westerman et al. (1987) also observed a decrease in the corrosion rate of mild steel in runs pressurized with H_2 in their study for the SRP. XRD analysis of the nonadherent corrosion products from the six-month experiment yielded a diffraction pattern for $(Ni,Fe)_6Fe_2(CO)_3(OH)_{16}.4H_2O$ (reevesite). However, based on the high Ni content obtained by chemical analysis of this phase, the lack of significant Ni in Brine A or ASTM A 366 steel, and the high Ni content of the Hastelloy C autoclave used for this run, Telander and Westerman (1993) concluded that $(Ni,Fe)_6Fe_2(CO)_3(OH)_{16}.4H_2O$ formed in this run because of reactions among the Brine A, steel, and autoclave. Furthermore, based on the Mg content of the corrosion products from this and the other runs started with pure H_2 at a pressure of 35, 69, or 70 atm, they concluded that the unidentified peaks in the diffractograms could have resulted from the same unidentifiable phase observed in the low- and high-pressure runs with initially pure N_2.

In six- and 12-month experiments with initially pure CO_2 at a pressure of 36 atm, the pressures increased rapidly, but stopped increasing after about two months due to passivation of the steel specimens (see Figure B-4). (These are the only high-pressure runs for which Telander and Westerman, 1993, presented pressure data.) These results imply that passivation will occur at high CO_2 partial pressures despite acidic conditions produced by dissolution of CO_2 in brine and the concomitant increase in the solubility of $FeCO_3$. Because passivation occurred much sooner in these high-pressure runs than in the low-pressure runs with initially pure CO_2, the corrosion rates obtained from the high- and low-pressure runs are not readily comparable. However, the average, six-month corrosion rate of two heats each of ASTM A 366 and ASTM A 570 steel was 29.7 μm per year (see Table B-5), about five times higher than the average corrosion rate of 6.30 μm per year observed with the same four heats of steel in the

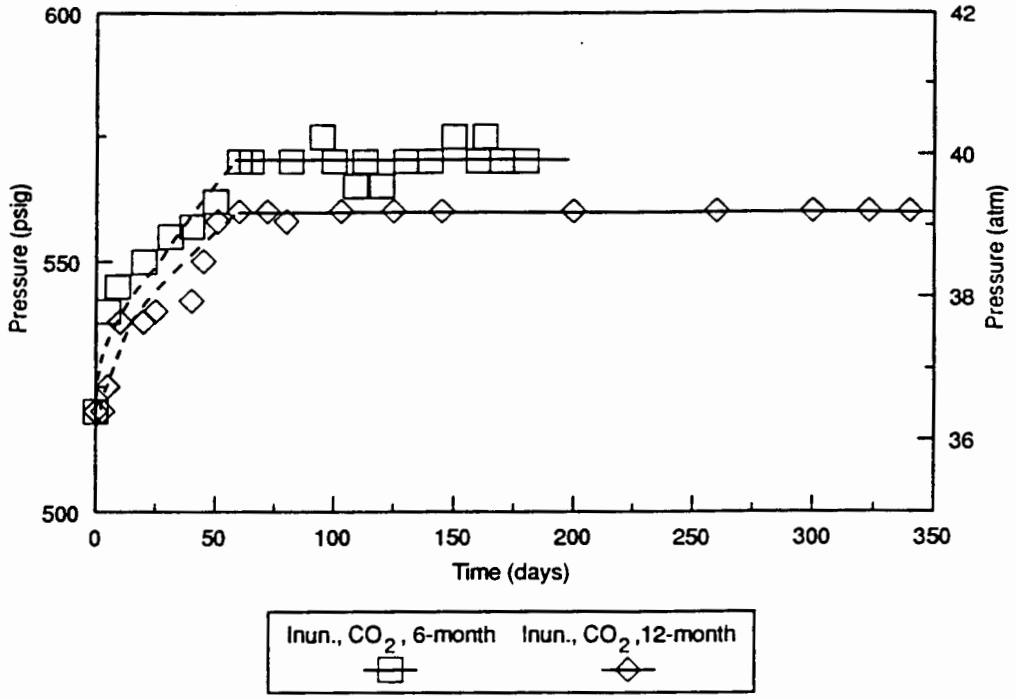

FLW/Brush/posepaper.pre

Figure B-4. Pressures measured during high-pressure corrosion experiments started with initially pure CO_2.

six-month, low-pressure runs with initially pure CO_2 (see Table B-3). Telander and Westerman (1993) did not complete the 12-month, high-pressure run in time for inclusion in their report. Posttest XRD analysis demonstrated that passivation resulted from formation of the adherent corrosion product $(Fe,Mn,Zn)CO_3$ (oligonite). Chemical analysis of this corrosion product revealed that the cations comprised 92.2% Fe, 6.1% Ca, 0.76% Mn, 0.31% Ni, 0.18% Zn and 0.17% Cu. The steel specimens were the source of the Fe and Mn, Brine A was the source of the Ca, and the Hastelloy C autoclave used for this run probably was the source of the Ni observed in this analysis. The reagents used to synthesize Brine A could have provided the Cu and Zn. Telander and Westerman (1993) did not report the quantity of CO_2 consumed during passivation under these conditions.

Finally, Telander and Westerman (1993) carried out two low-pressure experiments with crushed salt in the same autoclaves used for the high-pressure runs (see above). They placed 12 specimens of one heat of ASTM A 366 steel in two tiers in a stainless-steel-mesh baskets, filled the baskets with about 2 kg of coarse (2 to 6 mm diameter), particulate crushed salt from the WIPP underground workings, and suspended the baskets from the tops of the autoclaves. The total surface area of the specimens in each test was 0.033 m^2. To investigate the effect of capillary rise (brine wicking), Telander and Westerman (1993) added 890 ml of Brine A (see Table B-1) to one of the autoclaves. This was enough to inundate the crushed salt at the bottom

of the basket, but not enough to contact the bottoms of the specimens in the lower tier. They added 350 ml of Brine A to the other autoclave to examine the effects of vapor-phase transport of H_2O. In this run, the bottom of the basket was above the brine. They then added sufficient N_2 to pressurize the autoclaves to about 10 atm. They did not conduct duplicate runs under high-pressure, inundated conditions, or any runs under high-pressure, humid conditions.

Because capillary rise lithified the crushed salt in the first autoclave, it is unclear whether the corrosion rates reported by Telander and Westerman (1993) actually pertain to the entire duration of this experiment. (They did not report pressure data for this or the other low-pressure autoclave run.) Nevertheless, the average three-month corrosion rate of one heat of ASTM A 366 steel was 1.92 μm per year in the lower tier of specimens, and 1.15 μm per year in the upper tier. The rate reported for the lower tier was essentially identical to the average three-month rate of 1.94 μm per year observed with the same material in the low-pressure, seal-welded-container tests with initially pure N_2.

For the second autoclave, Telander and Westerman (1993) reported average three-month corrosion rates of 0.64 and 0.79 μm per year for the same heat of ASTM A 366 steel in the lower and upper tier of specimens, respectively. However, H_2O condensed on the underside of the autoclave head and dripped into the salt during this run. This resulted in partial saturation of the crushed salt with brine and some lithification of the salt. Therefore, these corrosion rates are not characteristic of those expected in the event of vapor-phase transport of H_2O.

B.1.2.1 EFFECTS OF ANOXIC CORROSION ON THE WATER CONTENT OF WIPP DISPOSAL ROOMS

Anoxic corrosion of steels and other Fe-base alloys by Reactions B.2 and B.3 will consume significant quantities H_2O. These reactions will consume at least 2 and 1.33 moles of H_2O per mole of Fe consumed, respectively. Furthermore, these reactions did not result in passivation of steels in experiments carried out by Telander and Westerman (1993). Therefore, as long as conditions remain favorable for formation of $Fe(OH)_2$ or Fe_3O_4, these reactions will continue to consume H_2O until one or both of the reactants are consumed or equilibrium is attained.

Although anoxic corrosion of steels and other Fe-base alloys by Reaction B.4 will consume 1 mole of H_2O per mole of Fe consumed, this reaction will probably result in passivation of these metals prior to consumption of significant quantities of H_2O. Reaction B.5, which will also passivate steels and other Fe-base alloys, and Reaction B.6 will not consume any H_2O.

B.2 Microbial Activity

Aerobic microbial consumption of cellulosics and, perhaps, plastics and rubbers will consume O_2 and produce CO_2 in WIPP disposal rooms. After depletion of the O_2 initially present and in the absence of radiolytically produced O_2, anaerobic microbial consumption of these materials will produce CO_2, N_2O, N_2, H_2S, H_2, and, perhaps, CH_4 and, possibly, consume CO_2 and H_2.

B.2.1 Significant Issues Pertaining to Microbial Activity in WIPP Disposal Rooms

Whether significant microbial gas production will occur in WIPP disposal rooms has been a controversial topic since the WIPP Project first began to study gas generation during the late 1970s. The most important issues pertaining to microbial activity have been whether: (1) microorganisms will be present in the repository when it is filled and sealed; (2) sterilization of the waste and other contents of the repository will prevent microbial activity; (3) microbes will survive for a significant fraction of the 10,000-year period of performance of the repository; (4) sufficient H_2O will be present; (5) sufficient quantities of biodegradable substrates will be present; (6) sufficient electron acceptors will be present and available; (7) enough nutrients, especially N and P, will be present and available. This subsection considers these issues and concludes that, although significant microbial gas generation is possible, it is by no means certain.

B.2.1.1 PRESENCE OF MICROORGANISMS IN WIPP DISPOSAL ROOMS

Halophilic, halotolerant, and nonhalopilic microorganisms will be present in WIPP disposal rooms when they are filled and sealed. Halophilic microbes can survive only in highly saline environments such as salt lakes and salt marshes. Halotolerant microbes prefer asaline environments, but can tolerate saline conditions. Nonhalophilic microbes can survive only in asaline environments.

Although the WIPP Project has carried out little, if any, characterization of the microbes in TRU waste, they are no doubt present when the waste is produced. Because most of these microbes probably have been or will be introduced to the waste by processes related to its production, packaging, and storage prior to emplacement in the repository, most of these microbes are probably nonhalophilic. However, some of the microbes in the waste, especially

those that lived on human skin in the presence of salt from perspiration, might be halotolerant or develop halotolerance when exposed to saline conditions. At least some of the microbes in the waste will probably survive storage, emplacement, and the period (probably on the order of decades) between filling and sealing of the repository and rupture of containers caused by room closure. The microbes in the waste could include numerous species capable of fermentation and methanogenesis once anaerobic conditions develop in the containers (see B.2.4). In fact, fermentation and methanogenesis, as well as other microbial processes, have probably occurred or will occur in many containers during storage, especially in those with high humidities. Exposure of the mainly nonhalophilic, nonhalotolerant microbes in the waste to the saline conditions expected after container rupture, however, will probably cause most of them to lyse. Although the halotolerant microbes could survive, and a few nonhalotolerant microbes could develop halotolerance when exposed to saline conditions, the most potentially significant microbes during most of the 10,000-year period of repository performance will be the halophilic microbes present in WIPP disposal rooms when they are filled and sealed.

Halophilic microorganisms capable of carrying out the respiratory pathways described below (see B.2.3 and B.2.4) probably exist throughout the WIPP underground workings. However, the source of these microbes is unclear. They have probably entered the WIPP underground workings since excavation on dust particles transported from the salt lakes in Nash Draw, nearby soils, and the WIPP tailings pile by wind and the mine ventilation system, or by various human vectors. The salt lakes in Nash Draw contain an abundance of halophilic and halotolerant microbes, which occur both in the waters in these lakes and in the underlying sediments. These lacustrine waters and the underlying sedimentary pore waters are concentrated brines with salinities similar to those of brines that could enter the repository after filling and sealing. It is also possible that the halophilic microbes that currently exist in the WIPP underground workings were present in the Salado Formation prior to excavation. In either case, these halophilic microbes have evolved under saline conditions. Therefore, they are better adapted to expected repository conditions than any halotolerant or potentially halotolerant microbes in the waste, and would probably affect the behavior of the repository more than halotolerant species. At least some of the halophilic microbes in the WIPP underground workings will probably survive until the interval between filling and sealing and container rupture. In fact, unless these microbes are present in the Salado Formation prior to excavation, waste emplacement will probably increase the number of microbes present.

The WIPP Project has not carried out a systematic survey to determine the numbers and types of microorganisms in TRU waste or the WIPP underground workings, nor has it attempted to determine the source(s) of these microbes. Such a survey would not be feasible or useful for the waste (most of these microbes will lyse when exposed to saline conditions), or useful for the

repository (waste emplacement could significantly alter the characteristics of the microbial population). Instead, investigators such as Francis and Gillow (1994) at Brookhaven National Laboratory (BNL) have collected halophilic, halotolerant, and nonhalophilic microbes from a variety of sources, including the salt lakes in Nash Draw and the WIPP underground workings, and enriched them in the laboratory. They have then subjected these microbes to various combinations of conditions possible in the repository after filling and sealing to quantify microbial gas-generation rates (see B.2.3 and B.2.4).

B.2.1.2 STERILIZATION OF THE WASTE AND OTHER CONTENTS OF WIPP DISPOSAL ROOMS

Sterilization of the contents of WIPP disposal rooms by autoclaving, irradiation, the use of biocides, or filtration (the four sterilization techniques used by microbiologists) is infeasible. Although autoclaving, irradiation, or biocides might delay the start of microbial activity in the repository to some extent or inhibit it somewhat thereafter, it would be very difficult, if not impossible, to defend the efficacy of these techniques. Therefore, they would not reduce the uncertainties in predictions of microbial gas generation significantly.

Autoclaving, typically carried out at 121°C and 18 psi for about 20 to 30 minutes, is the most common sterilization technique used by microbiologists. Although it would be feasible to sterilize the waste containers by autoclaving them prior to emplacement in the repository, recontamination would occur during emplacement. Furthermore, it would be impossible to autoclave either the exposed surfaces of the WIPP underground workings or the rock above, below, or behind these surfaces. (Microorganisms have probably penetrated the rock surrounding the excavations along fractures in the disturbed rock zone.)

It would also be feasible to irradiate the containers with γ radiation prior to emplacement, but recontamination would occur, and it would be infeasible to irradiate the surficial and subsurfical rock throughout the entire repository.

Chemical sterilization is feasible for solids with small volumes (up to a few cubic centimeters). However, it would be impossible to ensure a homogeneous distribution of a biocide or biocides throughout large volumes of solids such as those in the containers.

Microbiologists frequently use bacteriological filters, typically with a pore size of 0.25 μm, to sterilize thermolabile liquids. However, this method is infeasible for solids.

B.2.1.3 LONG-TERM SURVIVAL OF MICROORGANISMS IN WIPP DISPOSAL ROOMS

Although microorganisms will be present in WIPP disposal rooms when they are filled and sealed, it is by no means certain that they will survive long enough to affect the behavior of the repository significantly if, as expected, sealing the shafts and boreholes around the repository effectively isolates its contents from the surficial environment. Microbes occur in deep, subsurficial environments (DOE Subsurface Science Program's Taylorsville Working Group, 1994). However, it is generally unclear how and when they arrive in these environments. Therefore, it is also unclear how long they can survive there, especially under suboptimal conditions. Furthermore, it is difficult, if not impossible, to carry out microbial survival experiments for periods long enough to be relevant to the long-term performance of the WIPP. Therefore, it will be very difficult to determine whether the halophilic or halotolerant microbes that carry out any of the three potentially significant respiratory pathways (see 1.3.2 and B.2.4) will survive until containers rupture, brine enters the repository, the electron acceptors and nutrients in other types of waste diffuse through the brine to the waste containing cellulosics, and other potential substrates and the microbes that conduct preceding respiratory pathways render conditions favorable to their process.

B.2.1.4 PRESENCE OF WATER IN WIPP DISPOSAL ROOMS

Preliminary data summarized by Molecke (1979) suggested that the H_2O content of WIPP disposal rooms will not affect microbial gas-production rates significantly. However, Brush (1990) concluded that, with the possible exception of fermentation and methanogenesis (see B.2.4), the H_2O content of the repository could affect microbial activity significantly. Brush (1990) concluded that the repository H_2O content could be an important factor because electron acceptors and nutrients, if present in the waste or the surrounding Salado Formation, will for the most part require the presence of brine for diffusive transport from the waste or rock in which they occur (see B.2.1.6 and B.2.1.7) to waste containing substrates such as cellulosics, plastics, and rubbers (see B.2.1.5).

B.2.1.5 BIODEGRADABILITY OF SUBSTRATES IN WIPP DISPOSAL ROOMS

Molecke (1979), Brush and Anderson (1989), and Brush (1990) concluded that microorganisms in WIPP disposal rooms will use cellulosics as the substrate in preference to plastics and rubbers. However, after the depletion of cellulosics, microbes might consume plastics and rubbers. The studies summarized by Brush (1990) imply that high absorbed doses

of α radiation will make plastics and rubbers more biodegradable. Furthermore, slow (on the human time scale), nonradiolytic, inorganic reactions could also make them more biodegradable.

The preliminary data summarized by Molecke (1979) and recent results reported by Francis and Gillow (1994) (see B.2.4) imply that, if certain conditions are met, microbial consumption of cellulosics will result in significant gas production. However, the WIPP Project has carried out little work on microbial consumption of plastics and rubbers. Microbial consumption of plastics and rubbers is so slow that it would be very difficult, if not impossible, to use them to quantify gas production without first subjecting them to accelerated degradation reactions and/or carrying out unattainably long experiments. (The persistence of plastics and rubbers in landfills and the natural environment attests to their resistance to microbial consumption.) However, accelerated degradation of these materials prior to these experiments could convert them to materials with properties significantly different from those that will be present in the repository tens, hundreds or thousands of years after emplacement. For example, high absorbed doses of α radiation could produce an unrealistically biodegradable substrate if most of the plastics and rubbers in the repository receive doses significantly lower than those required for detectable gas generation in experiments that last only a few years.

B.2.1.6 PRESENCE AND AVAILABILITY OF ELECTRON ACCEPTORS IN WIPP DISPOSAL ROOMS

It is unclear whether the TRU waste to be emplaced in WIPP disposal rooms will contain sufficient quantities of electron acceptors for significant microbial gas production. The current version of U.S. DOE Carlsbad Area Office (1994) does not provide estimates of the quantities of NO_3^-, Fe(III) oxides and hydroxides, Mn(IV) oxides and hydroxides, and SO_4^{2-}, electron acceptors consumed by anaerobic microorganisms (see B.2.4), in the waste. There is no reason to suspect that significant quantities of Fe(III) and Mn(IV) oxides and hydroxides will be present in the waste. However, significant quantities of NO_3^- and SO_4^{2-} could be present in process sludges.

Intergranular brines and minerals from the Salado Formation at or near the stratigraphic horizon of the repository contain very limited quantities of NO_3^-, Fe, and Mn (Stein, 1985; Stein and Krumhansl, 1986 and 1988; Deal et al., 1989a, 1989b, 1991a and 1991b). However, the dissolved SO_4^{2-} concentration of these brines is on the order of a few hundred millimolar. Furthermore, the Salado Formation contains a few weight percent $CaSO_4$ (anhydrite) and $CaSO_4.2H_2O$ (gypsum). Dissolution of these minerals could replenish the SO_4^{2-} consumed during SO_4^{2-} reduction.

If sufficient NO_3^- and SO_4^{2-} are present in the waste and/or the surrounding Salado Formation, they will, for the most part, require container rupture and the presence of brine for diffusive transport from process sludges[1] to the plastic liners of the containers in which they occur, or to cellulosics, plastics, and rubbers in other containers. Therefore, even if enough NO_3^- and SO_4^{2-} are present, they will not necessarily be available to the microorganisms capable of using them as electron acceptors.

B.2.1.7 PRESENCE AND AVAILABILITY OF NUTRIENTS IN WIPP DISPOSAL ROOMS

It is also unclear whether sufficient nutrients, especially N and P, will be present for significant microbial gas production in WIPP disposal rooms. U.S. DOE Carlsbad Area Office (1994) does not provide estimates of the quantities of N and P in the waste. Intergranular brines from the Salado Formation contain very low concentrations of N and P (Deal et al., 1989b, 1991a, and 1991b) and there is no reason to suspect that Salado-Formation minerals contain significant P (Stein, 1985).

Furthermore, even if enough N and P are present in the waste or the surrounding Salado Formation, they will not necessarily be available to microorganisms until the containers have ruptured and brine is present for diffusive transport of these nutrients to waste containing cellulosics, plastics and rubbers.

B.2.2 Sequential Consumption of Electron Acceptors

Brush and Anderson (1989) and Brush (1990) applied the conceptual model of sequential consumption of electron acceptors by microorganisms in the natural environment (Froelich et al., 1979; Berner, 1980) to WIPP disposal rooms. Brush (1990) used this model and estimates of which potential electron acceptors will be present in significant quantities in the repository after filling and sealing (see B.2.1.6) to determine which respiratory pathways are significant, which are insignificant, and to predict the overall reactions for the potentially significant processes (see B.2.3 and B.2.4). Furthermore, Brush (1990) planned laboratory studies to quantify the effects of various factors on the rates at which halophilic microbes from the WIPP region produce gas by carrying out potentially significant respiratory pathways. Recently, Brush et al. (1994) used some of these reactions, slightly modified, and microbial gas-

---

[1] Some NO_3^- will be present at residues of HNO_3 on paper and cloth used for decontamination.

production rates from Molecke (1979) and Francis and Gillow (1994) (see B.2.3 and B.2.4) to simulate microbial gas generation in the reaction-path gas-generation model (see C.3).

In the natural environment, microorganisms oxidize organic matter by consuming the electron acceptor that yields the most free energy per mole of organic C consumed (Froelich et al., 1979; Berner, 1980). After the depletion of this electron acceptor, other microbes consume the next most efficient electron acceptor present. (However, facultative anaerobes consume O_2 as long as it is available, but can use other electron acceptors, such as NO_3^-, after the depletion of O_2.) If the environment remains favorable to microbial activity, sequential consumption of electron acceptors continues until microbes have consumed all of the substrate or substrates, all available electron acceptors, or all essential nutrients. In natural systems, the order of consumption of electron acceptors is O_2, NO_3^-, Mn(IV) oxides and hydroxides, Fe(III) oxides and hydroxides, SO_4^{2-}, organic acids, and CO_2. (In some systems, consumption of Mn(IV) oxides and hydroxides occurs prior to that of NO_3^-.) Microbiologists refer to microbes that consume O_2 as "aerobic" and to those that use any of the other electron acceptors listed above as "anaerobic." They refer to consumption of NO_3^-, Mn(IV) and Fe(III) oxides and hydroxides, SO_4^{2-}, organic acids, and CO_2 as "denitrification," "Mn(IV) reduction," "Fe(III) reduction," and "SO_4^{2-} reduction" and "methanogenesis," respectively.

For the sake of simplicity, Brush and Anderson (1989) and Brush (1990) described these respiratory pathways as though they will occur sequentially in WIPP disposal rooms. This is generally the case in natural systems such as lacustrine, estuarine, and marine sediments. The processes described below could occur sequentially in many locations in the repository, but could also occur simultaneously because of the heterogeneous nature of the TRU waste to be emplaced in the repository. Aerobic microbial activity, for example, could continue for lengthy periods near large, radionuclide-bearing particles because of continuous production of O_2 from radiolysis of H_2O in the waste and brine. Simultaneously, anaerobic microbial activity could occur in waste with low concentrations of radionuclides, but with large quantities of steels and other Fe-base alloys, Al and Al-base alloys, organic materials, or other reductants.

During any of these respiratory pathways, the degradation of organic matter is complex and involves several intermediate steps usually mediated by different microorganisms. Geochemists have described microbial activity by writing overall reactions representative of each process (Froelich et al., 1979; Berner, 1980; Brush and Anderson, 1989). They use various formulas such as CH_2O (a simplified formula for glucose) or $(CH_2O)_{106}\cdot(NH_3)_{16}\cdot(H_3PO_4)$ (the Redfield ratio) to represent the substrate, but do not include microbial synthesis of cellular material (biomass) in their reactions. Microbiologists, on the other hand, include synthesis of

biomass by adding formulae such as $C_5H_7O_2N$ to the right-hand side of their reactions. To illustrate this difference, both types of reactions appear below (see B.2.3 and B.2.4).

B.2.3 Aerobic Microbial Activity

Aerobic microorganisms consume O_2 as the electron acceptor and produce CO_2 and H_2O (see B.2.2).

Brush and Anderson (1989) concluded that aerobic microbial consumption of cellulosics will not have a significant, direct effect on the gas or H_2O contents of WIPP disposal rooms. (They assumed that neither aerobic nor anaerobic microorganisms would consume plastics and rubbers.) Brush and Anderson (1989) calculated, based on their 1988 estimate of the quantity of cellulosics in the CH TRU waste to be emplaced in the repository and the assumption that aerobic microbial activity will be the only O_2-consuming process, that the O_2 in mine air trapped in the repository at the time of filling and sealing, would only be sufficient to oxidize about 1.1 to 1.7% of the cellulosics, depending on the initial void volume assumed. Inclusion of the cellulosics in CH TRU waste boxes and in RH TRU waste would somewhat decrease this estimated range. Nevertheless, estimates of actinide solubilities presented by Trauth et al. (1992) and of the quantities of brine in the repository from Brush (see E) imply that brine radiolysis will produce O_2 at such low rates that aerobic microbial activity will continue to be unimportant throughout the 10,000-year period of performance of the repository.

The overall reactions for aerobic microbial activity as written by Berner (1980) and Brush (1990), respectively, are:

$$CH_2O + O_2 \Rightarrow H_2O + CO_2; \qquad \text{(B.7a)}$$

$$CH_2O + 0.11H^+ + 0.11NO_{3^-} + 0.21O_2 \Rightarrow 0.11C_5H_7O_2N + 0.67H_2O + 0.44CO_2 \qquad \text{(B.7b)}$$

In these reactions and the reactions for other potentially significant respiratory pathways (see B.2.4), CH_2O represents the substrate. In Reaction B.7b and the second equation for each of the other processes, $C_5H_7O_2N$ represents biomass.

A. J. Francis and his colleagues at BNL have carried out laboratory studies of aerobic (and anaerobic) microbial gas generation for the WIPP Project since May 1991. Francis and Gillow (1994) reported the results of short-term experiments conducted for periods from a few days to several months, and preliminary results from long-term experiments planned to continue

for up to a few years. The objectives of the short-term experiments were to: (1) evaluate and standardize the techniques used for the long-term experiments, especially sampling, storing, and enriching communities of microorganisms for use as inocula and sampling and analyzing gases; (2) obtain preliminary gas-generation data from various communities and pure strains of microbes using different substrates and electron acceptors. The objective of the long-term experiments is to quantify the range of microbial gas-generation rates that could occur in WIPP disposal rooms. Because the conditions under which microbial activity (if any) will occur are uncertain (see B.2.1), BNL personnel are studying the effects of several factors on microbial gas generation. These factors are: (1) the presence or absence of an inoculum containing halophilic microbes from the salt lakes in Nash Draw and the WIPP underground workings, and nonhalophilic microbes from laboratories at BNL; (2) whether conditions are humid or inundated; (3) the presence or absence of papers simulating the cellulosics in the TRU waste to be emplaced in the repository; (4) the presence or absence of amended nutrients; (5) the presence or absence of amended NO_{3-} (an electron acceptor); (6) the presence or absence of bentonite (a proposed backfill material); (7) whether conditions are initially oxic or anoxic. Because the long-term experiments simulate expected repository conditions better than the short-term experiments did, this review emphasizes the long-term experiments.

For their long-term, inundated experiments, Francis and Gillow (1994) used 160-ml glass serum bottles sealed with butyl-rubber stoppers and brine collected from G Seep in the WIPP underground workings (see Table B-1; Deal and Case, 1987; Deal et al., 1989a, 1989b, 1991a, and 1991b). (BNL personnel did not start humid runs in time for this review.) Depending on the combination of conditions studied in each experiment (see above), Francis and Gillow (1994) added a mixed inoculum, papers, nutrients, NO_{3-}, bentonite, and air or O_2-free N_2 to the bottles. The mixed inoculum consisted of brines and muds collected from the salt lakes in Nash Draw, brines from G Seep, and dust collected from laboratories at BNL (see Table B-6). Francis and Gillow (1994) reported that brines from G Seep contained $7.2 \cdot 10^4$ to $3.4 \cdot 10^6$ microbial cells per ml, and brines from the lakes contained $5.5 \cdot 10^6$ to $1.0 \cdot 10^7$ cells per ml (see Table B-7). (Not all of these cells were necessarily viable.) Most of these microorganisms were probably halophilic, but these brines could have contained some halotolerant species. The dust probably contained mainly nonhalophilic microbes, but could have contained some halotolerant species. Because Brush (1990) estimated that the cellulosics in the WIPP inventory will consist of about 70% paper, Francis and Gillow (1994) used papers as the substrate in most of these experiments. To simulate these papers, they added 1.25 g each Whatman #1 filter paper, Kimwipes, brown paper towels, and white paper towels, each cut into 1 cm-by-1 cm squares, to the bottles with cellulosics. In these experiments, papers were the sole source of organic C and energy. The final nutrient concentrations in the amended runs were 1.25 mM NH_4NO_3, 0.735 mM K_3PO_4,

Table B-6. Composition of the Mixed Inoculum Used in Long-Term Microbial Gas-Generation Experiments at BNL.

Source	Brine (ml)	Mud (ml)[1]	Dust (g)
Nash-Draw Lakes			
Laguna Quatro	40	60	0
Laguna Tres (South)	40	13	0
Lindsey Lake	40	50	0
Surprise Springs	40	25	0
WIPP Underground Workings			
G Seep	200	0	0
BNL Labs			
Building 318	0	0	2.5

[1] Added as slurry.

Table B-7. Microbial Populations in Brines from Nash Draw and G Seep.

Source	Population (cells/ml)
Nash-Draw Lakes	
Laguna Cinco	$6.8 \cdot 10^6$
Laguna Quatro	$1.0 \cdot 10^7$
Laguna Tres (South)	$9.0 \cdot 10^6$
Lindsey Lake	$7.0 \cdot 10^6$
Surprise Springs	$5.5 \cdot 10^6$
WIPP Underground Workings	
G Seep, Carboy #9	$7.2 \cdot 10^4$
G Seep, Carboy #23	$3.4 \cdot 10^6$

and 0.5 g per L yeast extract; the concentration of KNO_3 (when added as an electron acceptor) was 4.95 mM.

Francis and Gillow (1994) added 6.0 g of MX-80 bentonite, a standard bentonite used in other studies conducted for the WIPP Project, to several of the bottles. The total volume of solution (brine and any inoculum, nutrients, and NO_{3-}), papers, and bentonite in each bottle was 100 to 117 ml. Francis and Gillow (1994) used six replicate bottles for each combination of conditions that included papers and duplicate bottles for those that did not. They incubated the bottles at 30 $\pm$ 2°C.

Francis and Gillow (1994) reported the results of inundated, aerobic experiments after 0, 45, 69, 104, 132, 169, and 200 days (see Figures B-5 and B-6). (They will continue these runs for up to a few years.) Because they started these experiments with a gaseous phase consisting of air, Francis and Gillow (1994) refer to them as "aerobic." However, microbial consumption of O_2 probably resulted in anoxic conditions in at least some of these experiments, and at least some anaerobic microbial activity occurred in these "aerobic" runs. For their bentonite-free experiments, Francis and Gillow (1994) reported 200-day, total gas-generation rates of 0.001 ml per g of cellulosics per day under uninoculated, unamended conditions, -0.001 ml per g of cellulosics per day under inoculated, unamended conditions, 0.008 ml per g of cellulosics per day under inoculated, amended (nutrients only) conditions, and 0.023 ml per g of cellulosics per day under inoculated, amended (nutrients and NO_{3-}) conditions. The rate observed in the experiment carried out under inoculated, amended (nutrients and NO_{3-}) conditions, the highest rate observed in the bentonite-free, aerobic runs, probably includes gas production from microbial denitrification, an anaerobic process (see B.2.4). Francis and Gillow (1994) also analyzed for CO_2 and N_2O. However, they did not correct their results for the quantities of gases that dissolved in the brine present in these inundated experiments. They observed that with bentonite present, the 200-day, total gas-production rates increased to 0.003 ml per g of cellulosics per day under uninoculated, unamended conditions, 0.001 ml per g of cellulosics per day under inoculated, unamended conditions, 0.028 ml per g of cellulosics per day under inoculated, amended (nutrients only) conditions, and 0.034 ml per g of cellulosics per day under inoculated, amended (nutrients and NO_{3-}) conditions.

B.2.4 Anaerobic Microbial Activity

After the depletion of O_2, anaerobic respiration begins. During denitrification, microorganisms consume NO_{3-} as the electron acceptor and produce CO_2, N_2O and N_2. Significant quantities of NO_{3-} could be present in WIPP disposal rooms (see B.2.1.6).

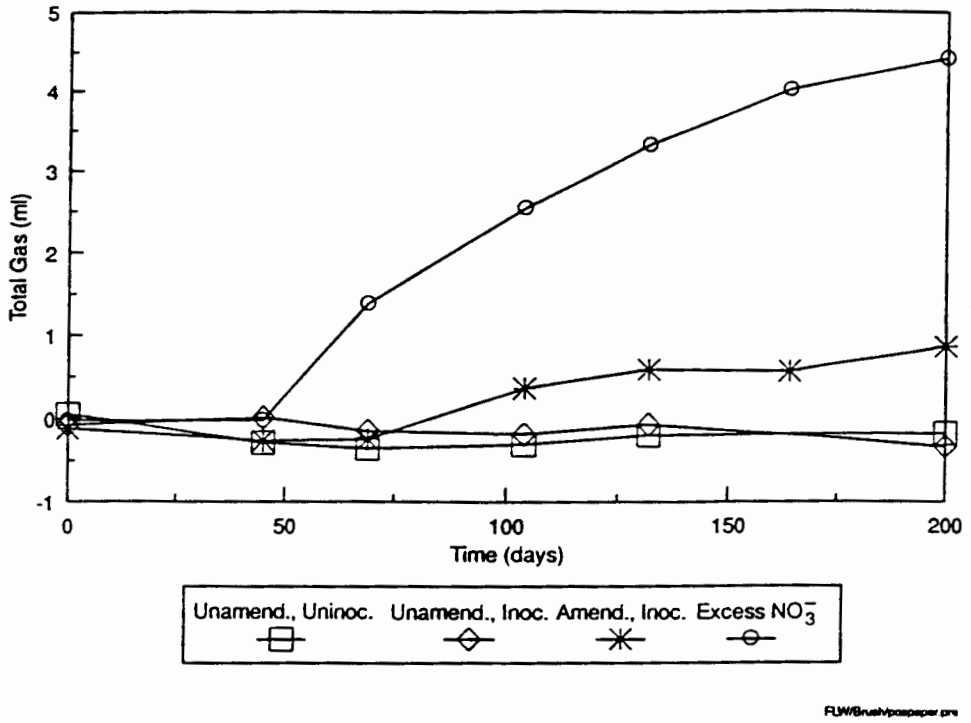

Figure B-5. Total quantities of gas produced in aerobic microbial experiments with cellulose.

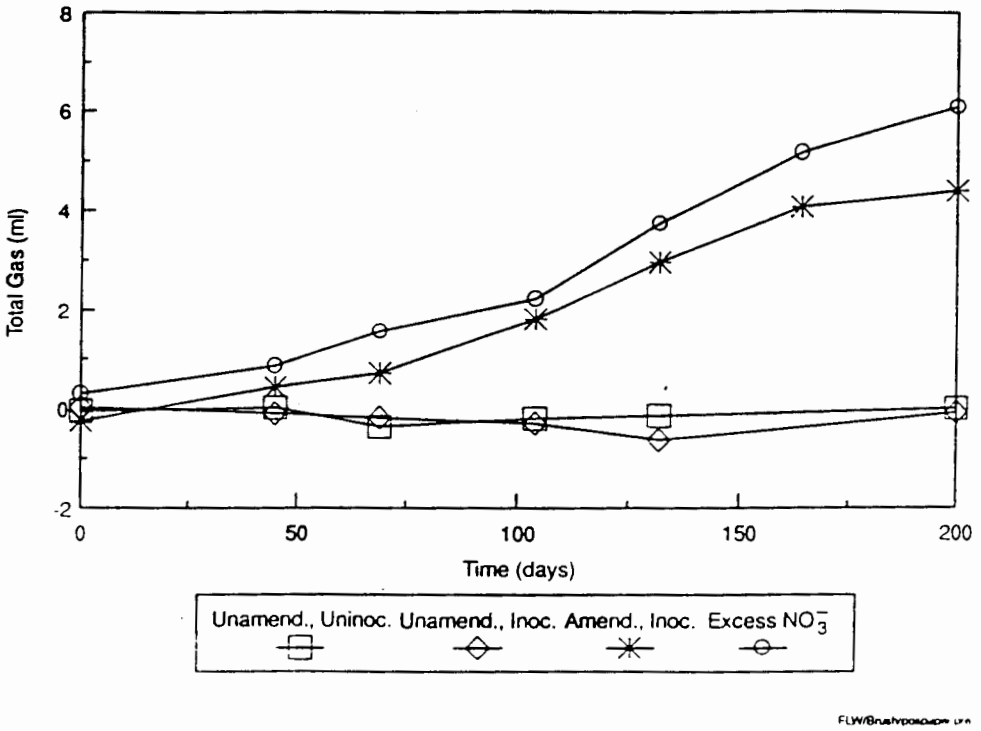

Figure B-6. Total quantities of gas produced in aerobic microbial experiments with cellulose and bentonite.

Therefore, denitrification is a potentially significant respiratory pathway from the standpoint of the gas and H_2O contents of the repository. Because significant denitrification could probably only occur with NO_{3-} from process sludges, it is only potentially significant after container rupture. Furthermore, it is also likely to be carried out by the halophilic or halotolerant microbes.

The overall reactions for microbial denitrification from Berner (1980) and Brush (1990), respectively, are:[1]

$$CH_2O + 0.8NO_{3-} \Rightarrow 0.6H_2O + 0.8OH^- + 1.0CO_2 + 0.4N_2;^1 \qquad \text{(B.8a)}$$

$$CH_2O + 0.46H^+ + 0.46NO_{3-} \Rightarrow 0.076C_5H_7O_2N + 0.96H_2O + 0.624CO_2 + 0.192N_2. \qquad \text{(B.8b)}$$

Incomplete reduction of NO_{3-} could result in the formation of N_2O along with or instead of N_2.

After the depletion of all available NO_{3-}, some microorganisms consume Mn(IV) oxides and hydroxides as electron acceptors (Lovley and Phillips, 1988). Because significant quantities of Mn(IV) oxides and hydroxides will not be present in WIPP disposal rooms or the surrounding Salado Formation (see B.2.1.6), Mn(IV) reduction will not have a significant, direct effect on the gas or H_2O content of the repository.

Subsequent to the depletion of any Mn(IV) oxides and hydroxides, some microorganisms consume Fe(III) oxides and hydroxides as electron acceptors (Lovley and Phillips, 1986 and 1988). Significant quantities of Fe(III) oxides and hydroxides will not be present in Salado-Formation brines or minerals (see B.2.1.6). Furthermore, the quantity of O_2 present in the air trapped in WIPP disposal rooms at the time they are filled and sealed will only be sufficient to oxidize about 0.4 to 1.1% of the drums in a room to Fe(III) oxides or hydroxides (see B.1.1). Moreover, radiolysis of H_2O in the waste and brine will probably not produce sufficient O_2 thereafter (see B.3.1) to form significant quantities of Fe(III) oxides or hydroxides. Finally, laboratory studies of anoxic corrosion imply that this process will produce Fe(II) hydroxides, carbonates, and sulfides, not Fe(III) oxides and hydroxides (see B.1.2). Therefore, Fe(III) reduction is not a potentially significant respiratory pathway.

---

[1] Reaction B.8a and some of the reactions below are modified slightly from Berner (1980) and Brush (1990) so that all of the microbially produced gas remains in the gaseous phase instead of dissolving to some extent in the aqueous phase. this facilitates comparison of the number of moles of gas produced per mole of organic C consumed by these reactions.

After the depletion of any Fe(III) oxides and hydroxides, obligately anaerobic microorganisms consume SO_4^{2-} as the electron acceptor and produce CO_2 and H_2S. Significant quantities of SO_4^{2-} will be present in WIPP disposal rooms and/or the surrounding Salado Formation (see B.2.1.6). Therefore, SO_4^{2-} reduction is a potentially significant respiratory pathway. Because significant SO_4^{2-} reduction could probably only occur with SO_4^{2-} from brine or process sludges, it is only potentially significant after container rupture and is likely to be conducted by the halophilic or halotolerant microbes.

The overall equations for microbial SO_4^{2-} reduction from Berner (1980) and Brush (1990) are:

$$CH_2O + 0.5SO_4^{2-} \Rightarrow OH^- + CO_2 + 0.5H_2S; \qquad \text{(B.9a)}$$

$$CH_2O + 0.58H^+ + 0.04NO_3^- + 0.34SO_4^{2-} \Rightarrow$$

$$0.04C_5H_7O_2N + 0.88H_2O + 0.18HS^- + 0.18H_2S + 0.4CO_2. \qquad \text{(B.9b)}$$

Fermentative microorganisms convert various substrates to acetic acid and other metabolic byproducts. Acetic acid could also be present in the waste. Methanogenic microbes then convert acetic acid to CH_4 and CO_2. Methanogens can also convert CO_2 and H_2 to CH_4 and H_2O. Because methanogenesis could occur without NO_3^- or SO_4^{2-} from process sludges or brine, it is the only potentially significant respiratory pathway prior to container rupture. Furthermore, it is also the only potentially significant process that could be carried out by the nonhalophilic or nonhalotolerant microbes present in the waste prior to emplacement. Of course, any microbial activity that occurs in unbreached containers would necessarily have to occur under humid conditions. Methanogenesis is also a potentially significant respiratory pathway under humid or inundated, saline conditions after container rupture, especially as NO_3^- and SO_4^{2-} are depleted.

The overall equations for microbial methanogenesis from Berner (1980) and Brush (1990) are:

$$2CH_2O \Rightarrow CH_4 + CO_2; \qquad \text{(B.10a)}$$

$$CH_2O + 0.04H^+ + 0.04NO_3^- \Rightarrow$$

$$0.04C_5H_7O_2N + 0.16H_2O + 0.36CH_4 + 0.44CO_2. \qquad \text{(B.10b)}$$

These reactions could produce significant quantities of gas. Another possible methanogenic reaction is:

$$CO_2 + 4H_2 \Rightarrow CH_4 + 2H_2O. \qquad \text{(B.10c)}$$

If both CO_2 (from denitrification, $SO_{4^{2-}}$ reduction, or fermentation) and H_2 (from anoxic corrosion or fermentation) are present, this reaction could consume significant quantities of gas. Clearly, Reactions B.10a, B.10b, and B.10c would have significantly different effects on the gas and H_2O contents of the repository.

Francis and Gillow (1994) carried out long-term, inundated, anaerobic experiments identical to the long-term, inundated, aerobic runs described above (see B.2.3), except that they started the anaerobic runs in a glove box containing O_2-free N_2, and used initially O_2-free N_2 as the gaseous phase in these runs (see Figures B-7 and B-8). After 200 days, the total gas-generation rates in their bentonite-free experiments were -0.004 ml per g of cellulosics per day under uninoculated, unamended conditions, 0.003 ml per g of cellulosics per day under inoculated, unamended conditions, 0.021 ml per g of cellulosics per day under inoculated, amended (nutrients only) conditions, and 0.039 ml per g of cellulosics per day under inoculated, amended (nutrients and NO_{3^-}) conditions. The 200-day, total gas-generation rates with bentonite present were -0.003 ml per g of cellulosics per day under uninoculated, unamended conditions, 0.007 ml per g of cellulosics per day under inoculated, unamended conditions, 0.013 ml per g of cellulosics per day under inoculated, amended (nutrients only) conditions, and 0.025 ml per g of cellulosics per day under inoculated, amended (nutrients and NO_{3^-}) conditions.

B.2.4.1 EFFECTS OF ANAEROBIC MICROBIAL ACTIVITY ON THE WATER CONTENT OF WIPP DISPOSAL ROOMS

It is unclear how anaerobic microbial consumption of cellulosics will affect the H_2O content of WIPP disposal rooms. Reactions B.8a through B.10b imply that microbial consumption of simple sugars will produce H_2O in most cases (see B.2.4), but hydrolysis of cellulosics will consume H_2O prior to the start of these reactions. Therefore, the net effect of microbial activity on the H_2O content of the repository is unclear. For the reaction-path gas-generation model (see C.3), Brush et al. (1994) used $C_6H_{10}O_5$, a simplified formula for cellulosics, to represent the substrate in Reactions C.12 through C.20. These equations suggest that, even after inclusion of hydrolysis, anaerobic microbial activity will produce H_2O. However, laboratory studies under expected WIPP conditions have not confirmed this yet.

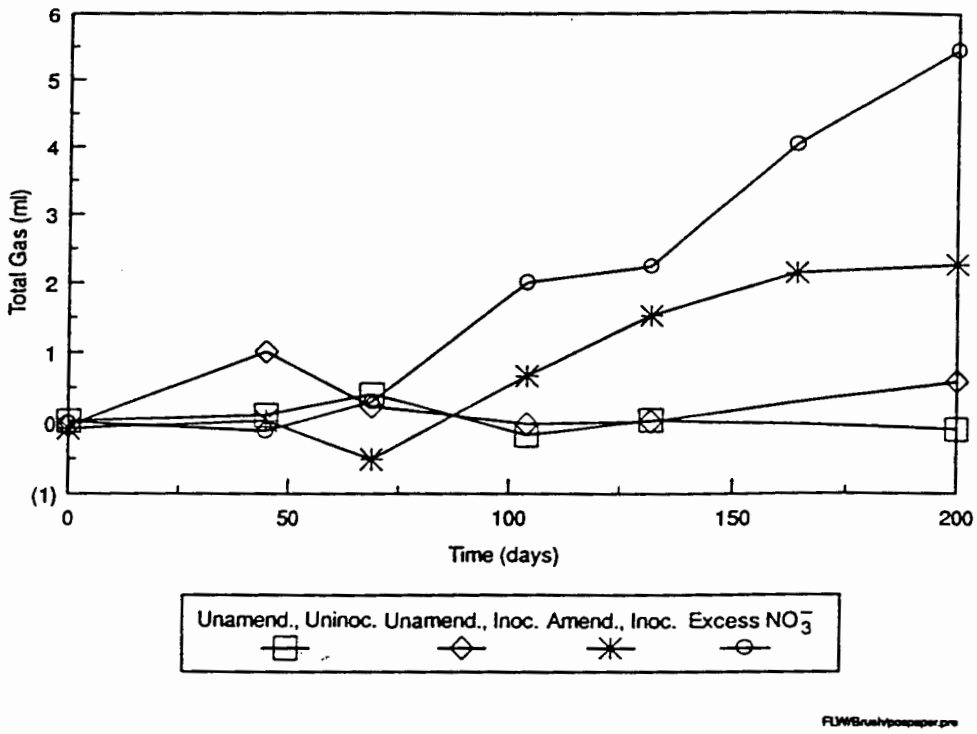

Figure B-7. Total quantities of gas produced in anaerobic microbial experiments with cellulose.

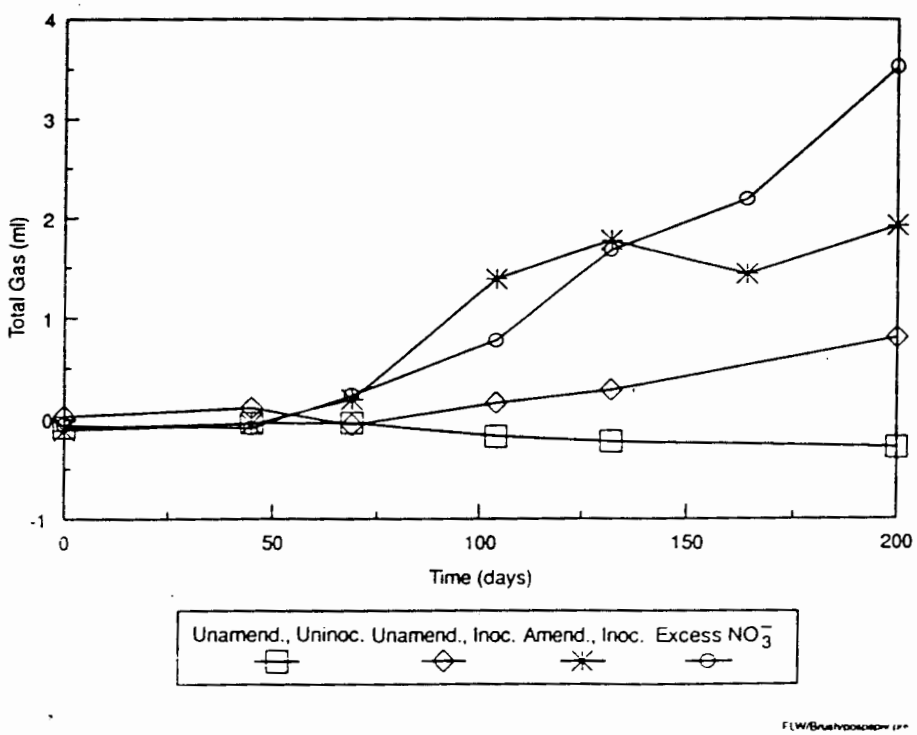

Figure B-8. Total quantities of gas produced in anaerobic microbial experiments with cellulose and bentonite.

It is also unclear how microbial consumption of plastics and rubbers will affect the H_2O content of the repository.

Quantification of the effects of anaerobic microbial activity on the H_2O content of the repository is essential to predict the extent of gas production from anoxic corrosion (see 1.3.1 and B.1.2) and brine radiolysis (see 1.3.3 and B.3.1), both of which require H_2O, and the quantity of brine available for the transport of radioactive waste constituents and other contaminants subject to aqueous-phase transport (see 1.1).

B.3 Radiolysis

Radiolysis of H_2O in the waste and brine in WIPP disposal rooms will consume H_2O and produce H_2 and O_2 or other oxidizing O-bearing species. Radiolysis of cellulosics, plastics and rubbers in the waste and, in the case of plastics, the container liners, will produce a variety of gases.

B.3.1 Radiolysis of Water in the Waste and Brine

D. T. Reed and his colleagues at Argonne National Laboratory have carried out laboratory studies of radiolysis for the WIPP Project since May 1989. Reed et al. (1993) reported the results of studies of the effects of dissolved ^{239}Pu concentration and brine composition on α radiolysis of WIPP brines. They conducted their study of the effects of dissolved ^{239}Pu concentration on brine radiolysis in 0.5 and 1.0 L glass flasks embedded in epoxy for additional strength. They used synthetic Brine A (see Table B-1 and Molecke, 1983) with dissolved ^{239}Pu concentrations of about $1 \cdot 10^{-8}$, $1 \cdot 10^{-6}$, and $1 \cdot 10^{-4}$ M for this study. Brine A is similar in composition to intergranular brines from the Salado Formation at or near the stratigraphic horizon of the WIPP underground workings (Stein and Krumhansl, 1986 and 1988; Deal et al., 1989a and 1989b; Brush, 1990; Deal et al., 1991a and 1991b). Reed et al. (1993) prepared $^{239}Pu(VI)$ stock solutions by evaporating about 50 mg of ^{239}Pu in a solution of $HClO_4$ to near dryness, dissolving the residues in triply distilled H_2O, analyzing for oxidation-state purity by ultraviolet-and-visible-absorption (UV-VIS) spectroscopy, and adjusting the pH to a nearly neutral value by adding NaOH. They then carried out serial dilutions of these stock solutions with Brine A to obtain 0.5 or 1.0 L of brine with the desired initial dissolved ^{239}Pu concentration. After allowing the solutions to equilibrate for three days, they analyzed them by α-scintillation counting and UV-VIS spectroscopy, and reported initial dissolved $^{239}Pu(VI)$ concentrations of $6.7 \cdot 10^{-9}$, $7.1 \cdot 10^{-9}$, $5.4 \cdot 10^{-7}$, $6.3 \cdot 10^{-7}$, $2.8 \cdot 10^{-4}$ and $3.4 \cdot 10^{-4}$ M.

Reed et al. (1993) conducted these duplicate runs at 31 ± 2°C for 155 or 162 days. They periodically sampled and analyzed the 6 to 61 ml headspaces for CO_2, H_2, N_2, and O_2 and used a pressure transducer to monitor the flasks with an initial dissolved Pu concentration of about $1 \cdot 10^{-4}$ M. They also analyzed a 3-ml sample of each brine periodically by UV-VIS spectroscopy to determine the oxidation state of the dissolved ^{239}Pu as a function of time.

Reed et al. (1993) reported that the dissolved ^{239}Pu concentrations did not change significantly during these experiments, except for the run with an initial dissolved ^{239}Pu concentration of $3.4 \cdot 10^{-4}$ M. Posttest analysis of the solution from this run implied that most of the ^{239}Pu precipitated during this run, probably because a crack in this flask allowed the Pu to react with the organic resin in the epoxy surrounding the flask. During these experiments, radiolysis of H_2O in Brine A produced H_2, but not O_2. This result is not surprising in view of the fact that O_2 is not a direct product of the radiolytic decomposition of H_2O. Instead, O_2 forms by the breakdown of O-bearing intermediate species, such as H_2O_2 in pure H_2O and, perhaps, ClO_{3-} or ClO_{4-} in brines. Given sufficiently high absorbed doses, the O_2-production rate would probably approach 50% that of H_2 in both pure H_2O and brines eventually. Therefore, the overall reaction for radiolysis of H_2O in the waste and brine in WIPP disposal rooms will be:

$$2H_2O \Leftrightarrow 2H_2 + O_2. \qquad \text{(B.11)}$$

It is also possible that these intermediate species will react with electron donors (reductants) such as steels, other Fe-base alloys, other metals, or organic matter before they produce O_2. Based on headspace H_2 analyses, Reed et al. (1993) reported $G(H_2)$ values of 1.3 and 1.4 molecules per 100 eV for the experiments with a dissolved ^{239}Pu concentration of about $1 \cdot 10^{-6}$ M and ≥ 0.8 and 1.1 molecules per 100 eV for the runs with a dissolved ^{239}Pu concentration of $1 \cdot 10^{-4}$ M. They could not determine $G(H_2)$ values for the experiments with a dissolved ^{239}Pu concentration of $1 \cdot 10^{-8}$ M because, the quantities of H_2 produced in these runs were too small.

Reed et al. (1993) carried out their study of the effects of brine composition on radiolysis identically to the study of the effects of dissolved Pu (see above), except that they used two brines collected from the WIPP underground workings, DH-36 and G Seep (see Table B-1 and Deal et al., 1989a, 1989b, 1991a, and 1991b) and synthetic ERDA-6 (see Table B-1 and Popielak et al., 1983). The brines from DH-36 and G Seep typify intergranular brines from the Salado Formation at or near the stratigraphic horizon of the WIPP underground workings; ERDA-6 brine simulates fluids that occur in isolated but occasionally large (on the order of 10^5 m^3) brine reservoirs in the underlying Castile Formation. The intended initial Pu(VI) concentration in these runs was about $1 \cdot 10^{-4}$ M; the actual values were $9.9 \cdot 10^{-5}$ to $1.9 \cdot 10^{-4}$ M. They conducted these runs for 182 days.

Reed et al. (1993) reported that the dissolved ^{239}Pu concentrations decreased by about 40 to 60% in some of these experiments. For example, it decreased from $1.1 \cdot 10^{-4}$ to $4.4 \cdot 10^{-5}$ M and from $1.4 \cdot 10^{-4}$ to $5.7 \cdot 10^{-5}$ M in the runs with brine from DH-36, from $1.4 \cdot 10^{-4}$ to $7.0 \cdot 10^{-5}$ M in one of the runs with brine from G Seep, and from $1.9 \cdot 10^{-4}$ to $1.1 \cdot 10^{-4}$ M in one of the runs with ERDA-6 brine. These decreases probably reflect precipitation of polymeric Pu during these runs, or adsorption of polymeric Pu by the flasks. They also observed H_2 production, but not O_2 production, during these experiments. Reed et al. (1993) reported $G(H_2)$ values of 0.8 to 1.5 molecules per 100 eV for the runs with brine from DH-36, but preferred the initial $G(H_2)$ values of 1.3 and 1.5 molecules per 100 eV. They reported $G(H_2)$ values of 0.7 to 1.5 molecules per 100 eV for the runs with brine from G Seep, but preferred the initial $G(H_2)$ values of 1.3 and 1.5 molecules per 100 eV. For the runs with ERDA-6 brine, they reported $G(H_2)$ values of 0.2 to 0.7 molecules per 100 eV, but favored their initial $G(H_2)$ values of 0.6 and 0.9 molecules per 100 eV. (The latter initial value is outside the range of final values because Pu precipitated during one of the runs with ERDA-6 brine.) ERDA-6 brine is the only one for which the $G(H_2)$ values are significantly less than those of the other brines. Reed et al. (1993) speculated that this might be because the Mg concentration of ERDA-6 brine is significantly less than those of the other brines.

Brush (see E) concluded that brine radiolysis will not produce gas at rates comparable to those expected for anoxic corrosion and microbial activity. He based this conclusion on calculations using the results of Reed et al. (1993) (see above), estimates of the quantities of brine that will enter WIPP disposal rooms after filling and sealing, and estimates of the concentrations of Pu, Am, Np, U, and Th in these brines from Trauth et al. (1992). (Laboratory and modeling studies of the chemical behavior of Pu, Am, Np, U, and Th under expected WIPP conditions are currently under way to replace the estimates of Trauth et al. (1992) with actual data.)

Reed et al. (1993) pointed out that the $G(H_2)$ values they observed with WIPP brines are only slightly lower than those reported for pure H_2O, about 1.6 molecules per 100 eV. Therefore, the conclusion that brine radiolysis will not produce gas at rates comparable to those expected for anoxic corrosion and microbial activity also applies to radiolysis of H_2O in the waste.

B.3.2 Radiolysis of Cellulosics, Plastics and Rubbers

The data summarized by Molecke (1979) imply that radiolysis of cellulosics, plastics, and rubbers would not be a significant, long-term gas-generation process in WIPP disposal rooms.

B.4 Processes that Consume Gas

$Ca(OH)_2$ (in hydrated cementitious materials) and CaO (a proposed backfill material) will consume CO_2. Brush (1990) described these reactions in detail.

Dissolution of gases (especially CO_2 and H_2S) in brine will also remove gas from WIPP disposal rooms. Cygan (1991) reviewed studies of dissolution of various gases in NaCl-bearing aqueous solutions. Because the solubilities of gases in these solutions are low under most conditions, dissolution will not significantly reduce the gas content of the repository unless the volume of brine is large and its pH is basic. Under these conditions, significant quantities of CO_2 or H_2S could dissolve in WIPP brines.

B.5 References

Berner, R.A. 1980. *Early Diagenesis: A Theoretical Approach.* Princeton, NJ: Princeton University Press.

Brush, L.H. 1990. *Test Plan for Laboratory and Modeling Studies of Repository and Radionuclide Chemistry for the Waste Isolation Pilot Plant.* SAND90-0266. Albuquerque, NM: Sandia National Laboratories.

Brush, L.H., and D.R. Anderson. 1989. "Potential Effects of Chemical Reactions on WIPP Gas and Water Budgets," *Systems Analysis, Long-Term Radionuclide Transport, and Dose Assessments, Waste Isolation Pilot Plant (WIPP), Southeastern New Mexico; March 1989.* Eds. A.R. Lappin, R.L. Hunter, D.P. Garber and P.B. Davies. SAND89-0462. Albuquerque, NM: Sandia National Laboratories. A-3 through A-30.

Brush, L.H., J.W. Garner, and L.J. Storz. 1994. "Development of a Gas Generation Model for the Waste Isolation Pilot Plant," *Scientific Basis for Nuclear Waste Management XVII, Materials Research Society Symposium Proceedings, Boston, MA, November 29-December 3, 1993.* Eds. A. Barkatt and R.A. Van Konynenburg. SAND93-1145C. Pittsburgh, PA: Materials Research Society. Vol. 333, 241-246.

Cygan, R.T. 1991. *The Solubility of Gases in NaCl Brine and a Critical Evaluation of Available Data.* SAND90-2848. Albuquerque, NM: Sandia National Laboratories.

Deal, D.E., and J.B. Case. 1987. *Brine Sampling and Evaluation Program Phase I Report.* DOE-WIPP-87-008. Carlsbad, NM: U.S. Department of Energy Waste Isolation Pilot Plant.

Deal, D.E., J.B. Case, R.M. Deshler, P.E. Drez, J. Myers, and J.R. Tyburski. 1989a. *Brine Sampling and Evaluation Program Phase II Report.* DOE-WIPP-87-010. Carlsbad, NM: U.S. Department of Energy Waste Isolation Pilot Plant.

Deal, D.E., R.J. Abitz, D.S. Belski, J.B. Case, M.E. Crawley, R.M. Deshler, P.E. Drez, C.A. Givens, R.B. King, B.A. Lauctes, J. Myers, S. Niou, J.M. Pietz, W.M. Roggenthen, J.R. Tyburski, and M.G. Wallace. 1989b. *Brine Sampling and Evaluation Program 1988 Report.* DOE-WIPP 89-015. Carlsbad, NM: U.S. Department of Energy Waste Isolation Pilot Plant.

Deal, D.E., R.J. Abitz, D.S. Belski, J.B. Clark, M.E. Crawley, and M.L. Martin. 1991a. *Brine Sampling and Evaluation Program 1989 Report.* DOE-WIPP 91-009. Carlsbad, NM: U.S. Department of Energy Waste Isolation Pilot Plant.

Deal, D.E., R.J. Abitz, J. Myers, J.B. Case, D.S. Belski, M.L. Martin, and W.M. Roggenthen. 1991b. *Brine Sampling and Evaluation Program 1990 Report.* DOE-WIPP 91-036. Carlsbad, NM: U.S. Department of Energy Waste Isolation Pilot Plant.

DOE Subsurface Science Program's Taylorsville Working Group (D. Balkwill, D.R. Boone, F.S. Colwell, T. Griffin, T.L. Kieft, R.M. Lehman, J.P. McKinley, S. Nierzwicki-Bauer, T.C. Onstott, H.-Y. Tseng, G. Gao, T.J. Phelps, D. Ringelberg, B. Russell. T. Stevens, D.C. White, and F.J. Wobber). 1994. "D.O.E. Seeks Origin of Deep Subsurface Bacteria," *EOS, Transactions, American Geophysical Union.* Vol. 75, no. 34, 385-396.

Francis, A.J., and J.B. Gillow. 1994. *Effects of Microbial Processes on Gas Generation Under Expected Waste Isolation Pilot Plant Repository Conditions.* SAND93-7036. Albuquerque, NM: Sandia National Laboratories.

Froelich, P.N., G.P. Klinkhammer, M.L. Bender, N.A. Luedtke, G.R. Heath, D. Cullen, P. Dauphin, D. Hammond, B. Hartman, and V. Maynard. 1979. "Early Oxidation of Organic Matter in Pelagic Sediments of the Eastern Equatorial Atlantic: Suboxic Diagenesis," *Geochimica et Cosmochimica Acta.* Vol. 43, no. 7, 1075-1090.

Lovley, D.R., and E.J.P. Phillips. 1986. "Organic Matter Mineralization with Reduction of Ferric Iron in Anaerobic Sediments," *Applied and Environmental Microbiology.* Vol. 51, no. 4, 683-689.

Lovley, D.R., and E.J.P. Phillips. 1988. "Novel Mode of Microbial Energy Metabolism: Organic Carbon Oxidation Coupled to Dissimilatory Reduction of Iron or Manganese," *Applied and Environmental Microbiology.* Vol. 54, no. 6, 1472-1480.

Molecke, M.A. 1979. *Gas Generation from Transuranic Waste Degradation: Data Summary and Interpretation.* SAND79-1245. Albuquerque, NM: Sandia National Laboratories.

Molecke, M.A. 1983. *A Comparison of Brines Relevant to Nuclear Waste Experimentation.* SAND83-0516. Albuquerque, NM: Sandia National Laboratories.

Popielak, R.S., R.L. Beauheim, S.R. Black, W.E. Coons, C.T. Ellingson, and R.L. Olsen 1983. *Brine Reservoirs in the Castile Formation, Waste Isolation Pilot Plant Project, Southeastern New Mexico.* TME 3153. Carlsbad, NM: U.S. Department of Energy WIPP Project Office.

Reed, D.T., S. Okajima, L.H. Brush, and M.A. Molecke. 1993. "Radiolytically-Induced Gas Production in Plutonium-Spiked WIPP Brine," *Scientific Basis for Nuclear Waste Management XVI, Materials Research Society Symposium Proceedings, Boston, MA, November 30-December 4, 1992.* Eds. C.G. Interrante, and R.T. Pabalan. SAND92-7283C. Pittsburgh, PA: Materials Research Society. Vol. 294, 431-438.

Simpson, J.P., and R. Schenk. 1989. "Corrosion Induced Hydrogen Evolution on High Level Waste Overpack Materials in Synthetic Groundwaters and Chloride Solutions," *Scientific Basis for Nuclear Waste Management XII, Materials Research Society Symposium Proceedings, Berlin, Germany, October 10-13, 1988.* Eds. W. Lutze and R.C. Ewing. Pittsburgh, PA: Materials Research Society. Vol. 127, 389-396.

Stein, C.L. 1985. *Mineralogy in the Waste Isolation Pilot Plant (WIPP) Facility Stratigraphic Horizon*. SAND85-0321. Albuquerque, NM: Sandia National Laboratories.

Stein, C.L., and J.L. Krumhansl. 1986. *Chemistry of Brines in Salt from the Waste Isolation Pilot Plant (WIPP), Southeastern New Mexico: A Preliminary Investigation*. SAND85-0897. Albuquerque, NM: Sandia National Laboratories.

Stein, C.L., and J.L. Krumhansl. 1988. "A Model for the Evolution of Brines in Salt from the Lower Salado Formation, Southeastern New Mexico," *Geochimica et Cosmochimica Acta*. Vol. 52, 1037-1046.

Telander, M.R., and R.E. Westerman. 1993. *Hydrogen Generation by Metal Corrosion in Simulated Waste Isolation Pilot Plant Environments*. SAND92-7347. Albuquerque, NM: Sandia National Laboratories.

Trauth, K.M., S.C. Hora, R.P. Rechard, and D.R. Anderson. 1992. *The Use of Expert Judgment to Quantify Uncertainty in Solubility and Sorption Parameters for Waste Isolation Pilot Plant Performance Assessment*. SAND92-0479. Albuquerque, NM: Sandia National Laboratories.

U.S. Department of Energy Carlsbad Area Office. 1994. *Waste Isolation Pilot Plant Transuranic Waste Baseline Inventory Report, Books 1 and 2*. CAO-94-1005, Rev. 0. Washington, DC: U.S. Department of Energy.

Westerman, R.E., J.H. Haberman, S.G. Pitman, K.H. Pool, K.C. Rhoads, and M.R. Telander. 1987. *Corrosion Behavior of A216 Grade WCA Mild Steel and Ti Grade 12 Alloy in Hydrothermal Brines, Salt Repository Project: Annual Report FY 1986*. PNL-SRP-6221. Richland, WA: Pacific Northwest Laboratory.

APPENDIX C: REVIEW OF WIPP GAS-GENERATION MODELS

CONTENTS OF APPENDIX C

C.1 The Rates-and-Potentials Model C-3
C.2 The Average-Stoichiometry Model C-4
C.3 The Reaction-Path Model C-7
C.4 References C-11

APPENDIX C: REVIEW OF WIPP GAS-GENERATION MODELS

This section describes three gas-generation models used or developed by the Waste Isolation Pilot Plant (WIPP) Project to date: (1) the rates-and-potentials model, used by Lappin et al. (1989) for systems analysis; (2) the average-stoichiometry model, currently incorporated in the multi-phase flow code Brine and Gas Flow (BRAGFLO) and used by WIPP Performance Assessment Division (1991) and Sandia WIPP Project (1992) for the 1991 and 1992 performance assessment (PA) calculations, respectively; (3) the reaction-path model of Brush et al. (1994), currently under development for eventual incorporation in BRAGFLO.

C.1 The Rates-and-Potentials Model

The rates-and-potentials model of Lappin et al. (1989) included two processes: (1) anoxic corrosion of steels and other Fe-base alloys; (2) microbial degradation of cellulosics and rubbers. Although Lappin et al. (1989) realized that radiolysis of H_2O in the waste and brine will produce H_2 and O_2 or other oxidizing, O-bearing species, and consume H_2O (see 1.3.3 and B.3.1), and that radiolysis of cellulosics, plastics, and rubbers in the waste and, in the case of plastics, the container liners, will produce a variety of gases, they assumed that this process would be unimportant relative to anoxic corrosion and microbial activity. They based this assumption on the data summarized by Molecke (1979), which showed that, in general, radiolysis of transuranic (TRU) waste produced gas at rates significantly lower than corrosion and microbial activity. The rates-and-potentials model also did not include interactions between anoxic corrosion and microbial activity, such as passivation of steels and other Fe-base alloys by microbially produced CO_2 or H_2S.

For their model, Lappin et al. (1989) simply estimated gas-production rates and potentials for anoxic corrosion and microbial activity, and divided the potentials by the rates to calculate gas production in WIPP disposal rooms. They did not specify which corrosion or microbial reactions would occur, only that these processes would occur and produce gas. Although they realized that anoxic corrosion will produce H_2 and that microbial activity will produce CO_2, CH_4, H_2, H_2S, and N_2, they did not predict the composition of the gaseous phase because of uncertainties as to which microbial respiratory pathways will occur in the repository.

Lappin et al. (1989) estimated an H_2-production rate of 1.70 moles per drum of waste per year for anoxic corrosion of steels and other Fe-base alloys. Laboratory studies of anoxic corrosion at Pacific Northwest Laboratory (PNL) had not yet yielded any H_2-production or

corrosion rates. Therefore, they based this estimate on a previous study for the WIPP Project (Molecke, 1979) and a more recent study for the Salt Repository Project for commercial spent fuel and high level waste (Haberman and Frydrych, 1988). Based on estimates by Brush and Anderson (1989) and Drez (1989) of the numbers of steel, contact-handled (CH) TRU waste containers (drums and boxes) to be emplaced in WIPP disposal rooms, the quantities of steel in these containers, and the quantity of Fe-base alloys in CH TRU waste, Lappin et al. (1989) estimated an H_2-production potential of 894 moles per drum. These estimates of the H_2-production rate and potential did not include the steels or other Fe-base alloys used for remote-handled (RH) TRU waste canisters and plugs or the Fe-base alloys contained in RH TRU waste. Although Lappin et al. (1989) realized that corrosion would consume significant quantities of H_2O, they assumed that sufficient brine would be present to produce 894 moles of H_2 per drum. Furthermore, laboratory studies at PNL had not yet demonstrated that CO_2 and H_2S, if present in sufficient quantities, passivate steels, or that anoxic corrosion and H_2 production do not occur under humid conditions. Therefore, they calculated that corrosion will produce H_2 at a constant rate of 1.70 moles per drum per year for 526 years.[1]

Lappin et al. (1989) estimated a microbial gas-production rate of 0.85 moles per drum per year for their model. Because laboratory studies of microbial activity had not yielded any gas-production rates since they were restarted by the WIPP Project in 1989, Lappin et al. (1989) used the arithmetic mean of the range of "the most probable overall average" gas-production rate from Molecke (1979) for this estimate. For their estimate of the microbial gas-production potential, Lappin et al. (1989) used the same assumptions made by M. A. Molecke for Sandia Laboratories (1979) and estimates by Drez (1989) of the quantities of cellulosics and rubbers in CH TRU waste to calculate a value of 606 moles of various gases per drum.[2] The most important of these assumptions was that microorganisms would consume all of the cellulosics and half of the rubbers, but none of the plastics in CH TRU waste. The other assumptions concerned the yields of various gases expected from microbial degradation of cellulosics and rubbers. Lappin et al. (1989) did not know whether microbial activity would produce or consume H_2O but they believed, based on data summarized by Molecke (1979), that microbial gas production was likely even under humid conditions. Therefore, they calculated that microbial activity will produce gas at a constant rate of 0.85 mole per drum per year for 713 years.

---

1 Lappin et al. (1989) did not believe that the use of three significant figures for these predictions was defensible. However, they reported them to three significant figures to facilitate verification of their calculations.

2 Because Sandia Laboratories (1979) did not describe the assumptions used for its estimate of the microbial gas-production potential, Lappin et al. (1989) described them based on information provided by M. A. Molecke.

corrosion rates. Therefore, they based this estimate on a previous study for the WIPP Project (Molecke, 1979) and a more recent study for the Salt Repository Project for commercial spent fuel and high level waste (Haberman and Frydrych, 1988). Based on estimates by Brush and Anderson (1989) and Drez (1989) of the numbers of steel, contact-handled (CH) TRU waste containers (drums and boxes) to be emplaced in WIPP disposal rooms, the quantities of steel in these containers, and the quantity of Fe-base alloys in CH TRU waste, Lappin et al. (1989) estimated an H_2-production potential of 894 moles per drum. These estimates of the H_2-production rate and potential did not include the steels or other Fe-base alloys used for remote-handled (RH) TRU waste canisters and plugs or the Fe-base alloys contained in RH TRU waste. Although Lappin et al. (1989) realized that corrosion would consume significant quantities of H_2O, they assumed that sufficient brine would be present to produce 894 moles of H_2 per drum. Furthermore, laboratory studies at PNL had not yet demonstrated that CO_2 and H_2S, if present in sufficient quantities, passivate steels, or that anoxic corrosion and H_2 production do not occur under humid conditions. Therefore, they calculated that corrosion will produce H_2 at a constant rate of 1.70 moles per drum per year for 526 years.[1]

Lappin et al. (1989) estimated a microbial gas-production rate of 0.85 moles per drum per year for their model. Because laboratory studies of microbial activity had not yielded any gas-production rates since they were restarted by the WIPP Project in 1989, Lappin et al. (1989) used the arithmetic mean of the range of "the most probable overall average" gas-production rate from Molecke (1979) for this estimate. For their estimate of the microbial gas-production potential, Lappin et al. (1989) used the same assumptions made by M. A. Molecke for Sandia Laboratories (1979) and estimates by Drez (1989) of the quantities of cellulosics and rubbers in CH TRU waste to calculate a value of 606 moles of various gases per drum.[2] The most important of these assumptions was that microorganisms would consume all of the cellulosics and half of the rubbers, but none of the plastics in CH TRU waste. The other assumptions concerned the yields of various gases expected from microbial degradation of cellulosics and rubbers. Lappin et al. (1989) did not know whether microbial activity would produce or consume H_2O but they believed, based on data summarized by Molecke (1979), that microbial gas production was likely even under humid conditions. Therefore, they calculated that microbial activity will produce gas at a constant rate of 0.85 mole per drum per year for 713 years.

---

1 Lappin et al. (1989) did not believe that the use of three significant figures for these predictions was defensible. However, they reported them to three significant figures to facilitate verification of their calculations.

2 Because Sandia Laboratories (1979) did not describe the assumptions used for its estimate of the microbial gas-production potential, Lappin et al. (1989) described them based on information provided by M. A. Molecke.

Based on the estimates described above, Lappin et al. (1989) calculated that anoxic corrosion and microbial activity would produce various gases at a combined rate of 2.55 moles per drum per year for 526 years after filling and sealing WIPP disposal rooms. Because laboratory studies at PNL had not yet revealed that CO_2 and H_2S passivate steels, they did not include this process during the 526-year period during which corrosion and microbial activity will produce gas simultaneously. From 526 to 713 years, microbial activity will produce gases at a rate of 0.85 moles per drum per year.

C.2 The Average-Stoichiometry Model

The average-stoichiometry model (WIPP Performance Assessment Division, 1991; Sandia WIPP Project, 1992) includes: (1) anoxic corrosion of steels and other Fe-base alloys; and (2) microbial degradation of cellulosics and rubbers. This model is similar to the rates-and-potentials model of Lappin et al. (1989) in that it does not include radiolysis or interactions between anoxic corrosion and microbial activity. Because the average-stoichiometry model is incorporated in BRAGFLO, gas production is coupled with brine and gas inflow and outflow. Moreover, because BRAGFLO uses a porosity surface to simulate room closure (Butcher and Mendenhall, 1993), it also couples gas production to room closure. In this position paper, "average-stoichiometry model" refers to a component of BRAGFLO, not a stand-alone gas-production model.

Perhaps the most significant difference between the rates-and-potentials model and the average-stoichiometry model is that the latter does not use gas-production potentials as input parameters. Instead, the average-stoichiometry model produces gas by corrosion or microbial activity until a reactant is consumed. Because BRAGFLO couples gas production with brine inflow and outflow, anoxic corrosion can consume all available H_2O prior to attaining its full gas-production potential. Thus, availability of H_2O, not steels and other Fe-base alloys, may limit anoxic corrosion and H_2 production. Therefore, other input parameters, not predetermined gas-production potentials, determine how much gas is produced in a given calculation. Input parameters that affect gas-production calculations by the average stoichiometry model include, in addition to gas-production rates, the initial quantities of steels and other Fe-base alloys, cellulosics, and H_2O in the waste, and the calculated quantity of brine that may seep into WIPP disposal rooms from the surrounding Salado Formation. For the 1991 and 1992 PA calculations, WIPP Performance Assessment Division (1991) and Sandia WIPP Project (1992) used gas-production rates provided by Brush (see D).

The average-stoichiometry model includes a weighted average of two anoxic-corrosion reactions, a simplified form of Reaction B.2 that produces $Fe(OH)_2.xH_2O$ in which x = 0 and Reaction B.3 (see B.1.2). WIPP Performance Assessment Division (1991) defined the average stoichiometry of Reactions B.2 and B.3 as:

$$Fe + ((4 + 2x)/3)H_2O \Leftrightarrow ((4 - x)/3)H_2 + xFe(OH)_2 + ((1 - x)/3)Fe_3O_4. \qquad (C.1)$$

In Reaction C.1, x is the mole fraction of Fe consumed by Reaction B.2. WIPP Performance Assessment Division (1991) and Sandia WIPP Project (1992) sampled the parameter x from a uniform distribution between 0 and 1, hence the name "average-stoichiometry" for this model. The code does not terminate Reaction C.1 at any pre-determined H_2 fugacity (roughly equivalent to the partial pressure). In particular, it does not terminate Reaction C.1 at an H_2 fugacity of 60 or 100 atm, the equilibrium H_2 fugacities for Reaction B.2 calculated by Brush (1990) and Simpson and Schenk (1989), respectively, or at an H_2 fugacity of 400 or 500 atm, the equilibrium H_2 fugacities for Reaction B.3 calculated by Brush (1990) and Simpson and Schenk (1989). Instead, it assumes that Reaction C.1 continues until one or both of the reactants are completely consumed regardless of the H_2 fugacity. Therefore, the average-stoichiometry model ignores the possible implications of whether Reaction B.2 or B.3 is predominant in the absence of CO_2 and H_2S (see B.1.2).

During a calculation, the code uses an effective corrosion rate consisting of a weighted average of the humid and inundated corrosion rates sampled for that calculation. The weighting depends on the quantities of steels and other Fe-base alloys in a waste panel in contact with brine and gas. The code assumes that the steels and other Fe-base alloys in contact with brine corrode and produce H_2 at the inundated rate and that those in contact with gas react at the humid rate. However, the code assumes that at least some brine must be present for corrosion to occur under humid conditions. At the start of each time step, it calculates the volume fractions of steels and other Fe-base alloys in contact with brine and gas from the initial quantities of these materials in a panel and the computed, time-dependent porosity and brine and gas saturation.

WIPP Performance Assessment Division (1991) and Sandia WIPP Project (1992) assumed that the humid and inundated corrosion rates are constant as long as these conditions persist in a given volume of the waste. Thus, they assumed that the sampled corrosion rates are independent of the "concentrations" of steels and other Fe-base alloys in the waste, the surface area of these materials, the total pressure, the composition of the aqueous phase (including pH and salinity), and the composition of the gaseous phase (including the humidity). The effects of some of these factors, such as the "concentration" of corroding metals, pressure, salinity and humidity, could indeed be modest. However, pH, CO_2, and H_2S affect corrosion of steels and

other Fe-base alloys significantly (see B.1.2). Therefore, Brush (see D) attempted to take some of these factors into consideration by estimating ranges for the rates of anoxic corrosion and H_2 production.

Although BRAGFLO does quantify the effects of Reaction C.1 on the H_2O content of WIPP disposal rooms, it does not calculate the reduction in porosity or other geomechanical effects caused by the precipitation of salts accompanying corrosion-induced consumption of H_2O from brine.

The average-stoichiometry model uses a generalized form of an overall reaction for microbial consumption of the potentially significant substrates in TRU waste (cellulosics, plastics, and rubbers) and concomitant gas production (WIPP Performance Assessment Division, 1991):

$$CH_2O + \text{unknowns} + \text{microorganisms} \Rightarrow y\text{gas} + \text{unknowns}. \qquad \text{(C.2)}$$

In Reaction C.2, CH_2O (a simplified formula for glucose) represents potentially significant microbial substrates, and y is a variable (see below). WIPP Performance Assessment Division (1991) and Sandia WIPP Project (1992) assumed that microorganisms could, depending on the rate of Reaction C.2, consume all of the cellulosics, half of the rubbers, and none of the plastics in the repository. WIPP Performance Assessment Division (1991) used Reaction C.2 to represent the microbial reactions of Brush and Anderson (1989), who listed overall reactions for several respiratory pathways that could occur in the repository to determine the range of the ratio of moles of gas produced per mole of organic C consumed. Brush and Anderson (1989) concluded that this ratio could vary from -1 in the case of aerobic respiration with complete consumption of CO_2 by dissolution in basic brine (their Reaction 17) to 5/3 in the case of microbial Fe_3O_4 reduction (their Reaction 20e*). (Brush and Anderson, 1989, used the asterisk in "Reaction 20e*" to distinguish it from "Reaction 20e," a similar but slightly different microbial reaction; the asterisk does not refer to a footnote in this position paper or their memorandum!) Although microbial reduction of Fe(III) oxides and hydroxides occurs in the natural environment, it is unclear whether microbes can use Fe_3O_4 as the electron acceptor. However, Brush and Anderson (1989) chose this reaction to bound the range of the ratio of moles of gas produced per mole of organic C consumed. WIPP Performance Assessment Division (1991) and Sandia WIPP Project (1992) sampled the parameter y in Reaction C.2 from a uniform distribution between 0 and 1. They chose a lower limit of 0 instead of -1 because they assumed that aerobic respiration is unlikely to be significant in the repository, a reasonable assumption in view of the conclusion that aerobic microbial activity would not have a significant, direct effect on the repository gas or H_2O content (see B.2.3). Although that assumption was

reasonable, the range of 0 to 1 neglected Reaction B.10c, which could, if it occurs, consume significant quantities of CO_2 and H_2 (see B.2.4). (Neither Brush and Anderson, 1989, nor Brush, 1990, included Reaction B.10c in their lists of possible microbial reactions.)

The code uses an effective microbial gas-production rate comprising a weighted average of the humid and inundated rates in a manner identical to that for anoxic corrosion. For microbial activity, the weighting depends on the quantities of cellulosics and rubbers in a waste panel in contact with brine and gas. The code assumes that microorganisms consume cellulosics and rubbers in contact with brine at the inundated rate, and that they consume cellulosics and rubbers in contact with gas at the humid rate. The code assumes that at least some brine must be present for microbial activity to occur under humid conditions.

WIPP Performance Assessment Division (1991) and Sandia WIPP Project (1992) assumed that the humid and inundated microbial gas-production rates are constant in those volumes of the waste that remain subject to these conditions. Thus, they assumed that the sampled microbial gas-production rates are independent of the concentrations, types and surface areas of cellulosics and rubbers in the waste, the numbers and types of microorganisms present, the concentrations of nutrients and electron acceptors, pressure, the composition of the aqueous phase, and the composition of the gaseous phase (including the concentrations or partial pressures of byproduct gases such as CO_2, N_2 and H_2S). Although the effects of some of these factors, such as the concentrations of cellulosics and rubbers, pressure, salinity, and humidity could be small, other factors could affect microbial activity significantly. These include the numbers and types of microbes, the concentrations of nutrients and electron acceptors, pH, and the concentrations or partial pressures of byproduct gases (see B.2). Brush (see D) tried to take some of these factors into account by estimating ranges for microbial gas-production rates.

Because it is unclear whether microbial degradation of the potentially significant substrates to be emplaced in the WIPP will result in net production or consumption of H_2O (see B.2.4.1)), WIPP Performance Assessment Division (1991) and Sandia WIPP Project (1992) assumed that microbial activity will have no net effect on the H_2O content of the repository.

C.3 The Reaction-Path Model

The reaction-path model (Brush et al., 1994) includes: (1) oxic and anoxic corrosion of steels and other Fe-base alloys, including passivation by the adherent corrosion products $FeCO_3$ and FeS, and depassivation caused by destabilization of these phases due to changes in the composition of the gaseous phase; (2) microbial degradation of cellulosics with sequential or

concurrent use of O_2, NO_3^-, FeO(OH), SO_4^{2-}, or CO_2 as the electron acceptor; (3) radiolysis of H_2O in the waste and brine; (4) consumption of CO_2 by $Ca(OH)_2$ (in hydrated cementitious materials) or CaO (a proposed backfill material).

The reaction-path model is similar to the average-stoichiometry model (see C.2) in that it uses input parameters such as the initial quantities of steels and other Fe-base alloys, cellulosics, and H_2O in the waste or brine, and gas-generation rates, but not gas-production potentials, to calculate gas generation in WIPP disposal rooms. One significant difference between these models is that the reaction-path model includes more gas-generation processes and requires more input parameters than the average-stoichiometry model. Furthermore, the reaction-path model includes interactions among these processes. Finally, because it has not yet been incorporated in BRAGFLO, the reaction-path model does not simulate interactions among gas generation, brine inflow and outflow, and room closure.

The reaction-path model includes one oxic-corrosion reaction (see Reaction B.1 in B.1.1) and five anoxic-corrosion reactions (Reactions B.2 through B.6 in B.1.2). (In the reaction-path model, the value of x in Reaction B.2 is 0.) It also includes the following reactions among Fe-bearing corrosion products:

$$Fe(OH)_2 + CO_2 \Leftrightarrow FeCO_3 + H_2O; \tag{C.3}$$

$$Fe(OH)_2 + H_2S \Leftrightarrow FeS + 2H_2O; \tag{C.4}$$

$$Fe(OH)_2 + 2H_2S \Leftrightarrow FeS_2 + 2H_2O + H_2; \tag{C.5}$$

$$FeCO_3 + H_2S \Leftrightarrow FeS + H_2O + CO_2; \tag{C.6}$$

$$FeCO_3 + 2H_2S \Leftrightarrow FeS_2 + H_2O + CO_2 + H_2; \tag{C.7}$$

$$3Fe(OH)_2 \Leftrightarrow Fe_3O_4 + 2H_2O + H_2; \tag{C.8}$$

$$Fe_3O_4 + 3CO_2 + H_2 \Leftrightarrow 3FeCO_3 + H_2O \tag{C.9}$$

$$Fe_3O_4 + H_2 + 3H_2S \Leftrightarrow 3FeS + 4H_2O; \tag{C.10}$$

$$Fe_3O_4 + 6H_2S \Leftrightarrow 3FeS_2 + 4H_2O + 2H_2. \tag{C.11}$$

The reaction-path model uses the following reactions to simulate gas production from microbial consumption of cellulosics:

$$C_6H_{10}O_5 + 6O_2 \Rightarrow 5H_2O + 6CO_2; \quad (C.12)$$

$$C_6H_{10}O_5 + 4.8H^+ + 4.8NO_{3^-} \Rightarrow 7.4\ H_2O + 6CO_2 + 2.4N_2; \quad (C.13)$$

$$C_6H_{10}O_5 + 24FeO(OH) + 7H_2O \Rightarrow 24Fe(OH)_2 + 6CO_2; \quad (C.14)$$

$$C_6H_{10}O_5 + 24FeO(OH) + 18CO_2 \Rightarrow 24FeCO_3 + 17H_2O; \quad (C.15)$$

$$C_6H_{10}O_5 + 24FeO(OH) + 24H_2S \Rightarrow 24FeS + 41H_2O + 6CO_2; \quad (C.16)$$

$$C_6H_{10}O_5 + 24FeO(OH) + 48H_2S \Rightarrow 24FeS_2 + 41H_2O + 6CO_2 + 24H_2; \quad (C.17)$$

$$C_6H_{10}O_5 + 24FeO(OH) \Rightarrow 8Fe_3O_4 + 9H_2O + 6CO_2 + 8H_2; \quad (C.18)$$

$$C_6H_{10}O_5 + 6H^+ + 3SO_{4^{2-}} \Rightarrow 5H_2O + 6CO_2 + 3H_2S; \quad (C.19)$$

$$C_6H_{10}O_5 + H_2O \Rightarrow 3CH_4 + 3CO_2. \quad (C.20)$$

Reactions C.12, C.13, C.19, and C.20 are similar to Reactions B.7a through B.10a (see B.2.3 and B.2.4), except that they use $C_6H_{10}O_5$, a simplified formula for cellulosics, instead of CH_2O, a simplified formula for glucose, to represent cellulosics in WIPP disposal rooms. Currently, the reaction-path model does not include gas production from microbial consumption of plastics and rubbers. To simulate microbial consumption of these materials, one would simply replace $C_6H_{10}O_5$ with formulae for various plastics and rubbers and add the resulting reactions to the model. The reaction-path model uses Reaction B.10c to simulate methanogenesis using CO_2 as the electron acceptor (see B.2.4).

The reaction-path model uses Reaction B.11 to simulate radiolysis of H_2O in the waste and brine. It does not, at this time, include radiolysis of cellulosics, plastics, and rubbers in the waste or, in the case of plastics, the container liners.

For consumption of CO_2 by $Ca(OH)_2$ or CaO, the reaction-path model includes the reactions:

$$Ca(OH)_2 + CO_2 \Leftrightarrow CaCO_3 + H_2O; \quad (C.21)$$

$$CaO + CO_2 \Leftrightarrow CaCO_3. \quad (C.22)$$

The code simulates corrosion, microbial activity, brine radiolysis, and CO_2 consumption, and the interactions among these processes by converting the reactants in Reactions B.1 through B.6 (see B.1.1 and B.1.2), B.11 (see B.3.1), and C.12 through C.22 (see above) to the products at the rates observed in laboratory studies of gas generation (see B.1.2, B.2.3, B.2.4 and B.3.1), or at rates estimated from studies carried out for applications other than the WIPP Project (see E). At the start of each time step, the code uses the partial pressures of CO_2, H_2, and H_2S in the gaseous phase and thermodynamically calculated, three-dimensional phase diagrams for the solid phases in the Fe-H_2O-CO_2-H_2-H_2S system to determine the solid corrosion product(s) stable at the start of that time step. Currently, the solid phases used to calculate these phase diagrams include Fe, $Fe(OH)_2$, Fe_3O_4, $FeCO_3$, FeS, and FeS_2. It then simulates corrosion, microbial activity, brine radiolysis, and CO_2 consumption by converting reactants (steels and other Fe-base alloys, cellulosics, H_2O, CO_2, etc.) to products (gases, corrosion products, H_2O, etc.) at experimentally observed or estimated rates. The quantities of the gases produced and consumed by Reactions B.2 through B.6, B.11, and C.3 through C.22 in turn determine the partial pressures of CO_2, H_2, and H_2S, and the corrosion product(s) stable at the start of the next time step. In addition to these gases, the model calculates the quantities of several other materials produced and consumed during each time step. These include other gases (O_2, N_2, and CH_4), H_2O, steels and other Fe-base alloys, corrosion products ($Fe(OH)_2$, Fe_3O_4, $FeCO_3$, FeS, and FeS_2), microbial substrate ($C_6H_{10}O_5$), electron acceptors (O_2, NO_3^-, FeO(OH), SO_4^{2-}, and CO_2) and materials that consume CO_2 ($Ca(OH)_2$ and CaO). (Some of these components appear more than once in this list because they are reactants or products of more than one reaction. However, the code does not distinguish between these multiple functions except in two cases described below.) It uses the ideal gas law to calculate the partial pressures of various gases and the total pressure. The code continues to convert reactants to gases, H_2O, and other products (or, in the case of gas- or H_2O-consuming reactions, it continues to convert gases or H_2O to condensed products) until a reactant is completely consumed, or until a reaction reaches equilibrium. The code calculates reaction paths by plotting points simultaneously depicting the common logarithms of the partial pressures of CO_2, H_2, and H_2S (the gases that determine the stabilities of observed or possible corrosion products) in the three-dimensional phase diagrams after each time step.

In general, the current version of the reaction-path model assumes that equilibrium is attained after the incremental conversion of reactants to products in each time step. For example, the code uses one or more of Reactions B.2 through B.6 to convert steels and other

Fe-base alloys to the solid corrosion product(s) stable (or, in the case of $Fe(OH)_2$, metastable) at the start of that time step. If one or more corrosion products are present at the end of a time step, the code then uses one or more of Reactions C.3 through C.11 to adjust the partial pressures of CO_2, H_2, and H_2S to values that simultaneously satisfy the equilibrium relationship(s) for these corrosion products. By adjusting the partial pressures of CO_2, H_2, and H_2S to their equilibrium values, these corrosion products are, in a sense, buffering the partial pressures of these gases. Only after one of these corrosion products is completely consumed are the partial pressures of CO_2, H_2, and H_2S free to deviate from values characteristic of equilibrium with that phase.

However, the reaction-path model does include disequilibrium behavior observed in laboratory studies of gas generation. For example, at low partial pressures of CO_2 and H_2S, the code can, at the user's discretion, convert steels and other Fe-base alloys to $Fe(OH)_2$, the experimentally observed anoxic-corrosion product, despite the fact that $Fe(OH)_2$ is thermodynamically unstable with respect to Fe_3O_4 under these conditions (see B.1.2). On the other hand, formation of Fe_3O_4 at low partial pressures of CO_2 and H_2S is also an option to determine the effects of possible long-term conversion of $Fe(OH)_2$ to Fe_3O_4.

Furthermore, the code simulates experimentally observed passivation of steels and other Fe-base alloys (see B.1.2) by "removing" these materials from the system once the experimentally observed passivation requirement is satisfied (formation of enough $FeCO_3$ or FeS on the surfaces of the steels and other Fe-base alloys to isolate them from additional corrosion). To determine whether the passivation requirement is met, the code distinguishes between the $FeCO_3$ or FeS that forms by corrosion of Fe, and thus adheres to corroding surfaces, and the $FeCO_3$ or FeS that, for example, replaces $Fe(OH)_2$ after it sloughs off the corroding surfaces. It is, of course, possible to add other disequilibrium phenomena to the reaction-path model if necessitated by results from additional laboratory studies of gas generation.

The current version of the reaction-path model assumes that the humid and inundated corrosion rates, the humid and inundated microbial gas-generation rates, the radiolytic gas-production rate, and the CO_2-consumption rate are constant as long as the conditions required for these processes persist in a given volume of the waste. Thus, it assumes that the sampled gas-generation rates are independent of parameters such as pH, the total pressure, the numbers and types of microorganisms present, and the concentrations of nutrients and electron acceptors. However, it is possible to add the effects of these factors to the model.

The reaction-path model is not a system-wide model. Therefore, it is necessary to use other models, such as the EQ3/6 geochemical software package (Daveler and Wolery, 1992;

Wolery, 1992a and 1992b; Wolery and Daveler, 1992), to address issues other than gas generation, such as the effects of high CO_2 partial pressures on pH or the effects of H_2O consumption on salinity.

C.4 References

Brush, L.H. 1990. *Test Plan for Laboratory and Modeling Studies of Repository and Radionuclide Chemistry for the Waste Isolation Pilot Plant.* SAND90-0266. Albuquerque, NM: Sandia National Laboratories.

Brush, L.H., and D.R. Anderson. 1989. "Potential Effects of Chemical Reactions on WIPP Gas and Water Budgets," *Systems Analysis, Long-Term Radionuclide Transport, and Dose Assessments, Waste Isolation Pilot Plant (WIPP), Southeastern New Mexico; March 1989.* Eds. A.R. Lappin, R.L. Hunter, D.P. Garber, and P.B. Davies. SAND89-0462. Albuquerque, NM: Sandia National Laboratories. A-3 through A-30.

Brush, L.H., J.W. Garner, and L.J. Storz. 1994. "Development of a Gas Generation Model for the Waste Isolation Pilot Plant," *Scientific Basis for Nuclear Waste Management XVII, Materials Research Society Symposium Proceedings, Boston, MA, November 29-December 3, 1993.* Eds. A. Barkatt and R.A. Van Konynenburg. SAND93-1145C. Pittsburgh, PA: Materials Research Society. Vol. 333, 241-246.

Butcher, B.M., and F.T. Mendenhall. 1993. *A Summary of the Models Used for the Mechanical Response of Disposal Rooms in the Waste Isolation Pilot Plant with Regard to Compliance with 40 CFR Part 191, Subpart B.* SAND92-0427. Albuquerque, NM: Sandia National Laboratories.

Daveler, S.A., and T.J. Wolery. 1992. *EQPT, A Data File Preprocessor for the EQ3/6 Software Package: User's Guide and Related Documentation (Version 7.0).* UCRL-MA-110662 PT II. Livermore, CA: Lawrence Livermore National Laboratory.

Drez, P.E. 1989. "Preliminary Quantitative Estimates of TRU Waste and Waste Containers to Be Emplaced in the Waste Isolation Pilot Plant: To Support Calculations for the Supplemental Environmental Impact Statement," *Systems Analysis, Long-Term Radionuclide Transport, and Dose Assessments, Waste Isolation Pilot Plant (WIPP), Southeastern New Mexico; March 1989.* Eds. A.R. Lappin, R.L. Hunter, D.P. Garber, and P.B. Davies. SAND89-0462. Albuquerque, NM: Sandia National Laboratories. A-117 through A-120.

Haberman, J.H., and D.J. Frydrych. 1988. "Corrosion Studies of A216 Grade WCA Steel in Hydrothermal Magnesium-Containing Brines," *Scientific Basis for Nuclear Waste Management XI, Materials Research Society Symposium Proceedings, Boston, MA, November 30-December 3, 1987.* Eds. M.J. Apted and R.E. Westerman. Pittsburgh, PA: Materials Research Society. Vol. 112, 761-772.

Lappin, A.R., R.L. Hunter, D.P. Garber, and P.B. Davies, ed. 1989. *Systems Analysis, Long-Term Radionuclide Transport, and Dose Assessments, Waste Isolation Pilot Plant (WIPP), Southeastern New Mexico; March 1989.* SAND89-0462. Albuquerque, NM: Sandia National Laboratories.

Molecke, M.A. 1979. *Gas Generation from Transuranic Waste Degradation: Data Summary and Interpretation.* SAND79-1245. Albuquerque, NM: Sandia National Laboratories.

Sandia Laboratories. 1979. *Summary of Research and Development Activities in Support of Waste Acceptance Criteria for WIPP.* SAND79-1305. Albuquerque, NM: Sandia National Laboratories.

Sandia WIPP Project. 1992. *Preliminary Performance Assessment for the Waste Isolation Pilot Plant, December 1992. Volume 3: Model Parameters.* SAND92-0700/3. Albuquerque, NM: Sandia National Laboratories.

Simpson, J.P., and R. Schenk. 1989. "Corrosion Induced Hydrogen Evolution on High Level Waste Overpack Materials in Synthetic Groundwaters and Chloride Solutions," *Scientific Basis for Nuclear Waste Management XII, Materials Research Society Symposium* Proceedings, *Berlin, Germany, October 10-13, 1988.* Eds. W. Lutze and R.C. Ewing. Pittsburgh, PA: Materials Research Society. Vol. 127, 389-396.

WIPP Performance Assessment Division. 1991. *Preliminary Comparison with 40 CFR Part 191, Subpart B for the Waste Isolation Pilot Plant, December 1991. Volume 3: Reference Data.* SAND91-0893/3. Eds. R.P. Rechard, A.C. Peterson, J.D. Schreiber, H.J. Iuzzolino, M.S. Tierney, and J.S. Sandha. Albuquerque, NM: Sandia National Laboratories.

Wolery, T.J. 1992a. *EQ3/6, A Software Package for Geochemical Modeling of Aqueous Systems: Package Overview and Installation Guide (Version 7.0).* UCRL-MA-110662-PT. I. Livermore, CA: Lawrence Livermore National Laboratory.

Wolery, T.J. 1992b. *EQ3NR, A Computer Program for Geochemical Aqueous Speciation-Solubility Calculations: Theoretical Manual, User's Guide, and Related Documentation (Version 7.0).* UCRL-MA-110662-PT. III. Livermore, CA: Lawrence Livermore National Laboratory.

Wolery, T.J., and S.A. Daveler. 1992. *EQ6, A Computer Program for Reaction-Path Modeling of Aqueous Geochemical Systems: Theoretical Manual, User's Guide, and Related Documentation (Version 7.0).* UCRL-MA-110662-PT. IV. Livermore, CA: Lawrence Livermore National Laboratory.

APPENDIX D: DATA USED IN THE 1991 AND 1992 WIPP PERFORMANCE ASSESSMENT CALCULATIONS

Date: July 8, 1991
To: D. R. Anderson, 6342
From: L. H. Brush, 6345
Subject: Current Estimates of Gas Production Rates, Gas Production Potentials, and Expected Chemical Conditions Relevant to Radionuclide Chemistry for the Long-Term WIPP Performance Assessment

Sandia National Laboratories

Albuquerque, New Mexico 87185

date July 8, 1991

to D. R. Anderson, 6342

L. H. Brush

from L. H. Brush, 6345

subject: Current Estimates of Gas Production Rates, Gas Production Potentials, and Expected Chemical Conditions Relevant to Radionuclide Chemistry for the Long-Term WIPP Performance Assessment

This memorandum justifies the estimates of gas production rates, gas production potentials, and expected chemical conditions relevant to radionuclide chemistry in WIPP disposal rooms for design-basis transuranic (TRU) waste provided to R. P. Rechard last month (Table 1). Many of these estimates are new; some are based on recently obtained data from laboratory studies of anoxic corrosion.

I will provide similar estimates for the Engineered Alternatives Task Force's (in prep.) Alternatives 2 and 6 by August 1, 1991.

ANOXIC CORROSION

R. E. Westerman (1990, 1991a) of Pacific Northwest Laboratory (PNL) has observed significant H_2 production from anoxic corrosion of two heats each of ASTM A 366 and ASTM A 570 steels by WIPP Brine A under inundated conditions when N_2 is present at low pressures (about 150 psig) in the headspace above the brine. The low-C, cold-rolled steel alloy ASTM A 366 simulates the drums to be emplaced in the repository; the medium-C, hot-rolled steel alloy ASTM A 570 simulates the boxes. The H_2 production rate was essentially constant during 3- and 6-month experiments; the average value for all four heats obtained from the 6-month experiments is 0.21 moles per m^2 of steel per year. Based on my estimate of 6 m^2 of steels per equivalent drum of waste, which includes steels used to fabricate waste containers (drums and boxes) and steels contained in the waste, this is equivalent to 1.26 mole of H_2 per drum per year. Westerman also reported an average corrosion rate of 1.72 μm of steel per year for the 6-month runs. The H_2 production rates of 0.2 moles per m^2 per year or 1 mole per drum per year and the corrosion rate of 2 μm per year are my best estimates for inundated conditions, rounded to one significant figure (Table 1).

Strictly speaking, the H_2 production rates and the corrosion rate are not equivalent. Although he obtained both rates from each

experiment, Westerman used independent techniques to obtain them (pressure measurements and posttest analysis of the headspace gases for the H_2 production rate and gravimetric, or weight-loss, analysis for the corrosion rate). These techniques agreed well, but not exactly, when applied to the 6-month experiments, but not as well for the 3-month experiments. (The best estimates described above are from the 6-month runs.) The discrepancies between these techniques probably result from uncertainties as to the identity and composition of the corrosion product or products formed during these experiments. (Characterization of the corrosion product is necessary to write the chemical reactions used to convert corrosion rates to H_2 production rates.) We are still attempting to characterize the corrosion product from these runs.

Although the H_2 production rate has been constant for 6 months when N_2 is present at low-pressures, the results of high-pressure experiments at PNL imply that the build-up of H_2 pressure would eventually reduce this rate significantly (Westerman, 1991b). After 6 months, the corrosion rate of two heats of ASTM A 366 steel under inundated conditions with H_2 at a pressure of 1,000 psig was 0.356 μm per year, 21.8% of the rate of 1.63 μm per year observed for the same two heats of ASTM A 366 steel under low-pressure, inundated conditions with N_2. Multiplying 1.72 μm per year, the average rate for all four heats, by 0.218 gives 0.375 μm per year, my estimate of the average corrosion rate for all four heats of steel at 1,000 psig H_2. However, at an N_2 pressure of 1,000 psig the corrosion rate of two heats of ASTM A 366 steel was 2.96 μm per year, 81.6% higher than the low-pressure, inundated rate of 1.63 μm per year observed for the same two heats of ASTM A 366 steel. The product of 1.72 μm per year and 1.82 is 3.13 μm per year, my estimated average corrosion rate for all four heats of steel at 1,000 psig N_2. Westerman did not report H_2 production rates for the high-pressure experiments. Furthermore, we have still not identified the corrosion product or products yet. However, the corrosion product appears to be the same phase that formed in the 6-month, low pressure experiments. It is thus possible to estimate an H_2 production rate by multiplying the 6-month, low-pressure rates of 0.21 moles per m^2 or 1.26 moles per drum of waste by 0.218 (1,000 psig H_2) and 1.82 (1,000 psig N_2) to obtain 0.046 moles per m^2 per year or 0.275 moles per drum per year (1,000 psig H_2) and 0.38 moles per m^2 per year or 2.29 moles per drum per year (1,000 psig N_2). At present, we do not have corrosion rates for any pressures other than 150 and 1,000 psig. Westerman will, however, report 12-month data for 500 psig H_2 and 1,000 psig H_2 in November or December 1991. The adjusted, measured corrosion rate of 3 μm per year and the estimated H_2 production rate of 0.4 mole per m^2 per year or 2 moles per drum per year with N_2 at 1,000 psig are my maximum estimates for inundated conditions, rounded to one significant figure (Table 1).

Under low-pressure, inundated conditions with CO_2, H_2 production occurred for about 3 months, then virtually stopped after 3 or 4 months due to formation of a passivating layer of $FeCO_3$, or siderite

(Westerman, 1991a). This suggests that, if microbially produced CO_2 were present, passivation of steel surfaces by $FeCO_3$ could stop H_2 production before the generation of significant quantities of this gas. However, we do not know the partial pressure of CO_2 required to form $FeCO_3$. Furthermore, crushing of drums and boxes during room closure could disrupt the layer of $FeCO_3$ and lead to some additional H_2 production. Nevertheless, the passivation observed after 3 or 4 months is the basis for my minimum estimates of 0 moles of H_2 per m^2 per year or 0 moles of H_2 per drum per year and 0 μm of steel per year for inundated conditions (Table 1).

Because we have still not identified the corrosion product or products, we cannot calculate the number moles of H_2O consumed per mole of Fe consumed or the number moles of H_2O consumed per mole of H_2 produced from anoxic corrosion of steels. However, the corrosion reaction that produces $Fe(OH)_2$ (amakinite) a possible corrosion product identified by Brush and Anderson (1988) and Brush (1990), would consume 2 moles of H_2O per mole of Fe consumed, or consume 2 moles of H_2O per mole of H_2 produced. The corrosion reaction that produces Fe_3O_4 (magnetite), another possible corrosion product, would consume 1.33 mole of H_2O per mole of Fe consumed, or consume 1 mole of H_2O per mole of H_2 produced. These values are probably typical of other corrosion reactions.

In 3- and 6-month, low-pressure, humid experiments with either CO_2 or N_2, Westerman (1990, 1991a) observed no H_2 production except for very limited quantities from corrosion of the bottom 10% of the specimens splashed with brine during pretest preparation of the containers. These results and modeling studies conducted by Davies (personal communication) suggested to me that anoxic corrosion could be self-limiting; small quantities of brine in the repository could produce H_2, increase the pressure, prevent additional brine inflow or even cause brine outflow, and thus prevent additional H_2 production. However, the thin film of brine introduced by capillary rise or condensation followed by dissolution of salts from the backfill, or H_2O absorbed by crushed salt or bentonite in the backfill, which will be in contact with drums and boxes, could cause additional anoxic corrosion of steels and H_2 production after brine is driven away from corroding steels.

Westerman (1991c) has just started a study to quantify H_2 production from anoxic corrosion of steels in contact with noninundated backfill materials and will report preliminary results by the end of September 1991. Until then, I propose the following arbitrarily estimated rates for humid conditions: minimum estimates of 0 moles of H_2 per m^2 of steel per year or 0 moles per drum of waste per year and 0 μm of steel per year; best estimates of 0.02 moles of H_2 per m^2 per year or 0.1 moles of H_2 per drum per year and 0.2 μm per year; and maximum estimates of 0.2 moles of H_2 per m_2 per year or 1 moles of H_2 per drum per year and 2 μm per year (Table 1).

Finally, I propose that the estimated gas production potential from

anoxic corrosion remain at 900 moles per drum of waste. This value, estimated by Brush and Anderson (1989), Lappin et al. (1989), and Brush (1990), is 60% of the total gas production potential.

MICROBIAL ACTIVITY

D. Grbic-Galic and her colleagues at Stanford University observed significant microbial gas production by halophilic microorganisms in brine collected from G Seep in the WIPP underground workings with glucose, a relatively biodegradable substrate, but did not report significant gas production with cellulose, a much less biodegradable substrate. Furthermore, brine from G Seep inhibited significant gas production by nonhalophilic microorganisms, although a few experiments did show some evidence for possible microbial activity. These results seem to suggest that microbial gas production may be significant under overtest conditions (relatively biodegradable substrates, amendment of brine with nutrients, etc.), but not under realistic conditions. However, I believe that, for the reasons described below, the results obtained by Grbic-Galic and her colleagues do not rule out significant microbial gas production.

First, N. Black of Stanford University, R. H. Vreeland of West Chester University, and I compared the recent study at Stanford University and studies carried out during the 1970s (Barnhart et al., 1980; Caldwell, 1981; Caldwell et al., 1988; Molecke, 1979; Sandia National Laboratories, 1979). We concluded, as others have before us (Molecke, 1979; Brush and Anderson, 1989; Lappin et al., 1989), that the earlier results implied significant microbial gas production under both realistic and overtest conditions.

Second, Vreeland observed significant degradation of filter paper by his enrichments of halophilic and halotolerant microorganisms from the salt lakes in Nash Draw. Although he could not quantify gas production rates from these experiments, the results suggest that microorganisms could consume paper under realistic conditions in WIPP disposal rooms. Paper constitutes 70% of the 10 kg of cellulosics per equivalent drum of contact handled TRU waste to be emplaced in the repository (Brush, 1990).

Third, Black, Vreeland, and I reviewed the methods used in the earlier and recent studies in detail. We concluded that the study at Stanford University was not sensitive enough to detect gas production rates equivalent to a few tenths of a mole of gas per drum of waste per year. Davies (1990) has demonstrated that gas production rates greater than about 0.1 mole per equivalent drum of waste per year are significant from the standpoint of the long-term performance of the repository.

Because the results obtained at Stanford University do not rule out significant microbial gas production under realistic conditions, I

propose using the same best estimate for the microbial gas production rate under inundated conditions proposed by Brush and Anderson (1989), Lappin et al. (1989), and Brush (1990), 1 mole of various gases per drum per year. However, I propose new minimum and maximum rates for inundated conditions, 0 and 5 moles per drum per year, respectively. The minimum estimate is analogous to the minimum estimate for anoxic corrosion under inundated conditions. The maximum estimate is Molecke's (1979) maximum estimate for microbial activity under inundated conditions. I also propose new minimum and best estimates for microbial gas production rates under humid conditions, 0 and 0.1 moles per drum per year. These estimates, both arbitrary, are analogous to the arbitrary minimum and best estimates for anoxic corrosion under humid conditions. The maximum estimate for microbial activity under humid conditions remains unchanged from the value estimated by Brush and Lappin (1990), 1 mole per drum per year (Table 1).

To convert these estimates of microbial gas production rates to units of moles per kg of cellulosics per year, I divided each rate by 10 kg of cellulosics per drum, the estimate used by Brush (1990), to obtain the estimates given in Table 1. Strictly speaking, this is inconsistent with the fact that the rate of 1 mole per drum per year is based on experiments carried out with simulated waste that included materials other than cellulosics (Molecke, 1979). It is also inconsistent with the assumption of Molecke (1979), Brush and Anderson (1979), and Lappin et al. (1989) that microorganisms will degrade 100% of the cellulosics, 50% of the Hypalon, and 50% of the Neoprene in the waste. However, about 90% of the microbial gas production potential (below) and hence 90% of the microbial gas production rate estimated by Brush and Anderson (1989) and Lappin et al. (1989) would result from biodegradation of cellulosics and only 5% each from Hypalon and Neoprene. Furthermore, Francis will use cellulosics as the sole substrate in his study of microbial gas production, at least initially. Finally, it will be much easier to use rates normalized only to the mass of cellulosics present than rates normalized to cellulosics, Hypalon, and Neoprene in performance-assessment calculations.

I also propose that the estimated gas production potential from microbial activity stay at 600 moles per drum of waste, the value estimated by Brush and Anderson (1989), Lappin et al. (1989), and Brush (1990). This is 40% of the total gas production potential.

RADIOLYSIS

D. T. Reed of Argonne National Laboratory is carrying out a low-pressure study of gas production by α radiolysis of Brine A as a function of dissolved Pu concentration. He has observed small, linear pressure increases from the solution with the highest dissolved Pu concentration, $1 \cdot 10^{-4}$ M, but does not have enough data to convert these rates to moles of gas per drum of waste per year yet. As

expected, he has not observed pressure increases yet from the solutions with lower dissolved Pu concentrations, $1 \cdot 10^{-6}$ and $1 \cdot 10^{-8}$ M. After completion of these 3-month experiments, Reed will carry out 2-month runs with a dissolved Pu concentration of $1 \cdot 10^{-4}$ M in other WIPP brines to determine the effect of compositional variations on the radiolytic gas production rate.

As soon as he obtains longer-term data from Brine A with a dissolved Pu concentration of $1 \cdot 10^{-4}$ M, data with lower dissolved Pu concentrations in Brine A, and results from other WIPP brines with a dissolved Pu concentration of $1 \cdot 10^{-4}$ M, Reed will calculate experimentally based radiolytic gas-production rates for the radionuclide concentrations estimated by the Radionuclide Source Term Expert Panel. In addition to rates in units of moles of gas per drum of waste per year, he will provide rates in moles per cubic meter of brine for various concentrations. Until then, I propose using the radiolytic gas production rates proposed by Brush and Lappin (1990), who estimated a minimum rate of $1 \cdot 10^{-7}$ mole of various gases per drum of waste per year, a best rate of $1 \cdot 10^{-4}$ mole per drum per year, and a maximum rate of $1 \cdot 10^{-1}$ mole per drum per year (Table 1).

EXPECTED CHEMICAL CONDITIONS RELEVANT TO RADIONUCLIDE CHEMISTRY

Development of the source term for radionuclide-transport calculations will require: (1) estimates of the quantity of each nonradioactive constituent of design-basis TRU waste to be emplaced in the repository; (2) predictions of the microenvironments (Eh, pH, and the concentrations of organic and inorganic ligands) for each nonradioactive waste constituent; (3) quantification of the chemical behavior of the important radionuclides in the waste for each of these microenvironments; (4) construction of a frequency distribution of radionuclide concentrations based on the relative quantity of each nonradioactive waste constituent and the concentration associated with that constituent.

Currently, inventories of radioactive and nonradioactive waste constituents and estimates of radionuclide concentrations in brines as a function of Eh and pH are available. However, the high priority placed on the gas issue in laboratory studies of repository chemistry has precluded efforts to predict microenvironment for waste constituents. Therefore, I propose that oxidizing, acidic conditions, oxidizing, basic conditions, reducing, acidic conditions, and reducing, basic conditions be considered equally probable for interpreting Eh-pH-dependent estimates of radionuclide concentrations in WIPP brines.

REFERENCES

Barnhart, B. J., E. W. Campbell, E. Martinez, D. E. Caldwell, and R. Hallett (1980). **Potential Microbial Impact on Transuranic Wastes Under Conditions Expected in the Waste Isolation Pilot Plant (WIPP), Annual Report, October 1, 1978-September 30, 1979.** LA-8297-PR, Los Alamos Scientific Laboratory, Los Alamos, NM.

Brush, L. H. (1990). **Test Plan for Laboratory and Modeling Studies of Repository and Radionuclide Chemistry for the Waste Isolation Pilot Plant**, SAND90-0266, Sandia National Laboratories, Albuquerque, NM.

Brush, L. H., and D. R. Anderson (1989). Estimates of Gas Production Rates, Potentials, and Periods, and Dissolved Radionuclide Concentrations for the WIPP Supplemental Environmental Impact Statement, unpublished memorandum to B. M. Butcher, February 14, 1989. Sandia National Laboratories, Albuquerque, NM.

Brush, L. H., and A. R. Lappin (1990). Additional Estimates of Gas Production Rates and Radionuclide Solubilities for Use in Models of WIPP Disposal Rooms, unpublished memorandum to D. R. Anderson, August 1, 1990. Sandia National Laboratories, Albuquerque, NM.

Caldwell, D. E. (1981). Microbial Biogeochemistry of Organic Matrix Transuranic Waste, unpublished report submitted to M. A. Molecke, June 17, 1981, University of New Mexico, Albuquerque, NM.

Caldwell, D. E., R. C. Hallett, M. A. Molecke, E. Martinez, and B. J. Barnhart (1988). **Rates of CO_2 Production From the Microbial Degradation of Transuranic Wastes under Simulated Geologic Isolation Conditions.** SAND87-7170, Sandia National Laboratories, Albuquerque, NM.

Davies, P. B. (1990). Results from Recent Variable-Rate Gas Simulations that Examine the Impact of Vapor-Limited ("Humid") Gas-Generation Rates, unpublished memorandum to L. H. Brush and A. R. Lappin, December 6, 1990. Sandia National Laboratories, Albuquerque, NM.

Engineered Alternatives Task Force (in prep.). **Evaluation of the Effectiveness and Feasibility of the Waste Isolation Pilot Plant Engineered Alternatives: Final Report of the Engineered Alternatives Task Force, Vol. I and II**, DOE/WIPP 91-007, Rev. 2, US Department of Energy Waste Isolation Pilot Plant, Carlsbad, NM.

Lappin, A. R., R. L. Hunter, D. P. Garber, and P. B. Davies, Eds. (1989). **Systems Analysis, Long-Term Radionuclide Transport, and Dose Assessments, Waste Isolation Pilot Plant (WIPP), Southeastern New Mexico; March, 1989.** SAND89-0462, Sandia National Laboratories, Albuquerque, NM.

Molecke, M. A. (1979). **Gas Generation from Transuranic Waste Degradation: Data Summary and Interpretation.** SAND79-1245, Sandia National Laboratories, Albuquerque, NM.

Sandia National Laboratories (1979). **Summary of Research and Development Activities in Support of Waste Acceptance Criteria for the WIPP.** SAND79-1305, Sandia National Laboratories, Albuquerque, NM.

Westerman, R. E. (1990). Corrosion of Low-Carbon Steel in Simulated Waste Isolation Pilot Plant (WIPP) Environments, Quarterly Progress Report for the Period July 1 - September 30, 1990, unpublished report submitted to L. H. Brush, September 28, 1990. Pacific Northwest Laboratory, Richland, WA.

Westerman, R. E. (1991a). Corrosion of Low-Carbon Steel in Simulated Waste Isolation Pilot Plant (WIPP) Environments, Progress Report for the Period October 1, 1990 to March 31, 1991, unpublished report submitted to L. H. Brush, March 29, 1991. Pacific Northwest Laboratory, Richland, WA.

Westerman, R. E. (1991b). April 1991 Monthly Report, Corrosion of Low-Carbon Steel in Simulated WIPP Environments, unpublished report submitted to L. H. Brush, April 26, 1991. Pacific Northwest Laboratory, Richland, WA.

Westerman, R. E. (1991c). May 1991 Monthly Report, Corrosion of Low-Carbon Steel in Simulated WIPP Environments, unpublished report submitted to L. H. Brush, May 28, 1991. Pacific Northwest Laboratory, Richland, WA.

TABLE 1. CURRENT ESTIMATES OF GAS PRODUCTION RATES

Process	Gas Production Rate (various units)		
	Minimum	Best	Maximum
Anoxic corrosion, inundated:[1]			
moles/m^2 · year	0	0.2	0.4
moles/drum · year	0	1	2
μm/year	0	2	3
Anoxic corrosion, humid:[1]			
moles/m^2 · year	0	0.02	0.2
moles/drum · year	0	0.1	1
μm/year	0	0.2	2
Microbial activity, inundated:			
moles/drum · year	0	1	5
moles/kg cellulosics · year	0	0.1	0.5
Microbial activity, humid:			
moles/drum · year	0	0.1	1
moles/kg cellulosics · year	0	0.01	0.1
Radiolysis of brine:			
moles/drum · year	0.0000001	0.0001	0.1

1. See text for estimates of H_2O consumption by anoxic corrosion of steels.

Distribution:

V. Daub, DOE/WPO
J. Carr, DOE/WPO
D. Blackstone, DOE/WPO
W. D. Arnold, Oak Ridge National Laboratory
J. N. Butler, Harvard University
G. R. Choppin, Florida State University
A. J. Francis, Brookhaven National Laboratory
J. B. Gillow, Brookhaven National Laboratory
J. K. Lanyi, University of California at Irvine
R. E. Meyer, Oak Ridge National Laboratory
H. Nitsche, Lawrence Livermore National Laboratory
D. T. Reed, Argonne National Laboratory
R. H. Vreeland, West Chester University
R. E. Westerman, Pacific Northwest Laboratory
6340 W. D. Weart
6341 R. C. Lincoln
6341 SWCF (6): XXXRC, XXXRC/AC, XXXRC/MA, XXXRC/R, XXXRNC, XXXRNC/SOL
6342 Staff
6343 T. M. Schultheis
6344 E. D. Gorham
6344 P. B. Davies
6345 B. M. Butcher
6345 Staff
6346 J. R. Tillerson

W. D. Arnold
Building 4500 North
Mail Stop 6201
Oak Ridge National Laboratory
Oak Ridge, TN 37831-6201

Dr. James N. Butler
Division of Applied Sciences
Harvard University
Cambridge, MA 02138

Dr. Gregory R. Choppin
Department of Chemistry
Florida State University
Tallahassee, FL 32306

Dr. Arokiasmy J. Francis
Department of Applied Science
Building 318-46
Brookhaven National Laboratory
Upton, NY 11973

Jeff Gillow
Department of Applied Science
Building 318-46
Brookhaven National Laboratory
Upton, NY 11973

Dr. Janos Lanyi
Department of Physiology and Biophysics
University of California at Irvine
Irvine, CA 92717

Dr. Robert E. Meyer
Building 4500 North
Mail Stop 6201
Oak Ridge National Laboratory
Oak Ridge, TN 37831-6201

Dr. Heino Nitsche
Mail Stop 70A-1150
Lawrence Berkeley
Laboratory
1 Cyclotron Rd.
Berkeley, CA 94720

Dr. Donald T. Reed
Chemical Technology Division
Argonne National Laboratory
9700 S. Cass Ave.
Argonne, IL 60439

Dr. Russell H. Vreeland
Department of Biology
West Chester University
West Chester, PA 19383

Dr. Richard E. Westerman
Battelle Pacific Northwest
Laboratory
PO Box 999
Richland, WA 99352

APPENDIX E: WIPP GAS-GENERATION DATA SUBMITTED FOR THE 1993 PERFORMANCE-ASSESSMENT CALCULATIONS AND THE SYSTEMS-PRIORITIZATION-METHOD-2 CALCULATIONS

Date: June 18, 1993
To: M. S. Tierney, 6342
From: L. H. Brush, 6348
Subject: Likely Gas-Generation Reactions and Current Estimates of Gas-Generation Rates for the Long-Term WIPP Performance Assessment

WP08524

Sandia National Laboratories

Albuquerque, New Mexico 87185

date: June 18, 1993

to: M. S. Tierney, 6342

L. H. Brush

SANDIA
WIPP CENTRAL FILE

from: L. H. Brush, 6348

subject: Likely Gas-Generation Reactions and Current Estimates of Gas-Generation Rates for the Long-Term WIPP Performance Assessment

INTRODUCTION

This memorandum identifies likely gas-generation reactions (Table 1), provides current estimates of humid and inundated gas-generation rates (Tables 2 and 3), and calculates the gas-generation potential for radiolysis of H_2O in brine by ^{239}Pu for the 1993 long-term WIPP performance-assessment (PA) calculations. A. R. Lappin, 6305, has provided estimates of gas-generation potentials for other processes.

I understand that because of severe time constraints and the higher priorities assigned to other changes in the models to be used for the 1993 PA calculations, you will not have time to incorporate the current version of the gas-generation model J. W. Garner and I provided to P. Vaughn in February 1993. Therefore, I understand you will use the same gas-generation model used in the 1991 and 1992 calculations. This approach consists of listing likely gas-generation reactions, calculating the average stoichiometric gas-production ratio of these reactions, estimating average gas-production rates, and allowing gas production to proceed until the total quantity of gas expected (the gas-generation potential) is attained for a given set of assumptions. I refer to this model as the "average-stoichiometry model." The assumptions include (but are not necessarily limited to): (1) the inventory of reactants (steels and other Fe-base alloys, Al and Al-base alloys, and, perhaps, other metals; cellulosics, plastics, and rubbers); (2) the extent to which these materials are convertible to gas (this is especially important in the case of plastics and rubbers); (3) whether sufficient H_2O will be available (this is especially significant in the case of reactions that occur only in the presence of brine, such as anoxic corrosion of steels). Of course, assumptions such as these are also necessary for the gas-generation model Garner and I are developing.

Given the severe time constraints and the higher priorities assigned to other improvements in the PA models, I concur with your

decision to retain the average-stoichiometry model used in the 1991 and 1992 PA calculations. However, I recommend using additional gas-generation reactions, if possible, and current estimates of gas-generation rates. I describe these reactions and rates below. Of course, I realize that there may not be time to make <u>any</u> changes in the average-stoichiometry model at this point.

Garner and I will continue to develop a thermodynamic and kinetic reaction-path gas-generation model. The current version of this model includes the following processes: (1) corrosion of steels and other Fe-base materials by O_2, H_2O, H_2O and CO_2, or H_2S; (2) passivation of steels by CO_2; (3) depassivation of steels by destabilization of $FeCO_3$; (4) microbial degradation of cellulosics with O_2, NO_3^-, Fe(III) hydroxide, or SO_4^{2-} as the electron acceptor; (5) consumption of CO_2 by $Ca(OH)_2$ (in cementitious materials) and CaO (a potential backfill additive). The main differences between the reaction-path model and the average-stoichiometry model used in the 1991 and 1992 PA calculations are that: (1) the reaction-path model includes more gas-producing reactions than the average-stoichiometry model; (2) the reaction-path model includes gas-consuming reactions; (3) the reaction-path model includes interactions among gas-producing and gas-consuming processes, such as passivation of steels by microbially-produced CO_2 and depassivation of steels due to consumption of CO_2 by $Ca(OH)_2$ and CaO. We will provide you with the latest version of this model as soon as you are ready to incorporate it in the PA models.

CORROSION

Oxic corrosion of steel waste containers (drums and boxes), Fe-base alloys in the waste, and, perhaps, other metals would consume O_2 in mine air trapped in WIPP disposal rooms at the time of filling and sealing. Oxic corrosion would also consume O_2 produced by radiolysis of H_2O in brine. After depletion of the O_2 initially present, anoxic corrosion of Fe-base and other metals could produce significant quantities of H_2, at least in microenvironments without radiolytically produced O_2. Other metals that could consume O_2 and produce H_2 include (but are not necessarily limited to) Al, Al-base alloys, Pb, and Pu. Oxic and anoxic corrosion could also consume significant quantities of brine and H_2O vapor.

Oxic Corrosion

Brush (1990) concluded that oxic corrosion of steels, other Fe-base alloys, and, perhaps, other metals would not have a significant, direct effect on the gas and H_2O budget of WIPP disposal rooms. However, this process could be important from the standpoint of the O_2 budget of the repository. The O_2 budget will in turn affect how soon the repository becomes anoxic after filling and sealing, the extent to which microenvironments dominated by brine radiolysis remain oxic, whether gas is consumed or produced, and which gases are consumed and

produced. The O_2 budget will also affect the oxidation state of radionuclides and hence their chemical behavior. Therefore, Garner and I have added the following reaction to the reaction-path gas-generation model to simulate oxic corrosion:

$$2Fe + H_2O + 1.5O_2 = 2\gamma FeO(OH) \qquad (1)$$

We are using this reaction because N. R. Sorensen, 1832, observed that $\gamma FeO(OH)$ (lepidocrocite) was the most abundant corrosion product in oxic, inundated experiments carried out for the Strategic Petroleum Reserve Project. Sorensen also observed Fe_3O_4 as a major corrosion product and $\beta FeO(OH)$ as a minor corrosion product. Therefore, Garner and I may also add an equation simulating the formation of Fe_3O_4. (Addition of an equation for $\beta FeO(OH)$ would not change the stoichiometry of Reaction 1).

For my best estimate of the O_2-consumption rate for oxic corrosion, I recommend 5 moles per m^2 of steel per year, the value (rounded off to one significant figure) reported by Molecke (1979). Lappin et al. (1989) estimated that there are 6 m^2 of steels and other Fe-base alloys per drum of CH TRU waste, 4 m^2 for CH TRU waste containers and an estimated 2 m^2 for the Fe-base alloys in CH TRU waste. (These values do not include steel or other Fe-base alloys in canisters or plugs to be used for RH TRU waste, any steels or other Fe-base alloys contained in RH TRU waste, or steels or other Fe-base alloys used for ground support in the WIPP underground workings.) Therefore, this rate is equivalent to 30 moles of O_2 per drum of CH TRU waste per year. I computed the oxic-corrosion rate as follows.

The rate at which Fe is consumed by Reaction 1 is:

$$((2 \text{ moles Fe}) / (1.5 \text{ moles } O_2)) \cdot 5 \text{ moles } O_2/(m^2 \cdot yr)$$
$$= 6.67 \text{ moles Fe}/(m^2 \cdot yr). \qquad (2)$$

(Only one of the figures in this and the following equations are significant, but I did not round off until the end of these calculations.) This rate is equivalent to:

$$6.67 \text{ moles}/(m^2 \cdot yr) \cdot 5.5847 \cdot 10^{-2} \text{ kg/mole}$$
$$= 3.7231 \cdot 10^{-1} \text{ kg}/(m^2 \cdot yr). \qquad (3)$$

In Equation 2, "$5.5847 \cdot 10^{-2}$ kg" is the mass of a mole of metallic Fe. The thickness of the layer of Fe removed from the surface per year is:

$$3.7231 \cdot 10^{-1}\ kg/(m^2 \cdot yr)\ /\ 7.86 \cdot 10^3\ kg/m^3$$

$$= 5 \cdot 10^{-5}\ m/yr. \qquad (4)$$

In Equation 4, "$7.86 \cdot 10^3\ kg/m^3$" is the density of metallic Fe. This rate is equivalent to about 50 μm of steel per year (Table 2). I cannot compare these estimates of O_2-consumption or corrosion rates with previous estimates because I did not estimate these rates for oxic corrosion of steels for the 1991 and 1992 PA calculations (see Brush, 1991).

My minimum estimates of O_2-consumption and corrosion rates for oxic corrosion of steels and other Fe-base alloys under inundated conditions, 0 moles per per m^2 of steel per year or 0 moles of O_2 per drum of CH TRU waste per year and 0 μm of steel per year (Table 2), are based on the possibility of passivation by formation of an adherent corrosion product (see Anoxic Corrosion below), or by precipitation of salts on the surfaces of corroding metals due to the consumption of H_2O during oxic corrosion of steels, other Fe-base alloys, and, perhaps, other metals. Although laboratory studies have not demonstrated these mechanisms yet, they are possible, especially (in the case of the latter mechanism) if microbial degradation of cellulosics and brine radiolysis also consume significant quantities of H_2O.

My maximum estimates of O_2-consumption and corrosion rates for oxic corrosion of steels and other Fe-base alloys under inundated conditions (Table 2) are based on estimates of the effects of pH on these rates. I have not yet considered the effects of total pressure, the partial pressures of gases expected in WIPP disposal rooms, or temperature on oxic corrosion. However, I have considered the effects of these factors on anoxic corrosion (see below); the analysis for anoxic corrosion suggests that pH is the most important of these factors. In the case of oxic corrosion, O_2-consumption and corrosion rates are inversely proportional to pH. I used the inverse relationship between pH and oxic-corrosion rates observed experimentally for applications other than the WIPP Project and estimates of the range of pH expected in WIPP disposal rooms after filling and sealing to estimate the maximum values of these rates.

I assume that the O_2-consumption rate of 5 moles per m^2 of steel per year (Molecke, 1979), which I used for my best estimate of this and other rates under inundated conditions (Table 2), pertains to Reaction 1 at a neutral or nearly neutral pH. Furthermore, I expect that the pH in WIPP disposal rooms will vary between about 3 and 12. Although obtained with deionized H_2O, the results of Uhlig and Revie (1963) suggest that the O_2-consumption and corrosion rates for oxic corrosion of steels are constant or essentially constant between a pH of about 4 and 10, that these rates are higher by about a factor of 1.5 at a pH of 3, and that they are lower by a factor of 0.6 at a pH of 11 and by a factor of 0.4 at a pH of 12. Therefore, the possibility of pH values as low as 3 in WIPP disposal rooms necessitates multiplying my

best estimates in Table 2 by a factor of 1.5:

$$1.5 \cdot 5 \text{ moles/m}^2 = 8 \text{ moles/(m}^2 \cdot \text{yr)}; \quad (5a)$$

$$1.5 \cdot 30 \text{ moles/(drum} \cdot \text{yr)} = 50 \text{ moles/(drum} \cdot \text{yr)}; \quad (5b)$$

$$1.5 \cdot 50 \ \mu\text{m/yr} = 80 \ \mu\text{m/yr}. \quad (5c)$$

These are my maximum estimates, rounded to one significant figure, of these rates under inundated conditions (Table 2). Because they are maximum estimates, I have rounded them up in all three cases. The effects of basic conditions on oxic corrosion need not be considered at this point because, although they decrease these rates, my minimum estimates are already 0 moles of O_2 per m^2 of steel per year, 0 moles of O_2 per drum of CH TRU waste per year, and 0 μm of steel per year because of possible passivation (see above).

My best estimates of O_2-consumption and corrosion rates for oxic corrosion of steels and other Fe-base alloys under humid conditions are 0.5 moles of O_2 per m^2 of steel per year, 3 moles of O_2 per drum of CH TRU waste per year, and 5 μm of steel per year (Table 3). I arbitrarily assume that these rates are one tenth of my current best estimates for oxic corrosion under inundated conditions (Table 2). I did not estimate these rates for oxic corrosion of steels for the 1991 and 1992 PA calculations (Brush, 1991).

My arbitrary minimum estimates of O_2-consumption and corrosion rates for oxic corrosion of steels and other Fe-base alloys under humid conditions are also 0 moles of O_2 per m^2 of steel per year, 0 moles of O_2 per drum of CH TRU waste per year, and 0 μm of steel per year (Table 3).

My maximum estimates of O_2-consumption and corrosion rates for oxic corrosion of steel and other Fe-base alloys under humid conditions are 5 moles of O_2 per m^2 of steel per year, 30 moles of O_2 per drum of CH TRU waste per year, and 50 μm of steel per year (Table 2). I arbitrarily assume that these rates are identical to my current best estimates for oxic corrosion under inundated conditions (Table 2).

If oxic-corrosion rates under humid conditions affect the overall performance of the repository significantly, laboratory studies will be necessary to replace these arbitrary estimates with experimentally-based results.

Anoxic Corrosion

Anoxic corrosion of steels, other Fe-base alloys, and, perhaps, other metals may, if brine is present, produce significant quantities

of H_2 and consume significant quantities of H_2O (Lappin et al., 1989; Brush, 1990).

I used thermodynamic calculations and laboratory studies carried out for applications other than the WIPP Project to predict the behavior of steels and other Fe-base alloys under expected WIPP conditions (see Brush, 1990). I am extending these thermodynamic calculations to support of the development of the reaction-path gas-generation model (see INTRODUCTION above).

R. E. Westerman and M. R. Telander of Pacific Northwest Laboratory (PNL) are carrying out laboratory studies of anoxic corrosion for the WIPP Project. So far, they have studied two heats each of the low-C steels ASTM A 366 and ASTM A 570 under inundated conditions (specimens immersed in Brine A) and humid conditions (specimens suspended above Brine A) with initially pure atmospheres of N_2, CO_2, and H_2S at low pressures (about 1 to 15 atm) at 30 ± 5°C. ASTM A 366 simulates the waste drums to be emplaced in the repository; ASTM A 570 simulates the boxes. Brine A is a synthetic brine that, although developed to simulate fluids equilibrated with K^+- and Mg^{2+}-bearing minerals in overlying potash-rich zones prior to entering the repository (Molecke, 1983), is coincidentally similar in composition to intergranular brines from the Salado Fm. at or near the stratigraphic horizon of the WIPP underground workings. Westerman and Telander have also conducted experiments with these steels under inundated conditions with initially pure N_2, CO_2, and H_2 at high pressures (about 35 or 70 atm). Finally, they have performed preliminary experiments with these steels in simulated backfill materials (crushed salt and a mixture of 70 wt % crushed salt and 30 wt % bentonite) at low pressures. Westerman and Telander also plan to study anoxic corrosion of Al and Al-base materials.

Telander and Westerman (in prep.) have identified three likely anoxic-corrosion reactions. At low fugacities (similar to partial pressures) of CO_2 and H_2S, the reaction observed in 3-, 6-, 12-, and 24-month experiments appears to be:

$$Fe + 2H_2O = Fe(OH)_2 + H_2. \qquad (6a)$$

However, Brush (1990) calculated that $Fe(OH)_2$ is unstable with respect to Fe_3O_4. Therefore, significant quantities of steels and other Fe-base alloys could eventually corrode via the reaction:

$$3Fe + 4H_2O = Fe_3O_4 + 4H_2. \qquad (6b)$$

At relatively high CO_2 fugacities, the experimentally observed reaction is:

$$Fe + H_2O + CO_2 = FeCO_3 + H_2. \quad (7)$$

Formation of the adherent corrosion product $FeCO_3$ (siderite) by this reaction will passivate steels and, presumably, other Fe-base alloys after the consumption of various quantities of CO_2. Currently, laboratory studies at PNL suggest a range of 0.33 to 2.2 moles of CO_2 per m^2 of steel for the amount of CO_2 required for passivation, depending on the CO_2 partial pressure and the pH of the brine. However, I do not recommend revision of the average-stoichiometry gas-generation model to include passivation. To avoid potential criticism, inclusion of this process would also necessitate the inclusion of depassivation, the simulation of which would require a reaction-path model such as the one Garner and I are developing.

Finally, at relatively high H_2S fugacities, the experimentally observed reaction appears to be:

$$Fe + 2H_2S = FeS_2 + 2H_2. \quad (8a)$$

Laboratory studies at PNL suggest that this reaction also passivates steels and other Fe-base alloys. However, I do not recommend revision of the average-stoichiometry model to include passivation by this reaction for the reasons given in connection with Equation 3 (above).

A literature review by Telander and Westerman (in prep.) and thermodynamic calculations for the reaction-path model have identified another possible reaction involving H_2S:

$$Fe + H_2S = FeS + H_2. \quad (8b)$$

The literature reviewed by Telander and Westerman (in prep.) suggests that this reaction does not passivate steels and other Fe-base alloys. Table 1 summarizes these anoxic-corrosion reactions.

In addition to these corrosion reactions, there exist numerous likely reactions among Fe-bearing corrosion products such as $Fe(OH)_2$, Fe_3O_4, $FeCO_3$, FeS, and FeS_2. Garner and I are incorporating these reactions in the reaction-path model to predict, among other things, if and when depassivation of steels will occur. I do not recommend revising the average-stoichiometry model to include reactions among corrosion products.

My best estimates of H_2-production and corrosion rates for anoxic corrosion of steels and other Fe-base alloys under inundated conditions are based on data reported by Telander and Westerman (in prep.) They obtained average H_2-production rates of 0.19, 0.21, 0.16, and 0.10 moles per m^2 of steel per year in experiments carried out under

inundated conditions with initially pure N_2 at low pressures (about 10 to 15 atm) for 3, 6, 12, and 24 months, respectively. Because there are 6 m^2 of steels and other Fe-base alloys per drum of CH TRU waste (Lappin et al., 1989), these rates are equivalent to 1.14, 1.26, 0.96, and 0.60 moles of H_2 per drum of CH TRU waste per year. The average corrosion rates in the 3-, 6-, 12-, and 24-month runs were 1.97, 1.72, 1.23, and 0.99 μm of steel per year. For my best estimates, I prefer values of 0.1 moles of H_2 per m^2 of steel per year or 0.6 moles of H_2 per drum of CH TRU waste per year and 1 μm of steel per year (see Table 2). These rates, from the 24-month experiments at PNL, are less by as much as about a factor of two than the rates observed in the 3-, 6-, and 12-month runs. Therefore, my best estimates are now half or about half those provided for the 1991 and 1992 PA calculations (Brush, 1991), 0.2 moles of H_2 per m^2 of steel per year, 1 mole of H_2 per drum of CH TRU waste per year, and 2 μm of steel per year, for which I used the 6-month results.

Strictly speaking, my best estimates of H_2-production and corrosion rates for anoxic corrosion of steels and other Fe-base alloys under inundated conditions (Table 2) pertain only to Reaction 6a, the reaction which apparently occurs with initially pure N_2 at low and high pressures. However, I arbitrarily assume that, at any given pH, Reactions 6b, 7, 8a, and 8b occur at the same rate as Reaction 6a. Therefore, my best estimates also apply to these reactions. Clearly, Reaction 7 proceeded much faster than Reaction 6a in low-pressure, inundated experiments at PNL, at least prior to passivation (below). However, this was probably because the pH of Brine A was much lower in runs with initially pure CO_2 at low pressures than in runs with initially pure N_2 at low pressures. I describe the effects of pH in the discussion of my maximum estimates for anoxic corrosion under inundated conditions (below).

My minimum estimates of H_2-production and corrosion rates for anoxic corrosion of steels and other Fe-base alloys under inundated conditions (Table 2) are based on passivation observed by Telander and Westerman (in prep.) in 6-, 12-, and 24-month, low-pressure (about 12 to 15 atm) experiments with initially pure CO_2. In these runs, the H_2-production and corrosion rates were high initially but decreased to 0 moles of H_2 per m^2 of steel per year or, 0 moles of H_2 per drum of CH TRU waste per year and 0 μm of steel per year after about 3 or 4 months due to passivation by Reaction 7 (above). Passivation at these pressures apparently required 0.33 moles of CO_2 per m^2 of steel, a very small quantity relative to the total microbial CO_2 production potential. My minimum estimates of these rates are identical to those provided for the 1991 and 1992 PA calculations (Brush, 1991). However, Telander and Westerman (in prep.) have now completed 12- and 24-month experiments, which confirm the results of the 6-month runs. Furthermore, since preparing their report, Westerman and Telander have also observed passivation in 6- and 12-month, high-pressure (about 36 to 40 atm) runs. These high-pressure tests partially address the concerns of those who claimed that high CO_2 partial pressures and concomitant acidification of brine would destabilize the passivating

film of $FeCO_3$ and restart anoxic corrosion and H_2 production. Experiments carried out to date suggest that these high CO_2 partial pressures increase the quantity of CO_2 required to passivate steels somewhat, from 0.33 to 2.2 moles per m^2 of steel. However, this requirement is still very small relative to the total microbial CO_2 production potential. On the other hand, these high CO_2 partial pressures apparently decrease the time required for passivation somewhat, from about 3 or 4 months to 2 months.

At least two other passivation mechanisms are possible. First, after a few days of H_2 production, Telander and Westerman (in prep.) have observed passivation of steels under inundated conditions with initially pure H_2S at low pressures (about 5 to 6 atm) for up to about 200 days. This is probably due to formation of the adherent corrosion product FeS_2 (pyrite) by Reaction 8a (above). Based on preliminary results obtained with the reaction-path model, Garner and I think that FeS_2 formation may be unlikely in WIPP disposal rooms. This is because H_2S fugacities high enough and CO_2 and H_2 fugacities low enough to stabilize FeS_2 may be unlikely, given expected stoichiometries for microbial gas-production reactions. Therefore, passivation by $FeCO_3$ appears more likely than passivation by FeS_2. However, the latter is still possible.

A second passivation mechanism is precipitation of salts on the surfaces of corroding metals due to the consumption of H_2O during anoxic corrosion (see Oxic Corrosion above).

The results of laboratory studies of anoxic corrosion at PNL demonstrate that passivation of steels, at least by $FeCO_3$, is a real phenomenon under at least some combinations of conditions expected in WIPP disposal rooms. However, based on preliminary results of modeling studies, Garner and I believe that depassivation of steels is also possible, especially if consumption of CO_2 by $Ca(OH)_2$ (in hydrated cementitious materials) and CaO (a potential backfill additive) decrease the fugacity of CO_2 below values required to stabilize $FeCO_3$. Nevertheless, minimum estimates of 0 moles of H_2 per m^2 of steel per year or 0 moles of H_2 per drum of CH TRU waste per year and 0 μm of steel per year seem justified at this time.

For my maximum estimates of H_2-production and corrosion rates for anoxic corrosion of steels and other Fe-base alloys under inundated conditions (Table 2), I estimated the effects of pH, pressure, and temperature on these rates. These H_2-production and corrosion rates are: (1) inversely proportional to pH; (2) proportional to the partial pressures of CO_2 and, probably, H_2S (both of these gases decrease the pH of any brine they are in contact with as their partial pressures increase); (3) proportional to the partial pressure of N_2 and hence the total pressure; (4) inversely proportional to the partial pressure of H_2; (5) probably proportional to temperature. I used estimated or experimentally measured relationships between these parameters and the H_2-production and corrosion rates, and estimates of the extreme values of these parameters in the repository after filling and sealing to

estimate the maximum values of these rates.

Telander and Westerman (in prep.) reported that the pH of Brine A, initially 6.7, increased to values of 8.3, 8.3, and 8.4 after the 6-, 12-, and 24-month, low-pressure experiments with initially pure N_2. (They did not report the pH of Brine A after the 3-month runs.) Therefore, the best estimates of these rates (Table 2) pertain to Reaction 6a at a neutral or nearly neutral pH. I expect that the pH in WIPP disposal rooms will vary between about 3 and 12. Although obtained for applications other than the WIPP Project, the results of Uhlig and Revie (1963) and Grauer et al. (1991) suggest that the H_2-production and corrosion rates for anoxic corrosion of steels are constant or essentially constant between a pH of about 4 and 10, that these rates are higher by about a factor of 50 at a pH of 3, and that they are lower by a factor of 0.05 at a pH of 11 and by a factor of 0.005 at a pH of 12. Therefore, the possibility of pH values as low as 3 in WIPP disposal rooms necessitates multiplying my best estimates in Table 2 by a factor of 50:

$$50 \cdot 0.10 \text{ moles/m}^2 = 5 \text{ moles/(m}^2 \cdot \text{yr)}; \tag{9a}$$

$$50 \cdot 0.60 \text{ moles/(drum} \cdot \text{yr)} = 30 \text{ moles/(drum} \cdot \text{yr)}; \tag{9b}$$

$$50 \cdot 1\ \mu\text{m/yr} = 50\ \mu\text{m/yr}. \tag{9c}$$

If acidification is caused by CO_2 or, perhaps, H_2S (see below), the increase in rates described above may only be temporary due to passivation of steels by $FeCO_3$ or, perhaps, FeS_2. However, organic acids produced by microbial degradation of cellulosics in the waste (below) could also acidify the brines in WIPP disposal rooms. These acids may not result in passivation of steels. The effects of basic conditions on anoxic corrosion need not be considered here because, although they decrease these rates, my minimum estimates are already 0 moles of H_2 per m^2 of steel per year or 0 moles of H_2 per drum of CH TRU waste per year and 0 μm of steel per year because of passivation (see above).

Based on the results of 6-month experiments, Telander and Westerman (in prep.) reported that an N_2 partial pressure of 73 atm increased the average corrosion rate of steels by about a factor of two from that observed at an N_2 partial pressure of 10 atm. Because 73 atm is about half of lithostatic pressure at the depth of the WIPP underground workings, I assume that total pressure (the effects of which should be equivalent to those of high N_2 partial pressure) could increase the H_2-production and corrosion rates for steels and other Fe-base alloys by as much as a factor of four. Therefore, the effect of lithostatic pressure on the rates estimated for the lowest pH expected in the repository necessitates multiplying the rates obtained from Equations

9a, 9b, and 9c by a factor of four:

$$4 \cdot 5 \text{ moles/m}^2 = 20 \text{ moles/(m}^2 \cdot \text{yr)}; \quad (10a)$$

$$4 \cdot 30 \text{ moles/(drum} \cdot \text{yr)} = 120 \text{ moles/(drum} \cdot \text{yr)}; \quad (10b)$$

$$4 \cdot 50\ \mu\text{m/yr} = 200\ \mu\text{m/yr}. \quad (10c)$$

High CO_2 and H_2S partial pressures should increase the H_2-production and corrosion rates for anoxic corrosion of steels and other Fe-base alloys under inundated conditions, at least prior to passivation, because the solubilities of these gases in aqueous solutions are proportional to their partial pressures and they form the weak, diprotic acids H_2CO_3 and H_2S after dissolution. Although weak, these acids do deprotonate to some extent, thus acidifying solutions in contact with these gases. However, I have already included the effects acidification on anoxic corrosion (see above).

The results of 6- and 12-month experiments carried out by Telander and Westerman (in prep.) suggest that H_2 partial pressures of 35, 69, and 70 atm decreased the average corrosion rate of steels by about a factor of five from that observed at the H_2 partial pressures in the low-pressure runs. High H_2 partial pressures have the opposite effect of high N_2 partial pressures (or total pressure) because H_2 is a product of Reactions 6a, 6b, 7, 8a, and 8b. The effects of high H_2 partial pressures on anoxic corrosion need not be addressed further because, although they decrease these rates, my minimum estimates are already 0 moles of H_2 per m^2 of steel per year or 0 moles of H_2 per drum of CH TRU waste per year and 0 μm of steel per year because of passivation.

Telander and Westerman (in prep.) have carried out all of their laboratory studies of anoxic corrosion at 30 ± 5°C. I assume that the temperature during their experiments was normally distributed about a value of 30°C. Therefore, their average rates pertain to this temperature. I also assume a temperature of 30 ± 3°C in WIPP disposal rooms after filling and sealing. This is slightly above the in situ temperature of 27°C at a subsurface depth of 2,150 feet because of the small amount of heat produced by RH TRU waste and, to a much lesser extent, by CH TRU waste. Finally, I assume that a 10°C increase in temperature would increase the rates of Reactions 6a, 6b, 7, 8a, and 8b by a factor of two. Therefore, the effect of a temperature of 33°C on the rates estimated for the lowest pH and highest total pressure expected in the repository, based on experiments carried out at 30 ± 5°C, requires multiplying the rates obtained from Equations 10a, 10b, and 10c by a factor of 1.23 (obtained from $2^{((33 - 30)/10)}$):

$$1.23 \cdot 20 \text{ moles}/(m^2 \cdot yr) = 20 \text{ moles}/(m^2 \cdot yr); \quad (11a)$$

$$1.23 \cdot 120 \text{ moles}/(\text{drum} \cdot yr) = 100 \text{ moles}/(\text{drum} \cdot yr); \quad (11b)$$

$$1.23 \cdot 200 \ \mu m/yr = 200 \ \mu m/yr. \quad (11c)$$

These are my maximum estimates, rounded to one significant figure, of these rates under inundated conditions (Table 2). They are significantly higher than those provided for the 1991 and 1992 PA calculations (Brush, 1991), 0.4 moles of H_2 per m^2 of steel per year or 2 moles of H_2 per drum of CH TRU waste per year and 3 μm of steel per year, because the combined effects of pH, high N_2 partial pressure or total pressure, and temperature have a much greater effect on these rates than high N_2 partial pressure, the only factor I included in my previous estimates of the maximum rates under inundated conditions.

My best estimates of H_2-production and corrosion rates for anoxic corrosion of steels and other Fe-base alloys under humid conditions are 0 moles of H_2 per m^2 of steel per year or 0 moles of H_2 per drum of CH TRU waste per year and 0 μm of steel per year (Table 3). These rates are less than those provided for the 1991 and 1992 PA calculations (Brush, 1991), 0.02 moles of H_2 per m^2 of steel per year or 0.1 moles of H_2 per drum of CH TRU waste per year and 0.2 μm of steel per year, which I arbitrarily assumed were one tenth of the best estimates provided at that time for inundated conditions. As of 1991, no H_2 production or corrosion had occurred in 3- and 6-month humid, low-pressure experiments with initially pure N_2 or CO_2, except for very limited H_2 production due to corrosion of some of the bottom 10% of the specimens splashed with brine during pretest preparation procedures. Since then, Telander and Westerman (in prep.) have obtained identical results from 6- and 12-month runs. These results confirm and extend the results of the 3- and 6-month runs. Therefore, I have reduced my best estimates as described above.

My minimum estimates of H_2-production and corrosion rates for anoxic corrosion of steels and other Fe-base alloys under humid conditions are also 0 moles of H_2 per m^2 of steel per year or 0 moles of H_2 per drum of CH TRU waste per year and 0 μm of steel per year (Table 3). These minimum estimates are identical to those provided for the 1991 and 1992 PA calculations (Brush, 1991).

My arbitrary maximum estimates of H_2-production and corrosion rates for anoxic corrosion of steels and other Fe-base alloys under humid conditions are 0.01 moles of H_2 per m^2 of steel per year or 0.06 moles of H_2 per drum of CH TRU waste per year and 0.1 μm of steel per year (Table 3). I arbitrarily assume that these rates are one tenth of my current best estimates for anoxic corrosion under inundated conditions. My maximum estimates for humid conditions are less than those provided for the 1991 and 1992 PA calculations (Brush, 1991), 0.2 moles of H_2

per m^2 of steel per year, 1 mole of H_2 per drum of CH TRU waste per year, and 2 μm of steel per year, which I arbitrarily assumed were identical to the best estimates provided at that time for inundated conditions.

If anoxic-corrosion rates under humid conditions significantly affect the behavior of the repository, additional laboratory studies will be necessary to replace these arbitrary estimates with actual experimental results.

MICROBIAL ACTIVITY

Microbial degradation of cellulosics and, perhaps, plastics and rubbers in the waste to be emplaced in WIPP disposal rooms may, if sufficient brine or H_2O vapor, nutrients, and viable microorganisms are present, produce or consume significant quantities of various gases and produce or consume significant quantities of H_2O (Lappin et al., 1989; Brush, 1990). The gases produced could include CO_2, CH_4, H_2S, N_2, and NH_3; the gases consumed could include CO_2, H_2 and O_2.

Brush (1990) applied the conceptual model of sequential usage of electron acceptors by microorganisms in natural environments (see, for example, Froelich et al., 1979; Berner, 1980) to WIPP disposal rooms. In natural environments, the observed sequence is aerobic respiration, NO_3^- reduction, reduction of Mn(IV) oxides and and hydroxides, reduction of Fe(III) oxides and and hydroxides, SO_4^{2-} reduction, and methanogenesis. Alternatively, reduction of Mn(IV) oxides and hydroxides may precede NO_3^- reduction. Based on which potential electron acceptors will be present in significant quantities in the repository after filling and sealing, I concluded that denitrification, SO_4^{2-} reduction, fermentation, and methanogenesis are potentially significant microbial processes (see Brush, 1990).

A. J. Francis and J. B. Gillow of Brookhaven National Laboratory (BNL) are carrying out laboratory studies of microbial gas production for the WIPP Project. Currently, they are conducting short- and long-term (up to 24-month) studies of microbial degradation of papers under inundated conditions with and without addition of electron acceptors and bentonite, amendment with nutrients, and inoculation with halophilic microorganisms from the WIPP Site and vicinity. They are also planning similar experiments under humid conditions and experiments with other potential substrates such as irradiated and unirradiated plastics and rubbers.

Aerobic Microbial Activity

I concluded that aerobic microbial activity will not affect the gas and H_2O budgets of WIPP disposal rooms directly (see Brush, 1990). However, this process could affect the O_2 budget of the repository significantly. The O_2 budget will in turn affect the chemical behavior

of the repository (see Oxic Corrosion above). Furthermore, Francis and Gillow (in prep.) have observed significant aerobic microbial activity. Therefore, Garner and I have added it to the reaction-path gas-generation model.

During aerobic microbial activity (or any other microbial process) the degradation of organic matter is complex and involves several intermediate steps usually mediated by different microorganisms. Geochemists have described microbial processes by writing simplified overall equations. Berner (1980) used the following equation to represent aerobic microbial activity:

$$CH_2O + O_2 = H_2O + CO_2. \tag{12}$$

This equation uses the formula CH_2O (a simplified formula for glucose) to represent the substrate (mainly papers and other cellulosics in the case of the WIPP) and does not include the synthesis of cellular material (biomass) by microorganisms. These approximations are certainly adequate for the average-stoichiometry gas-generation model, but may not be for the reaction-path model.

Anaerobic Microbial Activity

I also concluded that microbial denitrification could significantly affect the gas and H_2O budgets of WIPP disposal rooms (see Brush, 1990). Furthermore, Francis and Gillow (in prep.) have observed production of significant quantities of N_2O, a precursor of N_2 and an indicator of denitrification. According to Berner (1980), the overall equation for denitrification is:

$$CH_2O + 0.8H^+ + 0.8NO_3^- = 1.4H_2O + CO_2 + 0.4N_2. \tag{13}$$

Microbial reduction of Fe(III) oxides and hydroxides will not affect on the gas and H_2O budgets of WIPP disposal rooms significantly (Brush, 1990). However, Fe(III) reduction could affect the O_2 budget, which will in turn affect the chemical behavior of the repository (see Oxic Corrosion). Therefore, Garner and I added five possible Fe(III)-reduction reactions to the reaction-path model:

$$CH_2O + 4FeO(OH) + H_2O = 4Fe(OH)_2 + CO_2 \tag{14a}$$

$$CH_2O + 4FeO(OH) = 1.33Fe_3O_4 + 1.67H_2O + CO_2 + 1.33H_2 \tag{14b}$$

$$CH_2O + 4FeO(OH) + H_2O + 3CO_2 = 4FeCO_3 + 4H_2O \tag{14c}$$

$$CH_2O + 4FeO(OH) + 4H_2S = 4FeS + 7H_2O + CO_2 \quad (14d)$$

$$CH_2O + 4FeO(OH) + 8H_2S = 4FeS_2 + 7H_2O + CO_2 + 4H_2 \quad (14e)$$

Finally, microbial SO_4^{2-} reduction could affect the repository gas and H_2O budgets significantly (Brush, 1990). Francis and Gillow (in prep.) have not analyzed for H_2S, a product of SO_4^{2-} reduction. However, they have observed blackening, an indicator of SO_4^{2-} reduction, in some of their experiments. Berner (1980) gave the following overall equation for SO_4^{2-} reduction:

$$CH_2O + H^+ + 0.5SO_4^{2-} = H_2O + CO_2 + 0.5\ H_2S. \quad (15)$$

Finally, Brush (1990) concluded that microbial fermentation and methanogenesis could significantly affect the gas and H_2O budgets of WIPP disposal rooms. Francis and Gillow (in prep.) have not analyzed for CH_4, a product of methanogenesis. However, it would be almost impossible to rule out methanogenesis in the repository if other microbial processes are expected. Berner's (1980) overall equation for methanogenesis is:

$$2CH_2O = CH_4 + CO_2. \quad (16a)$$

However, the simultaneous presence of CO_2 and H_2 in the repository could facilitate the following reaction proposed by Francis and Gillow (in prep.):

$$CO_2 + 4H_2 = CH_4 + 2H_2O. \quad (16b)$$

Garner and I will include both of these equations in the reaction-path model and will probably use Equation 16b whenever both CO_2 and H_2 are present.

Francis and Gillow (in prep.) observed aerobic respiration, denitrification, and SO_4^{2-} reduction in their long-term study of microbial degradation of papers under inundated conditions. So far, the gas-production rates observed in these experiments have all been within the range estimated by Brush (1991) for the 1991 and 1992 PA calculations. There is probably no justification, at least on the basis of the results obtained by Francis and Gillow to date, for reducing the previously-estimated range. On the other hand, there is certainly no justification for extending it. Therefore, I recommend using the previously-provided rates again. My best estimate of the <u>total</u> microbial gas production rates from <u>all</u> of the processes

described in Reactions 12 through 16a (above) under inundated conditions is 0.1 moles of gas (CO_2, CH_4, H_2S and N_2) per kg of cellulosics per year. There are 10 kg of cellulosics per drum of CH TRU waste (Brush, 1990). (These values do not include any cellulosics in RH TRU waste.) Therefore, this rate is equivalent to 1 mole of gas per drum of CH TRU waste per year. My minimum estimate for inundated conditions is 0 moles of gas per kg of cellulosics per year or 0 moles of gas per drum of CH TRU waste per year. My maximum estimate is 0.5 moles of gas per kg of cellulosics per year or 5 moles of gas per drum of CH TRU waste per year.

Methanogenesis by Reaction 16b could consume significant quantities of CO_2 and especially H_2. Francis and Gillow (in prep.) have not observed this reaction yet. However, if it occurs under expected WIPP conditions, this reaction could consume a significant fraction of the CO_2 produced by microbial activity, the H_2 produced by anoxic corrosion, or even both, depending on the ratio of CO_2 to H_2O in the repository and the extent to which it proceeds. I have not estimated rates for this reaction yet. Predictions of the effects of this methanogenic reaction on the gas and H_2O budgets of the repository will require measurements of its rates of gas consumption under expected WIPP conditions and its incorporation in the reaction-path model Garner and I are developing. However, it may be possible to estimate the rate of Reaction 16b from studies carried out for application other than the WIPP Project.

Because Francis and Gillow (in prep.) have not reported any results for humid conditions yet, I recommend using the same microbial gas-production rates provided for the 1991 and 1992 PA calculations (Brush, 1991). My arbitrary best estimate of the total microbial gas production rates from all of the processes described in Reactions 12 through 16a (above) under humid conditions is 0.01 moles of gas per kg of cellulosics per year or 0.1 moles of gas per drum of CH TRU waste per year. My arbitrary minimum estimate for humid conditions is 0 moles of gas per kg of cellulosics per year or 0 moles of gas per drum of CH TRU waste per year. My arbitrary maximum estimate is 0.1 mole of gas per kg of cellulosics per year or 1 mole of gas per drum of CH TRU waste per year. I have not estimated any rates for methanogenesis by Reaction 16b yet.

Francis and Gillow are now carrying out laboratory studies of microbial gas production under conditions at BNL. Results from these studies will eventually replace these arbitrary estimates.

RADIOLYSIS

The rates of gas production from radiolysis of H_2O in brine and sludges in WIPP disposal rooms and radiolysis of cellulosics, plastics and rubbers in the waste will probably be significantly less than those expected from anoxic corrosion or microbial activity (Molecke, 1979;

Brush, 1990). However, even if these radiolytic gas-production rates are low, Garner and I will include radiolysis in the reaction-path gas-generation model we are developing to: (1) determine if, in the event that the rates and quantities of gas produced by anoxic corrosion and microbial activity turn out to be smaller than expected, radiolysis is still a minor gas-production mechanism; (2) predict the O_2 budget of the repository (see Oxic Corrosion above).

D. T. Reed and S. Okajima of Argonne National Laboratory (ANL) have quantified gas production from α radiolysis of WIPP brines as a function of dissolved ^{239}Pu concentration and brine composition. It is possible to use their results to calculate gas-production rates for other Pu isotopes, particulate Pu in contact with brine (colloids suspended in brine, undissolved particles in the waste, and precipitated particles), and other actinide elements dissolved, suspended, or otherwise in contact with brine. However, I did not have time to do so prior to submission of these estimates to PA. Instead, I considered only dissolved ^{239}Pu. I am currently gathering the information required to extend these calculations to include other Pu isotopes, particulate Pu, and important isotopes of other actinide elements. Eventually, Garner and I may include some or all of these other factors in the reaction-path model.

Reed and Okajima (in prep.) have observed H_2 production, but not O_2 production, from brine radiolysis in experiments carried out with ^{239}Pu. Recently, they have observed production of both H_2 and O_2 in runs conducted with ^{238}Pu. These studies and previous laboratory studies reviewed by Reed and Okajima (in prep.) suggest that, given sufficiently high absorbed doses, the O_2 production rate eventually approaches 50% that of H_2 in both pure H_2O and brines. Strictly speaking, O_2 is not a direct product of the radiolytic decomposition of H_2O. Instead, O_2 forms by the breakdown of O-containing intermediate species, such as H_2O_2 in pure H_2O and, possibly, ClO_3^- (chlorate) or ClO_4^- (perchlorate) in brines. On the other hand, it is possible that these intermediate species will react with electron donors (reductants), such as steels, other Fe-base alloys, other metals, or organic matter, before they produce significant O_2. However, to simplify brine radiolysis for the reaction-path model, Garner and I are using the equation:

$$H_2O = H_2 + 0.5O_2. \qquad (17)$$

Initially, we will assume that this process produces O_2 immediately. We may include a realistic induction period to account for the necessary build-up of O-containing intermediate species once the laboratory studies under way at ANL quantify the absorbed dose required to initiate O_2 production. We will then be able to calculate the time required to attain this dose as a function of the dissolved and suspended concentrations of radionuclides in WIPP brines. Until these results become available, the reaction-path model may overestimate the

time required for the repository to become anoxic and overestimate the proportion of the waste that remains oxic in microenvironments in which brine radiolysis is the predominant redox-determining process.

Reed and Okajima (in prep.) reported $G(H_2)$ values of 1.1 to 1.4 molecules per 100 eV for Brine A and ERDA-6, two synthetic WIPP brines, and DH-36 and G-Seep, two brines collected from the WIPP underground workings. The observed $G(H_2)$ values are independent of the dissolved ^{239}Pu concentration in these experiments. Garner and I plan to use units of moles of H_2, O_2, or H_2 plus O_2 per m^3 of brine per year in the reaction-path model. Therefore, I converted the results of Reed and Okajima (in prep.) from units of molecules per 100 eV to units of moles per m^3 of brine as follows.

For a dissolved ^{239}Pu concentration of 1 M, there are $2.39 \cdot 10^2$ g of ^{239}Pu per L of brine. The current estimate of the quantity of Pu to be emplaced in WIPP disposal rooms and the quantities of brine expected in the repository imply that there will not be enough Pu present to support an <u>average</u> Pu concentration of 1 M (see below). However, a <u>local</u> Pu concentration of 1 M may be possible in microenvironments in which Pu is highly soluble. Because there are $1 \cdot 10^3$ L of brine per m^3 of brine, the mass of ^{239}Pu per m^3 of brine is:

$$2.39 \cdot 10^2 \text{ g/L} \cdot 1 \cdot 10^3 \text{ L/m}^3 = 2.39 \cdot 10^5 \text{ g/m}^3. \qquad (18)$$

(Only two of the figures in this and the following equations are significant, but I did not round off until the end of these calculations.) The activity of ^{239}Pu per m^3 of brine is:

$$2.39 \cdot 10^5 \text{ g/m}^3 \cdot 0.0613 \text{ Ci/g} = 1.46507 \cdot 10^4 \text{ Ci/m}^3). \qquad (19)$$

In Equation 19, "0.0613 Ci/g" is the specific activity of ^{239}Pu. The disintegration rate of ^{239}Pu per m^3 of brine is:

$$1.46507 \cdot 10^4 \text{ Ci/m}^3 \cdot 3.7 \cdot 10^{10} \text{ (d/s)/Ci}$$
$$= 5.42076 \cdot 10^{14} \text{ d/(m}^3 \cdot \text{s)}. \qquad (20)$$

In Equation 20, "d" is the abbreviation for "disintegrations," not "days!" The energy-deposition rate per m^3 of brine is:

$$5.42076 \cdot 10^{14} \text{ d/(m}^3 \cdot \text{s)} \cdot 5.15 \text{ MeV/d}$$
$$= 2.79169 \cdot 10^{15} \text{ MeV/(m}^3 \cdot \text{s)}. \qquad (21)$$

In Equation 21, "5.15 MeV/d" is the average energy of an α particle emitted during the disintegration of ^{239}Pu. Changing units gives:

$$2.79169 \cdot 10^{15}\ \mathrm{MeV/(m^3 \cdot s)} \cdot 1 \cdot 10^{6}\ \mathrm{eV/MeV} \cdot 3.15576 \cdot 10^{7}\ \mathrm{s/yr}$$

$$= 8.80991 \cdot 10^{28}\ \mathrm{eV/(m^3 \cdot yr)}. \qquad (22)$$

I used a value of 1.25 molecules per 100 eV for $G(H_2)$ (the midpoint of the range of 1.1 to 1.4 molecules per 100 eV reported by Reed and Okajima (in prep.) for Brine A, ERDA-6, DH-36, and G-Seep) to calculate the number of molecules of H_2 produced per m^3 of brine per year:

$$8.80991 \cdot 10^{28}\ \mathrm{eV/(m^3 \cdot yr)} \cdot 1.25 \cdot 10^{-2}\ \mathrm{molecules/eV}$$

$$= 1.10124 \cdot 10^{27}\ \mathrm{molecules/(m^3 \cdot yr)}. \qquad (23)$$

The number of moles of H_2 produced per m^3 of brine per year is:

$$1.10124 \cdot 10^{27}\ \mathrm{molecules/(m^3 \cdot yr)} \ / \ 6.0225 \cdot 10^{23}\ \mathrm{molecules/mole}$$

$$= 1.8 \cdot 10^{3}\ \mathrm{moles/(m^3 \cdot yr)}. \qquad (24)$$

In Equation 24, "$6.0225 \cdot 10^{23}$ molecules/mole is Avogadro's number. Of course, "$1.8 \cdot 10^{3}$ moles/(m^3 · yr)" is actually the midpoint of a range of 1.6 to $2.0 \cdot 10^{3}$ moles/(m^3 · yr).

I repeated these calculations for dissolved ^{239}Pu concentrations of $1 \cdot 10^{-1}$, $1 \cdot 10^{-2}$, $1 \cdot 10^{-3}$, $1 \cdot 10^{-4}$, $1 \cdot 10^{-5}$, $1 \cdot 10^{-6}$, $1 \cdot 10^{-7}$, $1 \cdot 10^{-8}$, and $1 \cdot 10^{-9}$ M (see Table 4). Again, the quantity of Pu to be emplaced in WIPP disposal rooms and the quantities of brine expected in the repository imply that there will not be enough Pu present to support some of these <u>average</u> Pu concentrations (see below). I calculated O_2-production rates for the same dissolved ^{239}Pu concentrations in these brines by assuming a value of 0.625 molecules per 100 eV for $G(O_2)$ (half the midpoint of the observed range for $G(H_2)$) and neglecting the induction period for O_2 production from the breakdown of O-containing intermediate species (Table 4). (Bear in mind that O-containing intermediate species may react with electron donors in WIPP disposal rooms before they produce significant O_2.) Finally, I calculated total radiolytic gas-production rates by adding the H_2- and O_2-production rates (Table 4).

I converted these rates from units of moles of H_2, O_2, and H_2 plus O_2 per m^3 of brine per year to units of H_2, O_2, and H_2 plus O_2 per equivalent drum of CH TRU waste per year to compare them with the rates of gas production from anoxic corrosion and microbial activity. I

multiplied each of the rates in Table 4 by 135, 305, 525, or 815 m^3 of brine per WIPP disposal room to convert them to units of moles of H_2, O_2, and H_2 plus O_2 per room per year. B. M. Butcher used these estimates of the residual gas-accessible void volume in a WIPP disposal room and immediate vicinity for his recent calculations of gas-storage capacities. I then assumed that these volumes could become inundated. Of course, brine volumes less than 135 m^3 are entirely possible. Next, I divided Butcher's volumes by 6,800 drums of CH TRU waste per room to obtain units of moles of H_2, O_2, and H_2 plus O_2 per drum per year. Tables 5, 6, and 7 give these rates for H_2, O_2, and H_2 plus O_2, respectively.

To calculate the maximum <u>average</u> Pu concentrations as a function of brine volume and time (Table 8), I used the quantities of brine required to saturate the residual gas-accessible void volume in a WIPP disposal room (see above) and referred to the PA code DECAY to obtain the initial Pu inventory and decay predictions used for the most recent PA calculations (WIPP Performance Assessment Department, 1992). (PA personnel will also use this inventory for the round of calculations to be presented to the EPA in February 1994.) At each time (0, 100, 200, 500, 1,000, 2,000, 5,000, and 10,000 years), I added the quantities of ^{238}Pu, ^{239}Pu, ^{240}Pu, ^{241}Pu, ^{242}Pu, and ^{244}Pu present in both CH and RH TRU waste in the column labeled "Scaled Inventory" in the output files from the PA code DECAY. "Scaled inventory" refers to the quantity of Pu (or other) isotopes present in one WIPP disposal panel. I then divided these sums by 12.65, the number of equivalent WIPP disposal rooms in one panel. Next, I calculated the percentage of each isotope of Pu present at each time and calculated the average molecular weight of Pu at that time. I assumed that the molecular weight of each isotope has an integral value equal to its mass number. I then divided the total mass of Pu by 135,000, 305,000, 525,000, or 815,000 L, the quantities of brine present in 135, 305, 525, or 815 m^3 of brine, respectively. Finally, I divided the results by the average molecular weight of Pu at that time to obtain the concentrations shown in Table 8.

Clearly, both the dissolved ^{239}Pu and the volume of brine to which this concentration pertain will strongly affect the H_2-, O_2-, and H_2-plus O_2-production rates from brine radiolysis. If the dissolved ^{239}Pu concentration is low enough, these gas-production rates are obviously insignificant (see Tables 5, 6, and 7). On the other hand, if the dissolved ^{239}Pu concentration and the ^{239}Pu inventory are high enough, these gas-production rates can equal or even exceed those of anoxic corrosion and microbial activity, at least locally. Given a range of 135 to 815 m^3 of brine per room, the range of Pu solubilities and the Pu inventory assumed for WIPP disposal rooms will determine the range of radiolytic gas-production rates.

For my best estimates of the rates of gas production from brine radiolysis, I chose $6.0 \cdot 10^{-10}$ M, the midpoint of the range of Pu(V) solubilities estimated by the Radionuclide-Source-Term Expert Panel (Trauth et al., 1992). (The Expert Panel also estimated the same

midpoint for the range of Pu(IV) solubilities.) For ^{239}Pu, this dissolved concentration yields rates of $1.1 \cdot 10^{-6}$ moles of H_2 per m^3 per year, $5.4 \cdot 10^{-7}$ moles of O_2 per m^3 per year, and $1.6 \cdot 10^{-6}$ moles of H_2 plus O_2 per m^3 per year, equivalent to rates of $6.6 \cdot 10^{-8}$ moles of H_2 per drum per year, $3.3 \cdot 10^{-8}$ moles of O_2 per drum per year, and $9.9 \cdot 10^{-8}$ moles of H_2 plus O_2 per drum per year (Table 2). To convert from units of moles per m^3 per year to moles per drum per year, I used the average of the rates for 305 and 525 m^3 of brine per room in Tables 5, 6, and 7.

For my minimum estimates of the rates of gas production from brine radiolysis, I used the lower limit of the range of Pu solubilities estimated by the Expert Panel and 135 m^3, the lower limit of the range of residual gas-accessible void volume expected in a WIPP disposal room. (Of course, there could be less than 135 m^3 of brine in a room.) The Expert Panel estimated that, for expected repository conditions, the lower limit of the range of Pu solubilities is $2.5 \cdot 10^{-17}$ M, the value estimated for Pu(V). For ^{239}Pu, this dissolved concentration yields rates of $4.5 \cdot 10^{-14}$ moles of H_2 per m^3 per year, $2.2 \cdot 10^{-14}$ moles of O_2 per m^3 per year, and $6.7 \cdot 10^{-14}$ moles of H_2 plus O_2 per m^3 per year, equivalent to rates of $8.9 \cdot 10^{-16}$ moles of H_2 per drum per year, $4.5 \cdot 10^{-16}$ moles of O_2 per drum per year, and $1.3 \cdot 10^{-15}$ moles of H_2 plus O_2 per drum per year (Table 2).

It may be more difficult to defend estimates of the maximum rates of gas production from brine radiolysis. The Expert Panel estimated that the upper limit of the range of ~~Pu~~ solubilities is $5.5 \cdot 10^{-4}$ M, the value estimated for Pu(V). Assuming that all of the Pu present is $^{239}Pu(V)$, this estimate and 815 m^3 of brine per room (the upper limit of the range of residual gas-accessible void volume) yield upper limits of $9.9 \cdot 10^{-1}$ moles of H_2 per m^3 of brine per year, $5.0 \cdot 10^{-1}$ moles of O_2 per m^3 per year, and $1.5 \cdot 10^{0}$ moles of H_2 plus O_2 per m^3 per year (Table 2). Again, the current estimate of the quantity of Pu to be emplaced in the repository and 815 m^3 of brine per WIPP disposal room imply that there will not be enough Pu present to support an <u>average</u> Pu concentration of $5.5 \cdot 10^{-4}$ M (see above). These rates are equivalent to $1.2 \cdot 10^{-1}$ moles of H_2 per drum of CH TRU waste per year, $6.0 \cdot 10^{-2}$ moles of O_2 per drum per year, and $1.8 \cdot 10^{-1}$ moles of H_2 plus O_2 per drum per year (Table 2). These are my favorite estimates of the maximum gas-production rates from brine radiolysis. I like them because the Expert Panel is responsible for defending $5.5 \cdot 10^{-4}$ M as the upper limit of the range of Pu solubilities. A reasonable way to estimate the probability distribution for values within the range of gas-production rates from brine radiolysis is to assume the same probability distribution estimated by the Expert Panel for Pu(V) solubilities.

However, I believe that $5.5 \cdot 10^{-4}$ M may not be a defensible upper limit of the range of Pu solubilities. Pu(III) is probably more soluble than Pu(IV) and Pu(V), the only oxidation states for which the Expert Panel estimated solubilities. Furthermore, Pu(VI) could well turn out to be more soluble than Pu(III)! Presumably, the Expert Panel

did not estimate solubilities of Pu(III) and Pu(VI) because it accepted the hypothesis that Pu(III) and Pu(VI) will be unstable with respect to Pu(IV) and Pu(V) in WIPP disposal rooms and that Pu(IV) and Pu(V) will thus control the solubility of Pu. This hypothesis may be impossible to defend given the results of laboratory studies by Reed and Okajima (in prep.) in which Pu(VI) remained stable in WIPP brines for lengthy periods. They observed that Pu(VI) is the predominant form of Pu in Brine A and G Seep during stability experiments carried out for periods of over 300 and 400 days. (Stability runs are necessary to demonstrate that Pu remains in solution during an experiment to quantify gas production by brine radiolysis.) Reed and Okajima (in prep.) observed dissolved Pu(VI) concentrations on the order of 10^{-3} and 10^{-4} M in Brine A and G Seep during 300- and 400-day stability runs. Furthermore, they observed a Pu(VI) concentration of $2 \cdot 10^{-2}$ M in G Seep during an 80- or 90-day stability run. Because these experiments did not contain high concentrations of the inorganic ligand CO_3^{2-}, which could significantly increase both the stability and the solubility of Pu(VI), or any organic ligands, which could also increase the stability and solubility of Pu(VI), the results are clearly not worst-case. Nevertheless, ^{239}Pu concentrations on the order of 10^{-2} M would, if the inventory of ^{239}Pu were high enough, imply upper limits of the ranges of gas-production rates from brine radiolysis on the order of 10^1 moles of H_2, O_2, and H_2 plus O_2 per m^3 of brine per year (see Table 4) or 10^0 moles of H_2, O_2, and H_2 plus O_2 per drum of CH TRU waste per year (Tables 5, 6, and 7). These rates are similar to those expected from anoxic corrosion and microbial activity under inundated conditions.

If a significant fraction of Pu in WIPP disposal rooms is actually present as Pu(VI), its chemical behavior would probably be similar to that of its oxidation-state analog U(VI). G. R. Choppin observed dissolved U(VI) concentrations of about $1 \cdot 10^{-4}$ M in approximately 600-day dissolution experiments in Brine A at a pH of about 8 and $2 \cdot 10^{-3}$ M in 250-day precipitation runs under the same conditions at Florida State University. (Dissolution and precipitation experiments, also referred to as undersaturation and supersaturation runs, bracket the solubility by approaching equilibrium from opposite directions.) These results are similar to those of the ANL stability runs. Even worse, the Expert Panel's estimate of $1.0 \cdot 10^0$ M for the upper limit of the range of the solubility of U(VI) could apply to Pu(VI) as well. This would, if the inventory of ^{239}Pu were high enough, imply upper limits of the ranges of gas-production rates from brine radiolysis on the order of 10^3 moles of H_2, O_2, and H_2 plus O_2 per m^3 of brine per year (Table 4) or 10^2 moles of H_2, O_2, and H_2 plus O_2 per drum of CH TRU waste per year (Tables 5, 6, and 7). These rates are much higher than those expected from anoxic corrosion and microbial activity under inundated conditions.

Similarly, if a significant fraction of Pu is present as Pu(III), the Expert Panel's estimate of $1.4 \cdot 10^0$ M for the upper limit of the range of the solubilities of Am(III) and Cm(III) could apply to Pu(III). This would also imply very high upper limits of the ranges of

gas-production rates from brine radiolysis.

It is important to point out that such high solubilities may not persist indefinitely. For example, H. Nitsche of Lawrence Berkeley Laboratory observed dissolved Pu concentrations between about $1 \cdot 10^{-4}$ and $1 \cdot 10^{-3}$ M for over 1 year in a precipitation experiment started with initially pure Pu(VI) in Brine A at a pH of about 7. However, after about 400 days, the concentration of Pu dropped to between $1 \cdot 10^{-7}$ and $1 \cdot 10^{-6}$ M. This suggests that Pu(VI) may be unstable with respect to other, less soluble oxidation states and that, given enough time, the solubility of Pu will decrease to the ranges estimated by the Expert Panel for Pu(IV) and Pu(V). Therefore, it would probably be difficult at this time to defend upper limits of the ranges of gas-production rates from brine radiolysis based on a dissolved Pu(VI) concentration of $2 \cdot 10^{-2}$ M observed by Reed and Okajima (in prep.) during an 80- or 90-day stability experiment. It might even be difficult to defend upper limits based on Pu(VI) concentrations on the order of 10^{-4} or 10^{-3} M in several-hundred-day solubility or stability runs. These are the maximum <u>average</u> Pu concentrations that can be supported by the current inventory (see Table 8). Furthermore, even if Pu is highly soluble under some combinations of conditions in WIPP disposal rooms, brine radiolysis would, like anoxic corrosion, probably be self-limiting. This is because neither anoxic corrosion nor brine radiolysis seems to occur under humid conditions. Therefore, small quantities of brine in the repository may produce H_2 (in the case of anoxic corrosion) or H_2 and O_2 (in the case of brine radiolysis), increase the pressure, prevent additional brine inflow or even cause brine outflow, and thus prevent or greatly reduce additional gas production, at least by these mechanisms. However, I still feel that it may be difficult to rule out the possibility of very high (relative to anoxic corrosion and microbial activity) upper limits of the ranges of gas-production rates from brine radiolysis, at least in some microenvironments with high Pu solubilities. Furthermore, if the <u>average</u> Pu solubility turns out to be high, increasing the <u>quantity</u> of Pu to be emplaced in WIPP disposal rooms could significantly affect the gas budget of the repository, and perhaps its performance.

I calculated the gas-production potential for radiolysis of H_2O in brine by ^{239}Pu as follows. According to the initial Pu inventory and decay predictions used for the most recent PA calculations (WIPP Performance Assessment Department, 1992), there will be 568,600 g of ^{239}Pu in CH TRU waste and 14,280 g of ^{239}Pu in RH TRU waste per WIPP disposal panel at the time of emplacement. After 10,000 years, there will be 426,300 g of ^{239}Pu in CH TRU waste and 10,710 g of ^{239}Pu in RH TRU waste per panel. The mass of ^{239}Pu in one panel that will decay during the 10,000-year period of performance of the repository is:

$$(568{,}600 \text{ g} + 14{,}280 \text{ g}) - (426{,}300 \text{ g} + 10{,}710 \text{ g}) = 145{,}870 \text{ g}. \quad (25)$$

(I do not know how many of the figures in this and the following

equations are significant, but I suspect not more than one!) The mass of ^{239}Pu in an equivalent drum of CH TRU waste that will decay in 10,000 years is:

$$145{,}870 \text{ g/panel} / 86{,}000 \text{ drums/panel} = 1.69616 \text{ g/drum}. \quad (26)$$

I have included the ^{239}Pu in RH TRU waste in an "equivalent drum of CH TRU waste" for the sake of completeness, but this only increases the mass of ^{239}Pu per drum by about 2.5%! The number of ^{239}Pu disintegrations per drum in 10,000 years will be:

$$1.69616 \text{ g/drum} / 239 \text{ g/mole} \cdot 6.0225 \cdot 10^{23} \text{ d/mole}$$

$$= 4.27411 \cdot 10^{21} \text{ d}. \quad (27)$$

Assuming that all of the Pu in a drum dissolves in brine at the time of emplacement and remains dissolved throughout the 10,000-year period of performance of the repository is the worst-case assumption from the standpoint of radiolytic gas production. This assumption results in initial dissolved total Pu concentrations of $1.60 \cdot 10^{-3}$, $7.09 \cdot 10^{-4}$, $4.12 \cdot 10^{-4}$, or $2.65 \cdot 10^{-4}$, depending on the volume of brine per WIPP disposal room (see Table 8). Half of these values are higher than $5.5 \cdot 10^{-4}$ M, the upper limit of the range of Pu solubilities estimated by the Expert Panel. However, the laboratory studies of radionuclide chemistry described above have yielded dissolved Pu(VI) concentrations higher than $1.60 \cdot 10^{-3}$ M, at least so far. The total quantity of energy deposited in brine by decay of ^{239}Pu in 10,000 years is:

$$4.27411 \cdot 10^{21} \text{ d} \cdot 5.15 \text{ MeV/d} = 2.20117 \cdot 10^{28} \text{ eV}. \quad (28)$$

The number of moles of H_2 formed is:

$$2.20117 \cdot 10^{28} \text{ eV} \cdot 1.25 \text{ molecules/100 eV} /$$

$$6.0225 \cdot 10^{23} \text{ molecules/mole} = 4.57 \cdot 10^{2} \text{ moles/drum}. \quad (29)$$

In Equation 29, "1.25 molecules per 100 eV" is the midpoint of the range of $G(H_2)$ (1.1 to 1.4 molecules per 100 eV) reported by Reed and Okajima (in prep.) for three WIPP brines (see above) and "$6.0225 \cdot 10^{23}$ molecules/mole is Avogadro's number. Therefore, "$4.57 \cdot 10^{2}$ moles/drum" is actually the midpoint of a range of 4.02 to $5.12 \cdot 10^{2}$ moles per drum.

In addition to about 500 moles of H_2 per drum, the O_2-production potential for brine radiolysis by ^{239}Pu could be as high as about 250 moles per drum, depending on the induction period for O_2 production from the breakdown of O-containing intermediate species (above). However, Garner and I believe that oxic corrosion and aerobic microbial activity (above) will rapidly consume any O_2 produced by brine radiolysis. Therefore, we omit O_2 from the discussion that follows.

Although these results includes decay of ^{239}Pu but none of the other radionuclides in TRU waste, they are of the same order of magnitude as the H_2-production potential of 900 moles per drum from anoxic corrosion of steel CH TRU waste containers (drums and boxes) and steels and other Fe-base alloys in CH TRU waste (Brush, 1990). They are also similar to my calculated gas-production potential of 600 moles per drum from microbial degradation 100% of the cellulosics and 50% of the rubbers in CH TRU waste.

However, values of 500 moles of H_2 per drum and 750 moles of H_2 plus O_2 per drum for the gas-production potential from brine radiolysis by ^{239}Pu are probably far larger than what will actually be produced in WIPP disposal rooms. The assumption that all of the energy from decay of ^{239}Pu will be deposited in brine is probably far too pessimistic. It is much more likely that a significant fraction of this decay energy will be deposited in undissolved, particulate, Pu-bearing solids or other solids with which Pu is associated (cellulosics such as paper towels, articles of clothing, rubber gloves, other solids in sludges, etc.)

Preliminary results obtained after adding brine radiolysis to the PA code PANEL also suggest that actual radiolytic gas production will be much smaller than the gas-production potentials calculated above. (The addition of brine radiolysis to PANEL is the first step in the addition of brine radiolysis to the reaction-path gas-generation model.) PANEL calculates the quantities of radionuclides dissolved in brine in WIPP disposal rooms as a function of time. Currently, it uses either an internal analytical model or the two-phase flow code BRAGFLO to predict the quantity of Salado- or Castile-Fm. brine present as a function of time. It then uses Latin hypercube sampling of solubilities estimated by the Expert Panel to predict the solubilities of Pu and other important actinide elements, and uses the initial inventory and decay rates of individual isotopes of these elements to calculate the relative abundance of each dissolved radionuclide as a function of time. Garner added the equations used to calculate the gas-production potential from decay of ^{239}Pu (above) to PANEL and extended them to include other important α-emitting radionuclides in the WIPP inventory. For his preliminary calculations, Garner used predictions of brine inflow and outflow from BRAGFLO runs made for the last round of PA calculations (WIPP Performance Assessment Department, 1992), which included the average-stoichiometry gas-generation model. The brine volume in a panel varied with time in each vector (simulation). However, the gas-generation rates from anoxic corrosion and microbial activity and the dissolved concentration of each

radioactive element did not vary within a given vector, unless brine was completely consumed or the quantity of a radioactive element in the inventory limited its concentration to a value less than the sampled solubility.

The largest quantity of H_2 produced by brine radiolysis during the 10,000-year period of performance of the repository was 90 moles per drum, a value significantly smaller than the 500-mole-per-drum H_2-production potential from decay of ^{239}Pu calculated above. In this vector, the ^{241}Am was the largest contributor to radiolytic H_2 production. Furthermore, 50% of the 70 vectors produced less than 2 moles of H_2 per drum, a value less than 0.5% of the H_2-production potential.

Clearly, the difference between the H_2-production potential and the values calculated using PANEL suggest that gas production in WIPP disposal rooms may actually be far less than the gas-production potentials. The main reasons for this appear to be: (1) calculations of gas-production potentials often include worst-case assumptions; (2) these calculations also neglect interactions between or among processes; these interactions may significantly decrease the amount of gas produced.

CONSUMPTION OF GASES

The compounds $Ca(OH)_2$ (in hydrated cementitious materials and CaO (a potential backfill additive) could consume significant quantities of CO_2 and H_2S by the reactions:

$$Ca(OH)_2 + CO_2 = CaCO_3 + H_2O; \tag{30a}$$

$$Ca(OH)_2 + H_2S = CaS + 2H_2O; \tag{30b}$$

$$CaO + CO_2 = CaCO_3; \tag{31a}$$

$$CaO + H_2S = CaS + H_2O. \tag{31b}$$

In bench-scale laboratory experiments, $Ca(OH)_2$, dissolved in WIPP brines, reacts very rapidly with gaseous CO_2. Dissolved, hydrated CaO, solid $Ca(OH)_2$ and solid CaO would probably also react very rapidly with gaseous CO_2. However, the effects of transport phenomena must be incorporated in predictions of the rates of CO_2 and, perhaps, H_2S uptake by these compounds in WIPP disposal rooms. Furthermore, estimates of the quantities of hydrated cementitious materials and the concentrations of $Ca(OH)_2$ in these materials are necessary for room-

scale predictions. Therefore, I have not estimated rates for these reactions yet.

REFERENCES

Berner, R. A. (1980). **Early Diagenesis: A Theoretical Approach.** Princeton University Press, Princeton, NJ.

Brush, L. H. (1990). **Test Plan for Laboratory and Modeling Studies of Repository and Radionuclide Chemistry for the Waste Isolation Pilot Plant**, SAND90-0266, Sandia National Laboratories, Albuquerque, NM.

Brush, L. H. (1991). Current Estimates of Gas Production Rates, Gas Production Potentials, and Expected Chemical Conditions Relevant to Radionuclide Chemistry for the Long-Term WIPP Performance Assessment. In WIPP Performance Assessment Division, **Preliminary Comparison with 40 CFR Part 191, Subpart B for the Waste Isolation Pilot Plant**, December 1991, SAND91-0893/3, Sandia National Laboratories, Albuquerque, NM, pp. A-27 to A-36.

Brush, L. H., M. A. Molecke, R. E. Westerman, A. J. Francis, J. B. Gillow, R. H. Vreeland, and D. T. Reed (1992). **Laboratory Studies of Gas Generation for the Waste Isolation Pilot Plant.** Presented at the Materials Research Society's Symposium on the Scientific Basis for Nuclear Waste Management, Boston, Ma., November 30 to December 4, 1992.

Francis, A. J., and J. B. Gillow. **Effects of Microbial Processes on Gas Generation under Expected WIPP Conditions: Annual Report through 1992.** SAND93-7036, Sandia National Laboratories, Albuquerque, NM, in prep.

Froelich, P. N., G. P. Klinkhammer, M. L. Bender, N. A. Luedtke, G. R. Heath, D. Cullen, P. Dauphin, D. Hammond, B. Hartman, and V. Maynard (1979). Early Oxidation of Organic Matter in Pelagic Sediments of the Eastern Equatorial Atlantic: Suboxic Diagenesis, **Geochimica et Cosmochimica Acta**, Vol. 43, pp. 1075-1090.

Grauer, R., B. Knecht, P. Kreis, and J. P. Simpson (1991). Hydrogen Evolution from Corrosion of Iron and Steel in Intermediate Level Waste Repositories. In T. A. Abrajano, Jr., and L. H. Johnson, Eds., **Scientific Basis for Nuclear Waste Management XIV, Symposium held November 26-29, 1990, Boston, Massachusetts, U.S.A., Materials Research Society Symposia Proceedings**, Vol. 44, Materials Research Society, Pittsburgh, PA, pp. 295-302.

Lappin, A. R., R. L. Hunter, D. P. Garber, and P. B. Davies, Eds. (1989). **Systems Analysis, Long-Term Radionuclide Transport, and Dose Assessments, Waste Isolation Pilot Plant (WIPP), Southeastern New Mexico; March, 1989.** SAND89-0462, Sandia National Laboratories, Albuquerque, NM.

Molecke, M. A. (1979). Gas Generation from Transuranic Waste Degradation: Data Summary and Interpretation. SAND79-1245, Sandia National Laboratories, Albuquerque, NM.

Molecke, M. A. (1983). A Comparison of Brines Relevant to Nuclear Waste Experimentation. SAND83-0516, Sandia National Laboratories, Albuquerque, NM.

Reed, D. T., and S. Okajima. Radiation Effects Studies in Support of the Waste Isolation Pilot Plant: Progress Report for Fiscal Year 1992. SAND??-????, Sandia National Laboratories, Albuquerque, NM, in prep.

Telander, M. R., and R. E. Westerman. Hydrogen Generation by Metal Corrosion in Simulated WIPP Environments: Progress Report for Period November 1989 - December 1992. SAND92-7347, Sandia National Laboratories, Albuquerque, NM, in prep.

Trauth, K. M., S. C. Hora, R. P. Rechard, and D. R. Anderson (1992). The Use of Expert Judgement to Quantify Uncertainty in Solubility and Sorption Parameters for Waste Isolation PLant Performance Assessment, SAND92-0479, Sandia National Laboratories, Albuquerque, NM.

Uhlig, H. H., and R. W. Revie (1963). Corrosion and Corrosion Control: An Introduction to Corrosion Science and Engineering. John Wiley and Sons, New York, NY.

WIPP Performance Assessment Department (1992). Preliminary Performance Assessment for the Waste Isolation Pilot PLant, December 1992. Volume 4: Uncertainty and Sensitivity Analysis for 40 CFR 191, Subpart B. SAND92-0700/4, Sandia National Laboratories, Albuquerque, NM..

TABLE 1. GAS-GENERATION REACTIONS

Reaction	Abbreviation
Oxic corrosion of steels and other Fe-base materials:	
1. $2Fe + H_2O + 1.5O_2 = 2\gamma FeO(OH)$	Fe to $\gamma FeO(OH)$[1]
Anoxic corrosion of steels and other Fe-base materials:	
6a. $Fe + 2H_2O = Fe(OH)_2 + H_2$	Fe to $Fe(OH)_2$[2]
6b. $3Fe + 4H_2O = Fe_3O_4 + 4H_2$	Fe to Fe_3O_4[2]
7. $Fe + H_2O + CO_2 = FeCO_3 + H_2$	Fe to $FeCO_3$[2]
8a. $Fe + 2H_2S = FeS_2 + 2H_2$	Fe to FeS_2[2]
8b. $Fe + H_2S = FeS + H_2$	Fe to FeS[2]
Microbial degradation of cellulosics and, perhaps, plastics and rubbers:	
12. $CH_2O + O_2 = H_2O + CO_2$	Aerobic respiration[1]
13. $CH_2O + 0.8H^+ + 0.8NO_3^-$ $= 1.4H_2O + CO_2 + 0.4N_2$	Denitrification[2]

TABLE 1. GAS-GENERATION REACTIONS (cont.)

Reaction	Abbreviation
Microbial degradation of cellulosics and, perhaps, plastics and rubbers (cont.):	
14a. $CH_2O + 4FeO(OH) + H_2O$	
$= 4Fe(OH)_2 + CO_2$	Fe(III) reduction[1]
14b. $CH_2O + 4FeO(OH)$	
$= 1.33Fe_3O_4 + 1.67H_2O + CO_2 + 1.33H_2$	Fe(III) reduction[1]
14c. $CH_2O + 4FeO(OH) + H_2O + 3CO_2$	
$= 4FeCO_3 + 4H_2O$	Fe(III) reduction[1]
14d. $CH_2O + 4FeO(OH) + 4H_2S$	
$= 4FeS + 7H_2O + CO_2$	Fe(III) reduction[1]
14e. $CH_2O + 4FeO(OH) + 8H_2S$	
$= 4FeS_2 + 7H_2O + CO_2 + 4H_2$	Fe(III) reduction[1]
15. $CH_2O + H^+ + 0.5SO_4^{2-}$	
$= H_2O + CO_2 + 0.5\ H_2S$	SO_4^{2-} reduction[2]
16a. $2CH_2O = CH_4 + CO_2$	Methanogenesis[2]
16b. $CO_2 + 4H_2 = CH_4 + 2H_2O$	Methanogenesis[2]

TABLE 1. GAS-GENERATION REACTIONS (cont.)

Reaction	Abbreviation
Radiolysis:	
17. $H_2O = H_2 + 0.5O_2$	Radiolysis of brine[1]
Consumption of gases by cementitious materials and backfill additives:	
25a. $Ca(OH)_2 + CO_2 = CaCO_3 + H_2O$	$Ca(OH)_2$ to $CaCO_3$[2]
25b. $Ca(OH)_2 + H_2S = CaS + 2H_2O$	$Ca(OH)_2$ to CaS[2]
26a. $CaO + CO_2 = CaCO_3$	CaO to $CaCO_3$[2]
26b. $CaO + H_2S = CaS + H_2O$	CaO to CaS[12]

1. Probably will not have a significant, direct effect on the gas and H_2O budget of WIPP disposal rooms, but could be important from the standpoint of the O_2 budget of the repository (see text).

2. Could have a significant, direct effect on the gas and H_2O budget of the repository (see text).

TABLE 2. INUNDATED GAS-PRODUCTION RATES

Process	Gas-Production Rate		
	Minimum	Best	Maximum
Oxic corrosion of steels and other Fe-base materials:			
moles $O_2/(m^2$ steel · yr)	0	- 5	- 8
moles O_2/(drum · yr)	0[1]	- 30[1]	- 50[1]
μm steel/yr	0	50	80
Anoxic corrosion of steels and other Fe-base materials:			
moles $H_2/(m^2$ steel · yr)	0	0.1	20
moles H_2/(drum · yr)	0[1]	0.6[1]	100[1]
μm steel/yr	0	1	200
Microbial degradation of cellulosics (Reactions 12 through 16b):			
moles gas/(kg cellulose · yr)	0[2]	0.1[2]	0.5[2]
moles gas/(drum · yr)	0[1, 2]	1[1, 2]	5[1, 2]
Microbial degradation of cellulosics (Reaction 16b):			
moles gas/(kg cellulose · yr)	Not est.[3]	Not est.[3]	Not est.[3]
moles gas/(drum · yr)	Not est.[3]	Not est.[3]	Not est.[3]

TABLE 2. INUNDATED GAS-PRODUCTION RATES (cont.)

Reaction	Gas-Production Rate[1]		
	Minimum	Best	Maximum
Radiolysis of brine:			
moles $H_2/(m^3 \cdot yr)$	$4.5 \cdot 10^{-14}$	$1.1 \cdot 10^{-6}$	$9.9 \cdot 10^{-1}$
moles $H_2/(drum \cdot yr)$	$8.9 \cdot 10^{-16}$	$6.6 \cdot 10^{-8}$	$1.2 \cdot 10^{-1}$
moles $O_2/(m^3 \cdot yr)$	$2.2 \cdot 10^{-14}$	$5.4 \cdot 10^{-7}$	$5.0 \cdot 10^{-1}$
moles $O_2/(drum \cdot yr)$	$4.5 \cdot 10^{-16}$	$3.3 \cdot 10^{-8}$	$6.0 \cdot 10^{-2}$
moles $(H_2 + O_2)/(m^3 \cdot yr)$	$6.7 \cdot 10^{-14}$	$1.6 \cdot 10^{-6}$	$1.5 \cdot 10^{0}$
moles $(H_2 + O_2)/(drum \cdot yr)$	$1.3 \cdot 10^{-15}$	$9.9 \cdot 10^{-8}$	$1.8 \cdot 10^{-1}$
Consumption of CO_2 by cementitious materials and backfill additives:			
moles gas/(drum · yr)	Not est.[4]	Not est.[4]	Not est.[4]

1. Estimates do not include steels or other Fe-base alloys associated with RH TRU waste or steels or other Fe-base alloys used for ground support.

2. Gases produced by Reactions 12 through 16a could include CO_2, CH_4, H_2S, N_2, and NH_3 (see text).

3. Not estimated yet, but gases consumed by Reaction 16b could include significant quantities of CO_2 and especially H_2 (see text).

4. Not estimated yet, but gases consumed by $Ca(OH)_2$ and CaO in cementitious materials and backfill additives could include significant quantities of CO_2 and, perhaps, H_2S (see text).

TABLE 3. HUMID GAS-PRODUCTION RATES

Process	Gas-Production Rate		
	Minimum	Best	Maximum
Oxic corrosion of steels and other Fe-base materials:			
moles O_2/(m^2 steel · yr)	0	- 0.5	- 5
moles O_2/(drum · yr)	0[1]	- 3[1]	- 30[1]
μm steel/yr	0	5	50
Anoxic corrosion of steels and other Fe-base materials:			
moles H_2/(m^2 steel · yr)	0	0	0.01
moles H_2/(drum · yr)	0[1]	0[1]	0.06[1]
μm steel/yr	0	0	0.1
Microbial degradation of cellulosics (Reactions 12 through 16b):			
moles gas/(kg cellulose · yr)	0[2]	0.01[2]	0.1[2]
moles gas/(drum · yr)	0[1, 2]	0.1[1, 2]	1[1, 2]
Microbial degradation of cellulosics (Reaction 16b):			
moles gas/(kg cellulose · yr)	Not set.[3]	Not est.[3]	Not est.[3]
moles gas/(drum · yr)	Not est.[3]	Not est.[3]	Not est.[3]

TABLE 3. HUMID GAS-PRODUCTION RATES (cont.)

Process	Gas-Production Rate		
	Minimum	Best	Maximum
Radiolysis of brine:			
moles $H_2/(m^3 \cdot yr)$	0	0	0
moles $H_2/(drum \cdot yr)$	0	0	0
moles $O_2/(m^3 \cdot yr)$	0	0	0
moles $O_2/(drum \cdot yr)$	0	0	0
moles $(H_2 + O_2)/(m^3 \cdot yr)$	0	0	0
moles $(H_2 + O_2)/(drum \cdot yr)$	0	0	0
Consumption of gases by cementitious materials and backfill additives:			
moles gas/(drum · yr)	Not est.[4]	Not est.[4]	Not est.[4]

1. Estimates do not include steels or other Fe-base alloys associated with RH TRU waste or steels or other Fe-base alloys used for ground support.

2. Gases produced by Reactions 12 through 16a could include CO_2, CH_4, H_2S, N_2, and NH_3 (see text).

3. Not estimated yet, but gases consumed by Reaction 16b could include significant quantities of CO_2 and especially H_2 (see text).

4. Not estimated yet, but gases consumed by $Ca(OH)_2$ and CaO in cementitious materials and backfill additives could include significant quantities of CO_2 and, perhaps, H_2S (see text).

TABLE 4. RADIOLYTIC GAS-PRODUCTION RATES (mol/m^3 of brine·yr)[1, 2]

Dissolved ^{239}Pu Conc. (M)	Gas-Production Rate		
	H_2	O_2	$H_2 + O_2$
$1 \cdot 10^{0}$	$1.8 \cdot 10^{3}$	$0.9 \cdot 10^{3}$	$2.7 \cdot 10^{3}$
$1 \cdot 10^{-1}$	$1.8 \cdot 10^{2}$	$0.9 \cdot 10^{2}$	$2.7 \cdot 10^{2}$
$1 \cdot 10^{-2}$	$1.8 \cdot 10^{1}$	$0.9 \cdot 10^{1}$	$2.7 \cdot 10^{1}$
$1 \cdot 10^{-3}$	$1.8 \cdot 10^{0}$	$0.9 \cdot 10^{0}$	$2.7 \cdot 10^{0}$
$1 \cdot 10^{-4}$	$1.8 \cdot 10^{-1}$	$0.9 \cdot 10^{-1}$	$2.7 \cdot 10^{-1}$
$1 \cdot 10^{-5}$	$1.8 \cdot 10^{-2}$	$0.9 \cdot 10^{-2}$	$2.7 \cdot 10^{-2}$
$1 \cdot 10^{-6}$	$1.8 \cdot 10^{-3}$	$0.9 \cdot 10^{-3}$	$2.7 \cdot 10^{-3}$
$1 \cdot 10^{-7}$	$1.8 \cdot 10^{-4}$	$0.9 \cdot 10^{-4}$	$2.7 \cdot 10^{-4}$
$1 \cdot 10^{-8}$	$1.8 \cdot 10^{-5}$	$0.9 \cdot 10^{-5}$	$2.7 \cdot 10^{-5}$
$1 \cdot 10^{-9}$	$1.8 \cdot 10^{-6}$	$0.9 \cdot 10^{-6}$	$2.7 \cdot 10^{-6}$

1. Rates in moles per m^3 of brine per year calculated from experimentally measured values of $G(H_2)$ (see text).

2. Values in bold type may exceed the maximum <u>average</u> Pu concentration or <u>average</u> gas-production rate depending on the quantity of brine present and time (see text).

TABLE 5. RADIOLYTIC H_2-PRODUCTION RATES (mol/drum·yr)[1, 2]

Dissolved ^{239}Pu Conc. (M)	Brine Volume (m^3/room)			
	135	305	525	815
$1 \cdot 10^{0}$	$3.6 \cdot 10^{1}$	$8.1 \cdot 10^{1}$	$1.4 \cdot 10^{2}$	$2.2 \cdot 10^{2}$
$1 \cdot 10^{-1}$	$3.6 \cdot 10^{0}$	$8.1 \cdot 10^{0}$	$1.4 \cdot 10^{1}$	$2.2 \cdot 10^{1}$
$1 \cdot 10^{-2}$	$3.6 \cdot 10^{-1}$	$8.1 \cdot 10^{-1}$	$1.4 \cdot 10^{0}$	$2.2 \cdot 10^{0}$
$1 \cdot 10^{-3}$	$3.6 \cdot 10^{-2}$	$8.1 \cdot 10^{-2}$	$1.4 \cdot 10^{-1}$	$2.2 \cdot 10^{-1}$
$1 \cdot 10^{-4}$	$3.6 \cdot 10^{-3}$	$8.1 \cdot 10^{1-3}$	$1.4 \cdot 10^{-2}$	$2.2 \cdot 10^{-2}$
$1 \cdot 10^{-5}$	$3.6 \cdot 10^{-4}$	$8.1 \cdot 10^{-4}$	$1.4 \cdot 10^{-3}$	$2.2 \cdot 10^{-3}$
$1 \cdot 10^{-6}$	$3.6 \cdot 10^{-5}$	$8.1 \cdot 10^{-5}$	$1.4 \cdot 10^{-4}$	$2.2 \cdot 10^{-4}$
$1 \cdot 10^{-7}$	$3.6 \cdot 10^{-6}$	$8.1 \cdot 10^{-6}$	$1.4 \cdot 10^{-5}$	$2.2 \cdot 10^{-5}$
$1 \cdot 10^{-8}$	$3.6 \cdot 10^{-7}$	$8.1 \cdot 10^{-7}$	$1.4 \cdot 10^{-6}$	$2.2 \cdot 10^{-6}$
$1 \cdot 10^{-9}$	$3.6 \cdot 10^{-8}$	$8.1 \cdot 10^{-8}$	$1.4 \cdot 10^{-7}$	$2.2 \cdot 10^{-7}$

1. Rates in moles per drum per year calculated from values in moles per m^3 of brine per year (see text).

2. Values in bold type may exceed the maximum <u>average</u> H_2-production rate depending on the quantity of brine present and time (see text).

TABLE 6. RADIOLYTIC O_2-PRODUCTION RATES (mol/drum·yr)[1, 2]

Dissolved ^{239}Pu Conc. (M)	Brine Volume (m^3/room)			
	135	305	525	815
$1 \cdot 10^{0}$	$1.8 \cdot 10^{1}$	$4.0 \cdot 10^{1}$	$6.9 \cdot 10^{1}$	$1.1 \cdot 10^{2}$
$1 \cdot 10^{-1}$	$1.8 \cdot 10^{0}$	$4.0 \cdot 10^{0}$	$6.9 \cdot 10^{0}$	$1.1 \cdot 10^{1}$
$1 \cdot 10^{-2}$	$1.8 \cdot 10^{-1}$	$4.0 \cdot 10^{-1}$	$6.9 \cdot 10^{-1}$	$1.1 \cdot 10^{0}$
$1 \cdot 10^{-3}$	$1.8 \cdot 10^{-2}$	$4.0 \cdot 10^{-2}$	$6.9 \cdot 10^{-2}$	$1.1 \cdot 10^{-1}$
$1 \cdot 10^{-4}$	$1.8 \cdot 10^{-3}$	$4.0 \cdot 10^{-3}$	$6.9 \cdot 10^{-3}$	$1.1 \cdot 10^{-2}$
$1 \cdot 10^{-5}$	$1.8 \cdot 10^{-4}$	$4.0 \cdot 10^{-4}$	$6.9 \cdot 10^{-4}$	$1.1 \cdot 10^{-3}$
$1 \cdot 10^{-6}$	$1.8 \cdot 10^{-5}$	$4.0 \cdot 10^{-5}$	$6.9 \cdot 10^{-5}$	$1.1 \cdot 10^{-4}$
$1 \cdot 10^{-7}$	$1.8 \cdot 10^{-6}$	$4.0 \cdot 10^{-6}$	$6.9 \cdot 10^{-6}$	$1.1 \cdot 10^{-5}$
$1 \cdot 10^{-8}$	$1.8 \cdot 10^{-7}$	$4.0 \cdot 10^{-7}$	$6.9 \cdot 10^{-7}$	$1.1 \cdot 10^{-6}$
$1 \cdot 10^{-9}$	$1.8 \cdot 10^{-8}$	$4.0 \cdot 10^{-8}$	$6.9 \cdot 10^{-8}$	$1.1 \cdot 10^{-7}$

1. Rates in moles per drum per year calculated from experimentally measured values of $G(H_2)$ (see text).

2. Values in bold type may exceed the maximum <u>average</u> O_2-production rate depending on the quantity of brine present and time (see text).

TABLE 7. RADIOLYTIC GAS- (H_2 + O_2)-PRODUCTION RATES (mol/drum·yr)[1, 2]

Dissolved ^{239}Pu Conc. (M)	Brine Volume (m^3/room)			
	135	305	525	815
$1 \cdot 10^{0}$	$5.4 \cdot 10^{1}$	$1.2 \cdot 10^{2}$	$2.1 \cdot 10^{2}$	$3.2 \cdot 10^{2}$
$1 \cdot 10^{-1}$	$5.4 \cdot 10^{0}$	$1.2 \cdot 10^{1}$	$2.1 \cdot 10^{1}$	$3.2 \cdot 10^{1}$
$1 \cdot 10^{-2}$	$5.4 \cdot 10^{-1}$	$1.2 \cdot 10^{0}$	$2.1 \cdot 10^{0}$	$3.2 \cdot 10^{0}$
$1 \cdot 10^{-3}$	$5.4 \cdot 10^{-2}$	$1.2 \cdot 10^{-1}$	$2.1 \cdot 10^{-1}$	$3.2 \cdot 10^{-1}$
$1 \cdot 10^{-4}$	$5.4 \cdot 10^{-3}$	$1.2 \cdot 10^{-2}$	$2.1 \cdot 10^{-2}$	$3.2 \cdot 10^{-2}$
$1 \cdot 10^{-5}$	$5.4 \cdot 10^{-4}$	$1.2 \cdot 10^{-3}$	$2.1 \cdot 10^{-3}$	$3.2 \cdot 10^{-3}$
$1 \cdot 10^{-6}$	$5.4 \cdot 10^{-5}$	$1.2 \cdot 10^{-4}$	$2.1 \cdot 10^{-4}$	$3.2 \cdot 10^{-4}$
$1 \cdot 10^{-7}$	$5.4 \cdot 10^{-6}$	$1.2 \cdot 10^{-5}$	$2.1 \cdot 10^{-5}$	$3.2 \cdot 10^{-5}$
$1 \cdot 10^{-8}$	$5.4 \cdot 10^{-7}$	$1.2 \cdot 10^{-6}$	$2.1 \cdot 10^{-6}$	$3.2 \cdot 10^{-6}$
$1 \cdot 10^{-9}$	$5.4 \cdot 10^{-8}$	$1.2 \cdot 10^{-7}$	$2.1 \cdot 10^{-7}$	$3.2 \cdot 10^{-7}$

1. Rates in moles per drum per year calculated from experimentally measured values of $G(H_2)$ (see text).

2. Values in bold type may exceed the maximum <u>average</u> gas-production rate depending on the quantity of brine present and time (see text).

TABLE 8. MAXIMUM AVERAGE Pu CONCENTRATIONS IN BRINES IN WIPP DISPOSAL ROOMS (M)[1]

	Brine Volume (m^3/room)			
Time (yr)	135	305	525	815
0	$1.60 \cdot 10^{-3}$	$7.09 \cdot 10^{-4}$	$4.12 \cdot 10^{-4}$	$2.65 \cdot 10^{-4}$
100	$1.56 \cdot 10^{-3}$	$6.91 \cdot 10^{-4}$	$4.02 \cdot 10^{-4}$	$2.59 \cdot 10^{-4}$
200	$1.54 \cdot 10^{-3}$	$6.84 \cdot 10^{-4}$	$3.97 \cdot 10^{-4}$	$2.56 \cdot 10^{-4}$
500	$1.52 \cdot 10^{-3}$	$6.73 \cdot 10^{-4}$	$3.91 \cdot 10^{-4}$	$2.52 \cdot 10^{-4}$
1,000	$1.49 \cdot 10^{-3}$	$6.61 \cdot 10^{-4}$	$3.84 \cdot 10^{-4}$	$2.47 \cdot 10^{-4}$
2,000	$1.44 \cdot 10^{-3}$	$6.39 \cdot 10^{-4}$	$3.71 \cdot 10^{-4}$	$2.39 \cdot 10^{-4}$
5,000	$1.31 \cdot 10^{-3}$	$5.78 \cdot 10^{-4}$	$3.36 \cdot 10^{-4}$	$2.16 \cdot 10^{-4}$
10,000	$1.11 \cdot 10^{-3}$	$4.92 \cdot 10^{-4}$	$2.86 \cdot 10^{-4}$	$1.84 \cdot 10^{-4}$

1. Calculations include all isotopes of Pu expected in the repository, not just ^{239}Pu (see text).

Distribution:

J. N. Butler, Harvard University
A. J. Francis, Brookhaven National Laboratory
J. B. Gillow, Brookhaven National Laboratory
D. T. Reed, Argonne National Laboratory
R. H. Vreeland, West Chester University
R. E. Westerman, Pacific Northwest Laboratory
6115 P. B. Davies
6119 F. Gelbard, Acting
6121 J. R. Tillerson
6303 W. D. Weart
6305 S. A. Goldstein
6305 A. R. Lappin
6306 A. L. Stevens
6342 D. R. Anderson
6342 Staff
6343 V. Harper-Slaboszewicz
6345 R. C. Lincoln
6345 Staff
6347 D. R. Schafer
6347 Staff
6348 J. T. Holmes
6348 Staff
6352 SWCF (6): RC (WBS 1.1.1.1.3), RC/AC (WBS 1.1.1.1.3), RC/MA (WBS 1.1.1.1.3), RC/R (WBS 1.1.1.1.3), RC/BA (WBS 1.1.1.1.3), RC/GGM (WBS 1.1.1.2.5)